DESIGN OF SHELL-TYPE LIGANDS FOR LUMINESCENT LANTHANIDE COMPLEXES

By

Dita Davis

A thesis submitted to
The University of Birmingham
For the degree of
DOCTOR OF PHILOSOPHY

The University of Birmingham
October 2010

Abstract

Work undertaken for this thesis involve ligands with defined architectures for an investigation of structural and photophysical properties of luminescent lanthanide complexes. The ligand design presented herein is focusing on satisfying three main requirements, in order to maximise the ligand potential to act as an efficient sensitiser for the lanthanide luminescence;

- A strong, negative binding site containing 'hard' oxygen atoms, which bind strongly to lanthanides.
- Aromatic units acting as chromophores and as an encapsulating 'hydrophobic shell' in order to protect the lanthanide ion from solvent coordination.
- Separate binding and antenna domains, hence the chromophore group can be easily modified without affecting the binding unit.

A series of lanthanide complexes Ln(**tpOp**)$_3$, (where Ln = Eu, Tb, Sm, Dy, Nd, Er, Yb, Gd) based on tetraphenyl imidodiphosphate ligand (H**tpOp**) have been prepared in order to investigate the ligand ability to act as a sensitiser for *f-f* based luminescence for the visible and NIR emitting ions. It has been shown that the H**tpOp** ligand can efficiently populate the excited levels of visible lanthanides and to lesser extent can act as a suitable sensitiser for Yb^{3+} and Nd^{3+} NIR emitters.

Furthermore, novel bimetallic luminescent lanthanide complexes Ln_2(**bistpOp**)$_3$ (where Ln = Eu, Tb, Sm, Dy, Nd, Er, Yb, Gd) based on two imidodiphosphate binding sites have been prepared for the examination of dinuclear lanthanide complexes formation. The sensitising properties of the **bistpOp** have been investigated by luminescence spectroscopy.

A new ligand based on biphenyl sensitisers has been developed utilising an imidodiphosphate binding site (H**biphen**). The lanthanide complexes Ln(**biphen**)$_3$ (where Ln = Eu, Tb, Sm, Dy, Nd, Er, Yb, Gd) have been prepared and their photophysical properties analysed. The H**biphen** provided enhanced absorption to the lanthanide complexes but did not have a beneficial effect on the increase of visible luminescence of its complexes.

CONTENTS

III ABBREVIATIONS

δ	chemical shift
$\subset$	Cryptand
τ	luminescent lifetime
ε	molar absorption coefficient
Φ	(absolute) luminescence quantum yield
λ	Wavelength
ν	harmonic vibration number / frequency
λ_{em}	wavelength of emission
Φ_{ET}	energy transfer quantum yield
λ_{exc}	wavelength of excitation
Φ_{ISC}	intersystem crossing quantum yield
Φ_{Ln}	intrinsic (lanthanide) quantum yield
λ_{max}	absorption maximum
τ_{obs}	observed luminescent lifetime
$[Ru(bpy)_3]Cl_2$	tris(2,2'-bipyridyl)dichlororuthenium(II) hexahydrate
°C	(degrees) Celsius
$^1\pi\pi$	singlet state
$^1\pi\pi^*$	excited singlet state
2D	two dimensional
$^3\pi\pi$	triplet state
$^3\pi\pi^*$	excited triplet state
Å	Angstrom
amu	atomic mass unit
aq	Aqueous
Ar	Aromatic
bpy	Bipyridine
br	Broad
COSY	correlation spectroscopy
DMSO	Dimethylsulfoxide
DTPA	diethylenetriaminepentaacetic acid
E	Energy
ES	Electrospray
ET	energy transfer
EtOH	Ethanol
$h\nu$	photon
HPLC	High performance liquid chromatography
HSQC	heteronuclear single quantum correlation
IR	Infrared
ISC	Inter system crossing
J^2	coupling constant
J	total angular momentum
k	rate constant
K	(degrees) Kelvin
L	orbital quantum number
LED	light emitting diode
Ln	lanthanide
Ln*	excited lanthanide state
m	Meta
m	Multiplet
m/z	mass to charge ratio
MALDI	matrix assisted laser desorption ionisation
MeCN	Acetonitrile

MM2	molecular mechanics 2
MOF	metal-organic framework
MRI	magnetic resonance imaging
MS	mass spectrometry
NIR	Near infrared
NMR	nuclear magnetic resonance
o	Ortho
p	Para
PENDANT	polarisation enhancement during attached nucleus testing
Ph	Phenyl
PMT	photomultiplier tube
ppm	Parts per million
q	(number of) coordinated solvent molecules
q	Quaternary
r	Distance
s	Singlet
S	spin quantum number
S_0	singlet ground state
S_1	lowest singlet excited state
t	Triplet
T_1	triplet state
THF	Tetrahydrofuran
TOF	Time of flight
UV	Ultraviolet
UV-Vis	Ultra violet / visible
XRD	X-ray diffraction
ύ	wave number
Z_{eff}	effective nuclear charge

1.0. Introduction

1.1. Overview

An extensive amount of research is focusing on design of ligands that encapsulate rare earth ions and can act as suitable chromophores for sensitising visible and NIR emitting ions. This introduction is focused on the development of luminescent lanthanide complexes with organic sensitising ligands by the self-assembly approach.

1.2. The lanthanide elements

The lanthanide (Ln) elements consist a group of fifteen elements from lanthanum to lutetium with atomic numbers 57 to 71 and are positioned in the *f*-block between the *s* and *d* blocks in period 6. Their electronic configurations range from $[Xe]4f^{0}5d^{1}6s^{2}$ for La to $[Xe]4f^{14}5d^{1}6s^{2}$ for Lu. The fourteen 4*f* electrons are added with some irregularities in the case of the atomic electronic configuration, while the progression is perfectly regular from $4f^{1}$ to $4f^{14}$ in lanthanides. Hence, their chemistry is very similar. All lanthanides show a stable +3 oxidation state, as any further ionisation results in the *f* electrons being held too tightly to gain any energetic benefit from reaction. However, there are some exceptions where the +2 and +4 oxidation states are also observed.[1-3] The +2 oxidation state of europium is especially prevalent as the difference in redox potential is small; $Eu^{3+} + e^{-} \rightarrow Eu^{2+} = -0.43$ V.[4] The easily reducible europium leads to the presence of charge transfer bands in complexes of Eu^{3+}.[5]

The coordination numbers of lanthanide cations are in the range 6 to 12, depending on the steric demand of the ligand, although 8 and 9 are the most common.[6,7] Lower

coordination numbers tend to be a result of the bulkiness of the ligand preventing further donor atoms from coordinating to the lanthanide ion.[8] Across the *f* block there is a gradual and uniform reduction in ionic radius with increasing atomic number (Table 1.1) which is termed the "lanthanide contraction".[1] This is due to the nature of the 4*f* orbitals: they are directional and disperse, hence the addition of electrons into the 4*f* shell does not compensate for the increased nuclear charge,[9] so the effective nuclear charge (Z_{eff}) becomes high, and a contraction of orbitals occurs as a result. The lanthanides 4*f* orbitals are effectively shielded by the filled $5s^2$ and $5p^6$ orbitals, and therefore behave as core orbitals. Thus complexed Ln^{3+} ions behave as the free ions would and coordination of ligands to lanthanide ions is largely of an electrostatic nature. Hence, the geometry of the complexes is not dictated by crystal-field effects but by the properties of ligands. Lanthanide ions are highly labile and require strongly coordinating polydentate ligands to form stable complexes, due to this ionic behaviour.

Y^{3+} is commonly used as a substitute in complexes when the properties of Ln^{3+} ions would be unfavourable, such as NMR spectroscopy; where lanthanide ions produce an extensive paramagnetic line broadening. The Y^{3+} ion has an inert noble gas electron configuration, as well as a very similar ionic radius to that of the lanthanides, and its chemistry closely resembles to that of lanthanide ions (Table 1.1.).

Table 1.1. Some selected properties of yttrium and f–block atoms and trivalent cations. [a]Atomic radius values for M(III) with coordination number = 6.[1]

Element	Atomic number and chemical symbol	Isolated atom electronic configuration	M^{3+} electronic configuration	M^{3+} ionic radius[a] (Å)
Yttrium	$_{39}$Y	[Kr]4$d^1$5s^2	[Kr]	1.040
Lanthanum	$_{57}$La	[Xe]5$d^1$6s^2	[Xe]	1.172
Cerium	$_{58}$Ce	[Xe]4$f^1$5$d^1$6s^2	[Xe]4f^1	1.150
Praseodymium	$_{59}$Pr	[Xe]4$f^3$6s^2	[Xe]4f^2	1.130
Neodymium	$_{60}$Nd	[Xe]4$f^4$6s^2	[Xe]4f^3	1.123
Promethium	$_{61}$Pm	[Xe]4$f^5$6s^2	[Xe]4f^4	1.110
Samarium	$_{62}$Sm	[Xe]4$f^6$6s^2	[Xe]4f^5	1.098
Europium	$_{63}$Eu	[Xe]4$f^7$6s^2	[Xe]4f^6	1.087
Gadolinium	$_{64}$Gd	[Xe]4$f^7$5$d^1$6s^2	[Xe]4f^7	1.078
Terbium	$_{65}$Tb	[Xe]4$f^9$6s^2	[Xe]4f^8	1.063
Dysprosium	$_{66}$Dy	[Xe]4f^{10}6s^2	[Xe]4f^9	1.052
Holmium	$_{67}$Ho	[Xe]4f^{11}6s^2	[Xe]4f^{10}	1.041
Erbium	$_{68}$Er	[Xe]4f^{12}6s^2	[Xe]4f^{11}	1.030
Thulium	$_{69}$Tm	[Xe]4f^{13}6s^2	[Xe]4f^{12}	1.020
Ytterbium	$_{70}$Yb	[Xe]4f^{14}6s^2	[Xe]4f^{13}	1.008
Lutetium	$_{71}$Lu	[Xe]4f^{14}5$d^1$6s^2	[Xe]4f^{14}	1.001

1.3. Photophysical properties of Ln^{3+} ions

The electronic absorption of the lanthanides is due to the 4*f*-4*f* transitions between excited and ground state lanthanide levels. The *f-f* transitions are forbidden by a number of rules; the Laporte (parity, $\Delta L \neq 0$) selection rule prohibits the redistribution of electrons in the 4*f* subshell and the orbital angular momentum selection rule ($\Delta l = \pm 1$) also forbids the *f-f* transitions. Certain transitions are also forbidden by the spin conservation selection rule ($\Delta S = 0$). Transitions may become allowed due to weak

vibronic coupling; in this process a molecular vibration temporarily lowers the symmetry of the lanthanide ion. The 4*f* orbital may therefore acquire symmetry characteristics of surrounding orbitals e.g. partial *p* character. The transitions, as a consequence, grow in intensity as symmetry and orbital angular momentum are changed. The absorption spectra are sharp and line-like due to the effective shielding of the *f* orbitals by the filled $5s^2 5p^6$ orbitals, therefore 4*f* orbitals interact only very weakly with ligand orbitals. This means that the symmetry rules are not relaxed by the same ligand field effect as for *d*-orbitals and therefore the absorption of lanthanide ions is intrinsically very weak ($\varepsilon \leq 10$ dm^3 mol^{-1} cm^{-1}).[10]

1.4. Lanthanide emission

The selection rules which apply for light absorption also apply to the luminescence of the lanthanide ions, again, based on the 4*f*-4*f* transitions. The transitions are only partially allowed and so there is a low probability of a transition from an excited state to the ground state of the lanthanide. This leads to the extended radiative luminescent lifetimes typical of lanthanide-based emission.

The ligand field can affect some *f-f* transitions of lanthanide ions. This can result in significant changes in spectral intensity and signal profiles for some emission peaks in the spectrum resulting from changes in coordination properties. These transitions are termed hypersensitive transitions,[11] and generally occur when the change in term symbols observe the following selection rules: $|\Delta L| \leq 2$ and $|\Delta J| \leq 2$.[12] A typical example of such a hypersensitive transition is the Eu^{3+} based $^5D_0$ -> $^7F_2$ transition, which is particularly sensitive to change in either coordination or the magnetic properties.[13] Hence, hypersensitive transitions can be used to probe aspects of the lanthanide coordination structure and environment.[12]

Lanthanide luminescence occurs when an excited-state *f* electron relaxes to the ground state. The energy lost in relaxation is expelled in the form of a photon of light. This can occur in either the visible or near-infrared region, depending on the lanthanide ion. The lanthanides can be divided into three categories depending upon the type of emission characteristics they possess;[14]

1) La^{3+}, Gd^{3+}, Lu^{3+} and Y^{3+}: no 4*f* -> 4*f* transitions are possible in La^{3+}, Lu^{3+} and Y^{3+} due to their electronic structures, therefore no emission is observed for these ions. In the case of Gd^{3+}, the lowest excited level ($^6P_{7/2}$) lies at 32,150 cm^{-1}, which is too high to allow an efficient energy transfer from a sensitising ligand, hence Gd^{3+} subsequently emits in the UV region.[15]
2) Eu^{3+}, Tb^{3+}, Dy^{3+}, Sm^{3+} lanthanide ions emit in the visible region.
3) Pr^{3+}, Nd^{3+}, Ho^{3+}, Er^{3+}, Tm^{3+} and Yb^{3+} lanthanide ions are the near-infrared emitters.

The characteristic wavelengths of emission are dependent upon the energy gap between the excited luminescent state and the ground state. The energy level diagram displaying the ground and excited state is depicted in Figure 1.1.

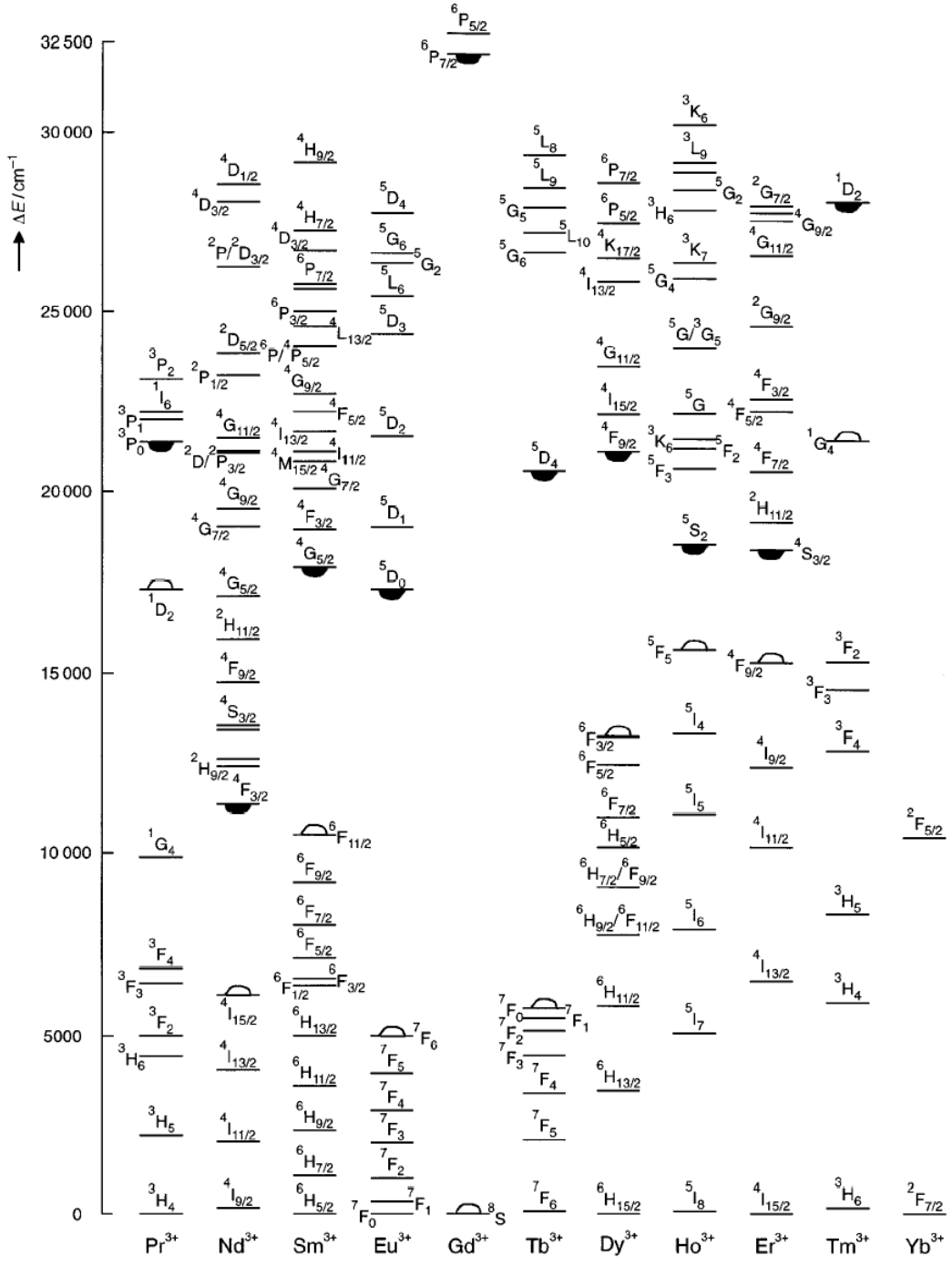

Figure 1.1. Term scheme[16,17] with energy levels of Ln^{3+} ions in aqueous solution; ◡ represents the lowest luminescent level, ⌓ represents the highest non-fluorescent level.

As the 4*f*-4*f* transitions are parity forbidden, the lifetimes of the excited states are long and often extended into the μs or ms range[13] which provides lanthanide based emitters with an advantage over organic or *d*–block based light emitters, which

typically display much shorter lifetimes of nano- to micro-seconds. The long-lived emission facilitates the use of time gated methods, which allow lanthanide luminescence to be distinguished from the shorter lived background fluorescence of many organic or biological systems (Figure 1.2).[18-22]

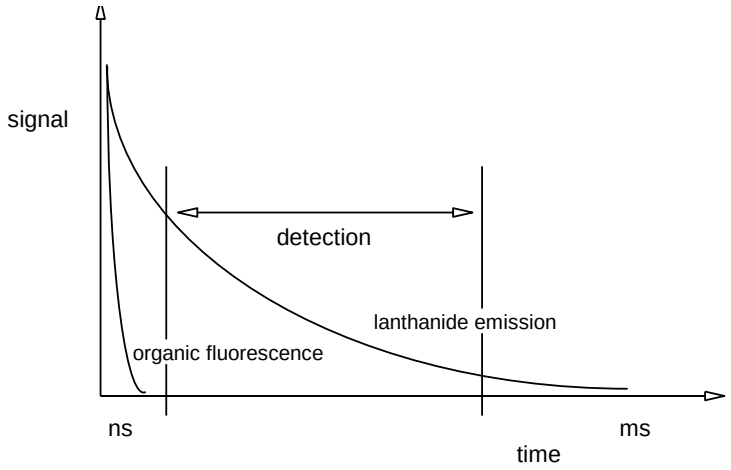

Figure 1.2. Elimination of the background organic fluorescence by time-resolved gating and detection of Ln^{3+} luminescence.

1.5. Non-radiative deactivation of the Ln^{3+} luminescence

Lanthanide luminescence is susceptible to quenching *via* non-radiative deactivation pathways. Theoretically lanthanides have very long radiative lifetimes, for example the lifetime of the $^5D_0$ level of Eu^{3+} in the absence of other deactivating pathways is 9.7 ms.[23] However, in practice the experimental values for lanthanide complexes in solution are substantially shorter, often around 0.1 to 2.0 ms. This reduction is primarily the result of non-radiative quenching of the excited lanthanide state back to the ground state of the lanthanide. The most significant of the possible mechanisms for this process is that of vibrational deactivation. This involves a “matching” of the energy gap between the excited and ground states of the lanthanide by the

vibrational modes of bond oscillators within the vicinity of the lanthanide effectively dissipating the energy of the excited state as vibrational energy throughout the surrounding molecules.

The ability of a given bond to quench luminescence is related to the frequency of the vibrational overtones of the bond in question. In this way the rate of energy transfer to bond vibrational states is dependent upon the number of the vibrational overtone best associated with the energy level of the lanthanide excited state, including how well matched these levels are. The vibrational quenching by water molecules bound to Ln^{3+} is one of the main competing deactivation pathways. For example, the lower energy vibrational overtone (ν = 3) of an O–H bond, deactivates the Eu^{3+} $^5D_0$ excited state far more efficiently than the higher energy vibrational overtone (ν = 5) of an O–D bond (Figure 1.3). This explains why luminescent lifetimes of lanthanide complexes are generally longer in D_2O than H_2O.

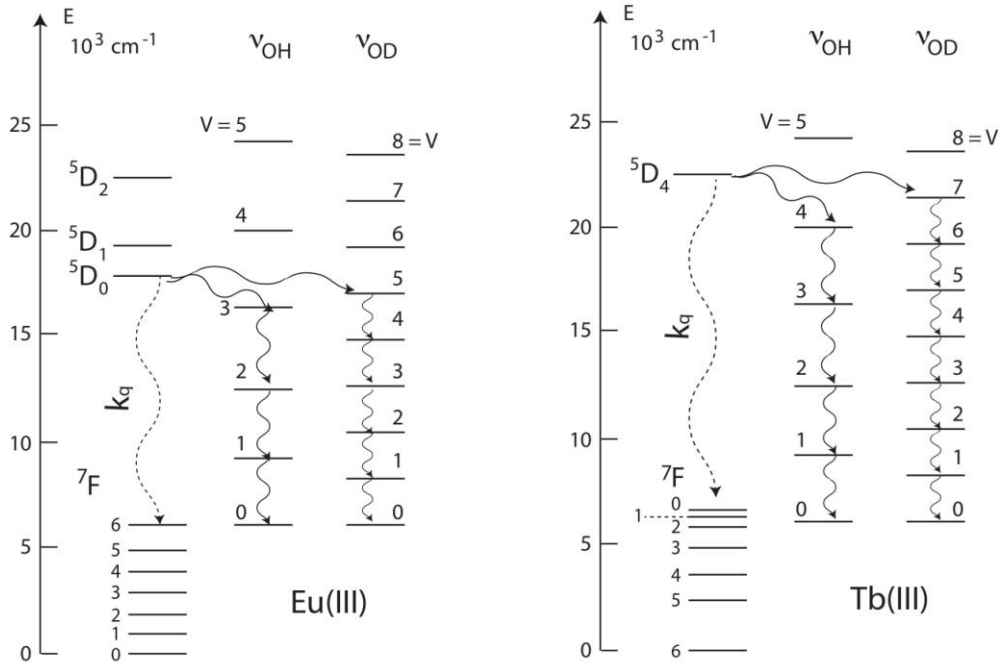

Figure 1.3. Radiationless deactivation of the excited state of Eu^{3+} and Tb^{3+} ions by OH and OD oscillators.[24]

The number of deactivating water molecules coordinated to Ln^{3+} ion in the inner-sphere, can be determined by measuring the luminescence lifetimes of the lanthanide excited states in H_2O and D_2O solution, as established by Horrocks and Sudnick.[25] The hydration number ***q*** (uncertainty ± 0.5) can be calculated by application of the equation 1.1;

$$q = A_{Ln3+}(k_H - k_D) \qquad \textbf{(eq. 1.1)}$$

Where A_{Ln3+} is an empirically determined factor of 4.2 for Tb^{3+} and 1.05 for Eu^{3+}, k_H and k_D are measured luminescence lifetimes (rates of decay in ms^{-1}), observed in protonated and deuterated solvent respectively.

1.6. Lanthanide emission *via* ligand sensitisation

As mentioned previously, the weak (Laporte forbidden) *f-f* absorption leads to inefficient direct excitation of Ln^{3+} ions, which is often only possible with high intensity excitation light, for example, from lasers. However, this problem can be overcome by use of the antenna effect.[26] The process of ligand sensitised lanthanide luminescence by intramolecular energy transfer from an organic chromophore was first reported in Eu^{3+} complexes based on β-diketonate ligands.[27] Absorption of a UV photon causes an excitation of the organic sensitiser from the singlet ground state (S_0) to the ligand singlet excited state (S_1). This state can transfer its energy by intersystem crossing to the longer lived, lower energy triplet state (T_1),[28-30] after which intramolecular energy transfer to the excited state of the lanthanide populates the emissive level of the Ln^{3+} ion. The excited energy is then lost by emission of light, which results in characteristic lanthanide emission spectra with each transition

corresponding to an emission band. The indirect excitation of Ln^{3+} ion is illustrated by a Jablonski diagram (Scheme 1.1).

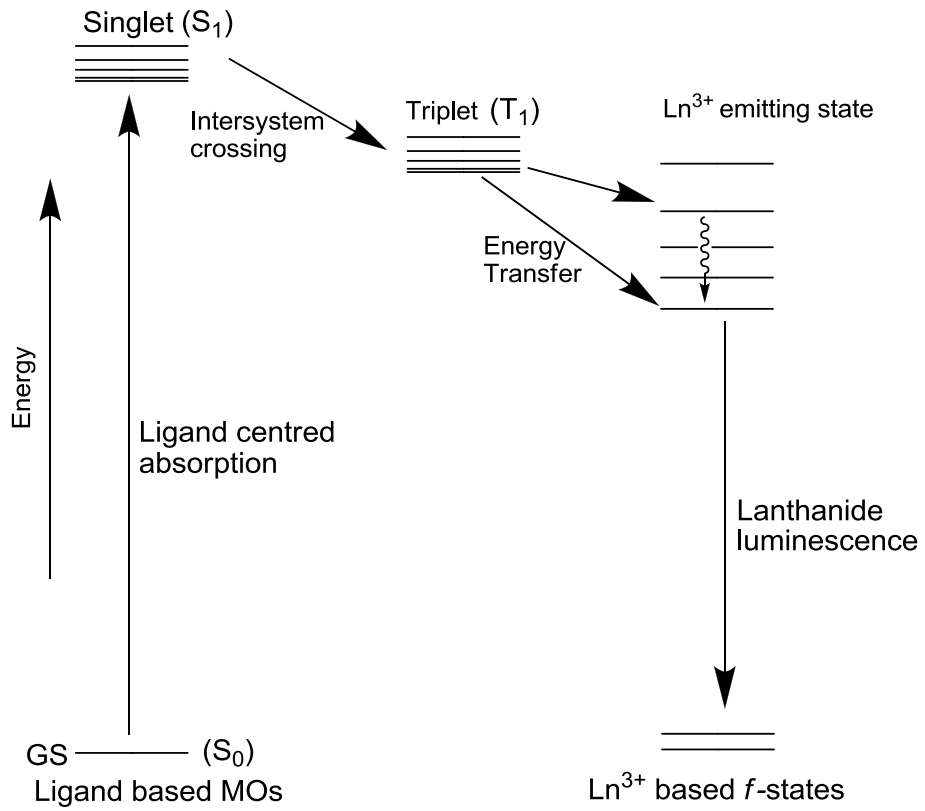

Scheme 1.1. Jablonski diagram of energy transfer from antenna to lanthanide ion.[31,32]

Intersystem crossing from S_1 to T_1 state is a spin forbidden process. However, the rate of intersystem crossing in the presence of lanthanide ion is enhanced due to the heavy-atom effect: this occurs as a consequence of the presence of the 'heavy' (high atomic mass) lanthanide ion, which gives rise to a significant degree of spin-orbit coupling, which provides a mechanism for intersystem crossing from the S_1 to T_1 state.[33]

The absorption, energy-transfer, emission (AETE) mechanism was established by studies with the $[Eu{\subset}bpy.bpy.bpy]^{3+}$ cryptand (Figure 1.4).[34]

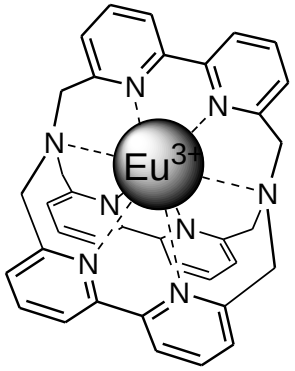

Figure 1.4. The structure of [Eu⊂bpy.bpy.bpy]$^{3+}$ cryptand.

The mechanism of energy transfer can proceed *via* two different migration paths.

1) The Förster type energy transfer involves overlap of energy levels and the energy transfer occurs through space. The rate of energy transfer is distance-dependent with dependence proportional to r^{-6}, where r is the distance between the Ln^{3+} and sensitising chromophore.[35] 2) The Dexter mechanism invokes energy transfer *via* an electron exchange between the excited chromophore and the Ln^{3+} ion acceptor through bond interaction.[36] In both mechanisms, the energy transfer is more efficient when the distance between the lanthanide ion and the chromophore is minimised.[37]

The overall emission efficiency of Ln^{3+} sensitised emission (Q_{Ln}^{L} in the complexes can be expressed by equation 1.2;

$$Q_{Ln}^{L} = \eta_{sens} \times Q_{Ln}^{Ln} \qquad \textbf{(eq. 1.2)}$$

Where η_{sens} is the sensitisation efficiency of energy transfer from the ligand to the Ln^{3+} ion and Q_{Ln}^{Ln} is the intrinsic luminescence quantum yield of the Ln^{3+}. The intrinsic

quantum yield can be calculated by equation 1.3, where τ_{rad} and τ_{obs} are the radiative and observed lifetimes.

$$Q_{Ln}^{Ln} = \tau_{obs} / \tau_{rad} \qquad \textbf{(eq. 1.3)}$$

Therefore, achieving a high efficiency in populating the excited state of lanthanides followed by lanthanide emission depends on various factors.

Firstly, the triplet energy of the sensitising chromophore, which is important for the efficiency of the energy transfer process. This is governed mainly by the degree of matching between the energy levels of the excited ligand triplet state (T_1) and the excited lanthanide levels. For maximum energy transfer efficiency the level of the donor triplet state should be higher (2,500 - 3,500 cm^{-1})[38] above that of the acceptor lanthanide level. If the gap between the energy levels is less than approximately 1,850 cm^{-1},[39] then thermally active back energy transfer competes to repopulate the ligand triplet state, and subsequently deactivates the T_1 back to the ground state.[34] On the other hand, if the energy gap is too large, the energy transfer efficiency is reduced, and therefore a compromise in the donor triplet energy level should be reached.[20]

Secondly, the efficiency of the intersystem crossing from the excited singlet state of the ligand to the excited triplet state. In lanthanide complexes the efficiency is aided by the heavy-atom effect. Thirdly, the overall emission efficiency also depends on the ability of the processes described above to compete effectively with other non-radiative deactivation processes that would otherwise quench *f-f* based emission. For example, the singlet excited state (S_1) can lose the energy through radiative decay such as fluorescence or non-radiative decay by collisions and vibration

interactions with the surrounding molecules.[40] Furthermore, the triplet state may also be quenched by interaction with molecular oxygen.[40] Vibrational interactions with other molecules, *i.e.* water or solvent molecules, can also result in energy lost of the excited lanthanide state.

1.7. Coordination of lanthanide ions

Classified as "hard acid" in character by the Pearson scheme,[41] Ln^{3+} ions will preferentially coordinate "hard donor" ligands such as anionic oxygen and nitrogen atoms rather than "soft donor" ligands, such as sulphur. The metal ions are hydrated in aqueous solution, and negatively charged oxygen donor ligands are required to displace water molecules from the primary coordination sphere. Neutral O and N donor atoms in general only bind the metal as components of multidentate ligands. Water molecules can be excluded from the primary coordination sphere of the ion by encapsulating it by using suitable chelators.

In summary, to ensure the suitability and optimisation of the properties of lanthanide complexes, a number of important considerations, which strongly influence photophysical properties, must be taken into account:

- The probability of transition from the ligand triplet state to the excited lanthanide state (T_1->Ln*) should be high. The triplet level of the chromophore should be sufficiently higher than the lanthanide acceptor state but not too close as to allow back energy transfer processes to take place.
- In order to minimise non-radiative pathways, the ligand should lack of an effective quenching oscillators such as N-H bonds and to less extend C-H bonds.

- The chelating ligand should provide an efficient shielding of the lanthanide ion in order to reduce the number of water molecules coordinated to Ln^{3+}, thus avoid non-radiative quenching by O-H oscillators.
- The sensitising unit should be in close proximity to the lanthanide ion, as both the Förster ($1/r^6$), and Dexter ($e^{-\alpha r}$) energy transfer processes are distance dependent.[42]
- For most applications, it is desirable that the complex shows high thermodynamic stability and kinetic inertness.
- The choice of lanthanide will affect the emission wavelength, lifetime, quantum yield, *etc.* of lanthanide complexes.

The recent published work in the area of self-assembled luminescence lanthanide complexes based on organic ligands, is therefore, focusing on finding ligands that reduce the importance of non-radiative processes, by excluding solvent molecules from Ln^{3+} coordination sphere. This is a well known strategy for optimising the luminescence lifetimes and quantum yields of lanthanide complexes.

1.8. Examples of visible emitting lanthanide complexes

A new tripodal ligand featuring salicylamide arms were reported by Song *et al.*[43] (Figure 1.5). This ligand architecture showed to be able to sensitise visible lanthanide ions (Tb^{3+}, Eu^{3+}, Dy^{3+} and Sm^{3+}). The reported quantum yields and lifetimes of powder samples displayed following trends; Tb^{3+} (19.8%, 1.2 ms) > Eu^{3+} (1.43%, 0.59 ms) > Dy^{3+} (0.94%, 0.02 ms) > Sm^{3+} (0.12%, 0.005 ms), which means that the energy transfer from the ligand to Tb^{3+} and Eu^{3+} is more effective than that to Dy^{3+} and Sm^{3+}. This behaviour is not surprising and can be rationalised by the

different energy gap between the excited luminescent states and the highest level of the ground state of these ions, previously discussed.

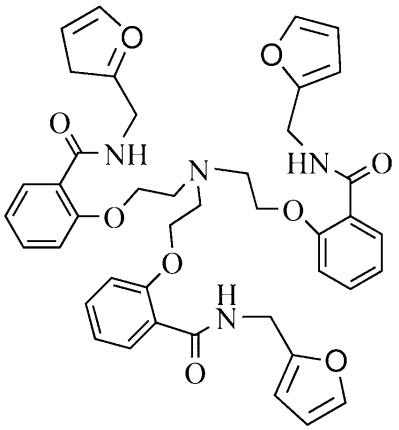

Figure 1.5. Structure of ligand used by Song *et al.*

After a successful design of 2-hydroxyisophthalamide chelating units,[44] Raymond e*t al.*[45] has presented photophysical studies of Eu^{3+} ion, coordinated by two 1-hydroxypyridin-2-one units bridged by an aryl group. The *o*-Phen-1,2-HOPO ligand (Figure 1.6) showed to be an efficient sensitiser for Eu^{3+} luminescence, yielding in overall quantum yield of 6.2% and the luminescence lifetime of 536 μs in H_2O, which was increased to 734 μs in D_2O. The time-resolved analysis of the luminescence of the $[Eu(o\text{-Phen-1,2-HOPO})_2]^-$ complex, showed no water molecules present in the inner-sphere.

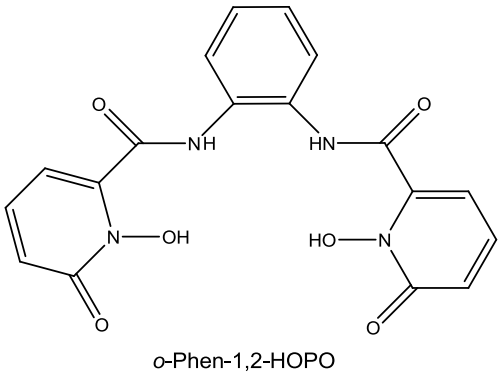

Figure 1.6. Strucutre of *o*-Phen-1,2-HOPO ligand, designed by Raymond *et al.*

Raymond and co-workers[46] also reported a new generation of lanthanide complexes based on 2-hydroxyisophthalamide (IAM) as chelating unit. The octadentate ligand yielded highly stable luminescence complexes with all four visible lanthanides (Tb^{3+}, Eu^{3+}, Sm^{3+} and Dy^{3+}) ions. The Tb^{3+} complex displayed a very high quantum yield of 59% and a luminescence lifetime of 2.6 ms in aqueous solution. In order to improve the solubility of these complexes, Samuel *et al.*[47] further modified the (IAM) ligand architecture by replacing the methyl amide by 2-methoxyethyl (MOE) amide group (Figure 1.7). Photophysical properties of the more soluble complex [Tb(H(2,2)-IAM-MOE)] remained unchanged (Φ_{tot} = 56%, τ = 2.6 ms). This was due the fact that the ligands energy triplet state were essentially the same for both ligands, regardless the substitution; (H(2,2)-IAM 23,350 cm^{-1} and H(2,2)-IAM-MOE 23,170 cm^{-1}). The exceptional performance of both Tb^{3+} complexes, could be explained by an excellent match between the T_1 state and $^5D_4$ emitting level of the Tb^{3+} ion, as well as very effective shielding of the lanthanide ion against water molecules in the inner-sphere.

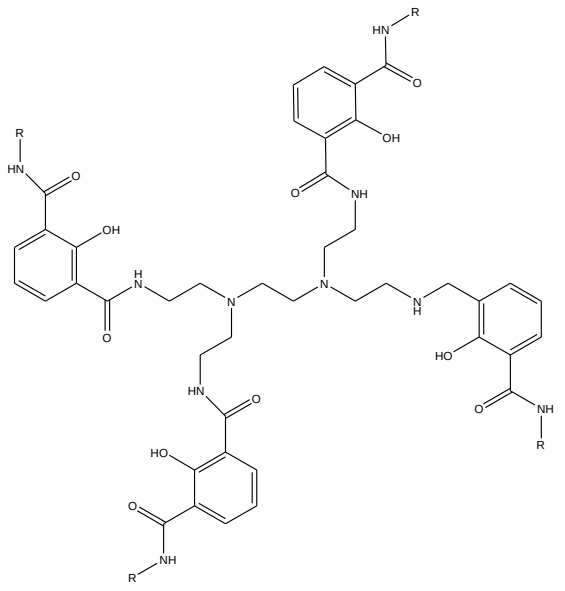

Figure 1.7. Structures of ligands based on the 2- hydroxyisophthalamide (IAM).

As the IAM chromophore showed to be a very good sensitiser for Tb^{3+} luminescence, Raymond's research group, used the same backbone as for the IAM chromophore combined with a 6-amide derivative of 1-hydroxy-pyridin-2-one (1,2-HOPO), which sensitised Eu^{3+} with high efficiency[48] and produced a new octadentate ligand (H(2,2)-1,2-HOPO), which is depicted in Figure 1.8.[49] The photophysical properties of $[Eu(H(2,2)\text{-}1,2\text{-}HOPO)]^-$ complex measured in aqueous solution showed reduction in the overall quantum yield (3.6%) and luminescence lifetime (480 μs). It was found that the H(2,2)-1,2-HOPO ligand, did not provide a protection from non-radiative deactivation and the intensity of Eu^{3+} luminescence was quenched by O-H oscillators of water molecule, coordinated to the Eu^{3+} ion.

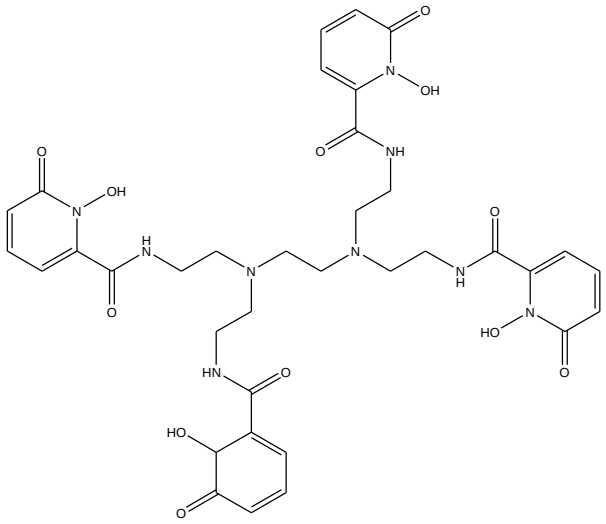

Figure 1.8. Structure of the H(2,2)-1,2-HOPO ligand.

De Cola and co-workers developed neutral, nine-coordinate lanthanide complexes (Figure 1.9).[50] It was found that the ligand acts as a better sensitiser for the Eu^{3+} ion with the quantum yield of 60% and the luminescence lifetime of 2.2 ms, compared to 7% and 0.2 ms observed for the Tb^{3+} analogue in acetonitrile solution. The bright luminescence of Eu^{3+} complex is due to the exclusion of solvent molecules from the

inner coordination sphere, as well as the good match of the triplet energy level of the ligand (22,700 cm^{-1}) with the emitting level ($^5D_0$; 17,500 cm^{-1}) of Eu^{3+} ion. In the case of the Tb^{3+} complex, the $^5D_4$ state lies too close to the triplet state of the ligand, therefore the back energy transfer into the triplet manifold limits the ligand's application to act as an efficient sensitiser for Tb^{3+} luminescence.

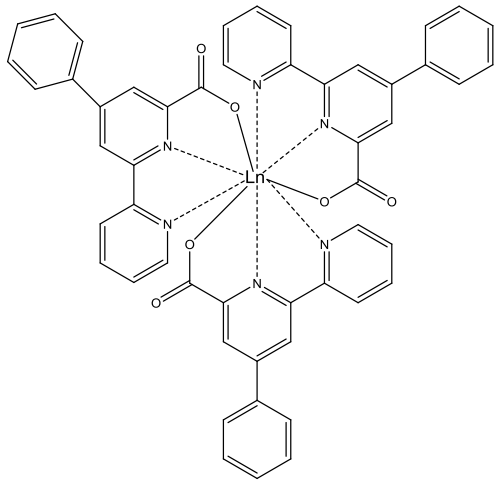

Figure 1.9. Structure of lanthanide complex used by De Cola and co-workers.

The new tripodal ligand containing salicylamide pendant arms was developed by Wang and co-workers,[51] and its structure is presented in Figure 1.10. The triplet energy level of the ligand was measured to be at 24,449 cm^{-1}, which made the ligand a suitable sensitiser for population of the visible emitting ions. All complexes displayed relatively high values of quantum yields and sizeable values of lifetimes for powder samples; Tb^{3+} (44%, 2.0 ms), Eu^{3+} (2.6%, 1.6 ms), Sm^{3+} (0.3%, 0.05 ms), Dy^{3+} (1.6%, 0.07 ms). The observed results are suggesting that the tripodal ligand provides a significant protection from non-radiative deactivation of Ln^{3+} ions by the solvent molecules.

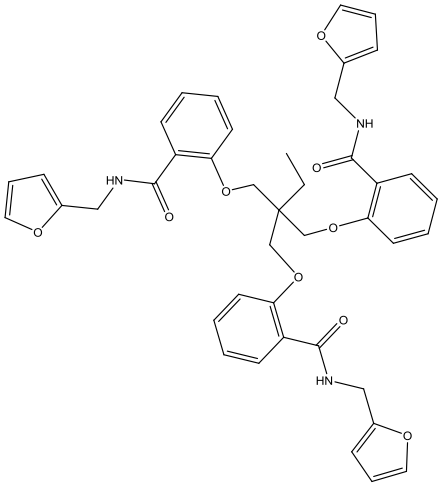

Figure 1.10. Structure of ligand designed by Wang and co-workers.

Another interesting example of ligand design was introduced by Hasegawa, Kawai *et al.*[52] Their work has focused on novel Eu^{3+} complexes, using tridentate phosphane oxide ligands with three hexafluoroacetylacetonate ligands (Figure 1.11). All three, nine-coordinated complexes showed to be highly luminescent with impressive quantum yields between 62 – 60%, and the luminescence lifetime values of ~ 1.2 ms in d_6-acetone.

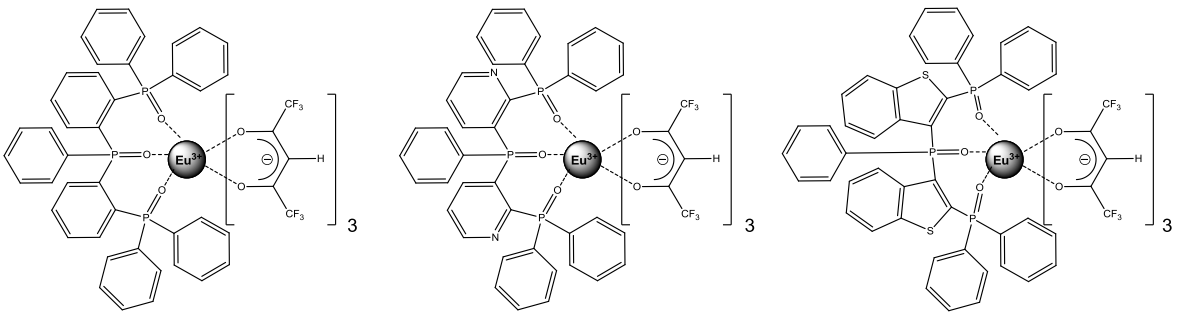

$Eu(hfa)_3(DPPPO)$ $Eu(hfa)_3(DPYPPO)$ $Eu(hfa)_3(DPBTPO)$

Figure 1.11. Structures of $Eu(hfa)_3(DPPPO)$, $Eu(hfa)_3(DPYPPO)$ and $Eu(hfa)_3(DPBTPO)$ complexes.

A similar approach as above was introduced by Robertson and co-workers for europium complexes based on the ligand architecture, which combined DPEPO with fluorinated β-diketonates.[53]

Also Biju e*t al.* studied the luminescence properties of new lanthanide heterocyclic β-diketonates with DPEPO as ancillary ligand.[54]

Feng *et al.* used similar approach of ligand design in order to saturate the coordination sphere around the Dy^{3+} by six oxygen atoms from three Hbfa ligand and two nitrogen atoms from the phen ligand (Figure 1.12).[55] The photophysical studies revealed that the Hbfa is more efficient antenna than the phen chromophore, hence the intramolecular energy transfer in the $Dy(bfa)_3$phen complex mainly occurs between the Hbfa unit and the Dy^{3+} ion. The complex exhibited a relatively high quantum yield of 0.2% with the luminescence lifetime of 0.7 μs in ethanol solution.

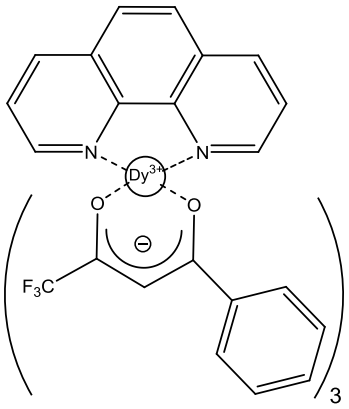

Figure 1.12. Structure of $Dy(bfa)_3$phen ligand.

Bünzli e*t al.* studied series of tridentate benzimidazole-substituted pyridine-2-carboxylic acids, with a halogen, methyl or alkoxy group in the 6-position of the

benzimidazole ring, with additional *N*-alkyl chain for enhanced solubility (Figure 1.13).[56] The ligands formed neutral, nine-coordinated complexes with Tb^{3+} and Eu^{3+} ions. This work was interested in the influence of different substituents introduced on the benzimidazole ring on their photophysical properties. It was found that all ligands could efficiently sensitised Eu^{3+} luminescence with overall quantum yields ranging from 43% to 71% in the solid state and between 42% and 52% in CH_2Cl_2. The values of luminescence lifetime were in range of 2.5 - 3 ms for the solid state samples and between 2.4 and 2.81 ms in CH_2Cl_2. The triplet energies of the ligands was found to be in the range of 21,300 – 18,760 cm^{-1} and decreases as a function of the substituents as (H, F, Cl) > CH_3 > Br > OC_8H_{17} > OCH_3. The photophysical properties of the Eu^{3+} complex with ligands $L8R^-$ remained the same for R = H, F, Cl and CH_3 substituents on the benzimidazole ring. In the case of the heavy bromide atom the triplet energy of the ligand was slightly lowered, which decreased values of quantum yield and lifetime in solid state samples. However, major changes were found for complexes containing alkoxy groups. The $^5D_0$ emitting level of the Eu^{3+} lied less than 2,050 cm^{-1} below the triplet level of EuL401 and EuL808 complex, which resulted in potential back-energy transfer from Eu^{3+} to the ligand.

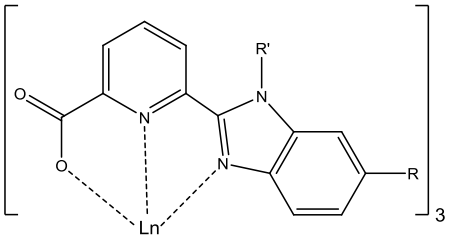

R' = CH_3
HL1: R = H

R' = C_4H_9
HL4Me: R = CH_3
HL4O1: R = OCH_3

R' = C_8H_{17}
HL8: R = H
HL8R: R = F, Cl, Br
HL8Me: R = CH_3
HL8O8: R = OC_8H_{17}

Figure 1.13. Lanthanide complexes studied by Bünzli *et al.*

Building on this previous work, Shavalleev *et al.* developed neutral, nine-coordinated Eu^{3+} complexes based on *N*-aryl-benzimidazole pyridine-2-carboxylic acid chelating unit (Figure 1.14).[57] The absorption spectra displayed identical trends, regardless to the R substituent, with the high ε, ranging from 50,000 - 56,000 dm^3 mol^{-1} cm^{-1}. Characteristic Eu^{3+} centred luminescence was observed for all complexes in solid state and CH_2Cl_2 solution. The quantum yields of ligand-sensitised Eu^{3+} luminescence were large 43 - 59% in solid state and 38 - 49% in CH_2Cl_2 solution. The observed lower efficiency in solution was due to energy losses within the ligands by collisional deactivation caused by solvent molecules. The ability of the ligand protecting the Eu^{3+} ion from non-radiative decay was also reflected on long luminescence lifetimes of 1.8 -2.6 ms in solid state and 2.2 - 2.7 ms in solution.

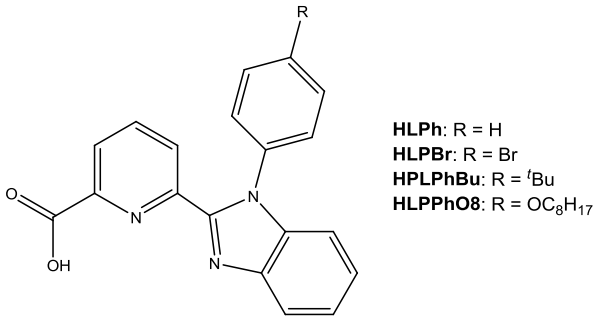

Figure 1.14. Structure of ligands developed by Shavalleev *et al.*

The photophysical properties of two new flexible exo-bidentate ligands incorporating a biphenyl skeleton bearing two salicylamide pendant arms have been studied by Guo *et al.*[58] The ligand **L2** has two hydrogen atoms in the 5- and 5'- positions on the biphenyl replaced by two bromide atoms (Figure 1.15). Luminescence properties of lanthanide complexes based on **L1** and **L2** has been studied in solid state and it was demonstrated that high extinction coefficients of the ligands due to salicylamide

pendant arms in the near UV-vis range provided an effective absorption of excitation energy, which promoted an effective energy transfer to all visible lanthanide ions (Tb^{3+}, Eu^{3+}, Dy^{3+} and Sm^{3+}). All four lanthanide complexes of **L1** displayed very high values of quantum yield with relatively long luminescence lifetimes; Tb^{3+} (29.8%, 1.6 ms), Eu^{3+} (10.4%, 1.1 ms), Dy^{3+} (5.6%, 0.073 ms), Sm^{3+} (0.73%, 0.061 ms). The luminescence efficiency of **L2** complexes was significantly reduced yielding in much lower values of quantum yield and luminescence lifetime; Tb^{3+} (7.41%, 1.2 ms), Eu^{3+} (2.97%, 0.57 ms), Dy^{3+} (0.43%, 0.014 ms), Sm^{3+} (0.21%, 0.01 ms). As the triplet level of the antenna changed only slightly (**L1**: 23, 474 cm^{-1}) by the bromide substitution on the biphenyl backbone (**L2**: 22,935 cm^{-1}), the quenching of luminescence in **L2** complexes was not due to the change of the nature of the T_1 state. The reduction of luminescence was caused by the deactivation pathway of methanol molecule, which was found to be coordinated to the Ln^{3+} ion.

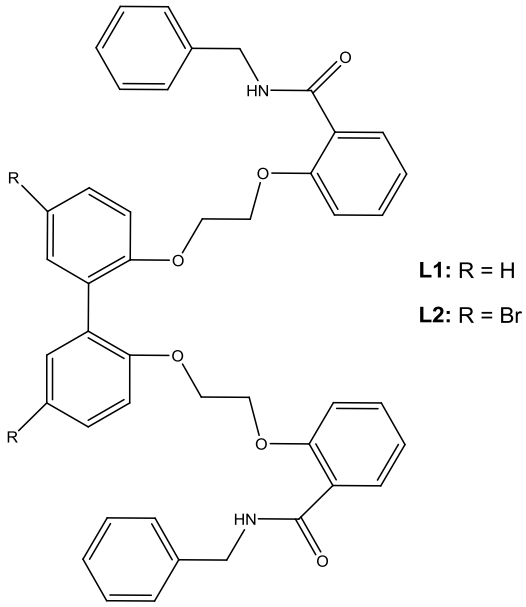

Figure 1.15. Structure of the organic ligands used by Guo *et al*.

Water soluble lanthanide complexes based on a 6''-carboxy-2,2':6',2''-terpyridine framework linked *via* a methylene bridge to *n*-butylamise were designed by Charbonnière *et al*.[59] (Figure 1.16). Photophysical properties Tb^{3+} and Eu^{3+} were studied by steady-state and time-resolved spectroscopy in aqueous solution. It was found that the systematic increase of the number of pyridyl rings resulted in big changes in the coordination and sensitising abilities of the ligands. Calculation of the hydration number revealed that all complexes have two water molecules presented in the inner sphere. The ligand **L1** showed to be the best sensitiser, which displayed relatively high values of quantum yield of 5.7% and 32% for Eu^{3+} and Tb^{3+} complexes, with the luminescence lifetimes of 390 μs and 850 μs, respectively, in H_2O, despite of two water molecules coordinated to the Eu^{3+} and Tb^{3+} ion.

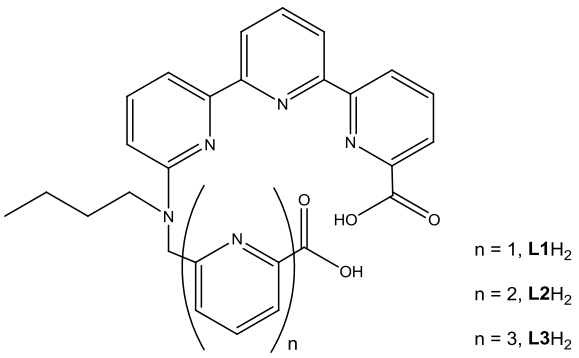

Figure 1.16. Structures of ligands used by Charbonnière *et a*l.

1.9. Examples of NIR emitting lanthanide complexes

Compared to the visible emitting ions, the low excited levels of NIR (Nd^{3+}, Yb^{3+}, Er^{3+}) ions are particularly sensitive to non-radiative quenching by the vibrational harmonics of O-H oscillators water as well as to N-H and C-H oscillators close to the lanthanide centre as demonstrated in Scheme 2.1.

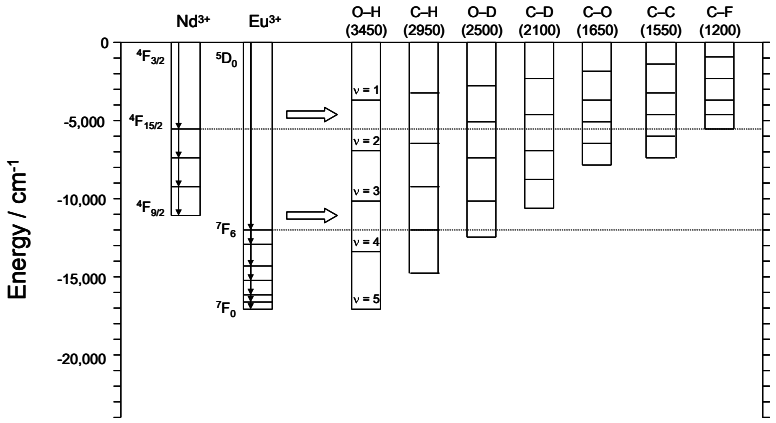

Scheme 2.1. Schematic representation of the vibrational energy quanta of various chemical bonds and comparisons with the electronic energy level gaps of Nd^{3+} and Eu^{3+} ions.

Therefore, the ligand design for the optimisation of the photophysical properties of NIR emitting lanthanides is focusing on the development of fully or partially fluorinated ligands or sulfonylaminate ligands or fully deauterated podand ligand architectures.[60 -70]

Zhen *et al.*[71] proposed a perfluorodiphenylphosphinic acid for a complexation with the Er^{3+} ion (Figure 1.17). The effect of fluorination of the organic ligands was noticeable from the observed luminescence lifetime of the longer component of 336 μs (89%) and the quantum efficiency of 0.98%.

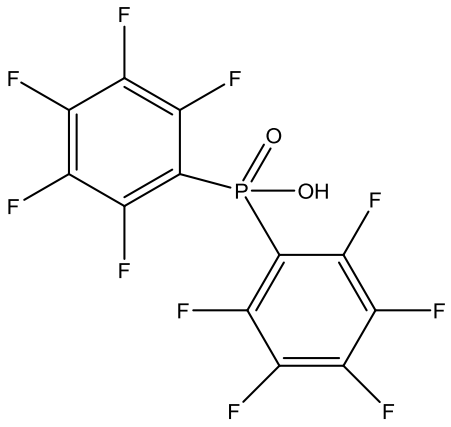

Figure 1.17. Structure of ligand used by Zhen and co-workers.

Since erbium tris(8-hydroxyquinoline) showed the possibility of being deposit on to silicon to produce organic electroluminescent diodes, which offers the opportunity of a cheap 1.5 μm emitter based on silicon technology[72], 8-hydroxyquinoline has been a chromophore incorporated in ligands design for sensitising NIR luminescence.

For example, Bünzli and co-workers developed lanthanide complexes (Nd^{3+}, Yb^{3+} and Er^{3+}) based on tripodal 8-hydroxyquinoline ligand, which has sulfonate groups on the aromatic rings for ensuring the water solubility.[73]

Another example of using the 8-hydroxyquinoline as chromophores with an additional carboxylate or tetrazole binding groups, was recently reported by Mazzanti *et al.*[74] New tri-anionic complexes were found be suitable for the NIR luminescence of Yb^{3+}, Nd^{3+} and Er^{3+} ions in solid state and in solution.

Nonat *et al.*[75] used similar approach of benefiting from the 8-hydroxyquinolinate moieties. In his work the pivotal amine group was replaced by an 1,4,7-triazacyclononane core.

An improved design of previously reported ligands[76] was reported by Shavaleev *et al.*[77] The benzoxazole-substituted 8-hydroxyquinoline ligands formed eight-coordinated complexes with Yb^{3+} ion and nine-coordinated complexes with Nd^{3+} ion (Figure 1.18). The introduction of new extended chromophore provided larger absorption coefficient in the visible region, which acted as an efficient sensitiser for the Yb^{3+} and Nd^{3+} emission. The lanthanide luminescence of Nd^{3+} ion was enhanced upon halogenations of the 5,7-position in the 8-hydroxyquinoline group yielding in the quantum yield of 0.33% and the luminescence lifetime of 1.82 μs in solid state. In the case of the Yb^{3+} complex the water molecule coordinated to the Yb^{3+} quenched the emission, therefore the observed lifetime and quantum yield are relatively small 0.8 μs and 0.09% respectively in the solid state.

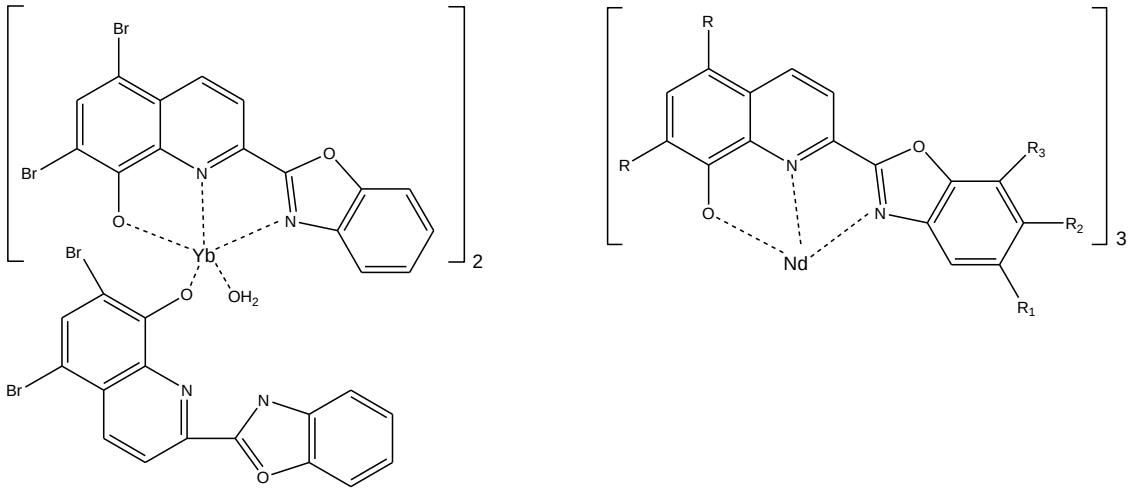

Figure 1.18. Nd^{3+} and Yb^{3+} lanthanide complexes designed by Shavaleev *et al.*

Huang and co-workers[78] introduced a new strategy of the ligand design by utilising the 8-hydroxyquinoline moiety attached to a rhodamine chromophore *via* carboxy-hydrazone linker (Figure 1.19). Two rigid tetradentate ligands provided a coordination number of eight for the Yb^{3+} ion, therefore completely excluding solvent molecules from the first coordination sphere. The efficient NIR emission was confirmed by a relatively high quantum yield of 1.1% in acetonitrile for the Yb^{3+} complex based on HQR1 ligands.

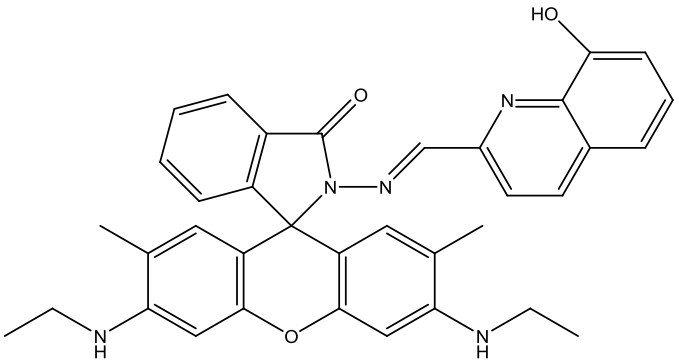

Figure 1.19. Structure of HQR1 ligand.

A very efficient ligand to lanthanide energy transfer and excellent protection of Nd^{3+}, Yb^{3+} and Er^{3+} ions from solvent molecules was demonstrated by Petoud and Zhang[79] (Figure 1.20). They used azulate moieties based ligand, which had a low-energy triplet state (14,300 cm^{-1}) hence could populate the emitting levels of NIR ions. The luminescence lifetime obtained in CD_3CN was 24.61 and 1.85 μs for Yb^{3+} and Nd^{3+} complex, respectively. The quantum yield of the Yb^{3+} complex was large with values of 3.8% in CH_3CN and 4.2% in CD_3CN.

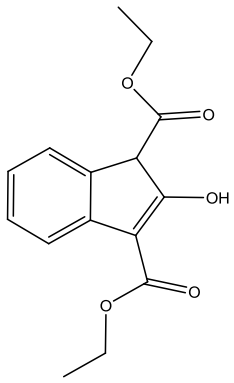

Figure 1.20. Structure of the HAz ligand.

Another successful example of the population of NIR emitted states of Nd^{3+}, Yb^{3+} and Er^{3+} ions was demonstrated by Bünzli *et al.*[80] (Figure 1.21). The tridentate ligand based on *N*-methylacridone heterocycle linked to the *N*-methylbenzimidazole pyridine-2-carboxilic acid formed neutral, stable complexes. The measured luminescence lifetimes and quantum yields were high in CD_3CN solution. The HL^{AB2} ligand showed to be the best sensitiser (T_1 = 16,450 cm^{-1}) for the Yb^{3+} ion with the lifetime of 33.5 μs and quantum yield of 1.20%, followed by 18.7 μs and 0.21% for the Nd^{3+} ion and 4.0 μs and 0.03% for Er^{3+} ion.

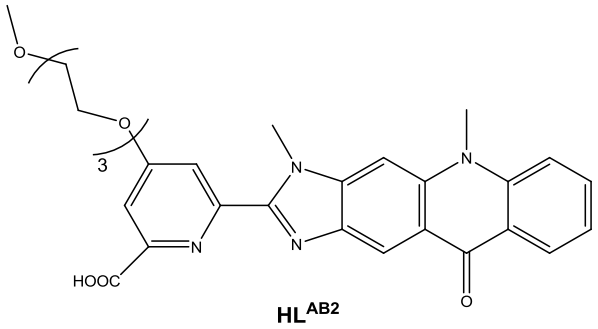

Figure 1.21. Structure of HL^{AB2} ligand.

Raymond *et al.*[81,82] studied the ability of tetradentate ligand based on the 1-methyl-3-hydroxy-pyridin-2-one chromophore to sensitised the luminescence of Yb^{3+} and Nd^{3+} ions. Complexes displayed the characteristic luminescence of the Yb^{3+} and Nd^{3+} ion. In the Nd^{3+} complex the decay time measured in D_2O was shorter (0.7 μs) compared to 25.3 μs observed for the Yb^{3+} complex. The better suitability of ligand to populate the emitting level of Yb^{3+} ion was also confirmed by the value of 0.22% of the quantum yield for Yb^{3+}.

1.10. Examples of bimetallic lanthanide complexes

Bünzli's and Pigeut's pioneering work[83] was the real breakthrough in the study of binuclear helicates formed by self-assembly. They designed a triple-stranded dinuclear Eu^{3+} helicate beased on a benzimidazole pyridyl ligand (Figure 1.22). The stability of the complex in aqueous media was enhanced by an introduction of negatively charged carboxylate groups.

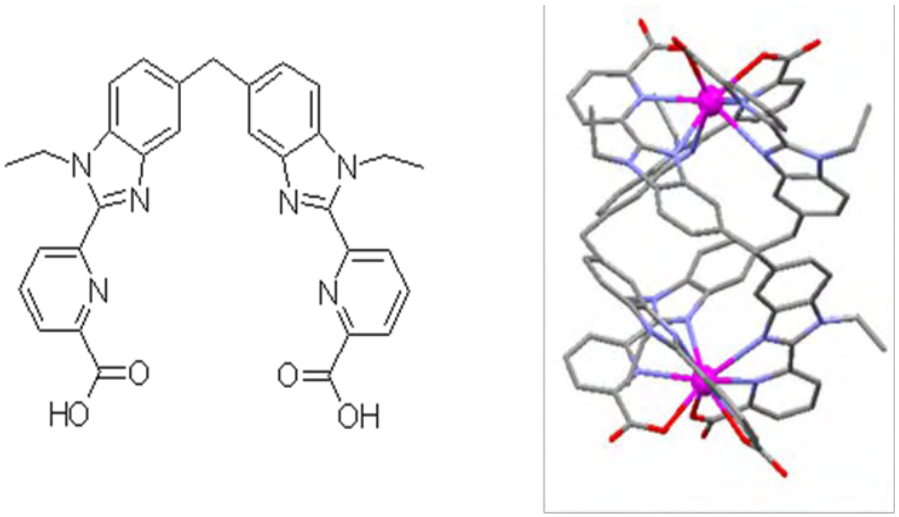

Figure 1.22. (a) The carboxylic functionalised benzimidazole pyridyl ligand, and **(b)** the XRD structure of the dinuclear Eu^{3+} triple stranded helical complex, synthesised by Bünzli and Piguet *et al*.

Building on this work, Bünzli, Pigeut and co-workers[84-86] developed stable binuclear helicates based on benzimidazole carboxylate ligands, which were able to act as a sensitiser for visible and NIR ions. The pyridine units could be substituted, for example by polyoxytheylene groups, which enhanced the solubility of complexes.

Ward and co-workers[87] investigated the coordination chemistry of lanthanide complexes based on bis-tridentate bridging ligands containing *N, N', O*-tridentate amide substituted pyrazolyl-pyridine chromophores linked by methylene units to an aromatic *o*, *m*, or *p*-phenylene spacer (Figure 1.23).

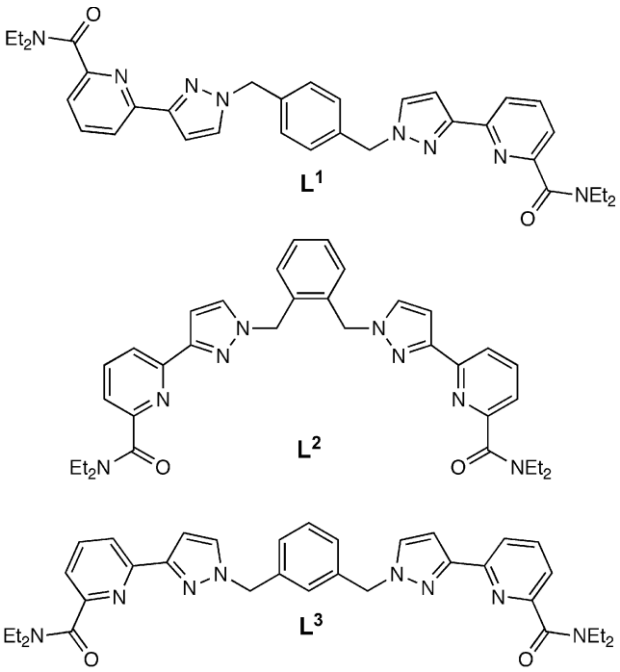

Figure 1.23. Strucutres of ligand designed by Ward and co-workers.

Our group synthesised and studied photophysical properties of new bimetallic complexes based on β-diketonate moieties. Generally, β-diketonate ligands are widely used because of their strong coordination ability, a negatively charged binding site which can coordinate to the Ln^{3+} ions through "hard" oxygen atoms. Furthermore, the high extinction coefficient in the UV region makes β-diketonate ligands good chromophores for sensitising Ln^{3+} ions. Also their position of the energy level of T_1 state is usually matched well with the excited state levels of most of the lanthanide ions. The H_2**L**^{1} and H_2**L**^{2} ligands incorporate two benzoyl β-diketonate sites linked together by a 1,3-phenylene spacer (Figure 1.24), which formed neutral homobimetallic triple stranded helicates with Ln^{3+} ions.[88] Due to the suitable position of the ligand triplet state, both ligands could efficiently sensitise Eu^{3+} and Sm^{3+} emission, as well as the NIR emission of Nd^{3+} ion. Despite three molecules of methanol bind to each Ln^{3+}, the luminescence lifetimes and quantum yields of

$Eu_2(\mathbf{L^1})_3$; (220 μs, 5.0%), $Sm_2(\mathbf{L^1})_3$; (13 μs, 0.16%) and $Nd_2(\mathbf{L^1})_3$; (1.5 μs, 0.6%) complexes were relatively high.

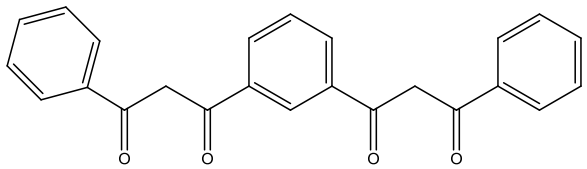

$\mathbf{H_2L^1}$

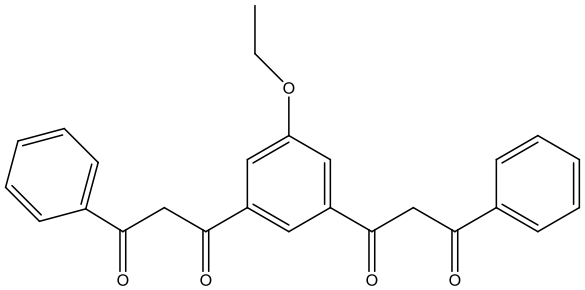

$\mathbf{H_2L^2}$

Figure 1.24 Structures of dinucleating ligands, H_2L^1 and H_2L^2

1.11. Our approach – shell type ligands

Our approach is to use sterically bulky ligands, which are designed to create a stabilising "hydrophobic shell" around the central lanthanide ion. Their coordination site is formed by a bidentate, negatively charged unit, consisting of hard oxygen donor capable of binding to the Ln^{3+} ions strongly. An important advantage of this kind of ligand design is that the binding site is independent of the aromatic chromophore groups. Hence, from the synthetic point of view the light-harvesting unit can be easily modified and fine tuned without affecting the binding unit of the ligand.

Previously in our research group, tetraphenyl imidodiphosphinate ligand H**tpip** (Figure 1.25) was studied.[8]

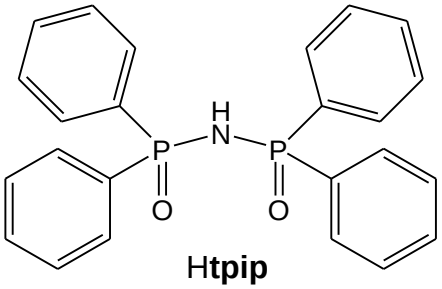

H**tpip**

Figure 1.25. The structure of the imidodiphosphinate ligand, H**tpip**.

It was found that the twelve aromatic rings of the three ligands surrounding lanthanide ion, can effectively shield the smaller lanthanide ion from solvent molecules, therefore minimising the quenching of luminescence. Also H**pip** ligand has not O-H and N-H bond, and relatively few C-H bonds in close proximity to the lanthanide ion, therefore the lanthanide complexes Ln(**tpip**)$_3$ showed very good photophysical properties and efficient lanthanide luminescence was observed for all four lanthanides emitting ions in the visible region. The H**tpip** ligand was also capable to sensitised the NIR emitting ions (Nd^{3+}, Yb^{3+} and Er^{3+}) with sizeable luminescence lifetimes in nondeuteurated solvents.[89]

In order to improve photophysical properties of visible lanthanides by exclusion of solvent molecules in the inner sphere, the *o*-tolyl analogue of H**tpip** was developed, H**Metpip** (Figure 1.26). The introduction of twelve CH_3- groups per complex provided a very good shielding of the Ln^{3+} against the solvent molecules. However, the luminescence lifetimes values were considerably shorter compared to those of **tpip**

complexes. It was found out that the presence of additional 36 C-H oscillators in the close proximity to the lanthanide ion could efficiently quench the luminescence.[8]

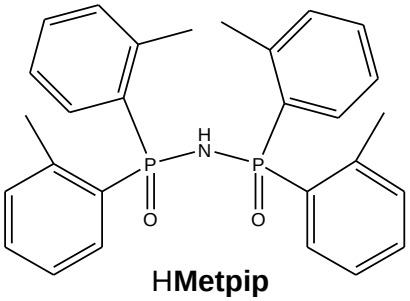

H**Metpip**

Figure 1.26. The structure of the imidodiphosphinate ligand, H**Metpip**.

In effort to minimise C-H quenching a new modified analogue of H**tpip** was designed. The phenyl moieties of the imidodiphosphinate ligand were fully fluorinated, therefore the H**F_{20}tpip** ligand lacks of C-H**,** N-H oscillators (Figure 1.27). For this reason the HF_{20}**tpip** ligand exhibited excellent photophysical properties, especially for the NIR emitting ions. The luminescence lifetimes measured in CD_3CN solution are the longest reported for NIR complexes based on organic chelating units.[90]

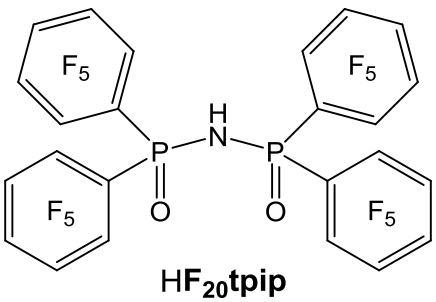

H**F_{20}tpip**

Figure 1.27. The structure of the fluorinated imidodiphosphinate ligand, H**F_{20}tpip**.

1.12. Applications of lanthanide complexes

The properties of many lanthanide complexes make them ideal for use in applications in which their photophysical characteristics are important.[15,91]

Many lanthanide complexes for electro-luminescent materials have been produced,[92] including photoactive polymers or gels,[93-95] and luminescent devices[31,96,97] such as light emitting diodes (LEDs),[98,99] or for organo-lanthanide phosphors for applications in new display technologies.[100-102] Lanthanide doped inorganic compounds are commonly used as the luminescent materials in lighting,[103] laser[104,105] and optical fibre applications,[106-108] in particular the use of lanthanide based materials to act as gain media in optical amplifiers.[109-111] The use of Er^{3+} complexes is particularly widespread due to the emission wavelength of the $^4I_{13/2} \rightarrow {}^4I_{15/2}$ transition at ~1,550 nm, falling within the NIR telecommunications window, typically between 1 and 1.6 μm, commonly used in glass fibre networks.[109,112] Within this context Nd^{3+} complexes are also useful due to the $^4F_{3/2} \rightarrow {}^4I_{11/2}$ transition occurring at ~1,060 nm.[15]

Luminescent labels are routinely used as an alternative to radioactive probes, due to disadvantages of the latter such as; the associated health risks, a short shelf life, and difficulties concerned with storage and disposal. Luminescent lanthanide complexes are commonly used to form the basis of highly sensitive fluoroimmunological diagnostic techniques[113,114] and many compounds have been developed for this purpose.[44,115-117]

Much research has focused upon the use of Eu^{3+} complexes for use as biological labels, because biological tissue is relatively transparent to red light.[118] However, the sensitised luminescence process often requires that such complexes must be excited by UV light, which is not desirable when working with biological systems. Lanthanide complexes that emit in the near infrared region can be sensitised by

ligands, such as organic dye derivatives, which can be excited with lower energy, longer wavelength radiation.[119]

The neutral DTPA-bis(amide) ligands and their Ln^{3+} complexes have been employed successfully in a number of important applications such as luminescent devices[120] to potential drug molecules[121] and biomarkers[122] as well as MRI contrast agents.[123]

1.13. Thesis outline

In this thesis the photophysical properties of lanthanide complexes have been examined. Since the intensity of the emission and choice of lanthanide both depend on the sensitiser, development of new chromophores based on imidodiphosphate binding sites suitable for visible emitting (Tb^{3+}, Eu^{3+}, Dy^{3+}, Sm^{3+}) and NIR emitting (Yb^{3+}, Nd^{3+}, Er^{3+}) were introduced.

Chapter two describes the preparation and full characterisation of neutral lanthanide complexes formed by a self-assembly of three imidodiphosphate ligands. The photophysical properties of visible and NIR complexes are examined in detail.

Chapter three is concerned with the synthesis, full characterisation and studies of luminescence properties of novel binuclear visible and NIR lanthanide complexes of pentaphenyl diimidotriphosphate ligand.

Chapter four is addressed to the preparation and full characterisation of new ligand tetrabiphenyl imidodiphosphate and luminescence studies of novel visible and NIR lanthanide complexes.

Chapter five provides conclusions and future work.

Chapter six details the experimental procedures used throughout the course of this work.

1.14. References

(1) Douglas, B.; McDaniel, D.; Alexander, J. *Concepts and Models of Inorganic Chemistry*; 3 ed.; John Wiley & Sons Inc.: New York, 1994.

(2) Evans, W. J. *Coord. Chem. Rev.* **2000**, *206*, 263.

(3) Wang, L.; Wang, S.; Zhao, X.; Sun, J. *J. Alloy. Compd.* **1995**, *225*, 174.

(4) Weast, R. C. *CRC Handbook of Chemistry and Physics*; 84 ed.; Chemical Rubber Company Co.: Ohio, 1971.

(5) Sabbatini, N.; Dellonte, S.; Ciano, M.; Bonazzi, A.; Balzani, V. *Chem. Phys. Lett.* **1984**, *107*, 212.

(6) Parker, D.; Dickins, R. S.; Puschmann, H.; Cossland, C.; Howard, J. A. K. *Chem. Rev.* **2002**, *102*, 1977.

(7) Cotton, S. *Lanthanides and Actinides*; Macmillan Education, 1991.

(8) Magennis, S. W.; Parsons, S.; Pikramenou, Z. *Chem. Eur. J.* **2002**, *8*, 5761.

(9) Kaltsoyannis, N.; Scott, P. *The F Elements*; Oxford Science Publications: Oxford, 1999.

(10) Binnemans, K.; Görller-Waldrand, C. *Chem. Phys. Lett.* **1995**, *235*, 163.

(11) Horrocks Jr., W. D.; Albin, M. *Progress in Inorganic Chemistry*; Wiley: New York, 1983; Vol. 31.

(12) Choppin, G. R.; Peterman, D. R. *Coord. Chem. Rev.* **1998**, *174*, 283.

(13) Choppin, G. R. *Lanthanide Probes in Life, Chemical & Earth Sciences*; Elsevier: Amsterdam, 1989.

(14) Moeller, T. *Comprehensive Inorganic Chemistry*; Pergamon Press: Oxford, 1971; Vol. 4.

(15) Bünzli, J.-C. G.; Piguet, C. *Chem. Soc. Rev.* **2005**, *34*, 1048.

(16) Stein, G.; Würzberg, E. *J. Chem. Phys.* **1975**, *62*, 208.

(17) Wolbers, M. P. O.; Van Veggel, F. C. J. M.; Snellink-Ruël, B. H. M.; Hofstraat, J. W.; Geurts, F. A. J.; Reinhoudt, D. N. *J. Chem. Soc., Perkin Trans. 2,* **1998**, 2141.

(18) Mathis, G. *Clin. Chem.* **1995**, *41*, 1391.

(19) Hanaoka, K.; Kikuchi, K.; Kojima, H.; Urano, Y.; Nagano, T. *J. Am. Chem. Soc.* **2004**, *126*, 12470.

(20) Parker, D. *Coord. Chem. Rev.* **2000**, *205*, 109.

(21) de Silva, A. P.; Gunaratne, H. Q. N.; Gunnlaugsson, T.; Huxley, A. J. M.; McCoy, C. P.; Rademacher, J. T.; Rice, T. E. *Chem. Rev.* **1997**, *97*, 1515.

(22) de Silva, A. P.; Fox, D. B.; Huxley, A. J. M.; Moody, T. S. *Coord. Chem. Rev.* **2000**, *205*, 41.

(23) Carnall, W. T. *Handbook on the Physics and Chemistry of Rare Earths*; North Holland: Amsterdam, 1979; Vol. 3.

(24) Bünzli, J.-C. G. and Choppin G. R. *Lanthanide Probes in Life, Chemical and Earth Sciences*, Elsevier Science Ltd., 1990.

(25) Horrocks Jr., W. D.; Sudnick, D. R. *Acc. Chem. Res.* **1981**, *14,* 384.

(26) Kobuke,Y. *Eur. J. Inorg. Chem.* **2006**, 2333.

(27) Weissman, S. J. *J. Chem. Phys.* **1942**, *10*, 214.

(28) Dawson, W. R.; Kropp, J. L.; Windsor, M. W. *J. Chem. Phys.* **1966**, *45*, 2410.

(29) Sager, W. F.; Filipescu, N.; Serafin, F. A. *J. Phys. Chem.* **1965**, *69*, 1092.

(30) Crosby, G. A.; Whan, R. E.; Alire, R. M. *J. Chem. Phys.* **1961**, *34*, 743.

(31) Sabbatini, N.; Guardigli, M.; Lehn, J. M. *Coord. Chem. Rev.* **1993,** *123*, 201.

(32) Crosby, G. A.; Whan, R. E.; Freeman, J. J. *J. Phys. Chem.* **1962,** *66,* 2493.

(33) Reinhard, C.; Güdel, H. U. *Inorg. Chem.* **2002**, *41*, 1048.

(34) Alpha, B.; Ballardini, R.; Balzani, V.; Lehn, J.-M.; Perathoner, S.; Sabbatini, N. *Photochem. Photobiol.* **1990**, *52*, 299.

(35) Foster, T. H. *Ann. Phys. 2.* **1984**, 55.

(36) Dexter, D. L. *J. Chem. Phys.* **1953**, 836.

(37) Kielar, F.; Montgomery, C. P.; New, E. J.; Parker, D.; Poole, R. A.; Richardson, S. L.; Stenson, S. P. A. *Org. Biomol. Chem.* **2007**, *5*, 2975.

(38) Eliseeva, S. V.; Bünzli, J.-C. G. *Chem. Soc. Rev.* **2010**, *39*, 189.

(39) Latva, M.; Takalo, H.; Mukkala, V.-M.; Matachescu, C.; Rodríguez-Ubis, J. C.; Kankare, J. *J. Lumin.* **1997**, *75*, 149.

(40) dos Santos, C. M. G.; Harte, A. J.; Quinn, S. J.; Gunnlaugsson, T. *Coord. Chem. Rev.* **2008,** *252*, 2512.

(41) Pearson, R. G. *J. Am. Chem. Soc.* **1963**, *84*, 3533.

(42) Turro, N. J. *Modern Molecular Photochemistry*; University Science Books: Sausalito, CA, 1991.

(43) Song, X.-Q.; Dong, W.-K.; Zhang, Y-J.; Liu, W.-S. *Luminescence* **2010,** *25,* 328.

(44) Petoud, S.; Cohen, S. M.; Bünzli, J.-C. G.; Raymond, K. N. *J. Am. Chem. Soc.* **2003,** *125,* 13324.

(45) D'Aléo, A.; Xu, J.; Moore, E. G.; Jocher, C.J.; Raymond, K. N. *Inorg. Chem.* **2008**, *47,* 6109.

(46) Petoud, S.; Muller, G.; Moore, E. G.; Xu, J.; Sokolnicki, J.; Riehl, J. P.; Le U. N.; Cohen, S. M.; Raymond, K. N. *J. Am. Chem. Soc.* **2007**, *129*, 77.

(47) Samuel A. P. S.; Moore, E. G.; Melchior, M.; Xu, J.; Raymond, K. N. *Inorg. Chem.* **2008**, *47*, 7535.

(48) D'Aléo, A.; Moore, E. G.; Szigethy, Xu, J.; Raymond, K. N. *Inorg. Chem.* **2009**, *48*, 9316.

(49) Seitz, M.; Do, K.; Ingram, A. J. Moore, E. G.; Muller, G.; Raymond, K. N. *Inorg. Chem.* **2009**, *48*, 8469.

(50) Kottas, G. S.; Mehlstäubl, M.; Fröhlich, R.; De Cola, L. *Eur. J. Inorg. Chem.* **2007**, 3465.

(51) Song, X.-Q.; Liu, W.-S.; Dou, W.; Zheng, J.-R.; Tang, X.-L.; Zhang, H.-R.; Wang, D.-Q. *Dalton. Trans.* **2008***,* 3582.

(52) Miyata, K.; Hasegawa, Y.; Kuramochi, Y.; Nakagawa, T.; Yokoo, T.; Kawai, T. *Eur. J. Inorg. Chem.* **2009**, 4777.

(53) Moudam, O.; Rowan, B. C.; Alamiry, M.; Richardson, P.; Richards, B. S.; Jones, A. C.; Robertson, N. *Chem. Commun.* **2009**, 6649.

(54) Biju, S.; Reddy, M. L. P.; Cowley, A. H.; Vasudevan, K. V. *Crystal Growth & Design.* **2009**, *9*, 3562.

(55) Feng, J.; Zhang, H.-J.; Song, S.-Y.; Li, Z.-F.; Sun, L.-N,; Xing, Y. *J. Lumin.* **2008**, *128,* 1957.

(56) Shavaleev, N. M.; Eliseeva, S. V.; Scopelliti, R.; Bünzli, J.-C. G. *Chem. Eur. J.* **2009**, *15,* 10790.

(57) Shavaleev, N. M.; Eliseeva, S. V.; Scopelliti, R.; Bünzli, J.-C. G. *Inorg. Chem.* **2010**, *49,* 3927.

(58) Guo, Y.; Dou, W.; Zhou, X.; Liu, W.; Qin, W.; Zang, Z.; Zhang, H.; Wang, D. *Inorg. Chem.* **2009**, *48,* 3581.

(59) Charbonnière, L.; Mameri, S.; Kadjane, P.; Platas-Iglesias, C.; Ziessel, R. *Inorg. Chem.* **2008**, *47,* 3748.

(60) Yanagida, S.; Hasegawa, Y.; Murakoshi, K.; Wada, Y.; Nakashimi, N.; Yamanaka, T. *Coord, Chem. Rev.* **1998**, *171*, 461.

(61) Comby, S.; Imbert, D.; Chauvin, A.-S.; Bünzli, J.-C. G. *Inorg. Chem.* **2006**, *45*, 732.

(62) Hasegawa, Y.; Ohkubo, T.; Sogabe, K.; Kawamura, Y.; Wada, Y.; Nakashima, N.; Yanagida, S. *Angew. Chem.* **2000**, 365.

(63) Xu, H.-B.; Chen, X.-M.; Zhang, Q.-S.; Zhang, L.-Y.; Chen, Z.-N. *Chem. Commun*. **2009**, 7318.

(64) Norton, K.; Kumar, G. A.; Dilks, J. L.; Emge, T. J.; Riman, R. E.; Brik, M. G.; Brennan, J. G. *Inorg. Chem*. **2009**, *48*, 3573.

(65) Feng, J.; Yu, J.-B.; Song, S.-Y.; Sun, L.-N.; Fan, W.-Q.; Guo, X.-M.; Dang, S.; Zhang, H.-J. *Dalton Trans*. **2009**, 2406.

(66) Nonat, A.; Imbert, D.; Pécaut, J.; Giraud, M.; Mazzanti, M. *Inorg. Chem*. **2009**, *48*, 4207.

(67) Lazarides, T.; Alamiry, M. A. H.; Adams, H.; Pope, S. J. A.; Faulkner, S.; Weinstein, J. A.; Ward, M. D. *Dalton Trans*. **2007**, 1484.

(68) Ahmed, Z.; Iftikhar, K. *Inorg. Chim. Acta.* **2010**, *363*, 2606.

(69) Valore, A.; Cariati, E.; Righetto, S.; Roberto, D.; Tessore, F.; Ugo, R.; Fragalà, I. L.; Fragalà, M. E.; Malandrino, G.; De Angelis, F.; Belpassi, L.; Ledoux-Rak, I.; Thi, K. H.; Zyss, J. *J. Am. Chem. Soc.* **2010**, *132*, 4966.

(70) Wu, J.; Li, H.-Y.; Xu, Q.-L.; Zhu, Y.-Ch.; Tao, Y.-M.; Li, H.-R.; Zheng, Y.-X.; Zuo, J.-L.; You, X.-Z. *Inorg. Chim. Acta.* **2010**, *363*, 2394.

(71) Song, L.; Hu, J.; Wang, J.; Liu, X.; Zhen, Z. *Photochem. Photobiol. Sci.* **2008**, *7,* 689.

(72) Gilling, W. P.; Curry, R. J. *Appl. Phys. Lett.* **1999**, *74*, 789.

(73) Comby, S.; Imbert, D.; Chauvin, A.S.; Bünzli, J.-C. G. *Chem. Commun.* **2007**, 732.

(74) Bozoklu, G.; Marchal, C.; Pécaut, J.; Imbert, D.; Mazzanti, M. *Dalton. Trans.* **2010**, *39,* 9112.

(75) Nonat, A.; Imbert, D.; Pécaut, J.; Giraud, M.; Mazzanti, M*. Inorg. Chem.* **2009**, *48,* 4207.

(76) Albrecht, M.; Osetska, O.; Klankermayer, J.; Fröhlich, R.; Gumy, F.; Bünzli, J.-C. G. *Chem. Commun.* **2007**, 1834.

(77) Shavaleev, N. M.; Scopelliti, R.; Gumy, F.; Bünzli, J.-C. G. *Inorg. Chem.* **2009**, *48,* 2908.

(78) Huang, W.; Wu, D.; Guo, D.; Zhu, X.; He, Ch.; Meng, Q.; Duan, Ch. *Dalton Trans.* **2009**, 2081.

(79) Zhang, J.; Petoud, S. *Chem. Eur. J.* **2008**, *14,* 1264.

(80) Deiters, E.; Gumy, F.; Bünzli, J.-C. G. *Eur. J. Inorg. Chem.* **2010,** 2723.

(81) Moore, E. G.; Szigethy, G.; Xu, J.; Pålsson, L.-O.; Beeby, A.; Raymond, K. N. *Angew. Chem. Int. Ed.* **2008**, *47,* 9500.

(82) Moore, E. G.; Xu, J.; Dodani, S. C.; Jocher, C. J.; D'Aléo, A.; Seitz, M.; Raymond, N. K. *Inorg. Chem.* **2010**, *49,* 4156.

(83) Elhabiri, M.; Scopelliti, R.; Bünzli, J.-C. G.; Piguet, C. *Chem. Commun.* **1998**, 2347.)

(84) Bünzli, J.-C. G. *Acc. Chem. Res.* **2006**, *39*, 53.

(85) Cantuel, M.; Gumy, F.; Bünzli, J.-C. G.; Piguet, C. *Dalton Trans.* **2006**, 2647.

(86) Terazzi, E.; Guénée, L.; Bocquet, B.; Lemonnier, J.-F.; Favera, N. D.; Piguet, C. *Chem. Eur. J.* **2009**, *15*, 12719.

(87) Ronson, T. K.; Adams, H.; Harding, L. P.; Pope, S. J. A.; Sykes, D.; Faulkner, S.; Ward, M. D. *Dalton Trans.* **2007**, 1006.

(88) Basset, A. P.; Magennis, S. W.; Glover, P. B.; Lewis, D. J.; Spencer, N.; Parsons, S.; Williams, R. M.; De Cola, L.; Pikramenou, Z. *J. Am. Chem. Soc.* **2004**, *126*, 9413.

(89) Bassett, A. P.; Van Deun, R.; Nockemann, P.; Glover, P. B.; Kariuki, B. M.; Van Hecke, K.; Van Meervelt, L.; Pikramenou, Z. *Inorg. Chem.* **2005**, *44*, 6140.

(90) Glover, P. B.; Bassett, A. P.; Nockemann, P.; Kariuki, B. M.; Van Deun, R.; Pikramenou, Z. *Chem. Eur. J.* **2007**, *13*, 6308.

(91) de Sá, G. F.; Malta, O. L.; de Mello Donegá, C.; Simas, A. M.; Longo, R. L.; Santa-Cruz, P. A.; da Silva Jr., E. F. *Coord. Chem. Rev.* **2000**, *196*, 165.

(92) Kido, J.; Okamoto, Y. *Chem. Rev.* **2002**, *102*, 2357.

(93) Smirnov, V. A.; Philippova, O. E.; Sukhadolski, G. A.; Khokhlov, A. R. *Macromolecules* **1998**, *31*, 1162.

(94) Smirnov, V. A.; Sukhadolski, G. A.; Philippova, O. E.; Khokhlov, A. R. *J. Phys. Chem. B* **1999**, *103*, 7621.

(95) Hasegawa, Y.; Sogabe, K.; Wada, Y.; Yanagida, S. *J. Lumin.* **2003**, *101*, 235.

(96) Bakker, B. H.; Goes, M.; Hoebe, N.; Van Ramesdonk, H. J.; Verhoeven, J. W.; Werts, M. H. V.; Hofstraat, J. W. *Coord. Chem. Rev.* **2000**, *208*, 3.

(97) Lin, Q.; Shi, C. Y.; Liang, Y. J.; Zheng, Y. X.; Wang, S. B.; Zhang, H. J. *Synthetic. Met.* **2000**, *114*, 373.

(98) Jiang, X.; Philan, G.; Carlson, B.; Liu, S.; Dalton, L.; Jen, A. K.-Y. *Macromol. Symp.* **2002**, *186*, 171.

(99) Aiga, F.; Iwanaga, H.; Amano, A. *J. Phys. Chem. A* **2005**, *109*, 11312.

(100) Shionoya, S.; Yen, W. M. *Phosphor Handbook*; CRC Press Inc.: Boca Raton, FL, U.S.A., 1999.

(101) Male, N. A. H.; Salata, O. V.; Christou, V. *Synthetic. Met.* **2002**, *126*, 7.

(102) Yu, G.; Liu, Y.; Wu, X.; Zhu, D. *Chem. Mater.* **2000**, *12*, 2537.

(103) Blasse, G.; Grabmaier, B. C. *Luminescent Materials*; Springer: Berlin, 1994.

(104) Hasegawa, Y.; Kawai, H.; Nakamura, K.; Yasuda, N.; Wada, Y.; Yanagida, S. *J. Alloy. Compd.* **2006**, *408-412*, 669.

(105) Reisfeld, R.; Jorgenson, C. K. *Laser and excited states of rare earths*; Springer: Berlin, 1977.

(106) Hasegawa, Y.; Wada, Y.; Yanagida, S.; Kawai, H.; Yasuda, N.; Nagamura, T. *Appl. Phys. Lett.* **2003**, *83*, 3599.

(107) Kuriki, K.; Koike, Y. *Chem. Rev.* **2002**, *102*, 2347.

(108) Digonet, M. J. F. *Rare earth doped fibre lasers and amplifiers*; 2nd ed.; Marcel Dekker Inc.: New York, 2001.

(109) Desurvire, E. *Erbium-doped Fibre Amplifiers*; John Wiley & Sons, 1994.

(110) Becker, P. C.; Olsson, N. A.; Simpson, J. R. *Erbium-doped fibre amplifiers: fundamentals and technology*; Academic Press: New York, 1999.

(111) Bjarlev, A. *Optical Fibre Amplifiers: Design and System Applications*; Artech House: Norwood, MA., 1993.

(112) Le Quang, A. Q.; Zyss, J.; Ledoux, I.; Truong, V. G.; Jurdyc, A.-M.; Jacquier, B.; Le, D. H.; Gibaud, A. *Chem. Phys.* **2005**, *318*, 33.

(113) Hemmilä, I. *Applications of Fluorescence in Immunoassays*; Wiley, 1991.

(114) Dickson, E. F. G.; Pollak, A.; Diamandis, E. P. *J. Photoch. Photobio. B* **1995**, *27*, 3.

(115) Hemmilä, I.; Mukkala, V.-M.; Takalo, H. *J. Alloy. Compd.* **1997**, *249*, 158.

(116) Hemmilä, I. *J. Alloy. Compd.* **1995**, *225*, 480.

(117) Mukkala, V.-M.; Takalo, H.; Liitti, P.; Hemmilä, I. *J. Alloy. Compd.* **1995**, *225*, 507.

(118) Diamandis, E. P.; Christopoulos, T. K. *Anal. Chem.* **1990**, *62*, 1149A.

(119) Werts, M. H. V.; Woudenberg, R. H.; Emmerink, P. G.; Van Gassel, R.; Hofstraat, J. W.; Verhoeven, J. W. *Angew. Chem. Int. Ed.* **2000**, *39*, 4542.

(120) Faulkner, S.; Pope, S. J. A. *J. Am. Chem. Soc.* **2003**, *125*, 10526.

(121) Scozzafava, A.; Menabuoni, L.; Mincione, F.; Supuran, C. T. *J. Med. Chem.* **2002**, *45*, 1466.

(122) Selvin, P. R.; Rana, T. M.; Hearst, J. E. *J. Am. Chem. Soc.* **1994**, *116*, 6029.

(123) Lauffer, R. B. *Chem. Rev.* **1987**, *87*, 901.

2.0. Luminescent Lanthanide Complexes Based on Tetraphenyl Imidodiphosphate Ligands

2.1. Introduction

Lanthanide complexes have attracted a lot of interest due to their potential applications because of the unique properties of the lanthanide ions. Therefore, the luminescence of lanthanides sensitisation by organic ligands has been widely investigated. Our research group previously studied photophysical properties of lanthanide complexes based on imidodiphosphinate ligands. Their bidentate, negatively charged binding site consisted of hard oxygen donors, provided a strong binding to the Ln^{3+} ions. The twelve aromatic rings of the three ligands created a stabilising hydrophobic shell around the central lanthanide ions. The Ln(**tpip**)$_3$ complexes showed very good luminescence properties, with high quantum yields and long luminescence lifetimes for both visible and NIR-emitting lanthanides.[1,2]

The flexibility of imidodiphosphinate ligands offers a wealth of possibilities for further derivitisation as the binding and antenna domains are not in conjugation. Therefore, we have built upon this and modified the H**tpip** ligand by changing the antenna groups. The H**tpOp** ligand was interesting to develop for two main reasons. Firstly, the substitution of phenyl groups for phenoxy was aimed to increase the solubility in polar solvents. Secondly, an introduction of oxygen on antenna groups of the ligand

was going to give more flexibility hence, providing a better shielding against quenching solvent molecules.

We report herein the synthesis, full characterisation and photophysical properties of tetraphenyl imidodiphosphate ligand H**tpOp** and its Ln(**tpOp**)$_3$ (Ln = Eu, Tb, Dy, Sm, Gd, Er, Nd, Yb) complexes.

2.2. Results and Discussion

2.2.1. Preparation and characterisation of HtpOp ligand

Two different procedures were explored in the preparation of H**tpOp** ligand.

The first procedure (Scheme 2.1) was mostly a modification of a previous published method from 1964.[3] However, the journal lacked NMR spectroscopic data, so a full NMR study was performed for the H**tpOp** ligand.

Tetraphenyl imidodiphosphate was prepared by one-pot condensation reaction of two equivalents of triphenyl phosphate with three equivalents of sodium amide. The sodium salt of tetraphenyl imidodiphosphate was converted into the pure H**tpOp** ligand under acidic condition in a reasonably good yield of 62%.

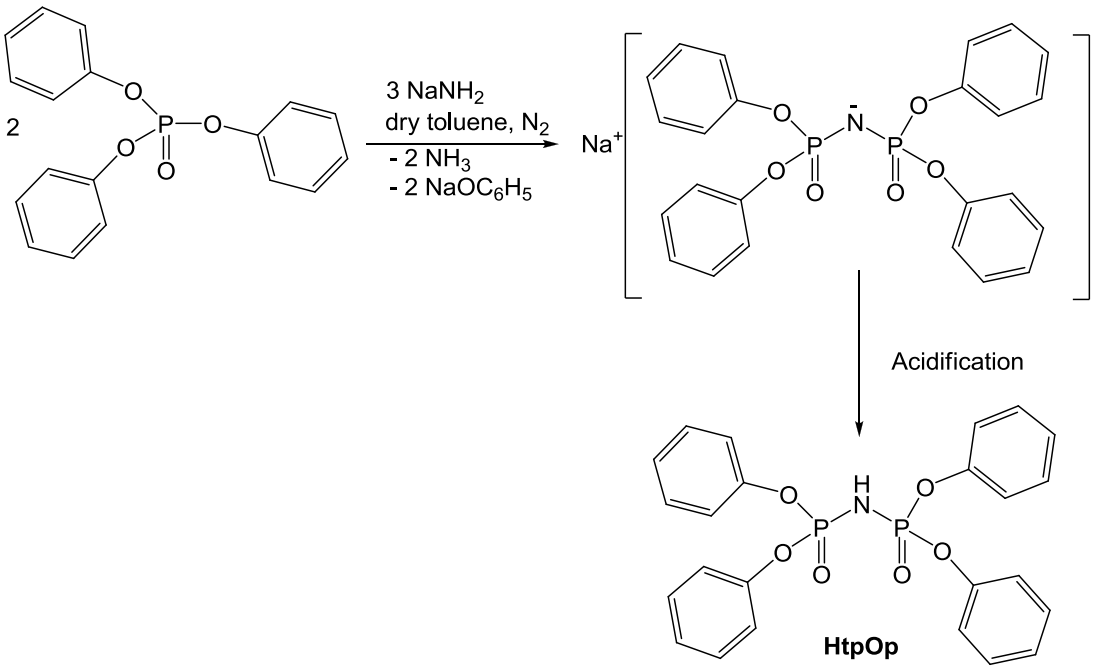

Scheme 2.1. Synthetic route I for preparation of H**tpOp.**

The second procedure for the preparation of the H**tpOp** ligand was adopted from a synthetic route, reported for unsymmetrical P-N-P ligands (Scheme 2.2).[4] The H**tpOp** was achieved by a condensation reaction between sodium salt of diphenyl

phosphoramidate and diphenyl chlorophosphate. The acidic work-up afforded the crude product, which was purified by recrystallisation, giving the desired product as a light brown solid in yield of 69%.

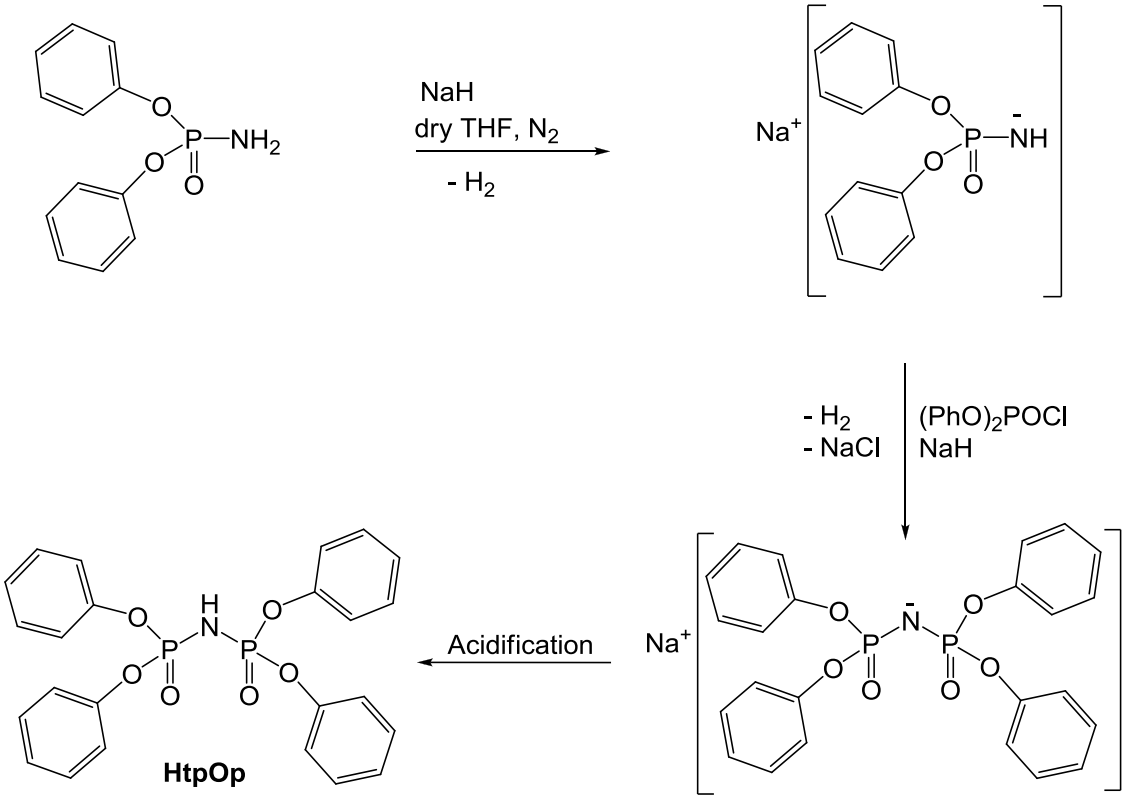

Scheme 2.2 Synthetic route II for preparation of H**tpOp**.

A comparison of the two procedures for the preparation of H**tpOp** concluded that the first synthetic route was a more convenient method, as it was less time consuming and secondly the ligand was isolated as pure without the need of any further purification such as recrystallisation.

The H**tpOp** has been fully characterised by ^{31}P, ^{13}C and ^{1}H NMR in $CDCl_3$, mass spectrometry and elemental analysis. The ligand was very soluble in solvents such as chloroform, acetonitrile, THF, ethanol and methanol.

The (-) ESI-MS of the ligand shows a peak at *m/z* 480 corresponding to $[M + H]^-$ (See Appendix A1).

The ^{1}H NMR spectrum of H**tpOp** in $CDCl_3$ shows a broad multiplet at range 7.11 - 7.24 ppm corresponding to the aromatic protons (Figure 2.1).

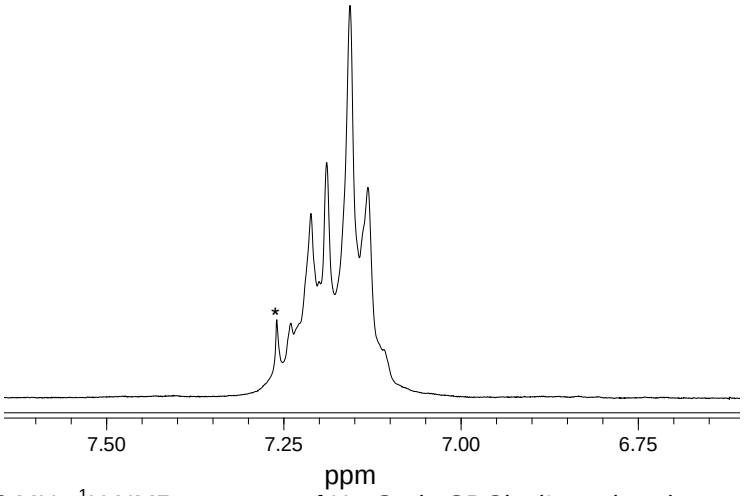

Figure 2.1. The 300 MHz ^{1}H NMR spectrum of H**tpOp** in $CDCl_3$. (* = solvent).

The ^{31}P NMR spectrum in $CDCl_3$ shows a single peak resonance at -9.7 ppm corresponding to the equivalent phosphorus atoms (Figure 2.2). The absence of a single peak at -16.5 ppm, which corresponds to the starting material triphenyl phosphate, provides evidence that the product was successfully isolated as pure solid. The phosphorus signal observed for H**tpOp** is shifted to a lower frequency by 31 ppm in comparison to H**tpip**[1], indicating that the phosphorus is more shielded in the presence of the phenoxide aromatic groups.

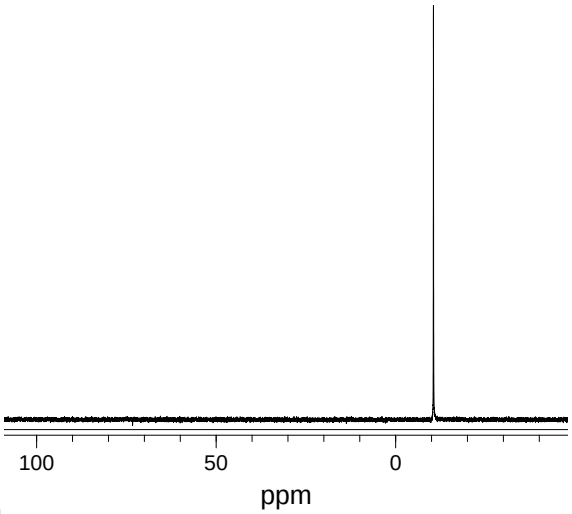

Figure 2.2 The 121 MHz ^{31}P NMR spectrum of H**tpOp** in $CDCl_3$.

The ^{13}C PENDANT NMR spectrum in chloroform (Figure 2.3) shows four resonances, as expected for the desired product. Carbon signals in the region 120 – 151 ppm correspond to the aromatic carbons of the phenoxide ring.

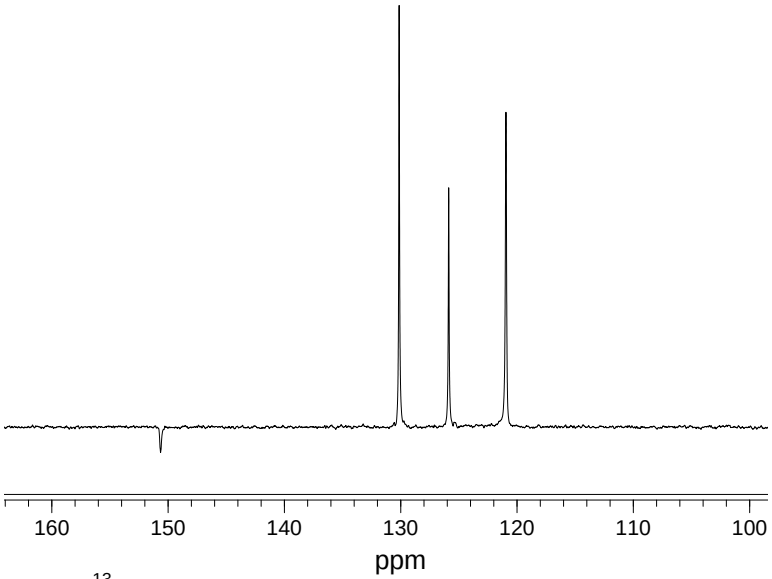

Figure 2.3. The 125 MHz ^{13}C NMR spectrum of H**tpOp** in $CDCl_3$.

The purity of the compound was also confirmed by melting point, elemental analysis and X-ray diffraction.

2.2.2. X – ray Crystallography of HtpOp

The crystal structure of H**tpOp** has been previously determined by single-crystal X-ray diffraction.[5] I also isolated crystals by slow evaporation of acetone solution over several weeks at room temperature (Figure 2.4). The crystallographic data for the ligand presented in Table 2.1 show that the crystals are monoclinic with the space group $P2_1/n$, whereas in the previous report the crystals were monoclinic with the space group $P2_1/c$. The rest of observed data for H**tpOp** are in good agreement with the published structure.[5]

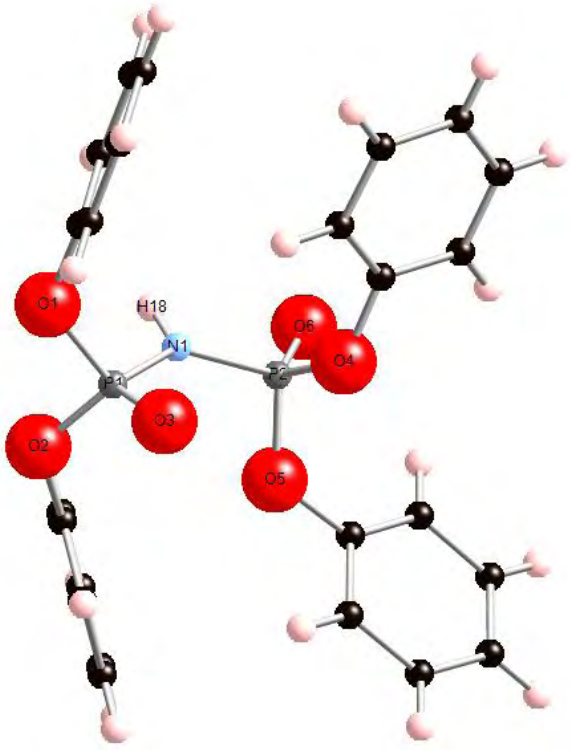

Figure 2.4. Molecular structure of H**tpOp** showing the atomic numbering scheme.

The Ht**pOp** ligand exists in the crystalline state in the phosphazane form. From the crystal structure it can be seen that the two donor atoms O(3) and O(6) of the imidophosphoryl group are in *trans* arrangement, with respect to each other. The hydrogen atom H(18) is chemically bonded at the nitrogen atom N(1) with the bond length of 0.860 Å.

The length of bonds P(1)-O(3) and P(2)-O(6) are almost equal at around 1.45 Å, which indicates double bonding between P and O with localised π-electrons. The P-N bonds N(1)-P(1) and N(1)-P(2) are almost identical single bonds at around 1.63 Å. Dimers are observed when two molecules are connected by the intermolecular hydrogen bonding N(1)-H(1)···O(6) with a 1.957 Å distance as shown in Figure 2.5.

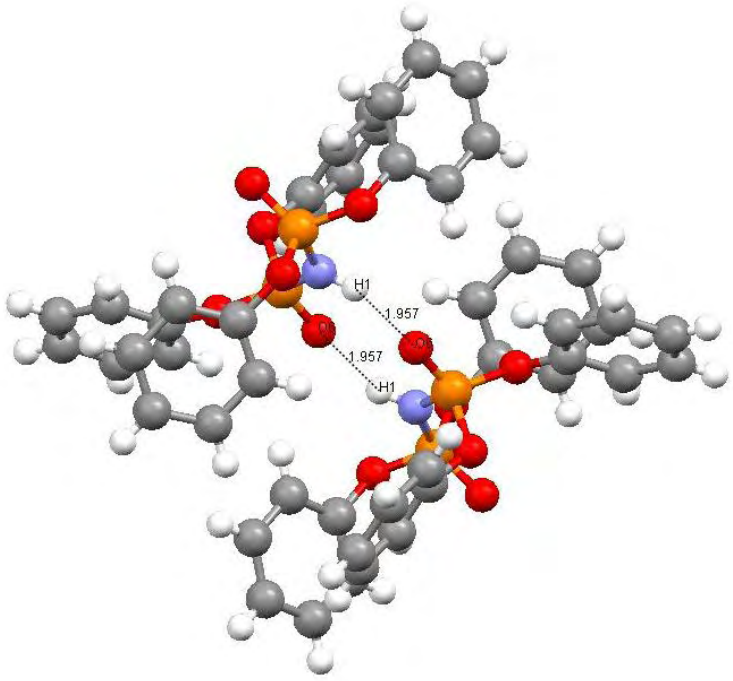

Figure 2.5 The single crystal XRD of H**tpOp** displaying the hydrogen bonded dimer.

Table 2.1. Crystal data and structure refinement for H**tpOp**.

Identification code	H**tpOp**	
Empirical formula	$C_{24}H_{21}NO_6P_2$	
Formula weight	481.36	
Temperature	296(2) K	
Wavelength	1.54178 Å	
Crystal system	Monoclinic	
Space group	$P2_1/n$	
Unit cell dimensions	a = 11.9924(7) Å	α= 90°
	b = 12.2955(7) Å	β= 96.820(4)°
	c = 16.2024(9) Å	γ = 90°
Volume	2372.2(2) $Å^3$	
Z	4	
Density (calculated)	1.348 Mg/m^3	
Absorption coefficient	2.011 mm^{-1}	
F(000)	1000	
Crystal size	0.5 x 0.15 x 0.15 mm^3	
Theta range for data collection	4.35 to 70.65°.	
Index ranges	-12<=h<=14, -13<=k<=14, -17<=l<=19	
Reflections collected	15063	
Independent reflections	4352 [R(int) = 0.0399]	
Completeness to theta = 70.65°	95.8 %	
Refinement method	Full-matrix least-squares on F^2	
Data / restraints / parameters	4352 / 0 / 298	
Goodness-of-fit on F^2	1.019	
Final R indices [I>2sigma(I)]	R1 = 0.0355, wR2 = 0.0886	
R indices (all data)	R1 = 0.0499, wR2 = 0.0969	
Largest diff. peak and hole	0.163 and -0.296 e.$Å^{-3}$	

In accordance with the crystal structure of the H**tpOp** ligand, the powder IR spectrum (Figure 2.6) shows absorption bands at 2,961 cm^{-1} and 2,753 cm^{-1} due to the N-H stretching vibrations. As the amine is involved in hydrogen bonding the NH stretching frequencies are lowered and broadened. The P=O stretching frequency centred at 1,184 cm^{-1} corresponds to the P(1)-O(3), P(2)-O(6) bonds. The sharp absorption band at 933 cm^{-1} is due to PNP stretching frequencies.[6]

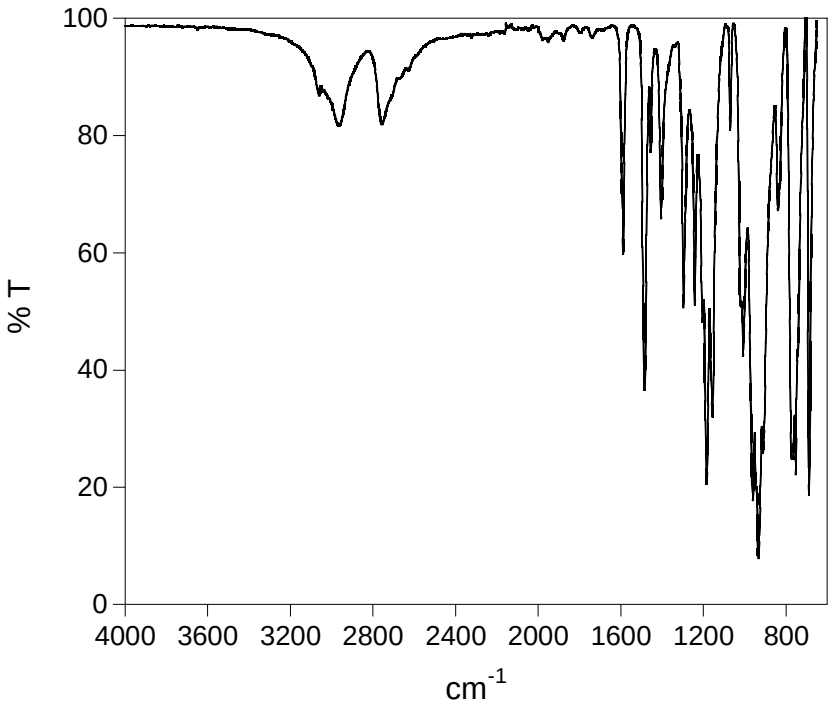

Figure 2.6. The IR spectrum of powder sample of H**tpOp**.

2.2.3. Preparation and characterisation of KtpOp

The preparation of **KtpOp** was attempted initially following the same method as that reported for the potassium salt of the H**tpip**[1], which included a reaction of the **tpip** ligand with methanolic KOH solution. However, attempts to prepare the K**tpOp** under same conditions were unsuccessful and the product was isolated in trace amounts, therefore the characterisation was not possible.

In order to optimise the formation and isolation of K**tpOp** salt, a new procedure was carried out using potassium hydride. Reaction of one equivalent of H**tpOp** with 1.2 equivalent of KH in THF (Scheme 2.3) gave K**tpOp** in a good yield of 88%. K**tpOp** was soluble in solvents such as methanol, ethanol, chloroform, acetone, and moderately soluble in water.

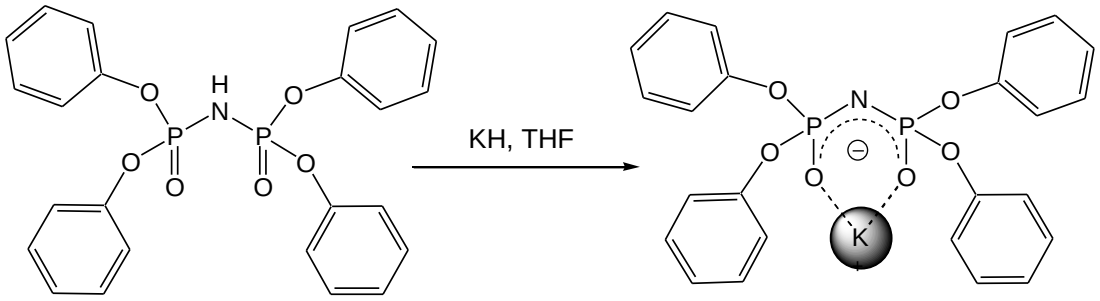

Scheme 2.3. Synthetic route to K**tpOp**.

The potassium salt of tetraphenyl imidodiphosphate has been identified using ^{31}P, ^{13}C and ^{1}H NMR in $CDCl_3$ and mass spectrometry.

The ^{31}P NMR resonance in K**tpOp** moves downfield upon deprotonation/ coordination compared to the free ligand. The appearance of a single peak at -7.2 ppm in the ^{31}P NMR spectra (Figure 2.7) confirmed the reaction was successful as there is no peak at -9.7 ppm corresponding to the unreacted H**tpOp** ligand.

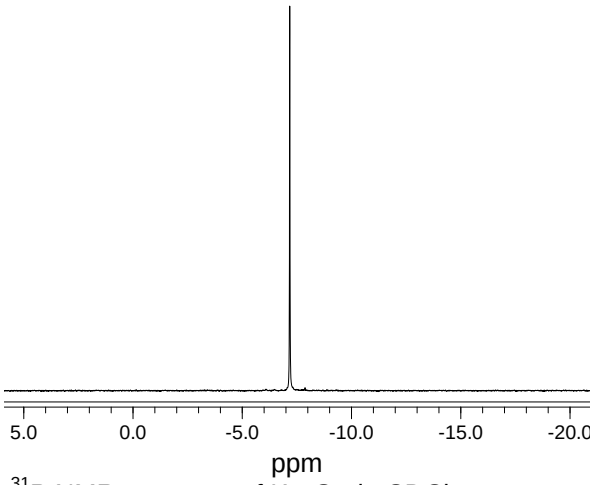

Figure 2.7. The 121 MHz ^{31}P NMR spectrum of K**tpOp** in $CDCl_3$.

The ^{1}H NMR spectrum of K**tpOp** in $CDCl_3$ displays a multiplet in the range 6.94 – 7.11 ppm, which is assigned to the aromatic protons of the phenoxide group of the **tpOp** ligand (Figure 2.8). The multiplet is slightly shifted upfield compare to the H**tpOp**.

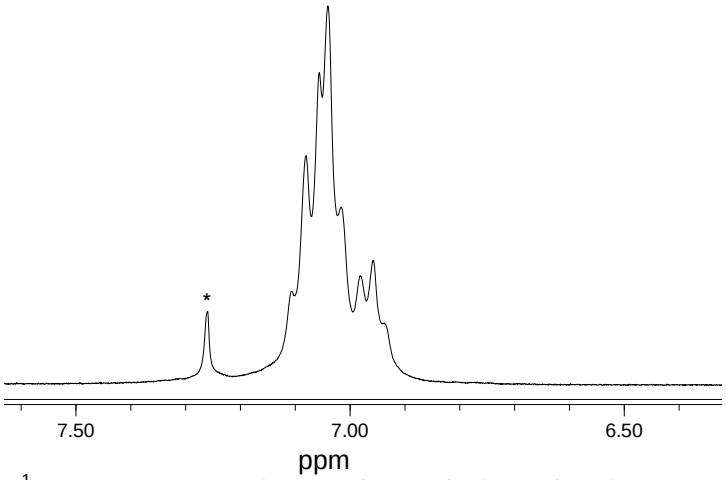

Figure 2.8. The 300 MHz ^{1}H NMR spectrum of K**tpOp** in $CDCl_3$. (* = solvent).

The ^{13}C NMR spectrum in $CDCl_3$ (Figure 2.9) displays four peaks corresponding to the correct number for the product.

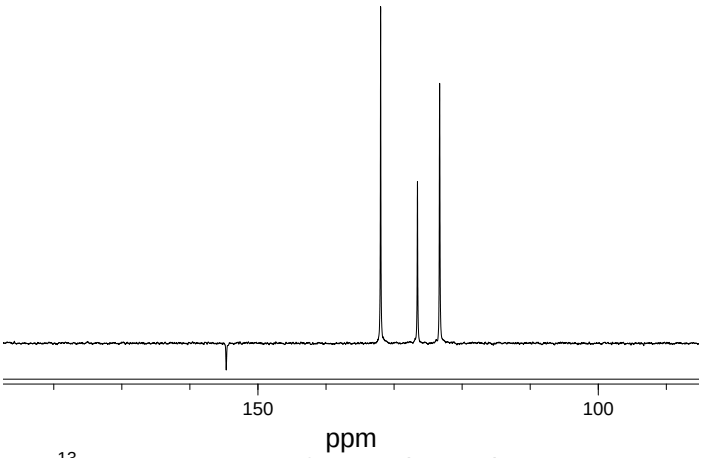

Figure 2.9. The 125 MHz ^{13}C NMR spectrum of K**tpOp** in $CDCl_3$.

Mass spectrometry provides another clear indication of K**tpOp** formation. The MALDI–TOF mass spectrum of the potassium salt of tetraphenyl imidodiphosphate displays signals at *m/z* = 519.6 and 557.6, corresponding to the $[M]^+$ and $[M + K]^+$ ion fragments.

2.2.4. X- ray Crystallography of KtpOp

X-ray quality crystals of the K**tpOp** were grown from aqueous solution by slow evaporation at room temperature. Details of the data collection and refinements for K**tpOp** are summarised in Table 2.2. The structure obtained by X-ray diffraction is shown in Figure 2.10. The K**tpOp** crystallises in the orthorhombic *P*bca space group.

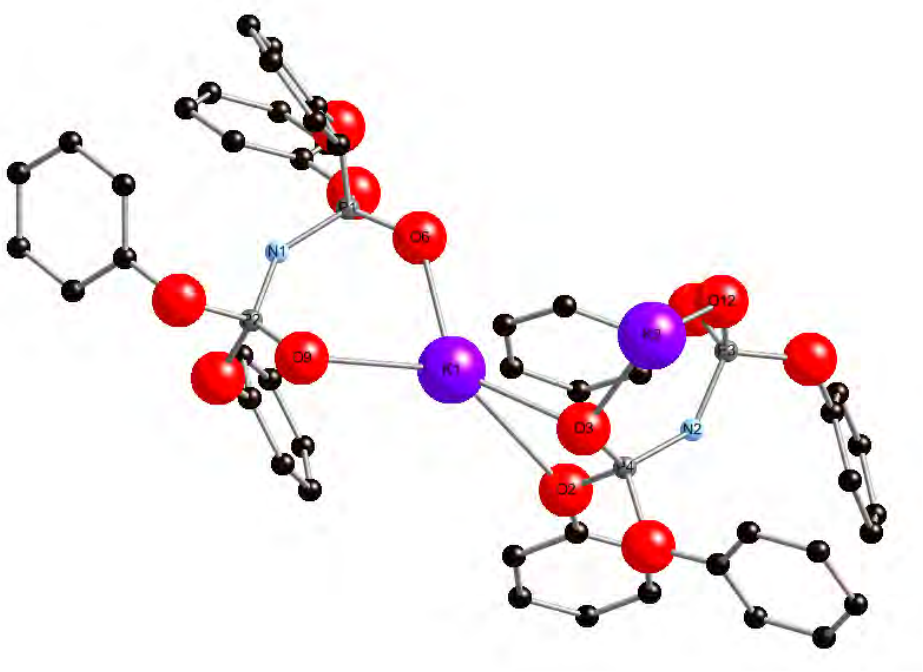

Figure 2.10. The X-ray crystal structure of K**tpOp** showing the atomic numbering scheme. (Hydrogen atoms are omitted for clarity).

The K**tpOp** structure contains two crystallographically independent molecules with similar crystallographic parameters. The P - N bonds P(1) - N(1) and P(2) - N(2) are almost identical at 1.552(4) and 1.554(4) Å respectively. The length of bonds P(1) - O(6) and P(2) - O (9) are 1.472(4) and 1.480(4) Å. The distances of P - N are shorter, in comparison to those observed for H**tpOp** (1.64 Å), whereas the P - O bond order is increased compare to P - O bond lengths of 1.46 Å of the free ligand. This is indicative of delocalisation of π-electrons around the binding unit.

The potassium ion K(1) is bound to two oxygen atoms O(6) and O(9) at distance of 2.658(4) and 2.837(4) Å respectively.

The aromatic moieties of the same ligand are involved in intramolecular interactions. The edge-to-face interaction between two phenoxide rings is observed with a 3.4 Å distance. There is also an evidence of a weak $\pi^{\cdots}\pi$ stacking within the ligand, as two rings are parallel and overlap distance of approximately 4 Å.

On average 1.5 disordered water molecules are also present in the unit cell, therefore K**tpOp** ligands are arranged in a hydrogen bonded network as displayed in Figure 2.11. The chain of ligands are formed by interactions involving bridging disordered water molecules.

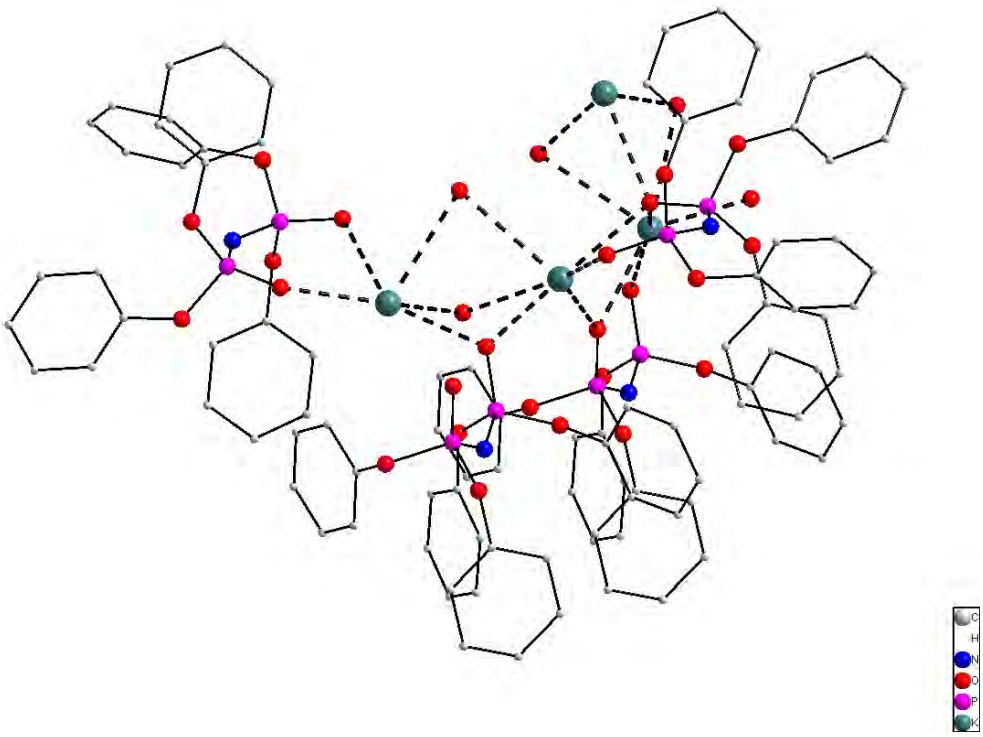

Figure 2.11. The X-ray crystal structure of KtpOp, showing the hydrogen bonded chain.

Table 2.2. Summary of the XRD single crystal structure data of K**tpOp**.

Identification code	**KtpOp**
Empirical formula	C_{24} H_{23} K N $O_{7.50}$ P_2
Formula weight	546.47
Temperature	293(2) K
Wavelength	1.54178 Å
Crystal system	Orthorhombic
Space group	Pbca
Unit cell dimensions	a = 8.023(2) Å α = 90°
	b = 36.423(10) Å β = 90°
	c = 35.590(10) Å γ = 90°
Volume	10401(5) $Å^3$
Z	16
Density (calculated)	1.396 Mg/m^3
Absorption coefficient	3.351 mm^{-1}
F(000)	4528
Crystal size	0.50 x 0.25 x 0.05 mm^3
Theta range for data collection	2.43 to 65.89°.
Index ranges	-8<=h<=9, -42<=k<=42, -37<=l<=41
Reflections collected	62917
Independent reflections	8764 [R(int) = 0.0878]
Completeness to theta = 65.89°	96.9 %
Max. and min. transmission	0.8503 and 0.2851
Refinement method	Full-matrix least-squares on F^2
Data / restraints / parameters	8764 / 0 / 643
Goodness-of-fit on F^2	1.027
Final R indices [I>2sigma(I)]	R1 = 0.0606, wR2 = 0.1306
R indices (all data)	R1 = 0.1092, wR2 = 0.1525
Largest diff. peak and hole	0.641 and -0.404 $e.Å^{-3}$

2.2.5. Preparation and characterisation of $Ln(tpOp)_3$ complexes, (Ln = Eu, Tb, Dy, Sm, Gd, Nd, Yb, Er) and $Y(tpOp)_3$

Two synthetic routes were explored in the preparation of $Ln(tpOp)_3$ complexes.

In the first procedure, the $Ln(tpOp)_3$ (Ln = Tb, Eu) complexes were prepared directly from the HtpOp ligand without a prior isolation of the potassium salt (Scheme 2.4).[7] However, there was a concern that this method did not result in good yields due to incomplete precipitation.

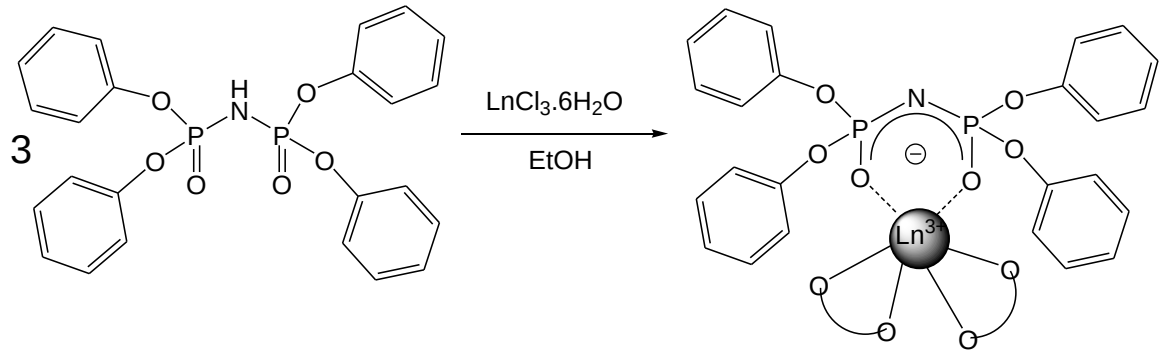

Scheme 2.4. Preparation of Ln(**tpOp**)$_3$ (I).

In the second method, the lanthanide complexes were prepared from the isolated KtpOp. The reaction of three equivalents of an alcoholic solution of KtpOp with one equivalent of aqueous alcoholic solution of $LnCl_3.6H_2O$ produced the corresponding $Ln(tpOp)_3$ complexes as a fine colourless powder with yields of 52 – 67% (Scheme 2.5). The complexes showed a good solubility in chloroform, acetone, acetonitrile, methanol and THF.

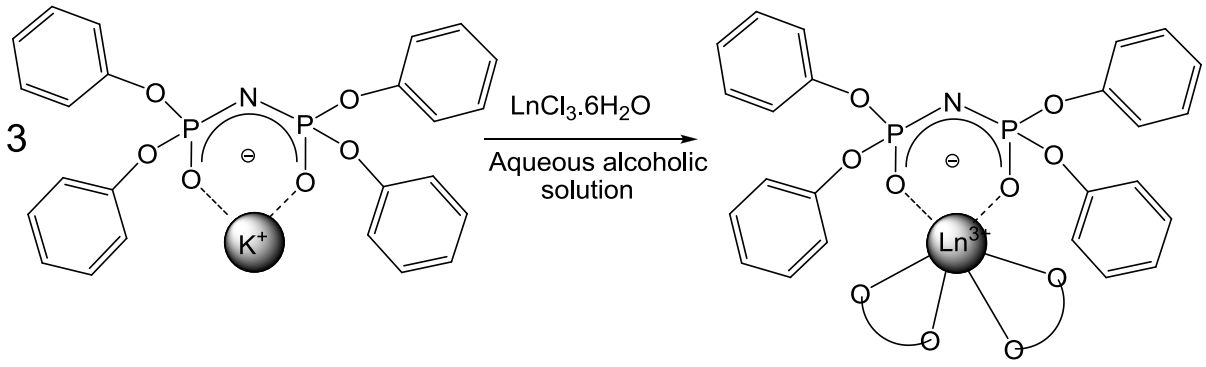

Scheme 2.5. Preparation of Ln(**tpOp**)$_3$ (II).

The complexes were characterised by ^{31}P, ^{1}H, ^{13}C NMR, mass spectrometry and the obtained results were consistent, regardless of the procedure. (No NMR spectra were acquired for Gd(tpOp)$_3$ due to the severe broadening caused by the highly paramagnetic Gd^{3+} ion.)

Upon coordination of tpOp ligand to Y^{3+}, the ^{31}P resonance of KtpOp moves downfield from δ = -7.2 to -4.2 ppm, due to the deshielding of the phosphorus atoms expected from the electron withdrawing effect of coordination. The presence of a single phosphorus peak, indicating one environment, and its chemical shift proves that the ligands are bound to Y^{3+} ion in solution.

The Ln(tpOp)$_3$ complexes can be separated into three groups by the signs of the ^{31}P chemical shifts with respect to the diamagnetic reference Y(tpOp)$_3$. The shifts of Dy^{3+}, Sm^{3+}, Yb^{3+} complexes remain similar to that of the Y(tpOp)$_3$ complex, whereas the Er^{3+}, Eu^{3+} and Tb^{3+} complexes show the greatest upfield ^{31}P shifts, while Nd^{3+} complex has the largest downfield shift.

The ^{31}P NMR spectra of the complexes have broadly similar features, with the exception of the characteristic differences that arise from the magnetic properties of the different Ln^{3+} ions. They all display a single resonance, indicating the presence of one phosphorus environment for the six phosphorus atoms of the complexes and confirm the equivalence of the ligands.

The ^{31}P NMR spectra of Sm^{3+} and Eu^{3+}, Nd^{3+} and Yb^{3+} complexes exhibit narrow bandwidths. Each spectrum displays a single peak: -80.0 ppm for Eu(**tpOp**)$_3$ (Figure 2.12), -4.0 ppm for Sm(**tpOp**)$_3$, -8.5 ppm for Yb(**tpOp**)$_3$ and 30.2 ppm for Nd(**tpOp**)$_3$ respectively (see Appendix A2 – A4).

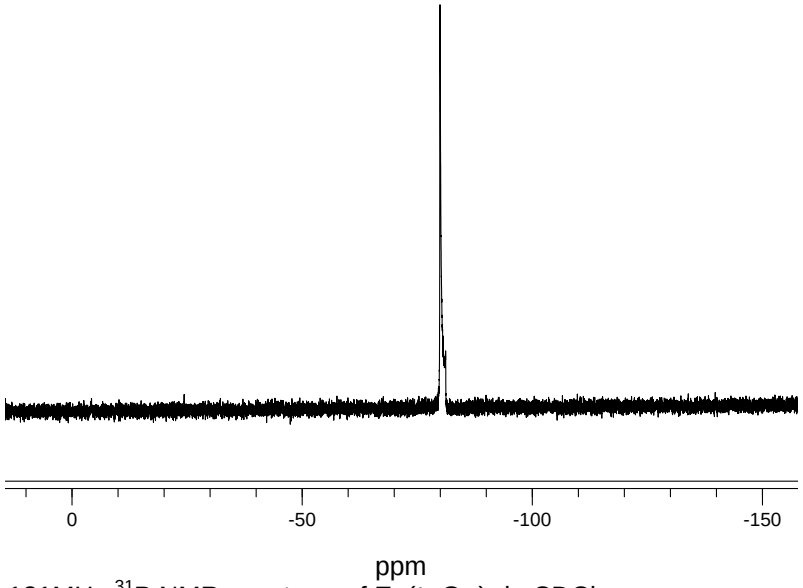

Figure 2.12. The 121MHz ^{31}P NMR spectrum of Eu(**tpOp**)$_3$ in $CDCl_3$.

In contrast, the Dy^{3+} and Tb^{3+} and Er^{3+} complexes undergo excessive line broadening as shown in (Figure 2.13) for Tb(**tpOp**)$_3$ complex as a representative example. The ^{31}P NMR spectra of Dy(**tpOp**)$_3$ and Er(**tpOp**)$_3$ in $CDCl_3$ also display a broad singlet peak paramagnetically sfifted to -2.2 ppm and -85.8 ppm respectively, (see Appendix A5 and A6) demonstrating again the high symmetry and chemical equivalence of the coordination environment.

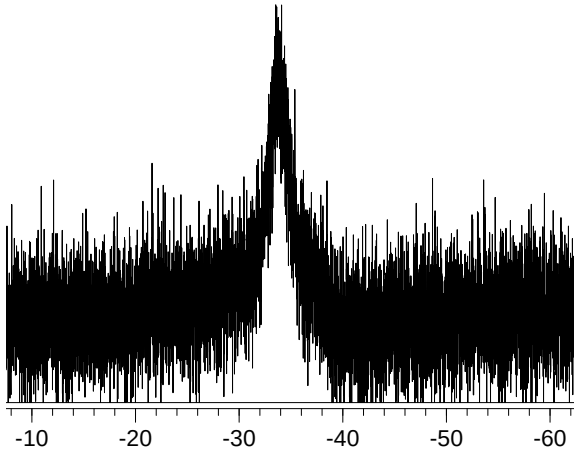

Figure 2.13. The 121 MHz ^{31}P NMR spectrum of Tb(**tpOp**)$_3$ in $CDCl_3$.

The observed significant changes in ^{31}P paramagnetic shifts and line broadening in the spectra of paramagnetic Ln(tpOp)$_3$ complexes arise from the influence of the 4*f* electrons of the lanthanide metals and the nuclei of the substrate. Two types of interaction between metal cation and ligand have been known; contact and pseudocontact interactions, and the resulting shifts referred to as the contact and pseudocontact shifts.[8,9,10]

The pseudocontact shift is caused by a dipolar interaction through space between the nucleus and the electron spin magnetisation of the paramagnetic Ln^{3+} ion. The magnitude of the pseuodocontact shifts is a function of the metal ion involved and the geometry of the nuclei of the ligand relative to the metal ion.[10,11] The second contribution to the shifts (the contact shift) is determined by covalent bonding interactions transferring unpaired electron density onto the ligand.[10,11] This interaction falls off rapidly with increasing distance, therefore the effect is greatest on ligand nuclei that are very close to the metal ion.

If the pseudocontact shift predominates, the theoretical order of ^{31}P to higher frequency should be Er > Yb > Eu > Sm > Nd > Tb > Dy.[10,11] But, if the contact interaction predominates, the order of ^{31}P shift to higher frequency should follow Tb > Dy > Er > Eu > Yb > Sm > Nd.[10,11] The observed patterns for the ^{31}P paramagnetic shifts of $Ln(tpOp)_3$ complexes across the series are not characteristic of shifts dominated by either pseudocontact or contact origins but rather a mixture of the two. In comparison, the ^{31}P shifts of $Ln(tpip)_3$ complexes were found to be purely contact shifts[1], whereas the phosphorus shift values for $Ln(F_{20}tpip)_3$ complexes followed a pseudocontact shift pattern.[12] The observed differences can be explained by the nature of the aromatic substrates. The $Ln(F_{20}tpip)_3$ complexes contain strong electron withdrawing pentafluorobenzene groups, which will pull some of the electron density away from the donor atoms, making the interaction more electrostatic and therefore making the pseudocontact contribution through space more significant. In contrast, the phenyl groups in $Ln(tpip)_3$ are electron donating, hence lessening the pseudocontact contribution.[1] Since the $Ln(tpOp)_3$ complexes contain the phenoxy groups, which are less electron withdrawing than pentafluorobenzene groups as well as less electron donating than the phenyl groups, both the contact shift and pseudocontact mechanisms are operating in the chemical shift series of the paramagnetic $Ln(tpOp)_3$ complexes.

The ^1H NMR spectra in $CDCl_3$ were recorded for all Ln(**tpOp**)$_3$ complexes. They display three signals in the intensity ratio of 2:1:2. These signals are sharp multiplets for the Eu^{3+} and Sm^{3+} (See Appendix A.7) complexes as shown in Figure 2.14 for Eu(**tpOp**)$_3$ complex, where a 7.3 Hz $^3J_{H,H}$ coupling and a 7.1 Hz $^3J_{H,H}$ coupling split the H-H protons into two triplets corresponding to H_b and H_c respectively. The

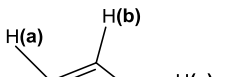

doublet centred at 6.78 ppm with a coupling constant of $^3J_{H,H}$ = 7.6 Hz is assigned as the *ortho* proton H_a.

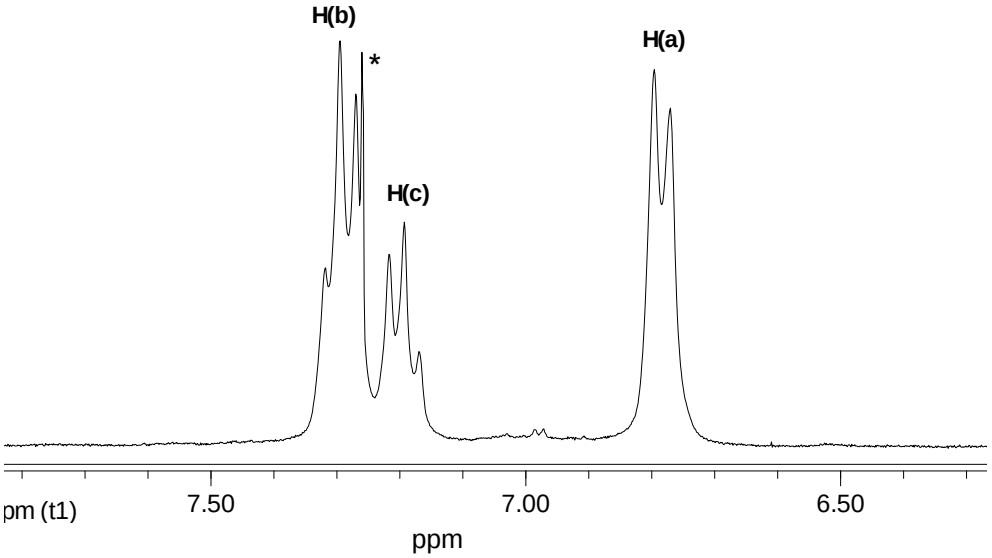

Figure 2.14. The 300 MHz ^{1}H NMR spectrum of Eu(**tpOp**)$_3$ in $CDCl_3$. Inset depicts part of the complex with the labelling scheme. (* = solvent).

In the cases of the Tb^{3+}, Dy^{3+} and Yb^{3+} complexes, a common feature is the broadening of the proton resonances into singlets as demonstrated in Figure 2.15 for Tb(**tpOp**)$_3$ complex.

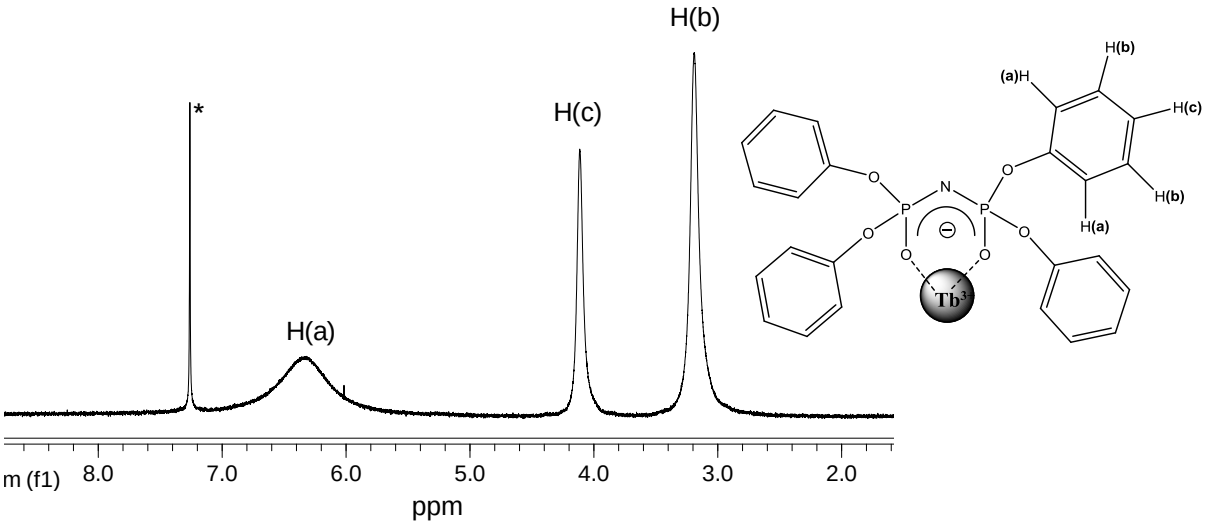

Figure 2.15. The 300 MHz ^{1}H NMR spectrum of Tb(**tpOp**)$_3$ in $CDCl_3$. Inset depicts part of the complex with the labelling scheme. (* = solvent).

The broadening effect is most noticeable for Nd(**tpOp**)$_3$ complex in which the aromatic signals, corresponding to 60H occur as a single band.

The equivalency of each of the phenoxide aromatic rings is confirmed by the ^{13}C PENDANT NMR. All complexes show four distinct carbon resonances in the region 120 - 164 ppm as demonstrated in Figure 2.16 for the Eu(**tpOp**)$_3$ complex.

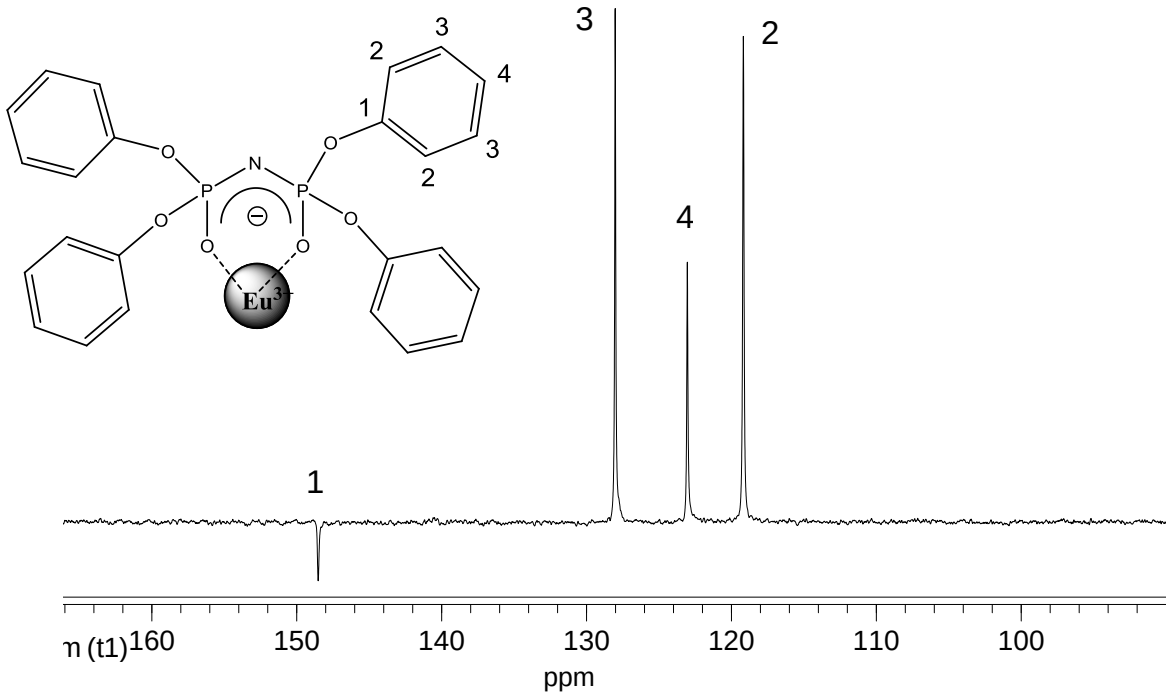

Figure 2.16. The 75 MHz ^{13}C NMR spectrum of Eu(**tpOp**)$_3$ in $CDCl_3$. Inset depicts part of the complex with the labelling scheme.

^{1}H-^{13}C HSQC and ^{1}H-^{1}H COSY NMR spectra of the Dy^{3+} and Eu^{3+} complexes (See Appendix A8 – A11) were obtained in order to fully assign the NMR environments. Observed correlations confirmed the correct assignments as predicted from ^{1}H and ^{13}C NMR studies above.

A summary of the NMR data of the Ln(**tpOp**)$_3$ complexes (Ln = Eu, Tb, Dy, Sm, Nd, Yb, Er) and Y(**tpOp**)$_3$ is given in Table 2.3.

Table 2.3. Summary of NMR data for Ln(**tpOp**)$_3$ (Ln = Eu, Tb, Dy, Sm, Nd, Er, Yb) and Y(**tpOp**)$_3$ complexes.

	δ $^{31}P\{^1H\}$ ($CDCl_3$)	δ^1H ($CDCl_3$)	δ $^{13}C\{^1H\}$ ($CDCl_3$)
Eu(**tpOp**)$_3$	- 80.0 (s)	7.29 (24H, t, ^3J (H,H) = 7.3 Hz, H_b) 7.19 (12H, t, ^3J (H,H) = 7.1 Hz, H_c) 6.78 (24H, d, ^3J (H,H) = 7.6 Hz, H_a)	148.5 (C1) 128.0 (C3) 123.0 (C4) 119.2 (C2)
Tb(**tpOp**)$_3$	- 33.8 (br,s)	6.35 (24H, br, H_a) 4.01 (12H, s, H_c) 3.21 (24H, s, H_b)	163.9 (C1) 126.2 (C3) 123.2 (C2) 121.2 (C4)
Dy(**tpOp**)$_3$	-2.2 (br,s)	5.66 (24H, br, H_a) 4.25 (12H,s, H_c) 3.32 (24H, s, H_b)	163.0 (C1) 128.2 (C3) 123.5 (C2) 120.5 (C4)
Sm(**tpOp**)$_3$	- 4.0 (s)	7.13 (24H, d, ^3J = 7.9 Hz, H_a) 7.02 (24H, t, ^3J = 7.5 Hz, H_b) 6.93 (12H, t, ^3J = 6.9 Hz, H_c)	151.5 (C1), 129.2 (C3) 124.2 (C4) 120.8 (C2)
Nd(**tpOp**)$_3$	30.2 (br,s)	6.73 – 6.80 (60H, m, Ar)	155.7 (C1) 131.6 (C3) 126.5 (C4) 123.4 (C2)
Er(**tpOp**)$_3$	-85.8 (br,s)	8.16 (24H, br, s, H_a) 7.76 (24H, br, s, H_b) 7.38 (12H, br, s, H_c)	147.2 (C1) 128.4 (C3) 123.5 (C2) 119.5 (C4)
Yb(**tpOp**)$_3$	-8.5 (s)	8.59 (24H, br, s,H_a) 7.81 (24H, br, s, H_b) 7.38 (12H, t, ^3J (H,H) = 7.3 Hz, H_c)	147.7 (C1) 128.5 (C3) 123.6 (C4) 119.5 (C2)
Y(**tpOp**)$_3$	-4.2 (s)	6.93 – 7.05 (60H, m, Ar)	150.7 (C1) 128.8 (C3) 123.9 (C2) 120.2 (C4)

Mass spectrometry also provides a clear indication of Ln(**tpOp**)$_3$ complexes formulation. The MAlDI-TOF or positive ion electrospray mass spectra of all complexes display correct *m/z* values corresponding to the $[M]^+$ or $[M + K]^+$ ion fragments. The distinctive isotopic patterns observed for all complexes match with the statistically predicted peak distribution as shown in Figure 2.17 for Sm(**tpOp**)$_3$ complex.

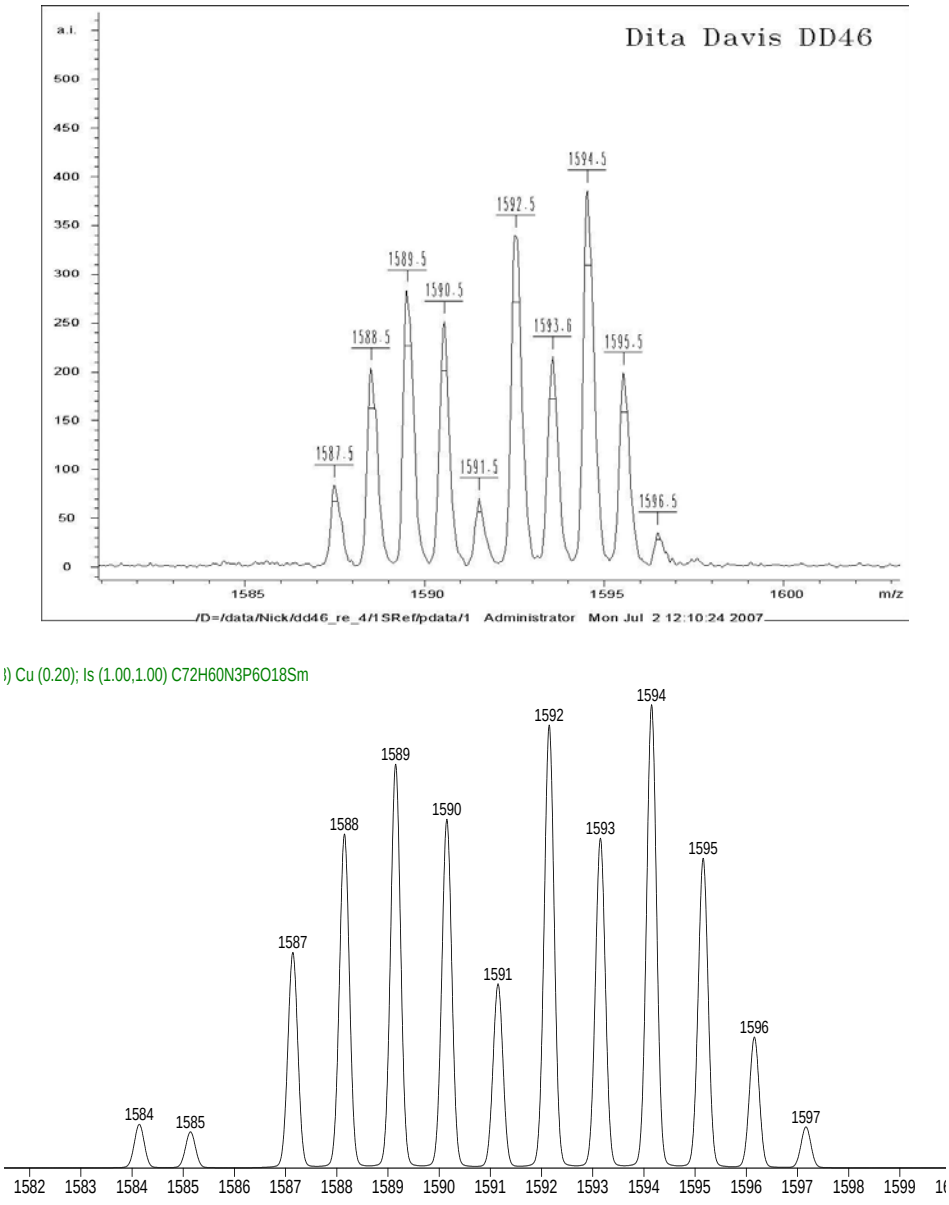

Figure 2.17. The expanded MALDI-TOF spectrum of Sm(**tpOp**)$_3$ (top) and its theoretical isotope pattern (bottom).

The powder IR spectrum of Dy(**tpOp**)$_3$ complex displays characteristic stretching vibrations of the P=O and PNP (Figure 2.18). The absorptions centred at 1,150 cm^{-1} are due to P=O vibrations, whereas the sharp band at 921 cm^{-1} corresponds to PNP stretching vibrations. As the coordination to Dy^{3+} ion take place through P=O groups, these frequencies are affected. Shifts in the P=O stretching frequencies from 1,184 cm^{-1} in H**tpOp** ligand to 1,155 cm^{-1} in Dy(**tpOp**)$_3$ complex show the involvement of phosphoryl oxygens in the complex formation with the Dy^{3+} ion. This is indicative of bond weakening and a decrease in double bond character of P=O as the electron density is drawn away by interaction with Dy^{3+} ion. Also this suggests that the electron density is delocalised within the complexes in the solid state. The broad absorption in the region of 3,250 cm^{-1} indicates the presence of solvent molecules in the complex, which is in agreement with the observed crystal structure of the Dy^{3+} complex.

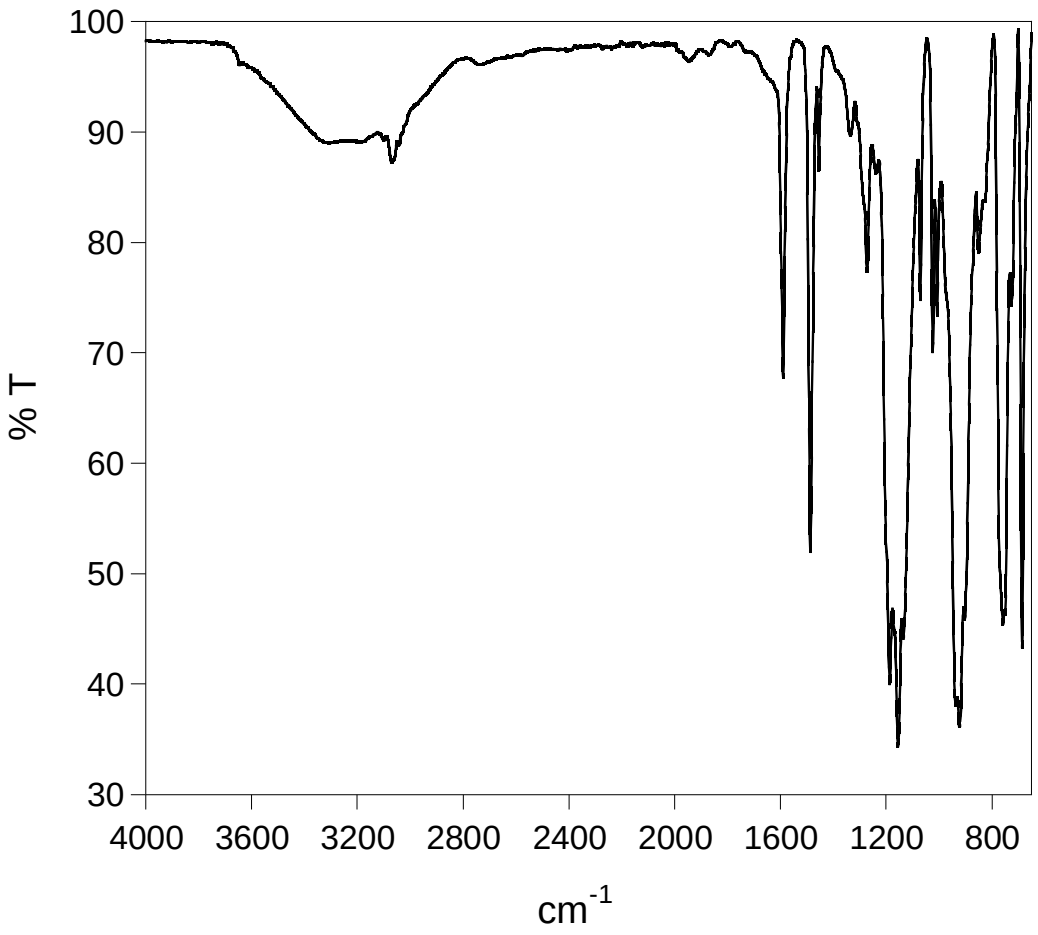

Figure 2.18. The powder IR spectrum of Dy(**tpOp**)$_3$ complex.

2.2.6. X- ray Crystallography Studies of Ln(tpOp)$_3$

In order to examine solid state structure of Ln(**tpOp**)$_3$ complexes, suitable single crystals for X-ray analysis were obtained by slow evaporation of chloroform, acetonitrile or hexane solutions over several weeks at room temperature. The X-ray diffraction crystal structures confirm the formulation of complexes. Each of the complexes contain one unique Ln^{3+} ion and three crystallographically independent imidodiphosphate ligands.

Details of crystal data and data collection parameters for Ln(**tpOp**)$_3$ (Ln = Eu, Tb, Dy, Gd, Er and Yb) are listed in Table 2.4. The complexes with different Ln^{3+} ions share similar structure properties. The Ln(**tpOp**)$_3$.EtOH (Ln = Tb, Eu, Dy, Gd, Er)

complexes all possess similar triclinic structures, belong to the *P*1 space group, with lanthanide ion being seven-coordinate; by three **tpOp** ligands and one additional molecule of ethanol.

In the case of Yb(**tpOp**)$_3$, the single crystal X-ray diffraction reveals that the complex crystallises in the monoclinic space group $P2_1/n$, and there are no other solvent molecules associated with the coordination sphere of the ytterbium ion.

Eu(**tpOp**)$_3$.EtOH

Crystals of Eu(**tpOp**)$_3$ were successfully grown for X-ray single crystal purposes by slow evaporation from chloroform solution at room temperature. The Eu^{3+} ion is coordinated by three bidentate **tpOp** ligands and one additional molecule of ethanol. The coordination geometry of the Eu^{3+} ion is best described as capped octahedral as demonstrated in Figure 2.19.

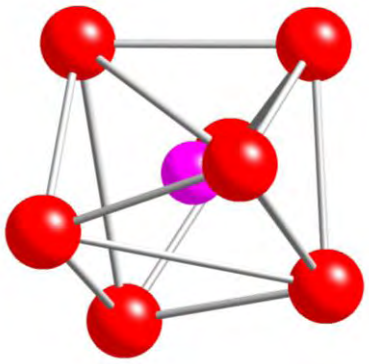

Figure 2.19. Coordination environment of Eu^{3+} in the Eu(**tpOp**)$_3$ complex. Heteroatoms: O, red; Eu^{3+}, pink.

The structure of Eu(**tpOp**)$_3$.EtOH is shown in Figure 2.20. The average bond length between the europium ion and the oxygen atoms is 2.344(6) Å, which is slightly shorter than that of europium and ethanol oxygen atom (2.379 Å). The average (P-O) and (P-N) bond lengths are 1.474(6) and 1.562(7) Å, respectively.

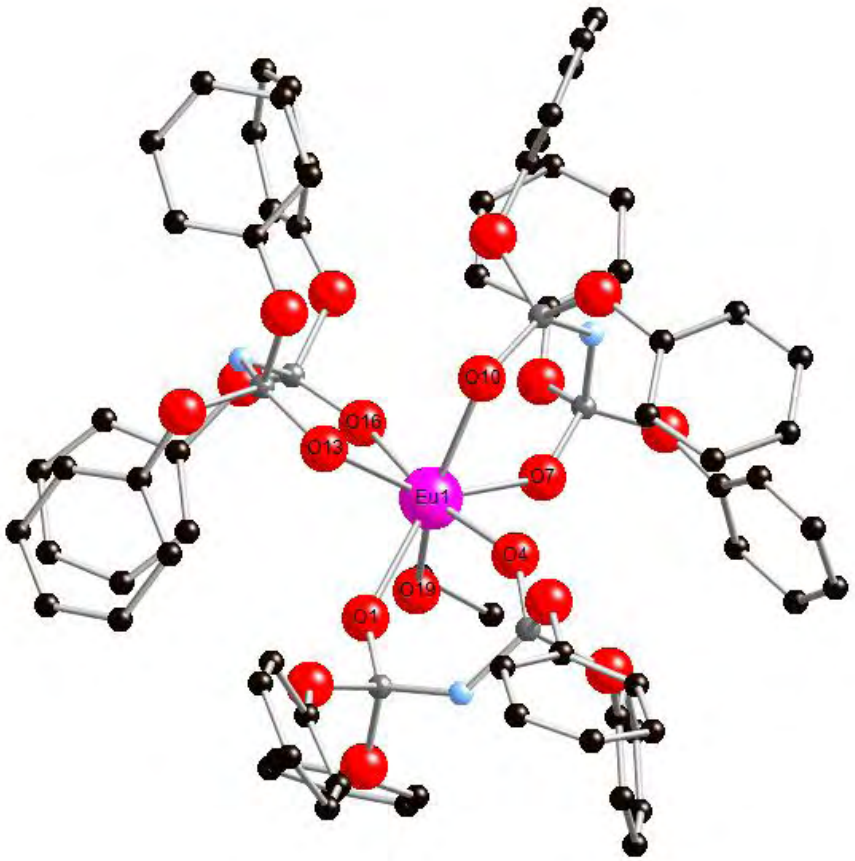

Figure 2.20. Molecular structure of Eu(**tpOp**)$_3$.EtOH complex. (Hydrogen atoms are omitted for clarity).

Tb(**tpOp**)$_3$.EtOH

In the case of Tb(**tpOp**)$_3$ crystals were grown from acetonitrile solution and a similar situation was found as seen for the Eu(**tpOp**)$_3$ complex. The central Tb^{3+} ion is coordinated by six oxygen atoms from three **tpOp** ligands and one oxygen atom from additional ethanol molecule (Figure 2.21). Thus, Tb^{3+} ion again exhibits a coordination number of seven. The coordination geometry of the central Tb^{3+} ion may be described again as capped octahedral.

The bond distances between the central metal and **tpOp** oxygens are not equal varying in the range of 2.363(6) and 2.284(6) Å. Additionally, the ethanol molecule is

directly coordinated to the Tb^{3+} ion *via* O(19) atom, with Tb(1)-O(19) distance at 2.409 Å. The average distances of (P-O) and (P-N) bonds are 1.477(6) and 1.567(8) Å respectively. The Tb-O bond lengths are comparable to the corresponding (Tb-O) bond lengths found in Tb(**tpip**)$_3$ complex.[1]

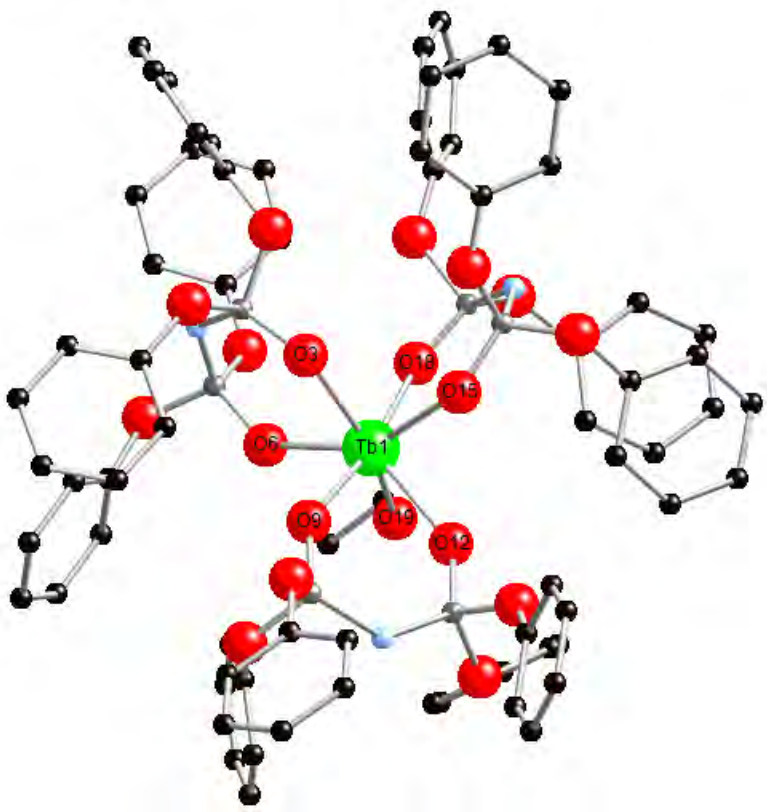

Figure 2.21. Molecular structure of Tb(**tpOp**)$_3$.EtOH complex. (Hydrogen atoms are omitted for clarity).

Gd(**tpOp**)$_3$.EtOH

Single crystals of Gd(**tpOp**)$_3$ were obtained by slow evaporation of acetonitrile solution at room temperature. The crystal structure of Gd(**tpOp**)$_3$.EtOH complex (Figure 2.22) reveals that the Gd^{3+} ion is chelated with six oxygen atoms from three **tpOp** ligands (O1, O4, O7, O10, O13, O16) and one oxygen atom (O19) from the

additional molecule of ethanol. The twelve phenoxide groups surround the lanthanide ion but the arrangement of ligands leave a gap on the side of the complex, which accommodates a molecule of ethanol. The Gd^{3+} centre adopts capped octahedral geometry. The (Gd-O) distances are in range 2.380(5) Å and 2.312(5) Å for the ligand and 2.424 Å for ethanol. The average bond lengths are 1.475(5) Å (P-O) and 1.565(6) Å (P-N).

Figure 2.22. Molecular structure of Gd(**tpOp**)$_3$.EtOH complex. (Hydrogen atoms are omitted for clarity).

Dy(**tpOp**)$_3$.EtOH

Single crystals of Dy(**tpOp**)$_3$ were grown from chloroform solution at room temperature. Once again, Dy^{3+} ion is surrounded by seven oxygen atoms, six of which are from the bidentate **tpOp** ligands and the other one from the coordinated ethanol molecule (Fig 2.23). The coordination polyhedron can be best described as capped octahedral geometry. The average (Dy-O) bond length in the structure is 2.306(4) Å. Average bond distances are calculated as (P-O) and (P-N) of 1.472(3) Å and 1.564(5) Å respectively.

This is comparable with the average (Tb-O) bond length in Tb(**tpOp**)$_3$ of 2.316(6) Å. Tb^{3+} has almost the same ionic radius as Dy^{3+} as they are adjacent in the lanthanide series.

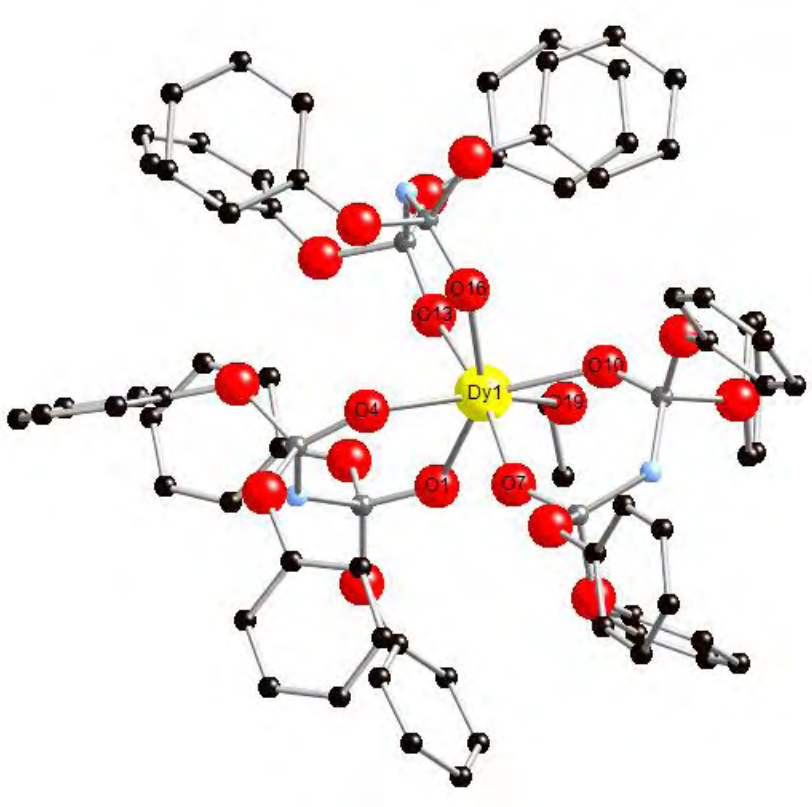

Figure 2.23. Molecular structure of Dy(**tpOp**)$_3$.EtOH complex. (Hydrogen atoms are omitted for clarity).

Er(**tpOp**)$_3$.EtOH

X-ray quality crystals were obtained by slow evaporation of acetonitrile solution at room temperature. The solid state structure of Er(**tpOp**)$_3$.EtOH in Figure 2.24 shows that it consists of three **tpOp** ligands coordinated around Er^{3+} ion in a bidentate fashion. There is also an additional ethanol molecule which is directly coordinated to Er^{3+} ion. The geometry around the Er^{3+} ion can be best described as capped octahedral. Average bond distances are calculated as (Er-O), (P-O) and (P-N) of 2.283(3), 1.476(3) and 1.564(4) Å respectively.

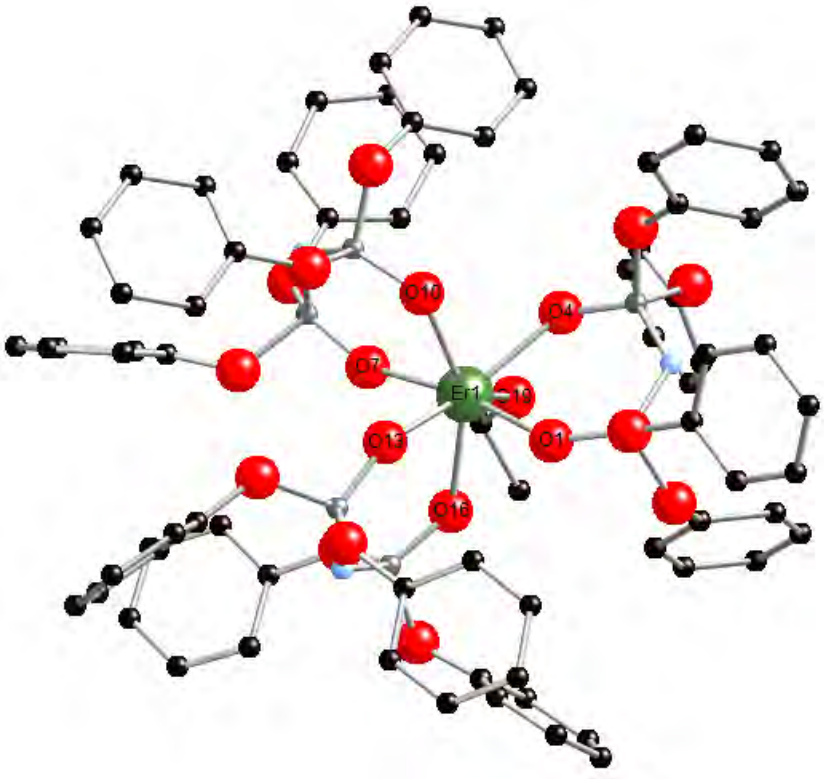

Figure 2.24. Molecular structure of Er(**tpOp**)$_3$.EtOH complex. (Hydrogen atoms are omitted for clarity).

Yb(**tpOp**)$_3$

Single crystals of Yb(**tpOp**)$_3$ suitable for X-ray diffraction analysis, were grown by slow evaporation from a chloroform solution at room temperature. The Yb(**tpOp**)$_3$ complex is composed of six-coordinate Yb^{3+} ion. The geometry at the metal ion is distorted octahedron as demonstrated in Figure 2.25.

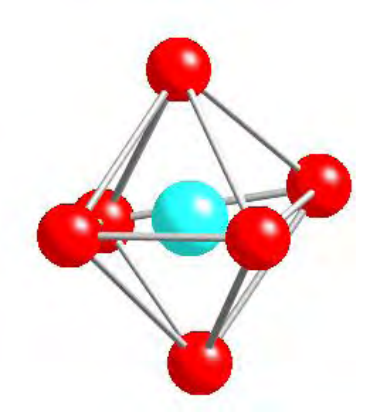

Figure 2.25. Coordination environment of Yb^{3+} in the Yb(**tpOp**)$_3$ complex. Heteroatoms: O, red; Yb^{3+}, blue.

Three **tpOp** ligands coordinate in a bidentate fashion and encapsulate the Yb^{3+} core, thus preventing the coordination solvent molecules. The coordination sphere of the lanthanide ion is therefore exclusively composed of oxygen atoms from the three **tpOp** ligands (Figure 2.26). The (Yb-O) distances compromised between 2.219(3) and 2.208(4) Å. The average bond distances of (P-O) and (P-N) are 1.489(4) and 1.566(4) Å respectively.

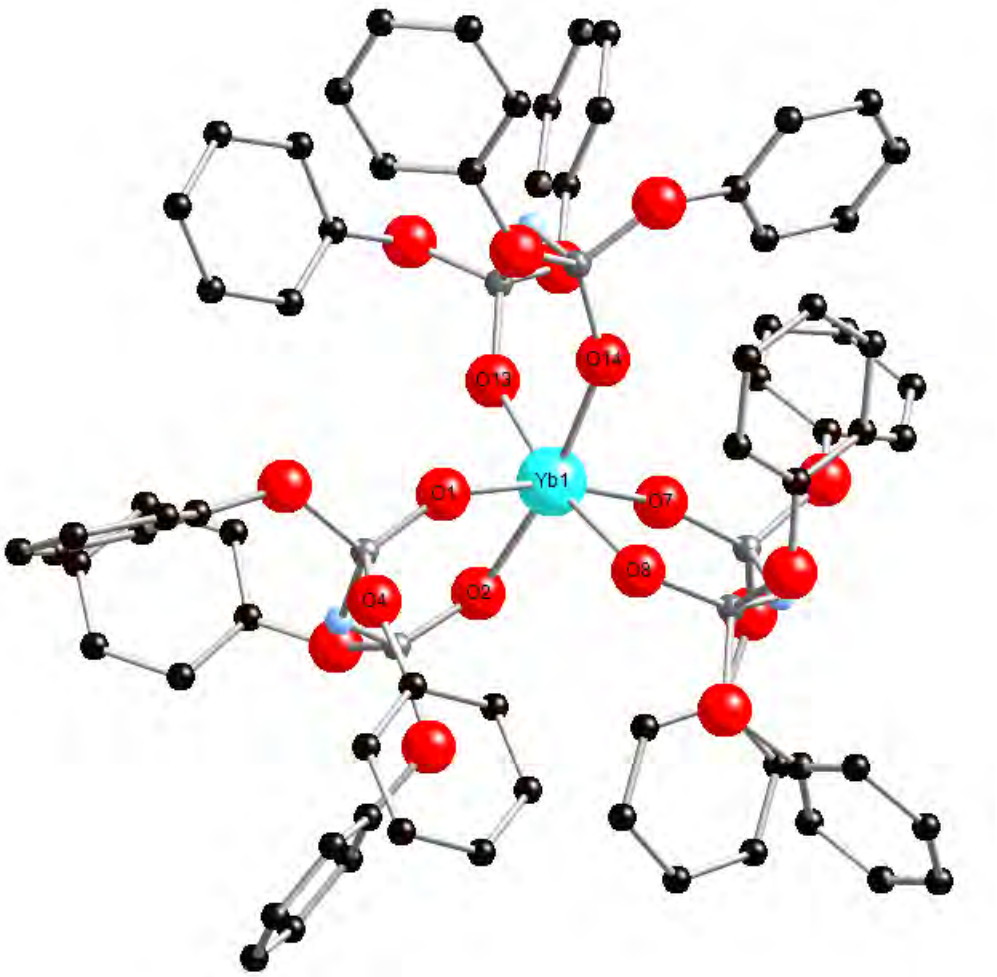

Figure 2.26. Molecular structure of Yb(**tpOp**)$_3$ complex. (Hydrogen atoms are omitted for clarity).

The obtained structure of Yb(**tpOp**)$_3$ compares well with the one previously reported, showing similar trends in ligand geometry and bond lengths.[13] The published structure shows the (Yb-O) bond distances ranging from 2.199(6) Å to 2.209(6) Å and the average bond lengths of 1.493(6) Å and 1.563(7) Å for (P-O) and (P-N) respectively.

In summary, a number of points can be noted from the crystal structures of the complexes presented above. The **tpOp** complexes have low coordination numbers of seven. The solid state structure of Yb(**tpOp**)$_3$ complex evidences a decrease of

the coordination number of the metal ion from seven to six as the ionic radius of the Ln^{3+} ion decreases.

The coordinated ethanol molecule to Ln^{3+} ions is the evidence that the hydrophobic shell of **tpOp** complexes remain partially ineffective at protecting larger lanthanides from solvent coordination.

The coordinated ligands are not equally strongly bonded to the metal ion as reflected in the different sets of bond lengths that decrease in the order Eu > Gd > Tb > Dy > Er > Yb as a result of lanthanide contraction.

In all studied Ln(**tpOp**)$_3$ complexes the P-O bond are elongated and the P-N distances are shorter when compared with the free ligand. For example, in the Er(**tpOp**)$_3$ complex the P-O bond length is changed from 1.46 Å to 1.48 Å and the P-N distances are shortened from 1.64 Å to 1.57 Å. This suggests that delocalisation of π-electrons occur in chelate rings.

The molecules are involved in intra-molecular interactions within single lanthanide complexes. These interactions include π-π stacking and the edge-on association between C-H and phenoxide rings; these play an important role in stabilising the hydrophobic shell formed by the twelve phenoxide groups around the central lanthanide.

Table 2.4. Summary of the XRD single crystal structure data of Ln(**tpOp**)$_3$ (Ln = Tb, Eu, Dy, Gd, Er, Yb)

	Tb(tpOp)$_3$.EtOH	***Eu(tpOp)$_3$.EtOH***	***Dy(tpOp)$_3$.EtOH***
Formula	$C_{74}H_{66}TbN_3O_{19}P_6$	$C_{74}H_{66}EuN_3O_{19}P_6$	$C_{74}H_{66}DyN_3O_{19}P_6$
M_r	1646.04	1639.08	1649.62
T [K]	296(2)	296(2)	296(2)
crystal system	Triclinic	Triclinic	Triclinic
space group	*P*1	*P*1	*P*1
a [Å]	9.9199(18)	9.8964(3)	9.922(3)
b [Å]	16.255(3)	16.2782(5)	16.246(4)
c [Å]	23.081(4)	23.1406(7)	23.040(6)
α [^{o}]	91.170(9)	91.065(2)	91.231(10)
β [^{o}]	91.642(9)	91.709(2)	91.801(10)
γ [^{o}]	98.003(8)	98.023(2)	98.019(13)
V [Å^3]	3682.8(11)	3688.74(19)	3674.7(18)
Z	2	2	2
ρ_{calcd} [Mg m^{-3}]	1.484	1.476	1.491
Absorption coefficient [mm^{-1}]	6.570	7.931	7.292
F(000)	1676	1672	1678
crystal size [mm^3]	0.35 x 0.10 x 0.10	0.30 x 0.10 x 0.05	0.20 x 0.20 x 0.20
θ range [^{o}]	1.92-56.30	1.91-58.98	1.92-65.88
index range	-10≤*h*≤10 -17≤*k*≤16 -24≤*l*≤23	-10≤*h*≤10 -17≤*k*≤18 -25≤*l*≤21	-11≤*h*≤11 -17≤*k*≤17 -25≤*l*≤24
reflections collected	23506	20533	23559
independent reflections	8845 (R_{int} = 0.0952)	9839 (R_{int} = 0.0748)	10888 (R_{int} = 0.0419)
Completeness to [^{o}] ([%])	56.30 (91.2)	58.98 (92.9)	65.88 (85.2)
max/min transm	0.5595/0.2070	0.6925/0.1995	0.3233/0.3233
GOF on F^2	1.011	1.033	1.030
Fina R_1, wR_2	0.0730,0.1513	0.0645,0.1377	0.0570,0.1318

	Gd(tpOp)$_3$.EtOH	***Er(tpOp)$_3$.EtOH***	***Yb(tpOp)$_3$***
Formula	$C_{74}H_{66}GdN_3O_{19}P_6$	$C_{74}H_{66}ErN_3O_{19}P_6$	$C_{72}H_{60}N_3YbO_{18}P_6$
M_r	1644.37	1654.38	1614.09
T [K]	296(2)	293(2)	296(2)
crystal system	Triclinic	triclinic	Monoclinic
space group	P1	P1	P21/n
a [Å]	9.9006(10)	9.9195(9)	18.678(4)
b [Å]	16.2816(15)	16.2284(14)	15.789(3)
c [Å]	23.129(2)	23.0008(18)	25.642(5)
α [^{o}]	91.086(5)	91.324(5)	90
β [^{o}]	91.714(6)	91.769(5)	108.144(6)
γ [^{o}]	98.060(5)	97.853(5)	90
V [Å^3]	3688.9(6)	3664.7(5)	7186(3)
Z	2	2	4

ρ_{calcd} [Mg m^{-3}]	1.480	1.499	1.492
μ [mm^{-1}]	7.659	3.982	4.274
F(000)	1674	1682	3268
crystal size [mm^3]	0.40 x 0.25 x 0.25	0.35 x 0.35 x 0.35	0.25 x 0.20 x 0.15
θ range [^{o}]	1.91/65.74	1.92/65.76	2.58/66.30
index range	-11≤*h*≤10	-10≤*h*≤11	-21≤*h*≤20
	-18≤*k*≤17	-18≤*k*≤16	-18≤*k*≤18
	-27≤*l*≤25	-26≤*l*≤26	-30≤*l*≤30
reflns collected independent reflns	23654 11050[R_{int} = 0.0483]	23804 11088 [R_{int} = 0.0320]	41595 12049 [R_{int} = 0.0781]
completeness to θ [^{o}] ([%])	65.74 (86.5)	65.76 (87.3)	66.30 (96.6)
max/min transm	0.2504/0.1496	0.3362/0.3362	0.5665/0.4146
GOF on F^2	1.023	1.029	1.048
Final R_1, wR_2	0.0670,0.1517	0.0469,0.1211	0.0514,0.0943

2.3. Photophysical properties of Ln(tpOp)$_3$

2.3.1. The visible emitting complexes

The absorption spectra of Ln(**tpOp**)$_3$ (Ln = Eu, Tb, Dy, Sm, Gd) in acetonitrile all show the similar profile as illustrated in Figure 2.27 for the Eu(**tpOp**)$_3$ complex. The absorption spectra exhibit an intense structured band with λ_{max} at 263 nm and two weaker bands at 257 nm and 269 nm respectively, which can be assigned to π -> π* transitions of the phenoxide aromatic groups, while the shoulder band at 290 nm can be identified as n -> π* transition of free ligand owing to its low absorption intensity.[14] The molar extinction coefficient value for the peak maximum at 263 nm is 4,800 dm^3 mol^{-1} cm^{-1}, which is approximately three times larger than H**tpOp,** which is consistent with the presence of three ligands per complex in solution.

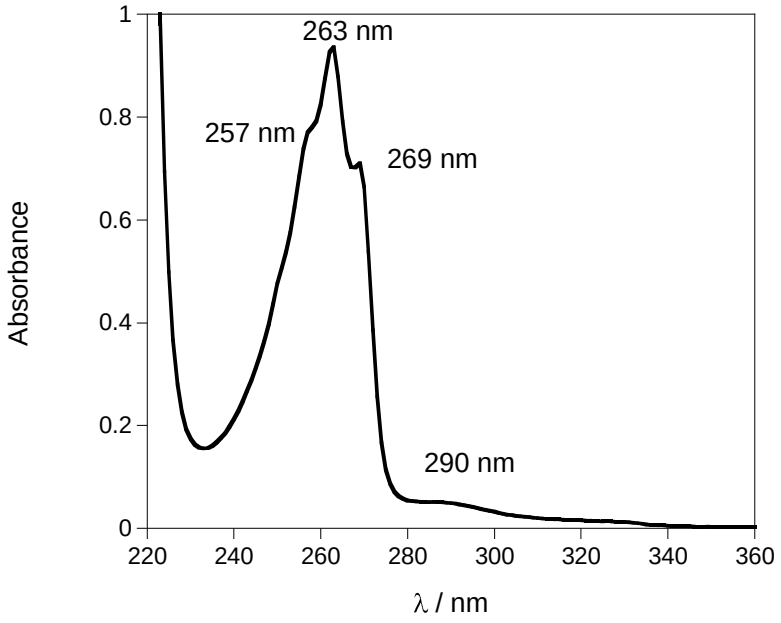

Figure 2.27. The absorption spectrum of Eu(**tpOp**)$_3$ in CH_3CN.

Since deprotonation of the ligand and its subsequent coordination to Ln^{3+} ion does not change the absorption spectrum of the ligand, this also confirms that the

phosphorus substituted phenoxide groups of **tpOp** can be considered as being remote from the imidodiphosphate binding unit.

Sensitisation of lanthanide emission by organic ligands typically occurs *via* an energy transfer process from the triplet energy level of the sensitiser to the luminescent energy level of the lanthanide.[15] The Gd(**tpOp**)$_3$ complex was prepared in order to determine the ligand-centred triplet state energy. The Gd^{3+} ion was chosen for the calculation of the ligand T_1 energy level because the heavy Gd^{3+} ion increases the rate of intersystem crossing from singlet (S_1) to triplet (T_1). In addition this ion cannot act as an energy acceptor from the excited ligand triplet state due to its lowest excited state ($^6P_{7/2}$), occurring at 32,150 cm^{-1}.[16] Therefore, a luminescence measurement in MeOH/EtOH 20:80 was performed at 77 K in order to enable the observation of phosphorescence of the ligand.

At room temperature Gd(**tpOp**)$_3$ spectrum in MeOH/EtOH (20:80) displays a broad emission with the band centred at 330 nm, which corresponds to the fluorescence of the **tpOp** ligand (Figure 2.28). Upon cooling the solution to 77 K the ligand phosphorescence is clearly observed and the spectrum exhibits the fine vibronic structure of the phosphorescent transitions (Figure 2.28).

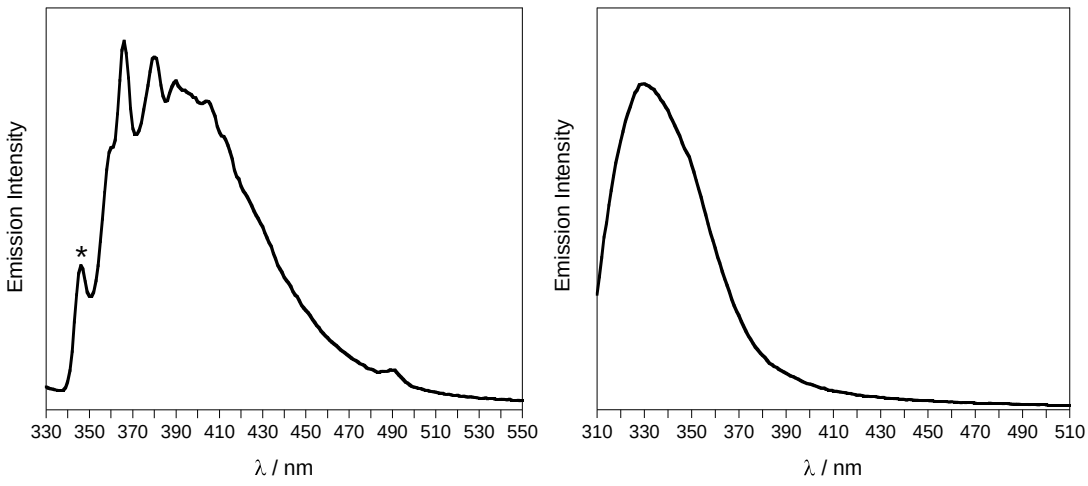

Figure 2.28. The emission spectra of Gd(**tpOp**)$_3$ at 77K (left) and room temperature (right) in MeOH/EtOH 20:80, λ_{exc} = 290 nm. * = scattered light.

The intensity of the peaks is determined by the Franck-Condon overlap between the upper and lower vibronic states in Gd(**tpOp**)$_3$. The $^3\pi$-π^* state of the ligand was evaluated to be 27,397 cm^{-1} from the 0-0 transition in the phosphorescence spectrum at 77 K. The energy of the progressive vibronic transitions was also calculated and the results are tabulated in Table 2.5. The triplet level energy is consistent with energy observed experimentally for phenol (28,089 cm^{-1}) in water.[17]

Table 2.5. Phosphorescent vibronic transitions in Gd(**tpOp**)$_3$ at 77 K.

λ_{max} (nm)	ν-ν'	Energy (cm^{-1})
365	0 – 0	27,397
379	0 – 1	26,385
388	0 – 2	25,773
404	0 – 3	24,752

The photophysical requirements for highly emissive compounds are related to the energy gap between singlet and triplet excited states of the ligand for an efficient intersystem crossing process. According to Reinhoudt's empirical rule[18] the intersystem crossing process is efficient when $\Delta E(^1\pi\pi^*)$ to $(^3\pi\pi^*)$ is at least 5,000 cm^{-1}. The singlet energy state for **tpOp** ligand was estimated by referencing the absorbance edge in Gd(**tpOp**)$_3$ complex, which is present at 34,483 cm^{-1}. Based on above experimental results the energy gap between the $^1\pi\pi^*$ and $^3\pi\pi^*$ level is 7,086 cm^{-1} thus suggesting the intersystem crossing processes in Ln(**tpOp**)$_3$ complexes are effective. Another key factor which affects the luminescence properties of complexes is the position of the ligand triplet level. The efficiency of the energy transfer from the ligand T_1 state to the lanthanide excited state depends on the energy difference between these levels. The emitting levels of Tb^{3+} ($^5D_4$; 20,500 cm^{-1}), Eu^{3+} ($^5D_0$; 17,200 cm^{-1}), Dy^{3+} ($^4F_{9/2}$; 21,100 cm^{-1}) and Sm^{3+} ($^4G_{5/2}$; 17,700 cm^{-1})[19] lie below the triplet state of ligand (27,397 cm^{-1}) and their energy gaps between ligand and metal-centred levels are too high to allow an effective back energy

transfer. Therefore the observed photoluminescent data of Gd(**tpOp**)$_3$ complex suggests that the **tpOp** ligand is suitable candidate to act as an efficient antenna sensitising the luminescence of visible emitting ions for these complexes. The schematic energy level diagram, which includes the triplet state energy levels of Gd complex and the energy transfer process to the Ln^{3+} excited states is shown in Scheme 2.6.

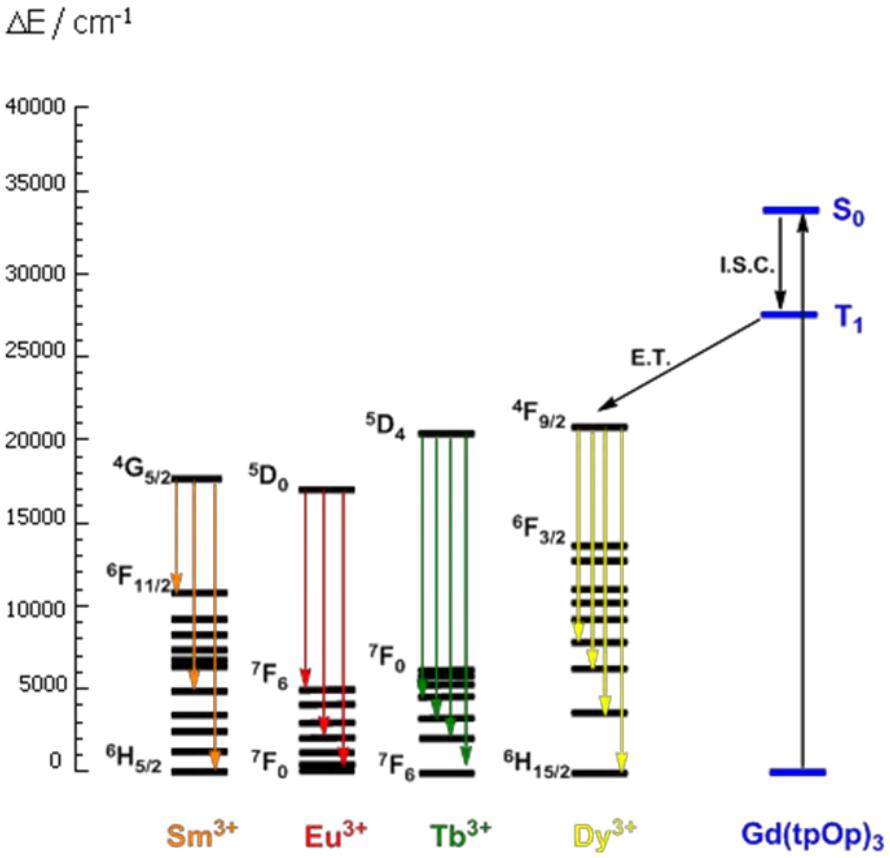

Scheme 2.6. Energy level diagram showing the lowest Ln^{3+} excited states and the estimated triplet state of the **tpOp** sensitiser in the Gd(**tpOp**)$_3$ complex.

The Ln(**tpOp**)$_3$ (Ln = Eu, Tb, Dy, Sm) complexes emit brightly at room temperature in acetonitrile and THF solutions, showing the typical narrow spectra of Ln^{3+} cations. The luminescence spectra of all Ln(**tpOp**)$_3$ complexes are dependent of excitation

wavelength as shown in a three dimensional plot of Tb(**tpOp**)$_3$ complex (Figure 2.29). The emission intensity is strongly enhanced upon excitation at ~ 290 nm.

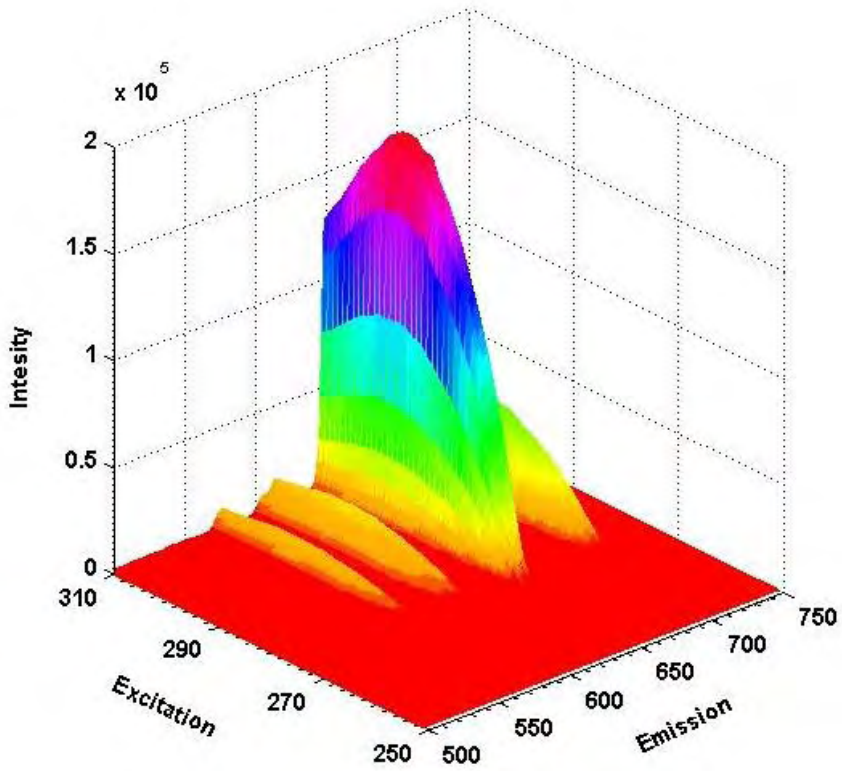

Figure 2.29. 3D view of the emission spectra of Tb(**tpOp**)$_3$ complex at different excitation wavelengths in dry CH_3CN.

For Eu(**tpOp**)$_3$ complex, excitation of the antenna at 290 nm leads to characteristic red emission from Eu^{3+} arising from $^5D_0$ -> ^7F_J transitions. The most intense hypersensitive band, corresponding to $^5D_0$ -> $^7F_2$ transition is observed at 612 nm (Figure 2.30). The non-degenerate $^7F_0$ level is not split giving the evidence that Eu^{3+} complex exists as a single luminescent species in solution.[20]

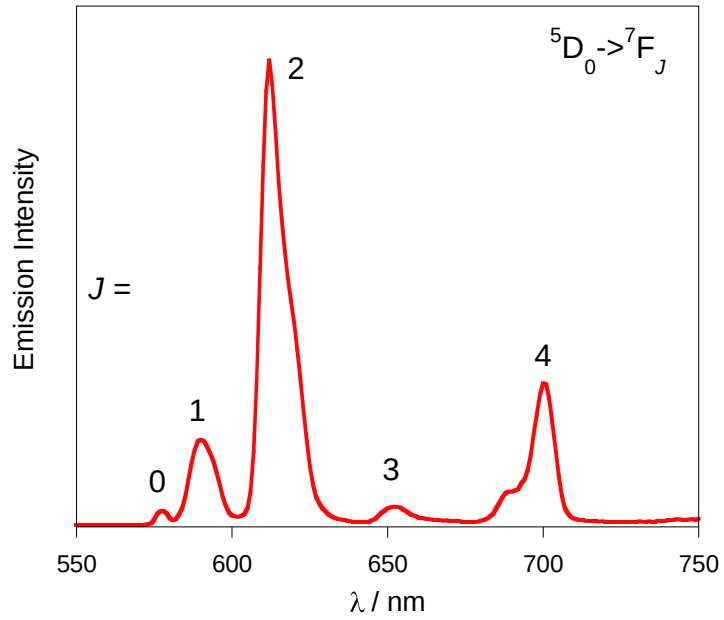

Figure 2.30. Emission spectrum of Eu(**tpOp**)$_3$ in dry CH_3CN, λ_{exc} = 290 nm.

Likewise, for Tb(**tpOp**)$_3$ complex, excitation of ligand at 290 nm populates the Tb^{3+} excited state, leading to strong green emission due to $^5D_4$ -> ^7F_J transitions with the most intense structured $^5D_4$ -> $^7F_5$ band with two peaks at 543 and 549 nm (Figure 2.31).

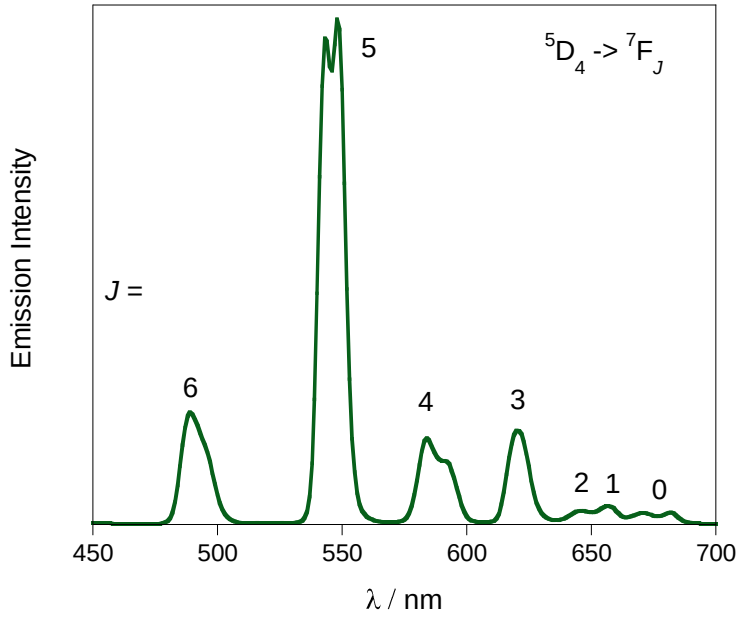

Figure 2.31. Emission spectrum of Tb(**tpOp**)$_3$ in dry CH_3CN, λ_{exc} = 290 nm.

The excitation of Dy(**tpOp**)$_3$ in the UV region is followed by fast relaxation to the $^4F_{9/2}$ state, from which radiative decay to the four ^6H_J states can be readily observed in the visible region of the emission spectrum (Figure 2.32). The typical yellow luminescence from Dy^{3+} ion displays the most intense band at 574 nm corresponding to the hypersensitive $^4F_{9/2}$ -> $^6H_{13/2}$ transition.

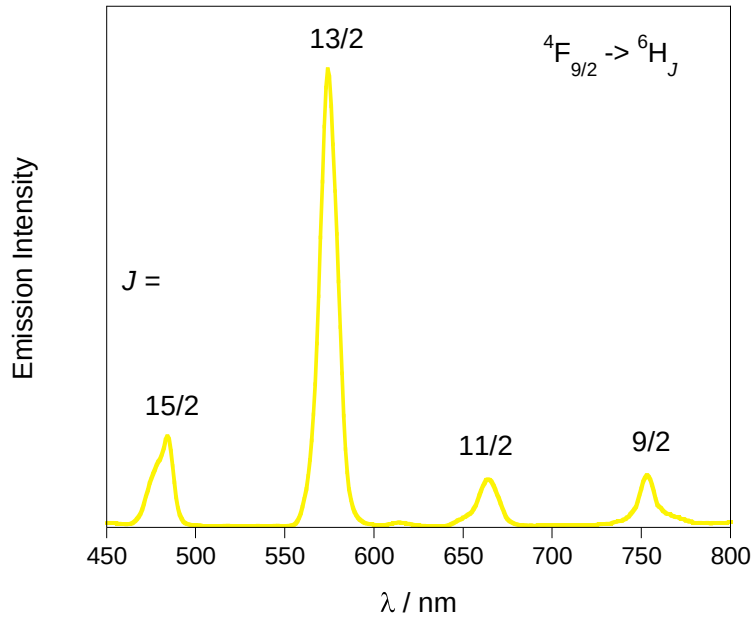

Figure 2.32. Emission spectrum of Dy(**tpOp**)$_3$ in dry CH_3CN, λ_{exc} = 290 nm.

Similarly, excitation of Sm(**tpOp**)$_3$ at 290 nm shows a strong orange emission of Sm^{3+} assigned to $^4G_{5/2}$ ->^6H_J (J = 5/2, 7/2, 9/2, 11/2) transitions with the most intense band at 645 nm corresponding to the $^4G_{5/2}$ -> $^6H_{9/2}$ transition (Figure 2.33).

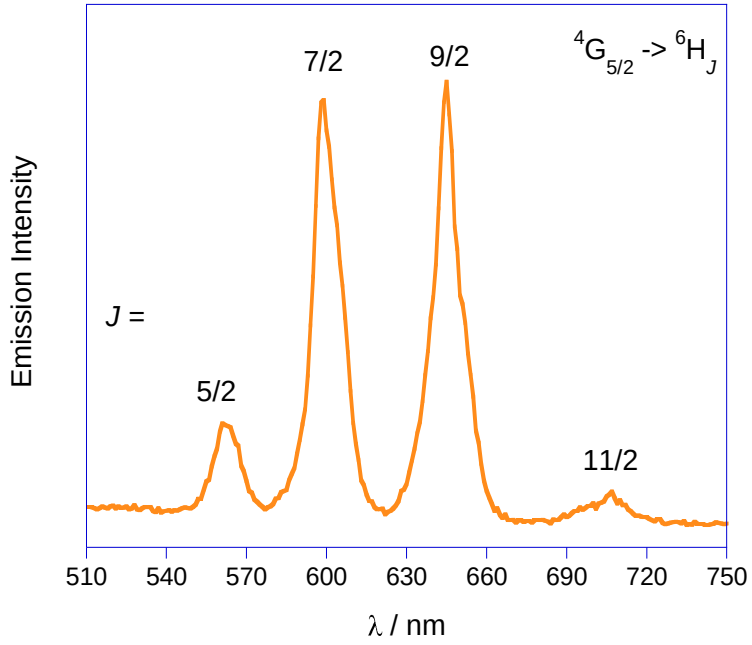

Figure 2.33. Emission spectrum of Sm(**tpOp**)$_3$ in dry CH_3CN, λ_{exc} = 290 nm.

The excitation spectrum in acetonitrile recorded for Dy(**tpOp**)$_3$ complex, monitoring on the strongest $^4F_{9/2}$ -> $^6H_{13/2}$ transition at 575 nm is present in Figure 2.34. The excitation profile shows a band with λ_{max} ~ 290 nm, corresponding to the ligand band in the absorption spectra of the complex.

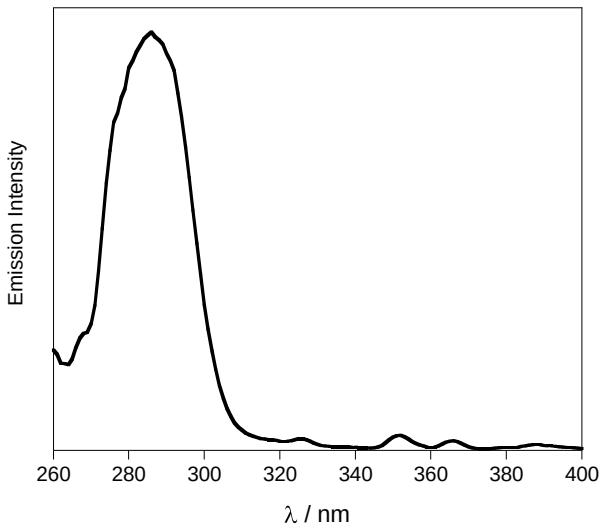

Figure 2.34. The corrected excitation spectrum of Dy(**tpOp**)$_3$ in CH_3CN, λ_{em} = 575 nm.

Excitation spectra of all Ln(**tpOp**)$_3$ complexes obtained by monitoring the metal centred emission are very similar. They are all dominated by strong band in the range of 260 - 310 nm with the maximum absorption at ~ 290 nm, confirming that the three coordinated **tpOp** ligands provide an efficient energy transfer to the Eu^{3+}, Tb^{3+}, Dy^{3+} and Sm^{3+} ions.

As Ln(**tpOp**)$_3$ complexes showed very good photophysical properties in solution, the solid-state photophysical properties were also investigated. The emission spectra of the powder samples give information about the symmetry of the ligand field around the lanthanide, by monitoring the splitting of the hypersensitive band. The emission spectra of powder samples of Eu^{3+}, Tb^{3+}, Dy^{3+} and Sm^{3+} complexes have been recorded. All of complexes were found to emit the characteristic line like emission of the metal ion upon excitation within the absorption band of the **tpOp** ligand.

The emission spectrum of powder sample of Eu(**tpOp**)$_3$ give an efficient red emission typical of Eu^{3+} ion. The hypersensitive band $^5D_0$ -> $^7F_2$ displays a split band into two peaks at 612 and 620 nm respectively (Figure 2.35). The splitting of this band, which is extremely sensitive to the nature and symmetry of the coordination environment, can be attributed to the distorted symmetry of the oxygen donor atoms around Eu^{3+} ion.[20] This is in line with the results of crystal structure analysis observed for the Eu(**tpOp**)$_3$ complex. The singlet band at 580 nm attributed to the $^5D_0$ -> $^7F_0$ transition indicates the presence of only single site symmetry Eu^{3+} ion, which is also in good agreement with the crystal structure results.

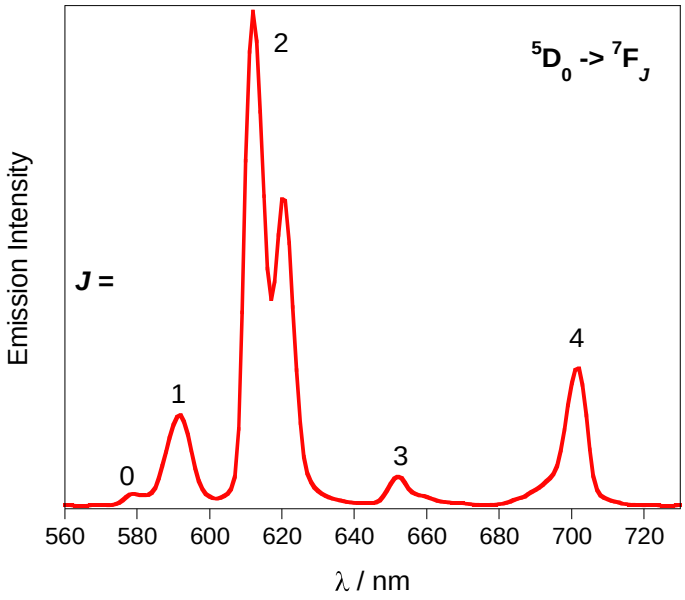

Figure 2.35. Emission spectrum of powder sample of Eu(**tpOp**)$_3$, λ_{exc}= 290 nm.

Similarly, the emission spectrum of powder sample for Tb(**tpOp**)$_3$ (Figure 2.36) is slightly different compared to the equivalent solution-phase spectrum. The hypersensitive $^5D_4$ -> $^7F_5$ transition is split stronger into two distinct bands at 541 and 548 nm.

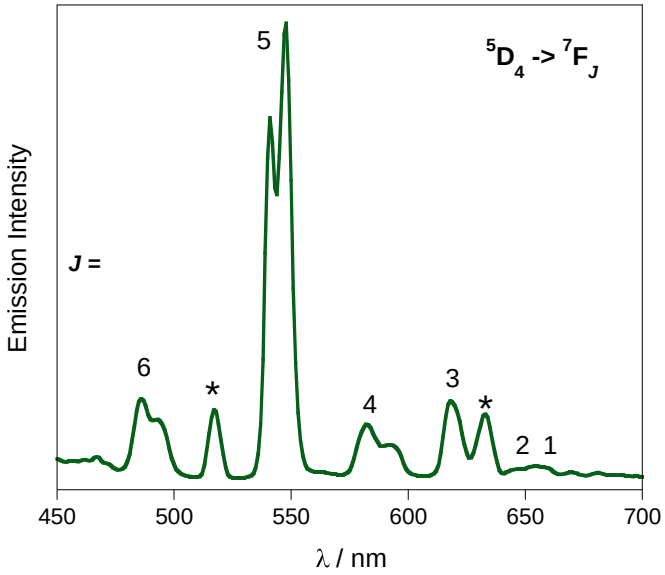

Figure 2.36. Emission spectrum of powder sample of Tb(**tpOp**)$_3$, λ_{exc}= 290 nm. * = scattered light.

Powder samples of Dy(**tpOp**)$_3$ and Sm(t**pOp**)$_3$ complexes display the same emission patterns as in solution. The emission spectrum of powder Dy(**tpOp**)$_3$ (Figure 2.37) shows the characteristic yellow line emission of 4*f*-4*f* transition of Dy^{3+} ion when excited by UV light, with the most intense band at 574 nm corresponding to the hypersensitive $^4F_{9/2}$ -> $^6H_{13/2}$ transition.

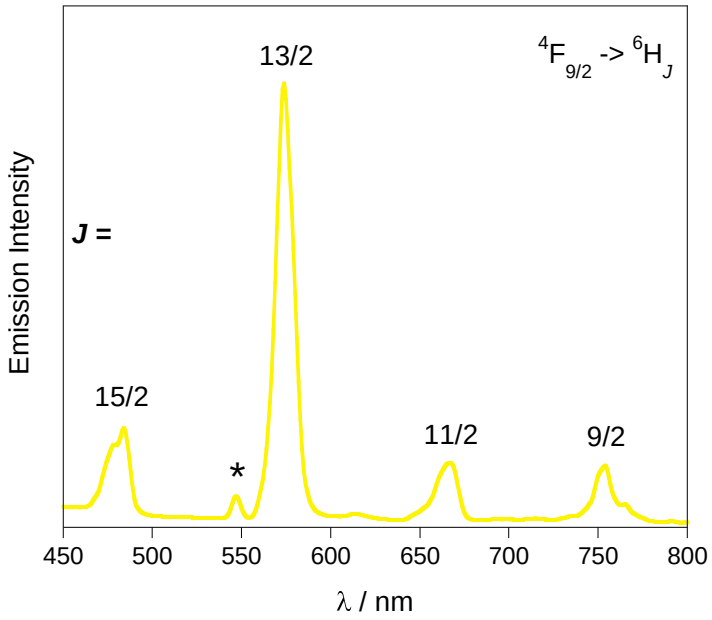

Figure 2.37. Emission spectrum of powder sample of Dy(**tpOp**)$_3$, λ_{exc}= 290 nm. * = scattered light.

Similarly, irradiation of powder sample of Sm(**tpOp**)$_3$ (Figure 2.38) with UV light at 290 nm leads to orange emission assigned to the $^4G_{5/2}$ -> ^6H_J transitions of Sm^{3+} (*J* = 5/2, 7/2, 9/2 and 11/2).

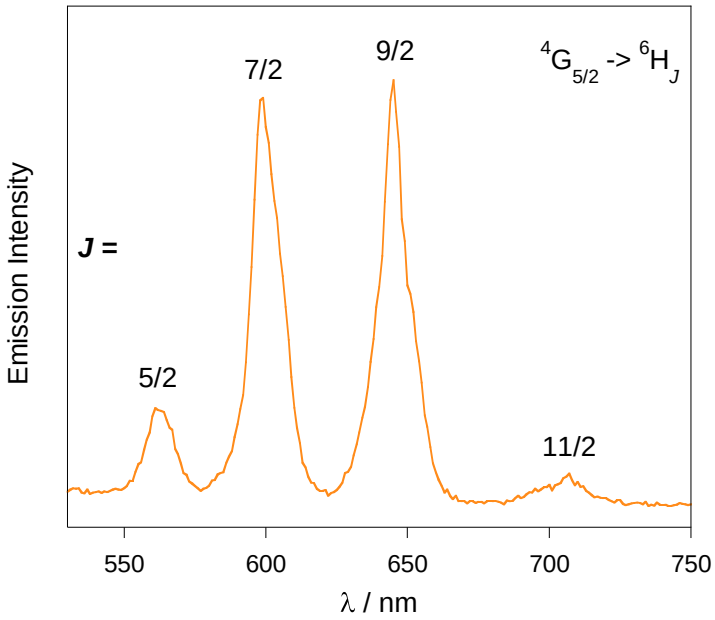

Figure 2.38. Emission spectrum of powder sample of Sm(**tpOp**)$_3$, λ_{exc}= 290 nm.

The reason behind more complex splitting of bands in the solid-state is due to different conformers of **tpOp** being locked in position, whereas in solution rotation of ligand around Ln^{3+} serves to raise the symmetry of the central metal ions coordination environment by averaging the environment, hence reducing the amount of fine splitting of the hypersensitive band.

Time-resolved spectroscopy was used for further determination of the photophysical processes involved in the luminescence of Ln(**tpOp**)$_3$ (Ln = Tb, Eu, Dy, Sm) complexes. The time-resolved measurements were obtained for powder and solutions samples and it was found that they all display relatively long luminescent lifetimes. The measured luminescence lifetimes of visible Ln(**tpOp**)$_3$ complexes, following excitation into ligand-centred bands (λ_{exc} = 290 nm) are summarised in Table 2.6.

In each case the decay profile was analysed as a single exponential component indicating the presence of a single emitting centre in solution as shown in Figure 2.39 for the Tb(**tpOp**)$_3$ complex.

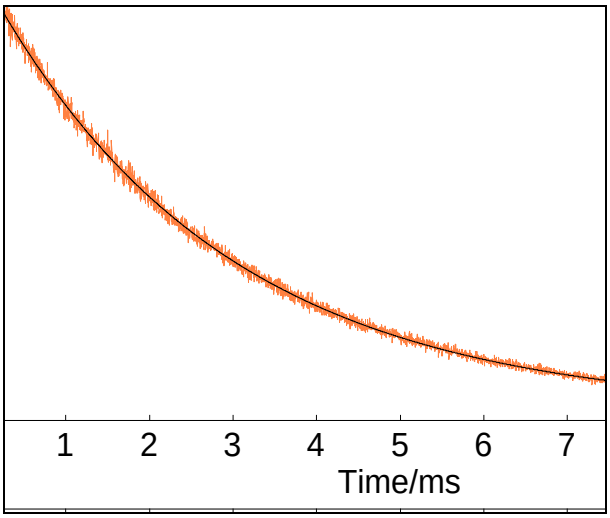

Figure 2.39. The fitted single-exponential decay of Tb(**tpOp**)$_3$ complex in dry CH_3CN, λ_{exc} = 290 nm and λ_{em} = 549 nm.

In the case of powder samples, the decay curves were fit to a double-exponential function.

Table 2.6. Luminescence lifetimes of the Tb^{3+} ($^5D_4$), Eu^{3+} ($^5D_0$), Dy^{3+} ($^4F_{9/2}$) and Sm^{3+} ($^4G_{5/2}$) levels in Ln(**tpOp**)$_3$ (Ln= Tb, Eu, Dy, Sm) (λ_{exc} = 290 nm). [a] = 10 mol dm^{-3}.

Complex	**Sample**	**τ / ms**
Tb(**tpOp**)$_3$	powder	1.7 (99.42%) 0.3 (0.58%)
	dry CH_3CN	3.1
	dry CH_3CN + H_2O[a]	2.0
Eu(**tpOp**)$_3$	powder	1.7 (74.44%) 0.8 (25.56%)
	dry CH_3CN	2.7
	dry CH_3CN + H_2O[a]	1.7 (92.51%) 0.6 (7.49%)
Dy(**tpOp**)$_3$	powder	0.2 (91.57%) 0.02 (8.43%)
	dry CH_3CN	0.2
Sm(**tpOp**)$_3$	powder	0.07 (77.83%)

		0.01 (22.17%)
	dry CH_3CN	0.1

Compared to the results in solid state, complexes in dry acetonitrile show a considerable lengthening of the luminescence lifetimes. The occurrence of the short component in the decay transient for powder samples reflects the presence of a different local environment around Ln^{3+} ions and is most likely attributed to the ethanol molecule that is coordinated directly to Ln^{3+} ion, which is in agreement with observed single-crystal X-ray structures of Ln(**tpOp**)$_3$ (Ln = Tb, Eu, Dy). The lifetimes of Eu(**tpip**)$_3$ and Tb(**tpip**)$_3$ complexes in the solid state are 2.2 and 3.1 ms,[1] respectively, which are much longer compared to the Eu(**tpOp**)$_3$ and Tb(**tpOp**)$_3$ complexes. In the single-crystal X-ray structures of Eu(**tpip**)$_3$ and Tb(**tpip**)$_3$ there were no solvent molecules coordinated directly to Ln^{3+} ion, therefore there was a lack of deactivating, non-radiative pathways.[1]

On the other hand, the results of lifetimes of Ln(**tpOp)**$_3$ complexes in dry acetonitrile compare favourably with the reported **tpip** complexes, where the measured lifetimes in dry acetonitrile were 1.8, 2.8, 0.15 and 0.18 ms for Eu^{3+}, Tb^{3+}, Sm^{3+} and Dy^{3+} **tpip** complexes, respectively.[1]

Even though the lifetimes of Dy(**tpOp**)$_3$ and Sm(**tpOp**)$_3$ in dry acetonitrile are shorter in comparison with Tb^{3+} and Eu^{3+} **tpOp** complexes, they are quite long relative to other Dy^{3+} and Sm^{3+} complexes based on organic chromophores, published in the literature. For example, lanthanide complexes based on a single phenanthroline chromophore and a flexibly diethylenetriamine tetracarboxylic acid unit, which acts as a coordination site for lanthanide, displayed the luminescence lifetime of 1.1 μs and 34 μs for Dy^{3+} and Sm^{3+} respectively, in D_2O.[21] Petoud *et al.*[22] reported the luminescence lifetime of 18 μs and 17 μs in MeOH for DyR(+)BnMe22IAM and

SmR(+)BnMe22IAM complexes, respectively. The R(+)BnMeH22IAM is the R(+) enantiomer of the octadentade ligand form from four 2-hydroxyisophthalamide chelating groups and chiral benzyl methyl substituents, which are linked by an alkylamino backbone.

The fast non-radiative deactivation of the excited state of the Dy^{3+} ion is due to the small energy gap between the excited level $^4F_{9/2}$ and the sublevels $^6H_{15/2}$, $^6H_{13/2}$, $^6H_{11/2}$ and $^6H_{9/2}$ of the ground state term.

The different lifetimes observed for Ln(**tpOp**)$_3$ complexes can be explained by the energy gap ΔE between the emissive state of the Ln^{3+} ion and the highest sublevel of its receiving ground state. The ΔE is for Dy^{3+} (7,850 cm^{-1}) and Sm^{3+} (7,400 cm^{-1}), whereas for Tb^{3+} and Eu^{3+} the gap is considerably larger at 14,800 cm^{-1} and 12,300 cm^{-1} respectively, therefore only the high energy O-H oscillators contribute to vibrational quenching.[23] The smaller gap for Dy^{3+} and Sm^{3+} results in lower frequency vibrations causing significant deactivation, hence the shorter values of the lifetimes.

Application of the lifetimes to the determination of the inner sphere solvation of Tb^{3+} and Eu^{3+} was undertaken using the relation in equation 2.1:

$$q = A\,(k_{H2O} - k_{CH3CN}) \qquad \textbf{(eq. 2.1)}$$

This equation can be used with CH_3CN as the solvent by measuring the lifetimes following the addition of equal amounts of H_2O to the CH_3CN solution. q (uncertainty ± 0.5) is the number of coordinated water molecules in the primary coordination sphere, A is a proportionality constant (A_{Eu} = 1.05, A_{Tb} = 4.2), k_{H2O} is observed decay rate constant in aqueous CH_3CN, k_{CH3CN} is the observed decay rate constant in dry CH_3CN.[24] The application of Equation 2.1 to the values presented in Table 2.6 give q

= 0.7 ± 0.5 and *q* = 0.3 ± 0.5 for Tb(**tpOp**)$_3$ and Eu(**tpOp**)$_3$ respectively, in aqueous CH_3CN.

The calculated *q* value suggests that complexes can bind to one water or solvent molecule to fill the coordination sphere. The same is expected for Dy^{3+} and Sm^{3+} **tpop** complexes, since they have analogous coordination chemistry. The fact that metal centres are not completely shielded from the environment is also evidenced by the X-ray crystal structures of Ln(**tpOp**)$_3$ (Ln = Tb, Dy, Eu) complexes, where an additional molecule of ethanol is coordinated to Ln^{3+} ion.

The obtained results are in agreement with the reported data for Ln(**tpip**)$_3$ compounds.[1] The calculated values of *q* for Tb(**tpip**)$_3$ and Eu(**tpip**)$_3$ are 1.5±0.5 and 0.71±0.5, respectively, in aqueous acetonitrile, suggesting that there is one water molecule coordinated to the metal ion. It can be seen from the obtained results that the introduction of an extra oxygen on chromophore groups in **tpOp** did not provide better shielding against quenching solvents molecules compare to the **tpip** ligand. However, despite the presence of a coordinated solvent molecule, the luminescence lifetimes of Ln(**tpOp**)$_3$ complexes are very promising values for the future ligand design based on a similar framework to that of H**tpOp**.

The overall efficiency of the sensitisation process for Ln(**tpOp**)$_3$ (Ln = Tb, Dy, Eu, Sm) was examined by measurements of luminescence quantum yields. The luminescence quantum yields were determined relative to a reference solution of quinine sulphate in 1N H_2SO_4 [25] and $[Ru(bpy)_3]Cl_2$ [26] in aerated H_2O corrected for the refractive index of solvents. The accuracy of these procedures was to be ± 10%.[1] All quantum yields were measured with aerated solutions upon excitation at 290 nm.

Table 2.7. Luminescence quantum yields for Ln(**tpOp**)$_3$ and Ln(**tpip**)$_3$[1] (Ln = Tb, Dy, Eu, Sm) complexes.

Complex	Φ λ_{exc} = 290 nm (dry CH_3CN)	Complex	Φ λ_{exc} = 273 nm (dry CH_3CN)
Tb(**tpOp**)$_3$	23%	Tb(**tpip**)$_3$	20%
Dy(**tpOp**)$_3$	5.8%	Dy(**tpip**)$_3$	-
Eu(**tpOp**)$_3$	1.7%	Eu(**tpip**)$_3$	1.3%
Sm(**tpOp**)$_3$	0.2%	Sm(**tpip**)$_3$	-

The results summarised in Table 2.7 show that **tpOp** antenna is clearly the most efficient sensitiser for Tb^{3+} with quantum yield of 23%, followed by Dy^{3+} with quantum yield of 5.8%. The process is less efficient in Eu(**tpOp**)$_3$ and Sm(**tpOp**)$_3$ with luminescence quantum yield of 1.7% and 0.2% respectively. The transition intensity follows the trend $Tb^{3+} > Dy^{3+} > Eu^{3+} > Sm^{3+}$, which means that the energy transfer from **tpOp** ligand to Tb^{3+} and Dy^{3+} is more effective than that to Eu^{3+} and Sm^{3+}. This behaviour can be rationalised by the ligand to metal energy transfer. The observation of stronger sensitisation of the Tb(**tpOp**)$_3$ and Dy(**tpOp**)$_3$ complexes than the Eu(**tpOp**)$_3$ and Sm(**tpOp**)$_3$ complexes is due to the larger energy gap between the ligand triplet state and the europium or samarium ion excited states.

Going from H**tpip** to H**tpOp** complexes, the overall quantum yields are improved. The observed values for Eu(**tpOp**)$_3$ and Tb(**tpOp**)$_3$ compare favourably with quantum yields of Ln(**tpip**)$_3$ complexes where obtained values are 1.3% for Eu(**tpip**)$_3$ and 20% for Tb(**tpip**)$_3$.[1] The overall quantum yield and sensitisation efficiency has been enhanced significantly for Dy(**tpOp**)$_3$. The value of 5.8% is very encouraging as it demonstrates that the **tpOp** ligand can act as very good antenna for Dy^{3+}. The observed increase of quantum yields, especially for Dy(**tpOp**)$_3$, when compared with Ln(**tpip**)$_3$ complexes is caused by suppression of radiationless transitions by the

introduction of oxygen on the phenyl rings in **tpOp** ligand. This is important, especially for Dy^{3+} ion, where the effect of C-H vibrational oscillations has a great ability to efficiently quench *f-f* transition. This is due to the good match between the emissive state of Dy^{3+} and the highest energy level state of the bond oscillators. Also the energy difference value for Dy^{3+} ($\Delta E \sim 7{,}900\ cm^{-1}$) is considerably smaller than the values for Eu^{3+} ($\Delta E \sim 12{,}300\ cm^{-1}$) and Tb^{3+} ($\Delta E \sim 14{,}800\ cm^{-1}$), hence the low energy vibrational states of bond oscillators quench effectively the excited states. For this reason, most of the studies in the field of luminescent lanthanide complexes based on organic ligands, have been devoted mainly to Eu^{3+} and Tb^{3+} compounds. However, a few reports on Dy^{3+} complexes based on organic antenna can be found in the literature. For example, the quantum yield reported for $Dy(BOPA)_3$ complex (BOPA = 3-(6-benzodioxanyl)-pyrazol-5-carboxylic acid) was 0.2% in water, 0.3% in acetonitrile and 0.4% in DMSO.27 Raymond at al. reported the absolute quantum yield measured in water to be 3% for Dy3+ lanthanide complex of octadentate ligand related to 2-hydroxyisophtalamide chelating units (H22IAM).28 Petoud *et al.*22 modified the structure of H22IAM ligand, which yielded the R(+) or S(-) enantiomeric forms of complexes. The quantum yields for Dy3+ and Sm3+ R(+) complexes recorded in MeOH were 1.3% and 0.8% respectively.

The main factor for great enhancement of the overall quantum yield for $Dy(\mathbf{tpOp})_3$ complex is the increased distance between C-H vibrations on the ligand core and Dy3+ ion. This is very important for the design of luminescence devices based on lanthanide metal ions which are very sensitive to the quenching of their Ln3+ excited states.

In order to investigate the stoichiometry of the lanthanide complexes, the titration of K**tpOp** versus $TbCl_3.6H_2O$ in methanol was performed (Figure 2.40).

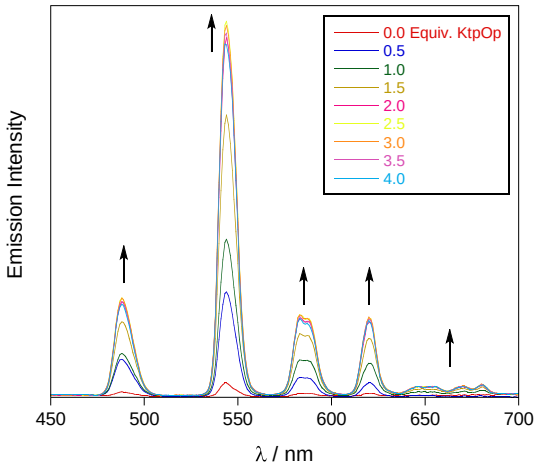

Figure 2.40. Emission spectra of titration of K**tpOp** against $TbCl_3.6H_2O$ in MeOH, λ_{exc} = 290 nm.

The emission intensity of Tb^{3+} ion increases until it reaches a plateau at about 2.5 equivalents of K**tpOp**, which does not confirm the expected binding stoichiometry of K**tpOp** to Tb^{3+} as 3:1 in solution (Figure 2.41). A likely explanation is that an error was introduced while weighing out the $TbCl_3.6H_2O$ salt, which was not dried before the experiment. Therefore not enough molar equivalents of Tb^{3+} were available to demonstrate 3:1 complexation.

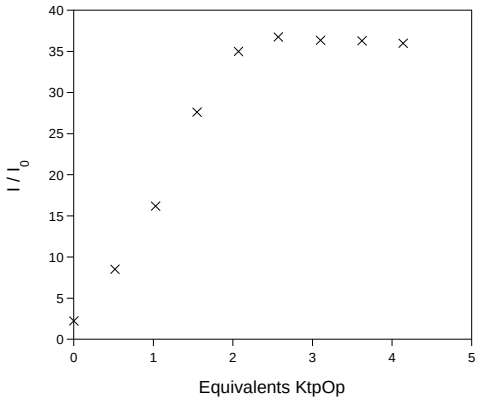

Figure 2.41. Relative integrated emission area *vs*. equivalents of K**tpOp**, upon titration of 30 μL methanolic solution of K**tpOp** (5.2×10^{-3} mol dm^{-3}) against $TbCl_3.6H_2O$ (1.0×10^{-4} mol dm^{-3}) in MeOH, λ_{exc} = 290 nm.

2.3.2. The NIR emitting complexes

The UV-vis absorption spectrum of Nd(**tpOp**)$_3$ in acetonitrile is shown in Figure 2.42. The spectrum exhibits a ligand-based band that is centred at 263 nm (ε_{263} = 4,798 dm^3 mol^{-1} cm^{-1}) with the structural bands at 257, 270 attributed to π->π* transitions of phenoxide moieties, while the shoulder at 290 nm can be assigned as n->π* transition. Absorption spectra for Yb(**tpOp**)$_3$ and Er(**tpOp**)$_3$ in acetonitrile are identical to that of Nd(**tpOp**)$_3$.

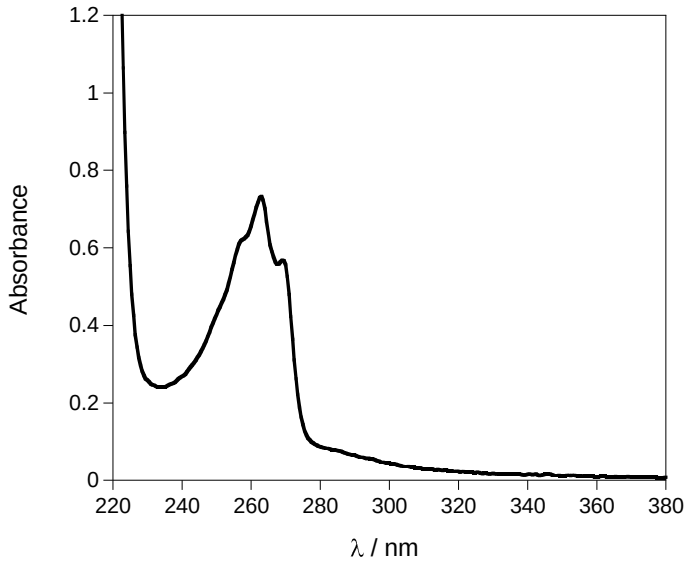

Figure 2.42. The absorption spectrum of Nd(**tpOp**)$_3$ in CH_3CN.

The NIR emitting complexes Nd(**tpOp**)$_3$, Yb(**tpOp**)$_3$ and Er(**tpOp**)$_3$ were studied in solution and solid state.

The Nd(**tpOp**)$_3$ and Yb(**tpOp**)$_3$ complexes in dry acetonitrile exhibit intense narrow band *f-f* based luminescence emission spectra in the NIR region. The luminescence intensity is not enhanced upon deoxygenation of the samples, indicating that oxygen quenching of the triplet state of **tpOp** is not competing with the energy transfer to the encapsulated lanthanide ion.

The Nd(**tpOp**)$_3$ spectrum shows an emissive behaviour upon excitation of the **tpOp** antenna chromophore at 290 nm. At room temperature sensitised emission is observed with three bands with peak maxima at 887, 1058 and 1328 nm. These are assigned to the luminescent transitions of $^4F_{3/2}$ -> ^4I_J (J = 9/2, 11/2, 13/2) respectively (Figure 2.43).

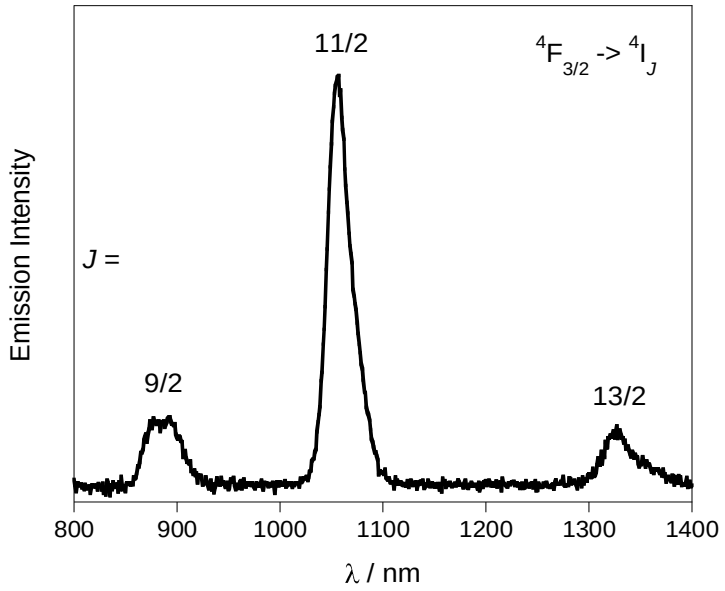

Figure 2.43. Emission spectrum of Nd(**tpOp**)$_3$ in dry CH_3CN, λ_{exc} = 290 nm.

Excitation of Yb(**tpOp**)$_3$ at 290 nm leads to infrared emission with maximum at 974 nm, corresponding to the $^2F_{5/2}$->$^2F_{7/2}$ transition for Yb^{3+} together with a broadened shoulder to low energy beyond 1000 nm (Figure 2.44).

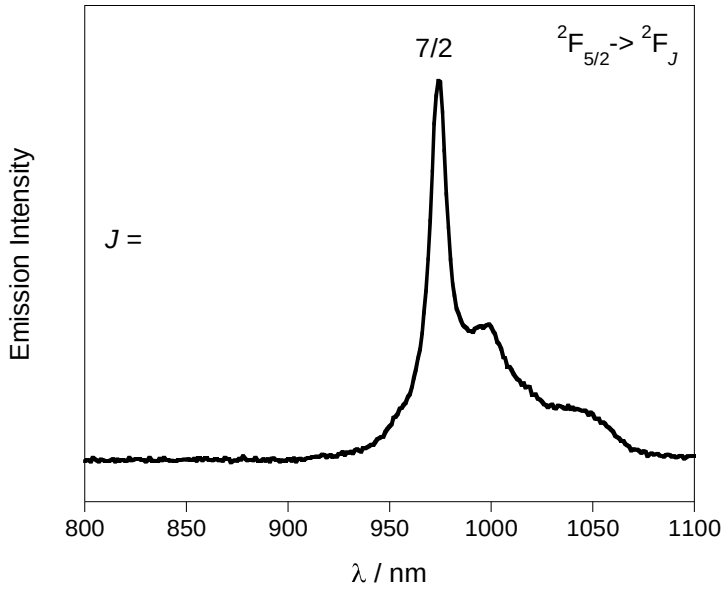

Figure 2.44. Emission spectrum of Yb(**tpOp**)$_3$ in dry CH_3CN, λ_{exc} = 290 nm.

The emission spectra of the Yb(**tpOp**)$_3$ and Nd(**tpOp**)$_3$ complexes confirm the suitability of the **tpOp** ligand as a sensitiser for these two NIR luminescent lanthanide ions. In the case of Er(**tpOp**)$_3$ complex no emission was observed. This can be either attributed to the solvent molecule coordinated to the Er^{3+} ion, which is in line with the observed X-ray data for Er(**tpOp**)$_3$, hence the CH oscillators efficiently quench the NIR luminescence of Er^{3+} ion. Or the triplet state energy level of **tpOp** (27,397 cm^{-1}) does not provide an efficient energy transfer to the emitting level of Er^{3+}($^4I_{13/2}$) at ~ 6,500 cm^{-1} as it is approximately 20,000 cm^{-1} higher. Hence, no further photophysical studies were performed on Er(**tpOp**)$_3$.

The excitation spectra of the lanthanide complexes in acetonitrile confirm that the ligand is responsible for sensitisation of Nd^{3+} and Yb^{3+} emission *via* the energy transfer process.

When the emission of the $^2F_{5/2}$ -> $^2I_{7/2}$ transition at 974 nm of the Yb(**tpOp**)$_3$ complex is monitored, an excitation profile that matches the absorption spectrum of the complex (Figure 2.45) is obtained. This demonstrates that an effective energy

transfer takes place from the ligand to the metal ion. Therefore, the aromatic phenoxide groups act as ligand sensitiser units for the *f-f* based Yb^{3+} and Nd^{3+} luminescence.

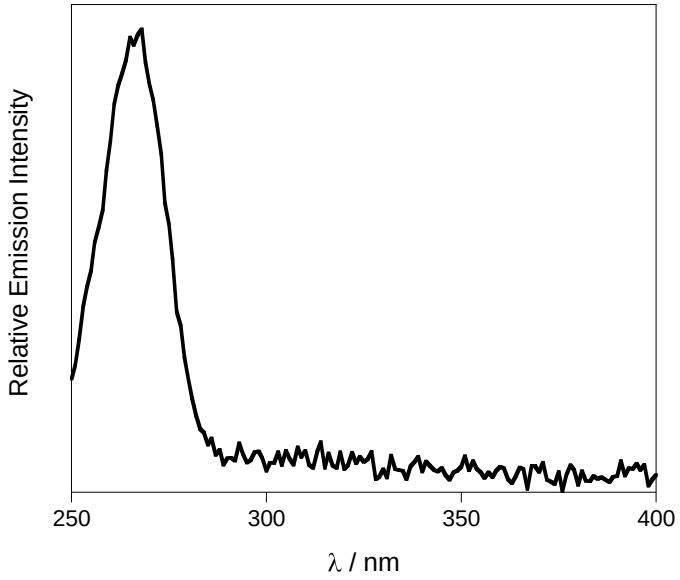

Figure 2.45. The excitation spectrum of Yb(**tpOp**)$_3$ in dry CH_3CN, λ_{em} = 974 nm.

The emission spectra of powder samples of Yb(**tpOp**)$_3$ and Nd(**tpOp**)$_3$ have been recorded at the room temperature.

Upon irradiation at λ_{exc} = 290 nm, Yb(**tpOp**)$_3$ displays NIR luminescence with a sharp band at 978 nm assigned to the $^2F_{5/2}$ -> $^2F_{7/2}$ transition, and broader bands at 1000 and 1045 nm due to vibronic transitions[29] (Figure 2.46).

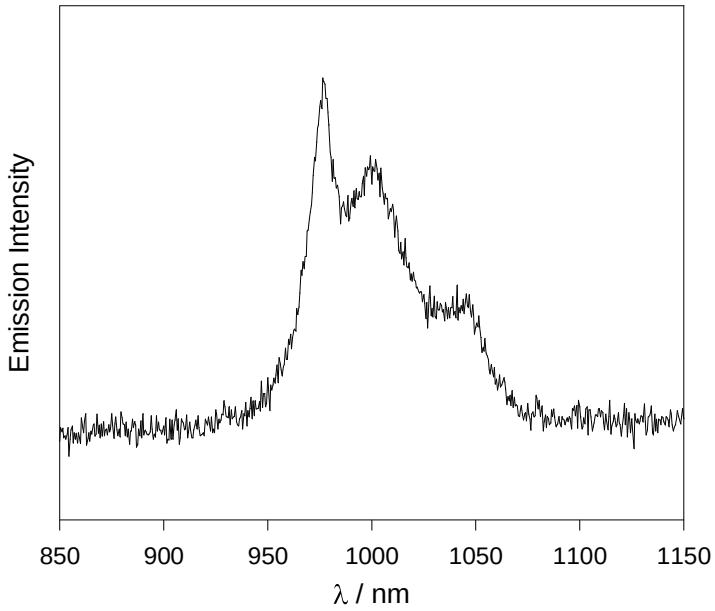

Figure 2.46. Emission spectrum of powder sample of Yb(**tpOp**)$_3$, λ_{exc} = 290 nm.

As can been seen in Figure 2.47, under excitation of 290nm, Nd(**tpOp**)$_3$ exhibits characteristic Nd^{3+} emission in the 800 - 1400 nm range, resulting from $^4F_{3/2}$ -> ^4I_J (J = 9/2, 11/2, 13/2) transitions. The main band at 1057 nm corresponds to the $^4F_{3/2}$ -> $^4I_{11/2}$ transition.

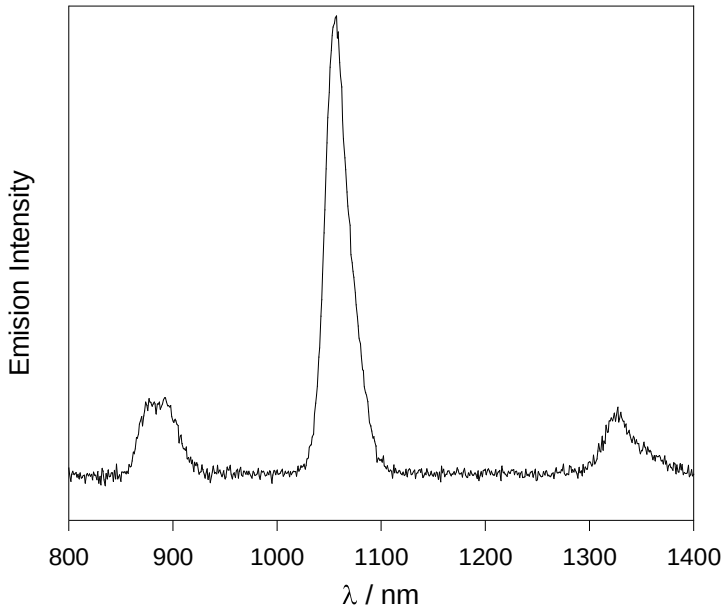

Figure 2.47. Emission spectrum of powder sample of Nd(**tpOp**)$_3$, λ_{exc} = 290 nm.

The luminescence lifetimes have been recorded in order to evaluate the coordination environment around the Ln^{3+} ions in Ln(**tpOp**)$_3$ (Ln = Nd^{3+}, Yb^{3+}) complexes.

The luminescence lifetimes of Nd ($^4F_{3/2}$) and Yb ($^2F_{5/2}$) excited states upon excitation at 290 nm were determined for Nd(**tpOp**)$_3$ and Yb(**tpOp**)$_3$ complexes in dry acetonitrile solution at the room temperature and the results are summarised in Table 2.8. The luminescence decays are all mono-exponential (Figure 2.48) indicating the presence of a single coordination environment around the lanthanide ion in complexes. The lifetime of powder samples were not obtained due to weak signals.

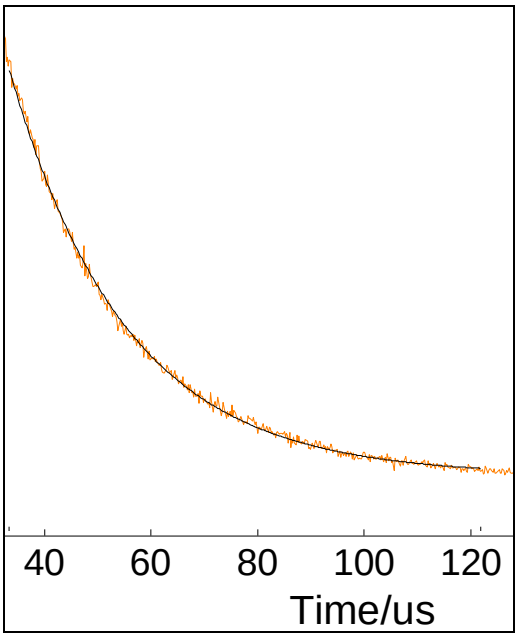

Figure 2.48. Fitted single-exponential decay of Yb(**tpOp**)$_3$ complex in dry CH_3CN, λ_{exc} = 290 nm and λ_{em} = 974 nm.

Table 2.8. Luminescence lifetimes (τ_{obs}) of the Nd^{3+} ($^4F_{3/2}$) and Yb^{3+} ($^2F_{5/2}$) levels in Nd(**tpOp**)$_3$ and Yb(**tpOp**)$_3$, λ_{exc} = 290 nm at RT.

Complex	**Sample**	τ_{obs} / μs
Nd(**tpOp**)$_3$	dry CH_3CN	3.3
Yb(**tpOp**)$_3$	dry CH_3CN	61.8

The obtained results for Yb(**tpOp**)$_3$ complex indicate that there is an absence of deactivating, non-radiative pathways in solution due to the solvent coordination. This was also confirmed by the X-ray structure analysis of Yb(**tpOp**)$_3$ complex, where the Yb^{3+} metal ion is protected toward external solvent interactions, which are excluded from the first coordination sphere.

Time-resolved luminescence measurements showed that the observed luminescence lifetimes of the Yb(**tpOp**)$_3$ and Nd(**tpOp**)$_3$ complexes in dry acetonitrile solutions at room temperature are relatively long and relate well with those based upon **tpip** ligands. Published results of luminescence lifetimes in dry acetonitrile solutions at room temperature for Yb(**tpip**)$_3$ and Nd(**tpip**)$_3$ complexes are 52.8 and 2.7 μs, respectively.[2] The luminescence lifetimes of Nd(**tpOp**)$_3$ and Yb(**tpOp**)$_3$ complexes in solution also compare well to decay times of the other NIR-emitting complexes based on organic ligands. An example of long decay times observed for Yb^{3+} and Nd^{3+} lanthanide complexes were demonstrated by Van Deun *et al.*[30] for the tetrakis β-diketone 1-phenyl-3-methyl-4-benzoyl-5-pyrazolone ligands, which are associated with the hemicyanine cationic chromophore. The decay time values of 46.4 μs for Yb^{3+} and 1.0 μs for Nd^{3+} complexes are measured in acetonitrile solution. On the other hand, the observed τ for Nd(**tpOp**)$_3$ and Yb(**tpOp**)$_3$ are not as good as the longest lifetimes values reported in the literature for Yb(**F_{20}tpip**)$_3$ and

Nd(**F_{20}tpip**)$_3$ complexes, which were prepared previously within our research group. The lifetimes were measured in CD_3CN and the obtained values were 1,111 μs and 44 μs for Yb(**F_{20}tpip**)$_3$ and Nd(**F_{20}tpip**)$_3$ respectively.[12] The long luminescence lifetimes of **F_{20}tpip** complexes can be explained by absence of high-energy C-H vibrations in complexes due to perflurinated phenyl chromophores.

The longer luminescence lifetime for Yb(**tpOp**)$_3$ compared to Nd(**tpOp**)$_3$ can be explained by Nd^{3+} being more sensitive to high energy oscillations than Yb^{3+}, and also the efficiency of quenching is increased due to Nd^{3+} having more electronic states at high energy than Yb^{3+}. According to the energy gap law, the smaller the harmonic number of vibrational quanta that is required to match the energy gap between the lowest luminescence state and the highest non-luminescence state of the lanthanide ion, the more effective the vibronic quenching will be. The number of harmonics needed to match the energy gap is larger for Yb^{3+} than for Nd^{3+} as shown in Scheme 2.7. The most intense radiative transition ($^4F_{3/2}$ -> $^4I_{11/2}$) of Nd^{3+} has an energy of 5,400 cm^{-1} which matches very well with the vibrational quantum number ν = 2 of the C-H bond vibrations (5,900 cm^{-1}), which leads to an efficient deactivation of the Nd^{3+} excited state and fast luminescence quenching.[31]

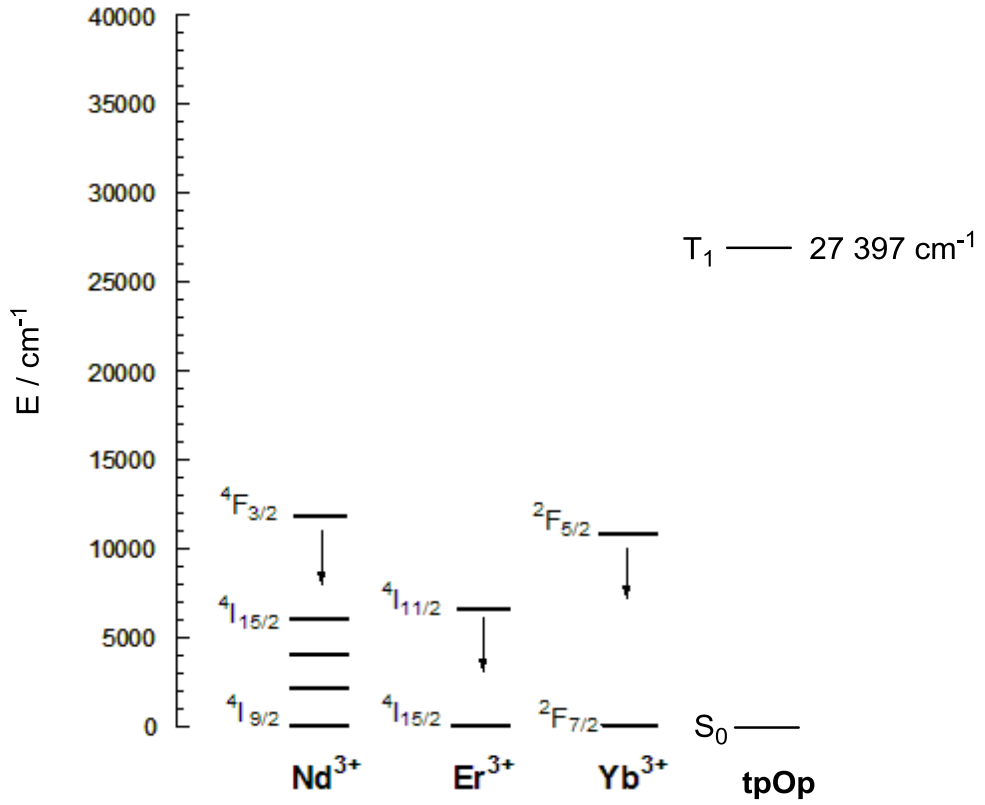

Scheme 2.7. The energy diagram of the 4*f* levels responsible for the lanthanide luminescence.

The overall efficiency of Ln^{3+} sensitised emission can be determined from the absolute quantum yield values (Φ_{tot}), which is regulated by the intersystem crossing efficiency (Φ_{ISC}), energy transfer efficiency (Φ_{ET}) and the lanthanide luminescence (Φ_{Ln}) as shown in Equation 2.2.[32,33]

$$\Phi_{tot} = \Phi_{ISC} \cdot \Phi_{ET} \cdot \Phi_{Ln} \qquad \textbf{(eq. 2.2)}$$

There are a few reports of the absolute quantum yields within the literature for Yb^{3+} and Nd^{3+} complexes. For example, Nonat *et al.*[34] have reported the absolute quantum yields of 0.016% for Nd^{3+} and 0.14% for Yb^{3+} complexes in aqueous solution, based on tripodal 8-hydroxy quinolinate ligands. The highest values of the absolute quantum yield for Yb^{3+} emitting lanthanide complex have been reported by Petoud and Zhang.[35] The Yb^{3+} complex based on the azulene moiety displayed an impressive quantum yield of 3.8% in CH_3CN and 4.2% in CD_3CN. The Nd^{3+} complex,

based on the same organic ligands, showed smaller, but still relatively high value of 0.45% in CH_3CN and 0.53% in CD_3CN,

Due to the lack of appropriate reference standard and the specialist technical equipment, the absolute quantum yield values (Φ_{tot}) for Nd(**tpOp**)$_3$ and Yb(**tpOp**)$_3$ complexes were not measured. However, it was possible to calculate the quantum yield of the lanthanide luminescence step from the observed luminescence lifetime (τ_{obs}) and the radiative lifetime values (τ_{rad}) by applying the Equation 2.3.[36,37] Estimates values of τ_{rad} in organic systems are 2,000 μs and 800 μs for Yb^{3+} and Nd^{3+} ions, respectively.[33]

$$\Phi_{Ln} = \tau_{obs} / \tau_{rad} \qquad \textbf{(eq. 2.3)}$$

This method refers only to the lanthanide based emission process (Φ_{Ln}) and takes no account of the efficiency of intersystem crossing (ISC) and energy transfer (ET) processes. However, the intrinsic quantum yield values can be calculated from values presented in Table 2.8 by applying the Equation 2.3.

Table 2.9. Calculated intrinsic quantum yield values (Φ_{Ln}) for Nd(**tpOp**)$_3$ and Yb(**tpOp**)$_3$ in dry CH_3CN.

Complex	**Φ_{Ln} (%)**
Nd(**tpOp**)$_3$	0.4
Yb(**tpOp**)$_3$	3.1

Calculated values of intrinsic quantum yield for Nd^{3+} and Yb^{3+} complexes in dry acetonitrile, illustrated in Table 2.9, are in line with those published for Nd(**tpip**)$_3$ (0.3%) and Yb(**tpip**)$_3$ (2.6%) complexes.[2] The obtained results indicate that C-H vibrations are not in close proximity to the Ln^{3+} centre, which makes the **tpOp** ligand a good sensitiser for Nd^{3+} and Yb^{3+} NIR- luminescence.

2.4. Conclusion

The luminescent Ln(**tpOp**)$_3$ (Ln = Tb, Dy, Eu, Sm, Gd, Nd, Yb, Er) complexes based upon tetraphenyl imidodiphosphate ligand H**tpOp**, have been synthesised and fully characterised.

The Ln(**tpOp**)$_3$ (Ln = Tb, Ey, Dy, Gd, Er, Yb) complexes were structurally authenticated by single-crystal X-ray diffraction. The X-ray crystal structures of complexes revealed that the twelve phenoxide groups present in the each complex, does not provide an effective shielding of larger lanthanides from solvent coordination. It was found out from the X-ray analysis that in addition to three **tpOp** ligands coordinate to the lanthanide in a bidentate fashion through oxygen atoms, there is also ethanol molecule coordinated directly to Ln^{3+}. However, in the case of Yb(**tpOp**)$_3$, the X-ray crystal study showed that the coordination sphere of the Yb^{3+} lanthanide ion is exclusively composed of oxygen atoms from the three **tpOp** ligands with absence of coordination solvent molecules.

The triplet energy level of the phenoxide moieties was evaluated by low temperature emission studies using Gd(**tpop**)$_3$. The lowest triplet state energy level of **tpOp** ligand indicates a good match to the resonance energy levels of Tb^{3+}, Dy^{3+}, Eu^{3+} and Sm^{3+}. In all of the complexes studied, excitation into ligand-centred bands is followed by energy transfer to the Ln^{3+} ion. All complexes exhibit strong characteristic emission of Ln^{3+} ion in solution and powder samples at the room temperature as well as relatively long lived visible luminescence lifetimes.

The most important result of this work is that **tpOp** can serve as an effective ligand for generating a high luminescence performances in Ln(**tpOp**)$_3$ complexes. A

luminescence study demonstrated that even though the introduction of oxygen on the aromatic chromophores does not improve the modulation of the first coordination sphere of the Ln^{3+} ions, still an impressive enhancement is achieved in the overall quantum yield for Dy(**tpOp**)$_3$ complex, compared to the Dy(**tpip**)$_3$ analogue. Remarkably, the luminescence efficiency of Dy(**tpOp**)$_3$ complex is greater than those of the previously reported in the literature for Dy^{3+} complexes based on organic chromophores.

The **tpOp** ligand is also suited as an efficient sensitiser for NIR emission. After ligand-mediated excitation, emission spectra of the Yb(**tpOp**)$_3$ and Nd(**tpOp**)$_3$ complexes show characteristic NIR luminescence of the corresponding Ln^{3+} ion through intramolecular energy transfer from **tpOp** to the Ln^{3+} ion.

The observed results demonstrate that improvements in luminescence efficiency can be achieved by straightforward synthetic tuning of the ligand aromatic chromophores.

2.5. Experimental

2.5.1. Materials

All reagents for synthesis were commercially available, purchased from Aldrich or Alfa Aesar and were used as received. NaH and KH were purchased as 60% and 35% dispersion in mineral oil which was removed prior to use by thorough washing with hexane or pentane.

Anhydrous toluene and THF were freshly distilled over sodium-benzophenone and sodium wire respectively, where required.

2.5.2. Preparation of tetraphenyl imidodiphosphate-HtpOp procedure 1

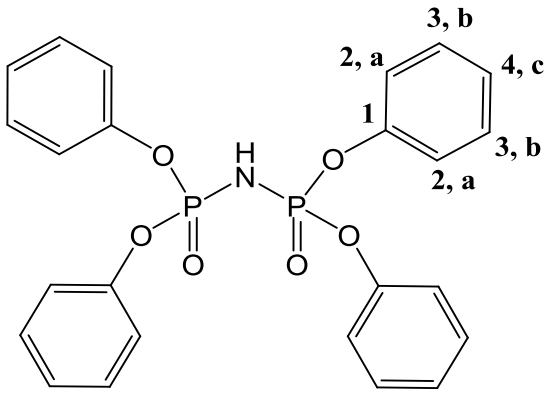

HtpOp

A suspension of triphenyl phosphate (6.01 g, 18.4 mmol) and sodium amide (1.51 g, 8.59 mmol) in dry toluene (60 cm^3) was heated at reflux for 4 h under N_2. During the

reaction foaming occurred due to elimination of ammonia gas. The resulting mixture was cooled to ~ 40^{o}C and water (50 cm^{3}) was added to dissolve the sodium phenoxide. The toluene layer was extracted, acidified with dilute HCl (9.2 cm^{3}, 1 M) and washed with water (2 x 20 cm^{3}). The volume of the solution was concentrated to ~ 4 cm^{3}, and hexane (40 cm^{3}) was added. The solution was then stirred until a white precipitate was formed. The precipitate was collected by filtration and washed with hexane (2 x 10 cm^{3}). This yielded the desired product as a fine white powder which was dried under vacuum (2.73 g, 62 %); m_p = 107 – 109 ^{o}C (literature value 110 – 112 ^{o}C) [12]; $\delta_P\{^1H\}$ (121 MHz, $CDCl_3$): - 9.7 (s); $\delta_C\{^1H\}$ (75 MHz, $CDCl_3$): 150.6 (C_1), 130.1 (C_3) 125.9 (C_4), 120.9 (C_2); δ_H (300 MHz, $CDCl_3$): 7.11 – 7.24 (20H, m, Ar); MS (ES$^-$) *m/z*: 480 [*M* - H]$^-$; elemental analysis calcd. (%) for $C_{24}H_{21}N_1O_6P_2$: C, 59.88; H, 4.40; N, 2.91; found C, 59.61; H, 4.20; N 2.98; UV/Vis (CH_3CN): λ in nm (log ε) 263 (3.2).

2.5.3. Preparation of tetraphenyl imidodiphosphate-HtpOp - procedure 2[4]

A solution of diphenyl phosphoramidate (2.57 g, 10.3 mmol) in dry THF (30 cm^{3}) was added to a suspension of NaH (1.21 g, 60% dispersion in mineral oil, 30.3 mmol) in dry THF (10 cm^{3}) at room temperature. The resulting mixture was stirred for 30 min before the dropwise addition of diphenyl chlorophosphate (2.73 g, 10.2 mmol) in dry THF (10 cm^{3}) over 15 min. The mixture was then stirred at reflux for 16 h. The reaction mixture was cooled to room temperature and quenched by the addition of MeOH (5 cm^{3}) in order to remove any excess of NaH. The volume of THF was reduced by half under vacuum and diluted HCl (27 cm^{3}, 2 M) was added. The mixture was then extracted with DCM (3 x 30 cm^{3}) and the combined extracts of the organic layer were dried over Na_2SO_4. The solvent volume was reduced to 30 cm^{3} in

vacuo and the solution stored in the freezer for 72 h. The resultant solid was recrystallised initially from acetone-water and subsequently from benzene-hexane and THF-hexane to yield tetraphenyl imidodiphosphate as a light brown solid (1.71 g, 69 %). $\delta_P\{^1H\}$ (121 MHz, $CDCl_3$): - 9.7 (s); $\delta_C\{^1H\}$ (75 MHz, $CDCl_3$): 150.5 (C_1), 130.0 (C_3), 125.7 (C_4), 120.8 (C_2); δ_H (300 MHz, $CDCl_3$): 7.02 – 7.23 (20H, m, Ar).

The data agree with those obtained by procedure one. This method was not followed further and was not used for the ligand batches used in the formation of complexes.

2.5.4. Preparation of KtpOp

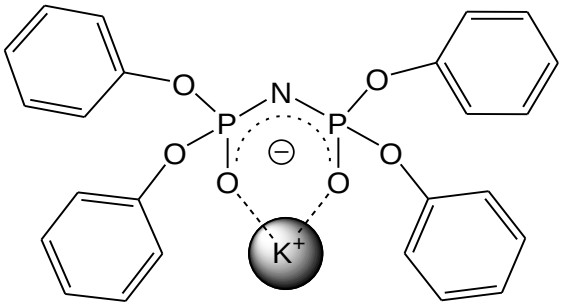

KtpOp

Potassium hydride (0.49 g, 35% dispersion in mineral oil, 3.69 mmol) was washed with pentane (3 x 5 cm^3) and dried *in vacuo* for 20 min. THF (8 cm^3) was added, followed by tetraphenyl imidodiphosphate (1.54 g, 3.20 mmol) dissolved in THF (15 cm^3). The resulting suspension was stirred for 1 h at room temperature. The solvent was removed *in vacuo* to yield a light brown viscous solution, which was dissolved in water (8 cm^3) and extracted with pentane (3 x 5 cm^3). The volume of the aqueous layer was reduced *in vacuo* and the residue transferred to the freezer overnight. The resulting light brown solid was washed with pentane (5 x 10 cm^3) and dried under vacuum, to yield the desired product (1.46 g, 88 %); $\delta_P\{^1H\}$ (121 MHz, $CDCl_3$): - 7.2

(s); $\delta_C\{^1H\}$ (75 MHz, $CDCl_3$): 155.1(C_1), 132.0 (C_3) 126.6 (C_4), 123.3 (C_2); δ_H (300 MHz, $CDCl_3$): 6.94 – 7.11 (20H, m, Ar); MALDI-MS *m/z*: 519.6 $[M]^+$, 557.6 $[M + K]^+$; elemental analysis calcd. (%) for $C_{24}H_{20}N_1O_6P_2K_1$(1/4 KCl): C, 53.57; H, 3.75; N, 2.60; found C, 53.64; H, 3.67; N 2.70.

2.5.5. Preparation of $Ln(tpOp)_3$ (Ln = Eu, Tb) – procedure 1[7]

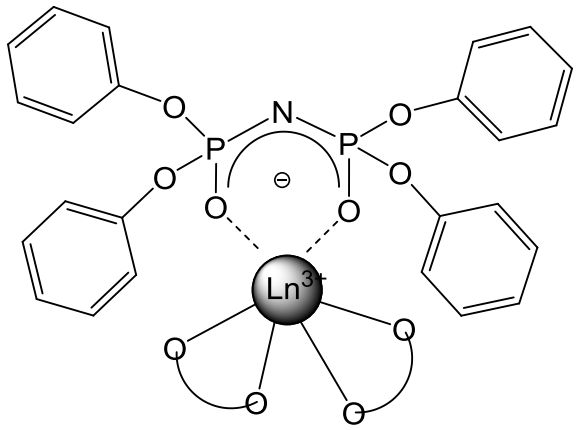

$Ln(tpOp)_3$

A solution of $LnCl_3.6H_2O$ (0.07 mmol, 1 equiv.) (Ln = Eu, Tb) in EtOH (1.5 cm^3) was added to the solution of tpOp (0.21 mmol, 3 equiv.) in EtOH (2.1 cm^3). The reaction mixture was cooled in the freezer for 2 h, after which time a small amount of precipitate had formed. The addition of water (15 cm^3) led to further precipitation. The precipitate was collected by filtration, washed with a minimum amount of EtOH (2 cm^3) and dried under vacuum.

$Tb(tpOp)_3$ – white solid (0.03 g, 28 %); $\delta_P\{^1H\}$ (121 MHz, $CDCl_3$): - 33.9 (br,s); δ_H (300 MHz, $CDCl_3$): 7.14 (24H, br, H_a), 4.00 (12H, s, H_c), 3.24 (24H, s, H_b); MS(ES^+): *m/z* 1600 $[M]^+$, 1622 $[M+Na]^+$; elemental analysis calcd. (%) for $C_{72}H_{60}N_3O_{18}P_6Tb$: C,

54.05; H, 3.78; N, 2.63; found C, 54.10; H, 3.63; N 2.67; UV/Vis (CH_3CN): λ in nm (log ε) 263 (3.7).

$Eu(tpOp)_3$ - white solid (0.05 g, 47 %); $\delta_P\{^1H\}$ (121 MHz, $CDCl_3$): -80.5 (s); MS(ES^+): *m/z* 1616 $[M+Na]^+$; elemental analysis calcd. (%) for $C_{72}H_{60}N_3O_{18}P_6Eu(H_2O)$: C, 53.68; H, 3.88; N, 2.61; found C, 53.48; H, 3.75; N 2.95; UV/Vis (CH_3CN): λ in nm (log ε) 263 (3.7).

2.5.6. Preparation of $Ln(tpOp)_3$ (Ln = Eu, Tb, Dy, Sm, Gd, Nd, Yb, Er) and $Y(tpOp)_3$ – procedure 2

To a stirring solution of KtpOp (3 equiv., 0.39 mmol) in EtOH (10 cm^3) a solution of $LnCl_3.6H_2O$ (1 equiv., 0.13 mmol) in aqueous EtOH (5 cm^3) was added dropwise. The resulting white suspension was then stored in the freezer over night, yielding a white, sticky precipitate, which could not be collected by filtration. The solvent was decanted off and the remaining solid was stirred vigorously with hexane (5 cm^3) to yield the product as a fine white powder. The powder was collected by filtration, washed with hexane (2 x 5 cm^3) and dried under vacuum.
Single crystals suitable for X-ray diffraction analysis were grown by slow evaporation of chloroform, acetonitrile or hexane solutions.

$Eu(tpOp)_3$ - (0.13 g, 63 %); $\delta_P\{^1H\}$ (121 MHz, $CDCl_3$): - 80.0 (s); $\delta_C\{^1H\}$ (75 MHz, $CDCl_3$): 148.5 (C_1), 128.0 (C_3), 123.0 (C_4), 119.2 (C_2); δ_H (300 MHz, $CDCl_3$): 7.29 (24H, t, ^3J (H,H) = 7.3 Hz, H_b), 7.19 (12H, t, ^3J (H,H) = 7.1 Hz, H_c), 6.78 (24H, d, ^3J

(H,H) = 7.6 Hz, H_a); MS(ES^+): *m/z* 1616 [*M*+Na]$^+$; elemental analysis calcd. (%) for $C_{72}H_{60}N_3O_{18}P_6Eu$: C, 54.28; H, 3.80; N, 2.64; found C, 54.14; H, 3.98; N 2.82; UV/Vis (CH_3CN): λ in nm (log ε) 263 (3.7).

$Tb(tpOp)_3$ - (0.12 g, 59%); $\delta_P\{^1H\}$ (121 MHz, $CDCl_3$): - 33.8 (br,s); $\delta_C\{^1H\}$ (75 MHz, $CDCl_3$): 163.9 (C_1), 126.2 (C_3), 123.2 (C_2), 121.2 (C_4); δ_H (300 MHz, $CDCl_3$): 6.35 (24H, br, H_a), 4.01 (12H, s, H_c), 3.21 (24H, s, H_b); MS(ES^+): *m/z* 1638 [*M*+K]$^+$; elemental analysis calcd. (%) for $C_{72}H_{60}N_3O_{18}P_6Tb$: C, 54.05; H, 3.78; N, 2.63; found C, 53.83; H, 4.02; N 2.79; UV/Vis (CH_3CN): λ in nm (log ε) 263 (3.7).

$Dy(tpOp)_3$ - (0.12 g, 58 %); $\delta_P\{^1H\}$ (121 MHz, $CDCl_3$): -2.2 (br,s); $\delta_C\{^1H\}$ (75 MHz, $CDCl_3$): 163.0 (C_1), 128.2 (C_3), 123.5 (C_2), 120.5 (C_4); δ_H (300 MHz, $CDCl_3$): 5.66 (24H, br, H_a), 4.25 (12H, s, H_c), 3.32 (24H, s, H_b); MS(ES^+): *m/z* 1643 [*M*+K]$^+$; elemental analysis calcd. (%) for $C_{72}H_{60}N_3O_{18}P_6Dy$: C, 53.93; H, 3.77; N, 2.62; found C, 54.10; H, 3.63; N 2.67; UV/Vis (CH_3CN): λ in nm (log ε) 263 (3.7).

$Sm(tpOp)_3$ - (0.11 g, 52 %); $\delta_P\{^1H\}$ (121 MHz, $CDCl_3$): - 4.0 (s); $\delta_C\{^1H\}$ (75 MHz, $CDCl_3$): 151.5 (C_1), 129.2 (C_3), 124.2 (C_4), 120.8 (C_2); δ_H (300 MHz, $CDCl_3$): 7.13 (24H, d, ^3J (H,H) = 7.9 Hz, H_a), 7.02 (24H, t, ^3J (H,H) = 7.5 Hz, H_b), 6.93 (12H, t, ^3J (H,H) = 6.9 Hz, H_c); MALDI - MS: *m/z* 1591.5 [*M*]$^+$; elemental analysis calcd. (%) for $C_{72}H_{60}N_3O_{18}P_6Sm$: C, 54.34; H, 3.80; N, 2.64; found C, 54.15; H, 3.92; N 2.67; UV/Vis (CH_3CN): λ in nm (log ε) 263 (3.7).

$Gd(tpOp)_3$ – (0.13 g, 58 %); MS(ES^+): *m/z* 1637 [*M*+K]$^+$; elemental analysis calcd. (%) for $C_{72}H_{60}N_3O_{18}P_6Gd$: C, 54.05; H, 3.78; N, 2.63; found C, 54.10; H, 3.94; N 2.66; UV/Vis (CH_3CN): λ in nm (log ε) 263 (3.6).

$Nd(tpOp)_3$ – (0.11 g, 56 %); $\delta_P\{^1H\}$ (121 MHz, $CDCl_3$): 30.2; $\delta_C\{^1H\}$ (75 MHz, $CDCl_3$): 155.7 (C_1), 131.6 (C_3), 126.5 (C_4), 123.4 (C_2); δ_H (300 MHz, $CDCl_3$): 6.73 – 6.80 (60H, m, Ar); MS(ES^+): *m/z* 1623 $[M+K]^+$; elemental analysis calcd. (%) for $C_{72}H_{60}N_3O_{18}P_6Nd$: C, 54.55; H, 3.81; N, 2.65; found C, 54.25; H, 3.63; N 2.77; UV/Vis (CH_3CN): λ in nm (log ε) 263 (3.7).

$Er(tpOp)_3$ – (0.14 g, 67 %); $\delta_P\{^1H\}$ (121 MHz, $CDCl_3$): - 85.8; $\delta_C\{^1H\}$ (75 MHz, $CDCl_3$): 147.2 (C_1), 128.4 (C_3), 123.5 (C_4), 119.5 (C_2); δ_H (300 MHz, $CDCl_3$): 8.16 (24H, br, s, H_a), 7.76 (24H, br, s, H_b), 7.38 (12H, br, s, H_c); MS(ES^+): *m/z* 1647 $[M+K]^+$; elemental analysis calcd. (%) for $C_{72}H_{60}N_3O_{18}P_6Er$: C, 53.77; H, 3.76; N, 2.61; found C, 53.70; H, 3.81; N 3.02; UV/Vis (CH_3CN): λ in nm (log ε) 263 (3.6).

$Y(tpOp)_3$ – (0.13 g, 66 %); $\delta_P\{^1H\}$ (121 MHz, $CDCl_3$): - 4.2; $\delta_C\{^1H\}$ (75 MHz, $CDCl_3$): 150.7 (C_1), 128.8 (C_3), 123.9 (C_4), 120.2 (C_2); δ_H (300 MHz, $CDCl_3$): 6.93 – 7.05 (60H, m, Ar); MS(ES^+): *m/z* 1569 $[M+K]^+$; elemental analysis calcd. (%) for $C_{72}H_{60}N_3O_{18}P_6Y$: C, 56.52; H, 3.95; N, 2.75; found C, 56.71; H, 3.94; N, 2.73; UV/Vis (CH_3CN): λ in nm (log ε) 263 (3.6).

$Yb(tpOp)_3$ – (0.13 g, 65 %); $\delta_P\{^1H\}$ (121 MHz, $CDCl_3$): -8.5 (s); $\delta_C\{^1H\}$ (75 MHz, $CDCl_3$): 147.7 (C_1), 128.5 (C_3), 123.6 (C_4), 119.5 (C_2); δ_H (300 MHz, $CDCl_3$): 8.59 (24H, br, s, H_a), 7.81 (24H, br, s, H_b), 7.38 (12H, t, ^3J (H,H) = 7.3 Hz, H_c); MS(ES^+): *m/z* 1653 $[M+K]^+$; elemental analysis calcd. (%) for $C_{72}H_{60}N_3O_{18}P_6Yb$: C, 53.58; H, 3.75; N, 2.60; found C, 53.59; H, 3.74, N, 2.59; UV/Vis (CH_3CN): λ in nm (log ε) 263 (3.6).

2.6. References

(1) Magennis, S. W.; Parsons, S.; Pikramenou, Z. *Chem. Eur. J.* **2002**, *8*, 576.

(2) Bassett, A. P.; Van Deun, R.; Nockemann, P.; Glover, P. B.; Kariuki, B. M.; Van Hecke, K.; Van Meervelt, L.; Pikramenou, Z. *Inorg. Chem.* **2005**, *44*, 6140.

(3) Nielsen, M. L. *Inorg. Chem.* **1964**, *3,* 1760.

(4) Necas, M.; Foreman, M. R. St J.; Marek, J.; Woollins, J. D.; Novosad, J. *New. J. Chem.* **2001,** *25,* 1256.

(5) Kulpe, S.; Seidel, I.; Herrmann, E. *Crystal Res. & Technol.* **1984**, *19,* 661.

(6) Lannert, K. P.; Joesten, M. D. *Inorg. Chem.* **1968**, *7*, 2048.

(7) Herrmann, E.; Hoàng, B. N.; Dreyer, R. *Z. Chem.* **1979**, *19*, 187.

(8) Reuben, J. *Progress in NMR Spectroscopy.* **1975**, *9,* 1.

(9) Drago, R. S. *Physical Methods in Chemistry.* Second ed.; Saunders, 1992.

(10) Bünzli, J.-C. G.; Choppin, G. R. Elsevier Science Ltd., 1990.

(11) Sherry, A. D.; Geraldes, C. F. G. C. *Lanthanide Probes in Life, Chemical and Earth Sciences*, eds. Bünzli, J.-C. G.; Choppin, G. R. Elsevier, Amsterdam, 1989, Ch.4.

(12) Glover, P. B.; Bassett, A. P.; Nockemann, P.; Kariuki, B. M.; Van Deun, R.; Pikramenou, Z. *Chem. Eur. J.* **2007**, *13*, 6308.

(13) Kulpe, S.; Seidel, I.; Szulzewsky, K. *Acta Cryst*. **1982**, *B32*, 2813.

(14) Zhang, F.; Hou, Y.; Du, Ch.; Wu, Y. *Dalton Trans.* **2009**, 7359.

(15) Sabbatini, N.; Guardigli, M.; Lehn, J.-M.; *Coord. Chem. Rev.* **1993**, *123*, 201.

(16) Bünzli, J.-C. G. “Spectroscopic Properties of Rare Earths” in *Optical Materials* (Ed.: Liu, G. K.), Springer-Verlag, Berlin, 2002.

(17) Mayer, G. V.; Bazyl, O. K.; Artyukhov, V. Y.; Sokolova, I. V. *Russ. Phys. J.* **1999**, *42*, 431.

(18) Steemers, F. J.; Verboom, W.; Reinhoudt, D. N.; Vander Tol, E. B.; Verhoeven, J. W. *J. Am. Chem. Soc.* **1995**, *117*, 9408.

(19) Carnall, W. T.; Fields, P. R.; Rajnak, K. *J. Chem. Phys.* **1968**, *49*, 4413.

(20) Klink, S. I.; Grave, L.; Reinhoudt, D. M.; Van Veggel, F.C. J. M.; Werts, M. H.; Geurts, F. A. J.; Hofstraat, J. W. *J. Phys. Chem. A.* **2000**, *104*, 5457.

(21) Quici, S.; Cavazzini, M.; Marzanni, G.; Accorsi, G.; Armaroli, N.; Ventura, B.; Barigelletti, F. *Inorg. Chem.* **2005**, *44*, 529.

(22) Petoud, S.; Muller, G.; Moore, E. G.; Xu, J.; Sokolnicki, J.; Riehl, J. P.; Le, U. N.; Cohen, S. M.; Raymond, K. N. *J. Am. Chem. Soc.* **2007**, *129*, 77.

(23) Stein, G.; Würzberg, E. *J. Chem. Phys*. **1975**, *62*, 208.

(24) Renaud, F.; Piguet, C.; Bernardinelli, G.; Bünzli, J.-C. G.; Hopfgartner, G. *J. Am. Chem. Soc.* **1999**, *121,* 9326.

(25) Meech, S. R.; Phillips, D. *J. Photochem.* **1983**, *23*, 193.

(26) Nakamaru, K. *Bull. Chem. Soc. Jpn.* **1982**, *55*, 2697.

(27) Tsvirko, M.; Meshkova, S.; Kiriiak, G.; Gorodnyuk, V. *J. Phys.; Conf. Ser*. **2007**, *79*, 012007.

(28) Petoud, S.; Cohen, S. M.; Bünzli, J.-C. G.; Raymond, K. N. *J. Am. Chem. Soc.* **2003,** *125,* 13324.

(29) Comby, S.; Imbert, D.; Vandevyver C.; Bünzli, J.-C. G. *Chem. Eur. J.* **2007**, *13*, 936.

(30) Van Deun, R.; Nockemann, P.; Parac-Vogt, T. N.; Van Hecke, K.; Van Meervelt, L.; Görller-Walrand, Ch.; Binnemans, K. *Polyhedron*, **2007**, 5441.

(31) Yanagida, S.; Hasegawa, Y.; Murakoshi, K.; Wada, Y.; Nakashimi, N.; Yamanaka, T. *Coord, Chem. Rev.* **1998**, *171*, 461.

(32) Werts, M. H. V.; Verhoeven, J. W.; Hofstraat, J. W. *J. Chem. Soc. Perkin Trans. 2.* **2000**, 433.

(33) Hofstraat, J. W.; Wolbers, M. P. O.; Van Veggel, F. C. J. M.; Reinhoudt, D. N.; Werts, M. H. V.; Verhoeven, J. W. *J. Fluoresc.* **1998**, *8*, 301.

(34) Nonat, A.; Imbert, D.; Pécaut, J.; Giraud, M.; Mazzanti, M. *Inorg. Chem.* **2009**, *48,* 4207.

(35) Zhang, J.; Petoud, S. *Chem. Eur. J.* **2008**, *14*, 1264.

(36) Klink, S. I.; Hebbink, G. A.; Grave, L.; Peters, F. G. A.; Van Veggel, F. C. J. M.; Reinhoudt, D. N.; Hofstraat, J. W. *Eur. J. Org. Chem.* **2000**, 1923.

(37) Werts, M. H. V.; Jukes, R. T. F.; Verhoeven, J. W. *Phys. Chem. Chem. Phys.* **2002**, *4*, 1542.

3.0. Dinuclear Lanthanide Complexes Based on Pentaphenyl Diimidotriphosphate Ligands

3.1. Introduction

In the last decade, following Bünzli's and Piguet's breakthrough in the study of bimetallic lanthanide assemblies[1] there has been an increasing interest in the design and synthesis of binuclear lanthanide complexes for the development of dual luminescent probes[2,3] and new photonic devices.[4-7] The synthesis of new homodinuclear lanthanide complexes has become an exciting field of study due to their unique photophysical properties. Our research group has been interested in self assembly strategies for the construction of lanthanide complexes, using versatile typologies of β-diketonate systems. Dinuclear lanthanide complexes based on two benzoyl β-diketonate sites linked together by a 1,3-phenylene spacer unit have been previously studied.[8] The approach taken in this chapter is to utilise a bidentate ligand based on the mononuclear analogue H**tpOp**. It was envisaged that two imidodiphosphate binding sites can be grafted on a single ligand. The pentaphenyl diimidotriphosphate (H_2**bistpOp**) ligand (Scheme 3.1) was chosen as an ideal candidate to investigate the possibility of forming aromatic groups and two strong chelating sites, would be promising features to lead to self- assembly process for formulation of homodinuclear lanthanide complexes Ln_2(**bistpOp**)$_3$. In this chapter the syntheses and photophysical properties of dinuclear complexes Ln_2(**bistpOp**)$_3$ (Ln = Eu, Tb, Sm, Dy, Gd, Yb, Er, Nd) have been reported.

3.2. Results and Discussion

3.2.1. Preparation and characterisation of H_2**bistpOp**

The procedure of the preparation of a dinucleating ligand was followed as described in the literature[9]. In this report it was demonstrated that the choice of reaction conditions, rate and order of addition and ratio of base to phosphoramidate can lead to the preparation of long -P-N-P- chain structures. The condensation reaction between diphenyl phosphoramidate and triphenyl phosphate, in the presence of base, did not proceed smoothly as reported.[9] It was found that two different pathways operate in the synthesis of the H_2**bistpOp** ligand. The reaction was also very sensitive to the order of addition of starting materials and the ratio of reagents, which resulted in two different reaction mechanisms. Firstly, when triphenyl phosphate was introduced first, followed by an addition of diphenyl phosphoramidate and NaH in 1:1:2 molar ratio respectively, the ^{31}P NMR investigation of the reaction showed a mixture of compounds. The observed product mixture was identified as the desired compound H_2**bistpOp** as well as the additional ligand H**tpOp** as shown in Scheme 3.1. Attempts to allow the product mixture to react with more diphenyl phosphoramidate and sodium hydride did not lead to any changes. The purification by silica column chromatography was not successful due to the poor separation.

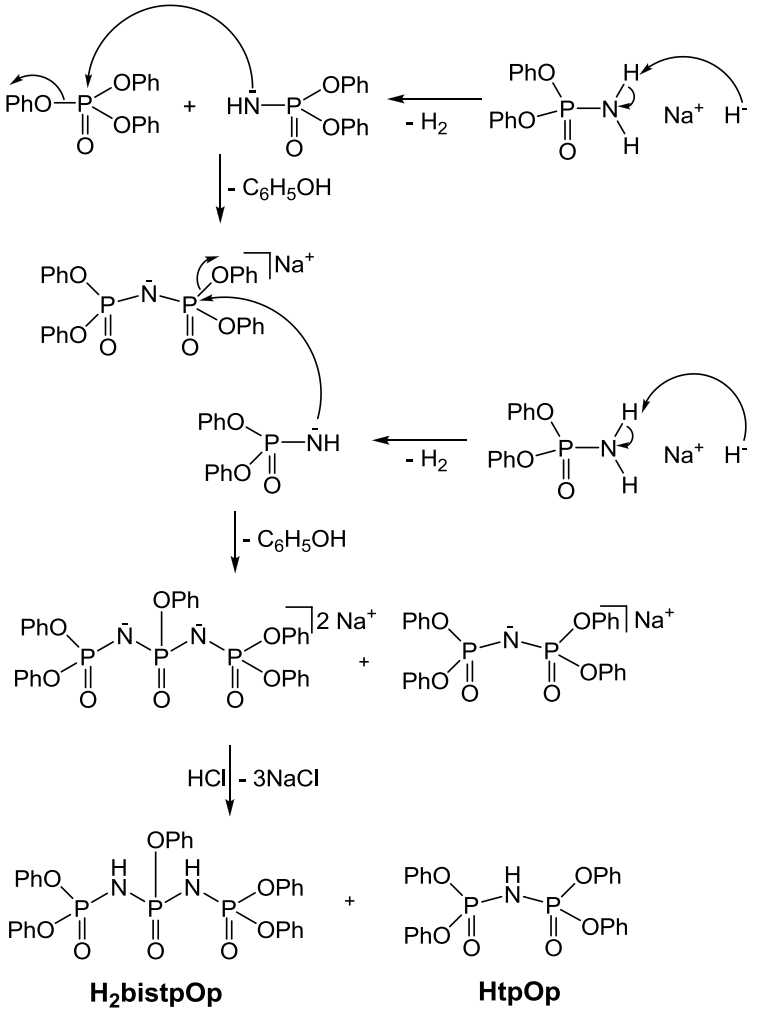

Scheme 3.1. Reaction mechanism I of synthetic route to H_2**bistpOp**.

Therefore, the order of starting materials introduced to the reaction and the ratio of reagents were modified to the introduction of diphenyl phosphoramidate and NaH, followed by triphenyl phosphate in 2:2:1 molar ratio respectively. Monitoring the reaction by ^{31}P NMR spectroscopy revealed that diphenyl phosphoramidate in the presence of NaH led to a head-to-tail self-condensation yielding triphenyl amidoimidodiphosphate as a by-product as illustrated in Scheme 3.2.

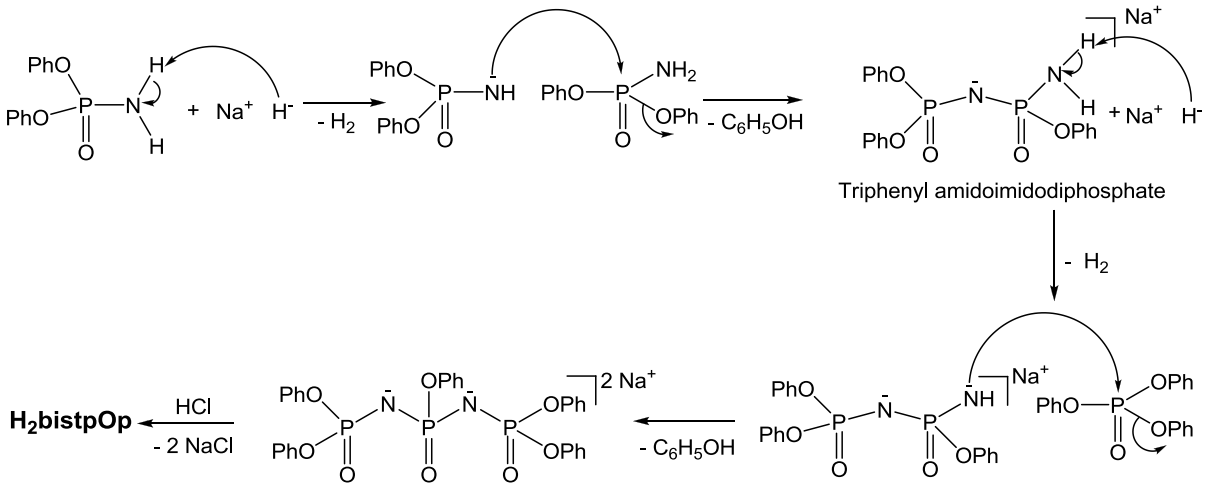

Scheme 3.2. Reaction mechanism II of synthetic route to H_2**bistpOp**.

However, in this case the increase of the concentration of base and triphenyl phosphate converted all by-product and the reaction was driven forward to yield selectively the H_2**bistpOp** ligand as the single product.

The H_2**bistpOp** was air-stable, soluble in chloroform, acetonitrile, THF, ethanol and methanol. It has been fully characterised by various spectroscopic techniques and elemental analyses.

The ^{31}P NMR spectrum in $CDCl_3$ (Figure 3.1) shows two resonances in a 1:2 ratio. A 11.1 Hz $^2J_{P,P}$ coupling splits the two outer phosphorus atoms into a doublet and a 11.1 Hz $^2J_{P,P}$ coupling gives a triplet pattern for the central phosphorus atom.

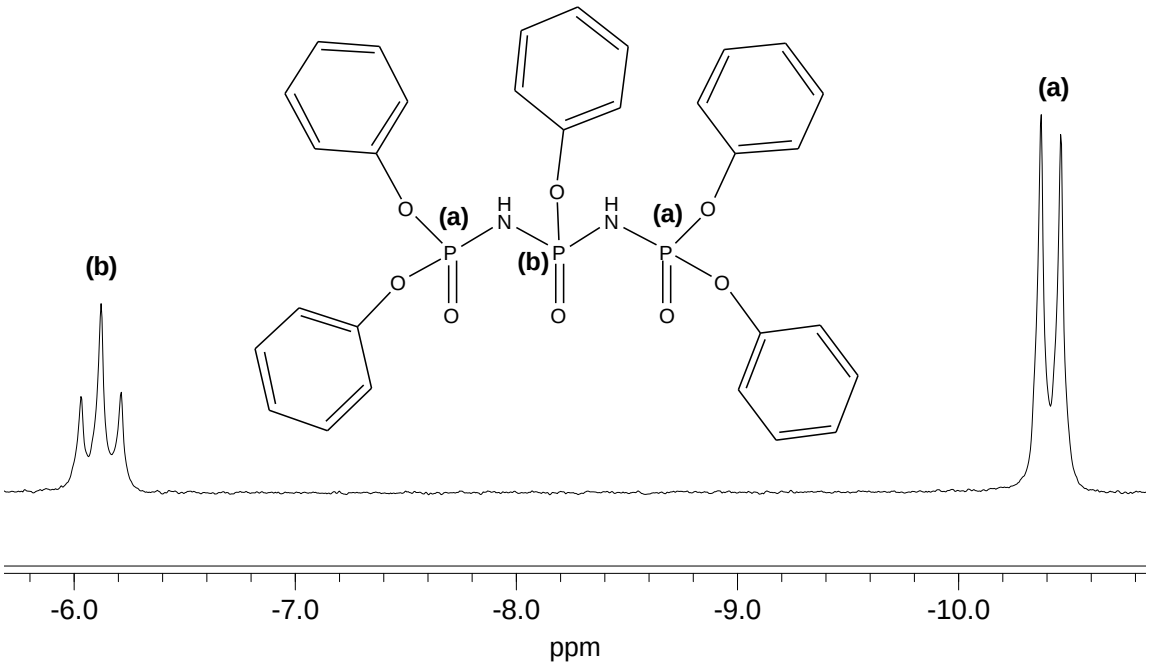

Figure 3.1. The 121 MHz ^{31}P NMR spectrum of H_2**bistpOp** in $CDCl_3$.

The ^{1}H NMR spectrum (Figure 3.2) of the ligand gives a multiplet in the range 7.0 – 7.2 ppm corresponding to the aromatic protons. However, the further investigation of the spectrum such as integration and multiplicities is impossible due to peaks overlapping.

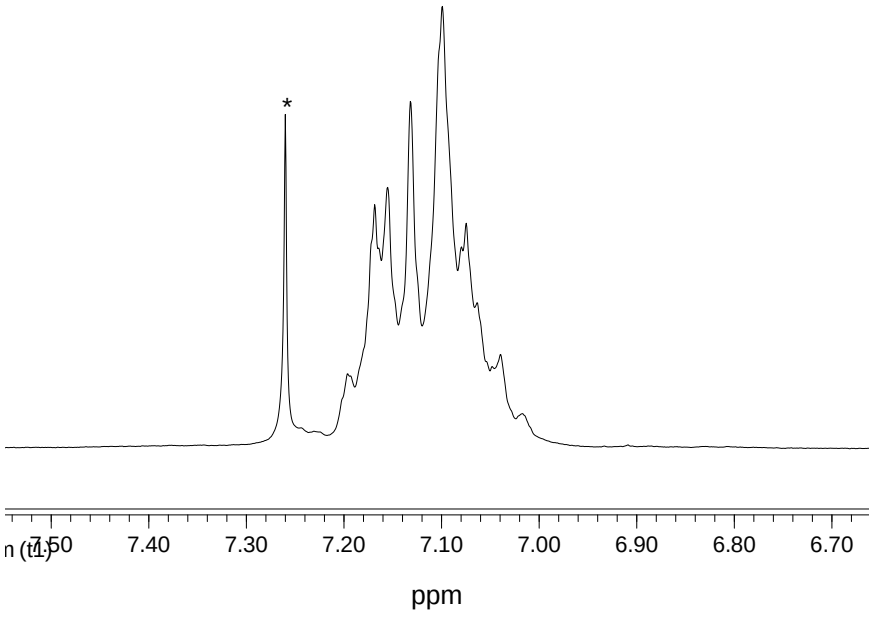

Figure 3.2. The 300 MHz ^{1}H NMR spectrum of H_2**bistpOp** in $CDCl_3$. (* = solvent).

The PENDANT ^{13}C NMR spectra of H_2**bistpOp** (See Appendix A1) displays 8 different carbon environments in the range of 150 - 121 ppm.

The positive mode electrospray mass spectrometry confirms the formulation of the ligand, displaying the intense peak at *m/z* = 659 corresponding to $[M + Na]^+$.

The UV-Vis spectrum of H_2**bistpOp** (Figure 3.3) exhibits dominant absorption at the maximum located at 261 nm (ε = 1739 dm^3 mol^{-1} cm^{-1}) and two weaker peaks at 255 and 268 nm. These bands are ascribed to the π->π* transition of the phenoxide moieties. If the observed absorption coefficient value is divided by five, for each phonoxide moiety present in H_2**bistpOp,** then the value corresponding to one phenoxide moiety is approximately 348 dm^3 mol^{-1} cm^{-1}. Therefore, observed ε value (1,739 dm^3 mol^{-1} cm^{-1}) is in good agreement with five phenoxide groups present in H_2**bistpOp** ligand compared to the H**tpOp** (ε_{263} = 1,410 dm^3 mol^{-1} cm^{-1}).

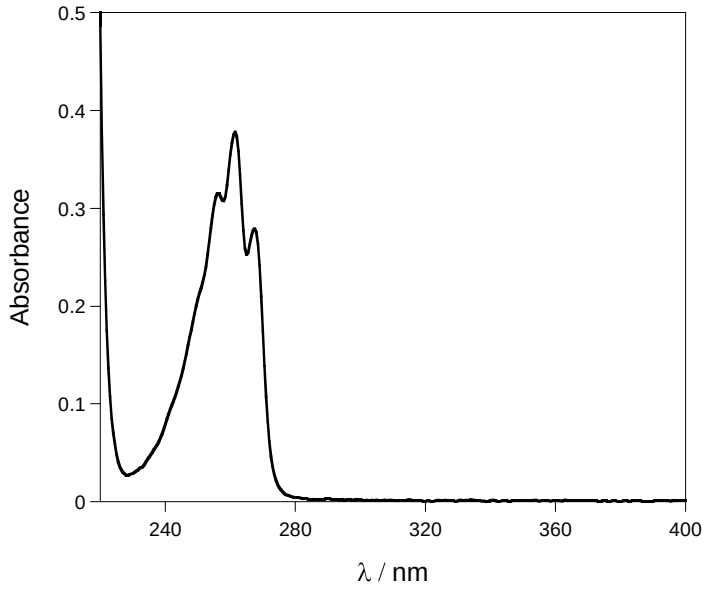

Figure 3.3. The UV-vis spectrum of H_2**bistpOp** in CH_3CN.

The solid state structure of the H_2bistpOp ligand has been further confirmed by X-ray diffraction analyses.

3.2. 2. X – ray Crystallography of H_2bistpOp

The slow evaporation of chloroform solution yielded crystals of sufficient quality for X-ray diffraction studies. Details of the crystal data, intensity measurements and structure refinements are summarised in Table 3.1.

The crystallographic data shows that H_2bistpOp crystallises in the triclinic space group P-1. The structure contains two crystallographically independent molecules in phosphazane form (Figure 3.4) with similar crystallographic parameters, therefore only one molecule of H_2bistpOp is described. The two donor atoms O(3) and O(5) in one chelate ring are in *cis* arrangement with respect to each other, whereas the oxygen atoms O(5) and O(8) in the second chelate ring have *anti* conformation. The O-P···P-O torsion angles in the two chalete rings of the ligand are 170.1° and 166.5°. The crystallographic P=O average bond distance is 1.46(5) Å, which indicate the double bonding between P and O with localised π-electrons. The P-N bonds P(1) – N(1), N(1) – P(2), P(2) – N(2) and P(3) – N(2) ranging from 1.67(5) to 1.63(6) Å. The P=O and P-N bond lengths are similar to those reported for the HtpOp ligand in Chapter 2. The hydrogen atoms H(1) and H(2) are chemically bonded at nitrogen N(1) and N(2) with the bond lengths of 0.88 Å.

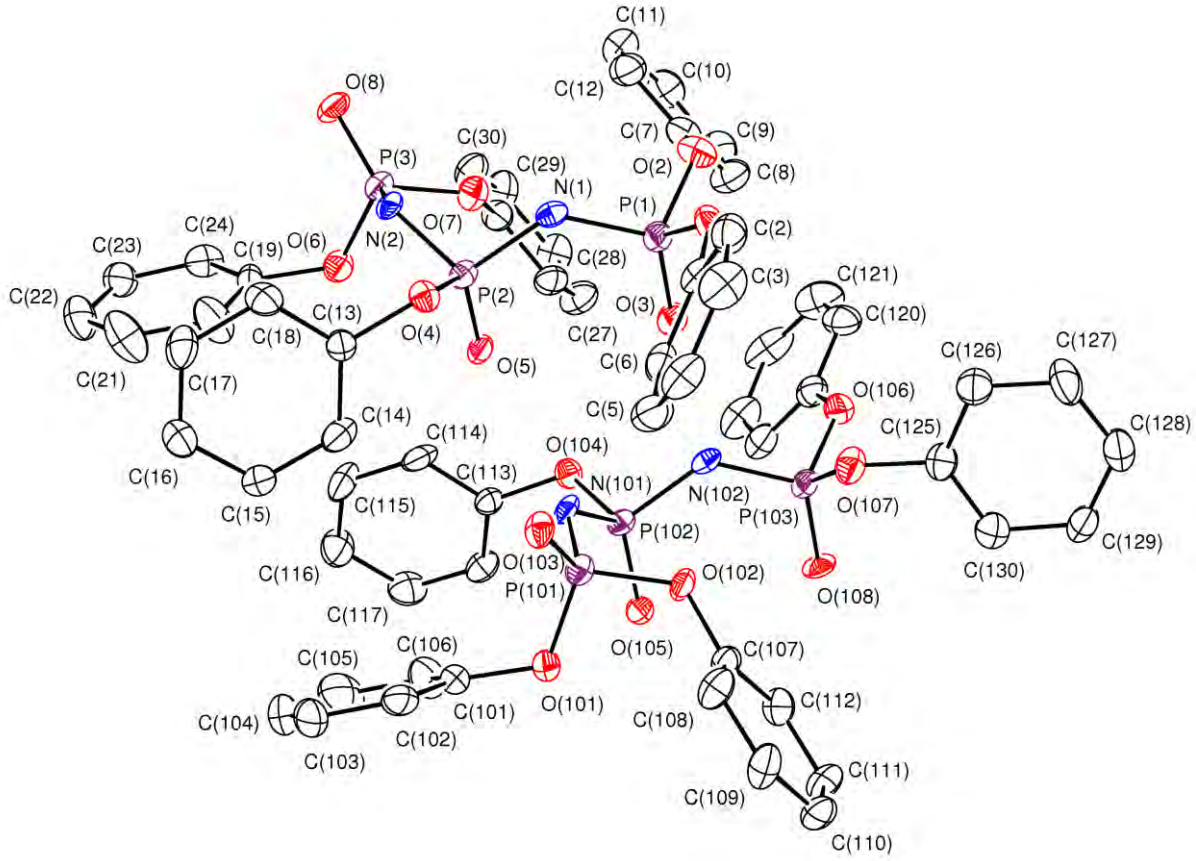

Figure 3.4. X-ray crystal structure of H_2**bistpOp** showing the atomic numbering scheme.

The crystallographicaly independent H_2**bistpOp** molecules are connected to one another by a network of hydrogen bonds (Figure 3.5). Hydrogen atoms located on the two nitrogen atoms of each ligand are involved in intermolecular hydrogen bonding with the phosphoryl oxygen atoms at a distance of 2.837(7) to 2.864(7) Å.

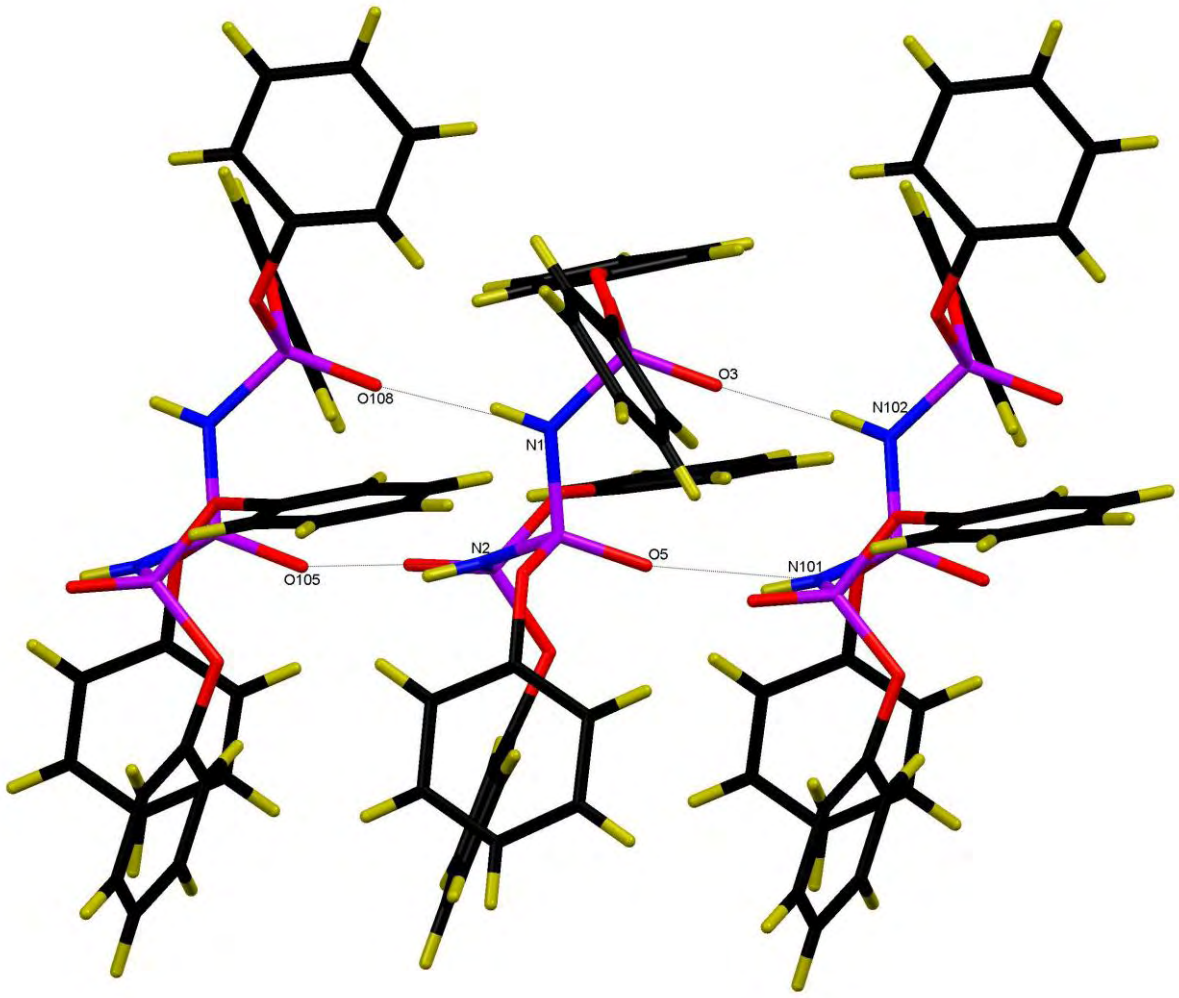

Figure 3.5. The solid state structure of H_2**bistpOp** showing the H-bonded chain structure.

Table 3.1. Summary of the XRD single crystal structure data of H_2**bistpOp**.

	H_2bistpOp	
Empirical formula	$C_{30}\ H_{27}\ N_2\ O_8\ P_3$	
Formula weight	636.45	
Temperature	120(2) K	
Wavelength	0.71073 Å	
Crystal system	Triclinic	
Space group	P -1	
Unit cell dimensions	a = 10.3971(3) Å	α= 75.526(2)°.
	b = 13.8413(4) Å	β= 79.698(2)°.
	c = 22.5648(6) Å	γ = 72.849(2)°.
Volume	2984.94(15) $Å^3$	
Z	4	
Density (calculated)	1.416 Mg/m^3	
Absorption coefficient	0.253 mm^{-1}	
F(000)	1320	
Crystal size	0.08 x 0.03 x 0.01 mm^3	
Theta range for data collection	3.08 to 25.03°.	
Index ranges	-12<=h<=12, -16<=k<=16, -26<=l<=26	
Reflections collected	43335	
Independent reflections	10509 [R(int) = 0.0991]	
Completeness to theta = 25.03°	99.4 %	
Absorption correction	Semi-empirical from equivalents	
Max. and min. transmission	0.9975 and 0.9800	
Refinement method	Full-matrix least-squares on F^2	
Data / restraints / parameters	10509 / 0 / 775	
Goodness-of-fit on F^2	1.129	
Final R indices [I>2sigma(I)]	R1 = 0.0965, wR2 = 0.1932	
R indices (all data)	R1 = 0.1587, wR2 = 0.2295	
Largest diff. peak and hole	1.134 and -0.485 e.$Å^{-3}$	

The solid IR spectrum of H_2**bistpOp** (Figure 3.6) contains two broad absorption bands at 3,070 and 2,724 cm^{-1} corresponding to the NH groups, involved in hydrogen bonding. The peaks at 1,184 and 1,156 cm^{-1} are assigned to the P=O stretching vibrations, whereas the sharp band at 938 cm^{-1} is characteristic of PNP stretching frequencies.

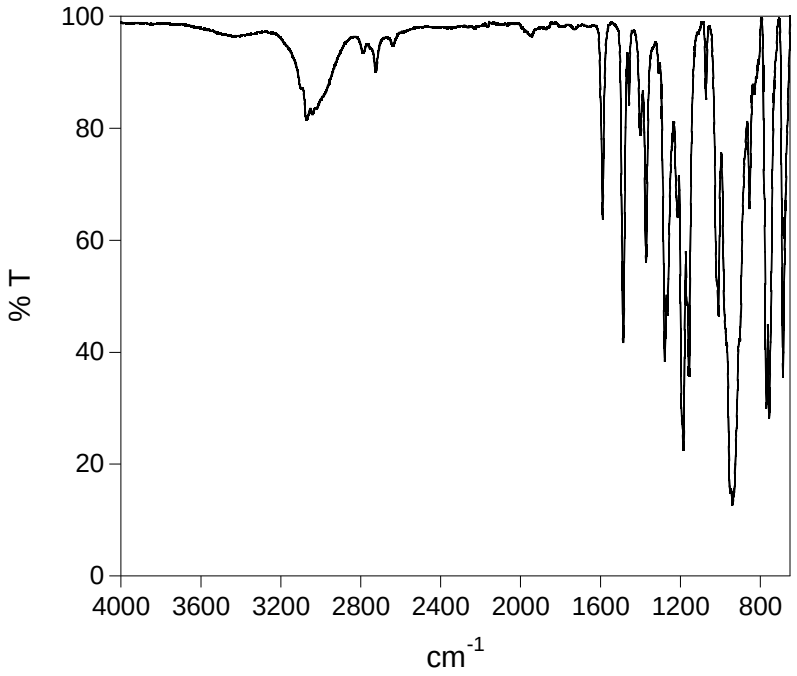

Figure 3.6. The IR spectrum of powder sample of H_2**bistpOp**.

3.3.3. Preparation and characterisation of K_2bistpOp

Deprotonation of the H_2**bistpOp** ligand with 2.1 equivalents of KH in THF (Scheme 3.3) gave the potassium salt of the pentaphenyl diimidotriphosphate in good yield. K_2**bistpOp** was soluble in solvents such as water, methanol, ethanol, acetone and moderately soluble in chloroform.

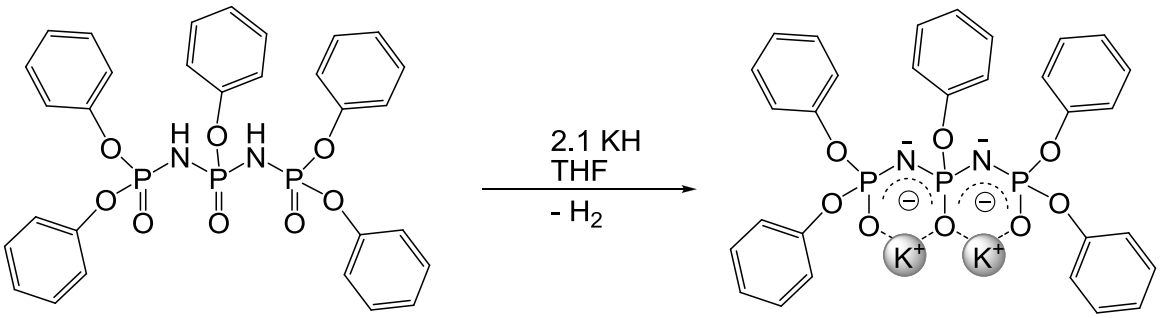

Scheme. 3.3. Synthetic route to K_2**bistpOp**.

The ^{31}P NMR spectrum in D_2O (Figure 3.7) shows two phosphorus resonances in 1:2 ratio. The triplet centred at -4.7 ppm has a coupling constant of $^2J_{P,P}$ = 45.1 Hz and is assigned as the central phosphorus atom. The doublet centred at -9.4 ppm has a coupling constant of $^2J_{P,P}$ = 44.9 Hz, which corresponds to two outer phosphorus atoms. Deprotonation/complexation of the H_2**bistpOp** to give K_2**bistpOp** results in a downfield shift of the phosporus nuclei.

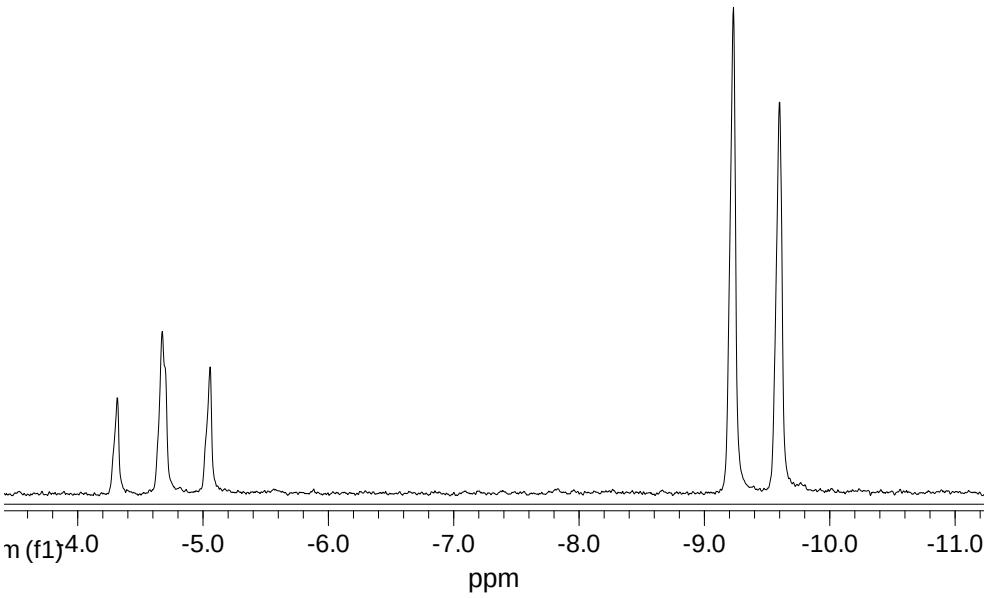

Figure 3.7. The 121 MHz ^{31}P NMR spectrum of K_2**bistpOp** in D_2O.

The ^{1}H NMR spectrum of K_2**bistpOp** in D_2O (Figure 3.8) displays a manifold of peaks in the aromatic region of the spectrum ranging from 7.26 – 7.01 ppm. The manifold corresponds to the aromatic CH protons on the phenoxide rings.

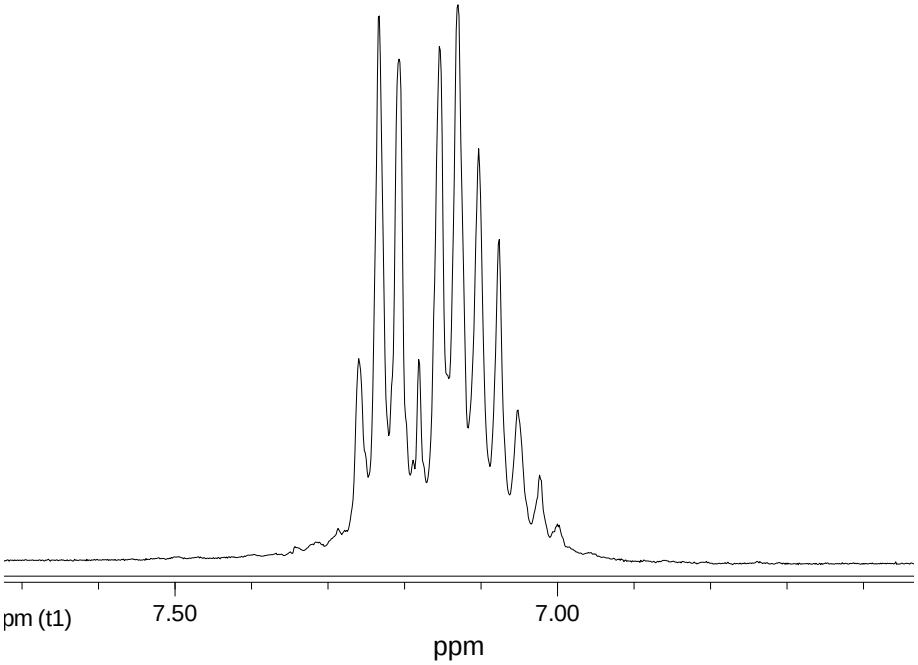

Figure 3.8. The 300 MHz ^{1}H NMR spectrum of K_2**bistpOp** in D_2O.

The ^{13}C NMR spectrum in D_2O displays the correct number of carbon resonances in the aromatic region.

3.3.4. Preparation and characterisation of $Ln_2(bistpOp)_3$ complexes, (Ln = Eu, Tb, Dy, Sm, Gd, Nd, Yb, Er) and $Y_2(bispOp)_3$

The title lanthanide complexes were prepared by reaction of three equivalents of an alcoholic solution of K_2**bistpOp** with two equivalents of aqueous alcoholic solution of $LnCl_3.6H_2O$ yielding the corresponding Ln_2(**bistpOp**)$_3$ complexes as a fine colourless

powder with yields of 58 – 80% (Scheme 3.4). The complexes showed a sufficient solubility in acetone, acetonitrile, methanol, ethanol and THF and chloroform.

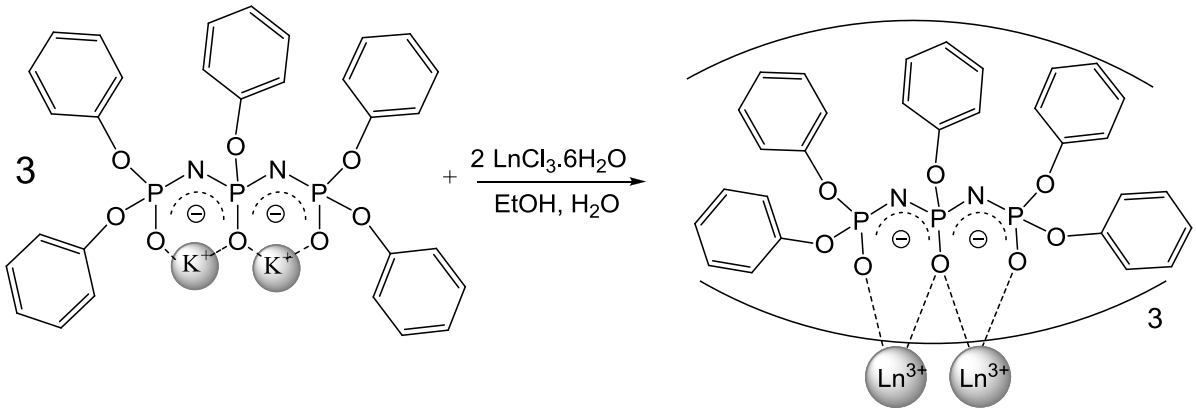

Scheme. 3.4. Synthetic route to Ln_2(**bistpOp**)$_3$ complexes.

The La_2(**bistpOp**)$_3$ and Y_2(**bistpOp**)$_3$ were also synthesised by the same approach as Ln_2(**bistpOp**)$_3$ and studied by NMR spectroscopy. The Y^{3+} ion was chosen because it is a good diamagnetic replacement for Eu^{3+}, whereas the La^{3+} has f^0 electronic configuration, therefore both ions can be used for NMR spectroscopy studies without producing paramagnetic line broadening in the NMR spectra. The ^{31}P, ^{1}H and ^{13}C NMR spectra of the La^{3+} and Y^{3+} complexes of **bistpOp** were obtained in $CDCl_3$ solution. The ^{31}P NMR spectra of La_2(**bistpOp**)$_3$ is illustrated in Figure 3.9. and Y_2(**bistpOp**)$_3$ display similar pattern. Each spectrum shows two resonances in 1:2 ratio at comparable chemical shifts. In both cases the triplet is broaden into a singlet and its resonance is shifted downfield, compare to the free ligand. The doublets centred at -10.1 ppm has a coupling constant of $^2J_{P,P}$ = 55.1 Hz for La_2(**bistpOp**)$_3$ whereas in Y_2(**bistpOp**)$_3$ the doublet is centred at -6.6 ppm with coupling constant of $^2J_{P,P}$ = 49.9 Hz.

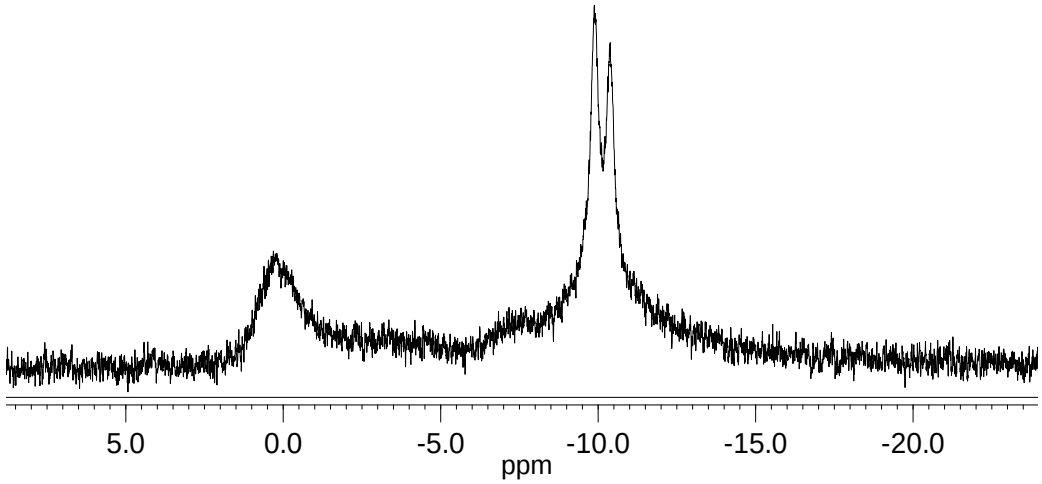

Figure 3.9. The 121 MHz ^{31}P NMR spectrum of La_2(**bistpOp**)$_3$ in $CDCl_3$.

The ^{1}H NMR spectra of the La_2(**bistpOp**)$_3$ (Figure 3.10) and Y_2(**bistpOp**)$_3$ complexes show multiplet signals in the region of 6.70 - 7.10 ppm corresponding to the aromatic protons of phenoxy groups. The multiplet is at lower frequency compared to the free ligand, which displayed a multiplet in the range 7.0 – 7.2 ppm.

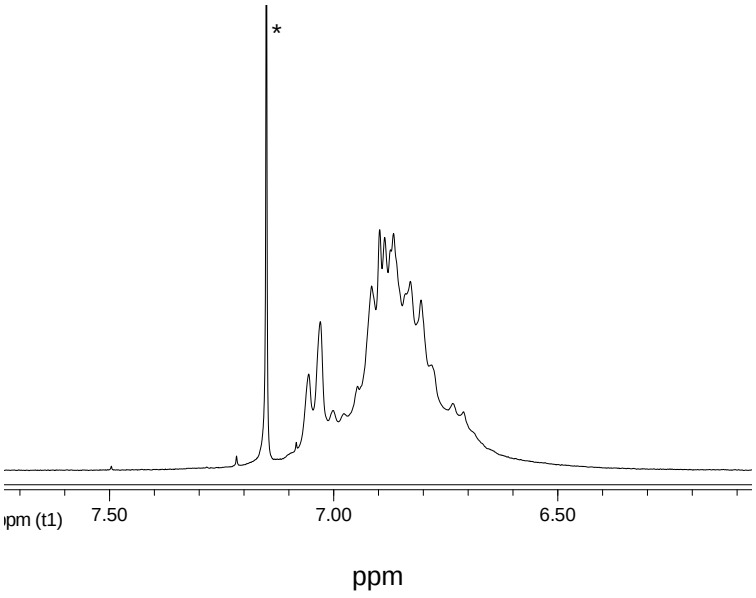

Figure 3.10. The 300 MHz ^{1}H NMR spectrum of La_2(**bistpOp**)$_3$ in $CDCl_3$. (* = solvent).

The symmetry of the complexes is confirmed by the ^{13}C NMR. The spectra show eight NMR peaks, in region of 153.3 – 121.2 ppm, for the 90 carbon nuclei of

La_2(**bistpOp**)$_3$ and Y_2(**bistpOp**)$_3$ complexes. The two quaternary carbons are distinguished by their opposing phase to the six CH carbons.

Only Eu_2(**bistpOp**)$_3$ and Sm_2(**bistpOp**)$_3$ complexes are suitable for ^{1}H and ^{13}C NMR analysis. The other complexes do not give meaningful NMR spectra, because of the very broad paramagnetic spectra, and their spectra are inconclusive.

The ^{1}H NMR spectrum of Eu_2(**bistpOp**)$_3$ in $CDCl_3$ (Figure 3.11) shows a different splitting pattern to the free ligand and to the diamagnetic complexes. The spectrum displays three singlet peaks in 2:2:1 ratio respectively, as well as a multiplet. The broad peak at 7.97 ppm can be assigned as protons H_d of the phenoxide rings attached to the middle phosphorus, which are deshielded the most in their adjacent position closest to Eu^{3+} ions. The protons H_e appears as slightly broadened singlet at 6.69 ppm and the singlet at 5.70 ppm is due to the proton H_f. The remaining aromatic protons H_a, H_b and H_c yield the multiplet at range of 7.02 – 7.37 ppm.

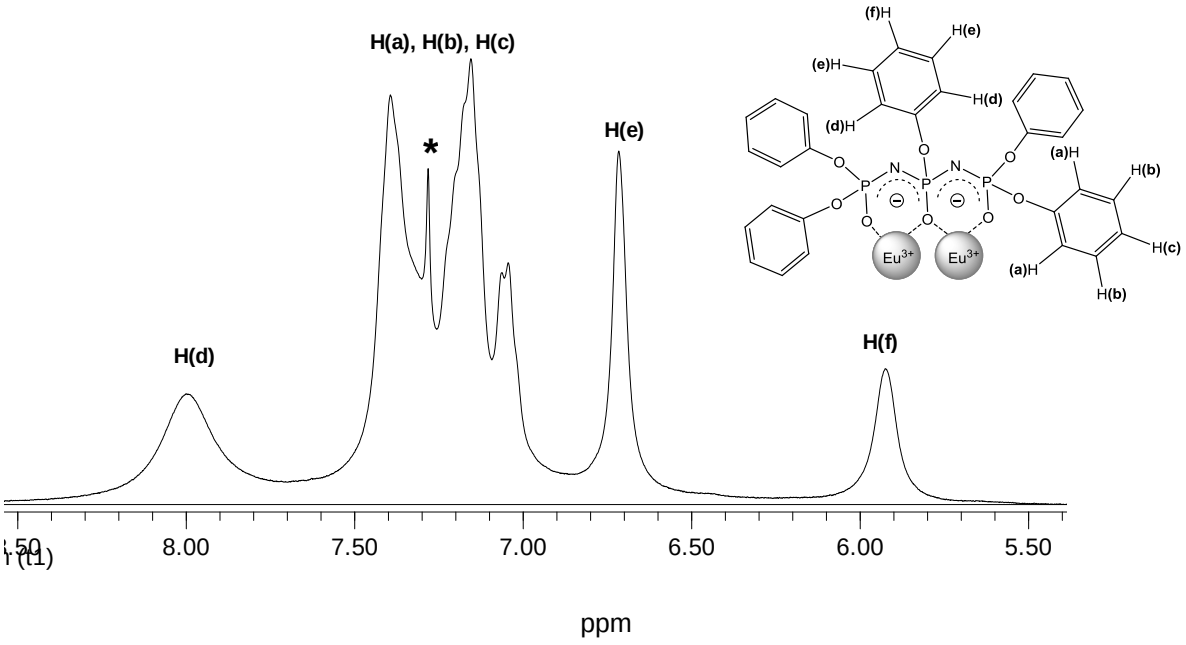

Figure 3.11. The 300 MHz ^{1}H NMR spectrum of Eu_2(**bistpOp**)$_3$ in $CDCl_3$, inset depicts the labelling scheme. (* = solvent).

The ^{1}H NMR spectrum of Sm_2(**bistpOp**)$_3$ displays a similar patter as above for the europium complex.

The ^{1}H-^{1}H COSY spectrum of Eu_2(**bistpOp**)$_3$ and Sm_2(**bistpOp**)$_3$ (See Appendix A2 and A3), display two separate spin systems diagram of cross peaks, which confirm the correct assignment made for both complexes.

Heteronuclear Single-Quantum Correlation (HSQC) spectra, which report ^{1}H-^{13}C correlation, allow the direct assignment of the aromatic CH resonances for Eu_2(**bistpop**)$_3$ and Sm_2(**bistpop**)$_3$ complexes (See Appendix A4 and A5). It is interesting to note that some of the carbon resonances are split into two separate signals as demonstrated in Figure 3.12. This is probably due to the slow interchange of ligand shell around the paramagnetic lanthanide ions.

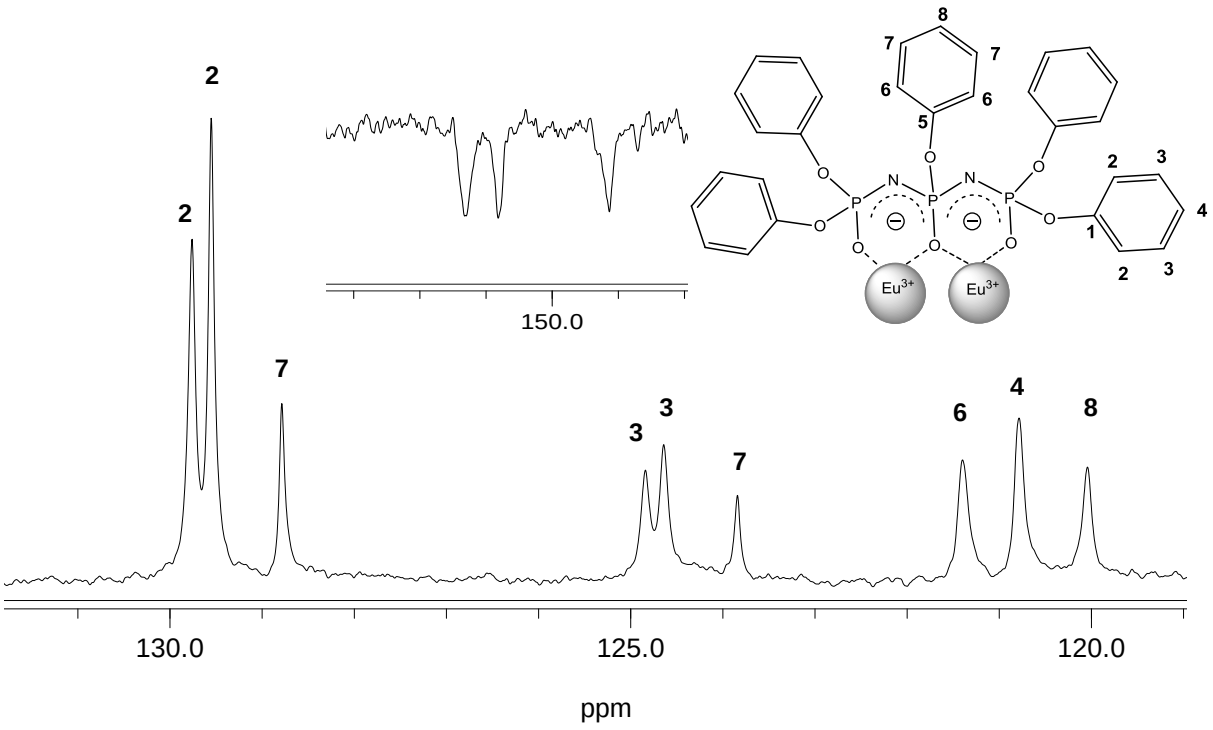

Figure 3.12. The 75 MHz ^{13}C NMR spectrum of Eu_2(**bistpOp**)$_3$ in $CDCl_3$. Inset depicts the labelling scheme.

Mass spectrometry provides another clear indication of complex formulation as MALDI (+ve) mass spectra were successfully obtained for Ln_2(**bistpOp**)$_3$ complexes. In all cases spectra of diamagnetic as well as paramagnetic **bistpOp** complexes show the signal occurring at the predicted mass-to-charge ratio value for the dinuclear species, confirming the formulation of the complexes in 3:2 ratio. In addition, the isotopic distributions of these peaks are in good agreement with the simulated ones as demonstrated in Figure 3.13 and 3.14. The fragments corresponding to 2:1 [Ln(**bistpOp**)$_2$ + 2H]$^+$ stoichiometries are also observed in every spectrum.

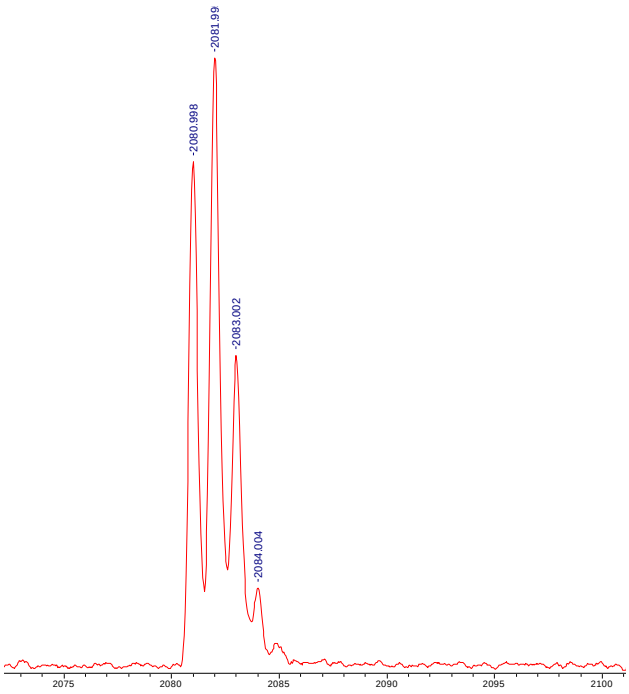

Figure 3.13. Expanded region of MALDI (+ve) mass spectrum of diamagnetic Y_2(**bistpOp**)$_3$ complex, demonstrating the *m/z* = 2081 peak assigned as the $[M + H]^+$ fragment (top), its calculated isotope distribution (bottom).

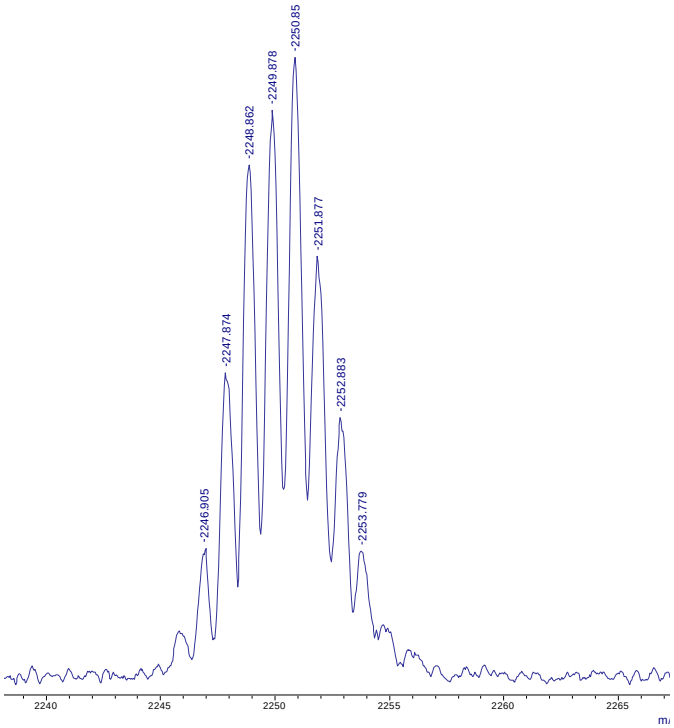

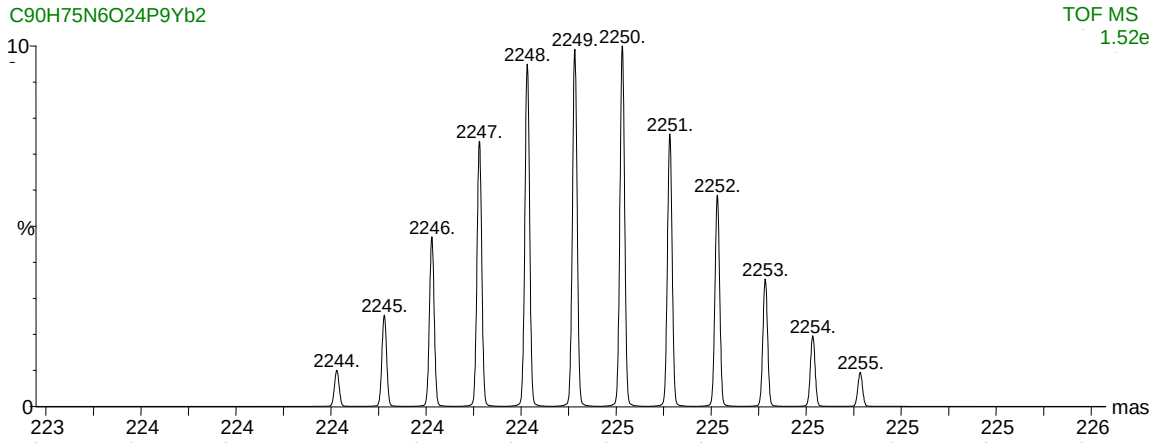

Figure 3.14 Expanded region of MALDI (+ve) mass spectrum of paramagnetic Yb_2(**bistpOp**)$_3$ complex, demonstrating the *m/z* = 2250 peak assigned as the $[M + H]^+$ fragment (top), its calculated isotope distribution (bottom).

The powder IR spectrum of Tb_2(**bistpOp**)$_3$ complex (Figure 3.15) contains a broad band at 1,194 and 1,137 cm^{-1} for the P=O groups. The band is slightly shifted to lower frequencies as a result of coordination to the Tb^{3+} ions. The strong band at 926 cm^{-1} is attributed to the PNP stretching frequency. In addition, there is a weak broad band in the range 3,100 - 3,600 cm^{-1} due to the water. This is in agreement with the elemental analysis for Tb_2(**bistpOp**)$_3$.

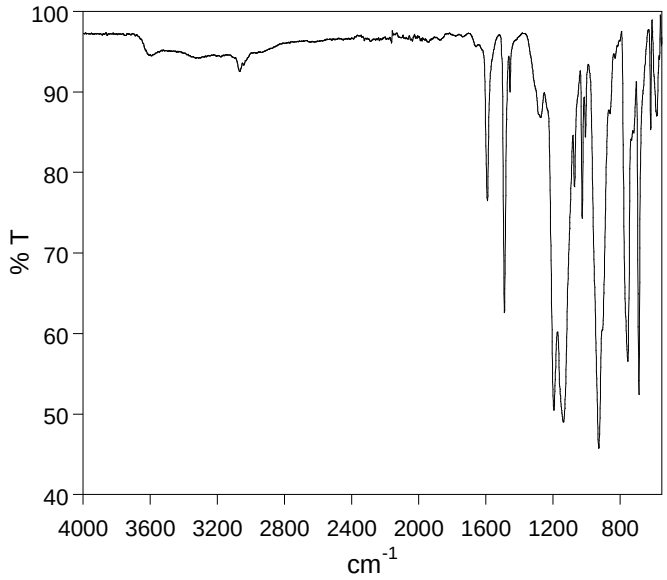

Fig. 3.15. The IR spectrum of powder sample of Tb_2(**bistpOp**)$_3$.

3.3. Photophysical properties of Ln_2(bistpOp)$_3$

3.3.1. Visible emitting complexes

UV-vis absorption spectra of Ln_2(**bistpOp**)$_3$ complexes were recorded in acetonitrile solution at room temperature. The spectra are dominated by the intense π->π*

transitions centred on the phenoxy core, with the maximum at 263 nm, and two weaker bands at 258 and 270 nm respectively, as illustrated in Figure 3.16 for Eu_2(**bistpOp**)$_3$ complex.

No significant changes occur in the shape of the absorption band upon formation of the lanthanide complexes, apart from the red shift of the maximum by 2 nm. The values of the absorption coefficients for the Ln_2(**bistpOp**)$_3$ complexes are 3 times higher than those of the free ligand, in line with the formation of 3:2 complexes. A similar spectral pattern is obtained for all Ln_2(**bistpOp**)$_3$ complexes.

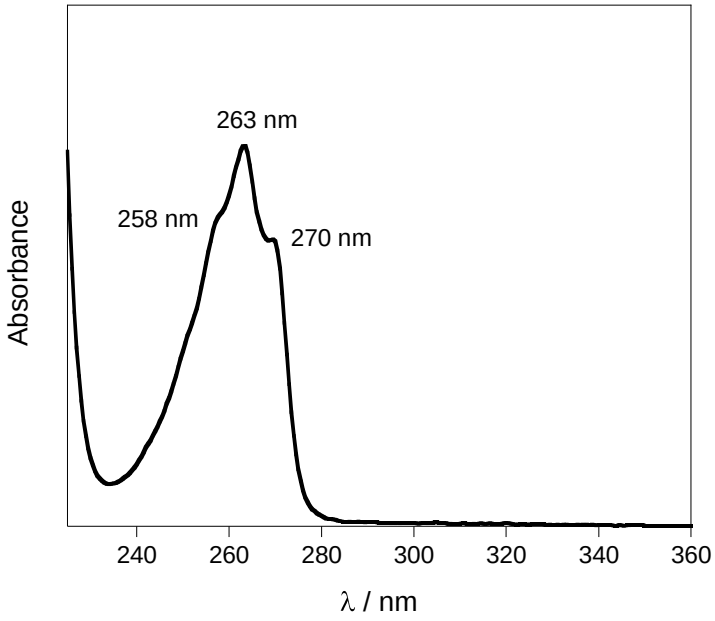

Figure 3.16. The absorption spectrum of Eu_2(**bistpOp**)$_3$ in dry CH_3CN.

The excitation spectra, recorded for the metal-centred emission of the visible Ln_2(**bistpOp**)$_3$ complexes in acetonitrile solution, overlap the absorption spectra of the ligand, which is firm evidence for the energy transfer from the ligand to the lanthanide, as demonstrated in Figure 3.17 for Tb_2(**bistpOp**)$_3$ complex.

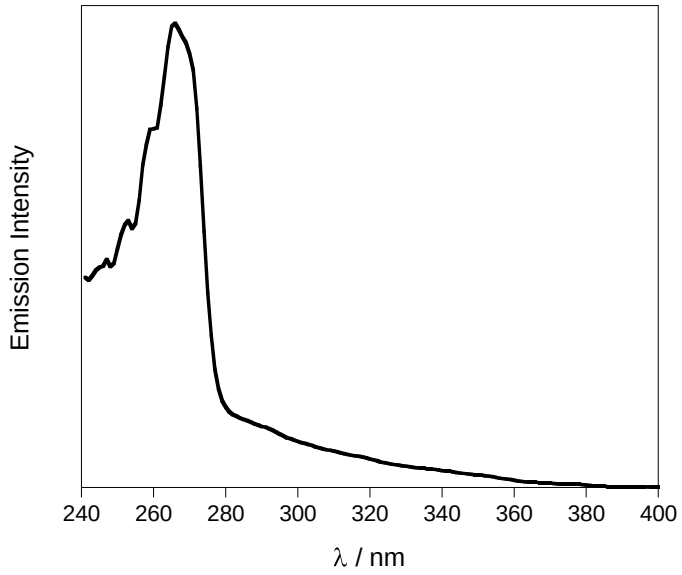

Figure 3.17. The excitation spectrum of Tb_2(**bistpOp**)$_3$ in CH_3CN, λ_{em} = 544 nm.

All of the complexes with luminescent visible lanthanides are found to emit the characteristic line-like emission of the metal ion in the solution upon excitation within the absorption band of the ligand and the emission intensity depends strongly on the lanthanide ion.

The Eu_2(**bistpOp**)$_3$ complex exhibits the characteristically intense transitions of the Eu^{3+} ion upon excitation at 270 nm as shown in Figure 3.18. Emission bands were observed at 577, 591, 612, 653 and 701 nm, and are attributed to the transitions from the excited $^5D_0$ state to different *J* levels of the lower ^7F_J state with *J* = 0, 1, 2, 3, and 4, respectively. The transition of highest intensity is dominated by the hypersensitive $^5D_0$ -> $^7F_2$ transition, which occurs at 612 and 621nm. This transition is much stronger than that of the $^5D_0$ -> $^7F_1$, which indicates that the environment of the Eu^{3+} ions is asymmetric.[10] The presence of only one peak in the region of the $^5D_0$ -> $^7F_0$ transition at 577 nm suggests the existence of a single chemical environment around Eu^{3+} ions.[10]

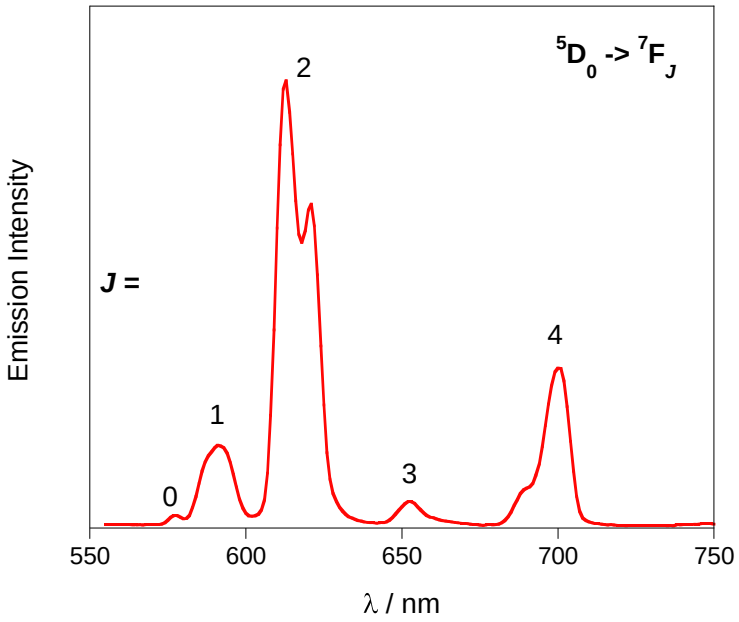

Figure 3.18. Emission spectrum of Eu_2(**bistpOp**)$_3$ in dry CH_3CN, λ_{exc} = 270 nm.

The excitation of the **bistpOp** antenna at 270 nm gave rise to characteristic green Tb^{3+} emission at 487, 544, 585, 619, 650, 668 and 681 nm for the deactivation of the $^5D_4$ excited state to the ground states ^7F_J (J = 6, 5, 4, 3, 2,1, 0), demonstrating its ability to populate the Tb^{3+} excited states (Fig. 3.19). The most intense emission band at 544 nm corresponds to the hypersensitive transition $^5D_4$ -> $^7F_5$.

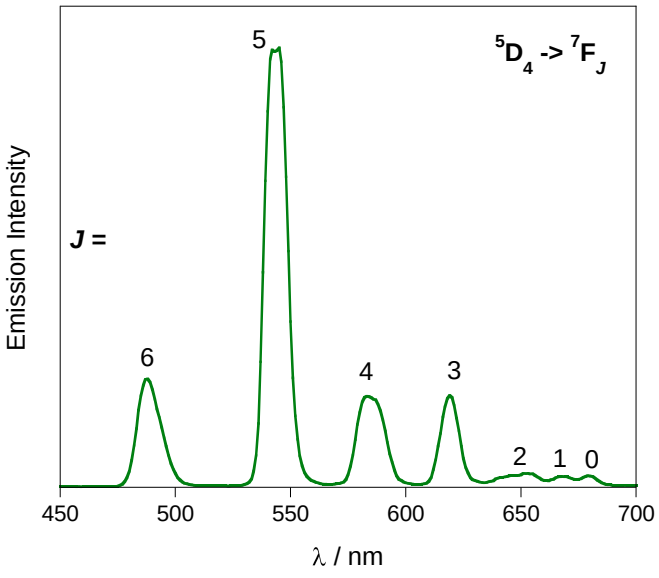

Figure 3.19. Emission spectrum of Tb_2(**bistpOp**)$_3$ in dry CH_3CN, λ_{exc} = 270 nm.

The emission spectrum of Dy_2(**bistpOp**)$_3$ complex (Figure 3.20), after ligand-mediated excitation at 270 nm shows sharp emission bands at 484, 576, 663 and 753 nm attributed to the transitions from the excited state $^4F_{9/2}$ to the $^6H_{15/2}$, $^6H_{13/2}$, $^6H_{11/2}$ and $^6H_{9/2}$ states of Dy^{3+} ion, respectively.

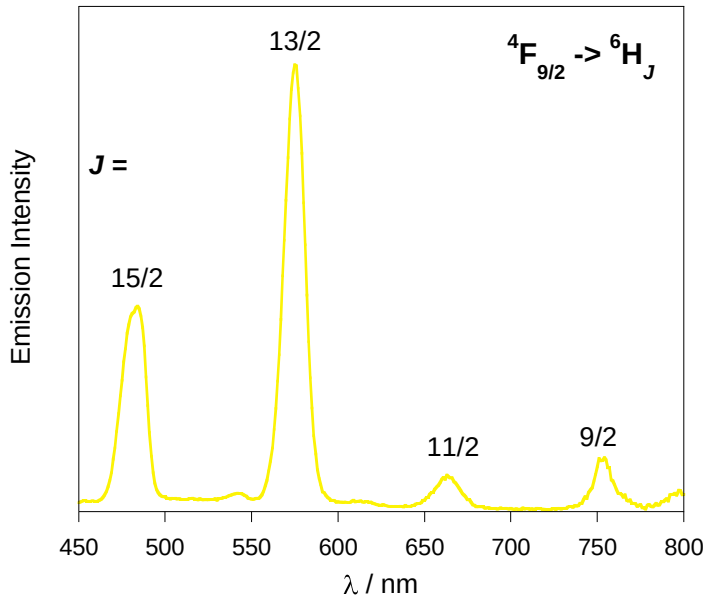

Figure 3.20. Emission spectrum of Dy_2(**bistpOp**)$_3$ in dry CH_3CN, λ_{exc} = 270 nm.

Under ligand excitation the Sm_2(**bistpOp**)$_3$ complex emits a weak characteristic metal-centred luminescence due to $^4G_{5/2}$ -> ^6H_J (J = 5/2, 7/2, 9/2) transitions. The most intense peak at 595 nm corresponds to the hypersensitive transition $^4G_{5/2}$ -> $^6H_{7/2}$ as illustrated in Figure 3.21.

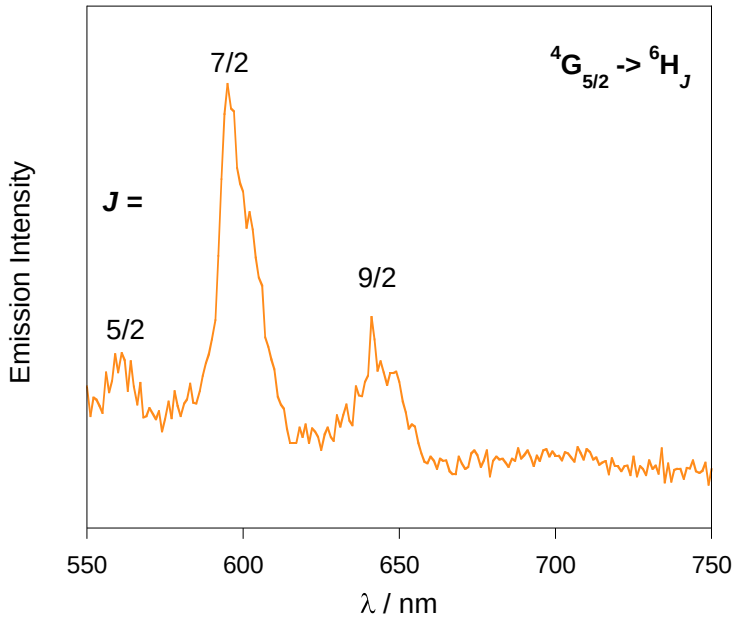

Figure 3.21. Emission spectrum of Sm_2(**bistpOp**)$_3$ in dry CH_3CN, λ_{exc} = 270 nm.

Excitation into the phenoxide absorption manifold of Tb_2(**bistpOp**)$_3$ complex in powder sample results in typical Tb^{3+} emission spectrum (Figure 3.22), comprised of one intense peak at 542 nm corresponding to the hypersensitive $^5D_4$ -> $^7F_5$ transition. The weaker bands at 489, 586 and 621 nm arising from the $^5D_4$ -> $^7F_6$, $^5D_4$ -> $^7F_4$ and $^5D_4$ -> $^7F_3$ transitions, respectively.

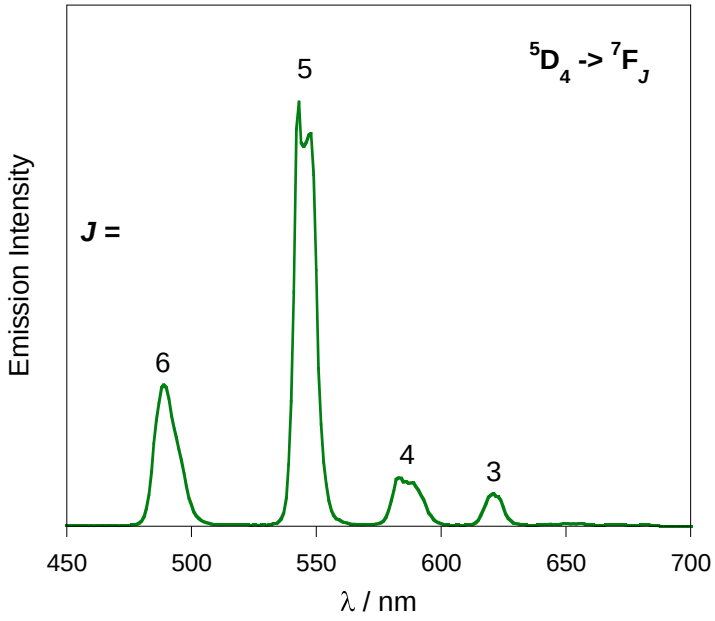

Figure 3.22. Emission spectrum of powder sample of Tb_2(**bistpOp**)$_3$, λ_{exc} = 270 nm.

Under ligand excitation, a powder emission spectrum of Eu_2(**bistpOp**)$_3$ (Figure 3.23) displays the characteristic $^5D_0$ -> ^7F_J (J = 0, 1, 2, 3, 4) transitions of Eu^{3+} with the hypersensitive $^5D_0$ -> $^7F_2$ transition at 613 nm as the most prominent one. The fine structure of the hypersensitive band is clearly different compared to the one in solution. This indicates that the symmetry around the europium ions in solution and solid state is not the same.

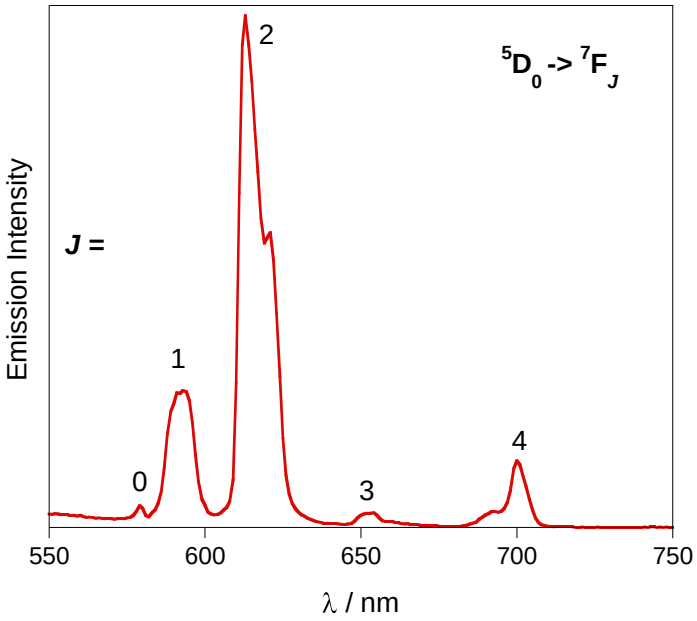

Figure 3.23. Emission spectrum of powder sample of Eu_2(**bistpop**)$_3$, λ_{exc} = 270 nm.

Powder samples of Dy_2(**bistpOp**)$_3$ and Sm_2(**bistpOp**)$_3$ complexes display the characteristic luminescence, but their efficiency in the solid state at room temperature is very low.

It is well documented from luminescence studies of trivalent lanthanide chelates[11] that the general mechanism for the sensitisation of Ln^{3+} ion luminescence *via* "antenna effect" involves the following steps. Firstly, the organic chromophore is excited to the first excited singlet state, followed by non-radiative intersystem

crossing from the singlet to triplet state. Then intramolecular energy transfer takes place, from the ligand-centred triplet state to the excited 4*f* states of the Ln^{3+} ion. Finally, the characteristic lanthanide emission is achieved by radiative transition from the lowest Ln^{3+} excited state to the ground state. Therefore, the intramolecular energy efficiency from the ligand to the Ln^{3+} is one of the most important factors determining the luminescence properties of lanthanide complexes.[11]

In an effort to demonstrate the energy transfer process, the ligand centred triplet excited state energy was measured from Gd_2(**bistpOp**)$_3$ complex. Because the Gd^{3+} ion lacks an appropriate positioned electronic acceptor level,[12] the phosphorescence of the ligand can be observed by luminescence measurement at 77 K. Excitation at 270 nm of Gd_2(**bistpOp**)$_3$ in MeOH/EtOH (20:80) solution, results in a ligand-centred emission, displaying one broadband with the maximum around 326 nm. Upon cooling the solution to 77K, the Gd_2(**bistpOp**)$_3$ spectrum reveals an intense structured emission band from 340 to 480 nm, assigned to phosphorescence from the ligand T_1 excited state (Figure 3.24). The lowest T_1 excited state energy is calculated at 28,736 cm^{-1}. The phosphorescence spectra shows resolved vibronic transitions and their calculated energies are summarised in Table 3.2. The singlet state energy level of the H_2**bistpOp** is estimated at 37,038 cm^{-1} by fluorescence and absorbance cross-section of Gd_2(**bistpOp**)$_3$.

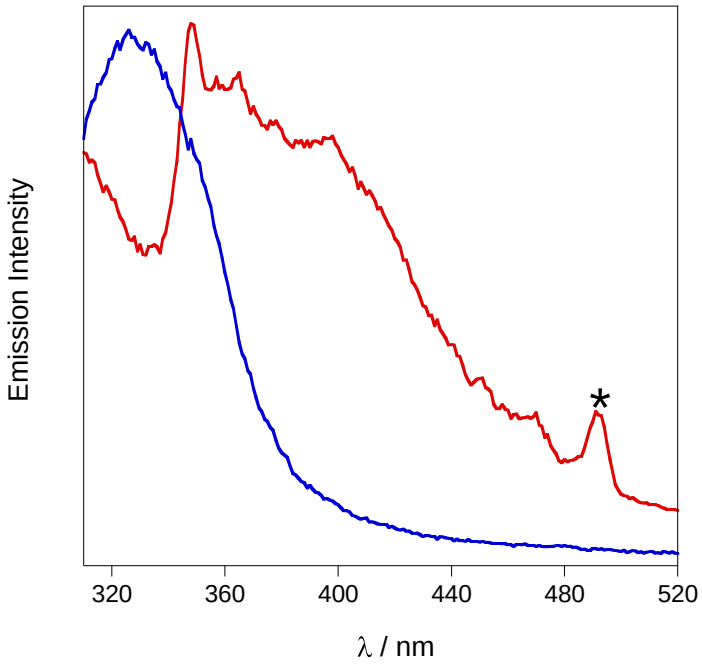

Figure 3.24. Room emission spectra (blue) and 77K (red) spectra of Gd_2(**bistpOp**)$_3$ in EtOH:MeOH (4:1), λ_{exc} = 270 nm. (* = scattered light).

Table 3.2. T_1 -> S_0 phoshorescent vibronic transitions in Gd_2(**bistpOp**)$_3$ at 77K.

λ_{max} (nm)	ν-ν'	Energy (cm^{-1})
348	0 - 0	28,736
365	0 - 1	27,397
378	0 - 2	26,455
397	0 - 3	25,189

The energy of the triplet state of **bistpOp** (28,736 cm^{-1}) is 1,339 cm^{-1} higher, when compared to the value obtained *via* an identical analysis for **tpOp** (27,397 cm^{-1}). Therefore, the increase of the energy gap can be expected to decrease the sensitisation efficiency from **bistpOp** ligand.

Luminescence efficiency has been assessed by quantum yield determination upon ligand excitation at 270 nm for Ln_2(**bistpOp**)$_3$ complexes (Ln = Tb, Ey, Dy and Sm). In the case of Dy_2(**bistpOp**)$_3$ and Sm_2(**bistpOp**)$_3$ complexes the emissions signals were detectable but no sufficiently intense for allowing the calculation of the quantum yield.

The quantum yield values were measured by using a relative method with quinine sulphate in 1N H_2SO_4[13] and $[Ru(bpy)_3]Cl_2$ in H_2O[14] for Tb_2(**bistpOp**)$_3$ and Eu_2(**bistpOp**)$_3$ respectively. The quantum yield of the Tb_2(**bistpOp**)$_3$ in CH_3CN was measured to be 10.4% and 0.72% for the Eu_2(**bistpOp**)$_3$ complex. One of the reasons behind the poor emission efficiency of Ln_2(**bistpOp**)$_3$ complexes is probably due to the inefficient energy transfer because of the large energy gap between the ligand triplet state and the excited state of lanthanides.

Comparison of the emission spectra of four solutions of same concentration of Ln_2(**bistpOp**)$_3$ complexes, allows that the transition intensity changes in order of $Tb^{3+} > Eu^{3+} > Dy^{3+} > Sm^{3+}$, which means that the energy transfer from the **bistpOp** ligand to Tb^{3+} and Eu^{3+} is more effective than that of Dy^{3+} and Sm^{3+}. If one considers the simplistic reasoning on energy gaps only, it is evident from Scheme 3.5. that Dy^{3+} ($^4F_{9/2}$; 21,100 cm^{-1}) and Tb^{3+} ($^5D_4$; 20,500 cm^{-1}) are better matched in energy to the proposed triplet level of the **bistpOp.**

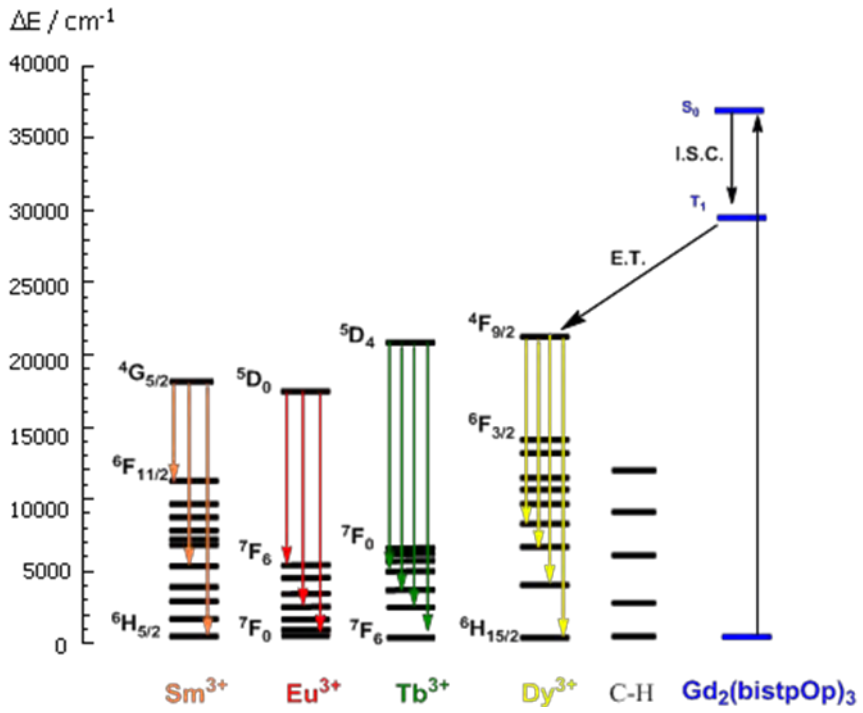

Scheme 3.5. Energy level diagram showing the lowest Ln^{3+} excited states and the estimated triplet state of the **bistpOp** sensitiser in the Gd_2(**bistpOp**)$_3$ complex.

However, from the photophysical studies reported above the more efficient emitters of **bistpOp** complexes are Tb^{3+} and Eu^{3+} ions. Therefore, consideration of the ligand triplet energy level does not give a full account of the experimental observations. This behaviour can be explained by differences in the vibrational levels of the lowest excited state and the highest ground state of Tb^{3+}, Eu^{3+}, Dy^{3+} and Sm^{3+} ions.

In the case of Eu^{3+} and Tb^{3+} the energy gaps are $\Delta E \sim 12{,}300$ and $\Delta E \sim 14{,}800$ cm^{-1} respectively, therefore only the high energy C-H oscillators contribute to the quenching of their luminescent states. On the other hand, Dy^{3+} and Sm^{3+} have considerably smaller energy gaps of $\Delta E \sim 7{,}900$ cm^{-1} and $\Delta E \sim 7{,}400$ cm^{-1} respectively, hence the effect of lower energy C-H vibrational oscillations has a great ability to efficiently quench the *f-f* transition.[15]

Another phenomenon causing the quantum yield reduction may be due to the close Ln^{3+}- Ln^{3+} distance, which results in concentration quenching, when the distance between Ln^{3+} ions themselves is less than 8.4 Å.[16] Despite the failed attempts to grow crystals suitable for XRD analysis, construction of a model of Y_2(**bistpOp**)$_3$ was achieved by molecular mechanic calculations, using the MM2 force field.[17] From the energy minimised model of Y_2(**bistpOp**)$_3$ complex, the measured distance between two metal centres is only ~ 3.7 Å (Figure 3.25), which further confirms the reasoning stated above.

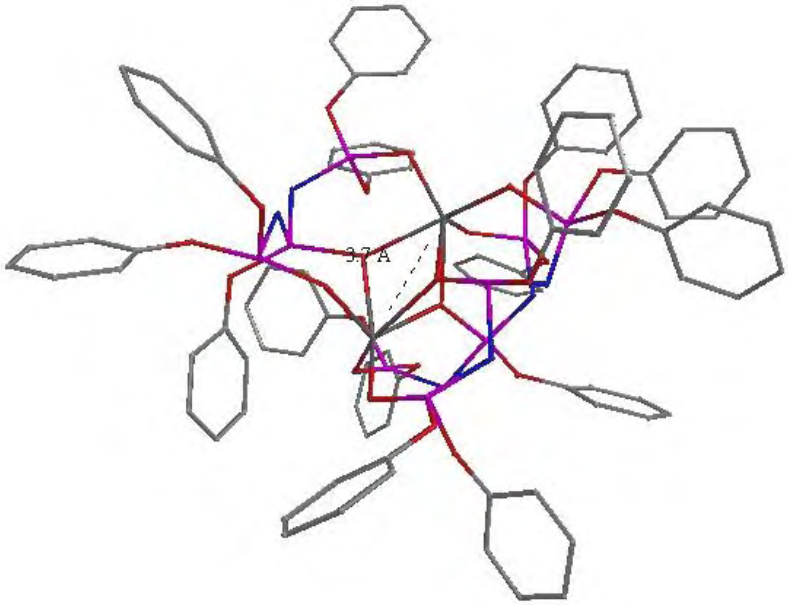

Figure. 3.25. Chem3D model of Y_2(**bistpOp**)$_3$.

In order to better characterise the sensitisation process, the luminescence lifetimes of Ln_2(**bistpOp**)$_3$ (Ln = Tb, Eu) complexes were determined in solution and solid state and results are presented in Table 3.3. In the case of Dy_2(**bistpOp**)$_3$ and Sm_2(**bistpOp**)$_3$ the signal was too small to adjust the value.

Table 3.3. Luminescence lifetimes of the Tb^{3+} ($^5D_4$), Eu^{3+} ($^5D_0$) levels in Ln_2(**bistpOp**)$_3$ (Ln = Tb, Eu) (λ_{exc} = 270 nm). [a] = 10 mol dm^{-3}.

	τ CH_3CN (ms)	**τ CH_3CN + H_2O[a] (ms)**	**τ powder**
Tb_2(**bistpOp**)$_3$	2.5	1.4	1.5
Eu_2(**bistpOp**)$_3$	1.4	0.6	0.9

The time-resolved emission profiles of Tb_2(**bistpOp**)$_3$ and Eu_2(**bistpOp**)$_3$ complexes reveal single-exponential decays as illustrated in Figure 3.26 for Tb_2(**bistpOp**)$_3$ complex. No significant improvements in fit were observed on applying a secondary exponential component to decay profiles, which indicates that two Ln^{3+} ions in complexes are located in the same parity sites.

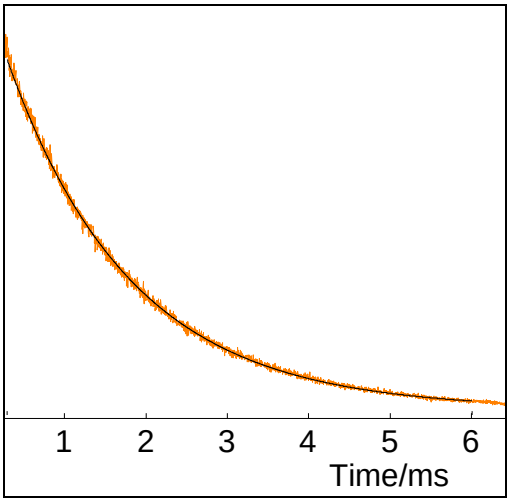

Figure 3.26. The fitted single- exponential decay of Tb_2(**bistpOp**)$_3$ in dry acetonitrile, λ_{exc} = 270 nm and λ_{em} = 544 nm.

Application of the lifetimes to the determination of the inner sphere solvation of Tb^{3+} and Eu^{3+} was undertaken using the relation in equation 3.1:

$$q = A\,(k_{H2O} - k_{CH3CN}) \qquad \textbf{(eq. 3.1)}$$

This equation can be used with CH_3CN as the solvent by measuring the lifetimes following the addition of equal amounts of H_2O to the CH_3CN solution. ***q*** (uncertainty ± 0.5) is the number of coordinated water molecules in the primary coordination sphere, ***A*** is a proportionality constant (A_{Eu} = 1.05, A_{Tb} = 4.2), $\boldsymbol{k_{H2O}}$ is observed decay rate in aqueous CH_3CN, $\boldsymbol{k_{CH3CN}}$ is the observed decay rate in dry CH_3CN.[18] The application of Equation 3.1 to the values presented in Table 3.3 give q = 1.3 ± 0.5 and q = 1.1 ± 0.5 for Tb_2(**bistpOp**)$_3$ and Eu_2(**bistpOp**)$_3$ respectively, in aqueous CH_3CN. The calculated q values suggest that one solvent molecule is coordinated to each Tb^{3+} and Eu^{3+} ions in Tb_2(**bistpOp**)$_3$ and Eu_2(**bistpOp**)$_3$ complexes, respectively. The same is expected for Dy^{3+} and Sm^{3+} **bistpOp** complexes, since they have analogous coordination chemistry.

Although the **bistpOp** ligand sensitise visible luminescence of Tb^{3+}, Eu^{3+}, Sm^{3+} and Dy^{3+} ions, coordinated water molecules and proximate C-H oscillators quench the excited states of these ions and limit their emission efficiency.

The luminescence properties of Ln_2(**bistpOp**)$_3$ complexes are not as good as other dinuclear complexes. As a comparison, quantum yields of 5% and 0.16% were reported for dinuclear Eu^{3+} and Sm^{3+} complexes based on bis-diketonate ligands, which were previously developed in our research group.[8] These ligands displayed good chromophoric and energy transfer properties for Sm^{3+} and Eu^{3+} ions due to the well matched position of the ligand-centred triplet states. Natrajan *et al.*[19] reported a high quantum yield of 50% and lifetime of 2.6 ms in aqueous solution for dinuclear terbium complex based on the septadentate chelate 5-Me-HXTA (*N,N*,-(2-hydroxy-5-methyl-1,3-xylylene)bis(*N*-(carboxymethyl)glycine). The high quantum yield and

lifetime value is due to the absence of solvent molecules in first coordination sphere. Bünzli *et al.*[20] showed high luminescence efficiency of Eu^{3+} bimetallic helicates with the quantum yields ranging between 24 – 19% and long luminescence lifetimes of 4.7 – 4.2 ms in D_2O and 2.4 ms in H_2O, with the hydration numbers of almost zero. Several other research groups reported better photophysical properties for dinuclear lanthanide helicates based upon organic ligands.[21,22]

The luminescence titration of K_2**bistpOp** with $TbCl_3 \cdot 6H_2O$ in MeOH was performed in order to further investigate the stoichiometry of the lanthanide complexes (Fig. 3.27). A plot of normalised emission intensity *vs*. equivalents of Tb^{3+} (Figure 3.28) shows a plateau at 2 equivalents of Tb^{3+} per three ligands in solution. After this point, the binding sites of the ligands in solution become saturated and no more Tb^{3+} is accommodated. The result clearly demonstrates the stoichiometry of Ln_2(**bistpOp**)$_3$ is 3:2 ligand to metal in solution.

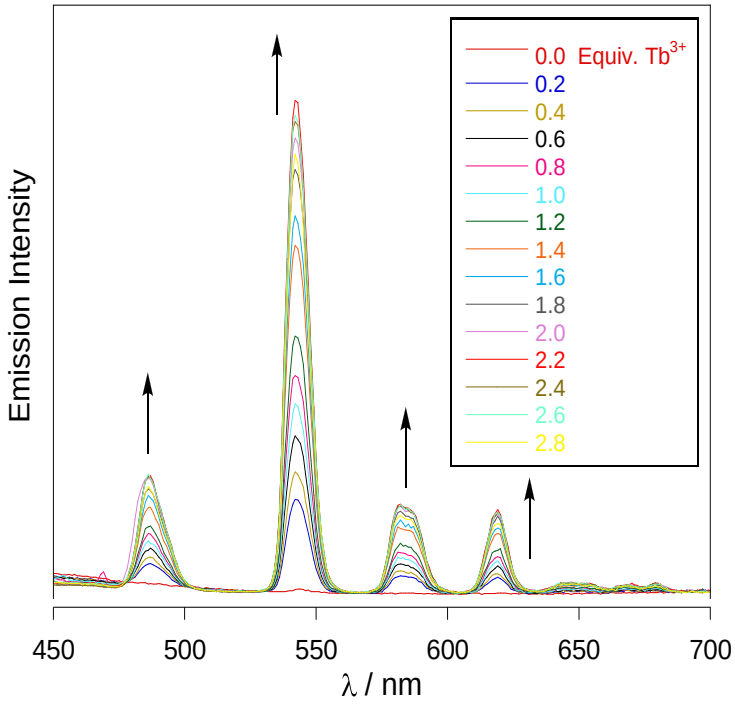

Figure 3.27. Emission spectra of titration of K_2**bistpOp** against $TbCl_3.6H_2O$ in MeOH, λ_{exc} = 270 nm.

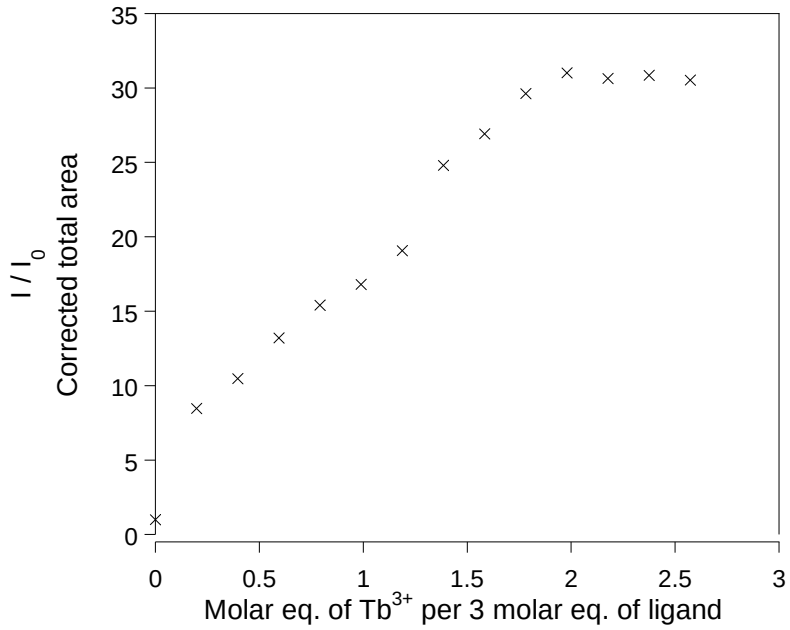

Figure 3.28. Plot of normalised emission intensity (I / I_0) *vs.* molar equivalents of Tb^{3+} per 3 molar equivalents of ligand in MeOH, λ_{exc} = 270 nm.

3.3.2. Photophysical properties of NIR emitting complexes

The absorption spectra of Ln_2(**bistpOp**)$_3$ (Ln = Yb, Nd, Er) in acetonitrile all display the structured absorbance with the maximum at 263 nm, which corresponds to the π–π* electronic transitions of phenoxide moieties as illustrated in Figure 3.29 for the Yb_2(**bistpOp**)$_3$ complex.

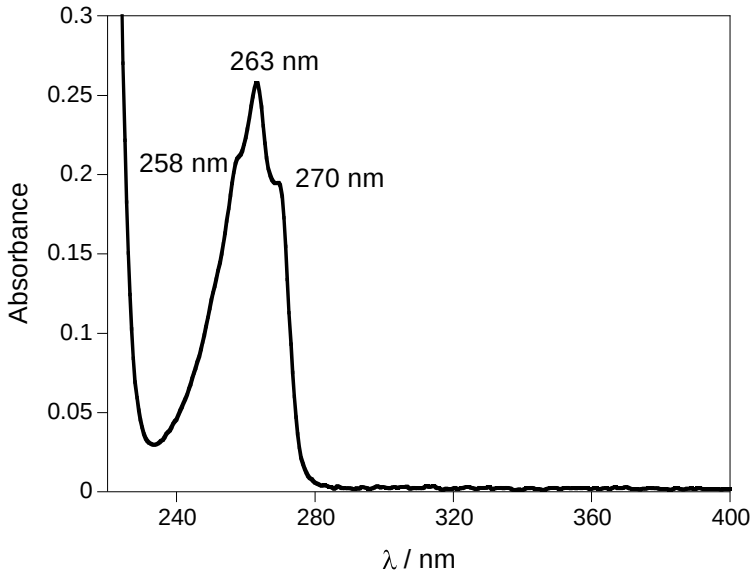

Figure 3.29. The absorption spectrum of Yb_2(**bistpOp**)$_3$ in CH_3CN.

As demonstrated in Figure 3.30, upon band excitation through the ligand at 270 nm in acetonitrile solution at room temperature, the Yb_2(**bistpOp**)$_3$ complex shows a weak luminescence corresponding to the *f-f* NIR transitions, which are characterised by a band in the 920 – 1100 nm range, assigned to the $^2F_{5/2}$ -> $^2F_{7/2}$ transition, with a maximum at 984 nm and broader component at longer wavelengths due to vibronic transitions.[23]

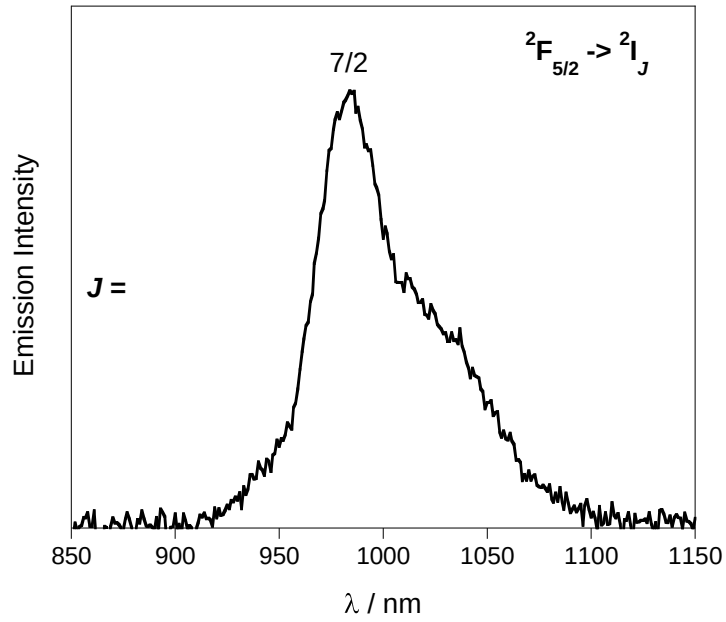

Figure 3.30. Emission spectrum of Yb_2(**bistpOp**)$_3$ in dry CH_3CN, λ_{exc} = 270 nm.

Sensitisation of the NIR luminescence by **bistpOp** is ascertained by the excitation spectrum of Yb_2(**bistpOp**)$_3$ (Figure 3.31) complex, which clearly demonstrates the antenna effect of the ligand with component matching the absorption bands of the electronic spectrum.

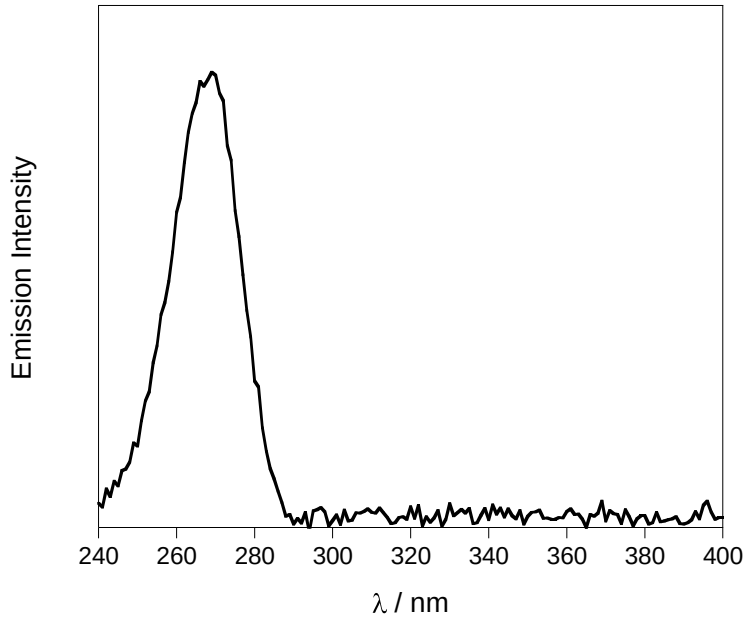

Figure 3.31. Excitation spectrum of Yb_2(**bistpOp**)$_3$ in dry CH_3CN, λ_{em} = 984 nm.

However, the weak metal-centred NIR emission observed for the Yb_2(**bistpOp**)$_3$ complex prevented us from measuring the corresponding lifetime.

In the case of Nd_2(**bistpOp**)$_3$ and Er_2(**bistpOp**)$_3$ complexes no emission was detected upon the ligand excitation at 270 nm. The poor luminescence properties of Yb_2(**bistpOp**)$_3$ and non emissive behaviour of Nd_2(**bistpOp**)$_3$ and Er_2(**bistpOp**)$_3$ complexes is not surprising. The reasons for this are 4-fold. Firstly, on the basis of the energy level of the ligand based triplet state, the triplet energy level of **bistpOp** is too high to provide an efficient sensitisation for the NIR lanthanide luminescence. Secondly, C-H vibrational oscillators, which have a great ability to efficiently quench *f-f* transitions, are located in the surrounding of the emitting ions. Thirdly, the probable presence of water molecules in the inner coordinated sphere of lanthanide centres quench luminescence performances of NIR Ln_2(**bistpOp**)$_3$ complexes as O-H vibrations are very efficient inhibitors of NIR luminescence. Fourthly, insufficient spacing (~ 3.7 Å) between two lanthanide ions results in concentration quenching.

However, it can be seen from Scheme 3.6 that in theory the energy transfer should be more efficient for Nd^{3+} because the $^4F_{3/2}$ state is higher in energy compared to the $^2F_{5/2}$ of Yb^{3+} ion.

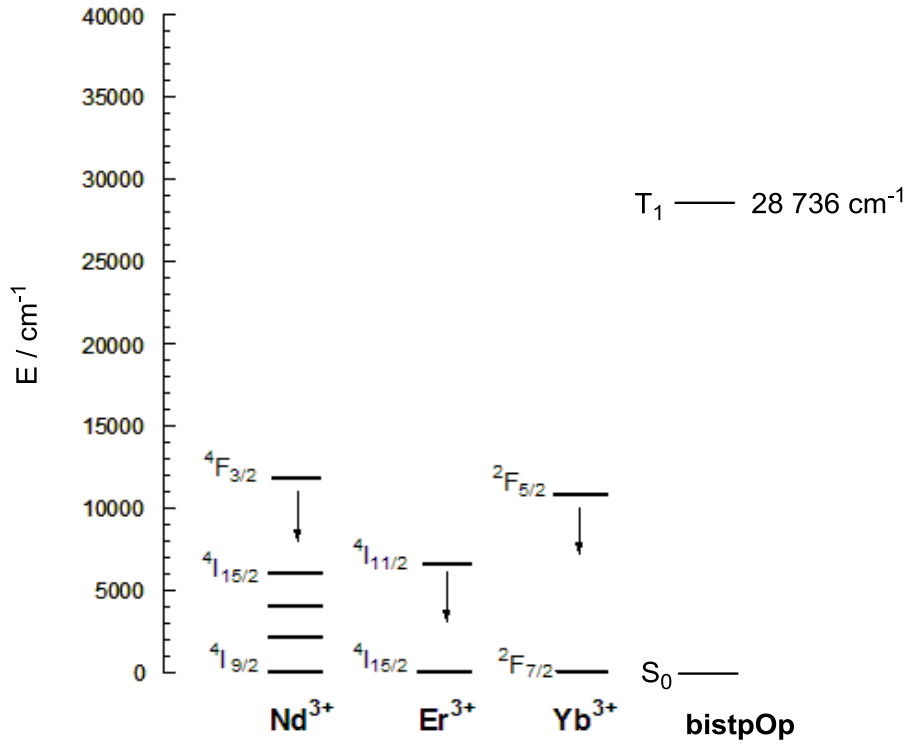

Scheme 3.6. The energy diagram of the 4f levels responsible for the lanthanide luminescence.

The poorer luminescence properties of Nd_2(**bistpOp**)$_3$ can be explained by Nd^{3+} being more sensitive to high energy oscillations than Yb^{3+}, due to more electronic states at high energy, which matches well with the C-H bond vibrations. Also the energy gap ΔE between the $^4F_{3/2}$ emissive state of Nd^{3+} and the $^4I_{15/2}$ highest sublevel (ΔE ~ 5,400 cm^{-1}) is smaller compare to the Yb^{3+} (ΔE ~ 10,250 cm^{-1}), hence it is easily matched by C-H and O-H vibrations, therefore the Nd^{3+} excited state gets more effectively quenched.[24]

3.4. Conclusion

In this chapter the H**bistpOp** ligand was synthesised and fully characterised. The self-assembly of three ligands around two Ln^{3+} ions led to formation of neutral dinuclear lanthanide Ln_2(**bistpOp**)$_3$ complexes. NMR spectroscopy and mass spectrometry has been used to characterise novel lanthanide complexes. The stochiometry of 3:2 ligand:metal in the lanthanide complexes was demonstrated by a titration of K_2**bistpOp** with $TbCl_3.6H_2O$.

The sensitising properties of the **bistpOp** ligand have been investigated by luminescence spectroscopy. Photophysical studies of the Gd_2(**bistpOp**)$_3$ complex at low temperature allowed the excited triplet state energy level of phenoxide moieties to be evaluated. The energy level of the ligand $^3\pi\pi^*$ state is too high, which prevents efficient population of the luminescent states of visible and in particularly near-infrared emitting Ln^{3+} ions. Poor photophysical properties can be also explained by an additional 15 C – H oscillators in **bistpOp** complexes compared to those of **tpOp**, as well as the short distance of ~ 3.7 Å between Ln^{3+} ions themselves, which results in concentration quenching. Furthermore, calculation of the number of inner-sphere solvent molecules in Ln_2(**bistpOp**)$_3$ showed that the **bistpOp** does not shield two lanthanide efficiently against the solvents coordination. The investigated Ln_2(**bistpOp**)$_3$ (Ln = Tb^{3+}, Eu^{3+}) have two water molecules present, one bound to each lanthanide ion. The same trend is expected for the rest of the complexes, since they have analogous coordination chemistry. Water coordinated molecules to Ln^{3+} ions render complexes amenable to quenching by O-H vibrations, especially in the case of the NIR-emitting ions. This is confirmed by the very short excited lifetimes and low quantum yields found for Ln_2(**bistpOp**)$_3$ complexes. Photophysical studies

into the visible emitting lanthanide complexes demonstrated that the ligand-to-Ln^{3+} energy transfer is most efficient for Tb^{3+} and Eu^{3+} ions.

Photophysical experiments of Nd_2(**bistpOp**)$_3$, Yb_2(**bistpOp**)$_3$ and Er_2(**bistpOp**)$_3$ complexes established that the **bistpOp** sensitiser was not suitable for population of the luminescent low lying states of Nd^{3+} and Er^{3+} ions. In the case of Yb_2(**bistpOp**)$_3$ complex, sensitisation of the Yb^{3+} luminescence was ascertained by the excitation spectrum, however, the observed emission was very weak in solution, which prevented further investigation of luminescence properties such as measurement of the luminescence lifetime.

3.5. Experimental

3.5.1. Materials

All reagents were purchased from Aldrich or Alfa Aesar and were used as received. NaH and KH were purchased as 60% and 35% dispersion in mineral oil which was removed prior to use by succesive washing with hexane or pentane.

Anhydrous toluene was freshly distilled over sodium-benzophenone.

3.5.2. Preparation of Pentaphenyl Diimidotriphosphate (H_2bistpOp)

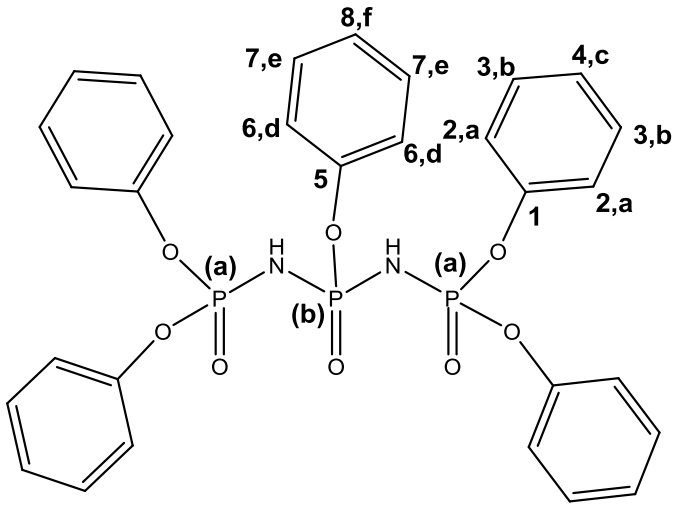

H_2bistpOp

A solution of diphenyl phosphoramidate (5.35 g, 21.48 mmol) and sodium hydride (0.82 g, 60% dispersion, 20.5 mmol) in dry toluene (75 cm^3) was stirred at room temperature for 15 mins. Then triphenyl phosphate (3.31 g, 10.1 mmol) in dry toluene (20 cm^3) was added and the mixture heated at reflux for 4 hours. The mixture was then cooled to room temperature and the suspension of NaH (0.82 g, 60% dispersion, 20.4 mmol) in dry toluene (10 cm^3) was added into the stirring

reaction mixture, followed by the addition of triphenyl phosphate (3.30 g, 10.1 mmol) in dry toluene (20 cm^3). The mixture was refluxed for 3 hours, after which time yellow-white suspension was formed. The mixture was then cooled to room temperature and water (200 cm^3) was added. The resulting two phases were separated and the aqueous layer was acidified with diluted HCl (35 cm^3, 1 M) resulting in formation of a white suspension. In order to remove phenol produced in reaction and unreacted triphenyl phosphate, the aqueous phase was repeatedly stirred with cyclohexane (50 cm^3) over night. The phases were separated and the resulting solid in the aqueous layer was collected by filtration. The crude product was then recrystallised from acetone-water (1:5) giving a white solid, which was dried under high vacuum to yield H_2bistpOp as the desired product (5.8 g, 90 %). Single crystals of H_2bistpOp suitable for an X-ray diffraction analysis were grown by slow evaporation from a chloroform solution. $^{31}P\{^1H\}$ NMR (121 MHz, $CDCl_3$): δ = - 6.1 (t, $^2J_{P,P}$ = 11.1 Hz), - 10.45 (d, $^2J_{P,P}$ = 11.1 Hz); $^{13}C\{H\}$ NMR (75 MHz, $CDCl_3$): δ = 150.2 (C_1), 150.1 (C_5), 129.6 (C_2), 129.5 (C_6), 125.3 (C_3), 125.2 (C_7), 120.7 (C_4), 120.5 (C_8); ^1H NMR (300 MHz, $CDCl_3$): δ = 7.02 – 7.20 (m, 25H, Ar); ES-MS(+): *m/z*: 659.1 $[M + Na]^+$; elemental analysis calcd. (%) for $C_{30}H_{27}N_3O_8P_3$: C, 56.61; H, 4.28; N, 4.40; found C, 56.60; H, 4.16; N 4.49; UV-Vis (CH_3CN) λ_{max} in nm (log ε): 261 (3.2).

3.5.3. Preparation of K_2bistpOp

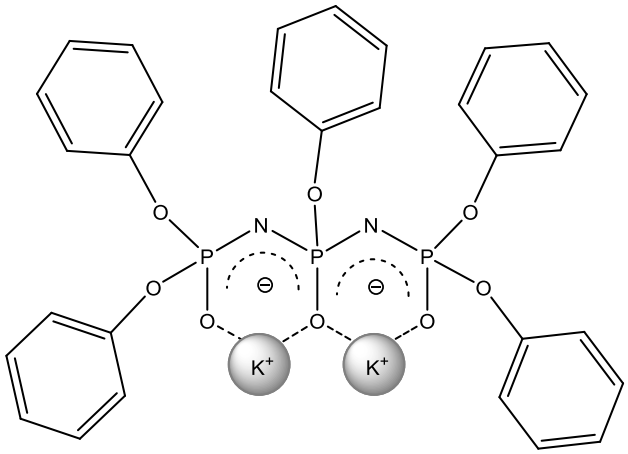

K_2bistpOp

Potassium hydride (0.49 g, 35% dispersion in mineral oil, 3.69 mmol) was washed with pentane (3 x 5 cm^3) and dried *in vacuo* for 20 min. THF (8 cm^3) was added, followed by pentaphenyl diimidodiphosphate (1.54 g, 3.20 mmol) dissolved in THF (15 cm^3). The resulting suspension was stirred for 1 h at room temperature. The solvent was removed *in vacuo* to yield a light brown viscous solution, which was dissolved in water (8 cm^3) and extracted with pentane (3 x 5 cm^3). The volume of the aqueous layer was reduced *in vacuo* and the resulting creamy solid was collected by filtration and washed with pentane (5 x 10 cm^3), dried under vacuum to yield the desired product (1.46 g, 85 %); $\delta_P\{^1H\}$ (121 MHz, D_2O): - 4.7 (t, $^2J_{P,P}$ = 45.1 Hz), - 9.4 (d, $^2J_{P,P}$ = 44.9 Hz); $\delta_C\{^1H\}$ (75 MHz, D_2O): 155.3(C_1), 154.3 (C_5), 130.0 (C_2), 129.6 (C_6), 124.2 (C_3), 123.0 (C_7), 122.3 (C_4), 122.0 (C_8); δ_H (300 MHz, D_2O): 7.0 – 7.26 (m, 25H, Ar); ES-MS(+) *m/z*: 712.7 $[M]^+$; elemental analysis calcd. (%) for $C_{30}H_{25}N_2O_6P_3K_2(H_2O)_2$: C, 48.13; H, 3.90; N, 3.74; found C, 47.91; H, 3.61; N 3.43.

3.5.4. Preparation of $Ln_2(bistpOp)_3$ (Ln = Eu, Tb, Dy, Sm, Gd, Nd, Yb, Er) and $Y_2(bistpOp)_3$

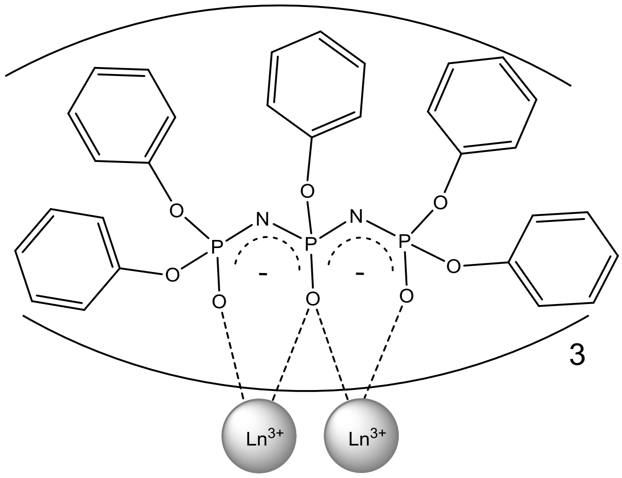

3

$Ln_2(bistpOp)_3$

To a stirring solution of K_2bistpOp (3 equiv., 0.21 mmol) in EtOH (20 cm^3) a solution of $LnCl_3.6H_2O$ (2 equiv., 0.14 mmol) in EtOH (5 cm^3) and H_2O (2 cm^3) were added dropwise. The resulting mixture was stirred for 1 hour at room temperature. The addition of water (10 cm^3) led to formation of white precipitate. The powder was collected by filtration, washed with hexane (2 x 5 cm^3) and dried under vacuum.

$Y_2(bistpOp)_3$ - (86.0 mg, 59 %); $\delta_P\{^1H\}$ (121 MHz, $CDCl_3$): 1.7 (br, s), - 6.6 (d, $^2J_{P,P}$ = 49.9 Hz); $\delta_C\{^1H\}$ (75 MHz, $CDCl_3$): 151.7 (C_1), 151.3 (C_5), 129.3 (C_2), 129.1 (C_6), 124.2 (C_3), 123.6 (C_7), 122.0 (C_4), 120.6 (C_8); δ_H (300 MHz, $CDCl_3$): 6.70 – 7.10 (m, 75H, Ar); MALDI-MS *m/z*: 2081 $[M+H]^+$,1359 $[M - Y(bistpOp) + 2H]^+$; elemental analysis calcd. (%) for $C_{90}H_{75}N_6O_{24}P_9Y_2(KCl)(H_2O)_{0.5}$: C, 49.94; H, 3.54; N, 3.88; found C, 49.02; H, 3.65; N, 3.94; UV-Vis (CH_3CN): λ in nm (log ε) 263 (3.8).

$La_2(bistpOp)_3$ - (113.1 mg, 74 %); $\delta_P\{^1H\}$ (121 MHz, $CDCl_3$): 0.3 (br, s), -10.1 (d, $^2J_{P,P}$ = 55.1 Hz); $\delta_C\{^1H\}$ (75 MHz, $CDCl_3$): 151.7 (C_1), 151.6 (C_5),129.1 (C_2), 128.8 (C_6), 123.9 (C_3), 123.1 (C_7), 120.8 (C_4), 120.6 (C_8); δ_H (300 MHz, $CDCl_3$): 6.92 – 7.10 (m, 75H, Ar); MALDI-MS *m/z*: 2180 $[M+H]^+$,1407 $[M$ - La(bistpOp) + $2H]^+$; elemental analysis calcd. (%) for $C_{90}H_{75}N_6O_{24}P_9La_2(KCl)(H_2O)_2$: C, 47.17; H, 3.47; N, 3.67; found C, 47.03; H, 3.71; N, 3.83; UV-Vis (CH_3CN): λ in nm (log ε) 263 (3.8).

$Eu_2(bistpOp)_3$ - (103.5 mg, 67 %); $\delta_C\{^1H\}$ (75 MHz, $CDCl_3$): 151.0, 150.8 (C_5), 149.1 (C_1), 129.8, 129.6 (C_2), 128.8 (C_7), 124.8, 124.6 (C_3), 123.8 (C_7), 121.4 (C_6), 120.8 (C_4), 120.0 (C_8); δ_H (300 MHz, $CDCl_3$): 7.97 (br,s, 6H, H_d), 7.02 – 7.37 (m, 60H, H_a, H_b, H_c), 6.69 (s, 6H, H_e), 5.90 (s, 3H, H_f); MALDI-MS *m/z*: 2209 $[M+H]^+$,1423 $[M$ - Eu(bistpOp) + $2H]^+$; elemental analysis calcd. (%) for $C_{90}H_{75}N_6O_{24}P_9Eu_2(H_2O)$: C, 48.58; H, 3.49; N, 3.78; found C, 48.79; H, 3.40; N, 3.85; UV-Vis (CH_3CN): λ in nm (log ε) 263 (3.7).

$Tb_2(bistpOp)_3$ - (121.3 mg, 78 %); MALDI-MS *m/z*: 2222 $[M+H]^+$,1429 $[M$ - Tb(bistpOp) + $2H]^+$; elemental analysis calcd. (%) for $C_{90}H_{75}N_6O_{24}P_9Tb_2(KCl)(H_2O)$: C, 46.72; H, 3.35; N, 3.63; found C, 46.74; H, 3.53; N, 3.78; UV-Vis (CH_3CN): λ in nm (log ε) 263 (3.8).

$Dy_2(bistpOp)_3$ - (124.8 mg, 80 %); MALDI-MS *m/z*: 2228 $[M+H]^+$, 1434 $[M$ - Dy(bistpOp)+ $2H]^+$; elemental analysis calcd. (%) for $C_{90}H_{75}N_6O_{24}P_9Dy_2(KCl)(H_2O)_{0.5}$: C, 46.74; H, 3.31; N, 3.64; found C, 46.92; H, 3.56; N, 3.85; UV-Vis (CH_3CN): λ in nm (log ε) 263 (3.7).

$Sm_2(bistpOp)_3$ - (114.4 mg, 74 %); $\delta_C\{^1H\}$ (75 MHz, d_6-acetone): 153.3 (C_5), 153.0 (C_1), 130.1, 120.0 (C_2), 129.2 (C_7), 124.7 (C_3), 124.4 (C_7), 123.5 (C_8), 122.0 (C_6) , 121.3 (C_4); δ_H (300 MHz, d_6-acetone): 7.61 (br, s, 6H, H_d), 6.95 – 7.21 (br, m, 66H, H_a, H_b, H_c, H_e), 6.81 (br, s, 3H, H_f) ; MALDI-MS *m/z*: 2204 $[M+H]^+$, 1422 $[M - Sm(bistpOp)+ 2H]^+$; elemental analysis calcd. (%) for $C_{90}H_{75}N_6O_{24}P_9Sm_2(KCl)(H_2O)_2$: C, 46.70; H, 3.44; N, 3.63; found C, 46.47; H, 3.54; N, 3.81; UV-Vis (CH_3CN): λ in nm (log ε) 263 (3.8).

$Gd_2(bistpOp)_3$ - (90.1 mg, 58 %); MALDI-MS *m/z*: 2219 $[M+H]^+$,1428 $[M - Gd(bistpOp)+2H]^+$; elemental analysis calcd. (%) for $C_{90}H_{75}N_6O_{24}P_9Gd_2(KCl)(H_2O)_{0.5}$: C, 46.97; H, 3.33; N, 3.65; found C, 46.69; H, 3.53; N, 3.81; UV-Vis (CH_3CN): λ in nm (log ε) 263 (3.8).

$Nd_2(bistpOp)_3$ - (85.9 mg, 63 %); MALDI-MS *m/z*: 2190 $[M+H]^+$,1419 $[M - Nd(bistpOp) + 2H]^+$; elemental analysis calcd. (%) for $C_{90}H_{75}N_6O_{24}P_9Nd_2(KCl)(H_2O)_2$: C, 46.95; H, 3.46; N, 3.65; found C, 46.68; H, 3.56; N, 3.89; UV-Vis (CH_3CN): λ in nm (log ε) 263 (3.7).

$Er_2(bistpOp)_3$ - (104.9 mg, 75 %); MALDI-MS *m/z*: 2237 $[M+H]^+$, 1436 $[M – Er(bistpOp) + 2H]^+$; elemental analysis calcd. (%) for $C_{90}H_{75}N_6O_{24}P_9Er_2(KCl)(H_2O)_{0.5}$: C, 46.57; H, 3.30; N, 3.62; found C, 46.36; H, 3.14; N, 3.61; UV-Vis (CH_3CN): λ in nm (log ε) 263 (3.8).

$Yb_2(bistpOp)_3$ - (102.4 mg, 69 %); MALDI-MS *m/z*: 2251 $[M+H]^+$, 1444 $[M - Yb(bistpOp) + 2H]^+$; *m/z* 1653 $[M+K]^+$; elemental analysis calcd. (%) for

$C_{90}H_{75}N_6O_{24}P_9Yb_2(KCl)(H_2O)_{0.3}$: C, 46.39; H, 3.27; N, 3.61; found C, 46.21; H, 3.36; N, 3.76; UV/Vis (CH_3CN): λ in nm (log ε) 263 (3.6).

3.6. References

1) Elhabiri, M.; Scopelliti, R.; Bünzli, J.-C. G.; Piguet, C. *Chem. Commun.* **1998,** 2347.
2) Chen, X.-Y.; Bretonniere, Y.; Pecaut, J.; Imbert, D.; Bünzli, J.-C.; Mazzanti, M. *Inorg. Chem.* **2007,** *13*, 346.
3) Martin, L. J.; Hahnke, M. J.; Nitz, M.; Wohnert, J.; Silvaggi, N. R.; Allen, K. N.; Schwalbe, H.; Imperiali, B. *J. Am. Chem. Soc.* **2007,** *129*, 7106.
4) Cantuel, M.; Gumy, F.; Bünzli, J.-C. G.; Piguet, C. *Dalton Trans.* **2006,** 2647.
5) Banerjee, S.; Kumar, G. A.; Riman, R. E.; Emge, T. J.; Brennan, J. G. *J. Am. Chem. Soc.* **2007,** *129,* 5926.
6) De Lill, D. T.; de Battencourt-Dias, A.; Cahill, C. L. *Inorg. Chem.* **2007,** *46*, 3960.
7) You, H.; Fang, J.; Wang, L.; Zhu, X.; Huang, W.; Ma, D. *Opt. Mater.* **2007,** *29*, 1514.
8) Glover, P. B.; Ashton, P. R.; Childs, L. J.; Rodger, A.; Kercher, M.; Williams, R. M.; De Cola, L.; Pikramenou, Z. *J. Am. Chem. Soc.* **2003**, *125*, 9918.
9) Nielsen, M. L. *Inorg. Chem.* **1964**, *3,* 1760.
10) Klink, S. I.; Grave, L.; Reinhoudt, D. M.; Van Veggel, F.C. J. M.; Werts, M. H.; Geurts, F. A. J.; Hofstraat, J. W. *J. Phys. Chem. A.* **2000,** *104*, 5457.
11) Sabbatini, N.; Guardigli, M.; Lehn, J.-M.; *Coord. Chem. Rev.* **1993**, *123*, 201.
12) Bünzli, J.-C. G. “Spectroscopic Properties of Rare Earths” in *Optical Materials* (Ed.: Liu, G. K.), Springer-Verlag, Berlin, 2002.
13) Meech, S. R.; Phillips, D. *J. Photochem.* **1983**, *23*, 193.
14) Nakamaru, K. *Bull. Chem. Soc. Jpn.* **1982**, *55*, 2697.
15) Stein, G.; Würzberg, E. *J. Chem. Phys.* **1975**, *62*, 208.
16) Jensen, T. B.; Scopelliti, R.; Bünzli, J.-C. G. *Chem. Eur. J.* **2007**, *13*, 8404.
17) Allinger, N. L. *J. Am. Chem. Soc.* **1977,** *95*, 8127.
18) Chauvin, A.-S.; Comby, S.; Song, B.; Vandevyver, C. D. B.; Bünzli, J.-C. G. *Chem. Eur. J.* **2008**, *14*, 1726.
19) Natrajan, L. S.; Timmins, P. L; Lunn, M.; Heath, S. L. *Inorg. Chem.* **2007**, *46*, 10877.
20) Deiters, E.; Song, B.; Chauvin, A.-S.; Vandevyver, C. D. B.; Bünzli, J.-C. G. *New. J. Chem.* **2008**, *32*, 1140.

21) Sultan, R.; Gadamsetti, S.; Swavey, S. *Inorg. Chim. Acta.* **2006**, *359*, 1233.
22) Irfanullah, M.; Iftikhar, K. *Inorg. Chem. Comm.* **2009**, *12*, 296.
23) Comby, S.; Imbert, D.; Vandevyver C.; Bünzli, J.-C. G. *Chem. Eur. J.* **2007**, *13*, 936.
24) Stein, G.; Würzberg, E. *J. Chem. Phys.* **1975**, *62*, 208.

4.0. Luminescent Lanthanide Complexes Based on Tetrabiphenyl Imidodiphosphate Ligands

4.1. Introduction

It was demonstrated in Chapter 2 that the H**tpOp** moiety can be used effectively for the sensitisation of the excited states of the visible and NIR-emitting lanthanide ions (Yb^{3+}, Nd^{3+}). Building on this previous work, an analogue of H**tpOp** was designed with biphenyl moieties as chromophores, H**biphen**. The biphenyl chromophore was selected because of its higher extinction coefficient due to the additional twelve aromatic rings, compared to the plain phenyl group, which would provide more efficient absorption of excitation energy, and therefore promote more effective energy transfer to the lanthanide ions.

It was expected that the H**biphen** would act as a more efficient sensitiser for Visible and NIR- emitting lanthanide ions.

Photophysical studies of the Ln^{3+} complexes of **biphen** were performed to determine how the substituent affect the ligand's excited state and Ln^{3+} emission.

4.2. Results and Discussion

4.2.1. Preparation and characterisation of tris-biphenyl phosphate

As the tris-biphenyl phosphate used in the synthesis for preparation of H**biphen** ligand was not commercially available, it had to be synthesised using an adapted procedure reported for triaryl phosphates (Scheme 4.1).[1]

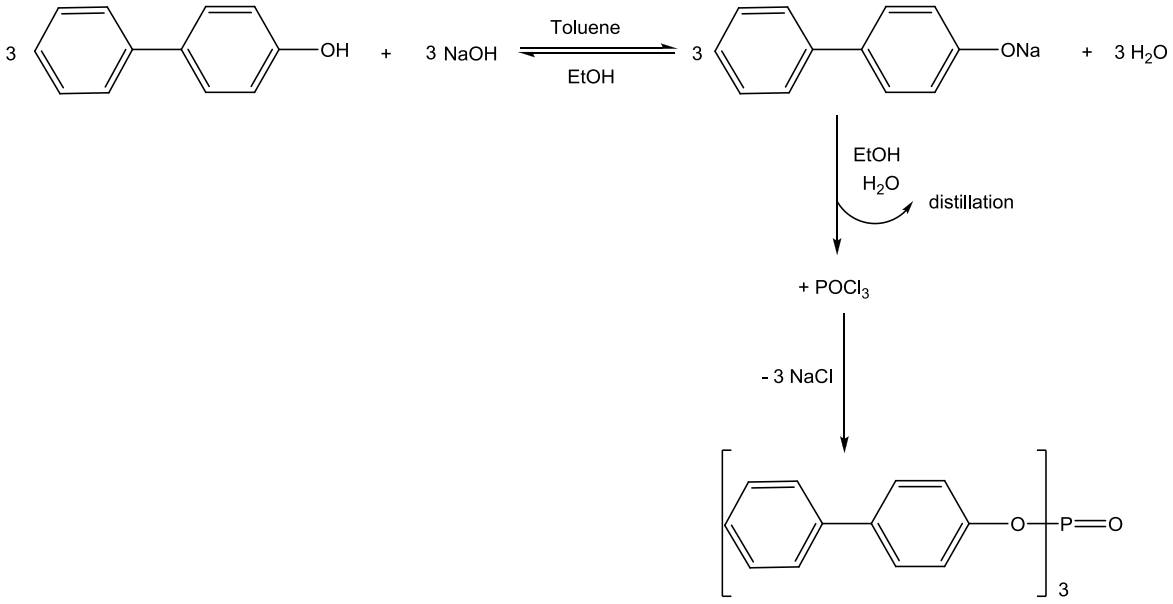

Scheme 4.1 Synthetic route to tris-biphenyl phosphate.

The tris-biphenyl phosphate was prepared by an one-pot reaction of 4-phenylphenol with sodium hydroxide in an excess of ethanol. The reaction mixture was dried by an azeotropic distillation with toluene to remove ethanol, yielding a suspension of anhydrous biphenyloxide, which was allowed to react with phosphorus oxychloride. The target compound was isolated in 83% yield after chromatography on silica. The

product was characterised by ^{31}P, ^{1}H and ^{13}C NMR spectroscopy in $CDCl_3$ and mass spectrometry.

The ^{31}P NMR spectrum (Figure 4.1) displays one phosphorus resonance, at -17.4 ppm as expected. The absence of a singlet peak at 4.3 ppm, corresponding to the phosphorus oxychloride, confirms the successful formation of the desired product. The phosphorus signal is in good agreement with the commercially available starting material triphenyl phosphate (-16.5 ppm), which was used for the synthesis of H**tpOp** ligand.

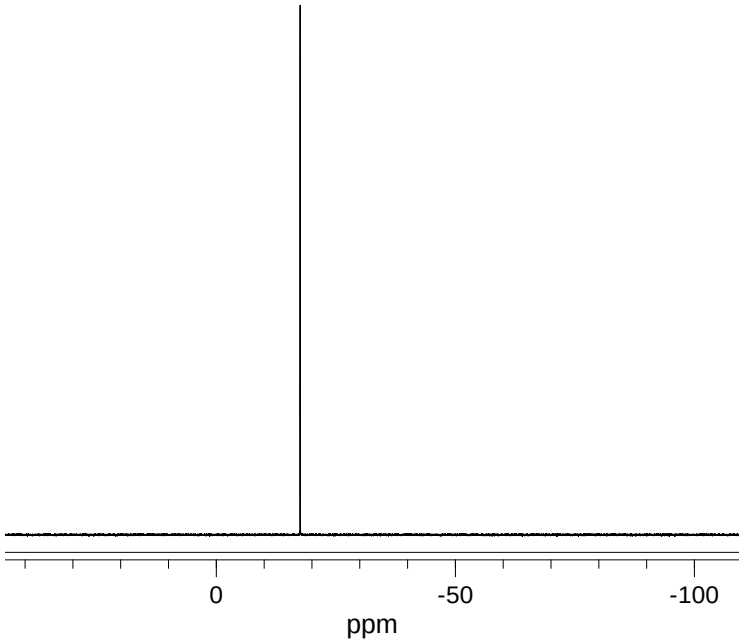

Figure 4.1. The 121 MHz ^{31}P NMR spectrum of tris-biphenyl phopshate in $CDCl_3$.

The ^{1}H NMR spectrum in $CDCl_3$ shows a multiplet in the region of 7.31 - 7.60 ppm, corresponding to the aromatic protons of three biphenyloxide rings. The ^{13}C NMR spectrum in $CDCl_3$ displays eight resonances as expected for the desired product. Carbon signals in the region of 120 - 151 ppm corresponding to the aromatic carbons of the biphenyloxide groups.

Positive-mode electrospray mass spectrometry displays an intense peak at *m/z* = 557, corresponding to the $[M + Na]^+$ adduct.

4.2.2. Preparation and characterisation of Hbiphen ligand

The H**biphen** ligand was synthesised following the reaction scheme adapted from a reported procedure for imidodiphosphate ligands (Scheme 4.2).[2]

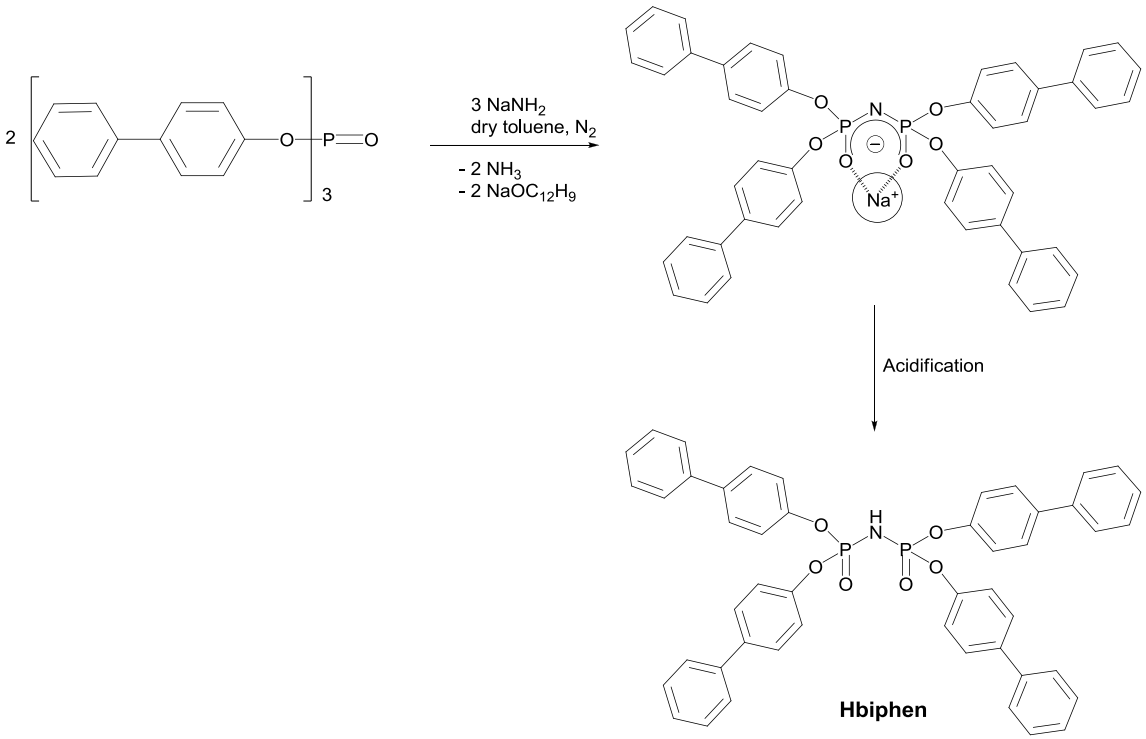

Scheme 4.2. Synthetic route to H**biphen**.

The H**biphen** was readily prepared by the condensation reaction between tris-biphenyl phosphate and sodium amide. The ligand was isolated as a Na**biphen** salt, which was established by an X-ray crystal structure determination, presented in Section 4.2.3. The final H**biphen** ligand was isolated by acidic work-up as a white powder in 82% yield.

The identity of the new H**biphen** ligand was confirmed from its ^{31}P NMR spectrum and it was further characterised by ^{1}H, ^{13}C NMR, mass spectrometry and elemental analysis.

The ^{31}P NMR spectrum in $CDCl_3$ (Figure 4.2) shows one singlet peak at -10.5 ppm for the two equivalent phosphorus atoms of the ligand. The absence of a single peak at -17.4 ppm, which corresponds to the starting material tris-biphenyl phosphate, confirms the successful formation of the H**biphen**. The frequency of phosphorus signal for H**biphen** is almost identical to the -9.5 ppm observed for the H**tpOp** ligand.

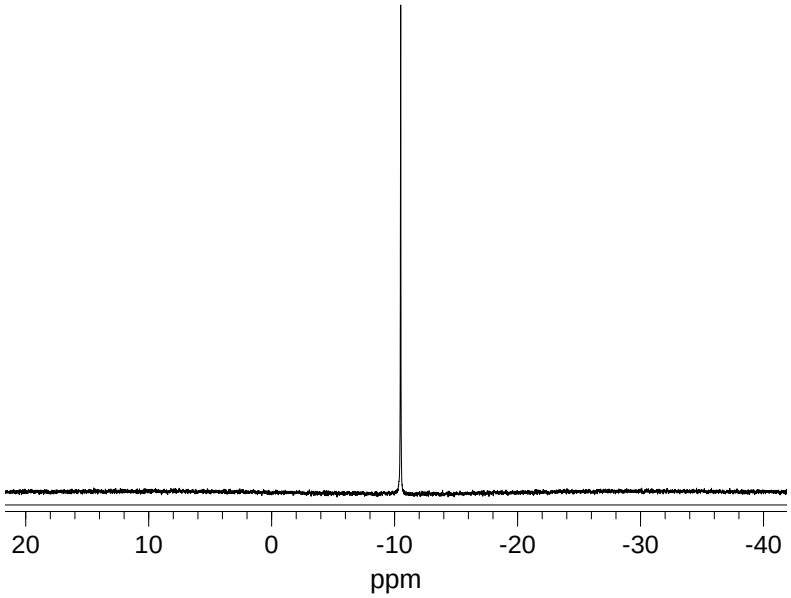

Figure 4.2. The 121 MHz ^{31}P NMR spectrum of H**biphen** in $CDCl_3$.

The ^{1}H NMR spectrum of H**biphen** in $CDCl_3$ shown in Figure 4.3 has the similar features as that of the tris-biphenyl phosphate. It exhibits a multiplet in the aromatic region, corresponding to the CH protons of the biphenyloxide rings.

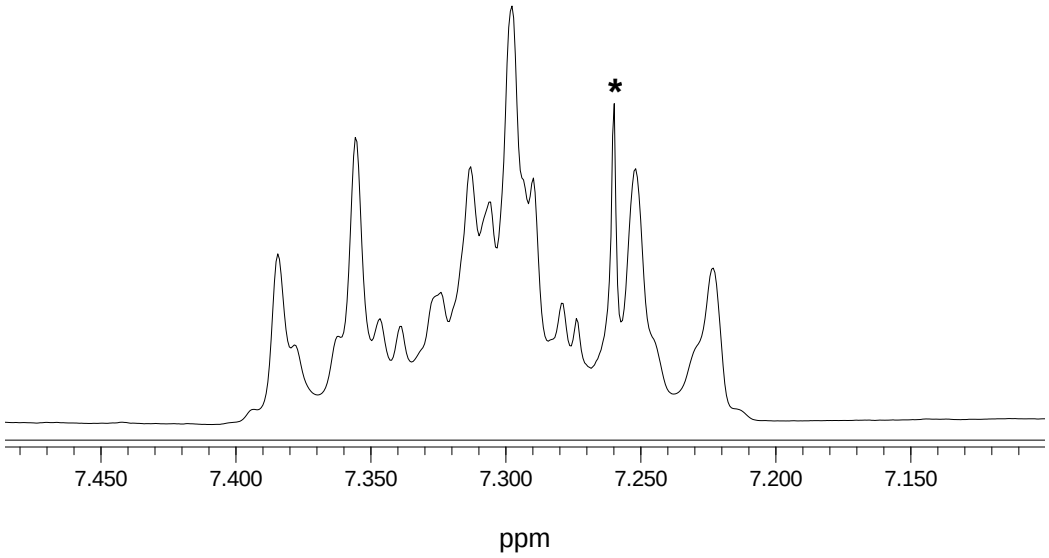

Figure 4.3. The 300 MHz ^{1}H NMR spectrum of H**biphen** in $CDCl_3$. (* = solvent).

The ^{13}C NMR spectrum in $CDCl_3$ displays eight signals in the aromatic section between 120 and 153 ppm corresponding to three quaternary and five CH signals.

The negative-mode mass spectrometry shows a peak at *m/z* = 784 corresponding to $[M - H]^-$.

The IR spectrum of powder sample of H**biphen** (Figure 4.4) displays broad bands at 3,060 and 3,032 cm^{-1} corresponding to the N-H stretching vibrations, as it is expected that the ligand is adopting a hydrogen bonded structure in the solid state. The free ligand H**biphen** shows sharp P=O stretch vibrations centred at 1,163 cm^{-1} as well as the sharp band centred at 953 cm^{-1} which is assigned as PNP stretching frequencies.

Positions of the IR bands observed for the H**biphen** are comparable to those corresponding bands in H**tpOp** and H_2**bistpOp** ligands.

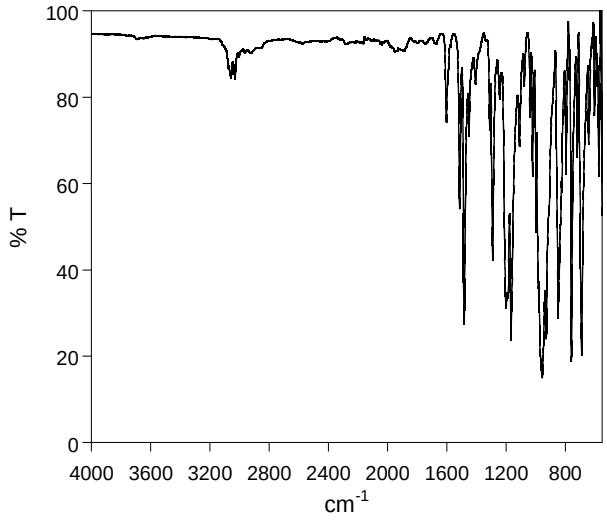

Figure 4.4. The IR spectrum of powder of H**biphen**.

The UV-vis absorption spectrum of the H**biphen** (Figure 4.5.) is dominated by an intense band corresponding to the ligand based π->π* transitions with a maximum at 255 nm (ε = 66,047 dm^3 mol^{-1} cm^{-1}). The UV-Vis profile and molar absorptivity of H**biphen** is consistent with that of biphenol[3] although obviously for the ligand, the absorption coefficient is approximately four times higher, as there are four chromophores of biphenyl present in the H**biphen**.

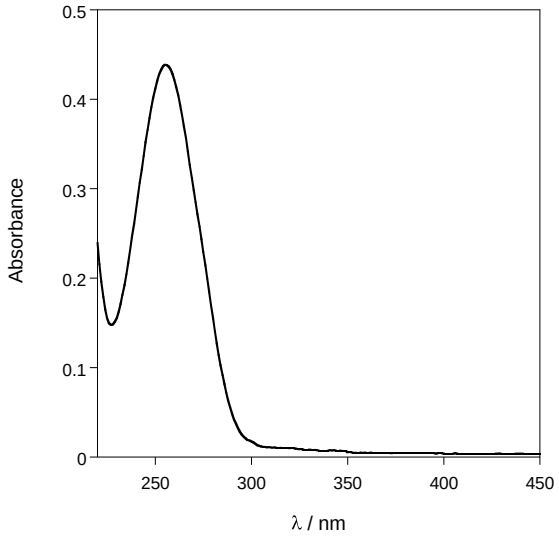

Fig 4.5. The UV-vis spectrum of H**biphen** in CH_3CN.

4.2.3. X-ray Crystallography of Nabiphen

Single crystals suitable for X-ray analysis could be obtained by slow evaporation of DMSO solution at room temperature. The single crystal X-ray structure of Na**biphen** ligand was determined and the crystal data and the data collection parameters are presented in Table 4.1.

The Na**biphen** crystallises in triclinic space group *P*-1. The crystal structure of Na**biphen** contains two independent molecules, which are connected *via* two bridging oxygen atoms from DMSO molecules. A similar trend of bond distances has been observed for both therefore only one is discussed herein. Sodium ion is five-coordinated by two oxygen atoms from **biphen** ligand, two bridging oxygen atoms from DMSO and one oxygen atom from directly coordinated DMSO, resulting in square pyramidal geometry as illustrated in Figure 4.6.

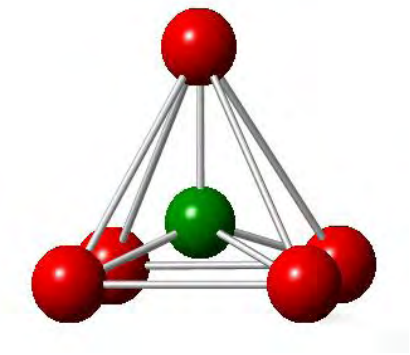

Figure 4.6. Coordination environment of Na^+ in the Na**biphen**. Heteroatoms: O, red; Na+, green.

The structure of Na**biphen** is depicted in Figure 4.7. The Na-O(**biphen**) bond lengths are 2.382(4) and 2.282(4) Å respectively, the Na-O(DMSO) corresponds to 2.281(4) Å, whereas Na-O(bridging) are slightly longer at 2.378(4) and 2.341(4) Å, respectively. Distances between P-N are 1.568(4) and 1.572(4) Å. The bond lengths

of P-O are almost identical at 1.474(4) and 1.473(4) Å. The P-N and P-O bond lengths are comparable to those of K**tpOp** ligand, presented in Chapter 2. In K**tpOp** the P-N bonds distances were 1.552(4) and 1.554(4) Å and P-O distances 1.472(4) and 1.480(4) Å, respectively. This is suggesting of delocalisation of π-electrons around the binding unit of Na**biphen** ligand.

Further examination of the Na**biphen** structure reveals a presence of strong intramolecular edge-to-face CH-π interactions between biphenyl rings with an average distance of 3.4 Å.

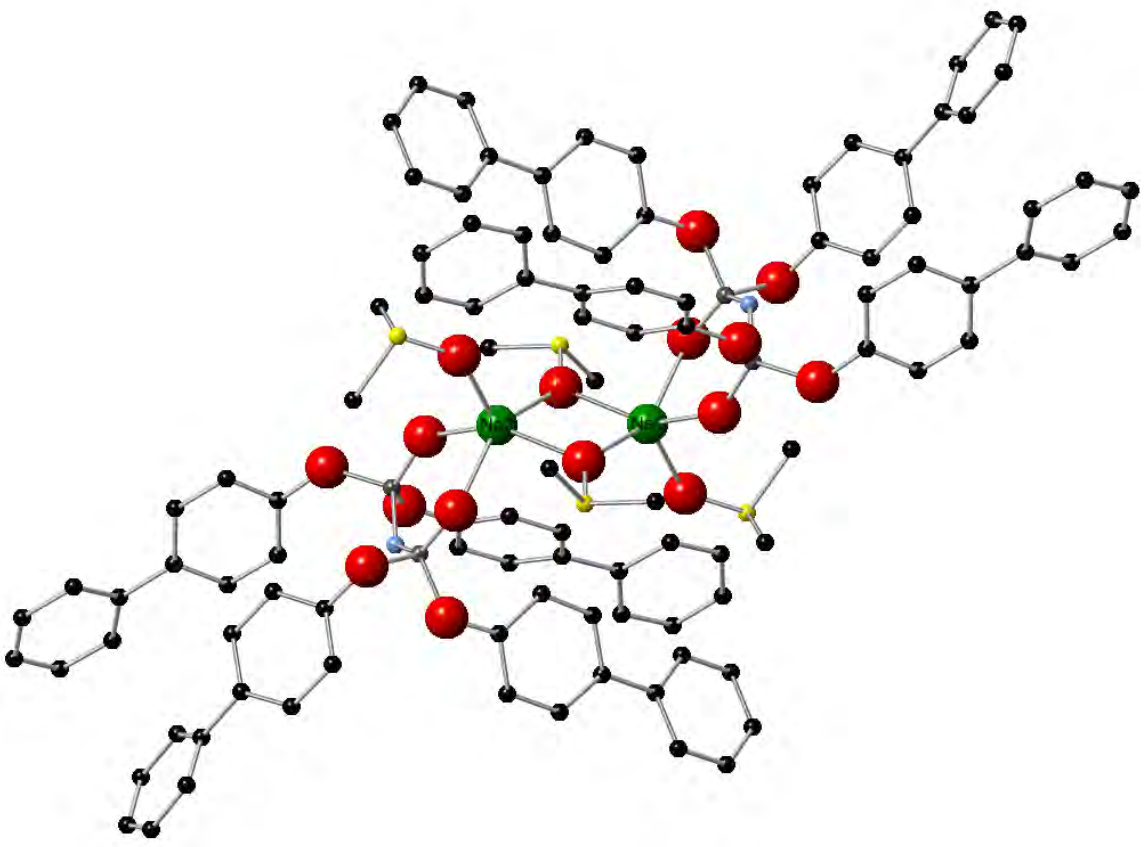

Figure 4.7. The X-ray crystal structure of dimer of Na**biphen** ligands.

Table 4.1. Crystal data and structure refinement for Na**biphen**.

Identification code	Na**biphen**	
Empirical formula	C_{52} H_{48} N Na O_8 P_2 S_2	
Formula weight	963.96	
Temperature	120(2) K	
Wavelength	1.54178 Å	
Crystal system	Triclinic	
Space group	P -1	
Unit cell dimensions	a = 9.5803(2) Å	α = 104.169(1)°
	b = 14.2838(2) Å	β = 101.659(1)°
	c = 17.8410(3) Å	γ = 90.511(1)°
Volume	2313.92(7) $Å^3$	
Z	2	
Density (calculated)	1.384 Mg/m^3	
Absorption coefficient	2.260 mm^{-1}	
F(000)	1008	
Crystal size	0.28 x 0.20 x 0.10 mm^3	
Theta range for data collection	6.40 to 66.59°.	
Index ranges	-11<=h<=10, -16<=k<=17, -20<=l<=20	
Reflections collected	14916	
Independent reflections	7494 [R(int) = 0.0227]	
Completeness to theta = 66.59°	91.6 %	
Absorption correction	Semi-empirical from equivalents	
Max. and min. transmission	0.8055 and 0.5702	
Refinement method	Full-matrix least-squares on F^2	
Data / restraints / parameters	7494 / 197 / 601	
Goodness-of-fit on F^2	1.435	
Final R indices [I>2sigma(I)]	R1 = 0.0823, wR2 = 0.2564	
R indices (all data)	R1 = 0.1165, wR2 = 0.3892	
Largest diff. peak and hole	1.083 and -1.037 $e.Å^{-3}$	

4.2.4. Preparation and characterisation of Kbiphen

Having established a successful synthesis of the ligand, the formation of its potassium precursor was carried out, by a reaction of H**biphen** with 1.2 equivalents of KH in THF (Scheme 4.3). The K**biphen** was isolated as a light brown powder in yield of 87%. The solid showed a good solubility in alcoholic solvents and chloroform.

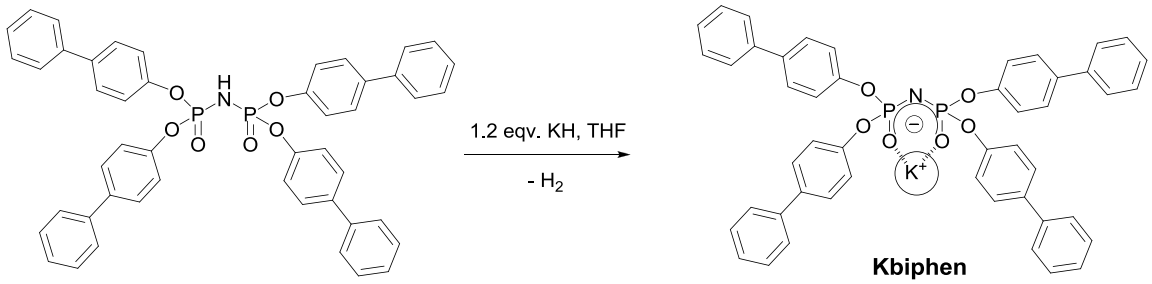

Scheme 4.3. Synthetic route to K**biphen**.

The K**biphen** was fully characterised by ^{31}P, ^{1}H, ^{13}C NMR spectroscopy, mass spectrometry and elemental analysis. The ^{31}P NMR spectrum in $CDCl_3$ (Figure 4.8.) shows one singlet peak at - 8.6 ppm for two equivalent phosphorus atoms of the K**biphen** ligand. The phosphorus resonance moves approximately by 2 ppm downfield upon coordination, compared to the free ligand.

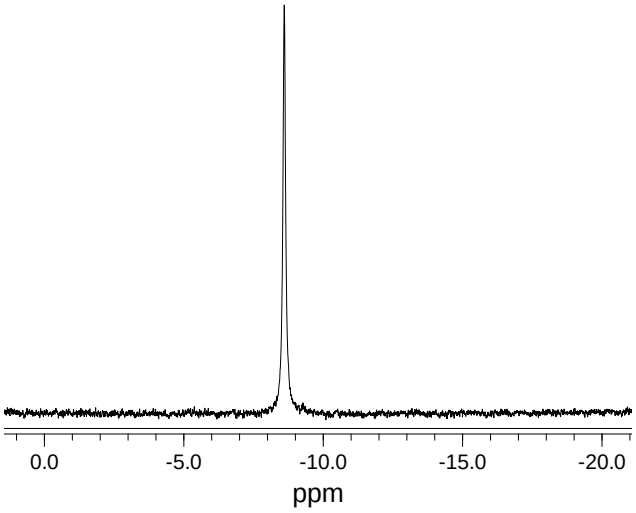

Figure 4.8. The 121 MHz ^{31}P NMR spectrum of K**biphen** in $CDCl_3$.

The ^{1}H NMR of K**biphen** in $CDCl_3$ shows a multiplet in the region of 6.79 – 7.41 ppm, corresponding to the 36 aromatic protons. The equivalence of each of the biphenyloxide aromatic rings is confirmed by the ^{13}C NMR spectrum (Figure 4.9), which displays eight distinct carbon resonances between 151 – 120 ppm.

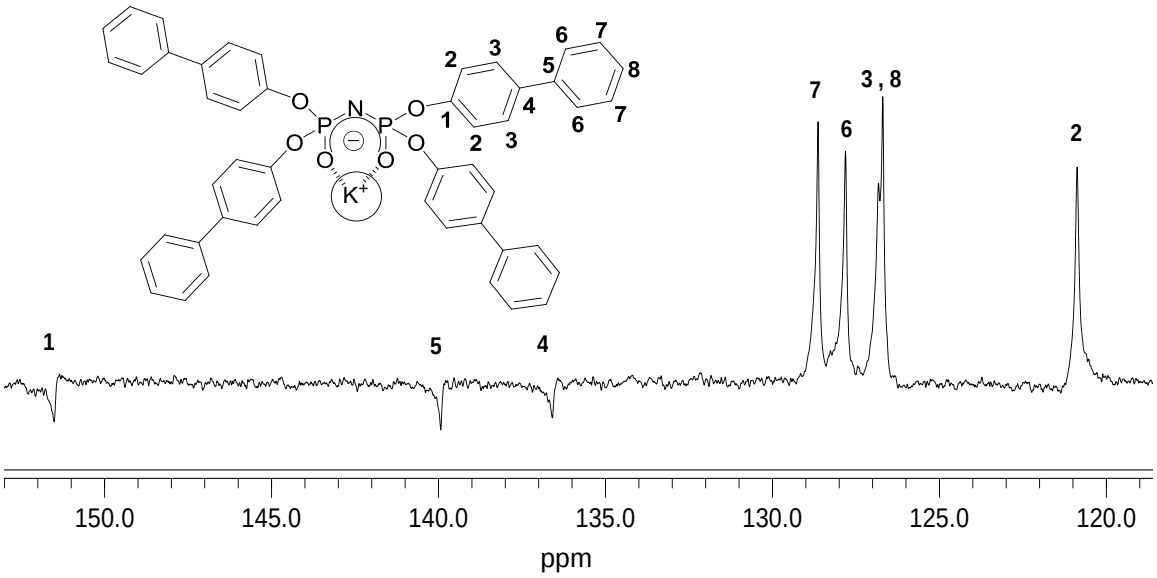

Figure 4.9. The 100 MHz ^{13}C NMR spectrum of K**biphen** in $CDCl_3$. Inset depicts the K**biphen** ligand with the labelling scheme.

The ES(+) spectrum of K**biphen** displays a signal at *m/z* = 823 corresponding to $[M]^+$.

4.2.5. Preparation and characterisation of Ln(biphen)$_3$ complexes, (Ln = Eu, Tb, Dy, Sm, Gd, Nd, Yb, Er) and Y(biphen)$_3$

A series of Ln(**biphen**)$_3$ complexes were traditionally synthesised by treatment of K**biphen** with $LnCl_3.6H_2O$ in 3:1 molar ratio, dissolved in hot aqueous ethanol (5:1) (Scheme 4.4.). The mononuclear complexes were isolated as colourless powders in 60 - 92% yields. The complexes were soluble in THF and, moderately soluble in alcoholic solvents, acetonitrile and chloroform. Ln(**biphen**)$_3$ complexes showed lower solubility than the analogous **tpOp** complexes, presumably due to the additional twelve phenyl rings.

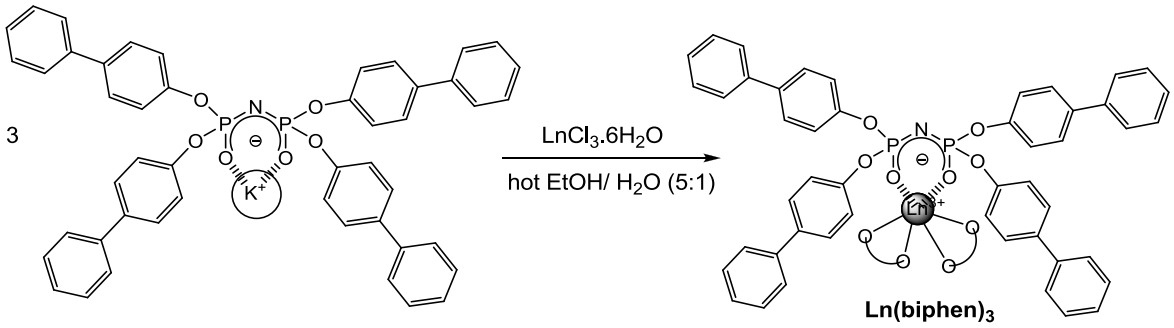

Scheme 4.4. Synthetic route to Ln(**biphen**)$_3$.

The new Ln(biphen)$_3$ (Ln = Eu, Tb, Dy, Sm, Nd, Yb, Er) complexes were fully characterised by ^{31}P, ^{1}H and ^{13}C NMR and mass spectrometry and elemental analysis. Due to the severe broadening caused by the highly paramagnetic Gd^{3+} ion no NMR spectra were acquired for Gd(tpOp)$_3$.

The diamagnetic lanthanide analogue Y(**biphen**)$_3$ was prepared in order to allow characterisation by NMR spectroscopy. Y^{3+} is a particularly good analogue for the Eu^{3+} cation due to the similarity in ionic radius to the lanthanide ions and its dominance of the +3 oxidation state.

The ^{31}P resonance of Y(biphen)$_3$ appears slightly downfield at -6.2 ppm compared to that of -8.6 ppm corresponding to the Kbiphen ligand because of the deshielding of the phosphorus atoms expected from the electron withdrawing effect of coordination. The presence of a single phosphorus peak, indicating one environment and its chemical shift proves that the ligands are bound to Y^{3+} ion in solution.

The lanthanide-induced shifts observed in the Ln(biphen)$_3$ complexes can be again separated into three groups by the signs of the ^{31}P chemical shifts with respect to the diamagnetic reference Y(biphen)$_3$. The Dy^{3+}, Er^{3+}, Eu^{3+} and Tb^{3+} complexes show the greatest upfield ^{31}P shifts, whereas the shifts of Sm^{3+} and Yb^{3+} complexes remain similar to that of the Y(biphen)$_3$ complex, while the Nd^{3+} complex has the largest downfield shift.

The ^{31}P NMR spectra of the complexes exhibit broadly similar features, with the exception of the characteristic differences that arise from the magnetic properties of the different Ln^{3+} ions. They all display a single resonance, indicating the presence of one phosphorus environment for the six phosphorus atoms of the complexes and confirm the equivalence of the ligands.

The ^{31}P NMR spectra of Eu^{3+}, Sm^{3+}, Yb^{3+} and Nd^{3+} complexes exhibit narrow bandwidths as demonstrated in Figure 4.10 (left) for Sm(biphen)$_3$, whereas the Dy^{3+},

Tb^{3+} and Er^{3+} complexes undergo excessive line broadening as depicted in Figure 4.10 (right) for Tb(biphen)$_3$ complex as a representative example.

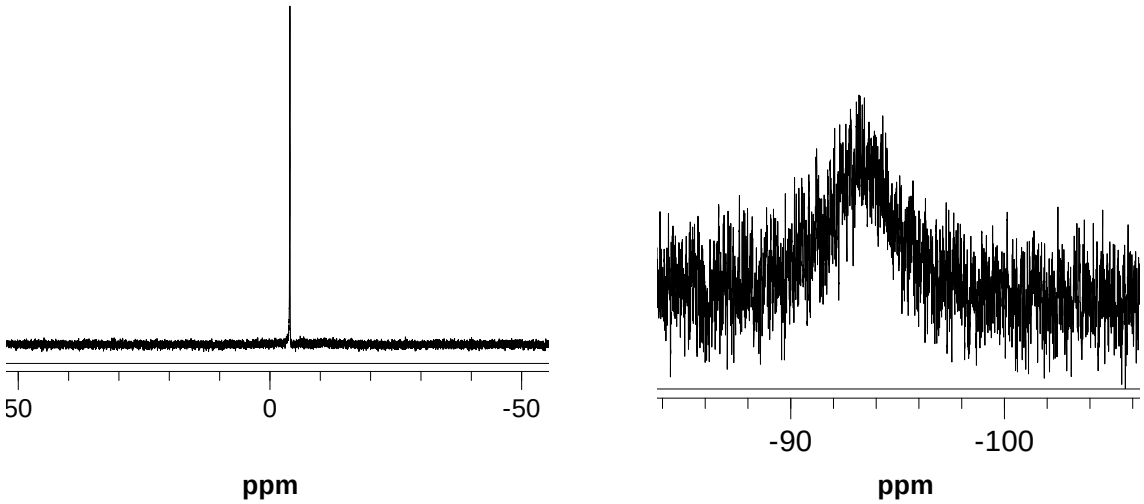

Figure 4.10. The 121 MHz ^{31}P NMR spectra of Sm(**biphen**)$_3$ (left) and Tb(**biphen**)$_3$ (right) in $CDCl_3$.

As already explained in Chapter 2, two main contributing interactions (contact and pseudocontact)[4,5,6] are responsible for the ^{31}P chemical shifts and line broadening in spectra of paramagnetic Ln(biphen)$_3$ complexes.

If the pseudocontact shift predominates, the theoretical order of ^{31}P to higher frequency should be Er > Yb > Eu > Sm > Nd > Tb > Dy.[7] But, if the contact interaction predominates, the order of ^{31}P shift to higher frequency should follow Tb > Dy > Er > Eu > Yb > Sm > Nd.[7] The observed patterns for the ^{31}P paramagnetic shifts of Ln(**biphen**)$_3$ complexes across the series are not characteristic of shifts dominated by either pseudocontact or contact origins but rather a mixture of the two. The introduction of extra twelve aromatic rings in Ln(**biphen**)$_3$ complexes makes a

very small difference in the chemical shifts in ^{31}P NMR spectra compared to those obtained for corresponding Ln(**tpOp**)$_3$ complexes.

The ^{1}H NMR spectra in $CDCl_3$ were recorded for all Ln(**biphen**)$_3$ complexes. The Tb^{3+}, Dy^{3+}, Yb^{3+} complexes showed a similar pattern as demonstrated in Figure 4.11 for the Tb(**biphen**)$_3$ complex. The spectrum displays four broad singlet peaks corresponding to the aromatic protons. The peaks corresponding to the H_a and H_b protons, which are closest to the metal ion, undergo the greatest broadening and shift to lower frequency. The resonances corresponding to the protons H_c, H_d, and H_e remain sharper, due to their distance from Tb^{3+} core.

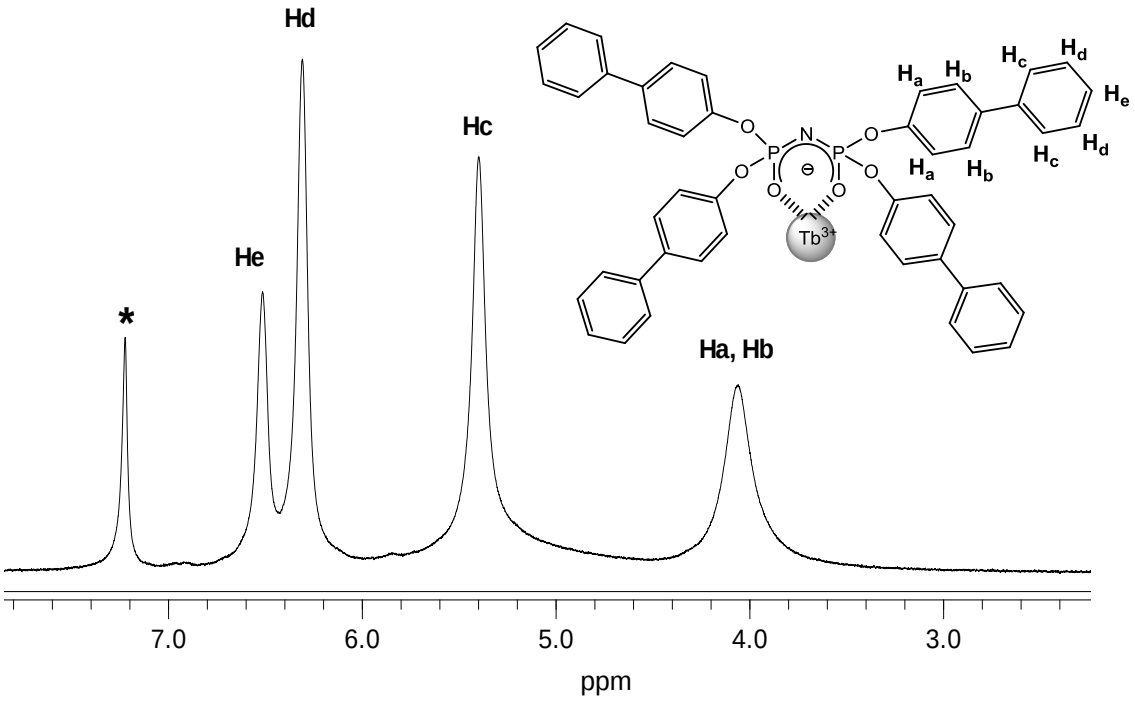

Figure 4.11. The 300 MHz ^{1}H NMR spectrum of Tb(**biphen**)$_3$ in $CDCl_3$. Inset depicts part of the complex with the labelling scheme. (* = solvent).

The ^{1}H NMR spectra of Ln(**biphen**)$_3$ (Ln = Eu, Sm, Er, Nd) complexes in $CDCl_3$ display broad multiplets in the range 7.08 – 6.65 ppm, which are assigned as the aromatic protons of the biphenyloxide groups of the **biphen** ligand.

The ^{13}C NMR spectra of Ln(**biphen**)$_3$ complexes in $CDCl_3$ exhibit similar patterns as shown in Figure 4.12 for the Eu(**biphen**)$_3$ complex, which is presented as a representative example. The spectrum reveals eight sets of signals in the aromatic region, in agreement with the 3-fold symmetry of the complex.

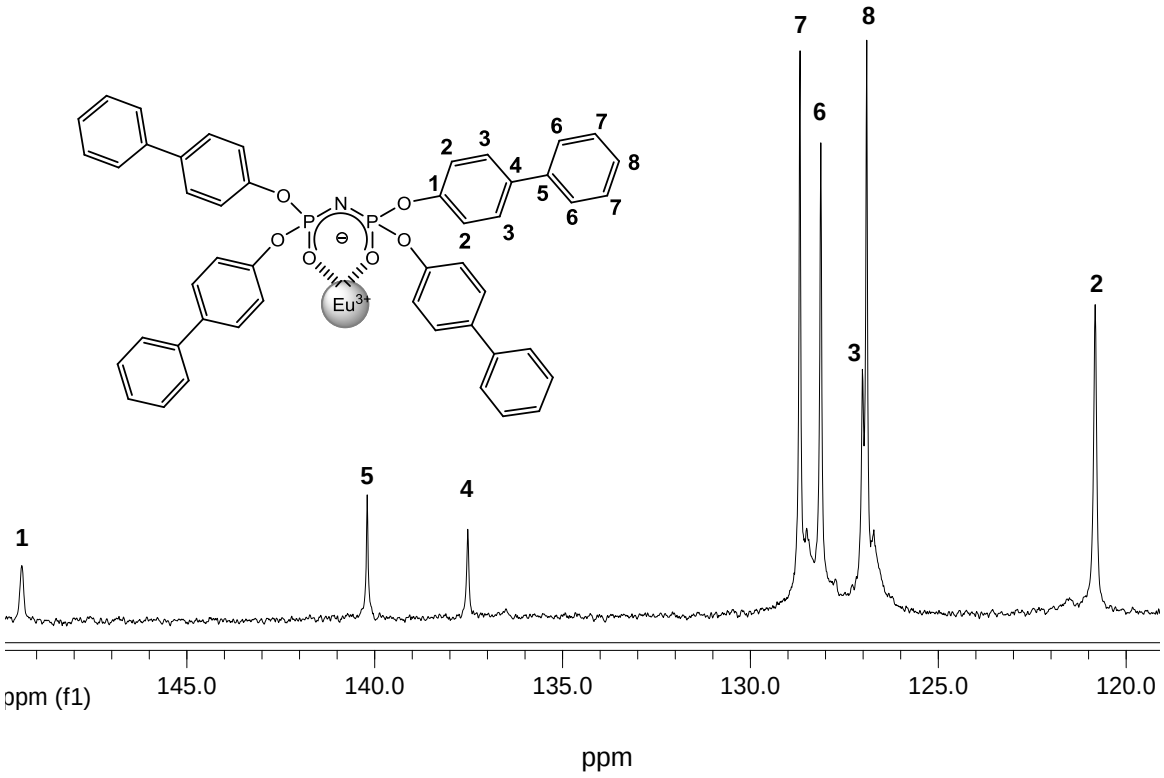

Figure 4.12. The 75 MHz ^{13}C NMR spectrum of Eu(**biphen**)$_3$ in $CDCl_3$. Inset depicts part of the complex with the labelling scheme.

^{1}H - ^{13}C HSQC and ^{1}H-^{1}H COSY spectra of Tb(**biphen**)$_3$ (See Appendix A1 and A2) demonstrated further verification of the correct assignments predicted from the ^{1}H and ^{13}C NMR studies for the Ln(**biphen**)$_3$ complexes.

The summary of NMR studies of Ln(**biphen**)$_3$ is presented in Table 4.2.

Table 4.2. Summary of NMR data for Ln(**biphen**)$_3$ (Ln = Eu, Td, Dy, Sm, Nd, Er, Yb) and Y(**biphen**)$_3$ complexes.

	δ $^{31}P\{^1H\}$ ($CDCl_3$)	δ^1H ($CDCl_3$)	$\delta^{13}C\{^1H\}$ ($CDCl_3$)
Eu(**biphen**)$_3$	- 81.5 (s)	7.08 - 7.40 (108H, m, Ar)	149.4 (C_1), 140.2 (C_5), 137.5 (C_4) 128.7 (C_7), 128.1 (C_6), 127.0 (C_3) 126.9 (C_8), 120.8 (C_2)
Tb(**biphen**)$_3$	- 93.2 (br,s)	6.66 (12H, s, H_e) 6.47 (24H, s, H_d) 5.55 (24H, s, H_c) 3.91 (48H, br,s, H_a, H_b)	150.1 (C_1), 142.6 (C_5), 138.2 (C_4) 130.3 (C_7), 127.6 (C_6), 126.1 (C_3) 125.3 (C_8), 120.8 (C_2)
Dy(**biphen**)$_3$	- 57.2 (br,s)	6.66 (12H, s, H_e) 6.46 (24H, s, H_d) 5.65 (24H, s, H_c) 4.18 (48H, br,s, H_a, H_b)	149.8 (C_1), 141.3 (C_5), 137.2 (C_4), 129.6 (C_7), 128.1 (C_6), 126.6 (C_3), 125.7 (C_8), 121.1 (C_2)
Sm(**biphen**)$_3$	- 4.0 (s)	6.89 - 7.27 (108H, m, Ar)	151.0 (C_1), 140.0 (C_5), 137.4 (C_4), 128.6 (C_7), 128.0 (C_6), 126.9 (C_3), 126.8 (C_8), 121.0 (C_2)
Nd(**biphen**)$_3$	29.2 (s)	7.43 (12H, br,s, H_e) 6.59 - 7.14 (96H, br,m, Ar)	152.3 (C_1), 140.0 (C_5), 137.2 (C_4), 128.5 (C_7), 127.9 (C_6), 126.6 (C_3), 126.4 (C_8), 121.2 (C_2)
Er(**biphen**)$_3$	-76.8 (br,s)	6.65 - 7.15 (108H, m, Ar)	149.8 (C_1), 140.3 (C_5), 138.0 (C_4), 128.7 (C_7), 128.5 (C_6), 127.3 (C_3), 126.2 (C_8), 121.1 (C_2)
Yb(**biphen**)$_3$	- 6.3 (s)	8.60 (12H, br,s, H_e) 7.82 (24H, br,s, H_d) 7.43 (24H, br,s, H_c) 7.29 - 7.31 (48H, br,m, H_a,H_b)	147.0 (C_1), 138.7 (C_5), 136.3 (C_4), 128.1 (C_7), 127.9 (C_6), 127.1(C_3), 126.9 (C_8), 119.4 (C_2)
Y(**biphen**)$_3$	- 6.2 (s)	7.04 - 7.16 (108H, m, Ar)	149.8 (C_1), 140.3 (C_5), 138.0 (C_4), 128.7 (C_7), 128.5 (C_6), 127.3 (C_3) 126.7 (C_8), 120.3 (C_2)

The correct identity of the Ln(**biphen**)$_3$ complexes can be also seen in MALDI TOF mass spectra. All the lanthanide complexes showed intense signals corresponding to $[M]^+$ and $[M+Na]^+$ respectively. The distinctive isotopic patterns observed for all complexes resemble the calculated isotopic distribution as shown in Figure 4.13 for Gd(**biphen**)$_3$ complex.

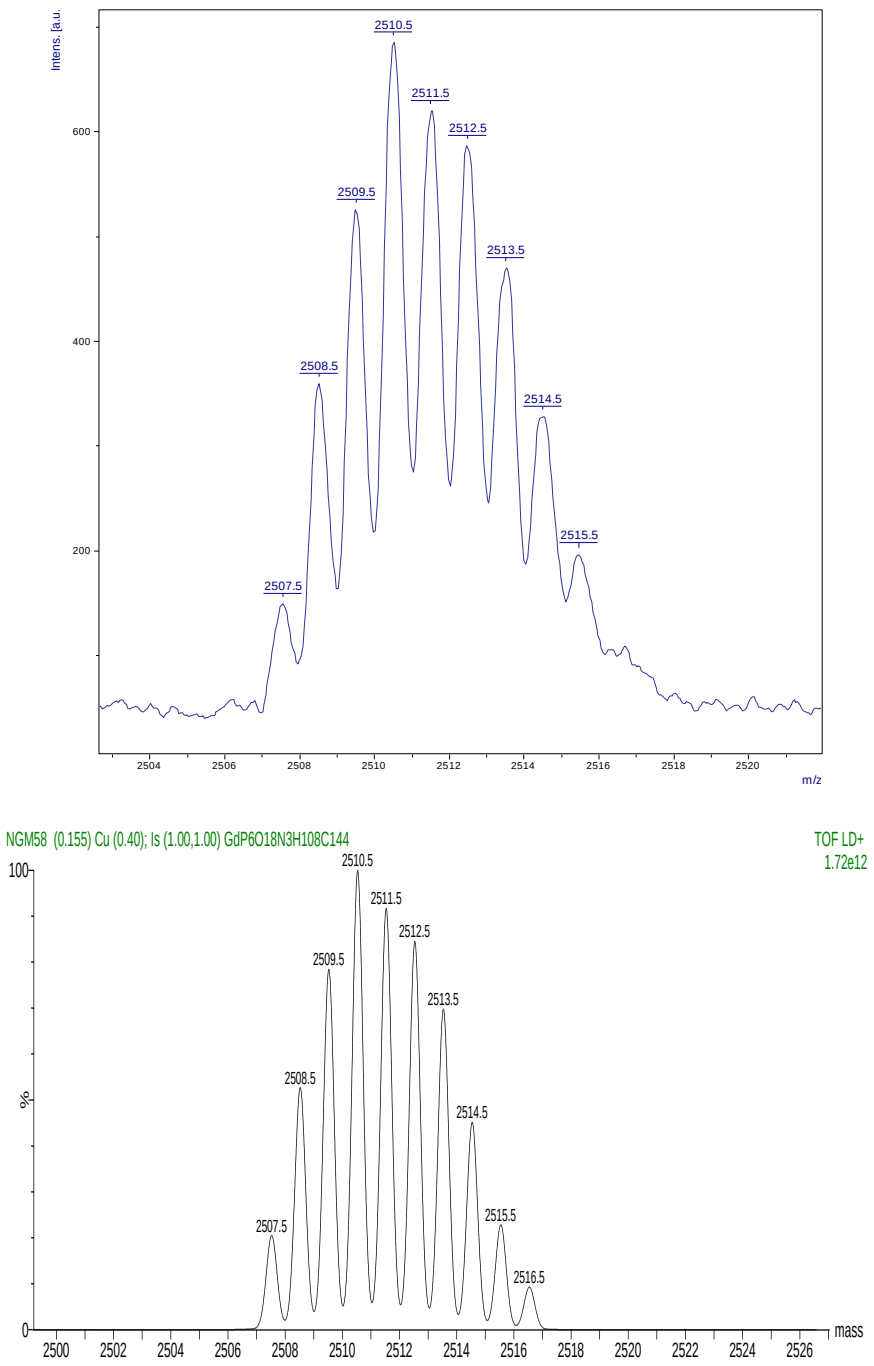

Figure 4.13. Experimental (top) and calculated isotopic distribution (bottom) of the Gb(**biphen**)$_3$ complex.

Elemental analysis and photophysical studies also confirmed the formation of the complexes.

The IR spectra of Nd(**biphen**)$_3$ was obtained on the powder sample (Figure 4.14). It displays characteristic P=O absorptions centred at about 1,140 cm^{-1}. Sharp bands centred at 914 cm^{-1} can be ascribed to the absorption of PNP stretch. Complexation of the ligands through P=O functions is reflected in the P=O vibrations, which are shifted toward lower wavenumbers by approximately 20 cm^{-1}. The present broad absorbance in the region between 3,000 and 3,600 cm^{-1} is attributed to the O-H stretching vibrations of coordinated water molecules.

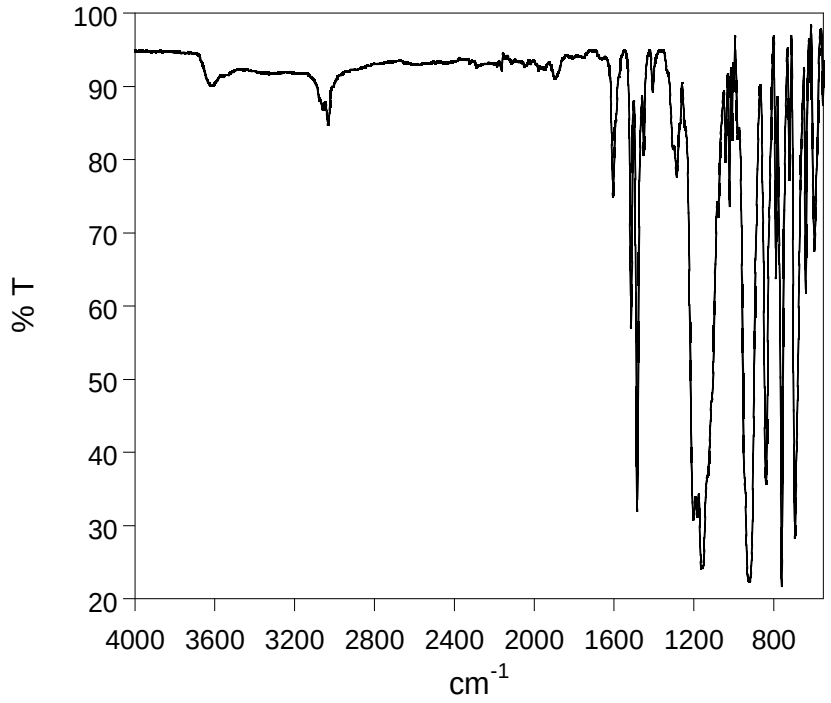

Figure 4.14. The IR spectrum of a powder sample of Nd(**biphen**)$_3$ complex.

4.3. Photophysical Properties of Ln(biphen)$_3$

4.3.1. The Visible Emitting Complexes

The absorption spectra of Ln(**biphen**)$_3$ complexes were recorded in THF, due to better solubility of complexes when compared to acetonitrile. All Ln(**biphen**)$_3$ show a broad electronic envelope centred at 255 nm, which can be assigned to the intramolecular π->π* ligand-based transitions of biphenyl moieties, as illustrated in Figure 4.15 for the Sm(**biphen**)$_3$ complex. The molar extinction coefficient value for the peak maximum at 255 nm is 199,262 dm^3 mol^{-1} cm^{-1} which is approximately three times larger compared to the free ligand. This confirms the presence of three ligands per complex in solution. The trends in the absorption spectra of Ln(**biphen**)$_3$ complexes are identical to the one observed for the free ligand. The absorption pattern is characteristic of transitions in biphenyl moieties.[3]

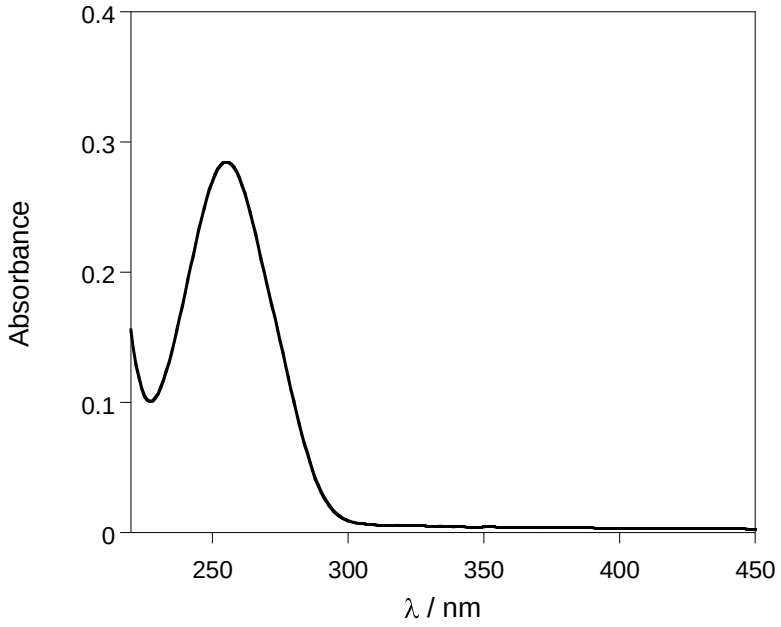

Figure 4.15. The absorption spectrum of Sm(**biphen**)$_3$ in THF.

The luminescence spectra of Ln(**biphen**)$_3$ complexes were recorded in THF and acetonitrile solution at room temperature. All complexes exhibit emission bands characteristic of the corresponding lanthanide ion, independent of excitation wavelength.

The luminescence spectrum upon ligand-centred excitation at 255 nm of Eu(**biphen**)$_3$ is shown in Figure 4.16. Characteristic Eu^{3+} bands are observed at 576, 589, 611, 651 and 689 nm, corresponding to the $^5D_0$->^7F_J transitions (J = 0, 1, 2, 3, 4). The emission spectrum has a single peak at 576 nm attributed to the $^5D_0$ -> $^7F_0$ transition, which suggests a low symmetry environment of the Eu^{3+} centre. The low symmetry is also confirmed by the highly intense $^5D_0$ -> $^2F_2$ hypersensitive transition at 611 nm, compared to the $^5D_0$ -> $^7F_1$.[8]

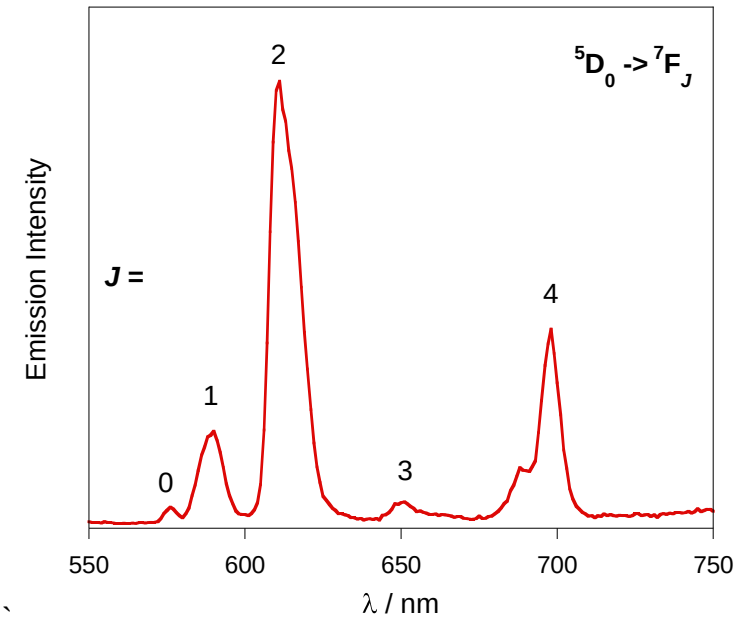

Figure 4.16. Emission spectrum of Eu(**biphen**)$_3$ in dry CH_3CN, λ_{exc} = 255 nm.

Under an excitation of 255 nm, Tb(**biphen**)$_3$ complex displays characteristic green narrow emission bands at 487, 542, 584, 619, 648, 671 and 679 nm, arising from

$^5D_4$ -> ^7F_J (J = 6 - 0) transitions of Tb^{3+} ion. The spectrum is dominated by the hypersensitive $^5D_4$ -> $^7F_5$ transition at 542 nm as demonstrated in Figure 4.17.

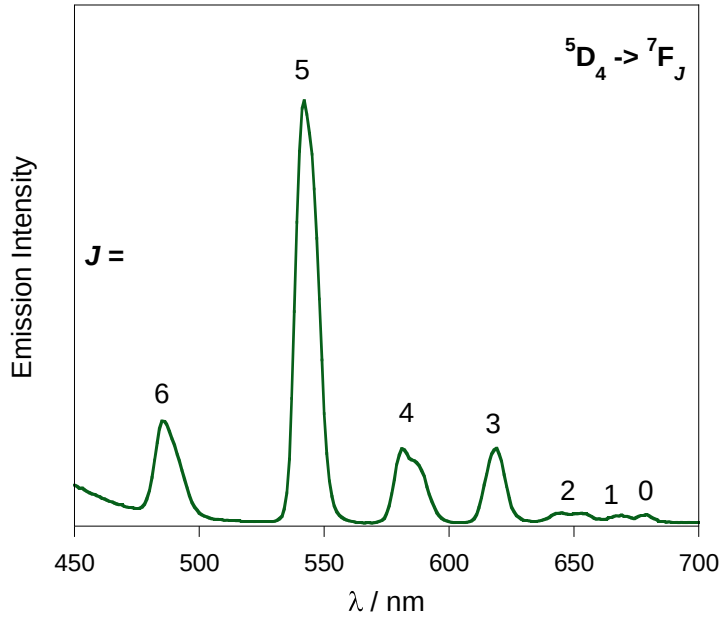

Figure 4.17. Emission spectrum of Tb(**biphen**)$_3$ in dry CH_3CN, λ_{exc} = 255 nm.

Likewise, for Dy(**biphen**)$_3$ complex, excitation of the ligand at 255 nm populates the Dy^{3+} excited state, leading to yellow line emission due to $^4F_{9/2}$ -> ^6H_J transitions (J = 15/2, 13/2, 11/2, 9/2) at 479, 573, 663 and 751 nm respectively. The most intense hypersensitive band at 573 nm, corresponds to the $^4F_{9/2}$ -> $^6H_{13/2}$ transition (Figure 4.18).

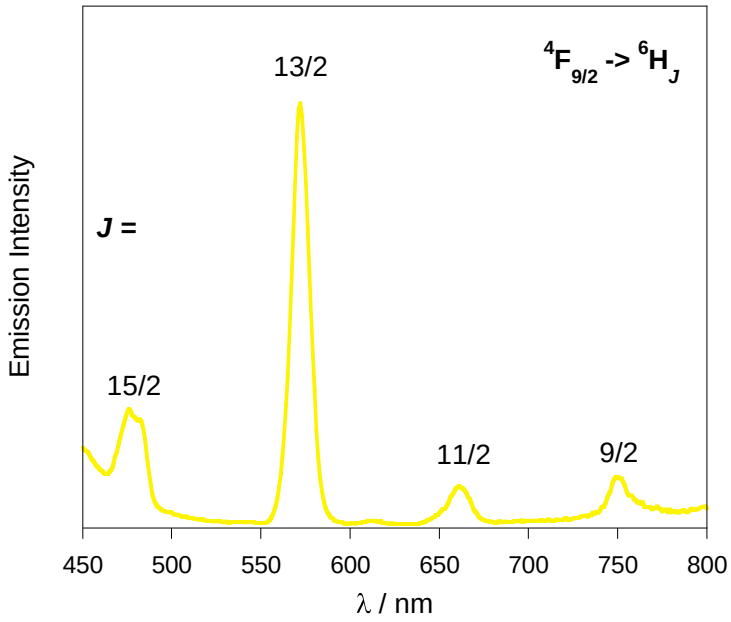

Figure 4.18. Emission spectrum of Dy(**biphen**)$_3$ in dry CH_3CN, λ_{exc} = 255 nm.

The excitation of Sm(**biphen**)$_3$ in the UV region is followed by fast relaxation to the $^4G_{5/2}$ state, from which radiative decay to the four ^6H_J levels (J = 5/2, 7/2, 9/2, 11/2) at 559, 594, 640 and 699 nm can be readily observed in the visible region of the emission spectrum (Figure 4.19).

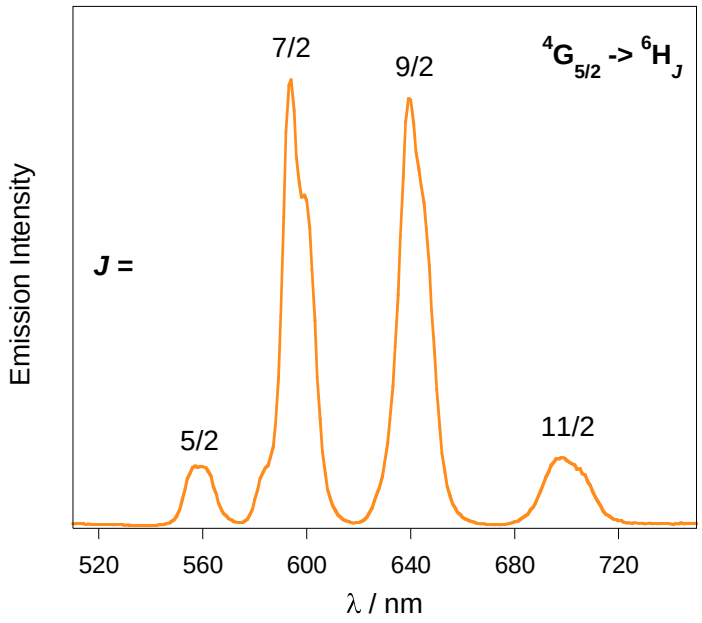

Figure 4.19. Emission spectrum of Sm(**biphen**)$_3$ in dry CH_3CN, λ_{exc} = 255 nm.

After a closer inspection, it was found that emission spectra of Tb(**biphen**)$_3$ and Dy(**biphen**)$_3$ complexes, in addition to typical Tb^{3+} and Dy^{3+} emission peaks, also reveal an intense band centred at 322 nm, which can be attributed to ligand-based fluorescence (Figure 4.20). The presence of a significant amount of ligand emission indicates that the intramolecular ligand to lanthanide energy transfer is incomplete in Tb(**biphen**)$_3$ and Dy(**biphen**)$_3$ complexes. The observation of ligand based emission due to incomplete energy transfer has been reported previously for various lanthanide complexes.[9-12]

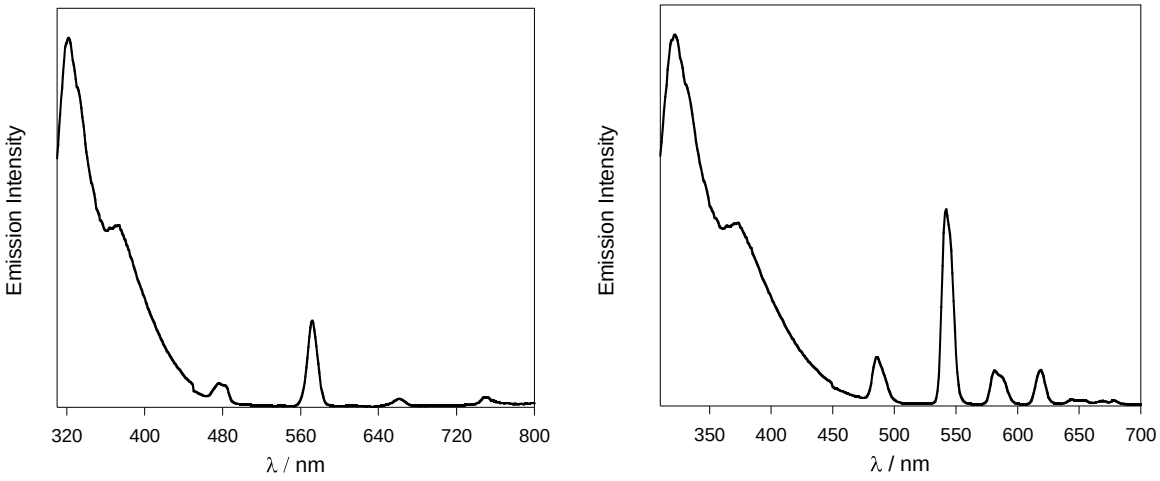

Figure 4.20. Emission spectra of Dy(**biphen**)$_3$ (left) and Tb(**biphen**)$_3$ (right) in dry CH_3CN, λ_{exc} = 255 nm.

The excitation spectrum of Tb(**biphen**)$_3$ complex monitored around the peak of the intense $^5D_4$ -> $^7F_5$ transition (542 nm) of the Tb^{3+} ion exhibits a broad band, which can be assigned to the π–π^* electronic transitions of **biphen** ligands (Figure 4.21). A close resemblance of the excitation spectrum to the UV-Vis absorption spectrum of the Tb(**biphen**)$_3$ is indicative of sensitised emission *via* energy transfer. The similar pattern has also been observed in excitation spectrum of other Ln(**biphen**)$_3$ complexes.

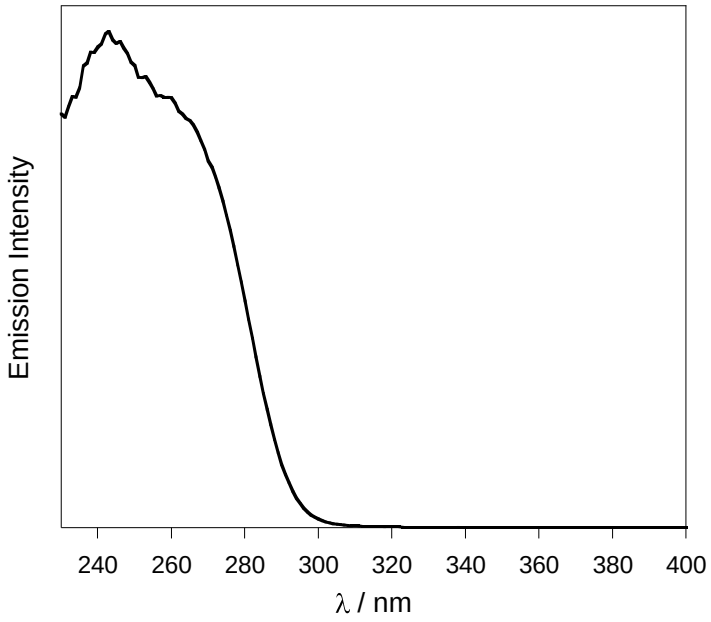

Figure 4.21. The corrected excitation spectrum of Tb(**biphen**)$_3$ in THF, λ_{em} = 542 nm.

It was found that the emission intensity of Ln(**biphen**)$_3$ depends strongly on the solvent. Enhanced emission intensity is observed in polar acetonitrile compared to those in non-polar THF. This phenomenon may be rationalised by the effect of environmental polarity. It has been reported that non-radiative rates are smaller in polar solvents.[13]

In order to better understand the symmetry around the central Ln^{3+} ion, the solid-state photophysical properties of Ln(**biphen**)$_3$ complexes were also investigated. Upon excitation into absorption band at 255 nm, complexes display the metal-based emission with the characteristic spectral distribution for the respective Ln^{3+} ion.

Figure 4.22 exhibits the emission spectrum of powder sample of Eu(**biphen**)$_3$. The characteristic red emission is observed, corresponding to the 4*f*-4*f* transitions of the $^5D_0$ excited state to the low-lying ^7F_J (J = 0, 1, 2, 3, 4) levels of Eu^{3+} ion. The $^5D_0$ -> $^7F_2$ transition at 614 nm dominates the whole emission spectrum. The broader

bandwidth of the hypersensitive $^5D_0$ -> $^7F_2$ transition and a significant reduced intensity of the $^5D_0$ -> $^7F_4$ transition are pointing to a different coordination environment around Eu^{3+} ion in the solid state.

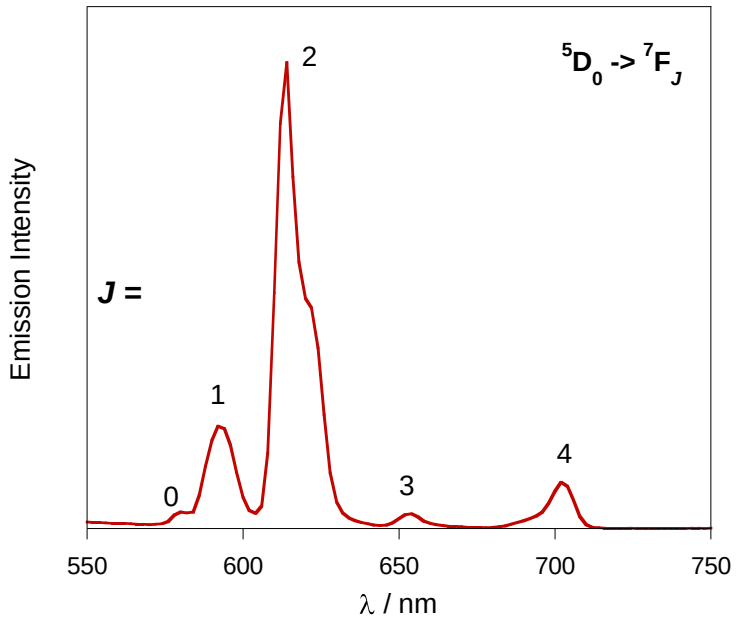

Figure 4.22. Emission spectrum of powder sample of Eu(**biphen**)$_3$, λ_{exc} = 255 nm.

Irradiation of powder sample of Dy(**biphen**)$_3$ upon the ligand based band at 255 nm leads to characteristic yellow line emission (Figure 4.23) with four main bands centred at 482, 575, 668 and 758 nm. These bands can be assigned as the $^4F_{9/2}$ -> ^6H_J (J = 15/2, 13/2, 11/2 and 9/2) transitions of Dy^{3+} ion. The most intense peak at 575 nm corresponds to the hypersensitive transition $^4F_{9/2}$ -> $^6H_{13/2}$. The overall shape of the spectrum is very similar to the one observed in solution.

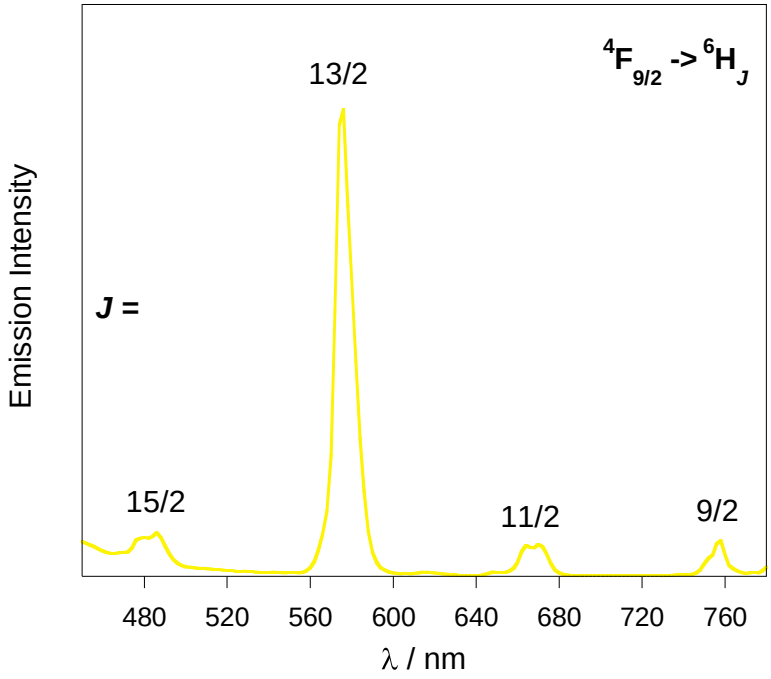

Figure 4.23. Emission spectrum of powder sample of Dy(**biphen**)$_3$, λ_{exc} = 255 nm.

The sensitisation process in powder sample of Sm(**biphen**)$_3$ leads to the strong orange *f-f* emission in the visible region due to the $^4G_{5/2}$ -> ^6H_J transitions (J = 5/2, 7/2, 9/2, 11/2) of Sm^{3+} at 563, 601, 648 and 709 nm (Figure 4.24). The spectrum pattern is almost identical compared to one recorded in solution, hence no significant changes in symmetry occur in solid state of Sm(**biphen**)$_3$ complex.

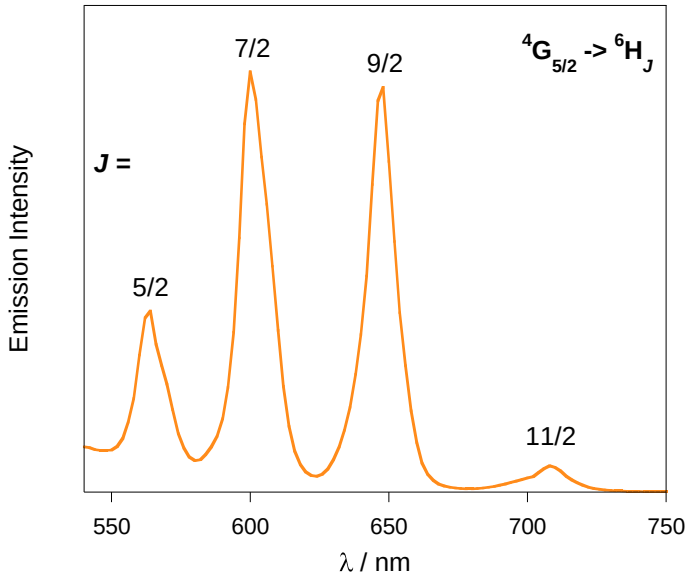

Figure 4.24. Emission spectrum of powder sample of Sm(**biphen**)$_3$, λ_{exc} = 255 nm.

The $^5D_4$ -> ^7F_J (J = 6-0) transitions of Tb^{3+} are observed for powder sample of Tb(**biphen**)$_3$ after excitation into the ligand-based π–π^* absorption band at 255 nm (Figure 4.25). The intense $^5D_4$ -> $^7F_5$ band is slightly split into two peaks at 544 and 548 nm, which is indicative of a less symmetrical environment around the Tb^{3+} ion in solid state.

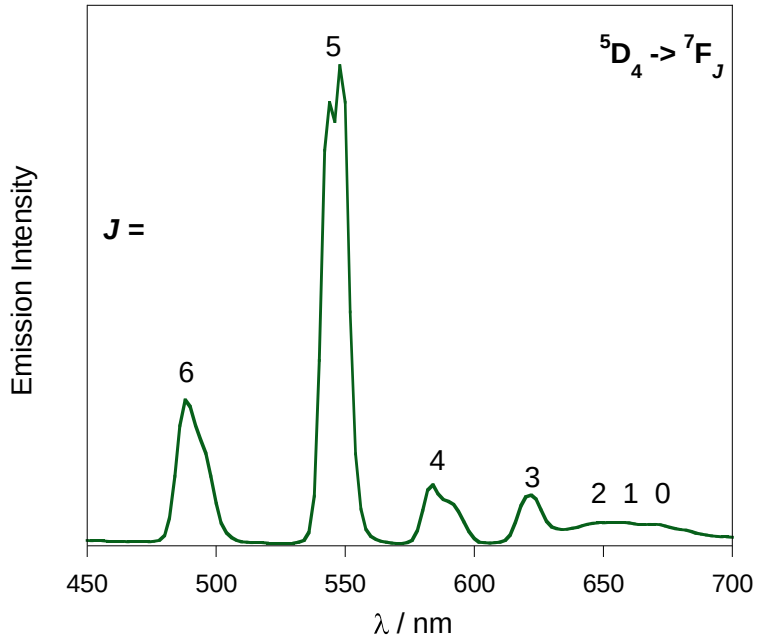

Figure 4.25. Emission spectrum of powder sample of Tb(**biphen**)$_3$, λ_{exc} = 255 nm.

Emission spectra of powder samples of Tb(**biphen**)$_3$ and Dy(**biphen**)$_3$ complexes, again display a broad ligand based emission band in additional to the characteristic peaks of Tb^{3+} and Dy^{3+} ion. However, the intensity of this band is considerably smaller compared to the equivalent solution-phase spectra as illustrated in Figure 4.26 for Tb(**biphen**)$_3$ complex.

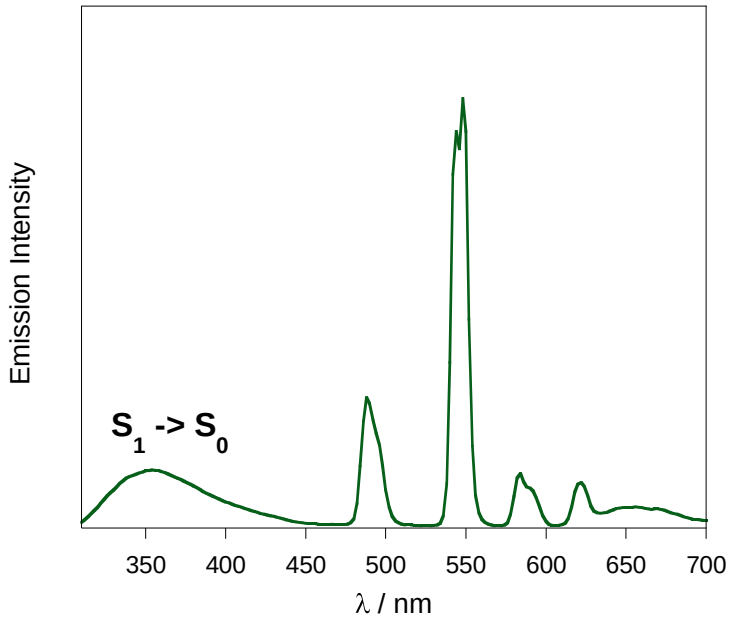

Figure 4.26. Emission spectrum of powder sample of Tb(**biphen**)$_3$, λ_{exc} = 255 nm.

Luminescence efficiency has been assessed by quantum yield determinations upon ligand excitation for each of the differing Ln(**biphen**)$_3$ complex, with results summarised in Table 4.3. The luminescence quantum yields were determined in dry acetonitrile solution using quinine sulphate in 1N H_2SO_4[14] and $[Ru(bpy)_3]Cl_2$ in aerated H_2O[15] as a reference.

Table 4.3. Luminescence quantum yields for Ln(**biphen**)$_3$ (Ln = Eu, Tb, Sm, Dy) complexes, λ_{exc} = 255 nm.

	Φ λ_{exc} = 255 nm (dry CH_3CN)
Eu(**bipehn**)$_3$	0. 5%
Tb(**bipehn**)$_3$	5.1%
Sm(**biphen**)$_3$	1.5%
Dy(**biphen**)$_3$	1.5%

Observed values of quantum yield indicate that the intersystem crossing and the energy transfer are affected in Tb^{3+}, Dy^{3+} and Eu^{3+} **biphen** complexes, resulting in an insufficient sensitisation process. However, it is noteworthy that the absolute quantum yield of 1.5% for Sm(**biphen**)$_3$ is relatively large for a Sm^{3+} containing compound. Generally, Sm^{3+} complexes display poor luminescence properties due to the energy gap between the lowest sublevel of $^4G_{5/2}$ and the highest sublevel of $^6F_{11/2}$ being around 7,400 cm^{-1}, which favours non-radiative de-excitation processes. Non-radiative deactivations are most pronounced in compounds with organic chromophores, which possess vibrations (C-H, O-H) of relatively high energy.[16]

In order to gain more information about the coordination environment and degree of quenching of the Ln^{3+}, time-resolved luminescence experiments at the maxima excitation and emission wavelengths in solution and powder of Ln(**biphen**)$_3$ complexes were determined at room temperature. The observed values are summarised in Table 4.4. The resultant decay curves for solution and powder samples are fitted by mono-exponential function, which is indicative of presence of single emissive species in Ln(**biphen**)$_3$ complexes. A typical decay profile is shown in Figure 4.27 for Tb(**biphen**)$_3$ complex.

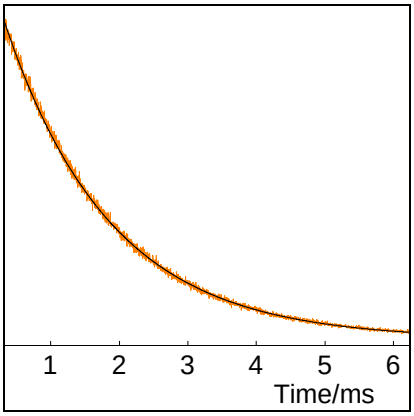

Figure 4.27. The fitted single-exponential decay of Tb(**biphen**)$_3$ complex in dry CH_3CN, λ_{exc} = 255 nm and λ_{em} = 542 nm.

Table 4.4. Luminescence lifetimes of the Tb^{3+} ($^5D_4$), Eu^{3+} ($^5D_0$), Dy^{3+} ($^4F_{9/2}$) and Sm^{3+} ($^4G_{5/2}$) levels in Ln(**biphen**)$_3$ (Ln= Tb, Eu, Dy, Sm) (λ_{exc} = 255 nm). [a] = 10 mol dm^{-3}.

Complex	**Sample**	τ / μs
Tb(**biphen**)$_3$	powder	1543
	dry CH_3CN	2131
	dry CH_3CN + H_2O[a]	1201
Eu(**biphen**)$_3$	powder	773
	dry CH_3CN	1915
	dry CH_3CN + H_2O[a]	537
Dy(**biphen**)$_3$	powder	95
	dry CH_3CN	181
Sm(**biphen**)$_3$	powder	71
	dry CH_3CN	116

The relative short luminescence lifetimes are suggesting that **biphen** ligand does not provide a significant level of protection from non-radiative deactivation of the Tb^{3+} and Eu^{3+} ions by solvent molecules.

Compared to the results in solid state, complexes in dry acetonitrile show a considerable lengthening of the luminescence lifetimes. This may be because molecules are densely packed and under the strong influence of neighbouring molecules in the solid state.

The different lifetime observed for each Ln^{3+} complex can be explained by considering the energy gap between the luminescent state and the highest *J* level of the ground state.[16] The ΔE is similar for Dy^{3+} (7,850 cm^{-1}) and Sm^{3+} (7,400 cm^{-1}) respectively, whereas for Eu^{3+} and Tb^{3+} the gap is considerably larger at 12,300 cm^{-1} and 14,800 cm^{-1}. Therefore, only the high energy O-H oscillators contribute to vibrational quenching for Eu^{3+} and Tb^{3+}. The smaller gap for Dy^{3+} and Sm^{3+} results in lower frequency vibrations, causing significant deactivation. This explains why the lifetimes of Dy(**biphen**)$_3$ and Sm(**biphen**)$_3$ complexes are much shorter than those of Tb(**biphen**)$_3$ and Eu(**biphen**)$_3$ complexes in dry acetonitrile.

Determination of the number of water molecules present in the inner coordination sphere of the Tb^{3+} and Eu^{3+} was done by using the equation 4.1:

$$q = A\,(k_{H2O} - k_{CH3CN}) \qquad \textbf{(eq. 4.1)}$$

This equation utilising observed lifetime differences in CH_3CN solution and CH_3CN solution containing the equal amounts of H_2O. *q* (uncertainty ± 0.5) is the number of coordinated water molecules in the primary coordination sphere, *A* is a proportionality constant (A_{Eu} = 1.05, A_{Tb} = 4.2), k_{H2O} is observed decay rate in aqueous CH_3CN, k_{CH3CN} is the observed decay rate in dry CH_3CN.[17]

The application of Equation (4.1) to the values presented in Table 4.4 give q = 1.5 ± 0.5 and q = 1.4 ± 0.5 for Tb(**biphen**)$_3$ and Eu(**biphen**)$_3$ respectively, in aqueous CH_3CN. Hydration numbers for Tb(**biphen**)$_3$ and Eu(**biphen**)$_3$ complexes in both cases correspond approximately up to two water molecules bound directly to the Tb^{3+} and Eu^{3+} ion to fill the coordination sphere. Since Sm^{3+} and Dy^{3+} complexes have analogous coordination chemistry, similar q values are expected for Sm(**biphen**)$_3$ and Dy(**biphen**)$_3$. The obtained results with Ln(**tpOp**)$_3$ complexes, where q values were calculated as q = 0.7 ± 0.5 and q = 0.3 ± 0.5 for Tb(**tpOp**)$_3$ and Eu(**tpOp**)$_3$ respectively, suggests that the degree of protection against non-radiative deactivation provided by three **biphen** ligands around the central lanthanide ions is reduced. Therefore, the introduction of extra phenyl ring on chromophore groups in **biphen** does not provide better shielding against quenching solvents molecules compare to the **tpOp** ligand.

In order to rationalise poor luminescence behaviour of the Ln(**biphen**)$_3$ complexes, the position of the lowest excited-state triplet energy was determined, using the Gd(**biphen**)$_3$ complex. As explained in Chapter two, the Gd(**biphen**)$_3$ allows the study of the **biphen** antenna luminescence in the absence of energy transfer, because Gd^{3+} ion facilitates the spin flip process of the ligand sensitiser from the singlet excited state to the triplet excited state by the heavy atom effect.[18] Also the Gd^{3+} ion has the lowest energy emitting state ($^6P_{7/2}$) at 32,150 cm^{-1}, therefore cannot accept any energy from the excited state of **biphen** as demonstrated in Scheme 4.5. Thus, the emission spectrum of the Gd(**biphen**)$_3$ complex shows exclusively ligand-centred emission.

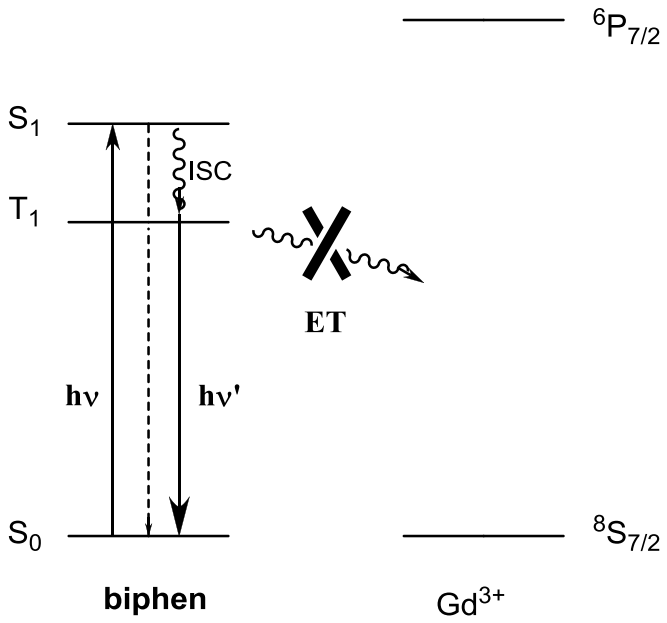

Scheme 4.5. Jablonski diagram of the phosphorescence process in Gd(**biphen**)$_3$.

Excitation at 255 nm of Gd(**biphen**)$_3$ in MeOH/EtOH (1:4) solution at room temperature, results in a ligand-centred fluorescence, displaying a broadband with a maximum around 322 nm as depicted in Figure 4.28. Phosphorescence does not usually occur at room temperature in the liquid state, because of the nature of the phosphorescent transition, which is very slow (with the lifetime up to minutes), and so is deactivated by numerous collisions with solvent leading to intersystem crossing to S_0 and subsequent vibrational deactivation. For that reason the phosphorescence spectrum of Gb(**biphen**)$_3$ was measured at 77 K in MeOH/EtOH (20:80) glass, the rigid matrix and low temperature favouring ligand-based phosphorescence.

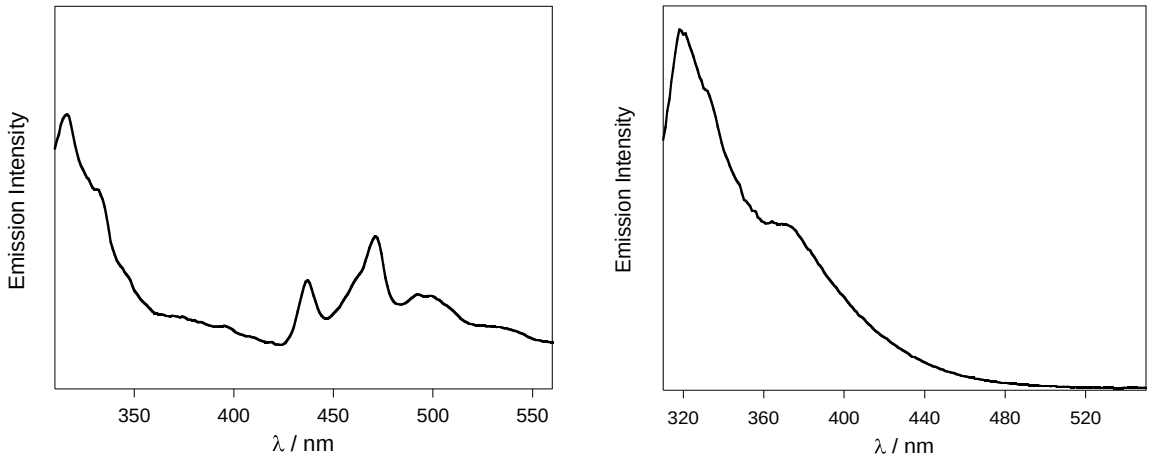

Figure 4.28. The emission spectra of Gd(**biphen**)$_3$ at 77K (left) and room temperature (right) in MeOH/EtOH 20:80, λ_{exc} = 255 nm.

The spectrum of Gd(**biphen**)$_3$ at 77 K (Figure 4.28) exhibits two distinct areas; one band around 320 nm, which can be attributed to ligand fluorescence, whereas the band centred at 470 nm is assigned to the ligand phosphorescence. The phosphorescence spectrum of the Gd(**biphen**)$_3$ also displays vibrational progressions attributable to ring-breathing modes. Their calculated energies are tabulated in Table 4.5.

Table 4.5. Phosphorescent vibronic transitions in Gd(**biphen**)$_3$ at 77 K.

λ_{max} (nm)	ν-ν'	Energy (cm^{-1})
437	0 - 0	22,883
467	0 - 1	21,413
490	0 - 2	20,408

It can be seen in the Scheme 4.6 that the position of the lowest triplet state T_1 was estimated to be 22,883 cm^{-1}. The lowest excited singlet state was calculated at 33, 333 cm^{-1} from the absorption edge of the Gb(**biphen**)$_3$ complex.

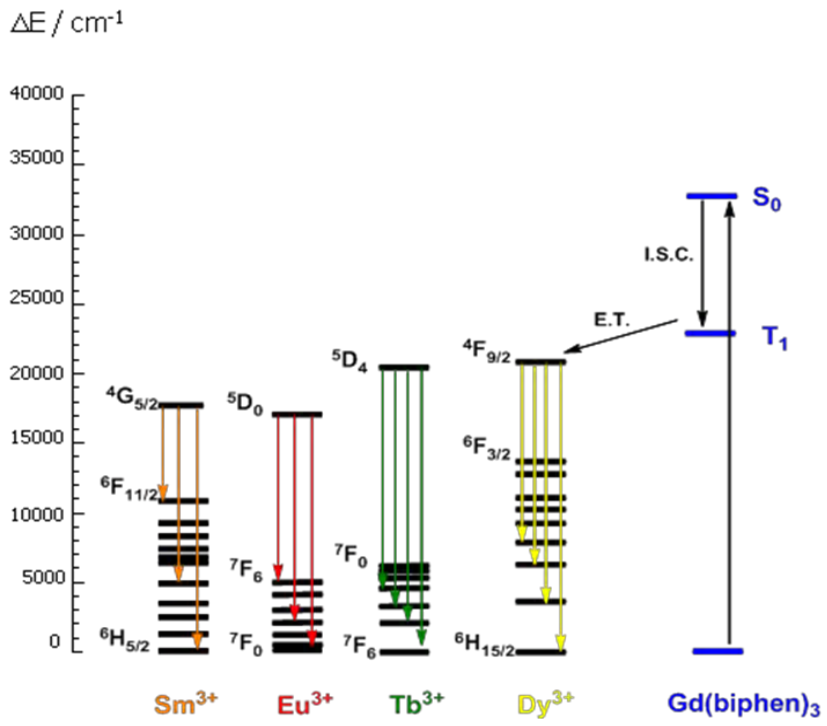

Scheme 4.6. Energy level diagram showing the lowest Ln^{3+} excited states and the estimated triplet state of the **biphen** sensitiser in the Gd(**biphen**)$_3$ complex.

The lowest excited singlet state and triplet state for the **biphen** ligand are ~ 10,500 cm^{-1} apart in energy, which suggests a relatively low rate of intersystem crossing, which may be contributing to low quantum yields. Furthermore, the position of the ligand triplet level is important when considering the emissive properties of the complexes because the efficiency of the energy transfer from the ligand T_1 state to the lanthanide excited state is strongly dependent on the energy difference between these levels.

Latva *et al.*[19] reported that the best intramolecular energy transfer from a triplet state of ligand to emitting $^5D_4$ level of Tb^{3+} ion occurs when the energy gap between triplet state of the ligand and the first emitting $^5D_4$ of the Tb^{3+} is higher than 2,000 cm^{-1}. Bünzli reported that optimal energy gap between triplet state of ligand and the emitting state of Ln^{3+} ions is between 2,500 – 3,500 cm^{-1}.[20] In the Tb(**biphen**)$_3$

complex, the gap between T_1 and $^5D_4$ emitting level is *ca*. 2,380 cm^{-1} and further reduced in Dy(**biphen**)$_3$ where the energy gap between T_1 and $^4F_{9/2}$ emitting level is only 1,783 cm^{-1}. The low energy of triplet state in **biphen** therefore limits its application to act as an efficient sensitiser for Tb^{3+} and Dy^{3+} because of the competing back energy transfer. This is in a good agreement with small values of quantum yield and lifetime observed for Tb(**biphen**)$_3$ and Dy(**biphen**)$_3$ complexes. On the other hand, the T_1 energy level for Eu(**biphen**)$_3$ and Sm(**biphen**)$_3$ lie ~ 5,700 cm^{-1} and ~ 5,200 cm^{-1} higher than the emitting excited 4*f* level ($^5D_0$; 17, 200 cm^{-1}) and ($^4G_{5/2}$; 17,700 cm^{-1}) of Eu^{3+} and Sm^{3+} ion. Therefore, **biphen** should act as a suitable sensitiser for Eu^{3+} and Sm^{3+} ions.

In comparison, values of luminescence lifetime and quantum yield for Eu^{3+}, Tb^{3+} and Dy^{3+} **biphen** complexes are much smaller compared to those previously reported in section 2.3.1 for Ln(**tpOp**)$_3$ complexes. Low luminescence performances of Ln(**biphen**)$_3$ complexes can be explained as follows:

Firstly, the triplet energy level of the **biphen** antenna (22,883 cm^{-1}) is significantly lowered in energy compared to the value of 27,397 cm^{-1} observed for the **tpOp.** Therefore, the change of the nature of triplet state position of **biphen** ligand is strongly effecting the photophysical properties of visible Ln(**biphen**)$_3$ complexes. The energy level of T_1 is too close in energy to the emitting levels of $^5D_4$ and $^4F_{9/2}$ of Tb^{3+} and Dy^{3+} ions, which results in the energy back-transfer. Thus, the **biphen** may be acting as a less efficient sensitiser for Tb^{3+} and Dy^{3+} ions. Furthermore, Tb(**biphen**)$_3$ and Dy(**biphen**)$_3$ display in addition to their metal-based emissions also a strong ligand fluorescence, which further confirms that the energy transfer from **biphen** to Tb^{3+} and Dy^{3+} is not efficient. This is another reason behind poor luminescence

behaviour of these two complexes. However, for Eu(**biphen**)$_3$ and Sm(**biphen**)$_3$ complexes, the emitting levels $^5D_0$ and $^4G_{5/2}$ of Eu^{3+} and Sm^{3+} ion respectively, are better matched in energy to the proposed triplet level of the **biphen**, therefore one would expect an efficient sensitisation of these ions.The Sm(**biphen**)$_3$ exhibited an intense luminescence of Sm^{3+} ion, with a relatively high quantum yield of 1.5 % and 116 μs luminescence lifetime in CH_3CN, which is indicative of an efficient ligand-to-metal energy transfer and an effective shielding of the Sm^{3+} ion from radiationless deactivation in spite of the presence of water molecules coordinated to the ion. On the other hand, Eu(**biphen**)$_3$ displayed unexpectedly a low quantum yield of 0.5% and relatively short lifetime of 1.9 ms in acetonitrile solution.

In summary, Ln(**biphen**)$_3$ complexes showed less efficient shielding of the lanthanide ions from water solvent molecules, which also resulted in a drop of the quantum yields and lifetimes for Ln(**biphen**)$_3$ complexes, relative to their **tpOp** analogues. The replacement of phenyl groups with biphenyl introduced 60 additional C-H oscillators per complex, in relatively close proximity to the lanthanide ion. As a consequence the effect of C-H vibrational oscillations had an ability to efficiently quench the luminescence of Ln(**biphen**)$_3$ complexes. The same line of reasoning applies to the case of significant decrease in lifetimes for Tb(**biphen**)$_3$ (2.1 ms) and Eu(**biphen**)$_3$ (1.9 ms) compared to those of 3.1 ms and 2.7 ms for Tb**(tpOp**)$_3$ and Eu(**tpOp**)$_3$ complexes.

Quantum yields of 5.1% and 1.5% for Tb(**biphen**)$_3$ and Dy(**biphen**)$_3$ are also very low compared to those of 23% and 5.8% for Tb(**tpOp**)$_3$ and Dy(**tpOp**)$_3$, respectively.

This is not surprising because the energy level of T_1 of the **tpOp** lies too high for competitive thermal back energy transfer.

4.3.2. The NIR Emitting Complexes

The UV-vis absorption spectrum of Yb(**biphen**)$_3$ in THF is shown in Figure 4.29. The spectrum exhibits an unstructured ligand-based band centred at around 255 nm (ε_{255} = 199,156 dm^3 mol^{-1} cm^{-1}) assigned as π-π* transitions of biphenyl moieties. Absorption spectra of Nd(**biphen**)$_3$ and Er(**biphen**)$_3$ in THF displayed a similar pattern to that of Yb(**biphen**)$_3$.

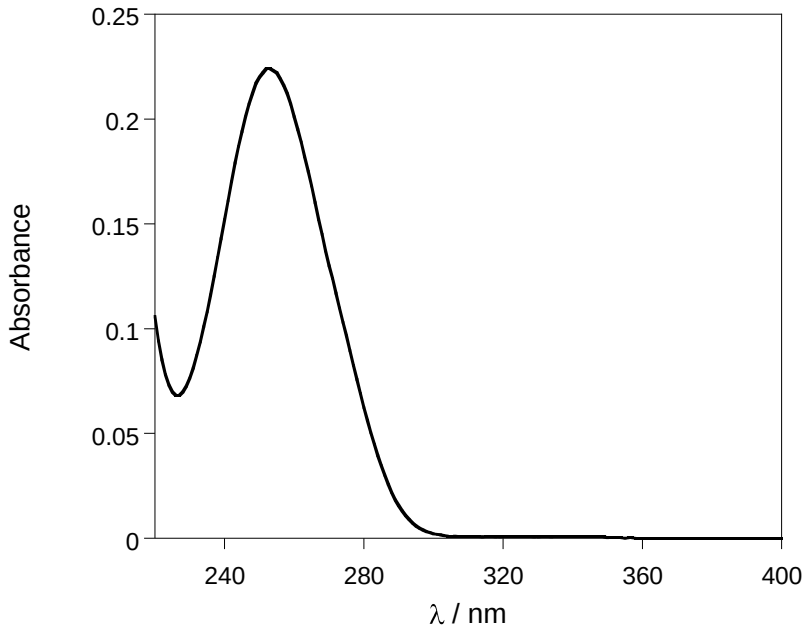

Figure 4.29. The absorption spectrum of Yb(**biphen**)$_3$ in THF.

The photophysical properties of Ln(**biphen**)$_3$ (Ln = Yb, Nd, Er) were examined in CH_3CN solution at room temperature. Upon excitation through ligand-based band, Yb(**biphen**)$_3$ and Nd(**biphen**)$_3$ complexes exhibit luminescence characteristic of the

corresponding Yb^{3+} and Nd^{3+} ion. However, the excitation of Er(**biphen**)$_3$ complex at 255 nm in acetonitrile solution, did not show any detectable emission.

Upon irradiation at 255 nm, the Yb(**biphen**)$_3$ complex exhibits good emissive behaviour. The typical emission band for $^2F_{5/2}$ -> $^2F_{7/2}$ transition at 975 nm is observed with extensive splitting due to vibronic coupling[21] (Figure 4.30).

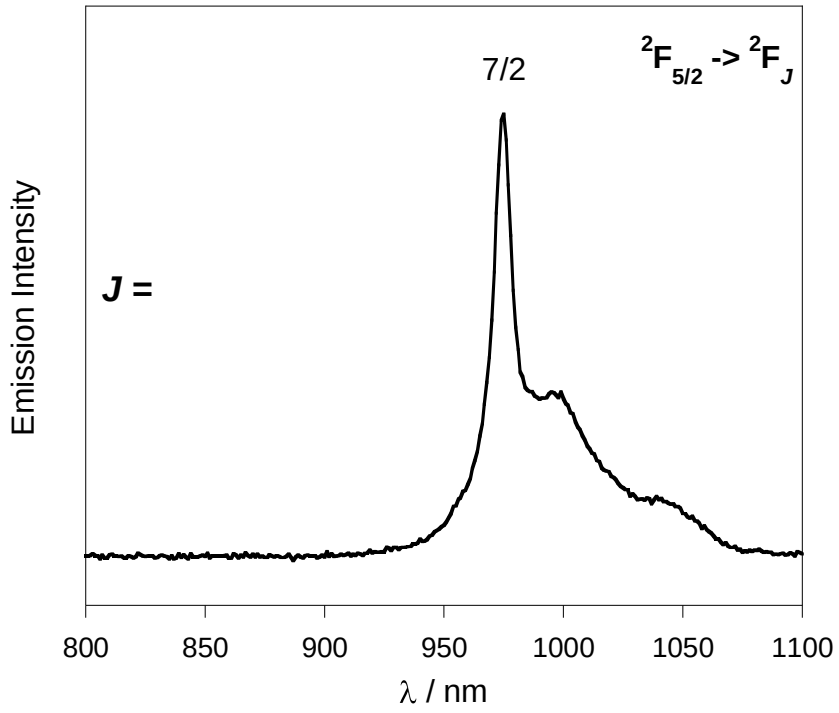

Figure 4.30. Emission spectrum of Yb(**biphen**)$_3$ in dry CH_3CN, λ_{exc} = 255 nm.

Excitation of Nd(**biphen**)$_3$ in acetonitrile solution at 255 nm yields the characteristic near infra-red emission at 890, 1055 and 1325 nm assigned to the $^4F_{3/2}$ -> ^4I_J (J = 9/2, 11/2 and 13/2) transitions of Nd^{3+} as shown in Figure 4.31.

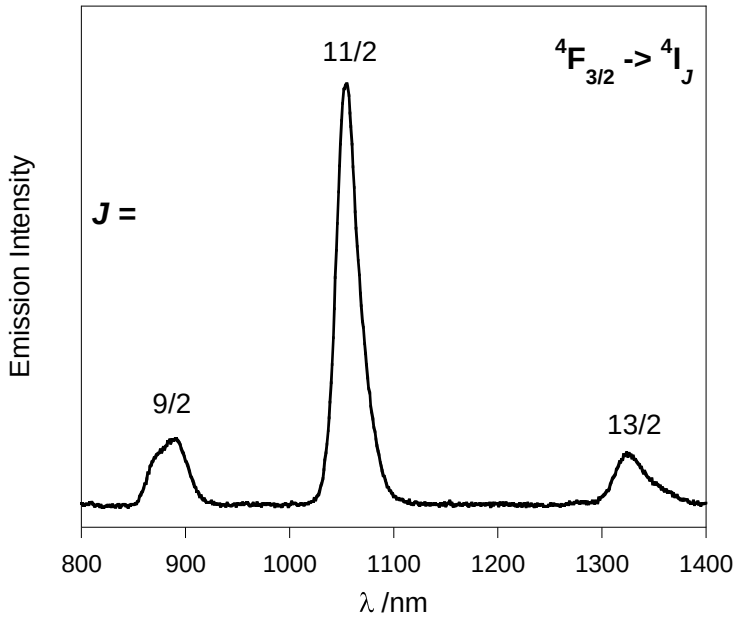

Figure 4.31. Emission spectrum of Nd(**biphen**)$_3$ in dry CH_3CN, λ_{exc} = 255 nm.

The excitation spectra of the lanthanide complexes in acetonitrile solution, confirm that the **biphen** is responsible for sensitisation of Yb^{3+} and Nd^{3+} emission *via* the energy transfer process. Monitoring of the strongest *f-f* transition at 975 nm ($^2F_{5/2}$ -> $^2F_{7/2}$) of Yb(**biphen**)$_3$ display an unstructured band from 240 – 300 nm (Figure 4.32). The excitation profile closely resembles the absorption spectrum of Yb(**biphen**)$_3$ demonstrating energy transfer from ligand to lanthanide ion to be responsible for the sensitised emission observed in Yb(**biphen**)$_3$.

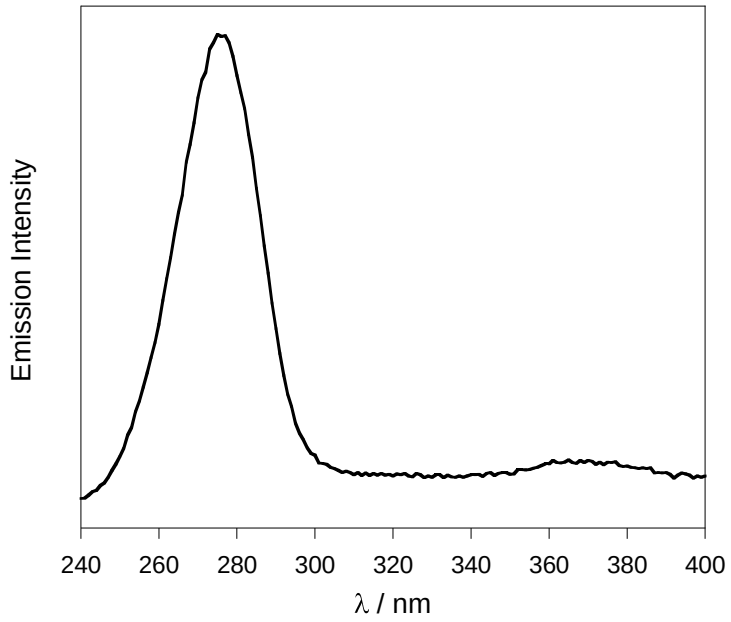

Figure 4.32. The excitation spectrum of Yb(**biphen**)$_3$ in CH_3CN, λ_{em} = 975 nm.

The photophysical properties of Yb(**biphen**)$_3$ and Nd(**biphen**)$_3$ complexes were also studied in solid state. The luminescence spectra exhibited peaks corresponding to the expected *f-f* NIR transitions of Yb^{3+} and Nd^{3+} ion, upon irradiation at 255 nm.

The powder sample of Nd(**biphen**)$_3$ display characteristic three bands in the range of 850 – 1400 nm (Figure 4.33), which can be assigned to $^4F_{3/2}$ -> $^4I_{9/2}$ (890 nm), $^4F_{3/2}$ -> $^4I_{11/2}$ (1,055 nm) and $^4F_{3/2}$ -> $^4I_{13/2}$ (1,328 nm) transitions of Nd^{3+} ion, respectively.

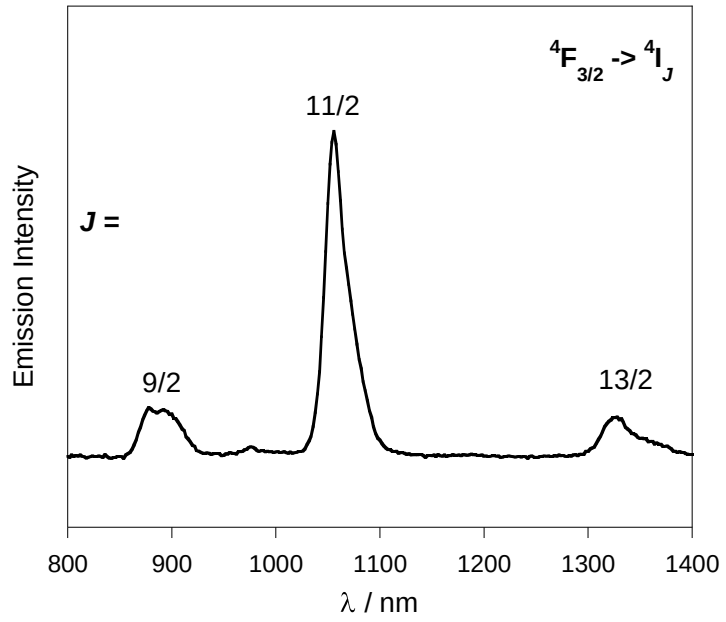

Figure 4.33. Emission spectrum of powder sample of Nd(**biphen**)$_3$, λ_{exc} = 255 nm.

Upon irradiation at 255 nm, the powder sample of Yb(**biphen**)$_3$ complex emits in the range of 950 - 1,100 nm, with the sharp band at 975 nm corresponding to the $^2F_{5/2}$ -> $^2F_{7/2}$ transition, and a broader vibronic component at longer wavelength as depicted in Figure 4.34.

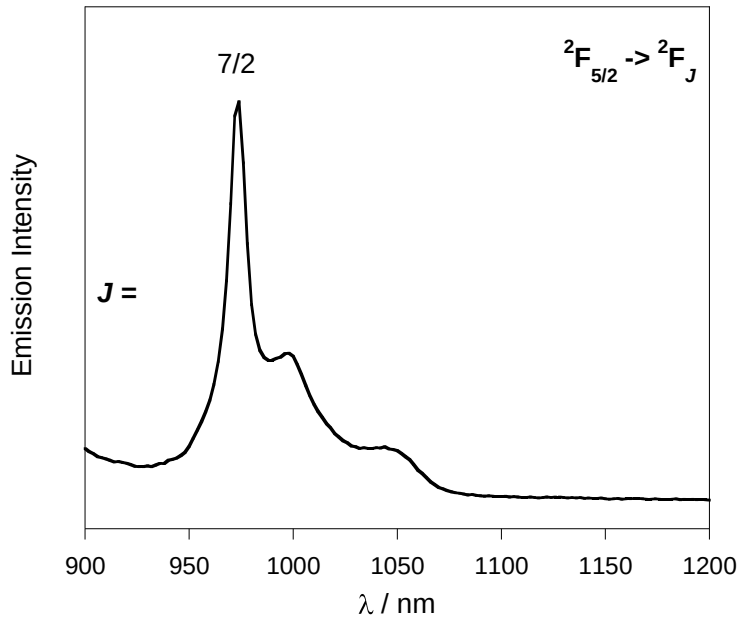

Figure 4.34. Emission spectrum of powder sample of Yb(**biphen**)$_3$, λ_{exc} = 255 nm.

The emission and excitation spectra of Yb(**biphen**)$_3$ and Nd(**biphen**)$_3$ complexes confirm the suitability of the **biphen** ligand in sensitising of NIR luminescence of Yb^{3+} and Nd^{3+} ion. This is in a good agreement with the position of the triplet energy of Gd(**biphen**)$_3$, which indicates that the level is suitable positioned for the energy transfer into the Near-emitting states of Nd^{3+} (11,200 cm^{-1}), Yb^{3+} (10,300 cm^{-1}) and Er^{3+} (6,500 cm^{-1}) as demonstrated in Scheme 4.7.

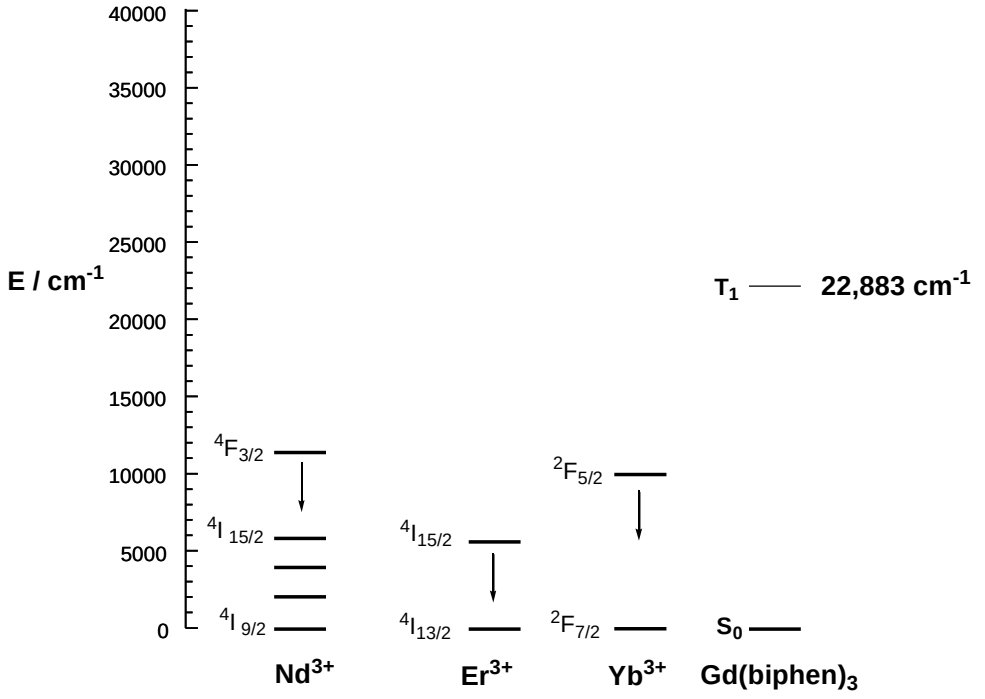

Scheme 4.7. The energy levels of the 4*f* levels responsible for the NIR luminescence.

However, in the case of Er(**biphen**)$_3$, the sensitisation of Er^{3+} ion is particularly difficult in the presence of water molecules in the inner coordination sphere due to O-H vibrations having a large quenching effect. Furthermore, the presence of 60 additional C-H overtones in Er(**biphen**)$_3$, which are resonant with the NIR emission of Er^{3+} ion, might also enhance the non-radiative decay of the $^4I_{13/2}$ electronic level,

due to vibrational couplings. Hence, photophysical properties of Er(**biphen**)$_3$ were not investigated any further.

To provide a better insight into how the effect of non-radiative deactivating pathways for NIR lanthanide emission varies between the solid state and in solution, the luminescence lifetimes of powder and solution samples of Yb(**biphen**)$_3$ and Nd(**biphen**)$_3$ complexes were measured.

The respective NIR luminescence decay curves obtained from time-resolved luminescence experiments can be fitted in all cases mono-exponentially, indicating the presence of only one emitting centre in solution and solid state as demonstrated in Figure 4.35 for Yb(**biphen**)$_3$ in dry acetonitrile solution. The obtained results of luminescence lifetimes are summarised in Table 4.6.

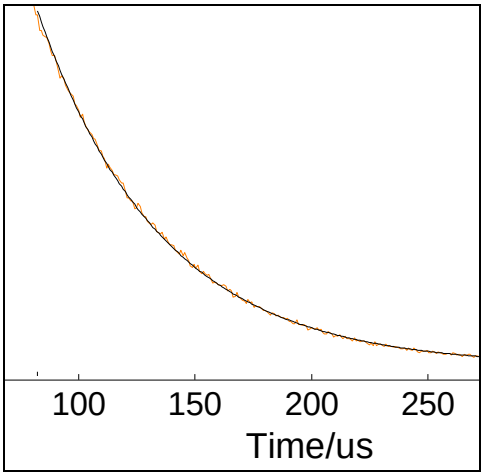

Figure 4.35. The fitted single-exponential decay of Yb(**biphen**)$_3$ complex in dry CH_3CN, λ_{exc} = 255 nm and λ_{em} = 975 nm.

Table 4.6. Luminescence lifetimes (τ_{obs}) of the Yb^{3+} ($^2F_{5/2}$) and Nd^{3+} ($^4F_{3/2}$) levels in Yb(**biphen**)$_3$ and Nd(**biphen**)$_3$, λ_{exc} = 255 nm at RT.

Complex	τ_{obs} / μs dry CH_3CN	τ_{obs} / μs d_6-DMSO	τ_{obs} / μs powder
Yb(**biphen**)$_3$	58.2	69.1	53.0
Nd(**biphen**)$_3$	4.5	11.5	4.3

Luminescence lifetimes obtained for Yb(**biphen**)$_3$ and Nd(**biphen**)$_3$ are sizeable and compare well with those reported for Yb(**tpop**)$_3$ (61.8 μs) and Nd(**tpOp**)$_3$ (3.3 μs) complexes in dry acetonitrile solution. Furthermore, the solvent effect on lifetimes was examined. The luminescence lifetimes were significantly enhanced in d_6-DMSO solution, which indicated that water solvent molecules coordinated to the Ln^{3+} ion were replaced by coordinating DMSO solvent. As the d_6-DMSO does not contain any high energy C-H or O-H vibrational oscillators, which would efficiently quench the NIR- emission of Yb^{3+} and Nd^{3+} ion, the significant improvement was observed in the luminescence lifetimes of Yb(**biphen**)$_3$ and Nd(**biphen**)$_3$ complexes.

Also the luminescence lifetimes for solid powders of Yb(**biphen**)$_3$ and Nd(**biphen**)$_3$ showed an improvement over those analogous **tpOp** of Yb^{3+} and Nd^{3+} complexes in solid state, where the lifetimes could not been detected due to weak signals. This behaviour can be anticipated to better ability of the **biphen** ligand transferring energy onto the NIR emissive levels of Nd^{3+} and Yb^{3+} as a direct consequence of more suitable lying triplet energy level of **biphen**.

The intrinsic quantum yield (Φ_{Ln}) of Nd(biphen)$_3$ and Yb(biphen)$_3$ complexes can be estimated by using the relationship defined in equation 4.2.[22,23]

$$\Phi_{Ln} = \tau_{obs} / \tau_{rad} \qquad \text{(eq. 4.2)}$$

Where τ_{obs} is the observed emission lifetime and τ_{rad} is the radiative decay. Estimated values of τ_{rad} in organic systems are 800 μs for Nd^{3+} and 2,000 μs for Yb^{3+}, respectively.[24] However, this method for the determination of quantum yield does not take into account other factors such as intersystem crossing efficiency or energy transfer process that other methods of quantum yield determination using optically dilute standards account for. Application of τ_{obs} values presented in Table 4.6 to the equation 4.2 gave the estimated intrinsic quantum yield 0.6% and 2.9% for Nd(**biphen**)$_3$ and Yb(**biphen**)$_3$ respectively. The calculated values of intrinsic quantum yield for Ln(**biphe**n)$_3$, Ln(**tpOp**)$_3$ and Ln(**tpip**)$_3$[25] (Ln = Nd, Yb) complexes are summarised in Table 4.7.

Table 4.7. Calculated intrinsic quantum yields (Φ_{Ln}) for Ln(**biphen**)$_3$, Ln(**tpOp**)$_3$ and Ln(**tpip**)$_3$ (Ln = Nd, Yb) in dry CH_3CN.

Complex	Φ_{Ln} (%)
Nd(**biphen**)$_3$	0.6
Nd(**tpOp**)$_3$	0.4
Nd(**tpip**)$_3$	0.3
Yb(**biphen**)$_3$	2.9
Yb(**tpOp**)$_3$	3.1
Yb(**tpip**)$_3$	2.6

The quantum yield values obtained for Nd(**biphen**)$_3$ and Yb(**biphen**)$_3$ compare very well to analogues **tpOp** and **tpip** Nd^{3+} and Yb^{3+} complexes. These results demonstrate the suitability of **biphen** moieties to sensitise emission of Nd^{3+} and Yb^{3+}. Despite the fact that quantum yields were not reported due to the absence of an appropriate standard reference and the lack of technical equipment, the obtained intrinsic quantum yields are still comparable to those results for complexes based on organic chromophores, which were specifically designed for near-infrared sensitisation by sulfonylaminate, deuterated or fluorinated ligands.[26-37]

4.4. Conclusion

In this chapter, a new bi-dentate tetrabiphenyl imidodiphosphate ligand was presented. The H**biphen** was easily modified, without changing the binding site for the complexation of lanthanide ions. H**biphen** has been successfully synthesised and fully characterised.

Lanthanide complexes have been formed by reaction of one lanthanide cation with three **biphen** ligands. Ln(**biphen**)$_3$ (Ln = Tb, Dy, Sm, Eu, Gd, Yb, Nd, Er) complexes have been isolated and fully characterised. Unfortunately, attempts to grow suitable crystals for X-ray analysis of Ln(**biphen**)$_3$ complexes were not successful.

The energy level of the triplet state was calculated for the Gd(**biphen**)$_3$ ligand, which revealed that the ligand was not suitable for an efficient sensitisation of Tb^{3+} and Dy^{3+} emission as the low lying energy of the triplet state resulted in energy back transfer.

The photophysical properties of visible emitting complexes have been investigated in solid state and solution at room temperature. UV-vis absorption and excitation spectra of Ln(**biphen**)$_3$ complexes displayed the similar pattern of a broad band, corresponding to π–π^* transitions of biphenyl moieties. All visible complexes showed characteristic emission of the corresponding lanthanide ion in solution and in the solid state, upon excitation of the antenna at 255 nm. In the case of Tb(**biphen**)$_3$ and Dy(**biphen**)$_3$, emission spectra also revealed a broad emission band corresponding to the ligand centred $^1\pi$–π^* state, which confirmed incomplete energy transfer.

The overall luminescence quantum yields of Ln(**biphen**)$_3$ (Ln = Tb, Dy, Eu, Sm) were measured in acetonitrile solution and were found to be rather weak. Especially for Tb^{3+}, Dy^{3+} and Eu^{3+} **biphen** complexes, with emission intensities in the order of Tb >> Dy ~ Sm >> Eu. Small values of quantum yield measurements of 5.1% and 1.5% also verified inefficient energy transfer in Tb^{3+} and Dy^{3+} complexes, due to energy back transfer between the **biphen** triplet energy level and the $^5D_4$ and $^4F_{9/2}$ excited state of Tb^{3+} and Dy^{3+} ion, respectively.

The presence of a de-excitation pathway involving energy back-transfer from the excited state of Tb^{3+} and Dy^{3+} to the ligand is also confirmed by short luminescence lifetimes. Furthermore, lifetime measurements of Ln(**biphen**)$_3$ complexes showed that solvent molecules are not excluded from the first coordination sphere and the Ln^{3+} ion can possibly bind up to two water molecules. Therefore, the additional of 12 phenyl rings on chromophores provided only enhanced absorption to the lanthanide complexes, but did not have expected beneficial effect on the increase of visible luminescence in Ln(**biphen**)$_3$ (Ln = Tb, Dy, Eu) complexes.

Near-infrared emitting complexes Ln(**biphen**)$_3$ (Ln = Yb, Nd, Er) have been also prepared and their photophysical properties investigated in the solid state and solution.

On the other hand, the electronic feature of the **biphen** ligand showed to be better suited for populating the NIR emitting excited states of Nd^{3+} and Yb^{3+}. With these two ions effective energy transfer took place from the ligand to the metal. The suitability of the **biphen** ligand as a sensitiser for NIR luminescence of Yb^{3+} and Nd^{3+} ion has

been demonstrated by the excitation spectra which matched well with absorption spectra and relatively long luminescence lifetimes of Ln(**biphen**)$_3$ (Ln = Yb, Nd).

It can be concluded that the **biphen** due to its triplet state located at lower energy compared to the **tpOp** ligand, is more efficient in sensitising the NIR-emitting Yb^{3+} and Nd^{3+} ions, in despite of the lower degree of protection against the non-radiative deactivations caused by presence of water molecules in the first coordination sphere.

4.5. Experimental

4.5.1. Materials

All reagents were purchased from Aldrich or Alfa Aesar and were used as received. KH was purchased as 35% dispersion in mineral oil which was removed prior to use by thorough washing with hexane.

Anhydrous toluene was freshly distilled over sodium-benzophenone.

4.5.2. Preparation of tris-biphenyl phosphate

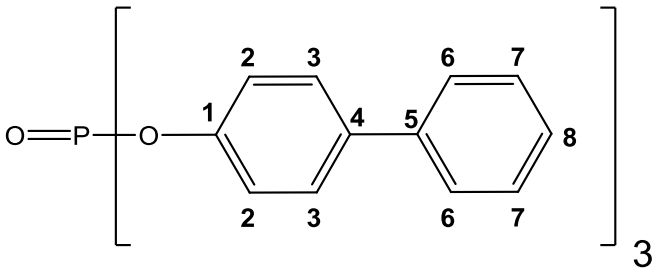

NaOH (1.12 g, 29.4 mmol) was dissolved in ethanol (17 cm^3) in a 3-necked flask equipped with a Dean and Stark head, dropping funnel, nitrogen inlet and mechanical stirrer. The suspension of 4-phenylphenol (5.00 g, 29.4 mmol) in dry toluene (15 cm^3) was added, then fractional distillation of the reaction mixture was carried out. The toluene-ethanol azeotrope (80^oC) was removed and the distillation was continued until the temperature reached the boiling point (110 ^oC) of toluene. At this point the reaction medium became light red. The reaction mixture was allowed to

cool to the room temperature and phosphorus oxychloride (1.44 g, 0.9 ml, 9.4 mmol) was introduced dropwise. The reaction mixture was then heated to reflux for 1.5 h then toluene was removed by distillation. The resulting white solid was washed with water (3 x 10 cm^3) in order to remove the sodium chloride. The crude product was purified on a silica column eluting with chloroform (R_f = 0.35) to yield tris-biphenyl phosphate (4.3 g, 83 %) as a white solid.

$\delta_P\{^1H\}$ (121 MHz, $CDCl_3$): - 17.4 (s); $\delta_C\{^1H\}$ (75 MHz, $CDCl_3$): 150.2 (C_1), 140.3 (C_5), 139.2, (C_4), 129.2 (C_7), 128.9 (C_6), 127.8 (C_3), 127.4 (C_8), 120.8 (C_2); δ_H (300 MHz, $CDCl_3$): 7.30 – 7.62 (m, 27H, Ar); ES-MS(+): *m/z*: 577.3 $[M + Na]^+$.

4.5.3. Preparation of tetrabiphenyl imidodiphosphate-Hbiphen

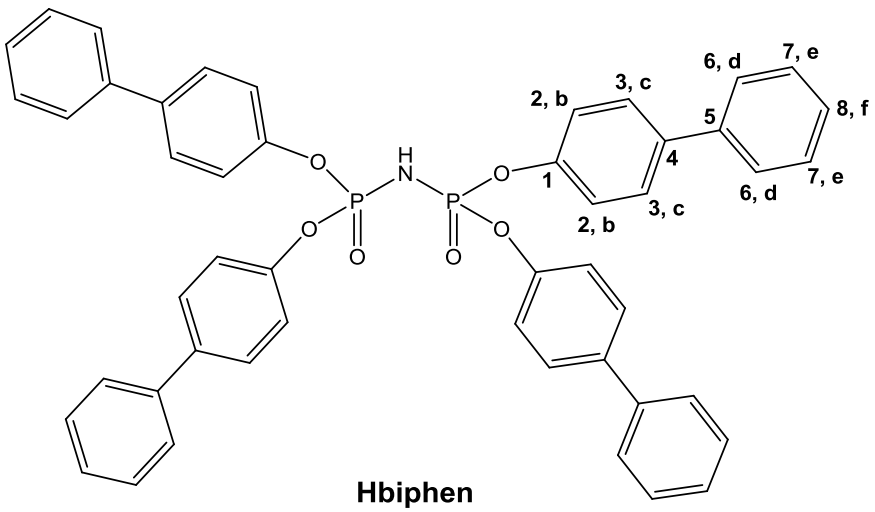

Hbiphen

A suspension of tris-biphenyl phosphate (8.83 g, 15.9 mmol) and sodium amide (1.24 g, 31.1 mmol) in dry toluene (80 cm^3) was heated at reflux for 4 h under N_2.

The resulting mixture was cooled to ~ 40^{o}C and water (50 cm^3) was added to dissolve the sodium biphenyloxide. The toluene layer was extracted, acidified with dilute HCl (5 cm^3, 6 M) and washed with water (2 x 30 cm^3). The volume of the solution was concentrated to ~ 6 cm^3, and hexane (40 cm^3) was added. The solution was then stirred until a white precipitate was formed. The white precipitate was collected by filtration and washed with hexane (2 x 10 cm^3). The desired product was dried under vacuum (5.13 g, 82 %); $\delta_P\{^1H\}$ (121 MHz, $CDCl_3$): - 10.5 (s); $\delta_C\{^1H\}$ (75 MHz, $CDCl_3$): 153.2 (C_1), 140.7 (C_5) 136.0 (C_4), 129.9 (C_7), 128.4 (C_6), 128.0 (C_3), 127.4 (C_8), 121.8 (C_2); δ_H (300 MHz, $CDCl_3$): 7.22 – 7.35 (m, 36H, Ar); MS-ES(-) *m/z*: 784 [*M* - H]$^-$; elemental analysis calcd. (%) for $C_{48}H_{37}N_1O_6P_2(C_7H_8)_{0.5}$: C, 74.36; H, 4.97; N, 1.68; found C, 74.61; H, 4.81; N, 1.55; UV/Vis (CH_3CN): λ in nm (log ε) 255 (4.8).

4.5.4. Preparation of Kbiphen

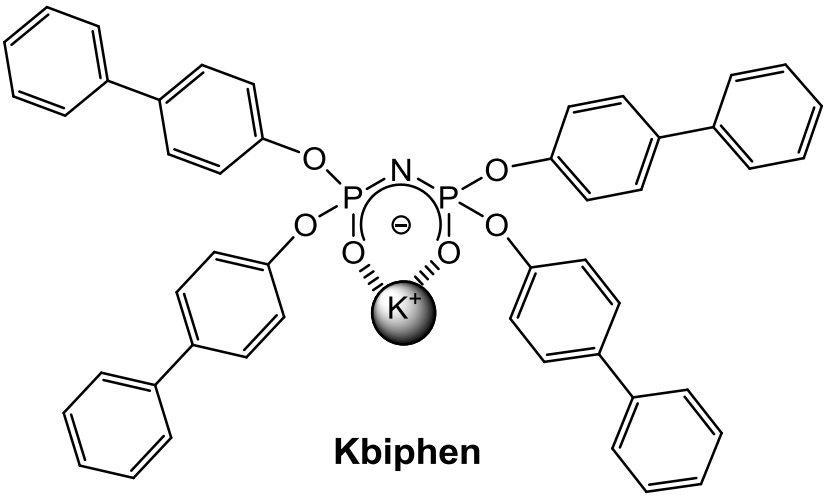

Kbiphen

Potassium hydride (0.41 g, 30% dispersion in mineral oil, 3.05 mmol) was washed with hexane (3 x 5 cm^3) and dried *in vacuo* for 20 min. THF (10 cm^3) was added, followed by tetrabiphenyl imidodiphosphate (2.00 g, 2. 43 mmol) dissolved in THF (20 cm^3). The resulting suspension was stirred for 1 h at room temperature. The solvent was reduced to 5 cm^3 *in vacuo*, which yielded in precipitation of a grey solid, which was collected by filtration and washed with water (10 cm^3). The solid was dried under vacuum, to yield the desired product (1.73 g, 87 %); $\delta_P\{^1H\}$ (121 MHz, $CDCl_3$): - 8.6 (s); $\delta_C\{^1H\}$ (75 MHz, $CDCl_3$): 151.5(C_1), 139.9 (C_5) 136.6 (C_4), 128.6 (C_7), 127.8 (C_6), 126.8 (C_3), 126.7 (C_8), 120.9 (C_2); δ_H (300 MHz, $CDCl_3$): 6.79 – 7.41 (36H, m, Ar); MS-ES(+) *m/z*: 823 $[M]^+$.

4.5.5. Preparation of Ln(biphen)$_3$ (Ln = Eu, Tb, Dy, Sm, Gd, Nd, Yb, Er) and Y(biphen)$_3$

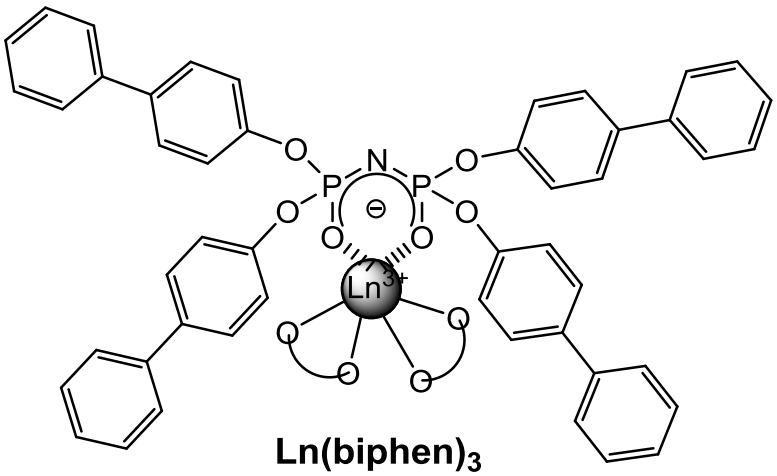

Ln(biphen)$_3$

To a stirring solution of Kbiphen (3 equiv., 0.24 mmol) in hot aqueous EtOH (5 cm^3) a solution of $LnCl_3.6H_2O$ (1 equiv., 0.08 mmol) in aqueous EtOH (5 cm^3) was added dropwise. A white precipitate was formed upon addition. The solid was collected by filtration, washed with water (2 x 5 cm^3) and dried under vacuum.

$Eu(biphen)_3$ - (0.14 g, 70 %); $\delta_P\{^1H\}$ (121 MHz, $CDCl_3$): - 81.5 (s); $\delta_C\{^1H\}$ (300 MHz, $CDCl_3$): 149.4 (C_1), 140.2 (C_5), 137.5 (C_4), 128.7 (C_7), 128.1 (C_6), 127.0 (C_3), 126.9 (C_8), 120.8 (C_2); δ_H (300 MHz, $CDCl_3$): 7.08 – 7.40 (108H, m, Ar); MALDI-MS: *m/z* 2506 $[M]^+$, 2529 $[M+Na]^+$;elemental analysis calcd. (%) for $C_{144}H_{108}N_3O_{18}P_6Eu(H_2O)_2$: C,68.03; H,4.44; N,1.65; found C,67.95; H,4.47; N,1.71; UV/Vis (THF): λ in nm (log ε) 255 (5.3).

$Tb(biphen)_3$ - (0.17 g, 87 %); $\delta_P\{^1H\}$ (121 MHz, $CDCl_3$): - 93.2 (br,s); $\delta_C\{^1H\}$ (75 MHz, $CDCl_3$): 150.1 (C_1), 142.6 (C_5), 138.2 (C_4), 130.3 (C_7), 127.6 (C_6), 126.1 (C_3), 125.3 (C_8), 119.8 (C_2); δ_H (300 MHz, $CDCl_3$): 6.66 (12H, s, H_e), 6.47 (24H, s, H_d), 5.55 (24H, s, H_c) 3.91 (48H, br, s, H_a, H_d); MALDI-MS: *m/z* 2513 $[M]^+$, 2536 $[M+Na]^+$; elemental analysis calcd. (%) for $C_{144}H_{108}N_3O_{18}P_6Tb(H_2O)(KCl)_{0.5}$: C,67.34; H,4.32; N,1.64; found C,67.13; H,4.44; N,1.69; UV/Vis (THF): λ in nm (log ε) 255 (5.3).

$Dy(biphen)_3$ - (0.15 g, 75 %); $\delta_P\{^1H\}$ (121 MHz, $CDCl_3$): - 57.2 (br,s); $\delta_C\{^1H\}$ (300 MHz, $CDCl_3$): 149.8 (C_1), 141.3 (C_5), 137.2 (C_4), 129.6 (C_7), 128.1 (C_6), 126.6 (C_3), 125.7 (C_8), 121.1 (C_2); δ_H (300 MHz, $CDCl_3$): 6.66 (12H, s, H_e), 6.46 (24H, s, H_d), 5.65 (24H, s, H_c), 4.18 (48H, br, s, H_a, H_b); MALDI-MS: *m/z* 2516 $[M]^+$, 2539 $[M+Na]^+$; elemental analysis calcd. (%) for $C_{144}H_{108}N_3O_{18}P_6Dy(H_2O)(KCl)$: C,66.28; H,4.25; N,1.61; found C,66.12; H,4.36; N,1.79 ; UV/Vis (THF): λ in nm (log ε) 255 (5.3).

$Sm(biphen)_3$ - (0.14 g, 72 %); $\delta_P\{^1H\}$ (121 MHz, $CDCl_3$): - 4.0 (s); $\delta_C\{^1H\}$ (300 MHz, $CDCl_3$): 151.0 (C_1), 140.0 (C_5), 137.4 (C_4), 128.6 (C_7), 128.0 (C_6), 126.9 (C_3), 126.8 (C_8). 121.0 (C_2); δ_H (300 MHz, $CDCl_3$): 6.89 - 7.27 (108H, m, Ar); MALDI-MS: *m/z* 2504 $[M]^+$, 2527 $[M+Na]^+$; elemental analysis calcd. (%) for $C_{144}H_{108}N_3O_{18}P_6Sm(H_2O)_{0.5}(KCl)$: C,66.82; H,4.24; N,1.62; found C,66.61 ; H,4.47; N,1.86; UV/Vis (THF): λ in nm (log ε) 255 (5.3).

$Gd(biphen)_3$ – (0.12 g, 60 %); MALDI-MS: *m/z* 2511 $[M]^+$, 2534 $[M+Na]^+$; elemental analysis calcd. (%) for $C_{144}H_{108}N_3O_{18}P_6Gd(H_2O)(KCl)$: C,66.42; H,4.26; N,1.61; found C,66.48; H,4.21; N,1.69; UV/Vis (THF): λ in nm (log ε) 255 (5.3).

$Nd(biphen)_3$ – (0.15 g, 77 %); $\delta_P\{^1H\}$ (121 MHz, $CDCl_3$): 29.2 (s); $\delta_C\{^1H\}$ (75 MHz, $CDCl_3$): 152.3 (C_1), 140.0 (C_5), 137.2 (C_4), 128.5 (C_7), 127.9 (C_6), 126.6 (C_3), 126.4 (C_8), 121.2 (C_2); δ_H (300 MHz, $CDCl_3$): 7.43 (12H, br, s, H_e), 6.59 – 7.14 (96H, br, m, Ar); MALDI-MS: *m/z* 2498 $[M]^+$, 2521 $[M+Na]^+$; elemental analysis calcd. (%) for $C_{144}H_{108}N_3O_{18}P_6Nd(H_2O)(KCl)$: C,66.75; H,4.28; N,1.62; found C,66.96; H,4.52; N,1.81; UV/Vis (THF): λ in nm (log ε) 255 (5.3).

$Er(biphen)_3$ – (0.18 g, 91 %); $\delta_P\{^1H\}$ (121 MHz, $CDCl_3$): - 76.8 ; $\delta_C\{^1H\}$ (75 MHz, $CDCl_3$): 149.8 (C_1), 140.3 (C_5), 138.0 (C_4), 128.7 (C_7), 128.5 (C_6), 127.3 (C_3), 126.2 (C_8), 121.1 (C_2); δ_H (300 MHz, $CDCl_3$): 6.65 – 7.15 (108H,m, Ar); MALDI-MS: *m/z* 2521 $[M]^+$, 2544 $[M+Na]^+$; elemental analysis calcd. (%) for $C_{144}H_{108}N_3O_{18}P_6Er(H_20)(KCl)_{0.5}$: C,67.12; H,4.30; N,1.63; found C,67.34; H,4.21; N,1.54; UV/Vis (THF): λ in nm (log ε) 255 (5.3).

Y(biphen)$_3$ – (0.17 g, 89 %); $\delta_P\{^1H\}$ (121 MHz, $CDCl_3$): - 6.2 (s); $\delta_C\{^1H\}$ (75 MHz, $CDCl_3$): 148.8 (C_1), 140.3 (C_5), 138.0 (C_4), 128.7 (C_7), 128.5 (C_6), 127.3 (C_3), 126.7 (C_8), 120.3 (C_2); δ_H (300 MHz, $CDCl_3$): 7.04 – 7.16 (108, m, Ar) ; MALDI-MS: *m/z* 2443 $[M]^+$, 2466 $[M+Na]^+$; elemental analysis calcd. (%) for $C_{144}H_{108}N_3O_{18}P_6Y(H_2O)$ (KCl): C,66.24; H,4.21; N,1.61; found C,66.40; H,4.06; N,1.44; UV/Vis (THF): λ in nm (log ε) 255 (5.3).

Yb(biphen)$_3$ – (0.13 g, 62 %); $\delta_P\{^1H\}$ (121 MHz, $CDCl_3$): - 6.3 (s); $\delta_C\{^1H\}$ (75 MHz, $CDCl_3$): 147.0 (C_1), 138.7 (C_5), 136.3 (C_4), 128.1 (C_7), 127.9 (C_6), 127.1 (C_3), 126.9 (C_8), 119.4 (C_2); δ_H (300 MHz, $CDCl_3$): 8.6 (12H, br, s, H_e), 7.82 (24H, br, s, H_d), 7.43 (24H, br, s, H_c), 7.29 – 7.31 (48H, br, m, H_a, H_b); MALDI-MS: *m/z* 2527 $[M]^+$, 2550 $[M+Na]^+$; elemental analysis calcd. (%) for $C_{144}H_{108}N_3O_{18}P_6Yb(H_2O)_{0.5}$(KCl): C,66.24; H,4.21; N,1.61; found C,66.45; H,4.15; N,1.54; UV/Vis (THF): λ in nm (log ε) 255 (5.3).

4.6. References

(1) Cajaiba Da Silva, J. F.; Nakayama, H. T.; Costa Neto, C. *Phosphorus, Sulfur, and Silicon.* **1997**, *131*, 71.

(2) Nielsen, M. L. *Inorg. Chem.* **1964**, *3,* 1760.

(3) Berlman, I. B. *Handbook of Fluorescence Spectra of Aromatic Molecules*; Academic Press, 1971.

(4) Reuben, J. *Progress in NMR Spectroscopy.* **1975**, *9,* 1.

(5) Drago, R. S. *Physical Methods in Chemistry.* Second ed.; Saunders, 1992.

(6) Bünzli, J.-C. G.; Choppin, G. R. Elsevier Science Ltd., 1990.

(7) Sherry, A. D.; Geraldes, C. F. G. C. *Lanthanide Probes in Life, Chemical and Earth Sciences*, eds. Bünzli, J.-C. G.; Choppin, G. R. Elsevier, Amsterdam, 1989, Ch.4.

(8) Klink, S. I.; Grave, L.; Reinhoudt, D. M.; Van Veggel, F.C. J. M.; Werts, M. H.; Geurts, F. A. J.; Hofstraat, J. W. *J. Phys. Chem. A.* **2000**, *104*, 5457.

(9) Deiters, E.; Gumy, F.; Bünzli, J.-C. G. *Eur. J. Inorg. Chem*. **2010**, 2723.

(10) Petoud, S.; Muller, G.; Moore, E. G.; Xu, J.; Sokolnicki, J.; Riehl, J. P.; Le, U. N.; Cohen, S. M.; Raymond, K. N. *J. Am. Chem. Soc.* **2007**, *129*, 77.

(11) Guo, Y.-L.; Wang, Y.-W.; Liu, W.-S.; Dou, W.; Zhong, X. *Spectrochimica Acta Part A.* **2007**, *67*, 624.

(12) Regulacio, M. D.; Pablico, M. H.; Vasquez, J. A.; Myers, P. N.; Gentry, S.; Prushan, M.; Tam-Chang, S.-W.; Stoll, S.L. *Inorg. Chem*. **2008**, *47*, 1512.

(13) Kim, H. Y.; Beak, N. S.; Kim, H. K. *Chem.Phys. Chem*. **2006**, *7*, 213.

(14) Meech, S. R.; Phillips, D. *J. Photochem.* **1983**, *23*, 193.

(15) Nakamaru, K. *Bull. Chem. Soc. Jpn.* **1982**, *55*, 2697.

(16) Carnall, W. T.; Fields, P. R.; Rajnak, K. *J. Chem. Phys.* **1968**, 49, 4413.

(17) Renaud, F.; Piguet, C.; Bernardinelli, G.; Bünzli, J.-C. G.; Hopfgartner, G. *J. Am. Chem. Soc.* **1999**, *121,* 9326.

(18) Bünzli, J.-C. G. “Spectroscopic Properties of Rare Earths” in *Optical Materials* (Ed.: Liu, G. K.), Springer-Verlag, Berlin, 2002.

(19) Latva, M.; Takalo, H.; Mukkala, V.-M.; Matachescu, C.; Rodriguez-Ubis, J. C.; Kankare, J. *J. Lumin*. **1997**, *75*, 149.

(20) Eliseeva, S. V.; Bünzli, J.-C. G. *Chem. Soc. Rev*. **2010**, *39*, 189.

(21) Comby, S.; Imbert, D.; Vandevyver C.; Bünzli, J.-C. G. *Chem. Eur. J.* **2007**, *13*, 936.

(22) Klink, S. I.; Hebbink, G. A.; Grave, L.; Peters, F. G. A.; Van Veggel, F. C. J. M.; Reinhoudt, D. N.; Hofstraat, J. W. *Eur. J. Org. Chem.* **2000**, 1923.

(23) Werts, M. H. V.; Jukes, R. T. F.; Verhoeven, J. W. *Phys. Chem. Chem. Phys.* **2002**, *4*, 1542.

(24) Hofstraat, J. W.; Wolbers, M. P. O.; Van Veggel, F. C. J. M.; Reinhoudt, D. N.; Werts, M. H. V.; Verhoeven, J. W. *J. Fluoresc.* **1998**, *8*, 301.

(25) Bassett, A. P.; Van Deun, R.; Nockemann, P.; Glover, P. B.; Kariuki, B. M.; Van Hecke, K.; Van Meervelt, L.; Pikramenou, Z. *Inorg. Chem.* **2005**, *44*, 6140.

(26) Yanagida, S.; Hasegawa, Y.; Murakoshi, K.; Wada, Y.; Nakashimi, N.; Yamanaka, T. *Coord, Chem. Rev.* **1998**, *171*, 461.

(27) Comby, S.; Imbert, D.; Chauvin, A.-S.; Bünzli, J.-C. G. *Inorg. Chem.* **2006**, *45*, 732.

(28) Hasegawa, Y.; Ohkubo, T.; Sogabe, K.; Kawamura, Y.; Wada, Y.; Nakashima, N.; Yanagida, S. *Angew. Chem.* **2000**, 365.

(29) Xu, H.-B.; Chen, X.-M.; Zhang, Q.-S.; Zhang, L.-Y.; Chen, Z.-N. *Chem. Commun*. **2009**, 7318.

(30) Norton, K.; Kumar, G. A.; Dilks, J. L.; Emge, T. J.; Riman, R. E.; Brik, M. G.; Brennan, J. G. *Inorg. Chem*. **2009**, 48, 3573.

(31) Feng, J.; Yu, J.-B.; Song, S.-Y.; Sun, L.-N.; Fan, W.-Q.; Guo, X.-M.; Dang, S.; Zhang, H.-J. *Dalton Trans*. **2009**, 2406.

(32) Nonat, A.; Imbert, D.; Pécaut, J.; Giraud, M.; Mazzanti, M. *Inorg. Chem*. **2009**, *48*, 4207.

(33) Lazarides, T.; Alamiry, M. A. H.; Adams, H.; Pope, S. J. A.; Faulkner, S.; Weinstein, J. A.; Ward, M. D. *Dalton Trans*. **2007**, 1484.

(34) Ahmed, Z.; Iftikhar, K. *Inorg. Chim. Acta.* **2010**, *363*, 2606.

(35) Valore, A.; Cariati, E.; Righetto, S.; Roberto, D.; Tessore, F.; Ugo, R.; Fragalà, I. L.; Fragalà, M. E.; Malandrino, G.; De Angelis, F.; Belpassi, L.; Ledoux-Rak, I.; Thi, K. H.; Zyss, J. *J. Am. Chem. Soc.* **2010**, *132*, 4966.

(36) Wu, J.; Li, H.-Y.; Xu, Q.-L.; Zhu, Y.-Ch.; Tao, Y.-M.; Li, H.-R.; Zheng, Y.-X.; Zuo, J.-L.; You, X.-Z. *Inorg. Chim. Acta.* **2010**, *363*, 2394.

(37) Song, L.; Hu, J.; Wang, J.; Liu, X.; Zhen, Z. *Photochem. Photobiol. Sci.* **2008**, *7*, 689.

5.0. Conclusions and future work

In this thesis different imidodiphosphate chelating ligands were examined for their suitability to efficiently sensitise visible and NIR lanthanide ions.

Photophysical studies of lanthanide complexes based on tetraphenyl imidodiphosphate ligand (H**tpOp**) revealed that the H**tpOp** can act as an efficient sensitiser for Vis lanthanides ions (Eu^{3+}, Tb^{3+}, Dy^{3+}, Sm^{3+}). The most important result of this work was strong yellow luminescence of the Dy(**tpOp**)$_3$ complex with a high quantum yield of 5.8%.

It was demonstrated that two lanthanide ions can coordinate when incorporating two **tpOp** binding sites, introducing a new binuclear ligand H_2**bistpOp**. The photophysical properties of neutral binuclear lanthanide Ln_2(**bistpOp**)$_3$ complexes showed that the high level of the ligand triplet state (T_1 = 28,736 cm^{-1}) prevents efficient population of the luminescent states of visible and in particularly near-infrared emitting Ln^{3+} ions.

The analogue of H**tpOp** with biphenyl moieties H**biphen** ligand was found to be an efficient sensitiser for NIR-emitting Yb^{3+} and Nd^{3+} ions in the solid state and solution. This behaviour can be explained by a better position of the **biphen** ligand triplet state (T_1 = 22,883 cm^{-1}) compared to T_1 = 27,397 cm^{-1} obtained for **tpOp**.

In future work it would be interesting to see if full fluorination of phenoxide rings in H**tpOp** ligand would further improve the photophysical properties of visible Ln(**tpOp**)$_3$

complexes and hence make them attractive candidates for application in luminescent devices.

Building on the effectiveness of **biphen** ligand to sensitise the NIR emitting ions (Nd^{3+} and Yb^{3+}), the next step would again be elimination of C-H bonds by full fluorination of biphenyloxide aromatic rings. This modification should enhance the NIR emission even further.

As the ligand **biphen** can enter a cyclodextrin cavity, Ln(**biphen**)$_3$ complexes could be possibly used as photoactive supramolecular devices. In such systems, a dye attached to a cyclodextrin acts as an energy donor with a Ln(**biphen**)$_3$ complex as an energy acceptor.

6.0. General Experimental

6.1. Materials and methods

All chemicals were purchased from Aldrich or Alfa Aesar and used without further purification unless stated. Solvents were purchased from Aldrich or Fisher and were degassed with dinitrogen and/or dried with appropriate molecular sieves or distilled over sodium/benzophenone if required. Deuterated solvents were Purchased from Goss Scientific or Aldrich and used as received. HPLC grade solvents were used in photophysical studies. Water was deionised using an Elga Option 3 water purifier. Column chromatography was performed on silica gel (Fluorochem or Merck, 40-63μm). Thin layer chromatography was carried out using Merck silica gel 60 F_{254} aluminium or Macherey-Nagel Polygram Sil G/UV_{254} pre-coated plastic sheets.

6.2. Equipment

^{1}H, $^{13}C\{^{1}H\}$, $^{31}P\{^{1}H\}$ and 2D NMR spectra were obtained using Brüker AC 300, AV 300, AV 400 spectrometers. ^{1}H and $^{13}C\{^{1}H\}$ NMR shofts were referenced to external SiMe4, whereas $^{31}P\{^{1}H\}$ shifts were referenced against external orthophosphoric acid. Electrospray mass spectra were recorded on a Micromass LC-TOF machine. MALDI-TOF mass spectra were recorded on a Brüker IV mass spectrometer. Elemental analyses were recorded on a Carlo Erber EA1110 Simultaneous CHNS elemental analyser. IR spectra of powder samples were recorded on a Perkin-Elmer Spectrum 100 FT-IR spectrometer.

Absorption spectra were recorded on a Shimadzu UV-3101PC UV-Vis-NIR spectrometer using matched pairs of 1 cm path length quartz cuvettes.

A suitable crystal of compounds were selected and datasets were measured on a Brüker SMART 6000 diffractometer ($\lambda_{Cu\text{-}K\alpha}$ = 1.54178 Å) at 120 K. The data collections were driven by SMART[1] and processed by SAINT.[2] An absorption correction was applied using SADABS.[3] The structures were solved in SIR2004[4] and were refined by a full-matrix least-squares procedure on F^2 in SHELXL-97.[5] All non-hydrogen atoms were refined with anisotropic displacement parameters. All hydrogen atoms were added at calculated positions and refined by use of a riding model with isotropic displacement parameters based on the equivalent isotropic displacement parameter (U_{eq}) of the parent atom. Figures were produced using ORTEP3[6] or CrystalMaker for Windows.

6.3. Photophysical studies

Luminescence experiments were carried out using a PTI fluorescence system. The illumination source was a PTI L-210M 75W xenon arc lamp. The detection system used a Shimadzu R298 PMT in a PTI model 814 analogue/photon counting multiplier. The emission monochromator was equipped with interchangeable 500 nm and 750 nm blazed gratings. Luminescence spectra of solution samples at ambient temperature were carried out at 90° to the excitation source using a 1 x 1 cm path length quartz cuvette with 4 transparent polished faces. Appropriate long-pass filters were used in every experiment. Excitation spectra were corrected for variation in lamp output in real time by using a reference beam correction profile. Spectra were recorded using PTI Felix fluorescence analysis software for Windows.

6.4. Quantum yield measurements

Quantum yield measurements were recorded using the optically dilute relative method, using the equation below:[8]

$$\Phi_x = \Phi_r \left[\frac{A_r(\lambda_r)}{A_x(\lambda_x)}\right]\left[\frac{I(\lambda_r)}{I(\lambda_x)}\right]\left[\frac{n_x^2}{n_r^2}\right]\left[\frac{D_x}{D_r}\right]$$

Where:

Φ_x = Quantum yield of sample
Φ_r = Quantum yield of reference
$A(\lambda)$ = Absorbance of sample at the exciting wavelength
$I(\lambda)$ = Relative intensity of exciting light at wavelength
n = Refractive index of the solvent
D = Integrated detector response

$[Ru(bpy)_3]Cl_2$ in aerated H_2O ($\Phi = 0.028$)[9] was used as the reference sample for Eu^{3+} and Sm^{3+} quantum yield measurements. Quinine sulphate in aerated 1N H_2SO_4 ($\Phi = 0.546$)[10] was used as the standard for Tb^{3+} and Dy^{3+} quantum yield measurements.

6.5. Time resolved emission spectroscopy

Visible emission lifetime spectra were recorded employing a Continuum Surelite I SSP class 4 pulsed Nd-YAG laser (10 Hz) as the excitation source using the 355 nm harmonic. The signal was collected as a direct output from the PMT to minimise the response time of the apparatus. Data were recorded on a LeCroy 9350AM 500 MHz oscilloscope, which was triggered by the laser, with an average of 500 shots. The lifetime data was analysed using Kaleidagraph software for the PC and fitted using a non-linear least-squares iterative technique (Marquardt-Levenberg algorithm).[11]

The lifetimes of NIR emission were obtained by using an Edinburgh instruments FLSPM920 equipped with a 100 W μF920H lamp.

6.6. References

1. *SMART V5.626: Software for the CCD Detector System*, **1997**, Bruker AXS Inc., Madison, Wisconsin, USA.

2. *SAINT V6.28A: Software for the CCD Detector System*, **1997**, Bruker AXS Inc., Madison, Wisconsin, USA.

3. Sheldrick, G. M. **2007**, *SADABS,* Bruker AXS Inc., Madison, Wisconsin, USA.

4. Burla, M. C.; Caliandro, R.; Camalli, M.; Carrozzini, B.; Cascarano, G. L.; De Caro, L.; Giacovazzo, C.; Polidori, G.; Spagna, R. **2004**, *SIR2004: An Improved Tool for Crystal Structure Determination and Refinement*, Italy.

5. Sheldrick, G. M. *Acta Cryst.*, **2008**, *A64*, 112-122.

6. Farrugia, L. J., *J. Appl. Crystallogr.* **1997**, *30*, 565.

7. FeliX 32, Photon Technology International Software, 2001.

8. Demas, J. N.; Crosby, G. A. *J. Phys. Chem*. **1971**, *75*, 991.

9. Nakamaru, K. *Bull. Chem. Soc. Jpn.* **1982**, *55*, 2697.

10. Meech, S. R.; Phillips, D. *J. Photochem.* **1983**, *23*, 193.

11. Kaleidagraph 3.51, Synergy Software, 2000.

Appendix A) Additional spectra

Chapter 2

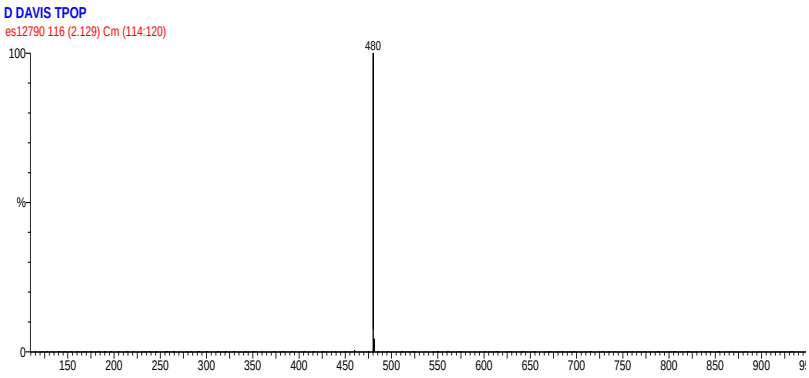

A1. The (-) ESI-MS of Ht**pOp**.

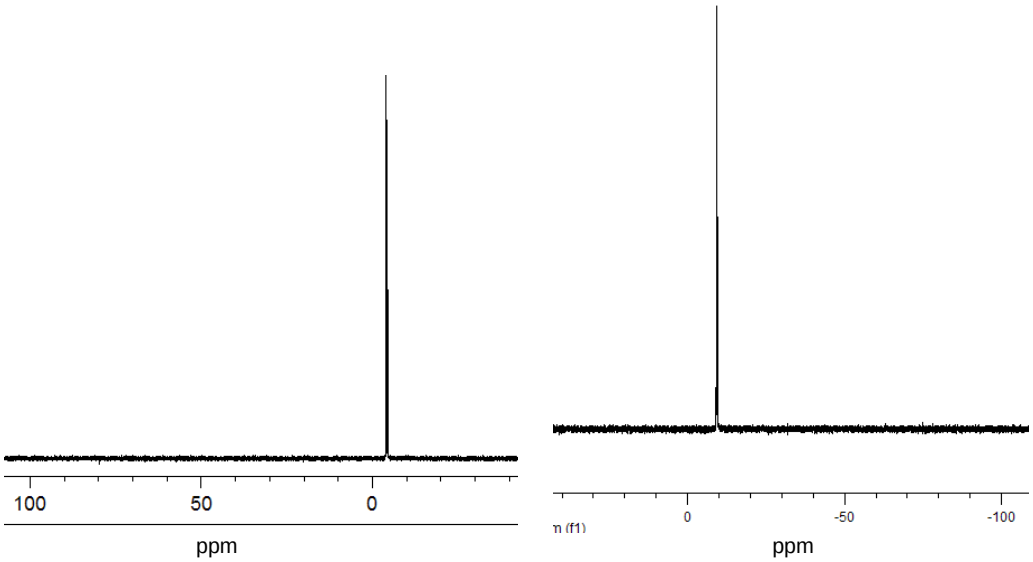

A2 and A3. The 121 MHz ^{31}P NMR spectra of Sm(**tpOp**)$_3$ (left) and Yb(**tpOp**)$_3$ (right) in $CDCl_3$.

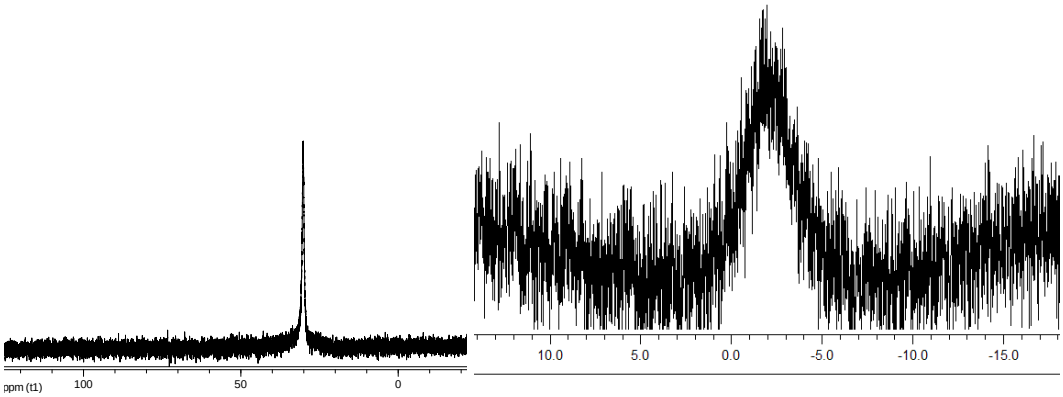

A4 and A5. The 121 MHz ^{31}P NMR spectra of Nd(**tpOp**)$_3$ (left) and Dy(**tpOp**)$_3$ (right) in $CDCl_3$.

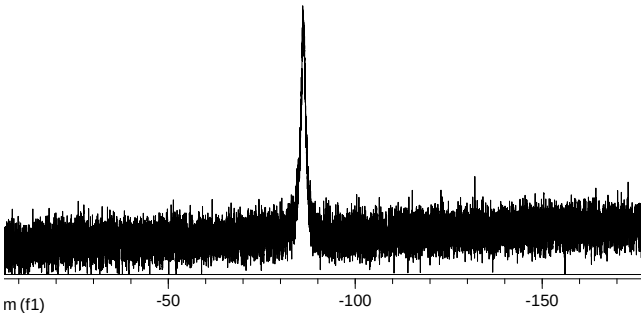

A6. The 121 MHz ^{31}P NMR spectrum of Er(**tpOp**)$_3$ in $CDCl_3$.

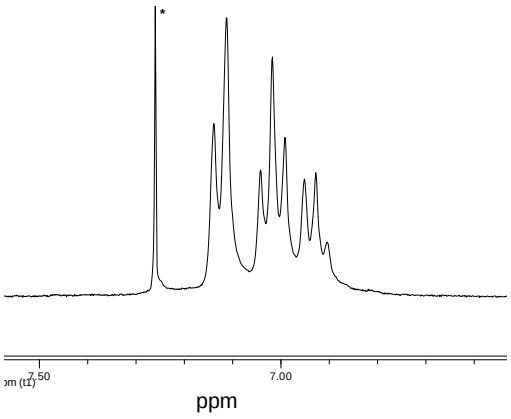

A7. The 300 MHz ^{1}H NMR spectrum of Sm(**tpOp**)$_3$ in $CDCl_3$.

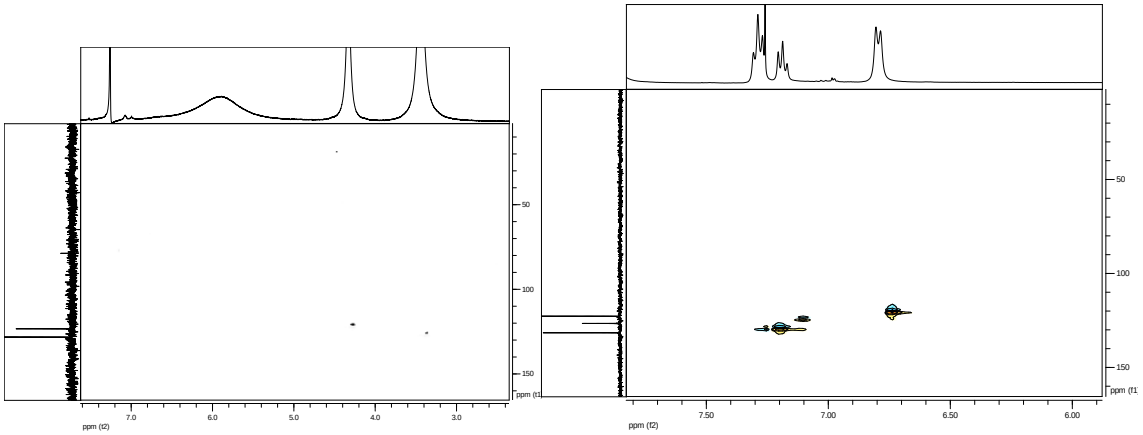

A8 and A9. ^{1}H-^{13}C HSQC NMR spectra of Dy(**tpOp**)$_3$ (left) and Eu(**tpOp**)$_3$ (right) in $CDCl_3$.

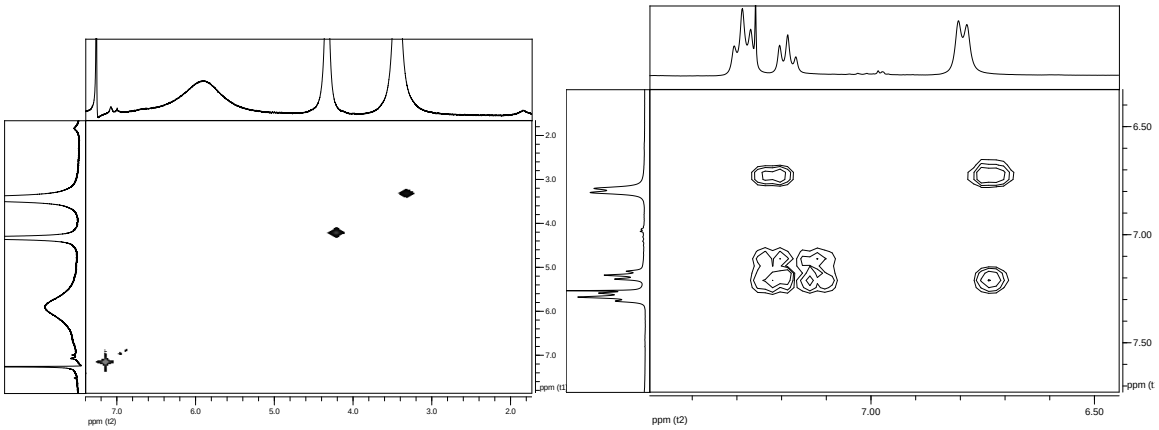

A10 and A11. The ^{1}H-^{1}H COSY NMR spectra of Dy(**tpOp**)$_3$ (left) and Eu(**tpOp**)$_3$ (right) in $CDCl_3$.

Chapter 3.

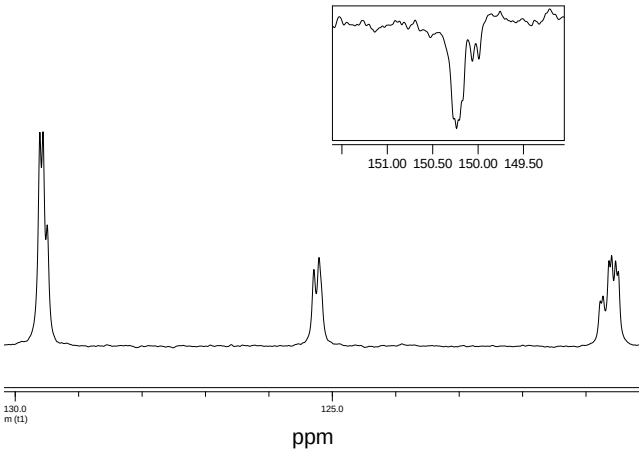

A1. The ^{13}C NMR spectrum of H_2**bistpOp** in $CDCl_3$.

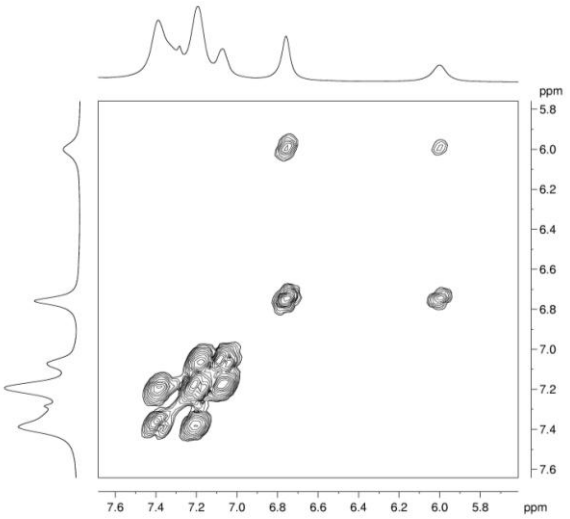

A2. The ^{1}H-^{1}H COSY NMR spectrum of Eu_2(**bistpOp**)$_3$ in $CDCl_3$.

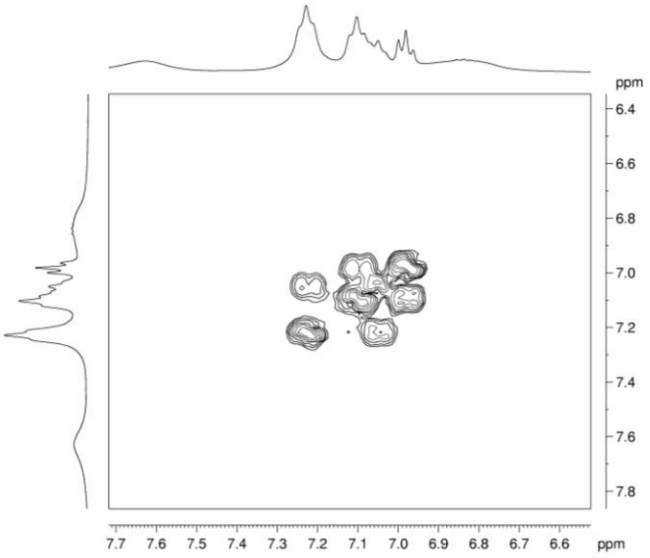

A3. The ^{1}H-^{1}H COSY NMR spectrum of Sm_2(**bistpOp**)$_3$ in $CDCl_3$.

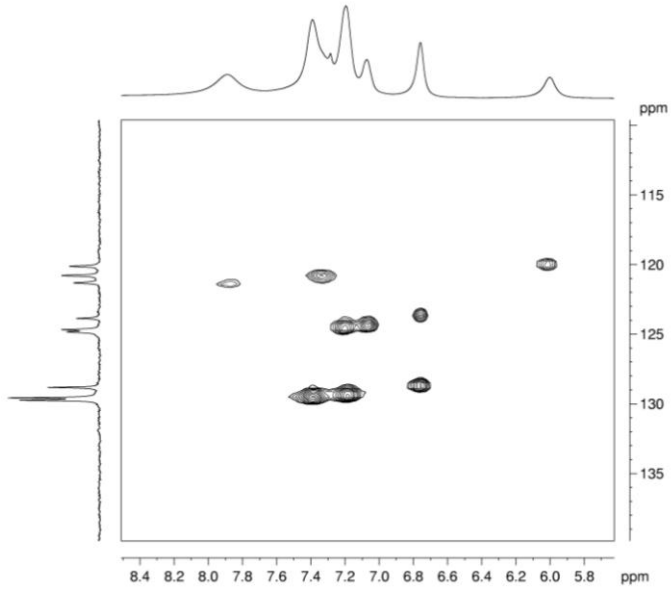

A4. ^{1}H-^{13}C HSQC NMR spectrum of Eu_2(**bistpOp**)$_3$ in $CDCl_3$.

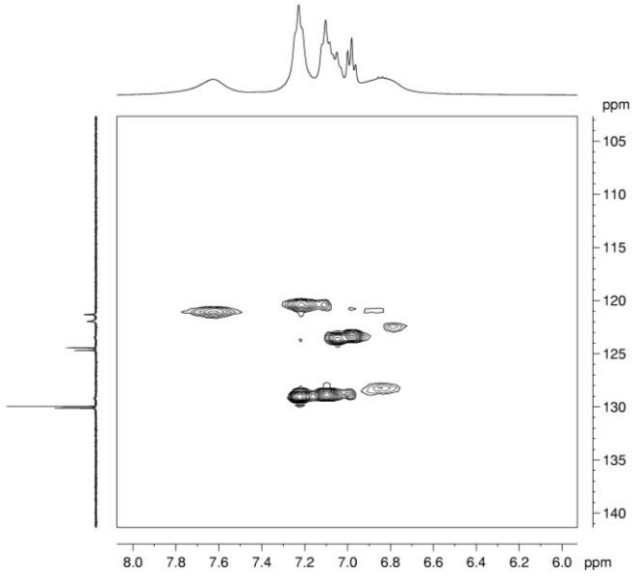

A5. ^{1}H-^{13}C HSQC NMR spectrum of Sm_2(**bistpOp**)$_3$ in $CDCl_3$.

Chapter 4

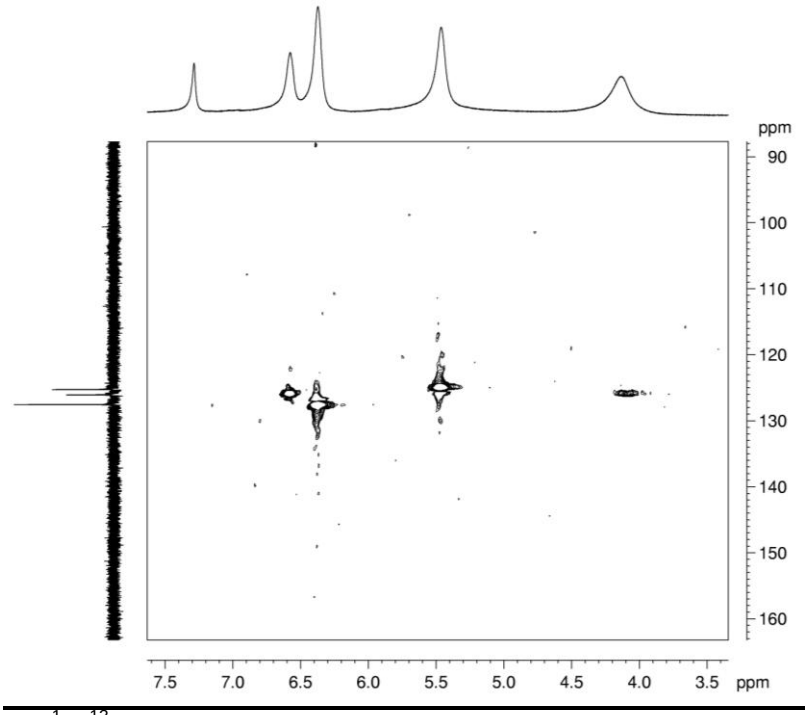

A1. ^{1}H-^{13}C HSQC NMR spectrum of Tb(**biphen**)$_3$ in $CDCl_3$.

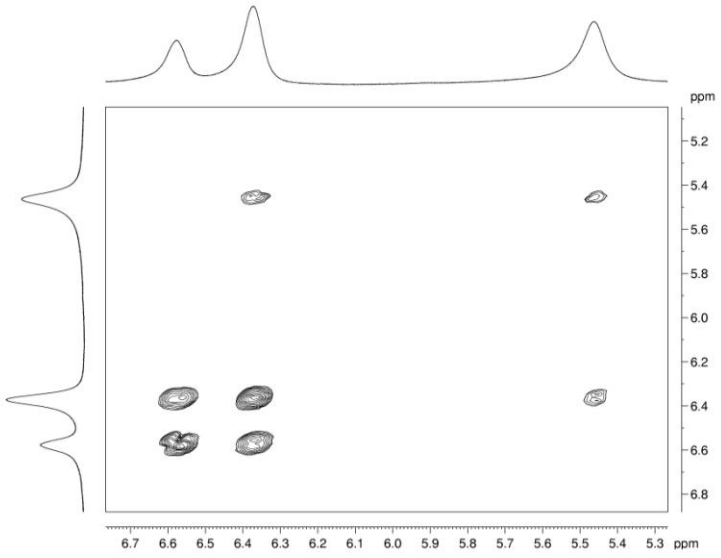

A2. The ^{1}H-^{1}H COSY NMR spectrum of Tb(**biphen**)$_3$ in $CDCl_3$.

APPENDIX B) X-RAY CRYSTALLOGRAPHIC DATA

B1 Crystallographic Data for HtpOp

Table 2. Atomic coordinates (x 10^4) and equivalent isotropic displacement parameters ($Å^2$x 10^3) for plig. U(eq) is defined as one third of the trace of the orthogonalized U^{ij} tensor.

	x	y	z	U(eq)
C(1)	6839(2)	6612(2)	321(1)	47(1)
C(2)	7731(2)	7290(2)	260(1)	59(1)
C(3)	7789(2)	8255(2)	703(2)	73(1)
C(4)	6968(2)	8520(2)	1187(2)	75(1)
C(5)	6083(2)	7838(2)	1233(2)	72(1)
C(6)	6007(2)	6867(2)	801(1)	59(1)
C(7)	7386(2)	2778(2)	-583(1)	56(1)
C(8)	6878(2)	1916(2)	-246(2)	70(1)
C(9)	7333(3)	885(2)	-344(2)	98(1)
C(10)	8247(4)	756(3)	-756(2)	110(1)
C(11)	8728(3)	1638(3)	-1087(2)	101(1)
C(12)	8300(2)	2663(2)	-1003(2)	73(1)
C(13)	9513(2)	5363(2)	2427(1)	45(1)
C(14)	10524(2)	5433(2)	2906(2)	68(1)
C(15)	10769(2)	6378(2)	3357(2)	84(1)
C(16)	10009(3)	7211(2)	3331(2)	77(1)
C(17)	9001(2)	7111(2)	2852(2)	77(1)
C(18)	8742(2)	6179(2)	2392(1)	62(1)
C(19)	9710(2)	2067(2)	1590(1)	46(1)
C(20)	8993(2)	1262(2)	1784(1)	61(1)
C(21)	9405(3)	434(2)	2312(2)	77(1)
C(22)	10512(3)	417(2)	2629(2)	76(1)
C(23)	11213(2)	1217(2)	2425(2)	73(1)
C(24)	10821(2)	2061(2)	1899(1)	60(1)
N(1)	8575(1)	4675(1)	426(1)	43(1)
O(1)	6762(1)	5638(1)	-141(1)	53(1)
O(2)	6924(1)	3824(1)	-526(1)	58(1)
O(3)	6742(1)	4194(1)	1021(1)	60(1)
O(4)	9218(1)	4372(1)	2013(1)	47(1)
O(5)	9242(1)	2878(1)	1041(1)	50(1)
O(6)	10642(1)	4452(1)	970(1)	51(1)
P(1)	7203(1)	4539(1)	277(1)	45(1)
P(2)	9511(1)	4124(1)	1114(1)	41(1)

Table 3. Bond lengths [Å] and angles [°] for plig.

C(1)-C(2)	1.369(3)	C(5)-C(6)	1.382(3)
C(1)-C(6)	1.372(3)	C(7)-C(12)	1.364(3)
C(1)-O(1)	1.409(2)	C(7)-C(8)	1.368(3)
C(2)-C(3)	1.383(3)	C(7)-O(2)	1.408(2)
C(3)-C(4)	1.370(4)	C(8)-C(9)	1.396(4)
C(4)-C(5)	1.362(4)		
C(9)-C(10)	1.359(5)	C(19)-C(24)	1.367(3)
C(10)-C(11)	1.367(5)	C(19)-C(20)	1.372(3)
C(11)-C(12)	1.374(4)	C(19)-O(5)	1.407(2)
C(13)-C(18)	1.361(3)	C(20)-C(21)	1.383(3)
C(13)-C(14)	1.363(3)	C(21)-C(22)	1.365(4)
C(13)-O(4)	1.415(2)	C(22)-C(23)	1.361(4)
C(14)-C(15)	1.384(3)	C(23)-C(24)	1.389(3)
C(15)-C(16)	1.368(4)	N(1)-P(2)	1.6327(15)
C(16)-C(17)	1.362(4)	N(1)-P(1)	1.6432(16)
C(17)-C(18)	1.382(3)	O(1)-P(1)	1.5749(14)

O(2)-P(1)	1.5727(14)	O(5)-P(2)	1.5661(14)
O(3)-P(1)	1.4469(14)	O(6)-P(2)	1.4608(13)
O(4)-P(2)	1.5677(13)		
C(2)-C(1)-C(6)	121.9(2)	C(24)-C(19)-O(5)	122.26(18)
C(2)-C(1)-O(1)	118.86(18)	C(20)-C(19)-O(5)	116.23(18)
C(6)-C(1)-O(1)	119.22(18)	C(19)-C(20)-C(21)	119.0(2)
C(1)-C(2)-C(3)	118.5(2)	C(22)-C(21)-C(20)	120.3(2)
C(4)-C(3)-C(2)	120.4(2)	C(23)-C(22)-C(21)	119.9(2)
C(5)-C(4)-C(3)	120.2(2)	C(22)-C(23)-C(24)	121.1(2)
C(4)-C(5)-C(6)	120.6(2)	C(19)-C(24)-C(23)	118.2(2)
C(1)-C(6)-C(5)	118.4(2)	P(2)-N(1)-P(1)	130.72(10)
C(12)-C(7)-C(8)	122.8(2)	C(1)-O(1)-P(1)	120.20(12)
C(12)-C(7)-O(2)	118.2(2)	C(7)-O(2)-P(1)	121.19(12)
C(8)-C(7)-O(2)	119.0(2)	C(13)-O(4)-P(2)	122.54(11)
C(7)-C(8)-C(9)	117.3(3)	C(19)-O(5)-P(2)	125.60(12)
C(10)-C(9)-C(8)	120.7(3)	O(3)-P(1)-O(2)	117.40(9)
C(9)-C(10)-C(11)	120.2(3)	O(3)-P(1)-O(1)	117.84(8)
C(10)-C(11)-C(12)	120.6(3)	O(2)-P(1)-O(1)	95.51(7)
C(7)-C(12)-C(11)	118.4(3)	O(3)-P(1)-N(1)	112.52(8)
C(18)-C(13)-C(14)	122.1(2)	O(2)-P(1)-N(1)	106.82(8)
C(18)-C(13)-O(4)	119.00(18)	O(1)-P(1)-N(1)	104.77(8)
C(14)-C(13)-O(4)	118.68(18)	O(6)-P(2)-O(5)	116.43(8)
C(13)-C(14)-C(15)	118.2(2)	O(6)-P(2)-O(4)	114.14(8)
C(16)-C(15)-C(14)	120.9(2)	O(5)-P(2)-O(4)	101.18(7)
C(17)-C(16)-C(15)	119.5(2)	O(6)-P(2)-N(1)	110.58(8)
C(16)-C(17)-C(18)	120.6(2)	O(5)-P(2)-N(1)	103.66(7)
C(13)-C(18)-C(17)	118.7(2)	O(4)-P(2)-N(1)	110.03(8)
C(24)-C(19)-C(20)	121.49(19)		

Symmetry transformations used to generate equivalent atoms:

Table 4. Anisotropic displacement parameters ($Å^2 x\ 10^3$)for plig. The anisotropic displacement factor exponent takes the form: $-2\pi^2[\ h^2 a^{*2} U^{11} + ... + 2\ h\ k\ a^*\ b^*\ U^{12}\ ]$

	U^{11}	U^{22}	U^{33}	U^{23}	U^{13}	U^{12}
C(1)	51(1)	44(1)	46(1)	6(1)	3(1)	10(1)
C(2)	60(1)	48(1)	71(1)	11(1)	20(1)	7(1)
C(3)	71(2)	48(1)	101(2)	6(1)	8(1)	-2(1)
C(4)	86(2)	58(2)	81(2)	-11(1)	4(1)	12(1)
C(5)	77(2)	72(2)	68(2)	-8(1)	19(1)	17(1)
C(6)	53(1)	64(1)	61(1)	3(1)	12(1)	7(1)
C(7)	64(1)	49(1)	51(1)	-10(1)	-9(1)	3(1)
C(8)	86(2)	58(2)	64(1)	-5(1)	-6(1)	-5(1)
C(9)	149(3)	53(2)	86(2)	-5(1)	-16(2)	-5(2)
C(10)	156(3)	73(2)	95(2)	-31(2)	-16(2)	43(2)
C(11)	108(2)	104(3)	89(2)	-29(2)	5(2)	39(2)
C(12)	75(2)	78(2)	65(2)	-13(1)	7(1)	9(1)
C(13)	56(1)	44(1)	35(1)	1(1)	9(1)	-3(1)
C(14)	63(1)	68(2)	70(2)	-11(1)	-8(1)	8(1)
C(15)	78(2)	88(2)	82(2)	-26(2)	-14(1)	-10(1)
C(16)	108(2)	59(2)	63(2)	-15(1)	11(1)	-10(1)
C(17)	104(2)	61(2)	65(2)	-11(1)	5(1)	22(1)
C(18)	65(1)	66(2)	53(1)	-6(1)	2(1)	13(1)
C(19)	62(1)	39(1)	37(1)	-2(1)	4(1)	6(1)
C(20)	69(1)	53(1)	60(1)	4(1)	2(1)	-7(1)
C(21)	113(2)	51(2)	67(2)	12(1)	7(2)	-10(1)
C(22)	119(2)	53(2)	53(1)	7(1)	-3(1)	18(1)
C(23)	77(2)	74(2)	63(2)	1(1)	-10(1)	20(1)
C(24)	62(1)	58(1)	58(1)	3(1)	1(1)	4(1)
N(1)	47(1)	41(1)	41(1)	7(1)	8(1)	-1(1)
O(1)	57(1)	48(1)	51(1)	1(1)	0(1)	11(1)
O(2)	61(1)	50(1)	60(1)	-6(1)	-7(1)	5(1)
O(3)	57(1)	61(1)	65(1)	10(1)	19(1)	-3(1)

O(4)	59(1)	45(1)	38(1)	2(1)	10(1)	-6(1)
O(5)	62(1)	39(1)	45(1)	2(1)	-4(1)	1(1)
O(6)	46(1)	63(1)	45(1)	9(1)	7(1)	0(1)
P(1)	45(1)	42(1)	47(1)	2(1)	6(1)	1(1)
P(2)	46(1)	41(1)	36(1)	3(1)	6(1)	0(1)

Table 5. Hydrogen coordinates (x 10^4) and isotropic displacement parameters ($Å^2$x 10^3) for plig.

	x	y	z	U(eq)
H(2)	8286	7107	-71	71
H(3)	8389	8726	671	88
H(4)	7015	9168	1486	90
H(5)	5524	8027	1558	86
H(6)	5406	6397	834	71
H(8)	6255	2012	37	85
H(9)	7008	281	-124	118
H(10)	8546	66	-814	132
H(11)	9351	1543	-1371	121
H(12)	8625	3265	-1228	87
H(14)	11036	4863	2929	82
H(15)	11458	6447	3682	101
H(16)	10180	7841	3637	92
H(17)	8482	7675	2834	92
H(18)	8054	6111	2065	74
H(20)	8240	1274	1565	74
H(21)	8927	-114	2451	93
H(22)	10787	-142	2984	91
H(23)	11966	1199	2641	87
H(24)	11302	2608	1761	71
H(1)	8846	5109	84	52

B2 Crystallographic Data for KtpOp

Table 2. Atomic coordinates (x 10^4) and equivalent isotropic displacement parameters ($Å^2$x 10^3) for ktpopm. U(eq) is defined as one third of the trace of the orthogonalized U^{ij} tensor.

	x	y	z	U(eq)		x	y	z	U(eq)
C(1)	2036(5)	-1787(1)	4360(1)	50(1)		C(25)	2905(5)	37(1)	3933(1)	41(1)
C(2)	1371(6)	-2128(1)	4314(1)	66(1)		C(26)	2400(6)	-321(1)	3884(1)	58(1)
C(3)	1613(8)	-2391(2)	4589(2)	88(2)		C(27)	1498(6)	-490(1)	4163(2)	70(1)
C(4)	2556(10)	-2306(2)	4899(2)	114(2)		C(28)	1110(6)	-306(2)	4486(1)	66(1)
C(5)	3201(10)	-1961(2)	4940(2)	124(3)		C(29)	1628(7)	49(2)	4532(1)	68(1)
C(6)	2969(7)	-1703(2)	4670(2)	78(2)		C(30)	2531(6)	220(1)	4254(1)	56(1)
C(7)	2038(5)	-1998(1)	3182(1)	51(1)		C(31)	3783(5)	1063(1)	3580(1)	45(1)
C(8)	1350(7)	-1829(1)	2876(1)	68(1)		C(32)	4543(6)	1066(1)	3920(1)	58(1)
C(9)	1136(8)	-2027(2)	2547(2)	90(2)		C(33)	4112(8)	1334(2)	4182(2)	81(2)
C(10)	1647(8)	-2383(2)	2529(2)	95(2)		C(34)	2930(8)	1590(2)	4087(2)	90(2)
C(11)	2307(7)	-2549(2)	2836(2)	91(2)		C(35)	2201(7)	1590(1)	3739(2)	79(2)
C(12)	2533(6)	-2357(1)	3167(2)	73(2)		C(36)	2626(6)	1326(1)	3483(1)	60(1)
C(13)	-3354(6)	-1327(2)	4218(2)	63(1)		C(37)	-1245(5)	972(1)	2995(1)	44(1)
C(14)	-2384(8)	-1455(2)	4497(2)	111(2)		C(38)	-1557(6)	1299(1)	3175(1)	60(1)
C(15)	-2138(13)	-1242(5)	4808(3)	196(7)		C(39)	-1150(6)	1622(1)	3002(2)	68(1)
C(16)	-2916(19)	-909(5)	4833(4)	216(10)		C(40)	-441(6)	1624(1)	2653(2)	64(1)
C(17)	-3915(16)	-781(2)	4549(3)	178(6)		C(41)	-145(6)	1298(1)	2472(1)	60(1)
C(18)	-4121(9)	-997(2)	4237(2)	107(2)		C(42)	-565(5)	970(1)	2643(1)	52(1)
C(19)	-3019(6)	-2313(1)	3613(1)	55(1)		C(43)	-1615(5)	392(1)	3980(1)	49(1)
C(20)	-1741(6)	-2539(1)	3501(2)	68(1)		C(44)	-2683(6)	226(2)	4233(1)	61(1)
C(21)	-1502(8)	-2866(2)	3688(2)	89(2)		C(45)	-3063(7)	402(2)	4564(2)	85(2)
C(22)	-2518(10)	-2962(2)	3975(2)	101(2)		C(46)	-2409(8)	741(2)	4640(2)	91(2)
C(23)	-3805(9)	-2737(2)	4082(2)	99(2)		C(47)	-1356(7)	908(2)	4386(2)	76(2)
C(24)	-4059(7)	-2407(2)	3901(2)	73(2)		C(48)	-953(6)	734(1)	4050(1)	58(1)

N(1)	-700(4)	-1686(1)	3715(1)	51(1)
N(2)	1301(4)	512(1)	3362(1)	39(1)
O(1)	1845(4)	-1501(1)	4107(1)	53(1)
O(2)	2315(3)	-1816(1)	3521(1)	54(1)
O(3)	1328(4)	-1157(1)	3524(1)	55(1)
O(4)	-3697(4)	-1552(1)	3917(1)	69(1)
O(5)	-3261(4)	-1984(1)	3413(1)	56(1)
O(6)	-2789(4)	-1325(1)	3281(1)	69(1)
O(7)	3894(3)	204(1)	3658(1)	48(1)
O(8)	4196(3)	792(1)	3314(1)	45(1)
O(9)	3730(3)	225(1)	2956(1)	50(1)
O(10)	-1692(3)	647(1)	3171(1)	56(1)
O(11)	-1280(3)	188(1)	3658(1)	47(1)
O(12)	-512(3)	21(1)	3014(1)	48(1)
O(13)	6019(4)	-406(1)	3294(1)	79(1)
O(14)	-5835(4)	-1026(1)	3124(1)	75(1)
O(15)	-7311(15)	-812(3)	2434(3)	72(3)
O(16)	-6390(20)	-992(4)	2350(4)	122(5)
O(17)	-8370(20)	-745(4)	2598(4)	127(5)
P(1)	1080(1)	-1521(1)	3695(1)	45(1)
P(2)	-2494(1)	-1612(1)	3567(1)	51(1)
P(3)	3176(1)	418(1)	3296(1)	37(1)
P(4)	-414(1)	331(1)	3280(1)	38(1)
K(1)	-917(2)	-665(1)	3305(1)	103(1)
K(2)	1587(1)	-22(1)	2401(1)	68(1)

Table 3. Bond lengths [Å] and angles [°] for ktpopm.

C(1)-C(2)	1.362(6)	N(2)-P(4)	1.553(3)	C(5)-C(6)-C(1)	119.6(6)
C(1)-C(6)	1.368(6)	N(2)-P(3)	1.561(3)	C(8)-C(7)-C(12)	121.2(5)
C(1)-O(1)	1.385(5)	O(1)-P(1)	1.592(3)	C(8)-C(7)-O(2)	122.6(4)
C(2)-C(3)	1.384(7)	O(2)-P(1)	1.586(3)	C(12)-C(7)-O(2)	116.2(4)
C(3)-C(4)	1.373(8)	O(3)-P(1)	1.471(3)	C(7)-C(8)-C(9)	119.4(5)
C(4)-C(5)	1.367(9)	O(3)-K(1)	2.658(3)	C(10)-C(9)-C(8)	119.8(6)
C(5)-C(6)	1.355(8)	O(4)-P(2)	1.593(3)	C(11)-C(10)-C(9)	120.2(6)
C(7)-C(8)	1.367(6)	O(5)-P(2)	1.585(3)	C(10)-C(11)-C(12)	120.9(6)
C(7)-C(12)	1.368(6)	O(6)-P(2)	1.478(3)	C(7)-C(12)-C(11)	118.5(6)
C(7)-O(2)	1.396(5)	O(6)-K(1)	2.835(3)	C(14)-C(13)-C(18)	122.3(6)
C(8)-C(9)	1.384(7)	O(7)-P(3)	1.614(3)	C(14)-C(13)-O(4)	119.0(6)
C(9)-C(10)	1.363(8)	O(8)-P(3)	1.590(3)	C(18)-C(13)-O(4)	118.5(6)
C(10)-C(11)	1.359(8)	O(9)-P(3)	1.469(3)	C(13)-C(14)-C(15)	119.1(9)
C(11)-C(12)	1.381(7)	O(9)-K(2)	2.766(3)	C(16)-C(15)-C(14)	119.3(13)
C(13)-C(14)	1.344(8)	O(9)-K(2)#1	2.770(3)	C(15)-C(16)-C(17)	121.5(11)
C(13)-C(18)	1.353(8)	O(10)-P(4)	1.590(3)	C(18)-C(17)-C(16)	118.1(11)
C(13)-O(4)	1.376(6)	O(11)-P(4)	1.599(3)	C(13)-C(18)-C(17)	119.8(8)
C(14)-C(15)	1.367(12)	O(11)-K(1)	3.365(3)	C(24)-C(19)-C(20)	121.7(5)
C(15)-C(16)	1.37(2)	O(12)-P(4)	1.475(3)	C(24)-C(19)-O(5)	120.4(5)
C(16)-C(17)	1.372(18)	O(12)-K(1)	2.727(3)	C(20)-C(19)-O(5)	117.8(5)
C(17)-C(18)	1.369(10)	O(12)-K(2)	2.758(3)	C(19)-C(20)-C(21)	118.7(6)
C(19)-C(24)	1.363(7)	O(12)-K(2)#2	2.761(3)	C(22)-C(21)-C(20)	120.2(6)
C(19)-C(20)	1.372(7)	O(13)-K(1)#3	2.633(4)	C(21)-C(22)-C(23)	120.7(6)
C(19)-O(5)	1.408(5)	O(13)-K(2)#1	2.879(4)	C(22)-C(23)-C(24)	120.0(6)
C(20)-C(21)	1.379(8)	O(15)-O(16)	1.029(15)	C(19)-C(24)-C(23)	118.5(6)
C(21)-C(22)	1.350(9)	O(15)-O(17)	1.060(15)	C(30)-C(25)-C(26)	120.6(4)
C(22)-C(23)	1.372(9)	O(15)-K(1)#2	2.907(12)	C(30)-C(25)-O(7)	120.0(4)
C(23)-C(24)	1.381(8)	O(15)-K(2)#4	3.014(12)	C(26)-C(25)-O(7)	119.3(4)
C(25)-C(30)	1.356(6)	O(16)-K(1)#2	2.646(15)	C(27)-C(26)-C(25)	119.1(4)
C(25)-C(26)	1.377(6)	O(17)-K(2)#4	2.725(15)	C(28)-C(27)-C(26)	120.6(5)
C(25)-O(7)	1.399(5)	O(17)-K(1)#4	3.256(17)	C(29)-C(28)-C(27)	119.5(5)
C(26)-C(27)	1.375(6)	P(1)-K(1)	3.7698(17)	C(28)-C(29)-C(30)	120.4(5)
C(27)-C(28)	1.369(6)	P(2)-K(1)	3.7893(19)	C(25)-C(30)-C(29)	119.8(4)
C(28)-C(29)	1.367(7)	P(3)-K(2)	3.7838(16)	C(32)-C(31)-C(36)	121.5(4)
C(29)-C(30)	1.377(6)	P(4)-K(2)#2	3.6496(16)	C(32)-C(31)-O(8)	119.9(4)
C(31)-C(32)	1.355(6)	P(4)-K(1)	3.6514(18)	C(36)-C(31)-O(8)	118.5(4)
C(31)-C(36)	1.378(6)	P(4)-K(2)	3.7423(16)	C(31)-C(32)-C(33)	119.3(5)
C(31)-O(8)	1.408(5)	K(1)-O(13)#4	2.633(4)	C(34)-C(33)-C(32)	118.9(5)
C(32)-C(33)	1.393(7)	K(1)-O(16)#1	2.646(15)	C(35)-C(34)-C(33)	121.3(5)
C(33)-C(34)	1.370(8)	K(1)-O(15)#1	2.907(12)	C(34)-C(35)-C(36)	119.7(5)
C(34)-C(35)	1.368(8)	K(1)-O(17)#3	3.256(17)	C(35)-C(36)-C(31)	119.2(5)
C(35)-C(36)	1.369(7)	K(1)-K(2)#2	3.9791(17)	C(42)-C(37)-C(38)	120.4(4)
C(37)-C(42)	1.364(6)	K(2)-O(17)#3	2.725(15)	C(42)-C(37)-O(10)	120.9(4)
C(37)-C(38)	1.376(6)	K(2)-O(12)#1	2.761(3)	C(38)-C(37)-O(10)	118.7(4)
C(37)-O(10)	1.389(5)	K(2)-O(9)#2	2.770(3)	C(39)-C(38)-C(37)	119.3(4)
C(38)-C(39)	1.366(7)	K(2)-O(13)#2	2.879(4)	C(38)-C(39)-C(40)	121.0(5)
C(39)-C(40)	1.367(7)	K(2)-O(15)#3	3.014(12)	C(39)-C(40)-C(41)	119.5(5)
C(40)-C(41)	1.372(6)	K(2)-P(4)#1	3.6496(16)	C(40)-C(41)-C(42)	119.9(5)
C(41)-C(42)	1.381(6)	K(2)-K(1)#1	3.9791(17)	C(37)-C(42)-C(41)	119.8(4)
C(43)-C(48)	1.375(6)	K(2)-K(2)#2	4.0727(11)	C(48)-C(43)-C(44)	121.3(4)
C(43)-C(44)	1.382(6)			C(48)-C(43)-O(11)	123.8(4)
C(43)-O(11)	1.395(5)	C(2)-C(1)-C(6)	121.0(5)	C(44)-C(43)-O(11)	114.9(4)
C(44)-C(45)	1.376(7)	C(2)-C(1)-O(1)	124.4(4)	C(45)-C(44)-C(43)	119.3(5)
C(45)-C(46)	1.368(8)	C(6)-C(1)-O(1)	114.7(4)	C(46)-C(45)-C(44)	120.4(6)
C(46)-C(47)	1.378(8)	C(1)-C(2)-C(3)	119.4(5)	C(45)-C(46)-C(47)	120.2(5)
C(47)-C(48)	1.391(7)	C(4)-C(3)-C(2)	119.3(6)	C(46)-C(47)-C(48)	120.3(6)
N(1)-P(1)	1.551(4)	C(5)-C(4)-C(3)	120.2(6)	C(43)-C(48)-C(47)	118.6(5)
N(1)-P(2)	1.557(3)	C(6)-C(5)-C(4)	120.5(7)	P(1)-N(1)-P(2)	140.2(2)

P(4)-N(2)-P(3)	137.1(2)	O(11)-P(4)-K(2)#2	99.07(11)	O(15)#1-K(1)-K(2)#2	48.9(2)
C(1)-O(1)-P(1)	127.3(3)	O(12)-P(4)-K(1)	41.47(11)	O(17)#3-K(1)-K(2)#2	83.1(3)
C(7)-O(2)-P(1)	124.1(3)	N(2)-P(4)-K(1)	121.01(12)	O(11)-K(1)-K(2)#2	69.36(6)
P(1)-O(3)-K(1)	129.54(16)	O(10)-P(4)-K(1)	130.88(12)	P(4)-K(1)-K(2)#2	56.95(3)
C(13)-O(4)-P(2)	124.8(3)	O(11)-P(4)-K(1)	66.96(11)	P(1)-K(1)-K(2)#2	159.06(5)
C(19)-O(5)-P(2)	120.0(3)	K(2)#2-P(4)-K(1)	66.05(3)	P(2)-K(1)-K(2)#2	121.57(4)
P(2)-O(6)-K(1)	119.57(18)	O(12)-P(4)-K(2)	39.07(11)	O(17)#3-K(2)-O(12)	82.0(4)
C(25)-O(7)-P(3)	124.6(2)	N(2)-P(4)-K(2)	85.55(12)	O(17)#3-K(2)-O(12)#1	100.4(4)
C(31)-O(8)-P(3)	120.5(2)	O(10)-P(4)-K(2)	108.74(12)	O(12)-K(2)-O(12)#1	159.08(9)
P(3)-O(9)-K(2)	123.69(15)	O(11)-P(4)-K(2)	141.00(11)	O(17)#3-K(2)-O(9)	97.0(3)
P(3)-O(9)-K(2)#1	141.58(16)	K(2)#2-P(4)-K(2)	66.85(3)	O(12)-K(2)-O(9)	78.33(8)
K(2)-O(9)-K(2)#1	94.72(8)	K(1)-P(4)-K(2)	74.17(4)	O(12)#1-K(2)-O(9)	80.75(8)
C(37)-O(10)-P(4)	124.2(2)	O(13)#4-K(1)-O(16)#1	90.7(4)	O(17)#3-K(2)-O(9)#2	116.2(3)
C(43)-O(11)-P(4)	127.1(3)	O(13)#4-K(1)-O(3)	151.52(11)	O(12)-K(2)-O(9)#2	80.74(9)
C(43)-O(11)-K(1)	144.7(2)	O(16)#1-K(1)-O(3)	93.1(4)	O(12)#1-K(2)-O(9)#2	115.71(9)
P(4)-O(11)-K(1)	87.11(11)	O(13)#4-K(1)-O(12)	77.09(9)	O(9)-K(2)-O(9)#2	137.47(11)
P(4)-O(12)-K(1)	117.54(15)	O(16)#1-K(1)-O(12)	95.4(3)	O(17)#3-K(2)-O(13)#2	75.6(3)
P(4)-O(12)-K(2)	121.24(15)	O(3)-K(1)-O(12)	130.47(10)	O(12)-K(2)-O(13)#2	127.57(10)
K(1)-O(12)-K(2)	108.75(10)	O(13)#4-K(1)-O(6)	79.00(10)	O(12)#1-K(2)-O(13)#2	72.61(9)
P(4)-O(12)-K(2)#2	115.60(15)	O(16)#1-K(1)-O(6)	61.0(3)	O(9)-K(2)-O(13)#2	150.31(9)
K(1)-O(12)-K(2)#2	92.93(9)	O(3)-K(1)-O(6)	78.25(9)	O(9)#2-K(2)-O(13)#2	68.42(9)
K(2)-O(12)-K(2)#2	95.09(8)	O(12)-K(1)-O(6)	145.98(10)	O(17)#3-K(2)-O(15)#3	20.5(3)
K(1)#3-O(13)-K(2)#1	92.29(10)	O(13)#4-K(1)-O(15)#1	72.1(3)	O(12)-K(2)-O(15)#3	101.7(2)
O(16)-O(15)-O(17)	151.6(18)	O(16)#1-K(1)-O(15)#1	20.7(3)	O(12)#1-K(2)-O(15)#3	80.0(2)
O(16)-O(15)-K(1)#2	65.2(11)	O(3)-K(1)-O(15)#1	113.7(3)	O(9)-K(2)-O(15)#3	95.7(2)
O(17)-O(15)-K(1)#2	139.8(12)	O(12)-K(1)-O(15)#1	82.5(2)	O(9)#2-K(2)-O(15)#3	124.7(2)
O(16)-O(15)-K(2)#4	143.8(12)	O(6)-K(1)-O(15)#1	67.2(2)	O(13)#2-K(2)-O(15)#3	67.3(2)
O(17)-O(15)-K(2)#4	64.2(11)	O(13)#4-K(1)-O(17)#3	127.3(3)	O(17)#3-K(2)-P(4)#1	120.1(4)
K(1)#2-O(15)-K(2)#4	84.4(3)	O(16)#1-K(1)-O(17)#3	50.9(4)	O(12)-K(2)-P(4)#1	155.19(7)
O(15)-O(16)-K(1)#2	94.1(12)	O(3)-K(1)-O(17)#3	75.0(3)	O(12)#1-K(2)-P(4)#1	21.37(6)
O(15)-O(17)-K(2)#4	95.3(12)	O(12)-K(1)-O(17)#3	73.3(3)	O(9)-K(2)-P(4)#1	87.15(7)
O(15)-O(17)-K(1)#4	161.8(13)	O(6)-K(1)-O(17)#3	103.5(3)	O(9)#2-K(2)-P(4)#1	97.29(7)
K(2)#4-O(17)-K(1)#4	96.0(5)	O(15)#1-K(1)-O(17)#3	61.7(3)	O(13)#2-K(2)-P(4)#1	72.80(8)
O(3)-P(1)-N(1)	119.50(18)	O(13)#4-K(1)-O(11)	66.04(9)	O(15)#3-K(2)-P(4)#1	99.6(2)
O(3)-P(1)-O(2)	111.25(17)	O(16)#1-K(1)-O(11)	137.0(4)	O(17)#3-K(2)-P(4)	97.0(3)
N(1)-P(1)-O(2)	109.31(18)	O(3)-K(1)-O(11)	124.91(9)	O(12)-K(2)-P(4)	19.69(6)
O(3)-P(1)-O(1)	106.66(16)	O(12)-K(1)-O(11)	45.95(8)	O(12)#1-K(2)-P(4)	142.13(7)
N(1)-P(1)-O(1)	109.35(18)	O(6)-K(1)-O(11)	138.50(10)	O(9)-K(2)-P(4)	63.87(6)
O(2)-P(1)-O(1)	98.70(16)	O(15)#1-K(1)-O(11)	118.3(2)	O(9)#2-K(2)-P(4)	85.27(7)
O(3)-P(1)-K(1)	32.94(12)	O(17)#3-K(1)-O(11)	115.1(3)	O(13)#2-K(2)-P(4)	144.78(8)
N(1)-P(1)-K(1)	86.90(14)	O(13)#4-K(1)-P(4)	75.32(8)	O(15)#3-K(2)-P(4)	114.9(2)
O(2)-P(1)-K(1)	132.90(12)	O(16)#1-K(1)-P(4)	116.2(3)	P(4)#1-K(2)-P(4)	135.87(5)
O(1)-P(1)-K(1)	117.65(11)	O(3)-K(1)-P(4)	127.02(8)	O(17)#3-K(2)-P(3)	100.9(3)
O(6)-P(2)-N(1)	120.3(2)	O(12)-K(1)-P(4)	20.99(6)	O(12)-K(2)-P(3)	61.15(6)
O(6)-P(2)-O(5)	107.80(18)	O(6)-K(1)-P(4)	154.17(8)	O(12)#1-K(2)-P(3)	98.16(7)
N(1)-P(2)-O(5)	109.14(18)	O(15)#1-K(1)-P(4)	101.7(2)	O(9)-K(2)-P(3)	18.84(6)
O(6)-P(2)-O(4)	110.1(2)	O(17)#3-K(1)-P(4)	90.0(3)	O(9)#2-K(2)-P(3)	121.87(7)
N(1)-P(2)-O(4)	108.61(19)	O(11)-K(1)-P(4)	25.93(5)	O(13)#2-K(2)-P(3)	169.06(8)
O(5)-P(2)-O(4)	98.72(17)	O(13)#4-K(1)-P(1)	134.35(8)	O(15)#3-K(2)-P(3)	105.9(2)
O(6)-P(2)-K(1)	40.60(13)	O(16)#1-K(1)-P(1)	90.8(4)	P(4)#1-K(2)-P(3)	100.83(4)
N(1)-P(2)-K(1)	86.13(14)	O(3)-K(1)-P(1)	17.52(6)	P(4)-K(2)-P(3)	45.31(3)
O(5)-P(2)-K(1)	145.43(13)	O(12)-K(1)-P(1)	147.96(7)	O(17)#3-K(2)-K(1)#1	65.5(4)
O(4)-P(2)-K(1)	105.59(13)	O(6)-K(1)-P(1)	62.33(7)	O(12)-K(2)-K(1)#1	147.12(8)
O(9)-P(3)-N(2)	121.42(17)	O(15)#1-K(1)-P(1)	110.2(2)	O(12)#1-K(2)-K(1)#1	43.20(6)
O(9)-P(3)-O(8)	106.85(16)	O(17)#3-K(1)-P(1)	86.8(3)	O(9)-K(2)-K(1)#1	109.20(7)
N(2)-P(3)-O(8)	107.63(16)	O(11)-K(1)-P(1)	131.57(7)	O(9)#2-K(2)-K(1)#1	108.49(7)
O(9)-P(3)-O(7)	108.52(16)	P(4)-K(1)-P(1)	141.58(5)	O(13)#2-K(2)-K(1)#1	41.40(7)
N(2)-P(3)-O(7)	109.15(16)	O(13)#4-K(1)-P(2)	91.07(8)	O(15)#3-K(2)-K(1)#1	46.6(2)
O(8)-P(3)-O(7)	101.40(15)	O(16)#1-K(1)-P(2)	76.1(3)	P(4)#1-K(2)-K(1)#1	57.00(3)
O(9)-P(3)-K(2)	37.47(11)	O(3)-K(1)-P(2)	62.65(7)	P(4)-K(2)-K(1)#1	161.10(5)
N(2)-P(3)-K(2)	83.97(12)	O(12)-K(1)-P(2)	165.44(8)	P(3)-K(2)-K(1)#1	127.68(4)
O(8)-P(3)-K(2)	124.82(11)	O(6)-K(1)-P(2)	19.83(7)	O(17)#3-K(2)-K(2)#2	88.2(4)
O(7)-P(3)-K(2)	125.97(11)	O(15)#1-K(1)-P(2)	85.8(2)	O(12)-K(2)-K(2)#2	42.48(6)
O(12)-P(4)-N(2)	119.48(16)	O(17)#3-K(1)-P(2)	108.6(3)	O(12)#1-K(2)-K(2)#2	157.30(7)
O(12)-P(4)-O(10)	111.25(17)	O(11)-K(1)-P(2)	136.11(7)	O(9)-K(2)-K(2)#2	119.30(7)
N(2)-P(4)-O(10)	108.02(16)	P(4)-K(1)-P(2)	161.30(5)	O(9)#2-K(2)-K(2)#2	42.61(6)
O(12)-P(4)-O(11)	105.59(15)	P(1)-K(1)-P(2)	45.49(3)	O(13)#2-K(2)-K(2)#2	89.56(7)
N(2)-P(4)-O(11)	111.41(16)	O(13)#4-K(1)-K(2)#2	46.31(8)	O(15)#3-K(2)-K(2)#2	106.4(2)
O(10)-P(4)-O(11)	99.21(15)	O(16)#1-K(1)-K(2)#2	68.6(4)	P(4)#1-K(2)-K(2)#2	139.82(4)
O(12)-P(4)-K(2)#2	43.03(11)	O(3)-K(1)-K(2)#2	157.48(9)	P(4)-K(2)-K(2)#2	55.49(3)
N(2)-P(4)-K(2)#2	149.09(13)	O(12)-K(1)-K(2)#2	43.87(6)	P(3)-K(2)-K(2)#2	100.78(4)
O(10)-P(4)-K(2)#2	70.58(12)	O(6)-K(1)-K(2)#2	102.33(8)	K(1)#1-K(2)-K(2)#2	127.20(3)

Symmetry transformations used to generate equivalent atoms:

#1 x+1/2,y,-z+1/2 #2 x-1/2,y,-z+1/2 #3 x+1,y,z #4 x-1,y,z

Table 4. Anisotropic displacement parameters ($Å^2 x\ 10^3$)for ktpopm. The anisotropic displacement factor exponent takes the form: $-2\pi^2[\ h^2 a^{*2} U^{11} + ... + 2\ h\ k\ a^*\ b^*\ U^{12}\ ]$

	U^{11}	U^{22}	U^{33}	U^{23}	U^{13}	U^{12}
C(1)	46(3)	56(3)	47(3)	0(2)	0(2)	2(2)
C(2)	75(4)	63(3)	61(3)	1(3)	-8(3)	2(3)
C(3)	105(5)	69(4)	91(5)	18(4)	8(4)	-1(3)
C(4)	139(7)	123(6)	81(5)	48(5)	-13(5)	3(5)
C(5)	154(7)	137(7)	80(5)	29(5)	-39(5)	-31(6)
C(6)	82(4)	89(4)	61(4)	7(3)	-16(3)	-15(3)
C(7)	43(3)	52(3)	59(3)	-15(2)	10(2)	2(2)
C(8)	94(4)	55(3)	57(3)	0(3)	1(3)	-6(3)
C(9)	111(5)	103(5)	56(4)	-10(3)	-3(3)	-17(4)
C(10)	92(5)	102(5)	92(5)	-50(4)	28(4)	-14(4)
C(11)	71(4)	67(4)	136(6)	-44(4)	0(4)	9(3)
C(12)	63(3)	59(3)	97(4)	-23(3)	-6(3)	8(3)
C(13)	61(3)	66(3)	60(3)	-11(3)	19(3)	-10(3)
C(14)	81(5)	182(8)	71(5)	-4(5)	7(4)	15(5)
C(15)	115(8)	400(20)	74(6)	-61(10)	13(5)	-37(10)
C(16)	214(16)	330(20)	107(8)	-131(12)	79(10)	-167(15)
C(17)	292(16)	87(5)	154(9)	-57(7)	132(10)	-77(7)
C(18)	169(7)	67(4)	84(5)	-7(4)	47(4)	2(4)
C(19)	53(3)	49(3)	62(3)	-7(2)	-19(2)	-6(2)
C(20)	62(3)	57(3)	85(4)	-12(3)	-12(3)	-4(3)
C(21)	81(4)	66(4)	119(5)	-12(4)	-23(4)	1(3)
C(22)	112(6)	68(4)	123(6)	11(4)	-40(5)	-8(4)
C(23)	115(6)	97(5)	86(5)	22(4)	-9(4)	-35(5)
C(24)	62(3)	83(4)	73(4)	-2(3)	-1(3)	-11(3)
C(25)	38(2)	47(2)	38(2)	6(2)	-6(2)	3(2)
C(26)	70(3)	53(3)	51(3)	-8(2)	8(2)	0(3)
C(27)	83(4)	53(3)	73(4)	6(3)	12(3)	-8(3)
C(28)	73(3)	77(4)	48(3)	15(3)	11(2)	-7(3)
C(29)	80(4)	77(4)	47(3)	-8(3)	8(3)	-4(3)
C(30)	68(3)	48(3)	52(3)	-8(2)	0(2)	-5(2)
C(31)	38(2)	42(2)	54(3)	-2(2)	2(2)	-7(2)
C(32)	58(3)	50(3)	66(3)	-4(2)	-9(3)	-10(2)
C(33)	94(4)	79(4)	68(4)	-18(3)	-11(3)	-23(4)
C(34)	95(5)	63(4)	111(5)	-42(4)	15(4)	-7(4)
C(35)	74(4)	53(3)	110(5)	-20(3)	-2(3)	10(3)
C(36)	53(3)	45(3)	81(4)	-6(3)	-7(3)	2(2)
C(37)	32(2)	48(3)	51(3)	6(2)	-5(2)	4(2)
C(38)	63(3)	62(3)	53(3)	-1(2)	0(2)	20(3)
C(39)	81(4)	47(3)	75(4)	-13(3)	-10(3)	18(3)
C(40)	65(3)	48(3)	79(4)	9(3)	-10(3)	2(3)
C(41)	63(3)	59(3)	57(3)	9(3)	5(2)	3(3)
C(42)	54(3)	46(3)	55(3)	-7(2)	-1(2)	8(2)
C(43)	39(2)	66(3)	42(3)	-1(2)	-2(2)	9(2)
C(44)	50(3)	90(4)	44(3)	16(3)	8(2)	3(3)
C(45)	81(4)	128(6)	47(3)	14(4)	14(3)	19(4)
C(46)	90(5)	142(6)	41(3)	-17(4)	-1(3)	37(4)
C(47)	75(4)	93(4)	60(3)	-21(3)	-12(3)	19(3)
C(48)	51(3)	72(3)	51(3)	-10(3)	-4(2)	6(3)
N(1)	41(2)	55(2)	57(2)	-1(2)	-6(2)	0(2)
N(2)	31(2)	40(2)	46(2)	0(2)	-1(1)	2(2)
O(1)	62(2)	44(2)	53(2)	-6(1)	-13(2)	-5(2)
O(2)	51(2)	55(2)	57(2)	-10(2)	-4(2)	10(2)
O(3)	55(2)	47(2)	64(2)	6(2)	-2(2)	1(2)
O(4)	50(2)	79(2)	80(2)	-28(2)	13(2)	-7(2)
O(5)	54(2)	52(2)	61(2)	-8(2)	-12(2)	-4(2)
O(6)	64(2)	58(2)	85(2)	10(2)	-8(2)	8(2)
O(7)	36(2)	60(2)	48(2)	14(1)	-2(1)	4(1)
O(8)	37(2)	42(2)	57(2)	1(1)	4(1)	-5(1)
O(9)	45(2)	57(2)	48(2)	-8(1)	2(1)	4(1)
O(10)	32(2)	59(2)	77(2)	22(2)	0(1)	5(1)
O(11)	45(2)	52(2)	43(2)	1(1)	7(1)	-7(1)
O(12)	42(2)	58(2)	44(2)	-5(1)	2(1)	-9(1)
O(13)	69(2)	59(2)	110(3)	11(2)	29(2)	12(2)

O(14)	62(2)	79(2)	83(2)	25(2)	-7(2)	-7(2)
P(1)	45(1)	41(1)	49(1)	-4(1)	-3(1)	2(1)
P(2)	46(1)	50(1)	58(1)	-6(1)	0(1)	1(1)
P(3)	33(1)	39(1)	38(1)	1(1)	-1(1)	1(1)
P(4)	33(1)	44(1)	38(1)	3(1)	-1(1)	-3(1)
K(1)	68(1)	63(1)	177(2)	48(1)	-14(1)	7(1)
K(2)	42(1)	114(1)	47(1)	-11(1)	5(1)	-5(1)

Table 5. Hydrogen coordinates (x 10^4) and isotropic displacement parameters ($Å^2$x 10^3) for ktpopm.

	x	y	z	U(eq)		x	y	z	U(eq)
H(2)	759	-2183	4099	80	H(26)	2667	-447	3664	69
H(3)	1142	-2623	4564	106	H(27)	1149	-732	4131	83
H(4)	2757	-2483	5081	137	H(28)	497	-421	4674	79
H(5)	3805	-1902	5155	149	H(29)	1371	175	4751	82
H(6)	3440	-1471	4696	93	H(30)	2883	462	4285	67
H(8)	1029	-1584	2888	82	H(32)	5345	891	3978	70
H(9)	645	-1916	2339	108	H(33)	4617	1340	4417	97
H(10)	1545	-2513	2305	114	H(34)	2619	1766	4262	108
H(11)	2611	-2795	2824	109	H(35)	1419	1769	3678	95
H(12)	3010	-2470	3376	88	H(36)	2140	1324	3245	72
H(14)	-1886	-1684	4478	134	H(38)	-2041	1301	3412	72
H(15)	-1449	-1323	5001	235	H(39)	-1357	1843	3124	81
H(16)	-2764	-766	5047	260	H(40)	-162	1845	2538	77
H(17)	-4437	-553	4567	213	H(41)	339	1297	2235	72
H(18)	-4787	-917	4040	128	H(42)	-385	749	2520	62
H(20)	-1051	-2472	3303	82	H(44)	-3141	-3	4179	74
H(21)	-638	-3021	3617	107	H(45)	-3767	290	4737	102
H(22)	-2344	-3182	4100	121	H(46)	-2676	859	4864	109
H(23)	-4506	-2807	4278	119	H(47)	-914	1138	4440	91
H(24)	-4921	-2251	3973	88	H(48)	-251	846	3877	70

B3 Crystallographic Data for $Tb(tpOp)_3$

Table 2. Atomic coordinates (x 10^4) and equivalent isotropic displacement parameters ($Å^2$x 10^3) for dd50m. U(eq) is defined as one third of the trace of the orthogonalized U^{ij} tensor.

	x	y	z	U(eq)		x	y	z	U(eq)
Tb(1)	823(1)	2782(1)	2554(1)	52(1)	C(24)	-1456(1)	-448(1)	1618(1)	82(4)
C(1)	3275(1)	231(1)	1316(1)	68(3)	C(25)	3995(1)	6053(1)	2139(1)	72(3)
C(2)	2235(1)	-397(1)	1144(1)	89(4)	C(26)	4750(1)	6347(1)	2635(1)	106(4)
C(3)	2506(1)	-1041(1)	779(1)	107(4)	C(27)	5423(1)	7157(1)	2663(1)	150(7)
C(4)	3816(1)	-1056(1)	586(1)	112(5)	C(28)	5339(1)	7673(1)	2194(1)	163(8)
C(5)	4856(1)	-428(1)	758(1)	114(5)	C(29)	4584(1)	7378(1)	1697(1)	140(6)
C(6)	4586(1)	216(1)	1123(1)	95(4)	C(30)	3912(1)	6568(1)	1670(1)	103(4)
C(7)	3700(1)	2704(1)	782(1)	55(3)	C(31)	-169(1)	5335(1)	1638(1)	65(3)
C(8)	3646(1)	3493(1)	1016(1)	67(3)	C(32)	-649(1)	6087(1)	1739(1)	88(4)
C(9)	3660(1)	4167(1)	653(1)	81(3)	C(33)	-2032(1)	6137(1)	1672(1)	98(4)
C(10)	3728(1)	4051(1)	57(1)	83(4)	C(34)	-2935(1)	5436(1)	1504(1)	96(4)
C(11)	3781(1)	3262(1)	-177(1)	80(3)	C(35)	-2455(1)	4684(1)	1403(1)	91(4)
C(12)	3767(1)	2588(1)	186(1)	65(3)	C(36)	-1072(1)	4633(1)	1470(1)	76(3)
C(13)	-1098(1)	2656(1)	399(1)	69(3)	C(37)	2736(1)	5575(1)	3978(1)	84(4)
C(14)	69(1)	3079(1)	166(1)	96(4)	C(38)	3963(1)	5373(1)	4200(1)	169(7)
C(15)	-9(1)	3792(1)	-149(1)	111(5)	C(39)	5004(1)	6000(1)	4374(1)	205(9)
C(16)	-1253(1)	4081(1)	-231(1)	103(4)	C(40)	4819(1)	6828(1)	4327(1)	236(11)
C(17)	-2420(1)	3657(1)	2(1)	91(4)	C(41)	3593(1)	7030(1)	4105(1)	203(9)
C(18)	-2342(1)	2945(1)	317(1)	84(4)	C(42)	2551(1)	6404(1)	3930(1)	142(6)
C(19)	-1345(1)	174(1)	1210(1)	65(3)	C(43)	-1689(1)	4720(1)	3528(1)	90(4)
C(20)	-1277(1)	-30(1)	625(1)	71(3)	C(44)	-2084(1)	4214(1)	3989(1)	148(6)
C(21)	-1320(1)	-856(1)	447(1)	85(4)	C(45)	-3390(1)	3774(1)	3991(1)	200(9)
C(22)	-1431(1)	-1478(1)	855(1)	94(4)	C(46)	-4301(1)	3840(1)	3531(1)	178(8)
C(23)	-1498(1)	-1274(1)	1440(1)	99(4)	C(47)	-3906(1)	4345(1)	3069(1)	185(8)

C(48)	-2600(1)	4785(1)	3068(1)	129(5)		N(2)	1406(8)	5265(4)	2782(3)	60(2)
C(49)	4583(1)	855(1)	3435(1)	74(3)		N(3)	1610(8)	1024(5)	3626(3)	59(2)
C(50)	5108(1)	502(1)	2952(1)	101(4)		O(1)	3006(7)	844(4)	1707(3)	66(2)
C(51)	5676(1)	-229(1)	3003(1)	130(5)		O(2)	3740(6)	2029(4)	1131(3)	61(2)
C(52)	5718(1)	-608(1)	3536(1)	119(5)		O(3)	2416(6)	2182(4)	2039(3)	61(2)
C(53)	5193(1)	-255(1)	4019(1)	112(5)		O(4)	-1025(10)	1918(5)	654(3)	110(3)
C(54)	4626(1)	477(1)	3968(1)	99(4)		O(5)	-1295(7)	976(5)	1408(3)	81(2)
C(55)	2400(1)	2365(1)	4641(1)	74(3)		O(6)	-318(7)	2425(4)	1670(3)	63(2)
C(56)	2142(1)	1945(1)	5154(1)	111(5)		O(7)	3457(6)	5236(4)	2102(3)	64(2)
C(57)	1427(1)	2287(1)	5585(1)	157(7)		O(8)	1222(7)	5321(4)	1675(3)	67(2)
C(58)	970(1)	3049(1)	5505(1)	149(6)		O(9)	1751(7)	3985(4)	2132(3)	61(2)
C(59)	1229(1)	3468(1)	4992(1)	145(6)		O(10)	1804(11)	4939(6)	3850(4)	135(4)
C(60)	1944(1)	3127(1)	4560(1)	101(4)		O(11)	-430(10)	5122(5)	3513(5)	137(4)
C(61)	575(1)	-700(1)	2883(1)	83(4)		O(12)	573(6)	3840(4)	3244(3)	59(2)
C(62)	-473(1)	-1345(1)	2964(1)	100(4)		O(13)	4097(7)	1590(4)	3357(3)	74(2)
C(63)	-208(1)	-2163(1)	2956(1)	117(5)		O(14)	3236(7)	2083(4)	4236(3)	69(2)
C(64)	1106(1)	-2335(1)	2868(1)	172(7)		O(15)	2373(6)	2550(4)	3280(2)	58(2)
C(65)	2155(1)	-1689(1)	2788(1)	205(9)		O(16)	434(9)	86(5)	2763(4)	111(3)
C(66)	1889(1)	-872(1)	2795(1)	148(6)		O(17)	-831(9)	358(6)	3539(4)	123(3)
C(67)	-1281(1)	804(1)	4059(1)	121(5)		O(18)	-26(7)	1476(4)	2831(3)	77(2)
C(68)	-1292(1)	248(1)	4509(1)	118(5)		O(19)	-1542(7)	2898(4)	2695(3)	78(2)
C(69)	-1711(1)	467(1)	5054(1)	138(6)		P(1)	2477(3)	1662(2)	1508(1)	58(1)
C(70)	-2118(1)	1242(1)	5148(1)	155(7)		P(2)	-253(3)	1750(2)	1229(1)	62(1)
C(71)	-2107(1)	1797(1)	4698(1)	178(7)		P(3)	1895(3)	4907(2)	2203(1)	59(1)
C(72)	-1689(1)	1578(1)	4153(1)	160(7)		P(4)	841(3)	4749(2)	3304(1)	65(1)
C(73)	-2749(15)	2293(10)		2552(7)	121(5)	P(5)	2714(3)	1818(2)	3600(1)	59(1)
C(74)	-3640(14)	2552(10)		2087(7)	136(6)	P(6)	303(3)	842(2)	3222(1)	66(1)
N(1)	1152(8)	1477(5)	1099(3)	60(2)						

Table 3. Bond lengths [Å] and angles [°] for dd50m.

Tb(1)-O(18)	2.284(6)	C(31)-C(32)	1.3900	C(67)-O(17)	1.500(11)
Tb(1)-O(9)	2.291(6)	C(31)-C(36)	1.3900	C(68)-C(69)	1.3900
Tb(1)-O(3)	2.314(6)	C(32)-C(33)	1.3900	C(69)-C(70)	1.3900
Tb(1)-O(15)	2.314(6)	C(33)-C(34)	1.3900	C(70)-C(71)	1.3900
Tb(1)-O(6)	2.328(6)	C(34)-C(35)	1.3900	C(71)-C(72)	1.3900
Tb(1)-O(12)	2.363(6)	C(35)-C(36)	1.3900	C(73)-O(19)	1.466(15)
Tb(1)-O(19)	2.409(7)	C(37)-O(10)	1.311(8)	C(73)-C(74)	1.477(17)
C(1)-O(1)	1.389(6)	C(37)-C(38)	1.3900	N(1)-P(2)	1.555(8)
C(1)-C(2)	1.3900	C(37)-C(42)	1.3900	N(1)-P(1)	1.586(8)
C(1)-C(6)	1.3900	C(38)-C(39)	1.3900	N(2)-P(4)	1.555(8)
C(2)-C(3)	1.3900	C(39)-C(40)	1.3900	N(2)-P(3)	1.563(8)
C(3)-C(4)	1.3900	C(40)-C(41)	1.3900	N(3)-P(6)	1.567(8)
C(4)-C(5)	1.3900	C(41)-C(42)	1.3900	N(3)-P(5)	1.576(8)
C(5)-C(6)	1.3900	C(43)-O(11)	1.328(9)	O(1)-P(1)	1.568(7)
C(7)-O(2)	1.378(6)	C(43)-C(44)	1.3900	O(2)-P(1)	1.600(7)
C(7)-C(8)	1.3900	C(43)-C(48)	1.3900	O(3)-P(1)	1.482(6)
C(7)-C(12)	1.3900	C(44)-C(45)	1.3900	O(4)-P(2)	1.560(8)
C(8)-C(9)	1.3900	C(45)-C(46)	1.3900	O(5)-P(2)	1.583(8)
C(9)-C(10)	1.3900	C(46)-C(47)	1.3900	O(6)-P(2)	1.491(6)
C(10)-C(11)	1.3900	C(47)-C(48)	1.3900	O(7)-P(3)	1.593(7)
C(11)-C(12)	1.3900	C(49)-O(13)	1.362(7)	O(8)-P(3)	1.580(7)
C(13)-O(4)	1.356(8)	C(49)-C(50)	1.3900	O(9)-P(3)	1.490(6)
C(13)-C(14)	1.3900	C(49)-C(54)	1.3900	O(10)-P(4)	1.559(9)
C(13)-C(18)	1.3900	C(50)-C(51)	1.3900	O(11)-P(4)	1.558(8)
C(14)-C(15)	1.3900	C(51)-C(52)	1.3900	O(12)-P(4)	1.467(6)
C(15)-C(16)	1.3900	C(52)-C(53)	1.3900	O(13)-P(5)	1.585(7)
C(16)-C(17)	1.3900	C(53)-C(54)	1.3900	O(14)-P(5)	1.573(7)
C(17)-C(18)	1.3900	C(55)-O(14)	1.380(7)	O(15)-P(5)	1.486(6)
C(19)-O(5)	1.366(7)	C(55)-C(56)	1.3900	O(16)-P(6)	1.628(9)
C(19)-C(20)	1.3900	C(55)-C(60)	1.3900	O(17)-P(6)	1.498(9)
C(19)-C(24)	1.3900	C(56)-C(57)	1.3900	O(18)-P(6)	1.447(7)
C(20)-C(21)	1.3900	C(57)-C(58)	1.3900		
C(21)-C(22)	1.3900	C(58)-C(59)	1.3900	O(18)-Tb(1)-O(9)	170.3(2)
C(22)-C(23)	1.3900	C(59)-C(60)	1.3900	O(18)-Tb(1)-O(3)	87.4(2)
C(23)-C(24)	1.3900	C(61)-O(16)	1.337(9)	O(9)-Tb(1)-O(3)	84.5(2)
C(25)-O(7)	1.361(6)	C(61)-C(62)	1.3900	O(18)-Tb(1)-O(15)	78.2(2)
C(25)-C(26)	1.3900	C(61)-C(66)	1.3900	O(9)-Tb(1)-O(15)	105.3(2)
C(25)-C(30)	1.3900	C(62)-C(63)	1.3900	O(3)-Tb(1)-O(15)	78.1(2)
C(26)-C(27)	1.3900	C(63)-C(64)	1.3900	O(18)-Tb(1)-O(6)	86.0(2)
C(27)-C(28)	1.3900	C(64)-C(65)	1.3900	O(9)-Tb(1)-O(6)	86.9(2)
C(28)-C(29)	1.3900	C(65)-C(66)	1.3900	O(3)-Tb(1)-O(6)	77.4(2)
C(29)-C(30)	1.3900	C(67)-C(68)	1.3900	O(15)-Tb(1)-O(6)	151.3(2)
C(31)-O(8)	1.383(7)	C(67)-C(72)	1.3900	O(18)-Tb(1)-O(12)	114.1(2)

O(9)-Tb(1)-O(12) 75.6(2)
O(3)-Tb(1)-O(12) 143.3(2)
O(15)-Tb(1)-O(12) 77.9(2)
O(6)-Tb(1)-O(12) 130.7(2)
O(18)-Tb(1)-O(19) 77.7(3)
O(9)-Tb(1)-O(19) 106.6(2)
O(3)-Tb(1)-O(19) 147.9(2)
O(15)-Tb(1)-O(19) 125.1(2)
O(6)-Tb(1)-O(19) 73.3(2)
O(12)-Tb(1)-O(19) 68.6(2)
O(1)-C(1)-C(2) 119.3(3)
O(1)-C(1)-C(6) 120.6(3)
C(2)-C(1)-C(6) 120.0
C(3)-C(2)-C(1) 120.0
C(2)-C(3)-C(4) 120.0
C(3)-C(4)-C(5) 120.0
C(6)-C(5)-C(4) 120.0
C(5)-C(6)-C(1) 120.0
O(2)-C(7)-C(8) 121.4(3)
O(2)-C(7)-C(12) 118.5(3)
C(8)-C(7)-C(12) 120.0
C(7)-C(8)-C(9) 120.0
C(8)-C(9)-C(10) 120.0
C(11)-C(10)-C(9) 120.0
C(10)-C(11)-C(12) 120.0
C(11)-C(12)-C(7) 120.0
O(4)-C(13)-C(14) 118.9(4)
O(4)-C(13)-C(18) 120.7(4)
C(14)-C(13)-C(18) 120.0
C(15)-C(14)-C(13) 120.0
C(14)-C(15)-C(16) 120.0
C(15)-C(16)-C(17) 120.0
C(18)-C(17)-C(16) 120.0
C(17)-C(18)-C(13) 120.0
O(5)-C(19)-C(20) 122.3(3)
O(5)-C(19)-C(24) 117.7(3)
C(20)-C(19)-C(24) 120.0
C(21)-C(20)-C(19) 120.0
C(22)-C(21)-C(20) 120.0
C(21)-C(22)-C(23) 120.0
C(24)-C(23)-C(22) 120.0
C(23)-C(24)-C(19) 120.0
O(7)-C(25)-C(26) 118.7(3)
O(7)-C(25)-C(30) 121.0(3)
C(26)-C(25)-C(30) 120.0
C(27)-C(26)-C(25) 120.0
C(26)-C(27)-C(28) 120.0
C(27)-C(28)-C(29) 120.0
C(28)-C(29)-C(30) 120.0
C(29)-C(30)-C(25) 120.0
O(8)-C(31)-C(32) 118.3(3)
O(8)-C(31)-C(36) 121.6(3)
C(32)-C(31)-C(36) 120.0
C(33)-C(32)-C(31) 120.0
C(32)-C(33)-C(34) 120.0
C(35)-C(34)-C(33) 120.0
C(34)-C(35)-C(36) 120.0
C(35)-C(36)-C(31) 120.0
O(10)-C(37)-C(38) 115.0(5)
O(10)-C(37)-C(42) 124.9(5)
C(38)-C(37)-C(42) 120.0
C(37)-C(38)-C(39) 120.0
C(40)-C(39)-C(38) 120.0
C(39)-C(40)-C(41) 120.0
C(42)-C(41)-C(40) 120.0
C(41)-C(42)-C(37) 120.0
O(11)-C(43)-C(44) 120.5(5)
O(11)-C(43)-C(48) 119.4(5)
C(44)-C(43)-C(48) 120.0
C(45)-C(44)-C(43) 120.0
C(46)-C(45)-C(44) 120.0
C(47)-C(46)-C(45) 120.0
C(46)-C(47)-C(48) 120.0
C(47)-C(48)-C(43) 120.0
O(13)-C(49)-C(50) 116.7(3)
O(13)-C(49)-C(54) 123.3(3)
C(50)-C(49)-C(54) 120.0
C(51)-C(50)-C(49) 120.0
C(50)-C(51)-C(52) 120.0
C(53)-C(52)-C(51) 120.0
C(52)-C(53)-C(54) 120.0
C(53)-C(54)-C(49) 120.0
O(14)-C(55)-C(56) 120.7(3)
O(14)-C(55)-C(60) 118.9(3)
C(56)-C(55)-C(60) 120.0
C(55)-C(56)-C(57) 120.0
C(56)-C(57)-C(58) 120.0
C(59)-C(58)-C(57) 120.0
C(60)-C(59)-C(58) 120.0
C(59)-C(60)-C(55) 120.0
O(16)-C(61)-C(62) 126.2(4)
O(16)-C(61)-C(66) 112.4(4)
C(62)-C(61)-C(66) 120.0
C(61)-C(62)-C(63) 120.0
C(64)-C(63)-C(62) 120.0
C(65)-C(64)-C(63) 120.0
C(64)-C(65)-C(66) 120.0
C(65)-C(66)-C(61) 120.0
C(68)-C(67)-C(72) 120.0
C(68)-C(67)-O(17) 105.7(3)
C(72)-C(67)-O(17) 134.2(3)
C(67)-C(68)-C(69) 120.0
C(70)-C(69)-C(68) 120.0
C(69)-C(70)-C(71) 120.0
C(70)-C(71)-C(72) 120.0
C(71)-C(72)-C(67) 120.0
O(19)-C(73)-C(74) 114.0(12)
P(2)-N(1)-P(1) 125.2(5)
P(4)-N(2)-P(3) 126.0(5)
P(6)-N(3)-P(5) 125.0(5)
C(1)-O(1)-P(1) 122.4(4)
C(7)-O(2)-P(1) 122.2(4)
P(1)-O(3)-Tb(1) 138.9(4)
C(13)-O(4)-P(2) 128.3(6)
C(19)-O(5)-P(2) 126.7(5)
P(2)-O(6)-Tb(1) 133.5(4)
C(25)-O(7)-P(3) 123.5(4)
C(31)-O(8)-P(3) 121.0(4)
P(3)-O(9)-Tb(1) 142.1(4)
C(37)-O(10)-P(4) 130.5(6)
C(43)-O(11)-P(4) 125.8(6)
P(4)-O(12)-Tb(1)139.0(4)
C(49)-O(13)-P(5) 125.3(5)
C(55)-O(14)-P(5) 122.1(5)
P(5)-O(15)-Tb(1)136.1(4)
C(61)-O(16)-P(6) 127.4(6)
P(6)-O(17)-C(67) 114.5(6)
P(6)-O(18)-Tb(1)140.1(4)
C(73)-O(19)-Tb(1) 129.0(7)
O(3)-P(1)-O(1) 106.5(4)
O(3)-P(1)-N(1) 118.2(4)
O(1)-P(1)-N(1) 112.1(4)
O(3)-P(1)-O(2) 110.4(4)
O(1)-P(1)-O(2) 98.7(4)
N(1)-P(1)-O(2) 109.2(4)
O(6)-P(2)-N(1) 119.0(4)
O(6)-P(2)-O(4) 111.1(4)
N(1)-P(2)-O(4) 110.7(5)
O(6)-P(2)-O(5) 107.2(4)
N(1)-P(2)-O(5) 110.3(4)
O(4)-P(2)-O(5) 96.1(5)
O(9)-P(3)-N(2) 117.3(4)
O(9)-P(3)-O(8) 112.0(4)
N(2)-P(3)-O(8) 109.1(4)
O(9)-P(3)-O(7) 105.9(4)
N(2)-P(3)-O(7) 111.6(4)
O(8)-P(3)-O(7) 99.6(4)
O(12)-P(4)-N(2) 119.3(4)
O(12)-P(4)-O(11) 111.8(4)
N(2)-P(4)-O(11) 107.4(5)
O(12)-P(4)-O(10) 105.8(5)
N(2)-P(4)-O(10) 110.8(5)
O(11)-P(4)-O(10) 100.0(6)
O(15)-P(5)-O(14) 110.5(4)
O(15)-P(5)-N(3) 118.9(4)
O(14)-P(5)-N(3) 108.7(4)
O(15)-P(5)-O(13) 107.4(4)
O(14)-P(5)-O(13) 98.3(4)
N(3)-P(5)-O(13) 111.2(4)
O(18)-P(6)-O(17) 118.4(5)
O(18)-P(6)-N(3) 119.1(4)
O(17)-P(6)-N(3) 110.1(5)
O(18)-P(6)-O(16) 100.7(5)
O(17)-P(6)-O(16) 94.0(5)
N(3)-P(6)-O(16) 110.7(5)

Symmetry transformations used to generate equivalent atoms:

Table 4. Anisotropic displacement parameters ($Å^2 x\ 10^3$)for dd50m. The anisotropic displacement factor exponent takes the form: $-2\pi^2[\ h^2 a^{*2} U^{11} + ... + 2\ h\ k\ a^*\ b^*\ U^{12}\ ]$

	U^{11}	U^{22}	U^{33}	U^{23}	U^{13}	U^{12}
Tb(1)	57(1)	47(1)	51(1)	1(1)	-1(1)	3(1)
C(1)	69(8)	52(7)	85(8)	2(6)	1(6)	17(6)
C(2)	78(9)	72(8)	114(10)	-15(7)	1(7)	4(7)
C(3)	85(9)	73(9)	163(12)	-31(8)	-15(9)	23(8)
C(4)	100(10)	104(10)	131(11)	-54(9)	-14(9)	27(9)
C(5)	94(10)	108(11)	144(12)	-46(9)	26(9)	29(8)

C(6)	78(9)	78(9)	124(10)	-17(7)	6(8)	-2(7)
C(7)	31(6)	66(7)	67(7)	6(6)	7(5)	1(5)
C(8)	64(7)	65(8)	70(8)	3(6)	-3(6)	1(6)
C(9)	69(8)	67(8)	105(9)	14(7)	5(7)	1(6)
C(10)	68(8)	95(9)	82(8)	26(7)	13(7)	-3(7)
C(11)	68(8)	94(9)	75(8)	-2(7)	16(6)	-2(7)
C(12)	53(7)	63(7)	77(8)	5(6)	9(6)	3(6)
C(13)	87(9)	76(8)	51(7)	3(6)	-21(6)	38(7)
C(14)	75(9)	137(12)	80(9)	-10(8)	19(7)	27(9)
C(15)	86(10)	153(13)	96(10)	18(9)	17(8)	18(9)
C(16)	110(11)	107(10)	95(9)	38(8)	-10(9)	23(9)
C(17)	74(8)	99(10)	104(10)	-9(8)	-24(7)	31(8)
C(18)	71(8)	100(10)	76(8)	-5(7)	6(7)	-1(7)
C(19)	39(6)	70(8)	80(8)	-29(6)	-7(6)	-6(6)
C(20)	50(7)	66(7)	91(8)	-2(6)	9(6)	-14(6)
C(21)	80(8)	91(9)	78(8)	-29(7)	28(7)	-13(7)
C(22)	86(9)	80(9)	104(10)	-27(7)	6(8)	-21(7)
C(23)	103(10)	85(9)	103(10)	3(8)	-7(8)	-6(8)
C(24)	75(8)	87(9)	81(9)	-12(7)	6(7)	1(7)
C(25)	47(7)	59(8)	108(9)	-8(7)	34(6)	-4(6)
C(26)	71(9)	105(10)	138(11)	-27(9)	29(8)	-6(8)
C(27)	95(11)	122(13)	216(17)	-78(12)	57(11)	-38(10)
C(28)	132(14)	88(11)	260(20)	-37(12)	97(14)	-36(10)
C(29)	139(14)	87(11)	199(16)	23(11)	74(12)	14(10)
C(30)	84(9)	76(9)	151(12)	19(8)	34(9)	10(7)
C(31)	77(8)	61(7)	58(7)	14(6)	10(6)	17(6)
C(32)	97(9)	81(9)	87(9)	4(7)	-10(7)	19(8)
C(33)	115(11)	103(10)	85(9)	7(8)	2(8)	46(9)
C(34)	74(9)	135(12)	89(9)	6(9)	11(7)	48(8)
C(35)	80(9)	110(10)	80(8)	-3(7)	-5(7)	8(8)
C(36)	82(9)	77(8)	72(8)	3(6)	2(7)	20(7)
C(37)	74(9)	107(10)	71(8)	-23(7)	-9(7)	18(8)
C(38)	165(16)	168(15)	164(15)	27(12)	-34(13)	-8(13)
C(39)	132(14)	260(20)	209(16)	60(17)	-73(13)	-23(15)
C(40)	185(18)	260(20)	222(18)	-24(18)	-68(15)	-99(18)
C(41)	199(18)	149(15)	237(18)	-96(13)	33(15)	-57(14)
C(42)	111(12)	107(12)	207(15)	-48(11)	11(11)	15(10)
C(43)	107(11)	71(9)	98(10)	1(7)	28(8)	27(8)
C(44)	101(12)	163(14)	185(15)	52(12)	23(11)	30(11)
C(45)	148(16)	158(15)	300(20)	90(15)	54(16)	28(14)
C(46)	103(13)	121(13)	310(20)	-1(15)	75(14)	1(11)
C(47)	139(15)	192(18)	231(18)	-81(15)	-6(15)	62(14)
C(48)	157(14)	132(12)	110(11)	-11(10)	27(11)	57(11)
C(49)	45(7)	84(9)	91(9)	-3(7)	13(6)	2(6)
C(50)	87(10)	99(10)	119(11)	9(9)	-1(8)	15(8)
C(51)	106(11)	113(12)	178(15)	-11(11)	16(11)	36(9)
C(52)	80(10)	90(10)	185(15)	1(10)	2(10)	11(8)
C(53)	89(10)	119(11)	140(12)	27(9)	6(9)	52(8)
C(54)	108(10)	100(10)	100(10)	24(8)	7(8)	47(8)
C(55)	85(8)	72(8)	62(8)	-2(6)	-21(7)	5(7)
C(56)	162(13)	101(10)	64(8)	26(7)	19(8)	-9(9)
C(57)	202(16)	169(15)	93(11)	0(11)	78(11)	-10(13)
C(58)	141(13)	168(16)	142(14)	-23(12)	32(12)	36(12)
C(59)	169(15)	155(14)	120(13)	-18(11)	-28(12)	61(12)
C(60)	136(12)	117(11)	55(8)	0(7)	0(8)	34(9)
C(61)	111(10)	43(7)	93(9)	14(6)	-24(8)	5(7)
C(62)	116(11)	70(9)	112(10)	-7(8)	10(8)	0(8)
C(63)	175(14)	66(9)	103(10)	-3(8)	-4(10)	-11(10)
C(64)	192(18)	120(13)	214(16)	-49(12)	-7(15)	73(13)
C(65)	158(16)	183(18)	278(19)	-76(17)	29(15)	37(14)
C(66)	108(12)	144(14)	185(14)	-6(12)	27(11)	-12(11)
C(67)	66(9)	158(14)	126(12)	62(11)	-9(9)	-40(9)
C(68)	93(10)	144(12)	114(12)	-6(10)	34(9)	2(9)
C(69)	134(13)	120(12)	157(14)	56(12)	5(11)	-3(10)
C(70)	149(14)	162(15)	157(14)	24(12)	59(12)	18(13)
C(71)	205(17)	144(14)	197(18)	22(13)	52(15)	54(13)
C(72)	145(14)	116(13)	215(17)	77(13)	-12(13)	0(11)
C(73)	102(11)	142(13)	122(12)	2(10)	20(10)	27(10)
C(74)	101(11)	154(14)	146(14)	25(11)	-50(10)	4(10)
N(1)	57(6)	58(5)	60(5)	-6(4)	0(4)	-6(4)
N(2)	67(6)	39(5)	73(6)	-1(4)	4(5)	11(4)
N(3)	66(6)	57(5)	50(5)	12(4)	-1(4)	-7(4)
O(1)	86(5)	59(5)	58(4)	2(4)	16(4)	20(4)
O(2)	53(4)	55(4)	74(5)	6(4)	6(4)	3(3)
O(3)	66(5)	60(4)	54(4)	-4(3)	-9(3)	6(4)

O(4)	178(9)	82(6)	77(6)	-10(5)	-43(6)	52(6)
O(5)	60(5)	75(5)	102(6)	-24(4)	-1(4)	-5(4)
O(6)	72(5)	57(4)	62(4)	-5(3)	-12(4)	19(4)
O(7)	52(4)	49(4)	92(5)	2(4)	10(4)	5(4)
O(8)	63(5)	66(5)	74(5)	23(4)	15(4)	8(4)
O(9)	75(5)	49(4)	57(4)	-6(3)	8(4)	4(4)
O(10)	187(10)	100(7)	91(6)	1(5)	-38(6)	-69(6)
O(11)	99(7)	79(6)	230(10)	-46(6)	92(7)	-6(5)
O(12)	64(5)	47(4)	64(4)	-2(3)	9(4)	0(3)
O(13)	60(5)	72(5)	92(5)	11(4)	19(4)	16(4)
O(14)	73(5)	77(5)	55(5)	-5(4)	-13(4)	10(4)
O(15)	59(4)	61(4)	48(4)	10(3)	-7(3)	-8(3)
O(16)	142(8)	90(6)	95(6)	3(5)	-24(6)	-3(6)
O(17)	82(6)	142(8)	131(8)	42(7)	-8(6)	-34(6)
O(18)	69(5)	61(5)	92(5)	26(4)	-32(4)	-18(4)
O(19)	46(5)	78(5)	105(6)	-27(4)	-2(4)	-8(4)
P(1)	62(2)	52(2)	58(2)	-3(1)	7(2)	6(2)
P(2)	81(2)	56(2)	52(2)	-3(1)	-13(2)	20(2)
P(3)	63(2)	48(2)	65(2)	4(1)	4(2)	7(2)
P(4)	67(2)	59(2)	65(2)	-15(2)	4(2)	-4(2)
P(5)	59(2)	62(2)	53(2)	4(1)	-4(1)	3(2)
P(6)	62(2)	62(2)	69(2)	13(2)	-9(2)	-13(2)

Table 5. Hydrogen coordinates (x 10^4) and isotropic displacement parameters ($Å^2$x 10^3) for dd50m.

	x	y	z	U(eq)		x	y	z	U(eq)
H(2)	1358	-387	1273	106		H(41)	3469	7584	4073	244
H(3)	1810	-1461	664	128		H(42)	1731	6539	3782	171
H(4)	3998	-1487	341	134		H(44)	-1475	4171	4297	177
H(5)	5733	-438	628	137		H(45)	-3654	3436	4299	240
H(6)	5281	637	1238	114		H(46)	-5175	3545	3531	213
H(8)	3601	3571	1415	81		H(47)	-4516	4389	2761	222
H(9)	3624	4695	810	97		H(48)	-2336	5123	2759	155
H(10)	3737	4501	-186	99		H(50)	5080	756	2595	122
H(11)	3826	3184	-576	96		H(51)	6027	-465	2680	157
H(12)	3803	2060	29	78		H(52)	6098	-1097	3570	142
H(14)	902	2886	221	115		H(53)	5221	-508	4376	134
H(15)	772	4075	-305	133		H(54)	4274	713	4291	119
H(16)	-1305	4557	-442	124		H(56)	2447	1436	5208	133
H(17)	-3253	3850	-53	109		H(57)	1253	2007	5928	188
H(18)	-3123	2661	473	100		H(58)	492	3277	5793	179
H(20)	-1203	386	352	85		H(59)	924	3978	4938	174
H(21)	-1275	-992	56	102		H(60)	2117	3407	4217	122
H(22)	-1459	-2030	736	112		H(62)	-1352	-1230	3022	120
H(23)	-1572	-1690	1713	119		H(63)	-909	-2595	3010	141
H(24)	-1501	-311	2009	98		H(64)	1284	-2882	2863	206
H(26)	4806	6002	2949	128		H(65)	3034	-1804	2729	247
H(27)	5928	7354	2995	180		H(66)	2591	-440	2742	178
H(28)	5789	8215	2212	196		H(68)	-1019	-270	4446	141
H(29)	4528	7723	1383	168		H(69)	-1718	96	5355	166
H(30)	3406	6371	1338	124		H(70)	-2398	1389	5513	186
H(32)	-45	6557	1852	106		H(71)	-2380	2316	4761	214
H(33)	-2353	6640	1740	118		H(72)	-1682	1950	3852	192
H(34)	-3860	5469	1460	115		H(73A)	-3274	2195	2898	145
H(35)	-3059	4214	1290	109		H(73B)	-2456	1771	2435	145
H(36)	-751	4130	1402	91		H(74A)	-4409	2130	2019	204
H(38)	4086	4819	4231	203		H(74B)	-3139	2633	1738	204
H(39)	5824	5864	4522	246		H(74C)	-3950	3063	2201	204
H(40)	5515	7247	4444	284						

B4 Crystallographic Data for $Eu(tpOp)_3$

Table 2. Atomic coordinates (x 10^4) and equivalent isotropic displacement parameters ($Å^2$x 10^3) for pcluseum. U(eq) is defined as one third of the trace of the orthogonalized U^{ij} tensor.

	x	y	z	U(eq)		x	y	z	U(eq)
Eu(1)	4169(1)	2218(1)	7453(1)	44(1)		C(52)	4051(19)	1968(16)	4530(8)	150(8)
C(1)	6652(1)	260(1)	6471(1)	76(3)		C(53)	3741(17)	1501(11)	5003(8)	133(6)
C(2)	7051(1)	759(1)	6008(1)	141(6)		C(54)	3001(15)	1832(9)	5439(5)	103(4)
C(3)	8363(1)	1194(1)	6004(1)	183(8)		C(55)	402(9)	4183(7)	6558(5)	64(3)
C(4)	9277(1)	1130(1)	6464(1)	149(7)		C(56)	-70(12)	4534(8)	7034(6)	92(4)
C(5)	8879(1)	631(1)	6927(1)	182(8)		C(57)	-651(15)	5262(9)	6972(8)	122(5)
C(6)	7566(1)	196(1)	6930(1)	132(5)		C(58)	-693(16)	5617(9)	6445(9)	125(6)
C(7)	2244(12)	-623(7)	6024(4)	73(3)		C(59)	-211(14)	5262(9)	5990(7)	111(5)
C(8)	1074(10)	-380(6)	5821(3)	168(7)		C(60)	362(4)	4533(3)	6021(2)	94(4)
C(9)	21(10)	-997(6)	5644(3)	225(10)		C(61)	6289(4)	4200(3)	5899(2)	112(5)
C(10)	178(10)	-1828(6)	5700(3)	208(10)		C(62)	6317(4)	4745(3)	5443(2)	108(4)
C(11)	1390(10)	-2040(6)	5933(3)	175(7)		C(63)	6754(4)	4514(3)	4906(2)	116(5)
C(12)	2444(10)	-1423(6)	6110(3)	124(5)		C(64)	7165(4)	3739(3)	4826(2)	152(6)
C(13)	5176(11)	-340(6)	8372(4)	57(3)		C(65)	7137(4)	3194(3)	5282(2)	185(8)
C(14)	5676(13)	-1076(7)	8266(5)	78(3)		C(66)	6699(4)	3425(3)	5819(2)	158(7)
C(15)	7053(17)	-1096(8)	8342(5)	94(4)		C(67)	4423(4)	5703(3)	7105(2)	81(3)
C(16)	7929(13)	-403(10)	8492(5)	86(4)		C(68)	5466(4)	6347(3)	7011(2)	90(4)
C(17)	7456(14)	316(8)	8594(5)	90(4)		C(69)	5205(4)	7164(3)	7033(2)	118(5)
C(18)	6056(12)	351(7)	8536(4)	73(3)		C(70)	3902(4)	7337(3)	7148(2)	176(8)
C(19)	969(10)	-1074(6)	7878(5)	70(3)		C(71)	2859(4)	6692(3)	7242(2)	212(10)
C(20)	241(12)	-1350(8)	7384(6)	101(4)		C(72)	3120(4)	5875(3)	7220(2)	147(6)
C(21)	-472(16)	-2191(11)	7349(8)	133(6)		C(73)	7770(12)	2729(8)	7431(5)	100(4)
C(22)	-306(18)	-2618(11)	7830(10)	141(7)		C(74)	8670(13)	2463(8)	7894(6)	121(5)
C(23)	394(17)	-2399(10)	8322(8)	133(6)		N(1)	3576(8)	-274(4)	7229(3)	57(2)
C(24)	1088(13)	-1569(7)	8340(6)	97(4)		N(2)	3840(7)	3516(4)	8913(3)	55(2)
C(25)	6058(12)	2322(6)	9618(4)	57(3)		N(3)	3403(7)	3978(4)	6371(3)	57(2)
C(26)	7337(12)	2074(8)	9680(5)	80(3)		O(1)	4431(6)	1146(4)	6764(2)	59(2)
C(27)	7426(13)	1347(9)	9996(6)	88(4)		O(2)	5430(8)	-135(4)	6508(5)	134(4)
C(28)	6261(16)	958(7)	10227(5)	92(4)		O(3)	3158(11)	48(5)	6157(3)	130(4)
C(29)	5055(14)	1228(9)	10136(5)	98(4)		O(4)	3227(6)	992(3)	7882(2)	58(2)
C(30)	4962(12)	1902(8)	9848(5)	82(3)		O(5)	3785(7)	-323(4)	8331(3)	64(2)
C(31)	6333(9)	4859(6)	8795(5)	62(3)		O(6)	1544(6)	-248(3)	7920(3)	62(2)
C(32)	6267(10)	5057(6)	9371(4)	66(3)		O(7)	5330(6)	2594(3)	8344(2)	55(2)
C(33)	6299(11)	5870(7)	9535(5)	74(3)		O(8)	6085(8)	3106(4)	9348(3)	89(2)
C(34)	6401(11)	6475(7)	9126(6)	82(3)		O(9)	6293(6)	4034(4)	8588(3)	69(2)
C(35)	6475(12)	6264(8)	8554(5)	89(4)		O(10)	2557(6)	2819(3)	7977(2)	53(2)
C(36)	6429(11)	5446(7)	8369(5)	72(3)		O(11)	1971(6)	4160(4)	8309(3)	61(2)
C(37)	1689(11)	4787(5)	8692(4)	56(2)		O(12)	1261(6)	2980(4)	8892(3)	56(2)
C(38)	394(12)	4770(7)	8879(5)	87(4)		O(13)	2614(6)	2464(3)	6723(2)	52(2)
C(39)	128(14)	5421(9)	9238(6)	113(5)		O(14)	1775(7)	2919(4)	5752(3)	65(2)
C(40)	1151(16)	6009(8)	9432(7)	116(5)		O(15)	895(7)	3421(4)	6629(3)	69(2)
C(41)	2427(13)	6021(7)	9237(6)	100(4)		O(16)	5007(7)	3550(4)	7181(3)	82(2)
C(42)	2716(11)	5394(6)	8864(5)	82(3)		O(17)	5832(9)	4614(8)	6460(5)	167(5)
C(43)	1307(8)	2283(6)	9237(4)	49(2)		O(18)	4595(10)	4930(5)	7215(4)	128(3)
C(44)	1242(9)	2399(6)	9827(4)	61(3)		O(19)	6570(6)	2127(4)	7296(3)	75(2)
C(45)	1216(9)	1718(8)	10174(4)	71(3)		P(1)	4144(3)	230(2)	6711(1)	60(1)
C(46)	1287(10)	931(7)	9941(5)	75(3)		P(2)	3087(3)	80(1)	7808(1)	52(1)
C(47)	1347(11)	846(7)	9356(5)	77(3)		P(3)	5259(3)	3260(2)	8778(1)	55(1)
C(48)	1364(9)	1517(6)	8992(4)	59(3)		P(4)	2511(2)	3339(1)	8507(1)	51(1)
C(49)	2606(11)	2591(7)	5361(4)	69(3)		P(5)	2286(2)	3194(2)	6394(1)	53(1)
C(50)	2904(16)	3021(8)	4877(6)	120(5)		P(6)	4715(3)	4155(2)	6768(1)	62(1)
C(51)	3600(20)	2693(13)	4454(8)	158(8)						

Table 3. Bond lengths [Å] and angles [°] for pcluseum.

Eu(1)-O(16)	2.315(6)	C(4)-C(5)	1.3900	C(17)-C(18)	1.397(14)
Eu(1)-O(13)	2.329(5)	C(5)-C(6)	1.3900	C(19)-C(24)	1.362(15)
Eu(1)-O(4)	2.334(6)	C(7)-O(3)	1.342(12)	C(19)-C(20)	1.367(15)
Eu(1)-O(10)	2.340(6)	C(7)-C(8)	1.350(13)	C(19)-O(6)	1.385(11)
Eu(1)-O(7)	2.359(5)	C(7)-C(12)	1.361(13)	C(20)-C(21)	1.451(18)
Eu(1)-O(1)	2.387(6)	C(8)-C(9)	1.3900	C(21)-C(22)	1.34(2)
Eu(1)-P(6)	3.535(2)	C(9)-C(10)	1.3900	C(22)-C(23)	1.33(2)
Eu(1)-P(3)	3.541(2)	C(10)-C(11)	1.3900	C(23)-C(24)	1.427(18)
Eu(1)-P(5)	3.564(2)	C(11)-C(12)	1.3900	C(25)-C(30)	1.330(14)
Eu(1)-P(4)	3.589(2)	C(13)-C(18)	1.363(13)	C(25)-C(26)	1.386(14)
C(1)-O(2)	1.294(8)	C(13)-C(14)	1.379(13)	C(25)-O(8)	1.427(11)
C(1)-C(2)	1.3900	C(13)-O(5)	1.382(11)	C(26)-C(27)	1.414(15)
C(1)-C(6)	1.3900	C(14)-C(15)	1.373(15)	C(27)-C(28)	1.365(16)
C(2)-C(3)	1.3900	C(15)-C(16)	1.356(16)	C(28)-C(29)	1.341(16)
C(3)-C(4)	1.3900	C(16)-C(17)	1.340(15)	C(29)-C(30)	1.308(15)

C(31)-C(32) 1.373(13)
C(31)-C(36) 1.381(13)
C(31)-O(9) 1.412(10)
C(32)-C(33) 1.364(13)
C(33)-C(34) 1.374(14)
C(34)-C(35) 1.366(14)
C(35)-C(36) 1.385(14)
C(37)-C(42) 1.360(13)
C(37)-C(38) 1.361(13)
C(37)-O(11) 1.402(10)
C(38)-C(39) 1.394(15)
C(39)-C(40) 1.353(17)
C(40)-C(41) 1.351(16)
C(41)-C(42) 1.389(14)
C(43)-C(48) 1.369(12)
C(43)-C(44) 1.381(12)
C(43)-O(12) 1.405(10)
C(44)-C(45) 1.378(13)
C(45)-C(46) 1.392(14)
C(46)-C(47) 1.364(14)
C(47)-C(48) 1.389(13)
C(49)-C(50) 1.350(14)
C(49)-C(54) 1.360(15)
C(49)-O(14) 1.389(12)
C(50)-C(51) 1.36(2)
C(51)-C(52) 1.33(2)
C(52)-C(53) 1.36(2)
C(53)-C(54) 1.406(18)
C(55)-C(56) 1.356(14)
C(55)-C(60) 1.378(11)
C(55)-O(15) 1.407(11)
C(56)-C(57) 1.395(17)
C(57)-C(58) 1.36(2)
C(58)-C(59) 1.324(19)
C(59)-C(60) 1.387(14)
C(61)-C(62) 1.3900
C(61)-C(66) 1.3900
C(61)-O(17) 1.558(13)
C(62)-C(63) 1.3900
C(63)-C(64) 1.3900
C(64)-C(65) 1.3900
C(65)-C(66) 1.3900
C(67)-O(18) 1.321(9)
C(67)-C(68) 1.3900
C(67)-C(72) 1.3900
C(68)-C(69) 1.3900
C(69)-C(70) 1.3900
C(70)-C(71) 1.3900
C(71)-C(72) 1.3900
C(73)-O(19) 1.453(12)
C(73)-C(74) 1.482(15)
N(1)-P(1) 1.541(8)
N(1)-P(2) 1.564(7)
N(2)-P(3) 1.558(8)
N(2)-P(4) 1.582(7)
N(3)-P(6) 1.558(7)
N(3)-P(5) 1.571(7)
O(1)-P(1) 1.481(6)
O(2)-P(1) 1.559(8)
O(3)-P(1) 1.585(8)
O(4)-P(2) 1.478(6)
O(5)-P(2) 1.576(6)
O(6)-P(2) 1.578(6)
O(7)-P(3) 1.474(6)
O(8)-P(3) 1.574(7)
O(9)-P(3) 1.587(7)
O(10)-P(4) 1.484(6)
O(11)-P(4) 1.577(6)
O(12)-P(4) 1.596(6)
O(13)-P(5) 1.491(6)
O(14)-P(5) 1.590(6)
O(15)-P(5) 1.584(7)
O(16)-P(6) 1.437(6)
O(17)-P(6) 1.459(8)
O(18)-P(6) 1.636(9)

O(16)-Eu(1)-O(13) 77.61(19)
O(16)-Eu(1)-O(4) 169.6(2)
O(13)-Eu(1)-O(4) 105.9(2)
O(16)-Eu(1)-O(10) 86.8(2)
O(13)-Eu(1)-O(10) 78.43(19)
O(4)-Eu(1)-O(10) 84.4(2)
O(16)-Eu(1)-O(7) 85.2(2)
O(13)-Eu(1)-O(7) 150.57(19)
O(4)-Eu(1)-O(7) 87.5(2)
O(10)-Eu(1)-O(7) 76.90(19)
O(16)-Eu(1)-O(1) 115.2(2)
O(13)-Eu(1)-O(1) 78.6(2)
O(4)-Eu(1)-O(1) 75.17(19)
O(10)-Eu(1)-O(1) 143.5(2)
O(7)-Eu(1)-O(1) 130.7(2)
O(16)-Eu(1)-P(6) 15.24(15)
O(13)-Eu(1)-P(6) 62.38(14)
O(4)-Eu(1)-P(6) 165.37(16)
O(10)-Eu(1)-P(6) 84.53(15)
O(7)-Eu(1)-P(6) 99.34(15)
O(1)-Eu(1)-P(6) 108.95(15)
O(16)-Eu(1)-P(3) 76.17(17)
O(13)-Eu(1)-P(3) 133.07(14)
O(4)-Eu(1)-P(3) 94.77(15)
O(10)-Eu(1)-P(3) 61.93(14)
O(7)-Eu(1)-P(3) 17.53(14)
O(1)-Eu(1)-P(3) 148.21(16)
P(6)-Eu(1)-P(3) 88.45(6)
O(16)-Eu(1)-P(5) 61.31(15)
O(13)-Eu(1)-P(5) 16.70(13)
O(4)-Eu(1)-P(5) 121.23(16)
O(10)-Eu(1)-P(5) 75.28(14)
O(7)-Eu(1)-P(5) 137.07(14)
O(1)-Eu(1)-P(5) 89.77(15)
P(6)-Eu(1)-P(5) 46.17(6)
P(3)-Eu(1)-P(5) 120.44(6)
O(16)-Eu(1)-P(4) 81.9(2)
O(13)-Eu(1)-P(4) 92.16(14)
O(4)-Eu(1)-P(4) 88.19(14)
O(10)-Eu(1)-P(4) 15.88(14)
O(7)-Eu(1)-P(4) 61.58(14)
O(1)-Eu(1)-P(4) 157.68(15)
P(6)-Eu(1)-P(4) 83.77(6)
P(3)-Eu(1)-P(4) 46.12(6)
P(5)-Eu(1)-P(4) 86.23(6)
O(2)-C(1)-C(2) 122.7(5)
O(2)-C(1)-C(6) 117.2(5)
C(2)-C(1)-C(6) 120.0
C(1)-C(2)-C(3) 120.0
C(2)-C(3)-C(4) 120.0
C(5)-C(4)-C(3) 120.0
C(4)-C(5)-C(6) 120.0
C(5)-C(6)-C(1) 120.0
O(3)-C(7)-C(8) 109.4(10)
O(3)-C(7)-C(12) 125.2(10)
C(8)-C(7)-C(12) 125.3(11)
C(7)-C(8)-C(9) 117.4(6)
C(8)-C(9)-C(10) 120.0
C(9)-C(10)-C(11) 120.0
C(12)-C(11)-C(10) 120.0
C(7)-C(12)-C(11) 117.1(6)
C(18)-C(13)-C(14) 119.6(10)
C(18)-C(13)-O(5) 121.0(9)
C(14)-C(13)-O(5) 119.4(10)
C(15)-C(14)-C(13) 118.7(11)
C(16)-C(15)-C(14) 121.5(11)
C(17)-C(16)-C(15) 120.2(12)
C(16)-C(17)-C(18) 119.6(12)
C(13)-C(18)-C(17) 120.3(11)
C(24)-C(19)-C(20) 122.6(11)
C(24)-C(19)-O(6) 118.9(11)
C(20)-C(19)-O(6) 118.5(11)
C(19)-C(20)-C(21) 119.5(14)
C(22)-C(21)-C(20) 113.0(16)

C(23)-C(22)-C(21) 130.9(19)
C(22)-C(23)-C(24) 114.5(16)
C(19)-C(24)-C(23) 119.4(14)
C(30)-C(25)-C(26) 121.7(10)
C(30)-C(25)-O(8) 124.6(11)
C(26)-C(25)-O(8) 113.2(10)
C(25)-C(26)-C(27) 117.0(10)
C(28)-C(27)-C(26) 117.8(11)
C(29)-C(28)-C(27) 121.5(12)
C(30)-C(29)-C(28) 121.2(13)
C(29)-C(30)-C(25) 120.7(12)
C(32)-C(31)-C(36) 122.9(9)
C(32)-C(31)-O(9) 122.6(10)
C(36)-C(31)-O(9) 114.5(9)
C(33)-C(32)-C(31) 118.9(10)
C(32)-C(33)-C(34) 120.1(10)
C(35)-C(34)-C(33) 120.0(10)
C(34)-C(35)-C(36) 121.7(11)
C(31)-C(36)-C(35) 116.4(10)
C(42)-C(37)-C(38) 122.1(10)
C(42)-C(37)-O(11) 119.0(9)
C(38)-C(37)-O(11) 118.9(9)
C(37)-C(38)-C(39) 117.8(11)
C(40)-C(39)-C(38) 120.6(12)
C(41)-C(40)-C(39) 120.5(12)
C(40)-C(41)-C(42) 120.0(11)
C(37)-C(42)-C(41) 118.8(11)
C(48)-C(43)-C(44) 121.7(9)
C(48)-C(43)-O(12) 121.0(8)
C(44)-C(43)-O(12) 117.2(8)
C(45)-C(44)-C(43) 118.5(9)
C(44)-C(45)-C(46) 121.4(10)
C(47)-C(46)-C(45) 118.1(10)
C(46)-C(47)-C(48) 122.1(10)
C(43)-C(48)-C(47) 118.2(10)
C(50)-C(49)-C(54) 121.3(13)
C(50)-C(49)-O(14) 117.3(12)
C(54)-C(49)-O(14) 121.2(10)
C(49)-C(50)-C(51) 119.9(15)
C(52)-C(51)-C(50) 119.9(18)
C(51)-C(52)-C(53) 122.1(19)
C(52)-C(53)-C(54) 118.1(16)
C(49)-C(54)-C(53) 118.5(13)
C(56)-C(55)-C(60) 122.3(10)
C(56)-C(55)-O(15) 117.0(10)
C(60)-C(55)-O(15) 120.7(9)
C(55)-C(56)-C(57) 118.6(13)
C(58)-C(57)-C(56) 119.8(16)
C(59)-C(58)-C(57) 120.0(16)
C(58)-C(59)-C(60) 122.9(14)
C(55)-C(60)-C(59) 116.3(9)
C(62)-C(61)-C(66) 120.0
C(62)-C(61)-O(17) 110.4(4)
C(66)-C(61)-O(17) 129.6(4)
C(63)-C(62)-C(61) 120.0
C(62)-C(63)-C(64) 120.0
C(65)-C(64)-C(63) 120.0
C(66)-C(65)-C(64) 120.0
C(65)-C(66)-C(61) 120.0
O(18)-C(67)-C(68) 125.3(5)
O(18)-C(67)-C(72) 113.3(5)
C(68)-C(67)-C(72) 120.0
C(67)-C(68)-C(69) 120.0
C(70)-C(69)-C(68) 120.0
C(69)-C(70)-C(71) 120.0
C(70)-C(71)-C(72) 120.0
C(71)-C(72)-C(67) 120.0
O(19)-C(73)-C(74) 113.4(11)
P(1)-N(1)-P(2) 126.7(5)
P(3)-N(2)-P(4) 125.7(5)
P(6)-N(3)-P(5) 125.7(5)
P(1)-O(1)-Eu(1) 138.6(3)
C(1)-O(2)-P(1) 126.8(5)
C(7)-O(3)-P(1) 129.2(8)
P(2)-O(4)-Eu(1) 141.8(4)

C(13)-O(5)-P(2) 122.3(6)	N(1)-P(2)-O(5) 109.0(4)	N(2)-P(4)-Eu(1) 93.0(3)
C(19)-O(6)-P(2) 124.5(6)	O(4)-P(2)-O(6) 105.8(3)	O(12)-P(4)-Eu(1)127.0(2)
P(3)-O(7)-Eu(1) 133.7(3)	N(1)-P(2)-O(6) 112.4(4)	O(13)-P(5)-N(3) 118.5(4)
C(25)-O(8)-P(3) 124.9(6)	O(5)-P(2)-O(6) 99.5(3)	O(13)-P(5)-O(15) 106.8(3)
C(31)-O(9)-P(3) 125.7(6)	O(7)-P(3)-N(2) 118.9(4)	N(3)-P(5)-O(15) 111.8(4)
P(4)-O(10)-Eu(1)138.6(3)	O(7)-P(3)-O(8) 110.8(4)	O(13)-P(5)-O(14) 110.4(3)
C(37)-O(11)-P(4) 123.9(6)	N(2)-P(3)-O(8) 111.5(4)	N(3)-P(5)-O(14) 108.9(4)
C(43)-O(12)-P(4) 121.7(5)	O(7)-P(3)-O(9) 106.5(4)	O(15)-P(5)-O(14) 98.6(4)
P(5)-O(13)-Eu(1)136.6(3)	N(2)-P(3)-O(9) 111.2(4)	O(13)-P(5)-Eu(1)26.7(2)
C(49)-O(14)-P(5) 122.3(6)	O(8)-P(3)-O(9) 95.3(4)	N(3)-P(5)-Eu(1) 93.3(3)
C(55)-O(15)-P(5) 125.5(6)	O(7)-P(3)-Eu(1) 28.8(2)	O(15)-P(5)-Eu(1)112.4(3)
P(6)-O(16)-Eu(1)139.7(4)	N(2)-P(3)-Eu(1) 95.2(3)	O(14)-P(5)-Eu(1)131.7(3)
P(6)-O(17)-C(61) 117.2(8)	O(8)-P(3)-Eu(1) 138.9(3)	O(16)-P(6)-O(17) 119.4(5)
C(67)-O(18)-P(6) 129.8(7)	O(9)-P(3)-Eu(1) 103.6(3)	O(16)-P(6)-N(3) 119.6(4)
O(1)-P(1)-N(1) 119.5(4)	O(10)-P(4)-O(11) 106.4(3)	O(17)-P(6)-N(3) 110.7(5)
O(1)-P(1)-O(2) 110.5(4)	O(10)-P(4)-N(2) 118.3(4)	O(16)-P(6)-O(18) 98.9(5)
N(1)-P(1)-O(2) 107.9(5)	O(11)-P(4)-N(2) 112.6(4)	O(17)-P(6)-O(18) 93.4(7)
O(1)-P(1)-O(3) 105.2(4)	O(10)-P(4)-O(12) 110.8(3)	N(3)-P(6)-O(18) 110.0(5)
N(1)-P(1)-O(3) 111.1(5)	O(11)-P(4)-O(12) 98.4(3)	O(16)-P(6)-Eu(1)25.1(2)
O(2)-P(1)-O(3) 101.1(6)	N(2)-P(4)-O(12) 108.5(4)	O(17)-P(6)-Eu(1)135.4(5)
O(4)-P(2)-N(1) 117.5(4)	O(10)-P(4)-Eu(1)25.6(2)	N(3)-P(6)-Eu(1) 94.6(3)
O(4)-P(2)-O(5) 111.1(4)	O(11)-P(4)-Eu(1)117.5(2)	O(18)-P(6)-Eu(1)112.2(3)

Symmetry transformations used to generate equivalent atoms:

Table 4. Anisotropic displacement parameters ($Å^2 x\ 10^3$)for pcluseum. The anisotropic displacement factor exponent takes the form: $-2\pi^2[\ h^2 a^{*2} U^{11} + ... + 2\ h\ k\ a^*\ b^*\ U^{12}\ ]$

	U^{11}	U^{22}	U^{33}	U^{23}	U^{13}	U^{12}
Eu(1)	52(1)	37(1)	43(1)	1(1)	-3(1)	2(1)
C(1)	89(8)	59(7)	85(8)	8(6)	19(6)	20(6)
C(2)	106(11)	148(12)	174(13)	42(11)	24(10)	35(9)
C(3)	191(15)	141(13)	225(16)	67(12)	30(13)	40(12)
C(4)	111(11)	118(11)	216(15)	-7(11)	44(11)	-2(9)
C(5)	155(14)	188(15)	209(16)	-62(13)	-12(12)	56(12)
C(6)	163(13)	123(11)	120(11)	-28(9)	26(10)	56(10)
C(7)	77(8)	78(8)	64(7)	-18(6)	-16(6)	18(7)
C(8)	171(14)	176(14)	152(13)	29(12)	-4(12)	12(12)
C(9)	206(17)	255(19)	211(17)	60(15)	-42(14)	29(15)
C(10)	164(14)	241(18)	188(15)	-48(13)	-65(12)	-61(13)
C(11)	202(15)	125(12)	184(14)	-63(11)	32(12)	-18(12)
C(12)	111(10)	75(8)	184(13)	-35(9)	17(9)	16(8)
C(13)	63(7)	48(6)	64(6)	14(5)	-1(5)	14(6)
C(14)	95(10)	57(7)	81(8)	4(6)	1(7)	9(7)
C(15)	124(12)	80(10)	90(9)	6(7)	9(8)	55(9)
C(16)	83(9)	106(11)	78(8)	9(8)	12(7)	40(9)
C(17)	88(10)	92(10)	84(9)	7(7)	-19(7)	0(8)
C(18)	81(9)	70(8)	70(7)	8(6)	-7(6)	17(7)
C(19)	53(6)	55(7)	101(8)	1(6)	27(6)	1(5)
C(20)	75(8)	98(9)	124(10)	-39(8)	27(7)	-12(7)
C(21)	118(11)	134(12)	139(12)	-59(10)	24(10)	-3(10)
C(22)	122(12)	109(11)	188(15)	-21(12)	61(12)	-2(9)
C(23)	137(12)	99(11)	174(14)	41(10)	64(11)	43(9)
C(24)	107(9)	62(7)	124(10)	21(7)	33(8)	8(7)
C(25)	77(8)	55(6)	39(5)	4(5)	-18(5)	7(6)
C(26)	65(9)	97(10)	72(8)	-13(7)	11(6)	-11(7)
C(27)	71(9)	104(10)	97(10)	-16(8)	-15(7)	43(8)
C(28)	117(12)	80(9)	81(9)	30(7)	-15(8)	24(9)
C(29)	85(10)	122(12)	87(9)	35(8)	-8(7)	18(9)
C(30)	58(8)	96(9)	93(9)	-3(8)	4(7)	17(7)
C(31)	43(6)	60(7)	79(8)	-25(6)	-1(5)	-1(5)
C(32)	64(7)	65(7)	64(7)	-6(6)	12(5)	-9(5)
C(33)	82(8)	68(8)	66(7)	-17(6)	5(6)	-9(6)
C(34)	73(8)	54(7)	110(10)	-20(7)	-1(7)	-13(6)
C(35)	117(11)	81(9)	66(8)	9(7)	-6(7)	-1(7)
C(36)	93(9)	62(7)	61(7)	2(6)	-1(6)	6(6)
C(37)	64(7)	40(6)	65(7)	1(5)	-2(5)	14(5)
C(38)	61(8)	80(8)	121(10)	-25(7)	13(7)	9(6)

C(39)	76(10)	116(11)	149(13)	-40(10)	17(9)	25(9)
C(40)	101(12)	93(10)	159(14)	-50(9)	4(10)	37(9)
C(41)	76(9)	66(8)	157(13)	-44(8)	-25(9)	12(7)
C(42)	68(8)	55(7)	120(10)	-20(7)	-1(7)	4(6)
C(43)	28(5)	54(6)	63(7)	0(5)	2(4)	1(4)
C(44)	63(7)	67(7)	54(7)	-7(5)	3(5)	12(5)
C(45)	50(7)	104(9)	57(7)	5(7)	19(5)	3(6)
C(46)	74(8)	69(8)	83(9)	28(7)	11(6)	5(6)
C(47)	86(9)	56(7)	90(9)	14(6)	5(7)	7(6)
C(48)	56(6)	54(6)	65(7)	-4(5)	3(5)	1(5)
C(49)	76(8)	88(9)	39(6)	4(6)	3(5)	-7(7)
C(50)	184(15)	94(10)	77(9)	10(8)	50(10)	-15(10)
C(51)	200(20)	174(19)	95(13)	11(14)	57(13)	3(16)
C(52)	141(15)	220(20)	96(14)	-21(16)	40(11)	53(16)
C(53)	155(15)	153(16)	101(13)	-37(12)	-25(11)	66(12)
C(54)	158(13)	98(10)	58(8)	-3(7)	-10(8)	43(9)
C(55)	39(6)	76(8)	77(8)	-4(6)	10(5)	3(5)
C(56)	94(10)	91(9)	94(10)	-13(8)	9(7)	23(8)
C(57)	100(11)	82(11)	183(18)	-33(11)	29(11)	9(9)
C(58)	104(12)	84(11)	190(20)	26(12)	16(13)	28(9)
C(59)	88(10)	114(12)	144(14)	41(10)	17(9)	48(9)
C(60)	89(9)	112(10)	90(9)	28(8)	12(7)	43(8)
C(61)	68(8)	172(13)	88(9)	41(9)	-8(7)	-21(8)
C(62)	99(9)	121(10)	102(9)	23(8)	12(8)	-2(8)
C(63)	114(10)	130(11)	99(9)	23(9)	29(8)	-8(8)
C(64)	143(12)	180(14)	138(12)	-2(11)	35(10)	37(11)
C(65)	222(16)	149(13)	194(16)	15(12)	43(14)	46(12)
C(66)	150(13)	135(12)	189(14)	71(12)	2(11)	13(10)
C(67)	105(9)	41(6)	92(8)	18(5)	-46(7)	1(6)
C(68)	91(8)	77(8)	101(9)	-13(7)	9(7)	9(7)
C(69)	182(13)	74(8)	91(9)	4(7)	-11(9)	3(9)
C(70)	195(15)	163(14)	182(14)	-70(11)	-32(12)	81(12)
C(71)	192(16)	202(16)	253(18)	-44(14)	40(14)	57(14)
C(72)	88(10)	163(13)	181(14)	15(11)	-9(10)	-18(10)
C(73)	85(9)	109(10)	103(10)	1(8)	7(8)	3(8)
C(74)	116(11)	124(12)	119(11)	-18(9)	-54(9)	22(9)
N(1)	67(5)	47(4)	59(5)	-4(4)	7(4)	17(4)
N(2)	55(5)	50(5)	53(5)	-10(4)	-2(4)	-9(4)
N(3)	61(5)	47(5)	62(5)	14(4)	-6(4)	4(4)
O(1)	77(5)	50(4)	49(4)	-5(3)	7(3)	2(3)
O(2)	91(6)	62(5)	244(11)	-45(6)	98(7)	-16(5)
O(3)	198(10)	94(6)	75(6)	4(5)	-45(6)	-52(7)
O(4)	79(5)	44(4)	51(4)	2(3)	10(3)	6(3)
O(5)	61(5)	68(4)	62(4)	26(3)	6(3)	6(3)
O(6)	55(4)	41(4)	88(5)	2(3)	10(3)	2(3)
O(7)	73(4)	51(4)	42(3)	-12(3)	-13(3)	17(3)
O(8)	124(7)	71(5)	73(5)	-12(4)	-35(4)	24(5)
O(9)	58(4)	66(5)	79(5)	-16(4)	12(3)	-4(3)
O(10)	60(4)	48(4)	50(4)	-4(3)	-4(3)	7(3)
O(11)	83(5)	49(4)	54(4)	-5(3)	6(3)	16(3)
O(12)	54(4)	53(4)	63(4)	4(3)	6(3)	12(3)
O(13)	60(4)	48(4)	44(3)	3(3)	-6(3)	-1(3)
O(14)	70(5)	70(4)	51(4)	1(3)	-16(3)	5(4)
O(15)	65(5)	67(5)	77(5)	11(4)	14(4)	16(4)
O(16)	84(5)	58(4)	92(5)	32(4)	-44(4)	-22(4)
O(17)	80(7)	254(13)	141(9)	97(9)	-33(6)	-75(7)
O(18)	177(9)	67(6)	133(8)	-4(5)	-50(7)	5(6)
O(19)	53(4)	75(5)	93(6)	-21(4)	-3(4)	-4(4)
P(1)	65(2)	52(2)	60(2)	-13(1)	5(1)	-1(1)
P(2)	59(2)	42(1)	56(2)	4(1)	5(1)	7(1)
P(3)	69(2)	50(2)	48(2)	-4(1)	-14(1)	15(1)
P(4)	57(2)	44(1)	52(2)	-2(1)	2(1)	6(1)
P(5)	55(2)	53(2)	49(1)	4(1)	-6(1)	5(1)
P(6)	66(2)	50(2)	65(2)	16(1)	-10(1)	-12(1)

Table 5. Hydrogen coordinates (x 10^4) and isotropic displacement parameters ($Å^2$x 10^3) for pcluseum.

	x	y	z	U(eq)		x	y	z	U(eq)

H(2)	6439	802	5700	169	H(41)	3111	6448	9352	121
H(3)	8630	1528	5694	220	H(42)	3596	5390	8735	98
H(4)	10155	1421	6461	179	H(44)	1216	2925	9988	73
H(5)	9490	588	7234	219	H(45)	1150	1786	10572	85
H(6)	7300	-138	7240	158	H(46)	1293	477	10179	90
H(8)	977	179	5800	201	H(47)	1378	322	9194	93
H(9)	-790	-855	5488	269	H(48)	1411	1447	8594	71
H(10)	-527	-2241	5582	250	H(50)	2632	3541	4834	144
H(11)	1495	-2596	5970	209	H(51)	3765	2974	4112	189
H(12)	3250	-1550	6279	148	H(52)	4594	1774	4251	180
H(14)	5093	-1551	8146	93	H(53)	4011	979	5036	160
H(15)	7393	-1595	8289	113	H(54)	2787	1538	5772	123
H(16)	8862	-427	8525	103	H(56)	-8	4295	7394	110
H(17)	8056	790	8702	108	H(57)	-1009	5504	7290	146
H(18)	5722	848	8609	88	H(58)	-1061	6109	6404	151
H(20)	204	-1000	7072	122	H(59)	-259	5513	5633	134
H(21)	-992	-2412	7027	159	H(60)	700	4294	5698	113
H(22)	-756	-3160	7818	169	H(62)	6042	5264	5497	130
H(23)	429	-2757	8629	159	H(63)	6773	4879	4601	139
H(24)	1616	-1366	8665	117	H(64)	7458	3584	4467	182
H(26)	8102	2371	9521	96	H(65)	7412	2675	5228	223
H(27)	8252	1140	10044	106	H(66)	6681	3060	6124	189
H(28)	6305	496	10454	110	H(68)	6338	6232	6934	108
H(29)	4270	930	10279	117	H(69)	5903	7595	6970	141
H(30)	4120	2090	9803	98	H(70)	3727	7883	7162	211
H(32)	6201	4645	9646	79	H(71)	1987	6808	7319	255
H(33)	6251	6014	9923	89	H(72)	2422	5444	7283	177
H(34)	6420	7028	9238	98	H(73A)	7479	3249	7550	120
H(35)	6559	6680	8283	107	H(73B)	8289	2827	7084	120
H(36)	6461	5301	7980	87	H(74A)	9432	2889	7968	181
H(38)	-290	4339	8770	105	H(74B)	8995	1960	7773	181
H(39)	-762	5451	9346	135	H(74C)	8165	2367	8240	181
H(40)	976	6409	9701	139	H(19)	6750	1797	7047	113

B5 Crystallographic Data for $Yb(tpOp)_3$

Table 2. Atomic coordinates (x 10^4) and equivalent isotropic displacement parameters ($Å^2$x 10^3) for ybtpop3m. U(eq) is defined as one third of the trace of the orthogonalized U^{ij} tensor.

	x	y	z	U(eq)		x	y	z	U(eq)	
C(1)	5541(4)	4875(4)	4217(2)	49(2)		C(30)	4998(4)	-711(4)	771(3)	63(2)
C(2)	6291(4)	4865(5)	4447(3)	71(2)		C(31)	5898(3)	2240(4)	865(2)	41(1)
C(3)	6638(5)	5442(6)	4850(3)	96(3)		C(32)	6079(3)	2230(4)	380(2)	57(2)
C(4)	6227(6)	6017(5)	5022(3)	85(3)		C(33)	6383(4)	2932(5)	221(3)	67(2)
C(5)	5472(5)	6034(5)	4787(3)	85(3)		C(34)	6509(4)	3653(5)	534(3)	66(2)
C(6)	5109(4)	5461(5)	4373(3)	71(2)		C(35)	6340(3)	3659(4)	1022(3)	59(2)
C(7)	4524(3)	5485(4)	2524(2)	42(2)		C(36)	6033(3)	2946(4)	1184(2)	49(2)
C(8)	4544(3)	6349(4)	2570(3)	60(2)		C(37)	2633(3)	2248(4)	1159(2)	45(2)
C(9)	4493(4)	6844(5)	2114(4)	77(2)		C(38)	2399(3)	2561(5)	1574(2)	66(2)
C(10)	4424(4)	6467(5)	1625(3)	78(2)		C(39)	1988(4)	2040(6)	1810(3)	77(2)
C(11)	4397(4)	5600(5)	1576(3)	68(2)		C(40)	1824(4)	1233(6)	1627(3)	83(3)
C(12)	4434(3)	5109(4)	2029(3)	54(2)		C(41)	2063(4)	923(5)	1208(3)	79(2)
C(13)	7485(3)	3911(4)	3628(2)	44(2)		C(42)	2478(3)	1435(5)	972(3)	61(2)
C(14)	7548(3)	3246(4)	3983(2)	56(2)		C(43)	3799(3)	3799(3)	233(2)	38(1)
C(15)	7940(4)	3376(5)	4534(3)	68(2)		C(44)	3062(3)	3934(4)	-75(2)	52(2)
C(16)	8258(4)	4149(6)	4707(3)	80(2)		C(45)	2900(4)	4028(5)	-632(3)	70(2)
C(17)	8195(4)	4788(5)	4345(3)	82(2)		C(46)	3455(5)	3980(4)	-873(3)	72(2)
C(18)	7798(4)	4685(4)	3791(2)	60(2)		C(47)	4179(5)	3864(5)	-559(3)	78(2)
C(19)	6784(3)	5248(4)	2351(2)	36(1)		C(48)	4364(4)	3767(4)	5(3)	63(2)
C(20)	6475(4)	5997(4)	2443(2)	53(2)		C(49)	5865(3)	1159(4)	4424(2)	42(2)
C(21)	6913(5)	6718(5)	2519(3)	74(2)		C(50)	5971(4)	2018(5)	4416(3)	64(2)
C(22)	7635(5)	6686(5)	2499(3)	80(2)		C(51)	5984(4)	2490(5)	4868(3)	80(2)
C(23)	7918(4)	5943(6)	2401(3)	75(2)		C(52)	5900(4)	2107(6)	5314(3)	84(3)
C(24)	7504(3)	5204(4)	2328(2)	55(2)		C(53)	5805(4)	1243(6)	5332(3)	83(3)
C(25)	4986(3)	-184(4)	1185(2)	40(1)		C(54)	5773(4)	761(5)	4872(3)	67(2)
C(26)	5339(3)	-395(4)	1725(2)	52(2)		C(55)	5708(3)	-877(4)	3350(2)	42(2)
C(27)	5696(4)	-1168(5)	1835(3)	65(2)		C(56)	6420(4)	-1217(4)	3504(2)	60(2)
C(28)	5699(4)	-1716(4)	1422(3)	69(2)		C(57)	6525(5)	-2029(5)	3705(3)	74(2)
C(29)	5355(4)	-1494(4)	894(3)	73(2)		C(58)	5941(5)	-2494(5)	3762(3)	77(2)

C(59)	5231(5)	-2131(5)	3619(3)	76(2)
C(60)	5105(4)	-1327(4)	3407(3)	60(2)
C(61)	3336(3)	1499(4)	3861(2)	46(2)
C(62)	3839(4)	1742(5)	4346(3)	67(2)
C(63)	3695(5)	1547(6)	4824(3)	86(3)
C(64)	3068(5)	1107(6)	4816(3)	92(3)
C(65)	2575(4)	877(6)	4334(3)	89(3)
C(66)	2699(4)	1055(5)	3841(3)	72(2)
C(67)	3072(3)	-156(4)	2426(3)	51(2)
C(68)	2461(4)	-683(4)	2367(3)	69(2)
C(69)	2339(5)	-1344(5)	2003(4)	97(3)
C(70)	2823(5)	-1499(5)	1705(4)	96(3)
C(71)	3426(4)	-974(5)	1764(3)	86(2)
C(72)	3544(4)	-292(4)	2123(3)	66(2)
N(1)	5896(2)	4441(3)	3125(2)	35(1)
N(2)	4261(3)	2124(3)	888(2)	41(1)
N(3)	4514(2)	646(3)	3384(2)	42(1)
O(1)	4734(2)	3436(2)	2984(1)	47(1)
O(2)	5910(2)	3146(2)	2489(1)	36(1)
O(3)	5178(2)	4242(3)	3836(1)	51(1)
O(4)	4565(2)	5023(3)	2996(2)	53(1)
O(5)	7129(2)	3759(2)	3071(1)	41(1)
O(6)	6343(2)	4504(2)	2256(1)	39(1)
O(7)	5132(2)	1571(2)	1829(1)	43(1)
O(8)	4172(2)	3047(2)	1707(1)	36(1)
O(9)	4568(2)	575(2)	1041(1)	46(1)
O(10)	5583(2)	1507(2)	997(2)	55(1)
O(11)	3007(2)	2793(3)	900(1)	49(1)
O(12)	3986(2)	3733(2)	811(1)	41(1)
O(13)	5534(2)	1483(2)	3094(1)	43(1)
O(14)	3930(2)	1690(2)	2575(1)	47(1)
O(15)	5900(2)	651(2)	3986(1)	46(1)
O(16)	5617(2)	-65(2)	3119(1)	46(1)
O(17)	3468(2)	1741(2)	3373(2)	51(1)
O(18)	3130(2)	515(3)	2783(2)	51(1)
P(1)	5118(1)	4248(1)	3210(1)	39(1)
P(2)	6273(1)	3943(1)	2749(1)	32(1)
P(3)	4878(1)	1494(1)	1221(1)	37(1)
P(4)	3893(1)	2879(1)	1105(1)	35(1)
P(5)	5347(1)	733(1)	3380(1)	39(1)
P(6)	3813(1)	1148(1)	3016(1)	42(1)
Yb(1)	4890(1)	2395(1)	2454(1)	33(1)

Table 3. Bond lengths [Å] and angles [°] for ybtpop3m.

C(1)-C(2)	1.339(8)	C(41)-C(42)	1.382(9)	O(5)-P(2)	1.580(4)
C(1)-C(6)	1.366(8)	C(43)-C(48)	1.359(8)	O(6)-P(2)	1.581(3)
C(1)-O(3)	1.414(7)	C(43)-C(44)	1.373(7)	O(7)-P(3)	1.487(3)
C(2)-C(3)	1.379(9)	C(43)-O(12)	1.415(6)	O(7)-Yb(1)	2.217(3)
C(3)-C(4)	1.349(10)	C(44)-C(45)	1.374(8)	O(8)-P(4)	1.492(3)
C(4)-C(5)	1.351(10)	C(45)-C(46)	1.365(9)	O(8)-Yb(1)	2.219(3)
C(5)-C(6)	1.398(10)	C(46)-C(47)	1.354(9)	O(9)-P(3)	1.578(4)
C(7)-C(12)	1.362(8)	C(47)-C(48)	1.385(8)	O(10)-P(3)	1.592(4)
C(7)-C(8)	1.369(8)	C(49)-C(54)	1.367(8)	O(11)-P(4)	1.579(4)
C(7)-O(4)	1.396(6)	C(49)-C(50)	1.372(8)	O(12)-P(4)	1.581(4)
C(8)-C(9)	1.386(9)	C(49)-O(15)	1.399(6)	O(13)-P(5)	1.489(4)
C(9)-C(10)	1.356(10)	C(50)-C(51)	1.373(9)	O(13)-Yb(1)	2.233(3)
C(10)-C(11)	1.375(9)	C(51)-C(52)	1.345(10)	O(14)-P(6)	1.488(4)
C(11)-C(12)	1.380(8)	C(52)-C(53)	1.378(10)	O(14)-Yb(1)	2.213(3)
C(13)-C(18)	1.363(8)	C(53)-C(54)	1.389(9)	O(15)-P(5)	1.582(4)
C(13)-C(14)	1.370(8)	C(55)-C(56)	1.373(8)	O(16)-P(5)	1.581(4)
C(13)-O(5)	1.397(6)	C(55)-C(60)	1.377(8)	O(17)-P(6)	1.580(4)
C(14)-C(15)	1.388(8)	C(55)-O(16)	1.400(7)	O(18)-P(6)	1.582(4)
C(15)-C(16)	1.369(10)	C(56)-C(57)	1.373(9)	P(1)-Yb(1)	3.4618(16)
C(16)-C(17)	1.351(10)	C(57)-C(58)	1.361(10)	P(2)-Yb(1)	3.4643(15)
C(17)-C(18)	1.391(8)	C(58)-C(59)	1.384(10)	P(3)-Yb(1)	3.4618(15)
C(19)-C(20)	1.366(8)	C(59)-C(60)	1.373(9)	P(4)-Yb(1)	3.4650(14)
C(19)-C(24)	1.368(7)	C(61)-C(62)	1.362(8)	P(5)-Yb(1)	3.4616(16)
C(19)-O(6)	1.412(6)	C(61)-C(66)	1.367(8)	P(6)-Yb(1)	3.4361(15)
C(20)-C(21)	1.379(9)	C(61)-O(17)	1.402(6)		
C(21)-C(22)	1.368(10)	C(62)-C(63)	1.368(9)	C(2)-C(1)-C(6)	120.7(6)
C(22)-C(23)	1.342(10)	C(63)-C(64)	1.357(10)	C(2)-C(1)-O(3)	120.4(6)
C(23)-C(24)	1.379(9)	C(64)-C(65)	1.340(10)	C(6)-C(1)-O(3)	118.8(6)
C(25)-C(30)	1.354(8)	C(65)-C(66)	1.383(9)	C(1)-C(2)-C(3)	120.3(7)
C(25)-C(26)	1.375(7)	C(67)-C(72)	1.360(8)	C(4)-C(3)-C(2)	120.4(8)
C(25)-O(9)	1.414(6)	C(67)-C(68)	1.382(8)	C(3)-C(4)-C(5)	119.3(8)
C(26)-C(27)	1.378(8)	C(67)-O(18)	1.384(7)	C(4)-C(5)-C(6)	121.1(7)
C(27)-C(28)	1.369(9)	C(68)-C(69)	1.371(10)	C(1)-C(6)-C(5)	118.0(7)
C(28)-C(29)	1.352(9)	C(69)-C(70)	1.374(10)	C(12)-C(7)-C(8)	120.5(6)
C(29)-C(30)	1.393(9)	C(70)-C(71)	1.368(10)	C(12)-C(7)-O(4)	122.5(6)
C(31)-C(36)	1.358(7)	C(71)-C(72)	1.390(9)	C(8)-C(7)-O(4)	116.9(6)
C(31)-O(10)	1.386(6)	N(1)-P(1)	1.565(4)	C(7)-C(8)-C(9)	119.7(7)
C(31)-C(32)	1.388(7)	N(1)-P(2)	1.571(4)	C(10)-C(9)-C(8)	119.7(7)
C(32)-C(33)	1.365(8)	N(2)-P(3)	1.560(4)	C(9)-C(10)-C(11)	120.7(7)
C(33)-C(34)	1.371(9)	N(2)-P(4)	1.562(4)	C(10)-C(11)-C(12)	119.5(7)
C(34)-C(35)	1.382(8)	N(3)-P(5)	1.565(4)	C(7)-C(12)-C(11)	119.9(6)
C(35)-C(36)	1.384(8)	N(3)-P(6)	1.570(5)	C(18)-C(13)-C(14)	122.8(6)
C(37)-C(38)	1.363(8)	O(1)-P(1)	1.496(4)	C(18)-C(13)-O(5)	119.3(5)
C(37)-C(42)	1.369(8)	O(1)-Yb(1)	2.208(4)	C(14)-C(13)-O(5)	117.7(6)
C(37)-O(11)	1.399(7)	O(2)-P(2)	1.485(4)	C(13)-C(14)-C(15)	118.2(6)
C(38)-C(39)	1.386(9)	O(2)-Yb(1)	2.223(3)	C(16)-C(15)-C(14)	120.0(7)
C(39)-C(40)	1.359(10)	O(3)-P(1)	1.575(4)	C(17)-C(16)-C(15)	120.4(7)
C(40)-C(41)	1.377(10)	O(4)-P(1)	1.584(4)	C(16)-C(17)-C(18)	121.2(7)

C(13)-C(18)-C(17) 117.4(6)
C(20)-C(19)-C(24) 121.6(6)
C(20)-C(19)-O(6) 119.7(5)
C(24)-C(19)-O(6) 118.6(5)
C(19)-C(20)-C(21) 118.4(6)
C(22)-C(21)-C(20) 120.8(7)
C(23)-C(22)-C(21) 119.4(7)
C(22)-C(23)-C(24) 121.8(7)
C(19)-C(24)-C(23) 118.0(7)
C(30)-C(25)-C(26) 121.3(6)
C(30)-C(25)-O(9) 117.2(5)
C(26)-C(25)-O(9) 121.4(5)
C(25)-C(26)-C(27) 118.1(6)
C(28)-C(27)-C(26) 121.3(6)
C(29)-C(28)-C(27) 119.7(7)
C(28)-C(29)-C(30) 120.1(7)
C(25)-C(30)-C(29) 119.5(6)
C(36)-C(31)-O(10) 123.6(5)
C(36)-C(31)-C(32) 119.8(6)
O(10)-C(31)-C(32) 116.6(5)
C(33)-C(32)-C(31) 120.0(6)
C(32)-C(33)-C(34) 120.7(6)
C(33)-C(34)-C(35) 119.3(6)
C(34)-C(35)-C(36) 120.0(6)
C(31)-C(36)-C(35) 120.2(5)
C(38)-C(37)-C(42) 122.0(6)
C(38)-C(37)-O(11) 118.4(6)
C(42)-C(37)-O(11) 119.5(5)
C(37)-C(38)-C(39) 118.7(7)
C(40)-C(39)-C(38) 120.1(7)
C(39)-C(40)-C(41) 120.7(7)
C(40)-C(41)-C(42) 119.7(8)
C(37)-C(42)-C(41) 118.8(7)
C(48)-C(43)-C(44) 122.1(5)
C(48)-C(43)-O(12) 118.5(5)
C(44)-C(43)-O(12) 119.3(5)
C(43)-C(44)-C(45) 118.1(6)
C(46)-C(45)-C(44) 120.9(6)
C(47)-C(46)-C(45) 119.7(6)
C(46)-C(47)-C(48) 121.0(7)
C(43)-C(48)-C(47) 118.1(6)
C(54)-C(49)-C(50) 121.6(6)
C(54)-C(49)-O(15) 117.5(6)
C(50)-C(49)-O(15) 120.7(5)
C(49)-C(50)-C(51) 119.2(7)
C(52)-C(51)-C(50) 119.9(8)
C(51)-C(52)-C(53) 121.5(8)
C(52)-C(53)-C(54) 119.2(7)
C(49)-C(54)-C(53) 118.5(7)
C(56)-C(55)-C(60) 121.2(6)
C(56)-C(55)-O(16) 117.3(5)
C(60)-C(55)-O(16) 121.5(6)
C(57)-C(56)-C(55) 119.0(7)
C(58)-C(57)-C(56) 121.3(7)
C(57)-C(58)-C(59) 118.8(7)
C(60)-C(59)-C(58) 121.4(7)
C(59)-C(60)-C(55) 118.3(7)
C(62)-C(61)-C(66) 121.5(6)
C(62)-C(61)-O(17) 118.4(6)
C(66)-C(61)-O(17) 120.0(6)
C(61)-C(62)-C(63) 118.9(7)
C(64)-C(63)-C(62) 120.7(7)
C(65)-C(64)-C(63) 119.6(7)
C(64)-C(65)-C(66) 121.7(7)
C(61)-C(66)-C(65) 117.5(7)
C(72)-C(67)-C(68) 120.2(7)
C(72)-C(67)-O(18) 124.6(6)
C(68)-C(67)-O(18) 115.2(6)
C(69)-C(68)-C(67) 119.3(7)
C(68)-C(69)-C(70) 121.0(8)
C(71)-C(70)-C(69) 119.5(8)
C(70)-C(71)-C(72) 119.8(8)
C(67)-C(72)-C(71) 120.2(7)
P(1)-N(1)-P(2) 126.9(3)
P(3)-N(2)-P(4) 128.6(3)
P(5)-N(3)-P(6) 126.6(3)
P(1)-O(1)-Yb(1) 137.5(2)
P(2)-O(2)-Yb(1) 137.37(19)
C(1)-O(3)-P(1) 124.6(3)
C(7)-O(4)-P(1) 123.9(3)
C(13)-O(5)-P(2) 125.8(3)
C(19)-O(6)-P(2) 121.1(3)
P(3)-O(7)-Yb(1) 137.4(2)
P(4)-O(8)-Yb(1) 137.2(2)
C(25)-O(9)-P(3) 125.4(3)
C(31)-O(10)-P(3) 124.0(3)
C(37)-O(11)-P(4) 121.5(3)
C(43)-O(12)-P(4) 122.3(3)
P(5)-O(13)-Yb(1) 135.9(2)
P(6)-O(14)-Yb(1) 135.5(2)
C(49)-O(15)-P(5) 124.2(3)
C(55)-O(16)-P(5) 124.3(3)
C(61)-O(17)-P(6) 124.9(4)
C(67)-O(18)-P(6) 128.4(4)
O(1)-P(1)-N(1) 117.9(2)
O(1)-P(1)-O(3) 105.3(2)
N(1)-P(1)-O(3) 111.6(2)
O(1)-P(1)-O(4) 110.2(2)
N(1)-P(1)-O(4) 109.6(2)
O(3)-P(1)-O(4) 100.9(2)
O(1)-P(1)-Yb(1) 25.53(13)
N(1)-P(1)-Yb(1) 92.57(16)
O(3)-P(1)-Yb(1) 121.56(16)
O(4)-P(1)-Yb(1) 120.37(16)
O(2)-P(2)-N(1) 118.1(2)
O(2)-P(2)-O(5) 109.0(2)
N(1)-P(2)-O(5) 110.1(2)
O(2)-P(2)-O(6) 104.82(19)
N(1)-P(2)-O(6) 112.0(2)
O(5)-P(2)-O(6) 101.41(19)
O(2)-P(2)-Yb(1) 25.75(12)
N(1)-P(2)-Yb(1) 92.36(16)
O(5)-P(2)-Yb(1) 123.31(15)
O(6)-P(2)-Yb(1) 117.54(14)
O(7)-P(3)-N(2) 117.4(2)
O(7)-P(3)-O(9) 110.5(2)
N(2)-P(3)-O(9) 106.6(2)
O(7)-P(3)-O(10) 110.4(2)
N(2)-P(3)-O(10) 110.3(2)
O(9)-P(3)-O(10) 100.1(2)
O(7)-P(3)-Yb(1) 25.67(14)
N(2)-P(3)-Yb(1) 91.75(16)
O(9)-P(3)-Yb(1) 122.90(15)
O(10)-P(3)-Yb(1) 123.63(16)
O(8)-P(4)-N(2) 117.0(2)
O(8)-P(4)-O(11) 110.6(2)
N(2)-P(4)-O(11) 110.4(2)
O(8)-P(4)-O(12) 106.7(2)
N(2)-P(4)-O(12) 110.8(2)
O(11)-P(4)-O(12) 100.0(2)
O(8)-P(4)-Yb(1) 25.81(14)
N(2)-P(4)-Yb(1) 91.60(16)
O(11)-P(4)-Yb(1) 119.62(14)
O(12)-P(4)-Yb(1) 124.06(14)
O(13)-P(5)-N(3) 117.4(2)
O(13)-P(5)-O(16) 105.7(2)
N(3)-P(5)-O(16) 112.5(2)
O(13)-P(5)-O(15) 111.5(2)
N(3)-P(5)-O(15) 109.4(2)
O(16)-P(5)-O(15) 98.8(2)
O(13)-P(5)-Yb(1) 26.67(13)
N(3)-P(5)-Yb(1) 92.19(17)
O(16)-P(5)-Yb(1) 110.91(14)
O(15)-P(5)-Yb(1) 133.02(16)
O(14)-P(6)-N(3) 117.0(2)
O(14)-P(6)-O(17) 106.4(2)
N(3)-P(6)-O(17) 111.4(2)
O(14)-P(6)-O(18) 111.6(2)
N(3)-P(6)-O(18) 109.4(2)
O(17)-P(6)-O(18) 99.6(2)
O(14)-P(6)-Yb(1) 26.83(14)
N(3)-P(6)-Yb(1) 93.06(16)
O(17)-P(6)-Yb(1) 107.48(15)
O(18)-P(6)-Yb(1) 135.37(16)
O(1)-Yb(1)-O(14) 91.17(14)
O(1)-Yb(1)-O(7) 167.63(13)
O(14)-Yb(1)-O(7) 99.35(14)
O(1)-Yb(1)-O(8) 91.48(13)
O(14)-Yb(1)-O(8) 93.22(13)
O(7)-Yb(1)-O(8) 81.52(12)
O(1)-Yb(1)-O(2) 81.61(12)
O(14)-Yb(1)-O(2) 170.00(12)
O(7)-Yb(1)-O(2) 88.67(13)
O(8)-Yb(1)-O(2) 93.87(13)
O(1)-Yb(1)-O(13) 99.91(14)
O(14)-Yb(1)-O(13) 81.22(13)
O(7)-Yb(1)-O(13) 88.19(13)
O(8)-Yb(1)-O(13) 167.38(13)
O(2)-Yb(1)-O(13) 93.16(12)
O(1)-Yb(1)-P(6) 87.82(10)
O(14)-Yb(1)-P(6) 17.67(9)
O(7)-Yb(1)-P(6) 104.16(10)
O(8)-Yb(1)-P(6) 110.65(9)
O(2)-Yb(1)-P(6) 153.57(9)
O(13)-Yb(1)-P(6) 64.78(9)
O(1)-Yb(1)-P(5) 101.18(10)
O(14)-Yb(1)-P(5) 63.91(10)
O(7)-Yb(1)-P(5) 89.35(10)
O(8)-Yb(1)-P(5) 153.75(9)
O(2)-Yb(1)-P(5) 110.57(9)
O(13)-Yb(1)-P(5) 17.42(9)
P(6)-Yb(1)-P(5) 47.90(4)
O(1)-Yb(1)-P(3) 154.59(10)
O(14)-Yb(1)-P(3) 98.42(10)
O(7)-Yb(1)-P(3) 16.90(9)
O(8)-Yb(1)-P(3) 64.66(9)
O(2)-Yb(1)-P(3) 90.99(8)
O(13)-Yb(1)-P(3) 104.77(10)
P(6)-Yb(1)-P(3) 108.04(4)
P(5)-Yb(1)-P(3) 104.17(4)
O(1)-Yb(1)-P(1) 16.98(9)
O(14)-Yb(1)-P(1) 108.11(10)
O(7)-Yb(1)-P(1) 152.03(10)
O(8)-Yb(1)-P(1) 91.56(9)
O(2)-Yb(1)-P(1) 64.66(9)
O(13)-Yb(1)-P(1) 100.92(10)
P(6)-Yb(1)-P(1) 103.65(4)
P(5)-Yb(1)-P(1) 107.20(4)
P(3)-Yb(1)-P(1) 145.43(3)
O(1)-Yb(1)-P(2) 64.74(9)
O(14)-Yb(1)-P(2) 154.97(10)
O(7)-Yb(1)-P(2) 105.40(10)
O(8)-Yb(1)-P(2) 94.03(9)
O(2)-Yb(1)-P(2) 16.87(9)
O(13)-Yb(1)-P(2) 95.73(9)
P(6)-Yb(1)-P(2) 143.80(3)
P(5)-Yb(1)-P(2) 112.15(4)
P(3)-Yb(1)-P(2) 106.34(3)
P(1)-Yb(1)-P(2) 47.79(3)
O(1)-Yb(1)-P(4) 108.50(10)
O(14)-Yb(1)-P(4) 92.52(9)
O(7)-Yb(1)-P(4) 64.83(9)
O(8)-Yb(1)-P(4) 17.02(9)
O(2)-Yb(1)-P(4) 96.31(9)
O(13)-Yb(1)-P(4) 151.05(10)
P(6)-Yb(1)-P(4) 110.03(4)
P(5)-Yb(1)-P(4) 142.44(4)
P(3)-Yb(1)-P(4) 47.93(4)
P(1)-Yb(1)-P(4) 107.87(4)
P(2)-Yb(1)-P(4) 101.22(3)

Symmetry transformations used to generate equivalent atoms:

Table 4. Anisotropic displacement parameters ($Å^2 x\ 10^3$)for ybtpop3m. The anisotropic displacement factor exponent takes the form: $-2\pi^2[\ h^2 a^{*2} U^{11} + ... + 2\ h\ k\ a^*\ b^*\ U^{12}\ ]$

	U^{11}	U^{22}	U^{33}	U^{23}	U^{13}	U^{12}
C(1)	68(5)	46(4)	34(3)	-2(3)	19(3)	2(4)
C(2)	68(5)	79(6)	57(4)	-29(4)	5(4)	16(4)
C(3)	88(6)	105(7)	75(5)	-39(5)	-4(5)	-2(5)
C(4)	132(8)	61(6)	53(5)	-12(4)	14(5)	13(6)
C(5)	118(8)	67(6)	74(5)	-27(5)	36(5)	20(5)
C(6)	75(5)	72(6)	69(5)	-3(4)	27(4)	17(4)
C(7)	31(3)	40(4)	55(4)	0(3)	13(3)	6(3)
C(8)	55(4)	51(5)	80(5)	-15(4)	27(4)	1(3)
C(9)	67(5)	38(5)	124(7)	-1(5)	26(5)	3(4)
C(10)	76(6)	67(6)	86(6)	31(5)	17(5)	8(4)
C(11)	76(5)	68(6)	50(4)	7(4)	6(4)	9(4)
C(12)	56(4)	45(4)	54(4)	1(4)	7(3)	8(3)
C(13)	33(3)	55(4)	38(3)	8(3)	4(3)	3(3)
C(14)	54(4)	56(5)	52(4)	13(4)	10(3)	6(3)
C(15)	67(5)	77(6)	53(4)	26(4)	9(4)	11(4)
C(16)	61(5)	122(8)	43(4)	0(5)	-5(4)	-2(5)
C(17)	83(6)	89(6)	57(5)	-9(5)	0(4)	-32(5)
C(18)	68(5)	58(5)	43(4)	7(3)	-1(3)	-19(4)
C(19)	32(3)	45(4)	31(3)	5(3)	9(3)	-9(3)
C(20)	47(4)	48(4)	67(4)	5(4)	21(3)	-1(3)
C(21)	90(6)	48(5)	81(5)	-2(4)	23(5)	-12(4)
C(22)	82(7)	74(6)	76(5)	7(5)	13(5)	-39(5)
C(23)	46(5)	105(7)	76(5)	17(5)	23(4)	-25(5)
C(24)	43(4)	71(5)	57(4)	5(4)	27(3)	0(4)
C(25)	36(3)	36(4)	45(3)	-5(3)	8(3)	-7(3)
C(26)	62(4)	40(4)	48(4)	0(3)	9(3)	2(3)
C(27)	77(5)	60(5)	53(4)	10(4)	14(4)	9(4)
C(28)	68(5)	42(4)	87(6)	0(4)	9(4)	8(4)
C(29)	85(6)	44(5)	78(5)	-24(4)	9(5)	9(4)
C(30)	83(5)	46(4)	48(4)	-12(4)	1(4)	-1(4)
C(31)	36(3)	46(4)	42(3)	-5(3)	15(3)	-1(3)
C(32)	59(4)	61(5)	52(4)	-13(4)	19(3)	-7(3)
C(33)	74(5)	84(6)	54(4)	-2(4)	36(4)	-16(4)
C(34)	68(5)	70(5)	67(5)	-3(4)	32(4)	-21(4)
C(35)	57(4)	60(5)	59(4)	-18(4)	17(4)	-21(4)
C(36)	52(4)	55(4)	42(3)	-8(3)	18(3)	-6(3)
C(37)	28(3)	60(5)	38(3)	11(3)	-2(3)	5(3)
C(38)	54(4)	91(6)	51(4)	-14(4)	13(3)	-7(4)
C(39)	57(5)	125(8)	51(4)	10(5)	22(4)	-1(5)
C(40)	51(5)	112(8)	90(6)	46(6)	27(5)	0(5)
C(41)	55(5)	64(5)	118(7)	21(5)	28(5)	1(4)
C(42)	51(4)	63(5)	73(5)	8(4)	25(4)	4(4)
C(43)	48(4)	30(3)	31(3)	5(3)	5(3)	-3(3)
C(44)	43(4)	58(4)	48(4)	17(3)	2(3)	2(3)
C(45)	60(5)	79(6)	51(4)	21(4)	-9(4)	-5(4)
C(46)	107(7)	60(5)	40(4)	12(4)	12(5)	-5(5)
C(47)	96(7)	92(6)	63(5)	21(5)	50(5)	18(5)
C(48)	53(4)	79(5)	53(4)	18(4)	12(4)	13(4)
C(49)	33(3)	53(4)	34(3)	0(3)	1(3)	1(3)
C(50)	73(5)	66(5)	57(4)	-8(4)	24(4)	-15(4)
C(51)	77(5)	78(6)	81(5)	-21(5)	21(4)	-11(5)
C(52)	75(6)	120(8)	49(5)	-26(5)	10(4)	0(5)
C(53)	83(6)	123(8)	49(4)	13(5)	27(4)	12(6)
C(54)	74(5)	79(6)	51(4)	9(4)	21(4)	1(4)
C(55)	53(4)	39(4)	34(3)	-1(3)	13(3)	-1(3)
C(56)	57(5)	59(5)	60(4)	21(4)	15(4)	11(4)
C(57)	81(6)	68(6)	66(5)	10(4)	12(4)	20(5)
C(58)	121(7)	49(5)	54(4)	6(4)	19(5)	5(5)
C(59)	114(7)	58(6)	69(5)	-16(4)	47(5)	-25(5)
C(60)	71(5)	51(5)	63(4)	-10(4)	27(4)	-4(4)
C(61)	42(4)	46(4)	51(4)	4(3)	17(3)	13(3)
C(62)	53(5)	75(5)	73(5)	-16(4)	21(4)	0(4)
C(63)	72(6)	124(8)	58(5)	-21(5)	14(4)	14(5)
C(64)	71(6)	151(9)	63(5)	9(6)	35(5)	31(6)

C(65)	55(5)	133(8)	86(6)	19(6)	30(5)	-14(5)
C(66)	47(4)	111(7)	59(4)	2(4)	17(4)	-15(4)
C(67)	41(4)	44(4)	61(4)	6(4)	4(3)	-8(3)
C(68)	62(5)	52(5)	88(5)	10(4)	18(4)	-17(4)
C(69)	82(6)	59(6)	139(8)	-14(6)	18(6)	-34(5)
C(70)	91(7)	64(6)	132(8)	-35(6)	30(6)	-19(5)
C(71)	68(5)	79(6)	107(6)	-32(5)	23(5)	-14(5)
C(72)	60(5)	63(5)	75(5)	-18(4)	23(4)	-20(4)
N(1)	39(3)	34(3)	32(2)	-1(2)	11(2)	-1(2)
N(2)	53(3)	38(3)	24(2)	-2(2)	2(2)	5(2)
N(3)	40(3)	42(3)	45(3)	10(2)	16(2)	1(2)
O(1)	49(2)	51(3)	49(2)	-10(2)	26(2)	-13(2)
O(2)	36(2)	34(2)	38(2)	-7(2)	13(2)	-5(2)
O(3)	71(3)	57(3)	31(2)	-8(2)	23(2)	-15(2)
O(4)	52(3)	58(3)	54(2)	0(2)	26(2)	11(2)
O(5)	32(2)	52(3)	32(2)	-3(2)	1(2)	3(2)
O(6)	41(2)	49(3)	26(2)	1(2)	8(2)	-10(2)
O(7)	48(2)	41(2)	31(2)	-5(2)	1(2)	4(2)
O(8)	44(2)	34(2)	26(2)	-1(2)	6(2)	4(2)
O(9)	50(3)	31(2)	45(2)	-4(2)	-3(2)	1(2)
O(10)	60(3)	39(3)	74(3)	2(2)	34(2)	4(2)
O(11)	33(2)	65(3)	43(2)	15(2)	5(2)	-7(2)
O(12)	52(2)	35(2)	32(2)	1(2)	8(2)	-4(2)
O(13)	35(2)	47(3)	41(2)	12(2)	5(2)	-3(2)
O(14)	35(2)	55(3)	45(2)	16(2)	6(2)	-11(2)
O(15)	45(2)	53(3)	35(2)	5(2)	5(2)	10(2)
O(16)	60(3)	43(3)	41(2)	6(2)	24(2)	9(2)
O(17)	48(3)	44(3)	63(3)	7(2)	22(2)	5(2)
O(18)	44(3)	54(3)	57(3)	-3(2)	18(2)	-14(2)
P(1)	42(1)	44(1)	33(1)	-5(1)	15(1)	-2(1)
P(2)	31(1)	35(1)	29(1)	-1(1)	7(1)	-3(1)
P(3)	40(1)	33(1)	35(1)	-4(1)	7(1)	-4(1)
P(4)	39(1)	36(1)	28(1)	3(1)	6(1)	-1(1)
P(5)	39(1)	43(1)	33(1)	7(1)	8(1)	3(1)
P(6)	35(1)	44(1)	45(1)	7(1)	11(1)	-5(1)
Yb(1)	36(1)	35(1)	28(1)	2(1)	7(1)	-6(1)

Table 5. Hydrogen coordinates (x 10^4) and isotropic displacement parameters ($Å^2$x 10^3) for ybtpop3m.

	x	y	z	U(eq)		x	y	z	U(eq)
H(2)	6578	4466	4334	85		H(38)	2513	3114	1697	79
H(3)	7160	5435	5004	116		H(39)	1824	2244	2094	92
H(4)	6461	6397	5300	102		H(40)	1548	887	1788	100
H(5)	5188	6433	4903	102		H(41)	1945	371	1083	94
H(6)	4590	5479	4208	85		H(42)	2649	1231	692	73
H(8)	4591	6603	2907	72		H(44)	2683	3960	90	63
H(9)	4506	7431	2142	92		H(45)	2405	4127	-848	84
H(10)	4394	6800	1320	94		H(46)	3336	4026	-1252	86
H(11)	4354	5346	1241	82		H(47)	4557	3850	-724	94
H(12)	4397	4523	1997	65		H(48)	4860	3682	220	75
H(14)	7335	2723	3859	67		H(50)	6032	2278	4107	77
H(15)	7987	2938	4784	82		H(51)	6052	3073	4867	96
H(16)	8518	4235	5076	96		H(52)	5906	2433	5618	100
H(17)	8422	5306	4468	98		H(53)	5763	987	5647	100
H(18)	7747	5126	3543	72		H(54)	5691	179	4870	81
H(20)	5982	6020	2453	64		H(56)	6825	-902	3472	72
H(21)	6714	7232	2586	89		H(57)	7005	-2265	3805	89
H(22)	7928	7174	2552	96		H(58)	6016	-3046	3894	92
H(23)	8407	5926	2381	90		H(59)	4832	-2439	3667	91
H(24)	7709	4692	2265	66		H(60)	4625	-1092	3305	73
H(26)	5337	-26	2007	62		H(62)	4274	2035	4354	80
H(27)	5939	-1321	2197	78		H(63)	4031	1718	5158	103
H(28)	5937	-2239	1504	83		H(64)	2980	965	5143	110
H(29)	5356	-1864	612	87		H(65)	2139	591	4331	107
H(30)	4770	-551	408	76		H(66)	2362	880	3509	86
H(32)	5992	1746	163	69		H(68)	2135	-590	2571	82
H(33)	6507	2921	-104	80		H(69)	1923	-1693	1957	117
H(34)	6707	4134	419	79		H(70)	2741	-1957	1466	116
H(35)	6432	4141	1241	71		H(71)	3756	-1074	1564	103
H(36)	5919	2951	1512	59		H(72)	3946	73	2157	79

B6 Crystallographic Data for $Dy(tpOp)_3$

Table 2. Atomic coordinates (x 10^4) and equivalent isotropic displacement parameters ($Å^2$x 10^3) for ddx2m. U(eq) is defined as one third of the trace of the orthogonalized U^{ij} tensor.

	x	y	z	U(eq)			x	y	z	U(eq)	
C(1)	-1341(6)	149(4)	1208(3)	59(2)			C(53)	-269(2)	-2162(1)	2976(1)	126(4)
C(2)	-1488(8)	-449(5)	1625(3)	72(2)			C(54)	-499(2)	-1338(1)	2982(1)	88(2)
C(3)	-1520(8)	-1258(5)	1440(4)	86(2)			C(55)	-1266(2)	764(1)	4087(1)	107(3)
C(4)	-1442(8)	-1464(5)	861(4)	82(2)			C(56)	-1303(2)	232(1)	4553(1)	106(3)
C(5)	-1321(7)	-863(5)	455(3)	73(2)			C(57)	-1744(2)	482(1)	5087(1)	115(3)
C(6)	-1276(3)	-41(2)	629(1)	63(2)			C(58)	-2148(2)	1263(1)	5155(1)	148(5)
C(7)	-1093(3)	2657(2)	396(1)	54(2)			C(59)	-2110(2)	1794(1)	4690(1)	180(7)
C(8)	-2334(3)	2950(2)	312(1)	74(2)			C(60)	-1669(2)	1545(1)	4155(1)	154(6)
C(9)	-2406(3)	3664(2)	-2(1)	83(2)			C(61)	4573(2)	841(1)	3428(1)	62(2)
C(10)	-1236(3)	4086(2)	-234(1)	89(3)			C(62)	5070(2)	478(1)	2942(1)	84(2)
C(11)	5(3)	3793(2)	-151(1)	96(3)			C(63)	5632(2)	-256(1)	2993(1)	112(3)
C(12)	77(3)	3079(2)	164(1)	78(2)			C(64)	5696(2)	-626(1)	3529(1)	112(3)
C(13)	3275(7)	215(4)	1309(3)	55(2)			C(65)	5199(2)	-263(1)	4015(1)	110(3)
C(14)	4553(8)	214(5)	1126(4)	84(2)			C(66)	4637(2)	471(1)	3964(1)	90(3)
C(15)	4835(10)	-424(6)	766(4)	105(3)			C(67)	2391(7)	2408(5)	4636(3)	64(2)
C(16)	3818(10)	-1027(6)	581(4)	103(3)			C(68)	2147(11)	1962(6)	5135(4)	106(3)
C(17)	2537(9)	-1034(5)	775(4)	98(3)			C(69)	1436(16)	2281(10)	5555(6)	160(6)
C(18)	2267(8)	-405(5)	1147(4)	79(2)			C(70)	964(13)	3026(11)	5501(6)	147(5)
C(19)	3683(5)	2716(4)	774(3)	49(2)			C(71)	1250(13)	3473(8)	5009(5)	134(4)
C(20)	3771(6)	2604(4)	185(3)	60(2)			C(72)	1990(11)	3155(6)	4565(4)	102(3)
C(21)	3789(7)	3276(5)	-167(3)	71(2)			C(73)	-2748(8)	2274(5)	2563(4)	83(2)
C(22)	3733(7)	4055(5)	68(4)	71(2)			C(74)	-3592(9)	2557(6)	2092(4)	108(3)
C(23)	3656(8)	4152(4)	649(4)	74(2)			N(1)	1142(5)	1488(3)	1097(2)	53(1)
C(24)	3639(7)	3490(4)	1016(3)	58(2)			N(2)	1389(5)	5253(3)	2780(2)	55(1)
C(25)	3989(7)	6052(4)	2130(4)	66(2)			N(3)	1607(5)	1030(3)	3624(2)	54(1)
C(26)	3882(9)	6547(5)	1666(4)	94(3)			O(1)	-326(4)	2416(2)	1670(2)	53(1)
C(27)	4574(14)	7359(7)	1690(7)	139(5)			O(2)	-1298(4)	975(3)	1419(2)	66(1)
C(28)	5295(18)	7607(9)	2180(10)	172(9)			O(3)	-1101(6)	1914(3)	657(2)	84(2)
C(29)	5399(13)	7139(10)	2659(8)	163(7)			O(4)	2402(4)	2183(2)	2036(2)	53(1)
C(30)	4711(9)	6338(6)	2625(4)	98(3)			O(5)	2999(5)	840(3)	1704(2)	60(1)
C(31)	-218(7)	5332(4)	1634(3)	55(2)			O(6)	3710(4)	2025(2)	1122(2)	53(1)
C(32)	-1084(7)	4633(5)	1466(3)	64(2)			O(7)	1733(4)	3975(2)	2123(2)	55(1)
C(33)	-2472(8)	4697(6)	1405(3)	81(2)			O(8)	3424(4)	5217(2)	2096(2)	59(1)
C(34)	-2948(9)	5423(7)	1507(4)	88(3)			O(9)	1180(4)	5303(3)	1670(2)	60(1)
C(35)	-2063(11)		6114(6)	1657(4)	94(3)		O(10)	554(4)	3824(2)	3238(2)	55(1)
C(36)	-673(2)	6087(1)	1733(1)	78(2)			O(11)	1843(8)	4923(4)	3846(2)	124(3)
C(37)	2776(2)	5571(1)	3969(1)	76(2)			O(12)	-430(6)	5101(3)	3521(4)	133(3)
C(38)	2521(2)	6386(1)	3915(1)	125(4)			O(13)	-24(5)	1473(3)	2826(2)	71(1)
C(39)	3510(2)	7042(1)	4093(1)	204(8)			O(14)	432(7)	77(3)	2758(3)	105(2)
C(40)	4755(2)	6883(1)	4325(1)	260(13)			O(15)	-852(6)	385(4)	3548(3)	112(2)
C(41)	5011(2)	6068(1)	4379(1)	227(10)			O(16)	2363(4)	2541(2)	3274(2)	49(1)
C(42)	4021(2)	5412(1)	4201(1)	153(5)			O(17)	4086(4)	1583(3)	3353(2)	65(1)
C(43)	-1671(2)	4703(1)	3536(1)	73(2)			O(18)	3229(4)	2089(3)	4237(2)	61(1)
C(44)	-2122(2)	4180(1)	3980(1)	129(4)			O(19)	-1544(4)	2867(3)	2703(2)	69(1)
C(45)	-3445(2)	3762(1)	3957(1)	205(9)			P(1)	-269(2)	1747(1)	1232(1)	51(1)
C(46)	-4318(2)	3869(1)	3489(1)	171(7)			P(2)	2468(2)	1665(1)	1505(1)	49(1)
C(47)	-3867(2)	4392(1)	3045(1)	176(7)			P(3)	1872(2)	4890(1)	2201(1)	50(1)
C(48)	-2544(2)	4810(1)	3068(1)	120(4)			P(4)	845(2)	4739(1)	3304(1)	57(1)
C(49)	563(2)	-709(1)	2882(1)	75(2)			P(5)	292(2)	843(1)	3222(1)	59(1)
C(50)	1854(2)	-904(1)	2776(1)	147(5)			P(6)	2706(2)	1816(1)	3596(1)	49(1)
C(51)	2084(2)	-1729(1)	2770(1)	213(9)			Dy(1)	817(1)	2775(1)	2552(1)	44(1)
C(52)	1022(2)	-2358(1)	2870(1)	180(7)							

Table 3. Bond lengths [Å] and angles [°] for ddx2m.

C(1)-C(6)	1.367(7)	C(4)-H(4)	0.9300	C(8)-H(8)	0.9300
C(1)-C(2)	1.378(10)	C(5)-C(6)	1.380(8)	C(9)-C(10)	1.3900
C(1)-O(2)	1.413(7)	C(5)-H(5)	0.9300	C(9)-H(9)	0.9300
C(2)-C(3)	1.368(11)	C(6)-H(6)	0.9300	C(10)-C(11)	1.3900
C(2)-H(2)	0.9300	C(7)-O(3)	1.361(6)	C(10)-H(10)	0.9300
C(3)-C(4)	1.375(11)	C(7)-C(8)	1.3900	C(11)-C(12)	1.3900
C(3)-H(3)	0.9300	C(7)-C(12)	1.3900	C(11)-H(11)	0.9300
C(4)-C(5)	1.361(11)	C(8)-C(9)	1.3900	C(12)-H(12)	0.9300

C(13)-C(14)	1.349(9)
C(13)-C(18)	1.353(9)
C(13)-O(5)	1.411(7)
C(14)-C(15)	1.377(11)
C(14)-H(14)	0.9300
C(15)-C(16)	1.357(12)
C(15)-H(15)	0.9300
C(16)-C(17)	1.359(12)
C(16)-H(16)	0.9300
C(17)-C(18)	1.380(10)
C(17)-H(17)	0.9300
C(18)-H(18)	0.9300
C(19)-C(24)	1.371(8)
C(19)-C(20)	1.374(9)
C(19)-O(6)	1.396(7)
C(20)-C(21)	1.371(9)
C(20)-H(20)	0.9300
C(21)-C(22)	1.374(10)
C(21)-H(21)	0.9300
C(22)-C(23)	1.350(10)
C(22)-H(22)	0.9300
C(23)-C(24)	1.381(9)
C(23)-H(23)	0.9300
C(24)-H(24)	0.9300
C(25)-C(26)	1.362(11)
C(25)-C(30)	1.363(11)
C(25)-O(8)	1.393(8)
C(26)-C(27)	1.398(14)
C(26)-H(26)	0.9300
C(27)-C(28)	1.34(2)
C(27)-H(27)	0.9300
C(28)-C(29)	1.36(2)
C(28)-H(28)	0.9300
C(29)-C(30)	1.382(15)
C(29)-H(29)	0.9300
C(30)-H(30)	0.9300
C(31)-C(32)	1.366(9)
C(31)-C(36)	1.382(7)
C(31)-O(9)	1.394(8)
C(32)-C(33)	1.398(10)
C(32)-H(32)	0.9300
C(33)-C(34)	1.350(11)
C(33)-H(33)	0.9300
C(34)-C(35)	1.356(12)
C(34)-H(34)	0.9300
C(35)-C(36)	1.391(10)
C(35)-H(35)	0.9300
C(36)-H(36)	0.9300
C(37)-O(11)	1.321(6)
C(37)-C(38)	1.3900
C(37)-C(42)	1.3900
C(38)-C(39)	1.3900
C(38)-H(38)	0.9300
C(39)-C(40)	1.3900
C(39)-H(39)	0.9300
C(40)-C(41)	1.3900
C(40)-H(40)	0.9300
C(41)-C(42)	1.3900
C(41)-H(41)	0.9300
C(42)-H(42)	0.9300
C(43)-O(12)	1.311(6)
C(43)-C(44)	1.3900
C(43)-C(48)	1.3900
C(44)-C(45)	1.3900
C(44)-H(44)	0.9300
C(45)-C(46)	1.3900
C(45)-H(45)	0.9300
C(46)-C(47)	1.3900
C(46)-H(46)	0.9300
C(47)-C(48)	1.3900
C(47)-H(47)	0.9300
C(48)-H(48)	0.9300
C(49)-O(14)	1.336(6)
C(49)-C(50)	1.3900
C(49)-C(54)	1.3900
C(50)-C(51)	1.3900
C(50)-H(50)	0.9300
C(51)-C(52)	1.3900
C(51)-H(51)	0.9300
C(52)-C(53)	1.3900
C(52)-H(52)	0.9300
C(53)-C(54)	1.3900
C(53)-H(53)	0.9300
C(54)-H(54)	0.9300
C(55)-C(56)	1.3900
C(55)-C(60)	1.3900
C(55)-O(15)	1.470(8)
C(56)-C(57)	1.3900
C(56)-H(56)	0.9300
C(57)-C(58)	1.3900
C(57)-H(57)	0.9300
C(58)-C(59)	1.3900
C(58)-H(58)	0.9300
C(59)-C(60)	1.3900
C(59)-H(59)	0.9300
C(60)-H(60)	0.9300
C(61)-O(17)	1.372(5)
C(61)-C(62)	1.3900
C(61)-C(66)	1.3900
C(62)-C(63)	1.3900
C(62)-H(62)	0.9300
C(63)-C(64)	1.3900
C(63)-H(63)	0.9300
C(64)-C(65)	1.3900
C(64)-H(64)	0.9300
C(65)-C(66)	1.3900
C(65)-H(65)	0.9300
C(66)-H(66)	0.9300
C(67)-C(72)	1.339(10)
C(67)-C(68)	1.383(10)
C(67)-O(18)	1.398(8)
C(68)-C(69)	1.351(14)
C(68)-H(68)	0.9300
C(69)-C(70)	1.364(17)
C(69)-H(69)	0.9300
C(70)-C(71)	1.374(16)
C(70)-H(70)	0.9300
C(71)-C(72)	1.408(14)
C(71)-H(71)	0.9300
C(72)-H(72)	0.9300
C(73)-O(19)	1.449(8)
C(73)-C(74)	1.470(11)
C(73)-H(73A)	0.9700
C(73)-H(73B)	0.9700
C(74)-H(74A)	0.9600
C(74)-H(74B)	0.9600
C(74)-H(74C)	0.9600
N(1)-P(1)	1.555(5)
N(1)-P(2)	1.582(5)
N(2)-P(4)	1.552(5)
N(2)-P(3)	1.563(5)
N(3)-P(6)	1.564(5)
N(3)-P(5)	1.567(5)
O(1)-P(1)	1.474(4)
O(1)-Dy(1)	2.319(4)
O(2)-P(1)	1.580(5)
O(3)-P(1)	1.587(5)
O(4)-P(2)	1.478(4)
O(4)-Dy(1)	2.302(4)
O(5)-P(2)	1.578(4)
O(6)-P(2)	1.590(4)
O(7)-P(3)	1.481(4)
O(7)-Dy(1)	2.291(4)
O(8)-P(3)	1.586(4)
O(9)-P(3)	1.590(4)
O(10)-P(4)	1.477(4)
O(10)-Dy(1)	2.347(4)
O(11)-P(4)	1.566(6)
O(12)-P(4)	1.560(6)
O(13)-P(5)	1.447(4)
O(13)-Dy(1)	2.273(4)
O(14)-P(5)	1.645(6)
O(15)-P(5)	1.500(6)
O(16)-P(6)	1.477(4)
O(16)-Dy(1)	2.302(4)
O(17)-P(6)	1.585(5)
O(18)-P(6)	1.584(4)
O(19)-H(19)	0.8200

C(6)-C(1)-C(2)	122.7(6)
C(6)-C(1)-O(2)	122.2(6)
C(2)-C(1)-O(2)	115.1(6)
C(3)-C(2)-C(1)	117.0(7)
C(3)-C(2)-H(2)	121.5
C(1)-C(2)-H(2)	121.5
C(2)-C(3)-C(4)	121.3(8)
C(2)-C(3)-H(3)	119.3
C(4)-C(3)-H(3)	119.3
C(5)-C(4)-C(3)	120.6(7)
C(5)-C(4)-H(4)	119.7
C(3)-C(4)-H(4)	119.7
C(4)-C(5)-C(6)	119.5(6)
C(4)-C(5)-H(5)	120.3
C(6)-C(5)-H(5)	120.3
C(1)-C(6)-C(5)	118.9(5)
C(1)-C(6)-H(6)	120.6
C(5)-C(6)-H(6)	120.6
O(3)-C(7)-C(8)	117.5(3)
O(3)-C(7)-C(12)	122.1(3)
C(8)-C(7)-C(12)	120.0
C(7)-C(8)-C(9)	120.0
C(7)-C(8)-H(8)	120.0
C(9)-C(8)-H(8)	120.0
C(10)-C(9)-C(8)	120.0
C(10)-C(9)-H(9)	120.0
C(8)-C(9)-H(9)	120.0
C(9)-C(10)-C(11)	120.0
C(9)-C(10)-H(10)	120.0
C(11)-C(10)-H(10)	120.0
C(12)-C(11)-C(10)	120.0
C(12)-C(11)-H(11)	120.0
C(10)-C(11)-H(11)	120.0
C(11)-C(12)-C(7)	120.0
C(11)-C(12)-H(12)	120.0
C(7)-C(12)-H(12)	120.0
C(14)-C(13)-C(18)	121.0(7)
C(14)-C(13)-O(5)	119.7(6)
C(18)-C(13)-O(5)	119.2(6)
C(13)-C(14)-C(15)	119.5(8)
C(13)-C(14)-H(14)	120.2
C(15)-C(14)-H(14)	120.2
C(16)-C(15)-C(14)	119.8(8)
C(16)-C(15)-H(15)	120.1
C(14)-C(15)-H(15)	120.1
C(15)-C(16)-C(17)	120.4(8)
C(15)-C(16)-H(16)	119.8
C(17)-C(16)-H(16)	119.8
C(16)-C(17)-C(18)	119.4(8)
C(16)-C(17)-H(17)	120.3
C(18)-C(17)-H(17)	120.3
C(13)-C(18)-C(17)	119.7(7)
C(13)-C(18)-H(18)	120.2
C(17)-C(18)-H(18)	120.2
C(24)-C(19)-C(20)	120.9(6)
C(24)-C(19)-O(6)	121.0(6)
C(20)-C(19)-O(6)	118.0(6)
C(21)-C(20)-C(19)	119.3(7)
C(21)-C(20)-H(20)	120.3
C(19)-C(20)-H(20)	120.3
C(20)-C(21)-C(22)	120.5(7)
C(20)-C(21)-H(21)	119.7
C(22)-C(21)-H(21)	119.7
C(23)-C(22)-C(21)	119.2(7)
C(23)-C(22)-H(22)	120.4
C(21)-C(22)-H(22)	120.4

C(22)-C(23)-C(24) 121.9(7)
C(22)-C(23)-H(23) 119.1
C(24)-C(23)-H(23) 119.1
C(19)-C(24)-C(23) 118.1(7)
C(19)-C(24)-H(24) 120.9
C(23)-C(24)-H(24) 120.9
C(26)-C(25)-C(30) 121.6(8)
C(26)-C(25)-O(8) 120.1(8)
C(30)-C(25)-O(8) 118.2(7)
C(25)-C(26)-C(27) 119.0(11)
C(25)-C(26)-H(26) 120.5
C(27)-C(26)-H(26) 120.5
C(28)-C(27)-C(26) 117.3(14)
C(28)-C(27)-H(27) 121.4
C(26)-C(27)-H(27) 121.4
C(27)-C(28)-C(29) 125.6(15)
C(27)-C(28)-H(28) 117.2
C(29)-C(28)-H(28) 117.2
C(28)-C(29)-C(30) 116.1(15)
C(28)-C(29)-H(29) 121.9
C(30)-C(29)-H(29) 121.9
C(25)-C(30)-C(29) 120.4(12)
C(25)-C(30)-H(30) 119.8
C(29)-C(30)-H(30) 119.8
C(32)-C(31)-C(36) 122.0(6)
C(32)-C(31)-O(9) 119.4(6)
C(36)-C(31)-O(9) 118.4(5)
C(31)-C(32)-C(33) 117.9(7)
C(31)-C(32)-H(32) 121.1
C(33)-C(32)-H(32) 121.1
C(34)-C(33)-C(32) 121.4(8)
C(34)-C(33)-H(33) 119.3
C(32)-C(33)-H(33) 119.3
C(33)-C(34)-C(35) 119.6(8)
C(33)-C(34)-H(34) 120.2
C(35)-C(34)-H(34) 120.2
C(34)-C(35)-C(36) 121.6(7)
C(34)-C(35)-H(35) 119.2
C(36)-C(35)-H(35) 119.2
C(31)-C(36)-C(35) 117.5(5)
C(31)-C(36)-H(36) 121.3
C(35)-C(36)-H(36) 121.3
O(11)-C(37)-C(38) 122.7(3)
O(11)-C(37)-C(42) 117.2(3)
C(38)-C(37)-C(42) 120.0
C(39)-C(38)-C(37) 120.0
C(39)-C(38)-H(38) 120.0
C(37)-C(38)-H(38) 120.0
C(38)-C(39)-C(40) 120.0
C(38)-C(39)-H(39) 120.0
C(40)-C(39)-H(39) 120.0
C(41)-C(40)-C(39) 120.0
C(41)-C(40)-H(40) 120.0
C(39)-C(40)-H(40) 120.0
C(40)-C(41)-C(42) 120.0
C(40)-C(41)-H(41) 120.0
C(42)-C(41)-H(41) 120.0
C(41)-C(42)-C(37) 120.0
C(41)-C(42)-H(42) 120.0
C(37)-C(42)-H(42) 120.0
O(12)-C(43)-C(44) 123.5(4)
O(12)-C(43)-C(48) 116.5(4)
C(44)-C(43)-C(48) 120.0
C(45)-C(44)-C(43) 120.0
C(45)-C(44)-H(44) 120.0
C(43)-C(44)-H(44) 120.0
C(44)-C(45)-C(46) 120.0
C(44)-C(45)-H(45) 120.0
C(46)-C(45)-H(45) 120.0
C(47)-C(46)-C(45) 120.0
C(47)-C(46)-H(46) 120.0
C(45)-C(46)-H(46) 120.0
C(46)-C(47)-C(48) 120.0
C(46)-C(47)-H(47) 120.0
C(48)-C(47)-H(47) 120.0
C(47)-C(48)-C(43) 120.0
C(47)-C(48)-H(48) 120.0
C(43)-C(48)-H(48) 120.0
O(14)-C(49)-C(50) 112.8(3)
O(14)-C(49)-C(54) 125.8(3)
C(50)-C(49)-C(54) 120.0
C(51)-C(50)-C(49) 120.0
C(51)-C(50)-H(50) 120.0
C(49)-C(50)-H(50) 120.0
C(50)-C(51)-C(52) 120.0
C(50)-C(51)-H(51) 120.0
C(52)-C(51)-H(51) 120.0
C(51)-C(52)-C(53) 120.0
C(51)-C(52)-H(52) 120.0
C(53)-C(52)-H(52) 120.0
C(54)-C(53)-C(52) 120.0
C(54)-C(53)-H(53) 120.0
C(52)-C(53)-H(53) 120.0
C(53)-C(54)-C(49) 120.0
C(53)-C(54)-H(54) 120.0
C(49)-C(54)-H(54) 120.0
C(56)-C(55)-C(60) 120.0
C(56)-C(55)-O(15) 112.9(2)
C(60)-C(55)-O(15) 127.0(2)
C(57)-C(56)-C(55) 120.0
C(57)-C(56)-H(56) 120.0
C(55)-C(56)-H(56) 120.0
C(58)-C(57)-C(56) 120.0
C(58)-C(57)-H(57) 120.0
C(56)-C(57)-H(57) 120.0
C(57)-C(58)-C(59) 120.0
C(57)-C(58)-H(58) 120.0
C(59)-C(58)-H(58) 120.0
C(58)-C(59)-C(60) 120.0
C(58)-C(59)-H(59) 120.0
C(60)-C(59)-H(59) 120.0
C(59)-C(60)-C(55) 120.0
C(59)-C(60)-H(60) 120.0
C(55)-C(60)-H(60) 120.0
O(17)-C(61)-C(62) 117.1(2)
O(17)-C(61)-C(66) 122.8(2)
C(62)-C(61)-C(66) 120.0
C(61)-C(62)-C(63) 120.0
C(61)-C(62)-H(62) 120.0
C(63)-C(62)-H(62) 120.0
C(64)-C(63)-C(62) 120.0
C(64)-C(63)-H(63) 120.0
C(62)-C(63)-H(63) 120.0
C(63)-C(64)-C(65) 120.0
C(63)-C(64)-H(64) 120.0
C(65)-C(64)-H(64) 120.0
C(64)-C(65)-C(66) 120.0
C(64)-C(65)-H(65) 120.0
C(66)-C(65)-H(65) 120.0
C(65)-C(66)-C(61) 120.0
C(65)-C(66)-H(66) 120.0
C(61)-C(66)-H(66) 120.0
C(72)-C(67)-C(68) 122.3(8)
C(72)-C(67)-O(18) 121.0(7)
C(68)-C(67)-O(18) 116.2(7)
C(69)-C(68)-C(67) 118.4(11)
C(69)-C(68)-H(68) 120.8
C(67)-C(68)-H(68) 120.8
C(68)-C(69)-C(70) 122.0(13)
C(68)-C(69)-H(69) 119.0
C(70)-C(69)-H(69) 119.0
C(69)-C(70)-C(71) 118.7(12)
C(69)-C(70)-H(70) 120.6
C(71)-C(70)-H(70) 120.6
C(70)-C(71)-C(72) 120.3(11)
C(70)-C(71)-H(71) 119.8
C(72)-C(71)-H(71) 119.8
C(67)-C(72)-C(71) 118.1(10)
C(67)-C(72)-H(72) 120.9
C(71)-C(72)-H(72) 120.9
O(19)-C(73)-C(74) 112.1(7)
O(19)-C(73)-H(73A) 109.2
C(74)-C(73)-H(73A) 109.2
O(19)-C(73)-H(73B) 109.2
C(74)-C(73)-H(73B) 109.2
H(73A)-C(73)-H(73B) 107.9
C(73)-C(74)-H(74A) 109.5
C(73)-C(74)-H(74B) 109.5
H(74A)-C(74)-H(74B) 109.5
C(73)-C(74)-H(74C) 109.5
H(74A)-C(74)-H(74C) 109.5
H(74B)-C(74)-H(74C) 109.5
P(1)-N(1)-P(2) 125.6(3)
P(4)-N(2)-P(3) 125.7(3)
P(6)-N(3)-P(5) 125.3(3)
P(1)-O(1)-Dy(1) 133.6(2)
C(1)-O(2)-P(1) 125.7(4)
C(7)-O(3)-P(1) 126.3(4)
P(2)-O(4)-Dy(1) 139.2(2)
C(13)-O(5)-P(2) 122.9(4)
C(19)-O(6)-P(2) 122.8(4)
P(3)-O(7)-Dy(1) 141.2(2)
C(25)-O(8)-P(3) 124.1(4)
C(31)-O(9)-P(3) 121.8(4)
P(4)-O(10)-Dy(1) 138.9(2)
C(37)-O(11)-P(4) 129.9(4)
C(43)-O(12)-P(4) 126.2(4)
P(5)-O(13)-Dy(1) 140.2(3)
C(49)-O(14)-P(5) 127.2(4)
C(55)-O(15)-P(5) 118.7(4)
P(6)-O(16)-Dy(1) 136.5(2)
C(61)-O(17)-P(6) 125.6(3)
C(67)-O(18)-P(6) 121.9(4)
C(73)-O(19)-H(19) 109.5
O(1)-P(1)-N(1) 118.5(2)
O(1)-P(1)-O(2) 106.8(3)
N(1)-P(1)-O(2) 111.1(3)
O(1)-P(1)-O(3) 110.5(2)
N(1)-P(1)-O(3) 111.9(3)
O(2)-P(1)-O(3) 95.6(3)
O(4)-P(2)-O(5) 106.6(2)
O(4)-P(2)-N(1) 117.5(3)
O(5)-P(2)-N(1) 112.5(3)
O(4)-P(2)-O(6) 111.4(2)
O(5)-P(2)-O(6) 98.8(2)
N(1)-P(2)-O(6) 108.5(2)
O(7)-P(3)-N(2) 118.1(3)
O(7)-P(3)-O(8) 105.5(2)
N(2)-P(3)-O(8) 111.8(3)
O(7)-P(3)-O(9) 111.4(3)
N(2)-P(3)-O(9) 108.8(3)
O(8)-P(3)-O(9) 99.7(2)
O(10)-P(4)-N(2) 119.0(3)
O(10)-P(4)-O(12) 110.5(3)
N(2)-P(4)-O(12) 107.8(4)
O(10)-P(4)-O(11) 106.2(3)
N(2)-P(4)-O(11) 110.7(3)
O(12)-P(4)-O(11) 101.0(4)
O(13)-P(5)-O(15) 118.0(3)
O(13)-P(5)-N(3) 118.6(3)
O(15)-P(5)-N(3) 110.3(3)
O(13)-P(5)-O(14) 100.3(3)
O(15)-P(5)-O(14) 95.9(4)
N(3)-P(5)-O(14) 110.3(3)
O(16)-P(6)-N(3) 118.7(3)
O(16)-P(6)-O(18) 110.4(2)
N(3)-P(6)-O(18) 108.5(3)
O(16)-P(6)-O(17) 107.6(2)
N(3)-P(6)-O(17) 111.2(3)
O(18)-P(6)-O(17) 98.6(3)
O(13)-Dy(1)-O(7) 169.87(16)
O(13)-Dy(1)-O(4) 87.59(17)
O(7)-Dy(1)-O(4) 84.21(14)
O(13)-Dy(1)-O(16) 78.13(14)
O(7)-Dy(1)-O(16) 105.85(14)

O(4)-Dy(1)-O(16) 78.14(14)	O(16)-Dy(1)-O(1) 151.15(14)	O(16)-Dy(1)-O(10) 78.33(14)
O(13)-Dy(1)-O(1) 85.86(15)	O(13)-Dy(1)-O(10) 114.02(17)	O(1)-Dy(1)-O(10) 130.42(14)
O(7)-Dy(1)-O(1) 86.56(15)	O(7)-Dy(1)-O(10) 76.07(14)	
O(4)-Dy(1)-O(1) 77.36(14)	O(4)-Dy(1)-O(10) 143.63(15)	

Symmetry transformations used to generate equivalent atoms:

Table 4. Anisotropic displacement parameters ($Å^2 x\ 10^3$)for ddx2m. The anisotropic displacement factor exponent takes the form: $-2\pi^2[\ h^2 a^{*2} U^{11} + ... + 2\ h\ k\ a^*\ b^*\ U^{12}\ ]$

	U^{11}	U^{22}	U^{33}	U^{23}	U^{13}	U^{12}
C(1)	40(4)	58(4)	73(5)	-23(4)	-3(3)	-10(3)
C(2)	85(6)	70(5)	55(5)	-5(4)	5(4)	-6(4)
C(3)	97(6)	79(6)	76(6)	4(5)	-1(5)	-11(5)
C(4)	80(6)	63(5)	95(7)	-24(5)	2(5)	-15(4)
C(5)	73(5)	71(5)	67(5)	-24(4)	19(4)	-13(4)
C(6)	64(5)	60(5)	62(5)	-3(3)	12(4)	-7(3)
C(7)	78(5)	42(4)	43(4)	-3(3)	-18(3)	14(3)
C(8)	53(5)	88(6)	77(5)	-10(4)	3(4)	0(4)
C(9)	75(5)	87(6)	93(6)	-10(5)	-26(5)	35(5)
C(10)	100(7)	80(6)	86(6)	26(5)	-20(5)	13(5)
C(11)	82(6)	121(8)	83(6)	15(5)	8(5)	7(5)
C(12)	64(5)	95(6)	75(5)	4(4)	10(4)	13(4)
C(13)	62(4)	41(4)	62(4)	-6(3)	0(3)	10(3)
C(14)	68(5)	70(5)	114(7)	-18(5)	10(5)	7(4)
C(15)	82(6)	97(7)	140(9)	-39(6)	31(6)	22(5)
C(16)	100(7)	86(7)	125(8)	-40(6)	2(6)	29(6)
C(17)	78(6)	81(6)	132(8)	-43(5)	-20(6)	18(5)
C(18)	62(5)	63(5)	114(7)	-13(4)	1(4)	14(4)
C(19)	30(3)	49(4)	65(5)	7(3)	4(3)	-2(3)
C(20)	54(4)	62(4)	64(5)	-3(4)	11(3)	6(3)
C(21)	60(5)	93(6)	58(5)	15(4)	13(4)	1(4)
C(22)	57(5)	76(6)	78(6)	27(4)	7(4)	-3(4)
C(23)	81(5)	51(5)	88(6)	6(4)	6(4)	-3(4)
C(24)	63(4)	52(4)	56(4)	-2(3)	0(3)	2(3)
C(25)	56(4)	45(4)	100(6)	0(4)	29(4)	6(3)
C(26)	100(7)	53(5)	132(8)	18(5)	35(6)	12(4)
C(27)	158(12)	71(8)	202(15)	41(8)	94(11)	36(8)
C(28)	145(13)	84(10)	280(30)	-61(12)	119(16)	-26(9)
C(29)	97(9)	156(13)	213(17)	-106(11)	60(10)	-55(9)
C(30)	76(6)	98(7)	112(8)	-32(6)	19(5)	-17(5)
C(31)	60(4)	56(4)	49(4)	10(3)	-1(3)	13(3)
C(32)	70(5)	64(5)	62(5)	-1(3)	3(4)	20(4)
C(33)	71(6)	93(6)	78(6)	0(5)	-10(4)	9(5)
C(34)	78(6)	119(8)	75(6)	7(5)	5(5)	45(6)
C(35)	129(8)	87(7)	83(6)	3(5)	12(6)	68(6)
C(36)	94(6)	61(5)	81(6)	0(4)	-2(5)	23(4)
C(37)	71(5)	87(6)	69(5)	-25(4)	-11(4)	14(4)
C(38)	99(7)	75(7)	198(12)	-50(7)	12(7)	9(5)
C(39)	249(18)	114(10)	221(16)	-91(10)	60(14)	-69(11)
C(40)	200(18)	350(30)	176(16)	-23(16)	-92(14)	-116(18)
C(41)	144(14)	300(20)	216(18)	73(17)	-71(12)	-36(14)
C(42)	147(11)	176(13)	136(11)	30(9)	-27(9)	27(9)
C(43)	95(6)	66(5)	66(5)	7(4)	31(4)	28(4)
C(44)	106(8)	167(11)	130(9)	57(8)	44(7)	54(7)
C(45)	133(12)	141(11)	360(20)	127(14)	106(14)	54(10)
C(46)	100(9)	90(9)	330(20)	0(10)	79(12)	10(7)
C(47)	118(10)	179(14)	238(17)	-96(13)	-37(11)	71(10)
C(48)	163(10)	107(8)	102(8)	-6(6)	16(8)	64(8)
C(49)	106(7)	42(4)	73(5)	5(3)	-32(5)	8(4)
C(50)	86(8)	175(12)	171(12)	7(10)	5(8)	-13(8)
C(51)	161(14)	203(17)	290(20)	-63(16)	37(14)	82(13)
C(52)	241(18)	160(13)	162(13)	-59(10)	-27(12)	121(13)
C(53)	234(14)	56(6)	82(7)	0(5)	-5(8)	0(7)
C(54)	90(6)	70(6)	98(6)	-11(4)	13(5)	-6(5)
C(55)	72(6)	161(10)	76(7)	39(7)	2(5)	-30(6)
C(56)	90(7)	122(8)	103(8)	24(6)	21(6)	-2(6)
C(57)	110(8)	138(9)	95(7)	41(7)	20(6)	2(7)
C(58)	138(10)	183(13)	130(10)	-5(9)	51(8)	31(9)
C(59)	252(18)	159(13)	150(13)	26(10)	63(12)	90(12)

C(60)	131(10)	94(8)	233(16)	74(10)	-20(10)	-5(7)
C(61)	39(4)	64(5)	80(5)	2(4)	0(3)	0(3)
C(62)	84(6)	78(6)	88(6)	-17(4)	8(5)	6(4)
C(63)	104(7)	78(7)	157(10)	-22(6)	20(7)	24(5)
C(64)	83(7)	81(7)	175(11)	9(7)	-2(7)	21(5)
C(65)	93(7)	114(8)	132(9)	43(7)	6(6)	45(6)
C(66)	88(6)	91(6)	99(7)	26(5)	9(5)	39(5)
C(67)	68(5)	69(5)	51(4)	-2(4)	-11(4)	-2(4)
C(68)	159(9)	89(6)	69(6)	16(5)	29(6)	8(6)
C(69)	202(14)	170(13)	106(10)	-8(9)	83(10)	3(11)
C(70)	144(11)	219(16)	85(9)	-29(10)	35(8)	47(11)
C(71)	166(11)	150(11)	100(9)	-43(8)	-28(8)	79(9)
C(72)	152(9)	99(7)	62(6)	-8(5)	-17(6)	50(6)
C(73)	68(5)	84(6)	93(6)	2(5)	-4(5)	0(4)
C(74)	98(7)	106(7)	118(8)	-10(6)	-34(6)	13(6)
N(1)	55(3)	53(3)	47(3)	-11(2)	4(3)	-6(2)
N(2)	73(4)	32(3)	61(4)	0(2)	4(3)	11(2)
N(3)	58(3)	53(3)	51(3)	8(2)	-6(3)	4(3)
O(1)	61(3)	52(3)	47(3)	-8(2)	-17(2)	14(2)
O(2)	52(3)	67(3)	76(3)	-19(2)	2(2)	-1(2)
O(3)	124(4)	61(3)	68(3)	-4(2)	-35(3)	23(3)
O(4)	58(3)	53(3)	48(3)	-6(2)	-4(2)	11(2)
O(5)	85(3)	50(3)	48(3)	-1(2)	4(2)	16(2)
O(6)	48(2)	48(3)	64(3)	3(2)	2(2)	8(2)
O(7)	74(3)	37(2)	54(3)	3(2)	13(2)	-2(2)
O(8)	54(3)	42(3)	82(3)	4(2)	9(2)	8(2)
O(9)	62(3)	62(3)	58(3)	17(2)	5(2)	7(2)
O(10)	67(3)	44(2)	50(3)	-5(2)	6(2)	0(2)
O(11)	191(7)	85(4)	72(4)	2(3)	-41(4)	-56(4)
O(12)	97(5)	59(4)	240(8)	-46(4)	92(5)	-13(3)
O(13)	64(3)	53(3)	89(4)	28(2)	-32(3)	-16(2)
O(14)	140(5)	73(4)	94(4)	-2(3)	-27(4)	-3(3)
O(15)	89(4)	123(5)	113(5)	45(4)	-13(4)	-34(4)
O(16)	56(3)	46(2)	41(2)	3(2)	-10(2)	-1(2)
O(17)	64(3)	64(3)	70(3)	9(2)	10(2)	13(2)
O(18)	68(3)	67(3)	45(3)	-1(2)	-14(2)	8(2)
O(19)	54(3)	65(3)	83(4)	-23(2)	-5(2)	-1(2)
P(1)	66(1)	45(1)	43(1)	-4(1)	-12(1)	11(1)
P(2)	55(1)	43(1)	48(1)	-3(1)	4(1)	5(1)
P(3)	57(1)	40(1)	55(1)	5(1)	3(1)	6(1)
P(4)	63(1)	49(1)	57(1)	-13(1)	5(1)	-2(1)
P(5)	62(1)	49(1)	62(1)	16(1)	-10(1)	-11(1)
P(6)	53(1)	49(1)	43(1)	3(1)	-4(1)	3(1)
Dy(1)	52(1)	37(1)	42(1)	0(1)	-4(1)	2(1)

Table 5. Hydrogen coordinates (x 10^4) and isotropic displacement parameters ($Å^2$x 10^3) for ddx2m.

	x	y	z	U(eq)		x	y	z	U(eq)
H(2)	-1562	-310	2015	86		H(29)	5904	7347	2991	195
H(3)	-1597	-1677	1711	104		H(30)	4739	5993	2940	118
H(4)	-1472	-2018	745	98		H(32)	-761	4132	1394	77
H(5)	-1269	-1005	64	87		H(33)	-3080	4228	1292	97
H(6)	-1204	376	358	76		H(34)	-3877	5450	1474	105
H(8)	-3116	2668	467	89		H(35)	-2393	6617	1712	113
H(9)	-3236	3860	-58	100		H(36)	-73	6559	1845	93
H(10)	-1284	4563	-444	106		H(38)	1688	6493	3760	150
H(11)	787	4075	-305	115		H(39)	3339	7587	4057	244
H(12)	907	2883	220	93		H(40)	5417	7322	4445	312
H(14)	5239	640	1243	101		H(41)	5844	5961	4534	272
H(15)	5721	-440	650	126		H(42)	4192	4866	4237	184
H(16)	3999	-1439	320	123		H(44)	-1538	4109	4293	155
H(17)	1849	-1458	658	117		H(45)	-3747	3412	4254	246
H(18)	1397	-406	1286	95		H(46)	-5203	3589	3473	205
H(20)	3818	2079	25	72		H(47)	-4451	4463	2732	211
H(21)	3840	3204	-566	85		H(48)	-2242	5160	2771	143
H(22)	3747	4510	-171	85		H(50)	2564	-483	2709	176
H(23)	3615	4679	806	89		H(51)	2948	-1860	2699	256
H(24)	3598	3567	1416	69		H(52)	1176	-2910	2866	216
H(26)	3355	6349	1339	113		H(53)	-979	-2583	3043	151
H(27)	4536	7711	1379	167		H(54)	-1363	-1207	3053	105
H(28)	5765	8145	2194	207		H(56)	-1033	-290	4507	127

H(57)	-1769	126	5399	138	H(69)	1263	1984	5891	192
H(58)	-2442	1429	5513	178	H(70)	457	3228	5791	176
H(59)	-2380	2317	4735	216	H(71)	954	3987	4969	161
H(60)	-1644	1900	3844	185	H(72)	2196	3454	4232	122
H(62)	5027	726	2583	101	H(73A)	-3285	2188	2907	100
H(63)	5965	-499	2668	134	H(73B)	-2475	1746	2449	100
H(64)	6072	-1117	3563	135	H(74A)	-4372	2146	2011	162
H(65)	5242	-511	4374	131	H(74B)	-3067	2638	1750	162
H(66)	4304	713	4289	108	H(74C)	-3887	3072	2208	162
H(68)	2465	1455	5181	127	H(19)	-1730	3216	2938	103

B7 Crystallographic Data for $Er(tpOp)_3$

Table 2. Atomic coordinates (x 10^4) and equivalent isotropic displacement parameters ($Å^2$x 10^3) for ertpopm. U(eq) is defined as one third of the trace of the orthogonalized U^{ij} tensor.

	x	y	z	U(eq)	x	y	z	U(eq)	
C(1)	-237(5)	5322(3)	1635(2)	55(1)	C(51)	2508(7)	-1039(4)	786(4)	96(2)
C(2)	-1120(6)	4626(4)	1467(2)	65(1)	C(52)	3809(8)	-1031(5)	588(4)	102(2)
C(3)	-2492(7)	4691(4)	1403(3)	79(2)	C(53)	4814(8)	-423(5)	769(4)	106(3)
C(4)	-2959(7)	5431(6)	1502(3)	88(2)	C(54)	4533(7)	216(4)	1135(3)	84(2)
C(5)	-2068(8)	6120(5)	1662(3)	94(2)	C(55)	3680(4)	2713(3)	782(2)	47(1)
C(6)	-685(2)	6089(1)	1740(1)	78(2)	C(56)	3619(5)	3487(3)	1022(2)	61(1)
C(7)	3946(2)	6018(1)	2146(1)	67(2)	C(57)	3656(6)	4159(4)	661(3)	71(2)
C(8)	3878(2)	6535(1)	1675(1)	93(2)	C(58)	3743(5)	4052(4)	72(3)	70(2)
C(9)	4561(2)	7343(1)	1706(1)	144(5)	C(59)	3807(6)	3275(4)	-161(3)	72(2)
C(10)	5312(2)	7633(1)	2207(1)	181(7)	C(60)	3785(5)	2597(4)	195(2)	61(1)
C(11)	5381(2)	7116(1)	2678(1)	165(6)	C(61)	-1346(5)	157(3)	1213(2)	56(1)
C(12)	4698(2)	6309(1)	2647(1)	97(2)	C(62)	-1514(6)	-447(4)	1615(2)	71(2)
C(13)	-1692(2)	4681(1)	3550(1)	71(2)	C(63)	-1558(7)	-1266(4)	1438(3)	86(2)
C(14)	-2472(2)	4836(1)	3063(1)	115(3)	C(64)	-1464(7)	-1462(4)	854(3)	81(2)
C(15)	-3806(2)	4446(1)	2990(1)	152(4)	C(65)	-1337(6)	-862(4)	455(3)	72(2)
C(16)	-4359(2)	3900(1)	3405(1)	140(4)	C(66)	-1285(5)	-32(4)	626(2)	65(1)
C(17)	-3579(2)	3745(1)	3892(1)	180(6)	C(67)	-1057(5)	2686(3)	380(2)	50(1)
C(18)	-2245(2)	4136(1)	3965(1)	133(4)	C(68)	-2315(6)	2958(4)	314(3)	74(2)
C(19)	2807(2)	5555(1)	3991(1)	74(2)	C(69)	-2366(7)	3684(4)	-18(3)	82(2)
C(20)	2444(2)	6342(1)	3905(1)	126(3)	C(70)	-1189(8)	4062(4)	-232(3)	85(2)
C(21)	3351(2)	7046(1)	4066(1)	203(7)	C(71)	-20(7)	3767(5)	-143(3)	94(2)
C(22)	4621(2)	6963(1)	4313(1)	245(10)	C(72)	52(6)	3087(4)	162(3)	74(2)
C(23)	4984(2)	6177(1)	4398(1)	201(7)	C(73)	-2735(6)	2270(4)	2562(3)	78(2)
C(24)	4077(2)	5472(1)	4237(1)	154(4)	C(74)	-3574(7)	2562(5)	2081(4)	103(2)
C(25)	-1258(2)	741(1)	4106(1)	87(2)	N(1)	1362(4)	5240(2)	2789(2)	56(1)
C(26)	-1596(2)	1488(1)	4140(1)	108(2)	N(2)	1605(4)	1032(2)	3622(2)	53(1)
C(27)	-2035(2)	1786(1)	4690(1)	161(4)	N(3)	1139(4)	1490(3)	1103(2)	53(1)
C(28)	-2127(2)	1222(1)	5180(1)	139(4)	O(1)	1704(4)	3957(2)	2133(1)	55(1)
C(29)	-1746(2)	468(1)	5088(1)	113(3)	O(2)	1165(3)	5286(2)	1675(2)	61(1)
C(30)	-1303(2)	237(1)	4554(1)	99(2)	O(3)	3397(3)	5200(2)	2102(2)	59(1)
C(31)	592(2)	-712(1)	2863(1)	72(2)	O(4)	547(3)	3809(2)	3244(1)	55(1)
C(32)	-519(2)	-1309(1)	2956(1)	82(2)	O(5)	-437(5)	5079(3)	3546(3)	134(3)
C(33)	-355(2)	-2146(1)	2966(1)	115(3)	O(6)	1859(6)	4902(3)	3854(2)	118(2)
C(34)	921(2)	-2385(1)	2884(1)	167(5)	O(7)	-43(4)	1483(2)	2828(2)	71(1)
C(35)	2032(2)	-1787(1)	2791(1)	199(7)	O(8)	-858(4)	394(3)	3555(2)	95(1)
C(36)	1867(2)	-951(1)	2781(1)	138(4)	O(9)	431(5)	83(3)	2752(2)	89(1)
C(37)	2404(6)	2400(3)	4645(2)	62(1)	O(10)	2357(3)	2548(2)	3267(1)	49(1)
C(38)	1968(8)	3149(5)	4574(3)	97(2)	O(11)	3236(4)	2097(2)	4234(1)	60(1)
C(39)	1242(10)	3461(6)	5017(4)	126(3)	O(12)	4077(4)	1592(2)	3344(2)	63(1)
C(40)	1000(11)	3027(9)	5513(5)	144(4)	O(13)	2379(3)	2185(2)	2047(1)	53(1)
C(41)	1454(13)	2277(8)	5569(4)	154(4)	O(14)	2975(4)	840(2)	1711(1)	60(1)
C(42)	2193(9)	1964(5)	5137(3)	107(3)	O(15)	3705(3)	2026(2)	1132(2)	55(1)
C(43)	4582(5)	836(3)	3421(3)	61(1)	O(16)	-332(3)	2422(2)	1680(1)	53(1)
C(44)	4651(7)	478(5)	3948(3)	91(2)	O(17)	-1302(3)	976(2)	1426(2)	65(1)
C(45)	5197(8)	-254(5)	3996(4)	105(3)	O(18)	-1117(5)	1920(2)	664(2)	78(1)
C(46)	5673(8)	-610(5)	3525(5)	113(3)	O(19)	-1534(3)	2865(2)	2702(2)	67(1)
C(47)	5642(8)	-243(5)	3000(5)	107(3)	P(1)	1848(1)	4875(1)	2208(1)	48(1)
C(48)	5060(6)	488(4)	2941(3)	83(2)	P(2)	831(1)	4720(1)	3314(1)	56(1)
C(49)	3251(5)	211(3)	1315(2)	56(1)	P(3)	299(1)	841(1)	3215(1)	58(1)
C(50)	2234(6)	-411(4)	1156(3)	77(2)	P(4)	2702(1)	1820(1)	3591(1)	48(1)

P(5)	2449(1)	1667(1)	1512(1)	47(1)	Er(1)	804(1)	2770(1)	2555(1)	42(1)
P(6)	-278(1)	1750(1)	1238(1)	50(1)					

Table 3. Bond lengths [Å] and angles [°] for ertpopm.

C(1)-C(2)	1.371(8)	C(57)-C(58)	1.368(8)	O(5)-C(13)-C(18)	127.4(3)
C(1)-C(6)	1.396(5)	C(58)-C(59)	1.369(9)	C(14)-C(13)-C(18)	120.0
C(1)-O(2)	1.400(6)	C(59)-C(60)	1.384(8)	C(15)-C(14)-C(13)	120.0
C(2)-C(3)	1.383(8)	C(61)-C(62)	1.360(8)	C(14)-C(15)-C(16)	120.0
C(3)-C(4)	1.363(9)	C(61)-C(66)	1.382(7)	C(17)-C(16)-C(15)	120.0
C(4)-C(5)	1.362(10)	C(61)-O(17)	1.401(6)	C(18)-C(17)-C(16)	120.0
C(5)-C(6)	1.386(8)	C(62)-C(63)	1.376(9)	C(17)-C(18)-C(13)	120.0
C(7)-O(3)	1.365(3)	C(63)-C(64)	1.382(9)	O(6)-C(19)-C(20)	117.0(3)
C(7)-C(8)	1.3900	C(64)-C(65)	1.350(9)	O(6)-C(19)-C(24)	123.0(3)
C(7)-C(12)	1.3900	C(65)-C(66)	1.388(8)	C(20)-C(19)-C(24)	120.0
C(8)-C(9)	1.3900	C(67)-C(72)	1.318(8)	C(21)-C(20)-C(19)	120.0
C(9)-C(10)	1.3900	C(67)-C(68)	1.385(7)	C(20)-C(21)-C(22)	120.0
C(10)-C(11)	1.3900	C(67)-O(18)	1.411(6)	C(21)-C(22)-C(23)	120.0
C(11)-C(12)	1.3900	C(68)-C(69)	1.424(9)	C(24)-C(23)-C(22)	120.0
C(13)-O(5)	1.322(5)	C(69)-C(70)	1.355(9)	C(23)-C(24)-C(19)	120.0
C(13)-C(14)	1.3900	C(70)-C(71)	1.325(9)	C(26)-C(25)-C(30)	123.0
C(13)-C(18)	1.3900	C(71)-C(72)	1.330(9)	C(26)-C(25)-O(8)	121.07(19)
C(14)-C(15)	1.3900	C(73)-O(19)	1.451(6)	C(30)-C(25)-O(8)	115.89(18)
C(15)-C(16)	1.3900	C(73)-C(74)	1.489(9)	C(25)-C(26)-C(27)	118.8
C(16)-C(17)	1.3900	N(1)-P(2)	1.553(4)	C(26)-C(27)-C(28)	118.4
C(17)-C(18)	1.3900	N(1)-P(1)	1.566(4)	C(29)-C(28)-C(27)	117.0
C(19)-O(6)	1.340(5)	N(2)-P(3)	1.566(4)	C(28)-C(29)-C(30)	121.1
C(19)-C(20)	1.3900	N(2)-P(4)	1.567(4)	C(25)-C(30)-C(29)	121.7
C(19)-C(24)	1.3900	N(3)-P(6)	1.560(4)	O(9)-C(31)-C(32)	121.3(2)
C(20)-C(21)	1.3900	N(3)-P(5)	1.570(4)	O(9)-C(31)-C(36)	117.7(2)
C(21)-C(22)	1.3900	O(1)-P(1)	1.482(3)	C(32)-C(31)-C(36)	120.0
C(22)-C(23)	1.3900	O(1)-Er(1)	2.262(3)	C(31)-C(32)-C(33)	120.0
C(23)-C(24)	1.3900	O(2)-P(1)	1.587(3)	C(34)-C(33)-C(32)	120.0
C(25)-C(26)	1.3022	O(3)-P(1)	1.582(4)	C(33)-C(34)-C(35)	120.0
C(25)-C(30)	1.3282	O(4)-P(2)	1.471(3)	C(36)-C(35)-C(34)	120.0
C(25)-O(8)	1.464(6)	O(4)-Er(1)	2.332(3)	C(35)-C(36)-C(31)	120.0
C(26)-C(27)	1.4434	O(5)-P(2)	1.560(5)	C(42)-C(37)-C(38)	122.4(7)
C(27)-C(28)	1.4651	O(6)-P(2)	1.579(5)	C(42)-C(37)-O(11)	117.2(6)
C(28)-C(29)	1.3435	O(7)-P(3)	1.455(4)	C(38)-C(37)-O(11)	120.0(5)
C(29)-C(30)	1.3777	O(7)-Er(1)	2.253(3)	C(37)-C(38)-C(39)	118.2(7)
C(31)-O(9)	1.349(4)	O(8)-P(3)	1.519(4)	C(40)-C(39)-C(38)	120.4(9)
C(31)-C(32)	1.3900	O(9)-P(3)	1.630(5)	C(41)-C(40)-C(39)	119.7(9)
C(31)-C(36)	1.3900	O(10)-P(4)	1.485(3)	C(40)-C(41)-C(42)	120.6(9)
C(32)-C(33)	1.3900	O(10)-Er(1)	2.281(3)	C(37)-C(42)-C(41)	118.6(9)
C(33)-C(34)	1.3900	O(11)-P(4)	1.589(3)	C(48)-C(43)-C(44)	121.0(6)
C(34)-C(35)	1.3900	O(12)-P(4)	1.579(4)	C(48)-C(43)-O(12)	116.2(5)
C(35)-C(36)	1.3900	O(13)-P(5)	1.482(3)	C(44)-C(43)-O(12)	122.8(5)
C(37)-C(42)	1.355(8)	O(13)-Er(1)	2.275(3)	C(43)-C(44)-C(45)	119.8(7)
C(37)-C(38)	1.357(8)	O(14)-P(5)	1.577(3)	C(46)-C(45)-C(44)	120.2(8)
C(37)-O(11)	1.399(7)	O(15)-P(5)	1.597(3)	C(45)-C(46)-C(47)	120.3(8)
C(38)-C(39)	1.391(11)	O(16)-P(6)	1.482(3)	C(46)-C(47)-C(48)	120.1(8)
C(39)-C(40)	1.366(14)	O(16)-Er(1)	2.297(3)	C(43)-C(48)-C(47)	118.5(7)
C(40)-C(41)	1.361(14)	O(17)-P(6)	1.581(4)	C(54)-C(49)-C(50)	121.9(5)
C(41)-C(42)	1.381(12)	O(18)-P(6)	1.589(4)	C(54)-C(49)-O(14)	119.0(5)
C(43)-C(48)	1.357(8)			C(50)-C(49)-O(14)	119.0(5)
C(43)-C(44)	1.359(9)	C(2)-C(1)-C(6)	121.9(5)	C(49)-C(50)-C(51)	119.2(6)
C(43)-O(12)	1.400(6)	C(2)-C(1)-O(2)	120.0(5)	C(50)-C(51)-C(52)	119.5(6)
C(44)-C(45)	1.377(9)	C(6)-C(1)-O(2)	118.1(4)	C(53)-C(52)-C(51)	120.3(6)
C(45)-C(46)	1.344(12)	C(1)-C(2)-C(3)	118.7(6)	C(52)-C(53)-C(54)	120.2(7)
C(46)-C(47)	1.361(12)	C(4)-C(3)-C(2)	120.8(7)	C(49)-C(54)-C(53)	118.9(6)
C(47)-C(48)	1.397(10)	C(5)-C(4)-C(3)	119.9(6)	C(60)-C(55)-C(56)	121.2(5)
C(49)-C(54)	1.349(8)	C(4)-C(5)-C(6)	121.8(6)	C(60)-C(55)-O(15)	117.9(4)
C(49)-C(50)	1.361(8)	C(5)-C(6)-C(1)	116.9(4)	C(56)-C(55)-O(15)	120.8(4)
C(49)-O(14)	1.412(6)	O(3)-C(7)-C(8)	120.68(17)	C(55)-C(56)-C(57)	119.1(5)
C(50)-C(51)	1.372(9)	O(3)-C(7)-C(12)	118.99(17)	C(58)-C(57)-C(56)	120.5(6)
C(51)-C(52)	1.380(10)	C(8)-C(7)-C(12)	120.0	C(57)-C(58)-C(59)	119.7(6)
C(52)-C(53)	1.352(10)	C(9)-C(8)-C(7)	120.0	C(58)-C(59)-C(60)	120.5(6)
C(53)-C(54)	1.384(9)	C(8)-C(9)-C(10)	120.0	C(55)-C(60)-C(59)	119.0(5)
C(55)-C(60)	1.368(7)	C(9)-C(10)-C(11)	120.0	C(62)-C(61)-C(66)	121.7(5)
C(55)-C(56)	1.370(7)	C(12)-C(11)-C(10)	120.0	C(62)-C(61)-O(17)	116.0(5)
C(55)-O(15)	1.392(6)	C(11)-C(12)-C(7)	120.0	C(66)-C(61)-O(17)	122.2(5)
C(56)-C(57)	1.384(8)	O(5)-C(13)-C(14)	112.6(3)	C(61)-C(62)-C(63)	119.4(6)

C(62)-C(63)-C(64)	119.5(6)	C(49)-O(14)-P(5)	123.0(3)	O(13)-P(5)-N(3)	117.9(2)
C(65)-C(64)-C(63)	120.9(6)	C(55)-O(15)-P(5)	122.6(3)	O(13)-P(5)-O(14)	106.52(19)
C(64)-C(65)-C(66)	120.4(6)	P(6)-O(16)-Er(1)	133.48(18)	N(3)-P(5)-O(14)	112.2(2)
C(61)-C(66)-C(65)	118.1(6)	C(61)-O(17)-P(6)	125.7(3)	O(13)-P(5)-O(15)	111.21(19)
C(72)-C(67)-C(68)	122.1(5)	C(67)-O(18)-P(6)	126.0(3)	N(3)-P(5)-O(15)	108.7(2)
C(72)-C(67)-O(18)	124.6(5)	O(1)-P(1)-N(1)	117.6(2)	O(14)-P(5)-O(15)	98.74(19)
C(68)-C(67)-O(18)	113.1(5)	O(1)-P(1)-O(3)	105.83(19)	O(16)-P(6)-N(3)	118.2(2)
C(67)-C(68)-C(69)	116.7(5)	N(1)-P(1)-O(3)	111.9(2)	O(16)-P(6)-O(17)	106.9(2)
C(70)-C(69)-C(68)	118.0(5)	O(1)-P(1)-O(2)	111.5(2)	N(3)-P(6)-O(17)	111.0(2)
C(71)-C(70)-C(69)	121.6(6)	N(1)-P(1)-O(2)	109.1(2)	O(16)-P(6)-O(18)	110.4(2)
C(70)-C(71)-C(72)	121.4(7)	O(3)-P(1)-O(2)	99.44(19)	N(3)-P(6)-O(18)	112.3(2)
C(67)-C(72)-C(71)	120.1(6)	O(4)-P(2)-N(1)	119.0(2)	O(17)-P(6)-O(18)	95.6(2)
O(19)-C(73)-C(74)	111.3(5)	O(4)-P(2)-O(5)	110.6(2)	O(7)-Er(1)-O(1)	170.22(13)
P(2)-N(1)-P(1)	125.3(3)	N(1)-P(2)-O(5)	108.3(3)	O(7)-Er(1)-O(13)	88.09(14)
P(3)-N(2)-P(4)	125.1(3)	O(4)-P(2)-O(6)	106.2(2)	O(1)-Er(1)-O(13)	84.27(12)
P(6)-N(3)-P(5)	125.3(2)	N(1)-P(2)-O(6)	110.3(3)	O(7)-Er(1)-O(10)	79.04(11)
P(1)-O(1)-Er(1)	141.8(2)	O(5)-P(2)-O(6)	100.9(4)	O(1)-Er(1)-O(10)	105.15(12)
C(1)-O(2)-P(1)	121.9(3)	O(7)-P(3)-O(8)	116.6(3)	O(13)-Er(1)-O(10)	77.62(11)
C(7)-O(3)-P(1)	123.8(2)	O(7)-P(3)-N(2)	118.7(2)	O(7)-Er(1)-O(16)	86.01(13)
P(2)-O(4)-Er(1)	139.0(2)	O(8)-P(3)-N(2)	109.5(2)	O(1)-Er(1)-O(16)	86.41(12)
C(13)-O(5)-P(2)	125.9(3)	O(7)-P(3)-O(9)	101.2(2)	O(13)-Er(1)-O(16)	77.84(11)
C(19)-O(6)-P(2)	131.3(3)	O(8)-P(3)-O(9)	97.1(3)	O(10)-Er(1)-O(16)	151.57(11)
P(3)-O(7)-Er(1)	139.7(2)	N(2)-P(3)-O(9)	111.2(2)	O(7)-Er(1)-O(4)	113.49(14)
C(25)-O(8)-P(3)	121.2(3)	O(10)-P(4)-N(2)	119.0(2)	O(1)-Er(1)-O(4)	76.20(11)
C(31)-O(9)-P(3)	128.4(3)	O(10)-P(4)-O(12)	107.00(19)	O(13)-Er(1)-O(4)	143.26(12)
P(4)-O(10)-Er(1)	135.99(18)	N(2)-P(4)-O(12)	111.5(2)	O(10)-Er(1)-O(4)	77.92(12)
C(37)-O(11)-P(4)	122.5(3)	O(10)-P(4)-O(11)	110.39(19)	O(16)-Er(1)-O(4)	130.46(11)
C(43)-O(12)-P(4)	125.3(3)	N(2)-P(4)-O(11)	108.6(2)		
P(5)-O(13)-Er(1)	139.0(2)	O(12)-P(4)-O(11)	98.5(2)		

Symmetry transformations used to generate equivalent atoms:

Table 4. Anisotropic displacement parameters ($Å^2 x\ 10^3$)for ertpopm. The anisotropic displacement factor exponent takes the form: $-2\pi^2[\ h^2 a^{*2} U^{11} + ... + 2\ h\ k\ a^*\ b^*\ U^{12}\ ]$

	U^{11}	U^{22}	U^{33}	U^{23}	U^{13}	U^{12}
C(1)	68(3)	56(3)	44(3)	12(2)	1(2)	18(2)
C(2)	69(4)	64(4)	64(3)	2(3)	-2(3)	15(3)
C(3)	71(4)	93(5)	74(4)	-1(3)	-9(3)	14(3)
C(4)	74(4)	131(7)	67(4)	6(4)	0(3)	45(4)
C(5)	115(6)	92(5)	87(5)	0(4)	3(4)	64(5)
C(6)	104(5)	58(4)	77(4)	-1(3)	0(4)	27(3)
C(7)	57(3)	45(3)	100(4)	-3(3)	25(3)	8(2)
C(8)	99(5)	58(4)	127(6)	21(4)	37(4)	15(3)
C(9)	154(8)	53(4)	237(12)	39(6)	110(9)	26(5)
C(10)	145(9)	82(7)	305(18)	-75(9)	126(11)	-33(6)
C(11)	100(6)	138(9)	239(13)	-111(9)	63(8)	-48(6)
C(12)	72(4)	94(5)	117(6)	-33(4)	18(4)	-11(4)
C(13)	80(4)	58(3)	79(4)	-2(3)	25(3)	22(3)
C(14)	138(7)	102(6)	113(6)	-12(5)	9(6)	47(6)
C(15)	158(10)	138(9)	170(11)	-28(8)	10(8)	60(8)
C(16)	86(6)	104(7)	232(14)	-4(8)	18(7)	24(5)
C(17)	121(8)	110(7)	319(18)	80(9)	96(10)	23(6)
C(18)	130(7)	156(9)	131(7)	66(7)	43(6)	65(6)
C(19)	88(4)	72(4)	58(3)	-26(3)	-17(3)	9(3)
C(20)	124(7)	73(5)	179(9)	-47(5)	11(6)	11(5)
C(21)	252(16)	129(10)	201(13)	-86(9)	28(12)	-53(10)
C(22)	270(20)	246(19)	177(14)	-6(13)	-70(13)	-112(16)
C(23)	139(10)	246(17)	189(12)	16(12)	-100(9)	-56(10)
C(24)	174(11)	169(10)	124(8)	22(7)	-45(7)	47(8)
C(25)	70(4)	99(5)	91(5)	18(4)	12(4)	-5(4)
C(26)	125(7)	95(6)	105(6)	23(5)	24(5)	16(5)
C(27)	205(12)	118(8)	178(11)	24(7)	54(9)	73(8)
C(28)	155(9)	150(9)	116(7)	9(7)	54(7)	20(7)
C(29)	124(7)	125(7)	91(6)	36(5)	21(5)	10(5)
C(30)	98(5)	108(6)	91(5)	32(5)	19(4)	8(4)
C(31)	100(5)	45(3)	69(4)	4(3)	-27(3)	7(3)
C(32)	88(4)	63(4)	93(5)	-1(3)	8(4)	-2(3)

C(33)	206(10)	60(4)	74(5)	3(4)	-5(5)	-4(5)
C(34)	251(16)	122(9)	140(9)	-30(7)	-11(10)	75(9)
C(35)	192(13)	158(12)	270(17)	-28(12)	48(12)	104(10)
C(36)	76(5)	161(9)	171(10)	3(8)	1(6)	-9(6)
C(37)	74(4)	62(3)	46(3)	-5(3)	-13(3)	-2(3)
C(38)	143(7)	95(5)	60(4)	-7(4)	-16(4)	49(5)
C(39)	157(8)	142(8)	89(6)	-35(6)	-24(6)	72(7)
C(40)	149(9)	192(12)	98(7)	-31(8)	38(6)	46(8)
C(41)	219(13)	145(9)	93(6)	1(6)	72(8)	-6(9)
C(42)	162(8)	86(5)	73(5)	21(4)	28(5)	10(5)
C(43)	44(3)	67(3)	71(4)	5(3)	-1(3)	10(2)
C(44)	92(5)	104(5)	87(5)	21(4)	9(4)	46(4)
C(45)	93(5)	110(6)	123(7)	41(5)	13(5)	48(5)
C(46)	77(5)	82(5)	186(10)	18(6)	3(6)	26(4)
C(47)	100(6)	78(5)	145(8)	-21(5)	16(5)	19(4)
C(48)	77(4)	80(4)	91(5)	-8(4)	4(4)	11(3)
C(49)	64(3)	45(3)	59(3)	-1(2)	-2(3)	15(2)
C(50)	65(4)	59(4)	107(5)	-16(3)	1(3)	16(3)
C(51)	84(5)	67(4)	137(6)	-34(4)	-27(4)	17(3)
C(52)	101(6)	89(5)	119(6)	-43(5)	-3(5)	35(4)
C(53)	84(5)	96(6)	143(7)	-33(5)	28(5)	25(4)
C(54)	72(4)	68(4)	112(5)	-22(4)	9(4)	8(3)
C(55)	40(2)	47(3)	53(3)	-1(2)	0(2)	0(2)
C(56)	65(3)	57(3)	59(3)	-2(3)	4(3)	1(2)
C(57)	77(4)	52(3)	82(4)	7(3)	5(3)	-1(3)
C(58)	57(3)	73(4)	78(4)	23(3)	3(3)	-3(3)
C(59)	61(3)	95(5)	57(3)	10(3)	8(3)	-1(3)
C(60)	57(3)	65(3)	57(3)	-6(3)	2(3)	3(2)
C(61)	40(3)	56(3)	67(3)	-22(3)	-1(2)	-5(2)
C(62)	86(4)	73(4)	51(3)	0(3)	1(3)	0(3)
C(63)	107(5)	67(4)	76(4)	3(3)	-1(4)	-13(3)
C(64)	84(4)	56(4)	96(5)	-18(4)	2(4)	-10(3)
C(65)	72(4)	68(4)	69(4)	-23(3)	13(3)	-13(3)
C(66)	60(3)	65(4)	63(3)	-5(3)	3(3)	-10(3)
C(67)	68(3)	46(3)	39(2)	-2(2)	-13(2)	18(2)
C(68)	56(3)	85(4)	75(4)	-12(3)	6(3)	-5(3)
C(69)	70(4)	90(5)	93(5)	-6(4)	-27(4)	39(4)
C(70)	96(5)	80(4)	80(4)	30(4)	-18(4)	15(4)
C(71)	78(5)	121(6)	82(5)	25(4)	2(4)	8(4)
C(72)	53(3)	93(5)	77(4)	5(4)	6(3)	16(3)
C(73)	54(3)	82(4)	93(5)	-1(3)	-7(3)	-6(3)
C(74)	86(5)	103(6)	117(6)	-10(5)	-28(4)	13(4)
N(1)	70(3)	41(2)	58(2)	-3(2)	3(2)	16(2)
N(2)	58(2)	51(2)	50(2)	10(2)	-6(2)	5(2)
N(3)	57(2)	58(2)	40(2)	-12(2)	3(2)	-6(2)
O(1)	76(2)	42(2)	46(2)	2(1)	12(2)	2(2)
O(2)	59(2)	63(2)	61(2)	20(2)	2(2)	9(2)
O(3)	57(2)	39(2)	82(2)	4(2)	6(2)	9(1)
O(4)	69(2)	48(2)	47(2)	-7(2)	3(2)	2(2)
O(5)	105(4)	59(3)	236(7)	-53(3)	88(4)	-8(2)
O(6)	182(5)	84(3)	70(3)	4(2)	-46(3)	-43(3)
O(7)	67(2)	53(2)	85(3)	26(2)	-32(2)	-16(2)
O(8)	79(3)	84(3)	113(4)	33(3)	-5(3)	-19(2)
O(9)	121(4)	65(3)	75(3)	1(2)	-16(3)	1(2)
O(10)	55(2)	46(2)	42(2)	4(1)	-11(1)	2(1)
O(11)	67(2)	67(2)	46(2)	1(2)	-16(2)	9(2)
O(12)	60(2)	66(2)	65(2)	12(2)	5(2)	11(2)
O(13)	58(2)	54(2)	48(2)	-8(2)	-7(2)	13(2)
O(14)	85(2)	50(2)	49(2)	-2(2)	3(2)	19(2)
O(15)	51(2)	53(2)	60(2)	2(2)	2(2)	9(2)
O(16)	62(2)	49(2)	50(2)	-7(2)	-15(2)	15(2)
O(17)	53(2)	63(2)	76(2)	-19(2)	4(2)	3(2)
O(18)	112(3)	57(2)	63(2)	-4(2)	-31(2)	14(2)
O(19)	50(2)	68(2)	79(3)	-22(2)	-2(2)	2(2)
P(1)	56(1)	36(1)	53(1)	4(1)	2(1)	7(1)
P(2)	63(1)	47(1)	54(1)	-13(1)	2(1)	-1(1)
P(3)	61(1)	49(1)	60(1)	16(1)	-11(1)	-9(1)
P(4)	52(1)	49(1)	42(1)	3(1)	-6(1)	4(1)
P(5)	55(1)	42(1)	44(1)	-3(1)	1(1)	6(1)
P(6)	64(1)	43(1)	42(1)	-3(1)	-14(1)	10(1)
Er(1)	51(1)	35(1)	40(1)	0(1)	-5(1)	3(1)

Table 5. Hydrogen coordinates (x 10^4) and isotropic displacement parameters ($Å^2$x 10^3) for ertpopm.

	x	y	z	U(eq)		x	y	z	U(eq)
H(2)	-802	4121	1398	78	H(41)	1264	1973	5902	185
H(3)	-3102	4224	1290	95	H(42)	2540	1464	5183	129
H(4)	-3885	5467	1460	105	H(44)	4329	727	4275	109
H(5)	-2397	6624	1720	112	H(45)	5237	-503	4355	126
H(6)	-84	6558	1857	94	H(46)	6025	-1110	3558	136
H(8)	3376	6340	1340	112	H(47)	6010	-480	2679	129
H(9)	4516	7688	1391	173	H(48)	5001	731	2580	99
H(10)	5769	8174	2228	217	H(50)	1364	-411	1295	92
H(11)	5883	7311	3013	199	H(51)	1823	-1466	670	116
H(12)	4743	5963	2962	116	H(52)	3994	-1446	328	122
H(14)	-2101	5200	2785	138	H(53)	5697	-435	648	128
H(15)	-4328	4549	2664	182	H(54)	5217	642	1255	101
H(16)	-5252	3639	3356	168	H(56)	3554	3559	1422	73
H(17)	-3949	3381	4169	216	H(57)	3621	4688	819	86
H(18)	-1723	4032	4291	160	H(58)	3758	4505	-169	84
H(20)	1594	6397	3740	151	H(59)	3866	3202	-561	87
H(21)	3108	7572	4009	243	H(60)	3841	2070	37	73
H(22)	5227	7435	4421	294	H(62)	-1597	-307	2005	85
H(23)	5833	6121	4563	241	H(63)	-1650	-1684	1709	103
H(24)	4320	4946	4294	185	H(64)	-1489	-2016	735	97
H(26)	-1555	1823	3817	129	H(65)	-1285	-1005	63	87
H(27)	-2253	2323	4732	193	H(66)	-1211	385	353	78
H(28)	-2435	1379	5538	167	H(68)	-3088	2680	478	88
H(29)	-1782	95	5390	136	H(69)	-3183	3892	-85	99
H(30)	-1027	-285	4506	119	H(70)	-1202	4540	-446	102
H(32)	-1372	-1149	3011	99	H(71)	768	4042	-298	112
H(33)	-1098	-2546	3028	139	H(72)	885	2895	222	88
H(34)	1031	-2944	2891	201	H(73A)	-3279	2186	2905	94
H(35)	2885	-1947	2736	239	H(73B)	-2459	1740	2449	94
H(36)	2610	-551	2719	166	H(74A)	-4353	2153	1995	154
H(38)	2151	3447	4238	116	H(74B)	-3039	2643	1741	154
H(39)	920	3969	4975	151	H(74C)	-3869	3079	2197	154
H(40)	528	3242	5811	173	H(19)	-1718	3206	2946	100

B8 Crystallographic Data for Gd(tpOp)$_3$

Table 2. Atomic coordinates (x 10^4) and equivalent isotropic displacement parameters ($Å^2$x 10^3) for ddx1m. U(eq) is defined as one third of the trace of the orthogonalized U^{ij} tensor.

	x	y	z	U(eq)		x	y	z	U(eq)
C(1)	11325(7)	4851(5)	8792(4)	57(2)		C(19)	6693(9)	4783(5)	8700(3)	58(2)
C(2)	11458(9)	5447(6)	8384(4)	73(3)		C(20)	5416(10)	4782(6)	8880(5)	88(3)
C(3)	11483(11)		6261(7)	8554(5)	92(3)	C(21)	5153(12)	5427(8)	9243(6)	111(4)
C(4)	11415(10)		6473(6)	9123(5)	83(3)	C(22)	6174(13)	6029(7)	9417(5)	105(4)
C(5)	11310(9)	5874(6)	9539(4)	77(3)		C(23)	7452(12)	6028(6)	9231(5)	103(4)
C(6)	11272(4)	5047(2)	9373(2)	67(2)		C(24)	7722(4)	5412(2)	8855(2)	84(3)
C(7)	11096(4)	2347(2)	9605(2)	53(2)		C(25)	9448(4)	5710(2)	7113(2)	75(3)
C(8)	12344(4)	2059(2)	9683(2)	73(3)		C(26)	8138(4)	5874(2)	7223(2)	148(5)
C(9)	12428(4)	1348(2)	9997(2)	84(3)		C(27)	7860(4)	6688(2)	7236(2)	201(8)
C(10)	11264(4)	924(2)	10233(2)	93(3)		C(28)	8892(4)	7337(2)	7138(2)	162(6)
C(11)	10016(4)	1212(2)	10156(2)	103(4)		C(29)	10201(4)	7173(2)	7028(2)	114(4)
C(12)	9932(4)	1924(2)	9841(2)	77(3)		C(30)	10479(4)	6360(2)	7015(2)	89(3)
C(13)	6317(7)	2285(5)	9237(3)	47(2)		C(31)	11274(4)	4229(2)	5908(2)	106(4)
C(14)	6242(8)	2388(5)	9822(4)	60(2)		C(32)	11683(4)	3450(2)	5852(2)	130(5)
C(15)	6229(8)	1719(6)	10169(4)	69(2)		C(33)	12133(4)	3189(2)	5324(2)	163(6)
C(16)	6263(9)	937(6)	9941(4)	71(2)		C(34)	12175(4)	3709(2)	4853(2)	147(5)
C(17)	6342(9)	840(6)	9356(4)	73(3)		C(35)	11766(4)	4488(2)	4909(2)	108(4)
C(18)	6351(8)	1509(5)	8994(4)	59(2)		C(36)	11316(4)	4748(2)	5437(2)	99(3)

C(37)	5406(8)	4172(6)	6560(4)	64(2)
C(38)	4920(11)	4530(7)	7040(5)	90(3)
C(39)	4339(13)	5246(8)	6983(7)	115(4)
C(40)	4301(12)	5615(8)	6461(8)	115(4)
C(41)	4807(12)	5266(8)	5995(6)	111(4)
C(42)	5343(5)	4535(3)	6041(2)	94(3)
C(43)	7591(5)	2600(3)	5370(2)	66(2)
C(44)	7885(5)	3038(3)	4868(2)	114(4)
C(45)	8610(5)	2707(3)	4437(2)	166(7)
C(46)	9042(5)	1937(3)	4507(2)	147(6)
C(47)	8748(5)	1499(3)	5009(2)	135(5)
C(48)	8023(5)	1830(3)	5440(2)	104(4)
C(49)	10193(9)	-333(5)	8366(3)	57(2)
C(50)	10661(12)		-1076(6)	8269(4) 81(3)
C(51)	12060(15)		-1104(8)	8337(5) 101(4)
C(52)	12950(12)		-399(10)	8493(4) 94(3)
C(53)	12450(11)		316(7)	8596(4) 83(3)
C(54)	11071(10)		365(6)	8537(4) 68(2)
C(55)	5980(9)	-1072(5)	7873(4)	68(2)
C(56)	5253(11)	-1344(7)	7379(5)	97(3)
C(57)	4534(14)	-2179(9)	7345(7)	132(5)
C(58)	4697(14)	-2628(9)	7826(8)	125(4)
C(59)	5389(14)	-2398(9)	8308(7)	126(4)
C(60)	6077(4)	-1570(2)	8339(2)	97(3)
C(61)	7232(4)	-593(2)	6040(2)	78(3)
C(62)	7448(4)	-1414(2)	6096(2)	120(4)
C(63)	6431(4)	-2054(2)	5920(2)	179(7)
C(64)	5198(4)	-1874(2)	5687(2)	204(8)
C(65)	4982(4)	-1053(2)	5631(2)	196(8)
C(66)	5999(4)	-413(2)	5807(2)	162(6)
C(67)	11681(4)	280(2)	6477(2)	76(3)
C(68)	12587(4)	200(2)	6937(2)	123(4)
C(69)	13904(4)	630(2)	6940(2)	168(6)
C(70)	14314(4)	1139(2)	6484(2)	145(5)
C(71)	13408(4)	1219(2)	6024(2)	169(6)
C(72)	12092(4)	789(2)	6021(2)	132(5)
C(73)	12765(11)		2728(7)	7433(5) 99(3)
C(74)	13646(13)		2454(8)	7905(5) 121(4)
N(1)	8851(6)	3517(4)	8903(3)	55(2)
N(2)	8388(6)	3975(4)	6373(3)	54(2)
N(3)	8580(7)	-271(4)	7225(3)	57(2)
O(1)	10336(5)	2584(3)	8337(2)	53(1)
O(2)	11288(5)	4034(3)	8588(2)	68(2)
O(3)	11084(7)	3095(4)	9349(3)	86(2)
O(4)	7564(5)	2813(3)	7972(2)	53(1)
O(5)	6265(5)	2972(3)	8888(2)	56(1)
O(6)	6974(6)	4158(3)	8309(2)	62(1)
O(7)	10027(6)	3544(3)	7174(3)	78(2)
O(8)	9582(9)	4923(4)	7234(3)	113(3)
O(9)	10840(8)	4630(5)	6443(4)	125(3)
O(10)	7616(5)	2462(3)	6721(2)	49(1)
O(11)	5900(5)	3421(4)	6638(2)	67(2)
O(12)	6765(6)	2915(3)	5758(2)	65(2)
O(13)	8232(5)	1004(3)	7881(2)	57(1)
O(14)	8793(6)	-320(3)	8333(2)	61(1)
O(15)	6549(5)	-242(3)	7913(2)	61(1)
O(16)	9436(5)	1151(3)	6764(2)	55(1)
O(17)	8166(9)	58(4)	6162(3)	127(3)
O(18)	10440(8)	-127(4)	6507(5)	141(4)
O(19)	11561(5)	2126(4)	7298(3)	72(2)
P(1)	10264(2)	3258(1)	8774(1)	53(1)
P(2)	7517(2)	3336(1)	8503(1)	50(1)
P(3)	9712(2)	4159(1)	6771(1)	61(1)
P(4)	7285(2)	3189(1)	6399(1)	50(1)
P(5)	8093(2)	88(1)	7805(1)	51(1)
P(6)	9146(2)	241(1)	6703(1)	58(1)
Gd(1)	9176(1)	2219(1)	7451(1)	44(1)

Table 3. Bond lengths [Å] and angles [°] for ddx1m.

C(1)-C(2)	1.362(12)	C(19)-C(24)	1.373(9)	C(37)-O(11)	1.392(10)
C(1)-C(6)	1.379(9)	C(19)-O(6)	1.412(9)	C(38)-C(39)	1.377(15)
C(1)-O(2)	1.398(9)	C(20)-C(21)	1.389(13)	C(38)-H(38)	0.9300
C(2)-C(3)	1.373(13)	C(20)-H(20)	0.9300	C(39)-C(40)	1.360(17)
C(2)-H(2)	0.9300	C(21)-C(22)	1.352(15)	C(39)-H(39)	0.9300
C(3)-C(4)	1.360(13)	C(21)-H(21)	0.9300	C(40)-C(41)	1.351(17)
C(3)-H(3)	0.9300	C(22)-C(23)	1.348(14)	C(40)-H(40)	0.9300
C(4)-C(5)	1.378(13)	C(22)-H(22)	0.9300	C(41)-C(42)	1.375(13)
C(4)-H(4)	0.9300	C(23)-C(24)	1.376(11)	C(41)-H(41)	0.9300
C(5)-C(6)	1.387(10)	C(23)-H(23)	0.9300	C(42)-H(42)	0.9300
C(5)-H(5)	0.9300	C(24)-H(24)	0.9300	C(43)-O(12)	1.373(7)
C(6)-H(6)	0.9300	C(25)-O(8)	1.340(8)	C(43)-C(44)	1.3900
C(7)-O(3)	1.366(7)	C(25)-C(26)	1.3900	C(43)-C(48)	1.3900
C(7)-C(8)	1.3900	C(25)-C(30)	1.3900	C(44)-C(45)	1.3900
C(7)-C(12)	1.3900	C(26)-C(27)	1.3900	C(44)-H(44)	0.9300
C(8)-C(9)	1.3900	C(26)-H(26)	0.9300	C(45)-C(46)	1.3900
C(8)-H(8)	0.9300	C(27)-C(28)	1.3900	C(45)-H(45)	0.9300
C(9)-C(10)	1.3900	C(27)-H(27)	0.9300	C(46)-C(47)	1.3900
C(9)-H(9)	0.9300	C(28)-C(29)	1.3900	C(46)-H(46)	0.9300
C(10)-C(11)	1.3900	C(28)-H(28)	0.9300	C(47)-C(48)	1.3900
C(10)-H(10)	0.9300	C(29)-C(30)	1.3900	C(47)-H(47)	0.9300
C(11)-C(12)	1.3900	C(29)-H(29)	0.9300	C(48)-H(48)	0.9300
C(11)-H(11)	0.9300	C(30)-H(30)	0.9300	C(49)-C(50)	1.372(12)
C(12)-H(12)	0.9300	C(31)-C(36)	1.3900	C(49)-C(54)	1.375(11)
C(13)-C(14)	1.367(10)	C(31)-C(32)	1.3900	C(49)-O(14)	1.389(10)
C(13)-C(18)	1.376(10)	C(31)-O(9)	1.491(10)	C(50)-C(51)	1.397(15)
C(13)-O(5)	1.398(9)	C(32)-C(33)	1.3900	C(50)-H(50)	0.9300
C(14)-C(15)	1.363(12)	C(32)-H(32)	0.9300	C(51)-C(52)	1.381(16)
C(14)-H(14)	0.9300	C(33)-C(34)	1.3900	C(51)-H(51)	0.9300
C(15)-C(16)	1.373(12)	C(33)-H(33)	0.9300	C(52)-C(53)	1.348(14)
C(15)-H(15)	0.9300	C(34)-C(35)	1.3900	C(52)-H(52)	0.9300
C(16)-C(17)	1.365(12)	C(34)-H(34)	0.9300	C(53)-C(54)	1.381(13)
C(16)-H(16)	0.9300	C(35)-C(36)	1.3901	C(53)-H(53)	0.9300
C(17)-C(18)	1.386(12)	C(35)-H(35)	0.9300	C(54)-H(54)	0.9300
C(17)-H(17)	0.9300	C(36)-H(36)	0.9300	C(55)-C(56)	1.364(13)
C(18)-H(18)	0.9300	C(37)-C(42)	1.350(10)	C(55)-C(60)	1.369(10)
C(19)-C(20)	1.342(12)	C(37)-C(38)	1.376(12)	C(55)-O(15)	1.390(9)

C(56)-C(57)	1.444(16)	C(1)-C(2)-C(3)	118.9(9)	C(26)-C(27)-C(28)	120.0
C(56)-H(56)	0.9300	C(1)-C(2)-H(2)	120.5	C(26)-C(27)-H(27)	120.0
C(57)-C(58)	1.359(19)	C(3)-C(2)-H(2)	120.5	C(28)-C(27)-H(27)	120.0
C(57)-H(57)	0.9300	C(4)-C(3)-C(2)	120.6(10)	C(29)-C(28)-C(27)	120.0
C(58)-C(59)	1.311(18)	C(4)-C(3)-H(3)	119.7	C(29)-C(28)-H(28)	120.0
C(58)-H(58)	0.9300	C(2)-C(3)-H(3)	119.7	C(27)-C(28)-H(28)	120.0
C(59)-C(60)	1.423(14)	C(3)-C(4)-C(5)	120.6(9)	C(30)-C(29)-C(28)	120.0
C(59)-H(59)	0.9300	C(3)-C(4)-H(4)	119.7	C(30)-C(29)-H(29)	120.0
C(60)-H(60)	0.9300	C(5)-C(4)-H(4)	119.7	C(28)-C(29)-H(29)	120.0
C(61)-O(17)	1.325(7)	C(4)-C(5)-C(6)	119.5(7)	C(29)-C(30)-C(25)	120.0
C(61)-C(66)	1.3900	C(4)-C(5)-H(5)	120.3	C(29)-C(30)-H(30)	120.0
C(61)-C(62)	1.3900	C(6)-C(5)-H(5)	120.3	C(25)-C(30)-H(30)	120.0
C(62)-C(63)	1.3900	C(1)-C(6)-C(5)	118.6(6)	C(36)-C(31)-C(32)	120.0
C(62)-H(62)	0.9300	C(1)-C(6)-H(6)	120.7	C(36)-C(31)-O(9)	112.4(3)
C(63)-C(64)	1.3900	C(5)-C(6)-H(6)	120.7	C(32)-C(31)-O(9)	127.5(3)
C(63)-H(63)	0.9300	O(3)-C(7)-C(8)	118.0(3)	C(31)-C(32)-C(33)	120.0
C(64)-C(65)	1.3900	O(3)-C(7)-C(12)	121.6(4)	C(31)-C(32)-H(32)	120.0
C(64)-H(64)	0.9300	C(8)-C(7)-C(12)	120.0	C(33)-C(32)-H(32)	120.0
C(65)-C(66)	1.3900	C(7)-C(8)-C(9)	120.0	C(34)-C(33)-C(32)	120.0
C(65)-H(65)	0.9300	C(7)-C(8)-H(8)	120.0	C(34)-C(33)-H(33)	120.0
C(66)-H(66)	0.9300	C(9)-C(8)-H(8)	120.0	C(32)-C(33)-H(33)	120.0
C(67)-O(18)	1.316(8)	C(10)-C(9)-C(8)	120.0	C(33)-C(34)-C(35)	120.0
C(67)-C(68)	1.3900	C(10)-C(9)-H(9)	120.0	C(33)-C(34)-H(34)	120.0
C(67)-C(72)	1.3900	C(8)-C(9)-H(9)	120.0	C(35)-C(34)-H(34)	120.0
C(68)-C(69)	1.3900	C(9)-C(10)-C(11)	120.0	C(34)-C(35)-C(36)	120.0
C(68)-H(68)	0.9300	C(9)-C(10)-H(10)	120.0	C(34)-C(35)-H(35)	120.0
C(69)-C(70)	1.3900	C(11)-C(10)-H(10)	120.0	C(36)-C(35)-H(35)	120.0
C(69)-H(69)	0.9300	C(12)-C(11)-C(10)	120.0	C(31)-C(36)-C(35)	120.0
C(70)-C(71)	1.3900	C(12)-C(11)-H(11)	120.0	C(31)-C(36)-H(36)	120.0
C(70)-H(70)	0.9300	C(10)-C(11)-H(11)	120.0	C(35)-C(36)-H(36)	120.0
C(71)-C(72)	1.3900	C(11)-C(12)-C(7)	120.0	C(42)-C(37)-C(38)	120.0(9)
C(71)-H(71)	0.9300	C(11)-C(12)-H(12)	120.0	C(42)-C(37)-O(11)	123.4(7)
C(72)-H(72)	0.9300	C(7)-C(12)-H(12)	120.0	C(38)-C(37)-O(11)	116.6(9)
C(73)-O(19)	1.456(11)	C(14)-C(13)-C(18)	120.5(8)	C(37)-C(38)-C(39)	119.3(11)
C(73)-C(74)	1.490(14)	C(14)-C(13)-O(5)	118.5(7)	C(37)-C(38)-H(38)	120.3
C(73)-H(73A)	0.9700	C(18)-C(13)-O(5)	120.8(7)	C(39)-C(38)-H(38)	120.3
C(73)-H(73B)	0.9700	C(15)-C(14)-C(13)	119.6(8)	C(40)-C(39)-C(38)	120.3(13)
C(74)-H(74A)	0.9600	C(15)-C(14)-H(14)	120.2	C(40)-C(39)-H(39)	119.9
C(74)-H(74B)	0.9600	C(13)-C(14)-H(14)	120.2	C(38)-C(39)-H(39)	119.8
C(74)-H(74C)	0.9600	C(14)-C(15)-C(16)	121.4(8)	C(41)-C(40)-C(39)	119.8(13)
N(1)-P(1)	1.552(7)	C(14)-C(15)-H(15)	119.3	C(41)-C(40)-H(40)	120.1
N(1)-P(2)	1.579(6)	C(16)-C(15)-H(15)	119.3	C(39)-C(40)-H(40)	120.1
N(2)-P(4)	1.564(6)	C(17)-C(16)-C(15)	118.6(8)	C(40)-C(41)-C(42)	120.6(12)
N(2)-P(3)	1.570(6)	C(17)-C(16)-H(16)	120.7	C(40)-C(41)-H(41)	119.7
N(3)-P(6)	1.553(6)	C(15)-C(16)-H(16)	120.7	C(42)-C(41)-H(41)	119.7
N(3)-P(5)	1.569(6)	C(16)-C(17)-C(18)	121.1(9)	C(37)-C(42)-C(41)	120.0(8)
O(1)-P(1)	1.488(5)	C(16)-C(17)-H(17)	119.5	C(37)-C(42)-H(42)	120.0
O(1)-Gd(1)	2.344(4)	C(18)-C(17)-H(17)	119.5	C(41)-C(42)-H(42)	120.0
O(2)-P(1)	1.581(6)	C(13)-C(18)-C(17)	118.7(8)	O(12)-C(43)-C(44)	117.8(3)
O(3)-P(1)	1.583(6)	C(13)-C(18)-H(18)	120.6	O(12)-C(43)-C(48)	121.9(3)
O(4)-P(2)	1.487(5)	C(17)-C(18)-H(18)	120.6	C(44)-C(43)-C(48)	120.0
O(4)-Gd(1)	2.332(5)	C(20)-C(19)-C(24)	121.6(7)	C(43)-C(44)-C(45)	120.0
O(5)-P(2)	1.601(5)	C(20)-C(19)-O(6)	119.6(8)	C(43)-C(44)-H(44)	120.0
O(6)-P(2)	1.577(6)	C(24)-C(19)-O(6)	118.6(6)	C(45)-C(44)-H(44)	120.0
O(7)-P(3)	1.440(6)	C(19)-C(20)-C(21)	118.5(9)	C(46)-C(45)-C(44)	120.0
O(7)-Gd(1)	2.312(5)	C(19)-C(20)-H(20)	120.8	C(46)-C(45)-H(45)	120.0
O(8)-P(3)	1.648(8)	C(21)-C(20)-H(20)	120.8	C(44)-C(45)-H(45)	120.0
O(9)-P(3)	1.498(7)	C(22)-C(21)-C(20)	120.2(10)	C(45)-C(46)-C(47)	120.0
O(10)-P(4)	1.480(5)	C(22)-C(21)-H(21)	119.9	C(45)-C(46)-H(46)	120.0
O(10)-Gd(1)	2.330(5)	C(20)-C(21)-H(21)	119.9	C(47)-C(46)-H(46)	120.0
O(11)-P(4)	1.585(6)	C(23)-C(22)-C(21)	120.9(10)	C(48)-C(47)-C(46)	120.0
O(12)-P(4)	1.589(5)	C(23)-C(22)-H(22)	119.6	C(48)-C(47)-H(47)	120.0
O(13)-P(5)	1.485(5)	C(21)-C(22)-H(22)	119.6	C(46)-C(47)-H(47)	120.0
O(13)-Gd(1)	2.321(5)	C(22)-C(23)-C(24)	119.7(9)	C(47)-C(48)-C(43)	120.0
O(14)-P(5)	1.589(6)	C(22)-C(23)-H(23)	120.1	C(47)-C(48)-H(48)	120.0
O(15)-P(5)	1.577(5)	C(24)-C(23)-H(23)	120.1	C(43)-C(48)-H(48)	120.0
O(16)-P(6)	1.472(5)	C(19)-C(24)-C(23)	118.9(6)	C(50)-C(49)-C(54)	121.1(9)
O(16)-Gd(1)	2.380(5)	C(19)-C(24)-H(24)	120.5	C(50)-C(49)-O(14)	118.1(8)
O(17)-P(6)	1.559(7)	C(23)-C(24)-H(24)	120.5	C(54)-C(49)-O(14)	120.6(8)
O(18)-P(6)	1.564(7)	O(8)-C(25)-C(26)	110.9(4)	C(49)-C(50)-C(51)	118.4(10)
O(19)-H(19)	0.8200	O(8)-C(25)-C(30)	127.6(4)	C(49)-C(50)-H(50)	120.8
		C(26)-C(25)-C(30)	120.0	C(51)-C(50)-H(50)	120.8
C(2)-C(1)-C(6)	121.8(7)	C(25)-C(26)-C(27)	120.0	C(52)-C(51)-C(50)	120.7(10)
C(2)-C(1)-O(2)	115.9(7)	C(25)-C(26)-H(26)	120.0	C(52)-C(51)-H(51)	119.7
C(6)-C(1)-O(2)	122.3(7)	C(27)-C(26)-H(26)	120.0	C(50)-C(51)-H(51)	119.7

C(53)-C(52)-C(51)	119.2(10)	P(1)-N(1)-P(2)	126.3(4)
C(53)-C(52)-H(52)	120.4	P(4)-N(2)-P(3)	125.5(4)
C(51)-C(52)-H(52)	120.4	P(6)-N(3)-P(5)	126.2(4)
C(52)-C(53)-C(54)	121.6(10)	P(1)-O(1)-Gd(1)	133.2(3)
C(52)-C(53)-H(53)	119.2	C(1)-O(2)-P(1)	126.2(5)
C(54)-C(53)-H(53)	119.2	C(7)-O(3)-P(1)	126.3(4)
C(49)-C(54)-C(53)	119.0(9)	P(2)-O(4)-Gd(1)	138.4(3)
C(49)-C(54)-H(54)	120.5	C(13)-O(5)-P(2)	122.0(4)
C(53)-C(54)-H(54)	120.5	C(19)-O(6)-P(2)	123.6(5)
C(56)-C(55)-C(60)	122.4(8)	P(3)-O(7)-Gd(1)	139.6(3)
C(56)-C(55)-O(15)	117.8(9)	C(25)-O(8)-P(3)	127.4(5)
C(60)-C(55)-O(15)	119.6(8)	C(31)-O(9)-P(3)	117.5(5)
C(55)-C(56)-C(57)	119.4(12)	P(4)-O(10)-Gd(1)	136.4(3)
C(55)-C(56)-H(56)	120.3	C(37)-O(11)-P(4)	125.6(5)
C(57)-C(56)-H(56)	120.3	C(43)-O(12)-P(4)	122.0(4)
C(58)-C(57)-C(56)	114.0(13)	P(5)-O(13)-Gd(1)	141.3(3)
C(58)-C(57)-H(57)	123.0	C(49)-O(14)-P(5)	121.3(5)
C(56)-C(57)-H(57)	123.0	C(55)-O(15)-P(5)	124.4(5)
C(59)-C(58)-C(57)	128.8(14)	P(6)-O(16)-Gd(1)	139.1(3)
C(59)-C(58)-H(58)	115.6	C(61)-O(17)-P(6)	129.5(6)
C(57)-C(58)-H(58)	115.6	C(67)-O(18)-P(6)	126.3(5)
C(58)-C(59)-C(60)	116.6(13)	C(73)-O(19)-H(19)	109.5
C(58)-C(59)-H(59)	121.7	O(1)-P(1)-N(1)	118.8(3)
C(60)-C(59)-H(59)	121.7	O(1)-P(1)-O(2)	107.0(3)
C(55)-C(60)-C(59)	118.8(8)	N(1)-P(1)-O(2)	110.4(3)
C(55)-C(60)-H(60)	120.6	O(1)-P(1)-O(3)	110.5(3)
C(59)-C(60)-H(60)	120.6	N(1)-P(1)-O(3)	111.8(4)
O(17)-C(61)-C(66)	115.4(5)	O(2)-P(1)-O(3)	95.9(3)
O(17)-C(61)-C(62)	124.4(5)	O(4)-P(2)-O(6)	106.9(3)
C(66)-C(61)-C(62)	120.0	O(4)-P(2)-N(1)	117.9(3)
C(63)-C(62)-C(61)	120.0	O(6)-P(2)-N(1)	112.3(3)
C(63)-C(62)-H(62)	120.0	O(4)-P(2)-O(5)	110.6(3)
C(61)-C(62)-H(62)	120.0	O(6)-P(2)-O(5)	98.4(3)
C(62)-C(63)-C(64)	120.0	N(1)-P(2)-O(5)	109.0(3)
C(62)-C(63)-H(63)	120.0	O(7)-P(3)-O(9)	119.3(4)
C(64)-C(63)-H(63)	120.0	O(7)-P(3)-N(2)	119.3(3)
C(65)-C(64)-C(63)	120.0	O(9)-P(3)-N(2)	109.8(4)
C(65)-C(64)-H(64)	120.0	O(7)-P(3)-O(8)	98.9(4)
C(63)-C(64)-H(64)	120.0	O(9)-P(3)-O(8)	95.1(5)
C(66)-C(65)-C(64)	120.0	N(2)-P(3)-O(8)	110.4(4)
C(66)-C(65)-H(65)	120.0	O(10)-P(4)-N(2)	119.0(3)
C(64)-C(65)-H(65)	120.0	O(10)-P(4)-O(11)	107.4(3)
C(65)-C(66)-C(61)	120.0	N(2)-P(4)-O(11)	111.1(3)
C(65)-C(66)-H(66)	120.0	O(10)-P(4)-O(12)	110.1(3)
C(61)-C(66)-H(66)	120.0	N(2)-P(4)-O(12)	108.7(3)
O(18)-C(67)-C(68)	117.1(5)	O(11)-P(4)-O(12)	98.6(3)
O(18)-C(67)-C(72)	122.9(5)	O(13)-P(5)-N(3)	117.8(3)
C(68)-C(67)-C(72)	120.0	O(13)-P(5)-O(15)	105.7(3)
C(67)-C(68)-C(69)	120.0	N(3)-P(5)-O(15)	112.0(3)
C(67)-C(68)-H(68)	120.0	O(13)-P(5)-O(14)	111.2(3)
C(69)-C(68)-H(68)	120.0	N(3)-P(5)-O(14)	109.0(3)
C(70)-C(69)-C(68)	120.0	O(15)-P(5)-O(14)	99.7(3)
C(70)-C(69)-H(69)	120.0	O(16)-P(6)-N(3)	119.2(3)
C(68)-C(69)-H(69)	120.0	O(16)-P(6)-O(17)	106.0(4)
C(69)-C(70)-C(71)	120.0	N(3)-P(6)-O(17)	110.6(4)
C(69)-C(70)-H(70)	120.0	O(16)-P(6)-O(18)	110.7(3)
C(71)-C(70)-H(70)	120.0	N(3)-P(6)-O(18)	107.1(4)
C(72)-C(71)-C(70)	120.0	O(17)-P(6)-O(18)	102.0(5)
C(72)-C(71)-H(71)	120.0	O(7)-Gd(1)-O(13)	169.8(2)
C(70)-C(71)-H(71)	120.0	O(7)-Gd(1)-O(10)	77.82(17)
C(71)-C(72)-C(67)	120.0	O(13)-Gd(1)-O(10)	105.72(17)
C(71)-C(72)-H(72)	120.0	O(7)-Gd(1)-O(4)	87.5(2)
C(67)-C(72)-H(72)	120.0	O(13)-Gd(1)-O(4)	83.97(17)
O(19)-C(73)-C(74)	112.6(9)	O(10)-Gd(1)-O(4)	78.28(17)
O(19)-C(73)-H(73A)	109.1	O(7)-Gd(1)-O(1)	85.61(19)
C(74)-C(73)-H(73A)	109.1	O(13)-Gd(1)-O(1)	87.11(17)
O(19)-C(73)-H(73B)	109.1	O(10)-Gd(1)-O(1)	151.03(17)
C(74)-C(73)-H(73B)	109.1	O(4)-Gd(1)-O(1)	77.38(17)
H(73A)-C(73)-H(73B)	107.8	O(7)-Gd(1)-O(16)	114.7(2)
C(73)-C(74)-H(74A)	109.5	O(13)-Gd(1)-O(16)	75.46(16)
C(73)-C(74)-H(74B)	109.5	O(10)-Gd(1)-O(16)	78.53(17)
H(74A)-C(74)-H(74B)	109.5	O(4)-Gd(1)-O(16)	143.30(17)
C(73)-C(74)-H(74C)	109.5	O(1)-Gd(1)-O(16)	130.33(17
H(74A)-C(74)-H(74C)	109.5		
H(74B)-C(74)-H(74C)	109.5		

Symmetry transformations used to generate equivalent atoms:

Table 4. Anisotropic displacement parameters ($Å^2 x\ 10^3$)for ddx1m. The anisotropic displacement factor exponent takes the form: $-2\pi^2[\ h^2 a^{*2} U^{11} + ... + 2\ h\ k\ a^*\ b^*\ U^{12}\ ]$

	U^{11}	U^{22}	U^{33}	U^{23}	U^{13}	U^{12}
C(1)	42(5)	53(5)	70(5)	-16(4)	-4(4)	-7(4)
C(2)	80(7)	74(7)	59(5)	-4(5)	1(5)	-1(5)
C(3)	111(9)	78(7)	80(7)	-4(6)	-1(6)	-5(6)
C(4)	82(7)	66(6)	94(8)	-14(6)	5(6)	-11(5)
C(5)	76(6)	86(7)	61(6)	-26(5)	15(5)	-20(5)
C(6)	64(6)	68(6)	62(5)	-4(4)	4(4)	-14(4)
C(7)	74(6)	47(5)	39(4)	-4(3)	-14(4)	15(4)
C(8)	50(6)	87(7)	77(6)	-10(5)	7(5)	-3(5)
C(9)	75(7)	85(7)	97(7)	-9(6)	-32(6)	33(6)
C(10)	115(9)	80(7)	84(7)	26(6)	-16(6)	17(7)
C(11)	86(8)	137(11)	86(8)	19(7)	-4(6)	15(7)
C(12)	67(6)	95(7)	70(6)	-2(5)	0(5)	16(5)
C(13)	34(4)	52(5)	55(5)	1(4)	3(3)	3(3)
C(14)	60(5)	55(5)	65(5)	-3(4)	10(4)	3(4)
C(15)	59(6)	94(7)	50(5)	2(5)	5(4)	-8(5)
C(16)	64(6)	71(7)	73(6)	24(5)	2(5)	-8(5)
C(17)	78(7)	50(6)	88(7)	4(5)	4(5)	-1(4)
C(18)	60(5)	54(5)	61(5)	1(4)	6(4)	2(4)
C(19)	68(6)	44(5)	63(5)	-1(4)	7(4)	14(4)
C(20)	65(7)	79(7)	119(8)	-20(6)	12(6)	6(5)
C(21)	83(8)	110(9)	145(11)	-42(8)	25(7)	30(7)
C(22)	91(9)	86(8)	139(10)	-52(7)	-1(7)	26(7)
C(23)	78(8)	70(7)	158(11)	-46(7)	-22(7)	17(6)
C(24)	71(7)	62(6)	120(8)	-15(6)	6(6)	13(5)
C(25)	96(6)	51(5)	77(5)	4(4)	-29(5)	13(5)
C(26)	129(8)	148(9)	160(9)	15(8)	8(7)	-13(7)
C(27)	186(11)	208(11)	217(11)	-27(9)	31(9)	55(9)
C(28)	180(10)	149(9)	166(9)	-31(8)	-10(8)	59(8)
C(29)	157(8)	80(6)	96(7)	0(5)	-10(6)	-10(6)
C(30)	89(6)	76(6)	96(6)	-5(5)	11(5)	-5(5)
C(31)	93(5)	117(5)	104(5)	7(4)	6(4)	-2(4)
C(32)	131(6)	126(6)	131(6)	15(5)	8(5)	11(4)
C(33)	170(7)	157(7)	165(7)	10(5)	8(5)	31(5)
C(34)	146(7)	153(7)	144(7)	-2(5)	19(5)	23(5)
C(35)	108(5)	115(5)	99(5)	20(4)	10(4)	3(4)
C(36)	99(5)	99(5)	98(5)	8(4)	5(4)	8(4)
C(37)	44(5)	74(6)	74(6)	5(5)	-1(4)	4(4)
C(38)	92(8)	84(8)	93(8)	-8(6)	12(6)	12(6)
C(39)	114(10)	82(9)	153(13)	-20(9)	16(9)	32(8)
C(40)	79(8)	82(9)	189(15)	14(10)	5(9)	24(6)
C(41)	88(8)	116(10)	143(11)	43(9)	20(8)	47(7)
C(42)	99(8)	85(8)	108(9)	28(7)	9(6)	41(6)
C(43)	73(6)	75(6)	44(5)	-2(4)	-6(4)	-10(5)
C(44)	175(12)	85(8)	73(7)	6(6)	22(7)	-14(8)
C(45)	232(19)	167(15)	88(9)	-14(10)	76(11)	-19(13)
C(46)	149(13)	198(17)	96(10)	-28(11)	35(9)	27(12)
C(47)	164(13)	161(13)	94(9)	-51(9)	-39(9)	87(11)
C(48)	158(11)	105(9)	57(6)	-10(6)	-21(6)	55(8)
C(49)	70(6)	55(5)	47(4)	11(4)	7(4)	14(4)
C(50)	104(9)	68(7)	74(6)	-2(5)	0(6)	25(6)
C(51)	123(11)	109(10)	86(8)	-3(7)	6(7)	72(9)
C(52)	78(8)	142(12)	70(7)	3(7)	-1(6)	41(8)
C(53)	73(7)	98(8)	74(6)	-4(6)	-9(5)	6(6)
C(54)	72(7)	65(6)	68(6)	-7(4)	3(5)	13(5)
C(55)	59(5)	57(5)	87(6)	-1(4)	22(4)	5(4)
C(56)	85(6)	91(6)	111(7)	-18(6)	22(6)	-8(5)
C(57)	122(8)	132(8)	140(8)	-47(7)	16(7)	8(7)
C(58)	122(8)	97(7)	156(9)	-24(7)	36(7)	12(6)

C(59)	127(8)	109(8)	147(8)	27(7)	39(7)	25(6)
C(60)	96(6)	73(6)	122(7)	16(6)	23(6)	9(5)
C(61)	72(6)	88(6)	74(5)	-18(5)	-14(5)	13(5)
C(62)	111(7)	92(7)	153(8)	-26(6)	5(7)	2(6)
C(63)	186(10)	155(9)	188(10)	-36(8)	24(8)	3(8)
C(64)	193(11)	214(11)	190(11)	-19(9)	-34(9)	-10(9)
C(65)	180(11)	214(11)	190(11)	19(9)	-30(8)	21(9)
C(66)	167(10)	164(10)	154(9)	23(8)	-17(8)	19(8)
C(67)	82(6)	69(5)	81(6)	-1(5)	19(5)	17(5)
C(68)	138(8)	120(8)	119(8)	-19(6)	16(7)	43(7)
C(69)	156(9)	176(10)	182(10)	-39(8)	-5(8)	60(8)
C(70)	122(8)	126(8)	184(10)	-7(8)	32(8)	-2(7)
C(71)	169(10)	148(9)	192(10)	44(8)	24(8)	25(8)
C(72)	121(8)	143(8)	137(8)	30(7)	25(7)	34(7)
C(73)	76(7)	102(8)	112(9)	1(7)	-2(6)	-8(6)
C(74)	115(10)	129(11)	116(10)	-5(8)	-44(8)	15(8)
N(1)	51(4)	59(4)	49(4)	-8(3)	3(3)	-11(3)
N(2)	58(4)	50(4)	53(4)	7(3)	-6(3)	5(3)
N(3)	69(4)	34(3)	69(4)	-1(3)	8(3)	13(3)
O(1)	66(3)	50(3)	43(3)	-9(2)	-17(2)	14(2)
O(2)	54(3)	69(4)	80(4)	-21(3)	4(3)	-1(3)
O(3)	135(6)	55(4)	69(4)	-6(3)	-32(4)	22(4)
O(4)	57(3)	55(3)	48(3)	-9(2)	-2(2)	10(2)
O(5)	53(3)	55(3)	62(3)	4(3)	3(3)	10(2)
O(6)	83(4)	51(3)	54(3)	-1(3)	2(3)	17(3)
O(7)	74(4)	53(3)	97(4)	29(3)	-40(3)	-20(3)
O(8)	164(7)	74(5)	97(5)	-2(4)	-35(5)	8(5)
O(9)	95(5)	127(6)	137(7)	50(5)	-25(5)	-45(5)
O(10)	53(3)	47(3)	43(3)	1(2)	-12(2)	-1(2)
O(11)	62(4)	65(4)	76(4)	16(3)	11(3)	13(3)
O(12)	72(4)	74(4)	46(3)	-3(3)	-18(3)	8(3)
O(13)	78(4)	38(3)	52(3)	0(2)	10(3)	2(2)
O(14)	60(4)	61(4)	64(3)	18(3)	7(3)	7(3)
O(15)	55(3)	43(3)	86(4)	3(3)	5(3)	8(2)
O(16)	66(3)	47(3)	52(3)	-8(2)	10(3)	2(2)
O(17)	191(8)	88(5)	76(5)	0(4)	-37(5)	-62(5)
O(18)	100(6)	62(4)	257(11)	-52(5)	95(6)	-8(4)
O(19)	53(4)	69(4)	90(5)	-25(3)	2(3)	-3(3)
P(1)	68(1)	45(1)	43(1)	-5(1)	-14(1)	12(1)
P(2)	60(1)	43(1)	47(1)	-2(1)	5(1)	4(1)
P(3)	63(1)	49(1)	65(1)	15(1)	-10(1)	-12(1)
P(4)	55(1)	48(1)	46(1)	2(1)	-7(1)	3(1)
P(5)	58(1)	39(1)	57(1)	6(1)	4(1)	5(1)
P(6)	62(1)	51(1)	57(1)	-13(1)	4(1)	-2(1)
Gd(1)	52(1)	36(1)	42(1)	1(1)	-4(1)	2(1)

Table 5. Hydrogen coordinates (x 10^4) and isotropic displacement parameters ($Å^2$x 10^3) for ddx1m.

	x	y	z	U(eq)		x	y	z	U(eq)	
H(2)	11531	5304	7996	87		H(18)	6380	1436	8595	71
H(3)	11547	6671	8279	110		H(20)	4723	4360	8764	106
H(4)	11439	7027	9233	99		H(21)	4272	5444	9366	134
H(5)	11265	6022	9927	93		H(22)	5993	6449	9669	126
H(6)	11212	4635	9647	80		H(23)	8147	6443	9356	123
H(8)	13123	2343	9525	87		H(24)	8588	5420	8708	101
H(9)	13263	1155	10049	101		H(26)	7448	5440	7288	178
H(10)	11320	448	10444	112		H(27)	6984	6797	7310	241
H(11)	9237	929	10314	123		H(28)	8706	7881	7147	195
H(12)	9096	2116	9789	92		H(29)	10891	7607	6962	137
H(14)	6201	2911	9983	72		H(30)	11356	6250	6941	106
H(15)	6195	1793	10567	83		H(32)	11655	3102	6167	156
H(16)	6234	483	10181	85		H(33)	12407	2668	5287	196
H(17)	6389	316	9198	88		H(34)	12476	3534	4500	177

H(35)	11794	4835	4594	130	H(58)	4258	-3172	7810	150
H(36)	11043	5270	5474	119	H(59)	5427	-2758	8613	151
H(38)	4983	4291	7400	108	H(60)	6583	-1370	8670	116
H(39)	3972	5479	7302	138	H(62)	8272	-1534	6252	144
H(40)	3927	6105	6425	138	H(63)	6575	-2603	5957	214
H(41)	4792	5523	5639	134	H(64)	4518	-2302	5569	245
H(42)	5663	4290	5716	113	H(65)	4158	-932	5475	235
H(44)	7596	3553	4821	137	H(66)	5855	136	5770	195
H(45)	8807	3000	4102	199	H(68)	12313	-141	7242	148
H(46)	9528	1716	4219	176	H(69)	14510	577	7248	202
H(47)	9037	984	5056	162	H(70)	15195	1427	6486	175
H(48)	7826	1537	5775	125	H(71)	13683	1560	5719	202
H(50)	10061	-1550	8162	97	H(72)	11486	842	5713	158
H(51)	12396	-1603	8275	121	H(73A)	12480	3252	7548	118
H(52)	13884	-417	8527	113	H(73B)	13294	2820	7088	118
H(53)	13048	788	8709	99	H(74A)	14425	2869	7977	182
H(54)	10742	863	8612	82	H(74B)	13946	1941	7790	182
H(56)	5221	-994	7068	117	H(74C)	13135	2375	8250	182
H(57)	4005	-2392	7023	159	H(19)	11766	1760	7083	108

B9 Crystallographic Data for H_2bistpOp

The hydrogen atoms were fixed as riding models. The hydrogen bonding is detailed in Table 6.
The SHELXL second parameter in WGHT is unusually large. Also the maximum residual electron density is a little high, 1.13 e.Å^{-3} at 0.80 Angstroms from H(2a). The crystal diffracted only very weakly and it is possible that these problems in the refinement are caused by a twinning of the dataset with the second component being too weak to be measured.

Table 2. Atomic coordinates (x 10^4) and equivalent isotropic displacement parameters (Å^{2}x 10^3) for 2008src1077. U(eq) is defined as one third of the trace of the orthogonalized U^{ij} tensor.

	x	y	z	U(eq)		x	y	z	U(eq)	
C(1)	784(7)	3620(6)	4499(3)	28(2)		N(2)	37(5)	2844(4)	2220(2)	19(1)
C(2)	-109(8)	3700(6)	5028(3)	33(2)		O(1)	542(5)	4481(4)	4002(2)	26(1)
C(3)	102(9)	2890(7)	5537(4)	40(2)		O(2)	238(5)	5628(4)	3068(2)	31(1)
C(4)	1154(8)	2018(7)	5514(4)	38(2)		O(3)	2542(5)	4250(4)	3140(2)	27(1)
C(5)	2026(8)	1956(6)	4972(4)	36(2)		O(4)	682(4)	1819(3)	3271(2)	21(1)
C(6)	1855(7)	2758(6)	4465(3)	29(2)		O(5)	2455(4)	2603(3)	2510(2)	21(1)
C(7)	398(7)	6159(6)	2451(3)	29(2)		O(6)	1525(5)	2698(4)	1170(2)	26(1)
C(8)	1501(8)	6567(6)	2243(4)	35(2)		O(7)	864(5)	4302(4)	1544(2)	28(1)
C(9)	1564(8)	7143(6)	1638(4)	39(2)		O(8)	-962(5)	3697(4)	1196(2)	30(1)
C(10)	562(8)	7323(6)	1272(4)	35(2)		P(1)	1079(2)	4485(1)	3300(1)	23(1)
C(11)	-522(8)	6898(6)	1493(4)	40(2)		P(2)	1025(2)	2732(1)	2752(1)	20(1)
C(12)	-602(8)	6296(6)	2093(4)	33(2)		P(3)	262(2)	3416(1)	1497(1)	22(1)
C(13)	1039(7)	804(5)	3149(3)	21(2)		C(101)	6665(7)	-253(5)	3141(3)	27(2)
C(14)	2377(7)	251(6)	3097(3)	30(2)		C(102)	6273(7)	-1122(6)	3467(4)	32(2)
C(15)	2682(8)	-728(6)	2995(4)	33(2)		C(103)	6325(8)	-1880(6)	3154(4)	41(2)
C(16)	1680(8)	-1161(6)	2943(4)	35(2)		C(104)	6774(9)	-1759(7)	2545(5)	49(2)
C(17)	340(8)	-597(6)	2997(4)	33(2)		C(105)	7183(10)	-884(8)	2226(4)	53(2)
C(18)	3(7)	403(6)	3099(3)	28(2)		C(106)	7136(8)	-116(6)	2531(3)	36(2)
C(19)	1383(7)	1832(5)	984(3)	24(2)		C(107)	6763(7)	1657(5)	4329(3)	22(2)
C(20)	1439(9)	912(6)	1411(4)	41(2)		C(108)	6467(7)	979(6)	4866(3)	28(2)
C(21)	1369(10)	68(7)	1204(4)	49(2)		C(109)	7379(8)	631(6)	5298(3)	33(2)
C(22)	1322(9)	123(7)	591(4)	40(2)		C(110)	8560(8)	944(6)	5190(3)	30(2)
C(23)	1283(8)	1044(6)	182(4)	35(2)		C(111)	8827(7)	1616(6)	4651(3)	27(2)
C(24)	1321(7)	1909(6)	369(3)	30(2)		C(112)	7926(7)	1978(6)	4213(3)	27(2)
C(25)	1731(7)	4779(5)	1083(3)	26(2)		C(113)	5892(7)	2448(5)	1453(3)	22(2)
C(26)	2935(7)	4775(6)	1256(3)	28(2)		C(114)	4829(7)	2074(6)	1383(3)	30(2)
C(27)	3763(8)	5298(6)	835(4)	36(2)		C(115)	5104(8)	1384(7)	999(4)	36(2)
C(28)	3403(8)	5809(6)	255(3)	35(2)		C(116)	6399(8)	1045(7)	718(4)	38(2)
C(29)	2184(8)	5784(6)	92(3)	37(2)		C(117)	7434(8)	1428(6)	806(4)	35(2)
C(30)	1333(8)	5266(6)	509(3)	33(2)		C(118)	7186(7)	2124(6)	1174(3)	27(2)
N(1)	352(5)	3745(4)	3073(3)	21(1)		C(119)	5700(7)	6286(6)	1960(4)	29(2)

C(120)	4931(8)	7284(6)	1764(4)	35(2)
C(121)	5068(10)	7739(7)	1138(4)	51(2)
C(122)	5932(9)	7191(8)	725(4)	50(3)
C(123)	6710(9)	6190(7)	932(4)	42(2)
C(124)	6594(8)	5727(6)	1560(4)	33(2)
C(125)	5512(7)	5410(6)	3976(3)	27(2)
C(126)	4324(8)	6013(6)	4207(4)	35(2)
C(127)	4392(9)	6615(7)	4608(4)	41(2)
C(128)	5601(9)	6621(6)	4751(4)	41(2)
C(129)	6783(8)	6022(6)	4503(4)	35(2)
C(130)	6751(8)	5389(6)	4109(4)	34(2)
N(101)	5052(5)	2148(4)	2881(2)	20(1)
N(102)	5356(5)	4036(4)	2711(3)	22(1)
O(101)	6681(5)	510(4)	3458(2)	24(1)
O(102)	5845(5)	2061(4)	3880(2)	23(1)
O(103)	4171(5)	1021(4)	3868(2)	24(1)
O(104)	5589(5)	3207(3)	1817(2)	21(1)
O(105)	7445(4)	2471(3)	2553(2)	21(1)
O(106)	5499(5)	5903(4)	2596(2)	27(1)
O(107)	5391(5)	4757(4)	3609(2)	30(1)
O(108)	7586(4)	4410(4)	2864(2)	26(1)
P(101)	5340(2)	1387(1)	3554(1)	21(1)
P(102)	6009(2)	2918(1)	2488(1)	18(1)
P(103)	6108(2)	4742(1)	2935(1)	23(1)

Table 3. Bond lengths [Å] and angles [°] for 2008src1077.

C(1)-C(6)	1.379(10)	C(25)-O(7)	1.415(8)	C(113)-O(104)	1.422(8)
C(1)-C(2)	1.381(10)	C(26)-C(27)	1.377(11)	C(114)-C(115)	1.381(11)
C(1)-O(1)	1.413(9)	C(26)-H(26)	0.9500	C(114)-H(114)	0.9500
C(2)-C(3)	1.389(11)	C(27)-C(28)	1.383(11)	C(115)-C(116)	1.380(11)
C(2)-H(2)	0.9500	C(27)-H(27)	0.9500	C(115)-H(115)	0.9500
C(3)-C(4)	1.373(12)	C(28)-C(29)	1.394(11)	C(116)-C(117)	1.394(11)
C(3)-H(3)	0.9500	C(28)-H(28)	0.9500	C(116)-H(116)	0.9500
C(4)-C(5)	1.393(11)	C(29)-C(30)	1.386(11)	C(117)-C(118)	1.364(11)
C(4)-H(4)	0.9500	C(29)-H(29)	0.9500	C(117)-H(117)	0.9500
C(5)-C(6)	1.376(11)	C(30)-H(30)	0.9500	C(118)-H(118)	0.9500
C(5)-H(5)	0.9500	N(1)-P(2)	1.651(6)	C(119)-C(124)	1.379(11)
C(6)-H(6)	0.9500	N(1)-P(1)	1.655(6)	C(119)-C(120)	1.383(10)
C(7)-C(12)	1.370(10)	N(1)-H(1)	0.8800	C(119)-O(106)	1.402(9)
C(7)-C(8)	1.382(11)	N(2)-P(3)	1.634(6)	C(120)-C(121)	1.395(12)
C(7)-O(2)	1.409(9)	N(2)-P(2)	1.666(5)	C(120)-H(120)	0.9500
C(8)-C(9)	1.398(11)	N(2)-H(2A)	0.8800	C(121)-C(122)	1.380(14)
C(8)-H(8)	0.9500	O(1)-P(1)	1.581(5)	C(121)-H(121)	0.9500
C(9)-C(10)	1.373(11)	O(2)-P(1)	1.573(5)	C(122)-C(123)	1.394(13)
C(9)-H(9)	0.9500	O(3)-P(1)	1.456(5)	C(122)-H(122)	0.9500
C(10)-C(11)	1.381(11)	O(4)-P(2)	1.572(5)	C(123)-C(124)	1.400(11)
C(10)-H(10)	0.9500	O(5)-P(2)	1.465(5)	C(123)-H(123)	0.9500
C(11)-C(12)	1.405(11)	O(6)-P(3)	1.584(5)	C(124)-H(124)	0.9500
C(11)-H(11)	0.9500	O(7)-P(3)	1.566(5)	C(125)-C(130)	1.365(10)
C(12)-H(12)	0.9500	O(8)-P(3)	1.454(5)	C(125)-C(126)	1.370(10)
C(13)-C(14)	1.376(10)	C(101)-C(106)	1.362(10)	C(125)-O(107)	1.411(8)
C(13)-C(18)	1.381(10)	C(101)-C(102)	1.376(10)	C(126)-C(127)	1.398(11)
C(13)-O(4)	1.428(8)	C(101)-O(101)	1.421(8)	C(126)-H(126)	0.9500
C(14)-C(15)	1.367(10)	C(102)-C(103)	1.388(11)	C(127)-C(128)	1.355(11)
C(14)-H(14)	0.9500	C(102)-H(102)	0.9500	C(127)-H(127)	0.9500
C(15)-C(16)	1.380(11)	C(103)-C(104)	1.355(13)	C(128)-C(129)	1.378(11)
C(15)-H(15)	0.9500	C(103)-H(103)	0.9500	C(128)-H(128)	0.9500
C(16)-C(17)	1.382(11)	C(104)-C(105)	1.386(14)	C(129)-C(130)	1.404(11)
C(16)-H(16)	0.9500	C(104)-H(104)	0.9500	C(129)-H(129)	0.9500
C(17)-C(18)	1.391(10)	C(105)-C(106)	1.389(12)	C(130)-H(130)	0.9500
C(17)-H(17)	0.9500	C(105)-H(105)	0.9500	N(101)-P(101)	1.637(6)
C(18)-H(18)	0.9500	C(106)-H(106)	0.9500	N(101)-P(102)	1.658(5)
C(19)-C(24)	1.378(10)	C(107)-C(112)	1.369(10)	N(101)-H(101)	0.8800
C(19)-C(20)	1.384(11)	C(107)-C(108)	1.383(10)	N(102)-P(103)	1.631(6)
C(19)-O(6)	1.417(8)	C(107)-O(102)	1.414(8)	N(102)-P(102)	1.660(6)
C(20)-C(21)	1.386(12)	C(108)-C(109)	1.380(10)	N(102)-H(10A)	0.8800
C(20)-H(20)	0.9500	C(108)-H(108)	0.9500	O(101)-P(101)	1.577(5)
C(21)-C(22)	1.375(11)	C(109)-C(110)	1.382(10)	O(102)-P(101)	1.568(5)
C(21)-H(21)	0.9500	C(109)-H(109)	0.9500	O(103)-P(101)	1.453(5)
C(22)-C(23)	1.370(11)	C(110)-C(111)	1.375(10)	O(104)-P(102)	1.574(5)
C(22)-H(22)	0.9500	C(110)-H(110)	0.9500	O(105)-P(102)	1.457(5)
C(23)-C(24)	1.378(11)	C(111)-C(112)	1.382(10)	O(106)-P(103)	1.590(5)
C(23)-H(23)	0.9500	C(111)-H(111)	0.9500	O(107)-P(103)	1.572(5)
C(24)-H(24)	0.9500	C(112)-H(112)	0.9500	O(108)-P(103)	1.459(5)
C(25)-C(26)	1.375(10)	C(113)-C(118)	1.375(10)		
C(25)-C(30)	1.376(10)	C(113)-C(114)	1.398(10)		
C(6)-C(1)-C(2)	121.7(7)	C(6)-C(1)-O(1)	122.4(6)	C(2)-C(1)-O(1)	115.9(7)

C(1)-C(2)-C(3)	118.4(7)	C(26)-C(25)-O(7)	116.1(6)	C(108)-C(109)-C(110)	120.7(7)
C(1)-C(2)-H(2)	120.8	C(30)-C(25)-O(7)	120.9(6)	C(108)-C(109)-H(109)	119.7
C(3)-C(2)-H(2)	120.8	C(25)-C(26)-C(27)	118.0(7)	C(110)-C(109)-H(109)	119.7
C(4)-C(3)-C(2)	121.1(7)	C(25)-C(26)-H(26)	121.0	C(111)-C(110)-C(109)	119.8(6)
C(4)-C(3)-H(3)	119.5	C(27)-C(26)-H(26)	121.0	C(111)-C(110)-H(110)	120.1
C(2)-C(3)-H(3)	119.5	C(26)-C(27)-C(28)	121.3(7)	C(109)-C(110)-H(110)	120.1
C(3)-C(4)-C(5)	119.1(8)	C(26)-C(27)-H(27)	119.3	C(110)-C(111)-C(112)	120.5(7)
C(3)-C(4)-H(4)	120.4	C(28)-C(27)-H(27)	119.3	C(110)-C(111)-H(111)	119.7
C(5)-C(4)-H(4)	120.4	C(27)-C(28)-C(29)	119.1(7)	C(112)-C(111)-H(111)	119.7
C(6)-C(5)-C(4)	120.9(8)	C(27)-C(28)-H(28)	120.4	C(107)-C(112)-C(111)	118.6(7)
C(6)-C(5)-H(5)	119.6	C(29)-C(28)-H(28)	120.4	C(107)-C(112)-H(112)	120.7
C(4)-C(5)-H(5)	119.6	C(30)-C(29)-C(28)	120.5(7)	C(111)-C(112)-H(112)	120.7
C(5)-C(6)-C(1)	118.8(7)	C(30)-C(29)-H(29)	119.8	C(118)-C(113)-C(114)	122.4(7)
C(5)-C(6)-H(6)	120.6	C(28)-C(29)-H(29)	119.8	C(118)-C(113)-O(104)	119.9(6)
C(1)-C(6)-H(6)	120.6	C(25)-C(30)-C(29)	118.2(7)	C(114)-C(113)-O(104)	117.6(6)
C(12)-C(7)-C(8)	123.0(7)	C(25)-C(30)-H(30)	120.9	C(115)-C(114)-C(113)	117.6(7)
C(12)-C(7)-O(2)	117.6(7)	C(29)-C(30)-H(30)	120.9	C(115)-C(114)-H(114)	121.2
C(8)-C(7)-O(2)	119.4(7)	P(2)-N(1)-P(1)	130.6(3)	C(113)-C(114)-H(114)	121.2
C(7)-C(8)-C(9)	117.0(7)	P(2)-N(1)-H(1)	114.7	C(116)-C(115)-C(114)	120.8(7)
C(7)-C(8)-H(8)	121.5	P(1)-N(1)-H(1)	114.7	C(116)-C(115)-H(115)	119.6
C(9)-C(8)-H(8)	121.5	P(3)-N(2)-P(2)	125.0(3)	C(114)-C(115)-H(115)	119.6
C(10)-C(9)-C(8)	121.8(7)	P(3)-N(2)-H(2A)	117.5	C(115)-C(116)-C(117)	119.7(7)
C(10)-C(9)-H(9)	119.1	P(2)-N(2)-H(2A)	117.5	C(115)-C(116)-H(116)	120.1
C(8)-C(9)-H(9)	119.1	C(1)-O(1)-P(1)	126.3(4)	C(117)-C(116)-H(116)	120.1
C(9)-C(10)-C(11)	119.7(7)	C(7)-O(2)-P(1)	122.5(4)	C(118)-C(117)-C(116)	120.7(7)
C(9)-C(10)-H(10)	120.2	C(13)-O(4)-P(2)	119.4(4)	C(118)-C(117)-H(117)	119.6
C(11)-C(10)-H(10)	120.2	C(19)-O(6)-P(3)	120.3(4)	C(116)-C(117)-H(117)	119.6
C(10)-C(11)-C(12)	119.9(7)	C(25)-O(7)-P(3)	126.2(4)	C(117)-C(118)-C(113)	118.7(7)
C(10)-C(11)-H(11)	120.0	O(3)-P(1)-O(2)	117.2(3)	C(117)-C(118)-H(118)	120.7
C(12)-C(11)-H(11)	120.0	O(3)-P(1)-O(1)	116.6(3)	C(113)-C(118)-H(118)	120.7
C(7)-C(12)-C(11)	118.6(7)	O(2)-P(1)-O(1)	94.1(3)	C(124)-C(119)-C(120)	122.4(7)
C(7)-C(12)-H(12)	120.7	O(3)-P(1)-N(1)	113.9(3)	C(124)-C(119)-O(106)	123.4(7)
C(11)-C(12)-H(12)	120.7	O(2)-P(1)-N(1)	105.5(3)	C(120)-C(119)-O(106)	114.2(7)
C(14)-C(13)-C(18)	122.2(7)	O(1)-P(1)-N(1)	107.4(3)	C(119)-C(120)-C(121)	118.6(8)
C(14)-C(13)-O(4)	119.9(6)	O(5)-P(2)-O(4)	116.1(3)	C(119)-C(120)-H(120)	120.7
C(18)-C(13)-O(4)	117.8(6)	O(5)-P(2)-N(1)	114.4(3)	C(121)-C(120)-H(120)	120.7
C(15)-C(14)-C(13)	118.5(7)	O(4)-P(2)-N(1)	102.8(3)	C(122)-C(121)-C(120)	120.4(8)
C(15)-C(14)-H(14)	120.7	O(5)-P(2)-N(2)	113.2(3)	C(122)-C(121)-H(121)	119.8
C(13)-C(14)-H(14)	120.7	O(4)-P(2)-N(2)	102.9(3)	C(120)-C(121)-H(121)	119.8
C(14)-C(15)-C(16)	121.2(7)	N(1)-P(2)-N(2)	106.2(3)	C(121)-C(122)-C(123)	120.2(8)
C(14)-C(15)-H(15)	119.4	O(8)-P(3)-O(7)	118.3(3)	C(121)-C(122)-H(122)	119.9
C(16)-C(15)-H(15)	119.4	O(8)-P(3)-O(6)	113.7(3)	C(123)-C(122)-H(122)	119.9
C(15)-C(16)-C(17)	119.6(7)	O(7)-P(3)-O(6)	101.5(3)	C(122)-C(123)-C(124)	120.1(9)
C(15)-C(16)-H(16)	120.2	O(8)-P(3)-N(2)	112.2(3)	C(122)-C(123)-H(123)	119.9
C(17)-C(16)-H(16)	120.2	O(7)-P(3)-N(2)	101.7(3)	C(124)-C(123)-H(123)	119.9
C(16)-C(17)-C(18)	120.3(7)	O(6)-P(3)-N(2)	108.2(3)	C(119)-C(124)-C(123)	118.3(8)
C(16)-C(17)-H(17)	119.9	C(106)-C(101)-C(102)	123.1(7)	C(119)-C(124)-H(124)	120.8
C(18)-C(17)-H(17)	119.9	C(106)-C(101)-O(101)	117.5(7)	C(123)-C(124)-H(124)	120.8
C(13)-C(18)-C(17)	118.1(7)	C(102)-C(101)-O(101)	119.3(7)	C(130)-C(125)-C(126)	122.9(7)
C(13)-C(18)-H(18)	120.9	C(101)-C(102)-C(103)	118.3(8)	C(130)-C(125)-O(107)	120.8(7)
C(17)-C(18)-H(18)	120.9	C(101)-C(102)-H(102)	120.8	C(126)-C(125)-O(107)	116.2(6)
C(24)-C(19)-C(20)	121.9(7)	C(103)-C(102)-H(102)	120.8	C(125)-C(126)-C(127)	118.0(7)
C(24)-C(19)-O(6)	118.4(6)	C(104)-C(103)-C(102)	119.8(8)	C(125)-C(126)-H(126)	121.0
C(20)-C(19)-O(6)	119.5(6)	C(104)-C(103)-H(103)	120.1	C(127)-C(126)-H(126)	121.0
C(19)-C(20)-C(21)	117.7(7)	C(102)-C(103)-H(103)	120.1	C(128)-C(127)-C(126)	120.9(8)
C(19)-C(20)-H(20)	121.2	C(103)-C(104)-C(105)	121.0(8)	C(128)-C(127)-H(127)	119.5
C(21)-C(20)-H(20)	121.2	C(103)-C(104)-H(104)	119.5	C(126)-C(127)-H(127)	119.5
C(22)-C(21)-C(20)	121.4(8)	C(105)-C(104)-H(104)	119.5	C(127)-C(128)-C(129)	119.9(7)
C(22)-C(21)-H(21)	119.3	C(104)-C(105)-C(106)	120.0(9)	C(127)-C(128)-H(128)	120.1
C(20)-C(21)-H(21)	119.3	C(104)-C(105)-H(105)	120.0	C(129)-C(128)-H(128)	120.1
C(23)-C(22)-C(21)	119.2(8)	C(106)-C(105)-H(105)	120.0	C(128)-C(129)-C(130)	120.7(7)
C(23)-C(22)-H(22)	120.4	C(101)-C(106)-C(105)	117.7(8)	C(128)-C(129)-H(129)	119.6
C(21)-C(22)-H(22)	120.4	C(101)-C(106)-H(106)	121.1	C(130)-C(129)-H(129)	119.6
C(22)-C(23)-C(24)	121.4(7)	C(105)-C(106)-H(106)	121.1	C(125)-C(130)-C(129)	117.5(7)
C(22)-C(23)-H(23)	119.3	C(112)-C(107)-C(108)	122.2(6)	C(125)-C(130)-H(130)	121.3
C(24)-C(23)-H(23)	119.3	C(112)-C(107)-O(102)	117.3(6)	C(129)-C(130)-H(130)	121.3
C(23)-C(24)-C(19)	118.4(7)	C(108)-C(107)-O(102)	120.4(6)	P(101)-N(101)-P(102)	124.2(3)
C(23)-C(24)-H(24)	120.8	C(109)-C(108)-C(107)	118.1(6)	P(101)-N(101)-H(101)	117.9
C(19)-C(24)-H(24)	120.8	C(109)-C(108)-H(108)	120.9	P(102)-N(101)-H(101)	117.9
C(26)-C(25)-C(30)	122.9(7)	C(107)-C(108)-H(108)	120.9	P(103)-N(102)-P(102)	129.5(3)

P(103)-N(102)-H(10A)	115.2	O(102)-P(101)-O(101)	101.1(3)	N(101)-P(102)-N(102)	106.0(3)
P(102)-N(102)-H(10A)	115.2	O(103)-P(101)-N(101)	112.4(3)	O(108)-P(103)-O(107)	116.5(3)
C(101)-O(101)-P(101)	118.9(4)	O(102)-P(101)-N(101)	102.5(3)	O(108)-P(103)-O(106)	114.0(3)
C(107)-O(102)-P(101)	124.5(4)	O(101)-P(101)-N(101)	107.8(3)	O(107)-P(103)-O(106)	101.0(3)
C(113)-O(104)-P(102)	121.0(4)	O(105)-P(102)-O(104)	116.7(3)	O(108)-P(103)-N(102)	115.6(3)
C(119)-O(106)-P(103)	124.9(5)	O(105)-P(102)-N(101)	113.1(3)	O(107)-P(103)-N(102)	101.7(3)
C(125)-O(107)-P(103)	124.5(4)	O(104)-P(102)-N(101)	103.9(3)	O(106)-P(103)-N(102)	106.3(3)
O(103)-P(101)-O(102)	116.7(3)	O(105)-P(102)-N(102)	114.3(3)		
O(103)-P(101)-O(101)	115.0(3)	O(104)-P(102)-N(102)	101.4(3)		

Table 4. Anisotropic displacement parameters ($Å^2 x\ 10^3$)for 2008src1077. The anisotropic displacement factor exponent takes the form: $-2\pi^2[\ h^2 a^{*2} U^{11} + ... + 2\ h\ k\ a^*\ b^*\ U^{12}\ ]$

	U^{11}	U^{22}	U^{33}	U^{23}	U^{13}	U^{12}
C(1)	26(4)	34(4)	27(4)	-3(3)	-10(3)	-12(3)
C(2)	30(4)	40(5)	33(4)	-16(4)	-1(3)	-11(4)
C(3)	38(5)	57(6)	24(4)	-6(4)	2(4)	-18(4)
C(4)	36(5)	50(5)	30(4)	-3(4)	-9(4)	-20(4)
C(5)	32(4)	35(5)	40(5)	-2(4)	-13(4)	-8(4)
C(6)	27(4)	37(4)	30(4)	-13(3)	-2(3)	-15(3)
C(7)	30(4)	23(4)	29(4)	-5(3)	-2(3)	-2(3)
C(8)	27(4)	38(5)	41(5)	-2(4)	-8(4)	-11(4)
C(9)	40(5)	39(5)	41(5)	-5(4)	3(4)	-21(4)
C(10)	45(5)	27(4)	29(4)	0(3)	-4(4)	-8(4)
C(11)	36(5)	43(5)	44(5)	-12(4)	-10(4)	-11(4)
C(12)	28(4)	28(4)	43(5)	-3(4)	-8(4)	-8(3)
C(13)	24(4)	20(4)	19(3)	-3(3)	-4(3)	-6(3)
C(14)	23(4)	39(5)	31(4)	-9(3)	-7(3)	-10(3)
C(15)	24(4)	32(4)	45(5)	-16(4)	-11(3)	-1(3)
C(16)	39(5)	24(4)	42(5)	-9(4)	-10(4)	-5(4)
C(17)	33(4)	36(4)	37(4)	-12(4)	3(3)	-21(4)
C(18)	20(4)	27(4)	31(4)	-6(3)	6(3)	-7(3)
C(19)	20(4)	27(4)	30(4)	-15(3)	2(3)	-9(3)
C(20)	66(6)	31(4)	21(4)	-7(3)	-1(4)	-7(4)
C(21)	76(7)	31(5)	34(5)	-7(4)	10(4)	-14(5)
C(22)	49(5)	38(5)	38(5)	-21(4)	4(4)	-14(4)
C(23)	37(5)	36(5)	33(4)	-14(4)	-9(4)	-3(4)
C(24)	28(4)	38(4)	21(4)	-5(3)	-1(3)	-5(3)
C(25)	24(4)	25(4)	28(4)	-5(3)	0(3)	-8(3)
C(26)	29(4)	26(4)	29(4)	0(3)	-12(3)	-4(3)
C(27)	28(4)	40(5)	40(5)	-1(4)	-6(4)	-14(4)
C(28)	40(5)	38(5)	27(4)	-1(4)	2(3)	-21(4)
C(29)	49(5)	45(5)	22(4)	-5(4)	-6(4)	-19(4)
C(30)	36(4)	37(4)	28(4)	-2(3)	-13(3)	-12(4)
N(1)	9(3)	27(3)	27(3)	-7(3)	3(2)	-7(2)
N(2)	13(3)	21(3)	26(3)	-4(2)	-2(2)	-10(2)
O(1)	26(3)	26(3)	28(3)	-14(2)	2(2)	-7(2)
O(2)	28(3)	24(3)	36(3)	-5(2)	-2(2)	0(2)
O(3)	21(3)	30(3)	34(3)	-11(2)	-2(2)	-10(2)
O(4)	21(3)	22(2)	19(2)	-6(2)	2(2)	-6(2)
O(5)	17(2)	25(3)	24(2)	-9(2)	-4(2)	-8(2)
O(6)	24(3)	29(3)	26(3)	-8(2)	-2(2)	-9(2)
O(7)	29(3)	29(3)	28(3)	-5(2)	-4(2)	-12(2)
O(8)	21(3)	40(3)	33(3)	-12(2)	-11(2)	-7(2)
P(1)	20(1)	24(1)	26(1)	-8(1)	-2(1)	-7(1)
P(2)	17(1)	24(1)	19(1)	-6(1)	-2(1)	-6(1)
P(3)	20(1)	27(1)	22(1)	-6(1)	-5(1)	-8(1)
C(101)	26(4)	21(4)	36(4)	-8(3)	-11(3)	-3(3)
C(102)	30(4)	24(4)	41(5)	0(3)	-15(4)	-4(3)
C(103)	33(5)	27(4)	68(6)	-13(4)	-9(4)	-11(4)
C(104)	48(6)	40(5)	69(7)	-32(5)	-20(5)	-3(4)
C(105)	54(6)	55(6)	44(5)	-24(5)	-4(4)	2(5)
C(106)	47(5)	33(4)	27(4)	-8(3)	0(4)	-9(4)
C(107)	22(4)	26(4)	20(3)	-7(3)	-5(3)	-5(3)
C(108)	27(4)	39(4)	25(4)	-2(3)	-1(3)	-21(3)

C(109)	49(5)	32(4)	24(4)	2(3)	-12(4)	-23(4)
C(110)	32(4)	36(4)	24(4)	-7(3)	-13(3)	-3(3)
C(111)	15(4)	44(5)	25(4)	-9(3)	2(3)	-13(3)
C(112)	30(4)	27(4)	25(4)	-5(3)	0(3)	-13(3)
C(113)	23(4)	23(4)	21(4)	-3(3)	-8(3)	-5(3)
C(114)	16(4)	45(5)	29(4)	-12(4)	-8(3)	-2(3)
C(115)	33(5)	51(5)	34(4)	-16(4)	-8(4)	-19(4)
C(116)	32(5)	48(5)	41(5)	-25(4)	4(4)	-11(4)
C(117)	28(4)	42(5)	33(4)	-10(4)	3(3)	-6(4)
C(118)	21(4)	35(4)	28(4)	-3(3)	-1(3)	-14(3)
C(119)	29(4)	25(4)	37(4)	-2(3)	-10(3)	-11(3)
C(120)	24(4)	32(4)	47(5)	-5(4)	-2(4)	-6(3)
C(121)	47(6)	45(5)	54(6)	15(5)	-13(5)	-16(5)
C(122)	42(5)	70(7)	39(5)	19(5)	-16(4)	-33(5)
C(123)	39(5)	62(6)	28(4)	0(4)	1(4)	-30(5)
C(124)	34(4)	37(4)	34(4)	-3(4)	-11(4)	-16(4)
C(125)	30(4)	29(4)	25(4)	-5(3)	0(3)	-15(3)
C(126)	23(4)	45(5)	42(5)	-20(4)	3(3)	-10(4)
C(127)	39(5)	45(5)	49(5)	-31(4)	12(4)	-16(4)
C(128)	43(5)	39(5)	50(5)	-24(4)	-6(4)	-11(4)
C(129)	30(4)	44(5)	39(5)	-17(4)	-10(4)	-11(4)
C(130)	32(4)	33(4)	39(5)	-11(4)	-5(4)	-9(4)
N(101)	14(3)	28(3)	22(3)	-9(2)	-3(2)	-10(2)
N(102)	13(3)	27(3)	26(3)	-5(3)	-5(2)	-7(2)
O(101)	23(3)	24(3)	28(3)	-11(2)	-4(2)	-5(2)
O(102)	25(3)	24(3)	25(3)	-6(2)	-10(2)	-10(2)
O(103)	21(3)	28(3)	28(3)	-10(2)	4(2)	-14(2)
O(104)	24(3)	22(2)	19(2)	-6(2)	-1(2)	-6(2)
O(105)	18(2)	21(2)	25(3)	-6(2)	-2(2)	-6(2)
O(106)	25(3)	23(3)	36(3)	-8(2)	-5(2)	-6(2)
O(107)	28(3)	37(3)	30(3)	-12(2)	-1(2)	-15(2)
O(108)	9(2)	36(3)	32(3)	-10(2)	-3(2)	-4(2)
P(101)	20(1)	24(1)	21(1)	-5(1)	-2(1)	-9(1)
P(102)	14(1)	23(1)	19(1)	-4(1)	-2(1)	-6(1)
P(103)	18(1)	26(1)	27(1)	-9(1)	-4(1)	-8(1)

Table 5. Hydrogen coordinates (x 10^4) and isotropic displacement parameters ($Å^2$x 10^3) for 2008src1077.

	x	y	z	U(eq)	x	y	z	U(eq)	
H(2)	-849	4295	5043	39	H(102)	5975	-1202	3895	38
H(3)	-491	2939	5908	48	H(103)	6045	-2483	3366	49
H(4)	1285	1466	5864	45	H(104)	6810	-2280	2333	58
H(5)	2747	1351	4951	43	H(105)	7496	-810	1799	63
H(6)	2464	2718	4099	35	H(106)	7423	484	2321	44
H(8)	2184	6461	2498	42	H(108)	5660	759	4936	34
H(9)	2322	7418	1477	47	H(109)	7192	171	5673	39
H(10)	614	7738	868	42	H(110)	9185	696	5488	36
H(11)	-1213	7014	1239	48	H(111)	9637	1834	4578	33
H(12)	-1334	5989	2248	40	H(112)	8111	2440	3839	32
H(14)	3073	544	3131	36	H(114)	3949	2287	1591	36
H(15)	3602	-1119	2958	39	H(115)	4394	1139	928	43
H(16)	1909	-1842	2872	42	H(116)	6584	554	466	46
H(17)	-353	-893	2963	39	H(117)	8322	1202	608	42
H(18)	-914	799	3134	33	H(118)	7894	2380	1236	33
H(20)	1522	861	1831	49	H(120)	4322	7652	2049	42
H(21)	1354	-561	1492	59	H(121)	4565	8430	996	62
H(22)	1316	-471	454	48	H(122)	5996	7497	297	61
H(23)	1229	1088	-241	42	H(123)	7321	5821	648	50
H(24)	1304	2543	80	36	H(124)	7117	5045	1706	40
H(26)	3188	4423	1654	34	H(126)	3478	6022	4099	42
H(27)	4598	5307	946	44	H(127)	3580	7026	4783	50
H(28)	3980	6172	-29	42	H(128)	5633	7038	5022	49
H(29)	1934	6124	-308	44	H(129)	7630	6036	4598	42
H(30)	499	5248	402	39	H(130)	7560	4963	3943	41
H(1)	-539	3921	3133	25	H(101)	4344	2148	2718	23
H(2A)	-659	2575	2337	23	H(10A)	4474	4285	2707	26

Table 6. Hydrogen bonds for 2008src1077 [Å and °].

D-H...A	d(D-H)	d(H...A)	d(D...A)	<(DHA)
N(1)-H(1)...O(108)#1	0.88	2.02	2.837(7)	154.6
N(2)-H(2A)...O(105)#1	0.88	1.98	2.828(7)	160.5
N(101)-H(101)...O(5)	0.88	1.98	2.816(7)	157.9
N(102)-H(10A)...O(3)	0.88	2.08	2.864(7)	148.1

Symmetry transformations used to generate equivalent atoms:
#1 x-1,y,z

B10 Crystallographic Data for Nabiphenp

Table 2. Atomic coordinates (x 10^4) and equivalent isotropic displacement parameters ($Å^2$x 10^3) for 2008ZP2. U(eq) is defined as one third of the trace of the orthogonalized U^{ij} tensor.

	x	y	z	U(eq)		x	y	z	U(eq)	
C(1)	2993(6)	-1644(4)	1898(3)	37(2)		C(34)	3726(6)	677(4)	478(3)	34(2)
C(2)	5742(8)	-1987(6)	2250(4)	53(2)		C(35)	2031(6)	2328(4)	-773(3)	31(2)
C(3)	1247(7)	-1399(5)	4506(3)	42(2)		C(36)	2067(6)	3302(4)	-772(3)	38(2)
C(4)	1732(7)	-444(5)	6022(4)	45(2)		C(37)	1442(6)	3601(5)	-1437(3)	39(2)
C(5)	-272(6)	927(4)	1764(3)	33(2)		C(38)	738(7)	2949(5)	-2114(3)	42(2)
C(6)	-1477(6)	1407(4)	1909(3)	32(2)		C(39)	665(6)	1983(5)	-2122(3)	40(2)
C(7)	-2117(6)	1961(4)	1411(3)	31(2)		C(40)	1305(6)	1677(4)	-1460(3)	36(2)
C(8)	-1559(6)	2039(4)	762(3)	35(2)		C(41)	5704(5)	2734(4)	3794(3)	29(2)
C(9)	-399(6)	1498(4)	596(3)	35(2)		C(42)	5532(6)	2418(4)	4432(3)	35(2)
C(10)	241(6)	931(4)	1085(3)	33(2)		C(43)	5975(6)	3023(4)	5193(3)	33(2)
C(11)	-2104(6)	2731(4)	294(3)	34(2)		C(44)	6586(6)	3943(4)	5305(3)	29(2)
C(12)	-3558(6)	2887(5)	106(3)	39(2)		C(45)	6771(6)	4241(4)	4643(3)	36(2)
C(13)	-4056(7)	3563(4)	-301(3)	40(2)		C(46)	6301(6)	3652(4)	3891(3)	35(2)
C(14)	-3100(7)	4103(5)	-541(4)	46(2)		C(47)	7154(6)	4570(4)	6123(3)	31(2)
C(15)	-1647(7)	3953(5)	-366(4)	45(2)		C(48)	7586(6)	4170(4)	6765(3)	35(2)
C(16)	-1166(6)	3276(5)	46(4)	40(2)		C(49)	8134(6)	4730(4)	7509(3)	36(2)
C(17)	1111(6)	2230(4)	4222(3)	31(2)		C(50)	8247(6)	5729(5)	7633(3)	41(2)
C(18)	330(6)	3043(4)	4415(3)	32(2)		C(51)	7797(7)	6141(4)	7014(4)	42(2)
C(19)	700(6)	3648(4)	5167(3)	30(2)		C(52)	7236(6)	5581(4)	6263(3)	35(2)
C(20)	1839(6)	3493(4)	5732(3)	30(2)		N(1)	2807(4)	1415(3)	2783(3)	27(2)
C(21)	2551(6)	2646(4)	5521(3)	33(2)		O(1)	4185(5)	-1940(3)	3296(2)	38(2)
C(22)	2212(6)	2013(4)	4771(3)	31(2)		O(2)	3479(4)	-165(3)	5121(2)	35(2)
C(23)	2341(6)	4187(4)	6509(3)	32(2)		O(3)	1999(4)	90(3)	3442(2)	34(2)
C(24)	1427(6)	4826(4)	6874(3)	36(2)		O(4)	381(4)	389(3)	2263(2)	32(2)
C(25)	1961(6)	5483(4)	7592(3)	37(2)		O(5)	680(4)	1651(3)	3460(2)	33(2)
C(26)	3384(7)	5530(4)	7958(3)	38(2)		O(6)	5052(4)	417(3)	3103(2)	34(2)
C(27)	4290(6)	4900(4)	7605(3)	33(2)		O(7)	4554(4)	877(3)	1837(2)	33(2)
C(28)	3785(6)	4250(4)	6892(3)	32(2)		O(8)	5347(4)	2165(3)	3017(2)	32(2)
C(29)	3971(5)	1283(4)	1231(3)	30(2)		P(1)	1619(1)	850(1)	3021(1)	29(2)
C(30)	3615(6)	2250(4)	1336(3)	31(2)		P(2)	4383(1)	1167(1)	2736(1)	30(2)
C(31)	3013(6)	2577(4)	687(3)	31(2)		Na(1)	4326(2)	-346(2)	3954(1)	30(2)
C(32)	2723(6)	1979(4)	-79(3)	32(2)		S(1)	4105(2)	-2370(1)	2427(1)	37(2)
C(33)	3132(6)	1019(4)	-169(3)	31(2)		S(2)	1897(1)	-239(1)	5105(1)	34(2)

Table 3. Bond lengths [Å] and angles [°] for 2008ZP2.

C(1)-S(1)	1.788(6)	C(2)-H(2B)	0.9800	C(4)-S(2)	1.769(6)
C(1)-H(1A)	0.9800	C(2)-H(2C)	0.9800	C(4)-H(4A)	0.9800
C(1)-H(1B)	0.9800	C(3)-S(2)	1.766(6)	C(4)-H(4B)	0.9800
C(1)-H(1C)	0.9800	C(3)-H(3A)	0.9800	C(4)-H(4C)	0.9800
C(2)-S(1)	1.769(7)	C(3)-H(3B)	0.9800	C(5)-O(4)	1.376(7)
C(2)-H(2A)	0.9800	C(3)-H(3C)	0.9800	C(5)-C(6)	1.384(8)

C(5)-C(10)	1.396(8)	C(25)-C(26)	1.381(9)	C(44)-C(45)	1.392(8)
C(6)-C(7)	1.387(8)	C(25)-H(25)	0.9500	C(44)-C(47)	1.503(7)
C(6)-H(6)	0.9500	C(26)-C(27)	1.385(8)	C(45)-C(46)	1.381(8)
C(7)-C(8)	1.397(8)	C(26)-H(26)	0.9500	C(45)-H(45)	0.9500
C(7)-H(7)	0.9500	C(27)-C(28)	1.370(8)	C(46)-H(46)	0.9500
C(8)-C(9)	1.399(8)	C(27)-H(27)	0.9500	C(47)-C(48)	1.393(8)
C(8)-C(11)	1.478(8)	C(28)-H(28)	0.9500	C(47)-C(52)	1.403(8)
C(9)-C(10)	1.390(8)	C(29)-O(7)	1.375(6)	C(48)-C(49)	1.366(8)
C(9)-H(9)	0.9500	C(29)-C(34)	1.381(7)	C(48)-H(48)	0.9500
C(10)-H(10)	0.9500	C(29)-C(30)	1.401(8)	C(49)-C(50)	1.390(9)
C(11)-C(16)	1.388(8)	C(30)-C(31)	1.374(8)	C(49)-H(49)	0.9500
C(11)-C(12)	1.399(8)	C(30)-H(30)	0.9500	C(50)-C(51)	1.373(9)
C(12)-C(13)	1.377(9)	C(31)-C(32)	1.394(8)	C(50)-H(50)	0.9500
C(12)-H(12)	0.9500	C(31)-H(31)	0.9500	C(51)-C(52)	1.379(8)
C(13)-C(14)	1.388(10)	C(32)-C(33)	1.409(8)	C(51)-H(51)	0.9500
C(13)-H(13)	0.9500	C(32)-C(35)	1.483(8)	C(52)-H(52)	0.9500
C(14)-C(15)	1.394(10)	C(33)-C(34)	1.383(8)	N(1)-P(2)	1.568(4)
C(14)-H(14)	0.9500	C(33)-H(33)	0.9500	N(1)-P(1)	1.572(4)
C(15)-C(16)	1.381(9)	C(34)-H(34)	0.9500	O(1)-S(1)	1.506(4)
C(15)-H(15)	0.9500	C(35)-C(40)	1.392(8)	O(1)-Na(1)	2.281(4)
C(16)-H(16)	0.9500	C(35)-C(36)	1.391(8)	O(2)-S(2)	1.513(4)
C(17)-C(22)	1.381(8)	C(36)-C(37)	1.384(8)	O(2)-Na(1)	2.341(4)
C(17)-O(5)	1.385(6)	C(36)-H(36)	0.9500	O(2)-Na(1)#1	2.378(4)
C(17)-C(18)	1.397(8)	C(37)-C(38)	1.374(9)	O(3)-P(1)	1.474(4)
C(18)-C(19)	1.382(7)	C(37)-H(37)	0.9500	O(3)-Na(1)	2.382(4)
C(18)-H(18)	0.9500	C(38)-C(39)	1.378(9)	O(4)-P(1)	1.604(4)
C(19)-C(20)	1.387(7)	C(38)-H(38)	0.9500	O(5)-P(1)	1.611(4)
C(19)-H(19)	0.9500	C(39)-C(40)	1.388(8)	O(6)-P(2)	1.473(4)
C(20)-C(21)	1.403(8)	C(39)-H(39)	0.9500	O(6)-Na(1)	2.282(4)
C(20)-C(23)	1.478(7)	C(40)-H(40)	0.9500	O(7)-P(2)	1.598(4)
C(21)-C(22)	1.393(8)	C(41)-C(42)	1.361(8)	O(8)-P(2)	1.605(4)
C(21)-H(21)	0.9500	C(41)-C(46)	1.384(8)	P(2)-Na(1)	3.426(2)
C(22)-H(22)	0.9500	C(41)-O(8)	1.398(6)	Na(1)-O(2)#1	2.378(4)
C(23)-C(28)	1.406(8)	C(42)-C(43)	1.398(8)	Na(1)-S(2)	3.381(2)
C(23)-C(24)	1.406(8)	C(42)-H(42)	0.9500	Na(1)-Na(1)#1	3.576(4)
C(24)-C(25)	1.387(8)	C(43)-C(44)	1.385(7)		
C(24)-H(24)	0.9500	C(43)-H(43)	0.9500		

S(1)-C(1)-H(1A)	109.5	C(8)-C(7)-H(7)	119.7	C(19)-C(18)-H(18)	120.6
S(1)-C(1)-H(1B)	109.5	C(7)-C(8)-C(9)	118.6(5)	C(17)-C(18)-H(18)	120.6
H(1A)-C(1)-H(1B)	109.5	C(7)-C(8)-C(11)	121.1(5)	C(18)-C(19)-C(20)	122.5(5)
S(1)-C(1)-H(1C)	109.5	C(9)-C(8)-C(11)	120.2(5)	C(18)-C(19)-H(19)	118.7
H(1A)-C(1)-H(1C)	109.5	C(10)-C(9)-C(8)	121.2(5)	C(20)-C(19)-H(19)	118.7
H(1B)-C(1)-H(1C)	109.5	C(10)-C(9)-H(9)	119.4	C(19)-C(20)-C(21)	116.6(5)
S(1)-C(2)-H(2A)	109.5	C(8)-C(9)-H(9)	119.4	C(19)-C(20)-C(23)	123.1(5)
S(1)-C(2)-H(2B)	109.5	C(9)-C(10)-C(5)	118.7(5)	C(21)-C(20)-C(23)	120.3(5)
H(2A)-C(2)-H(2B)	109.5	C(9)-C(10)-H(10)	120.6	C(22)-C(21)-C(20)	122.8(5)
S(1)-C(2)-H(2C)	109.5	C(5)-C(10)-H(10)	120.6	C(22)-C(21)-H(21)	118.6
H(2A)-C(2)-H(2C)	109.5	C(16)-C(11)-C(12)	117.5(6)	C(20)-C(21)-H(21)	118.6
H(2B)-C(2)-H(2C)	109.5	C(16)-C(11)-C(8)	120.4(5)	C(17)-C(22)-C(21)	118.0(5)
S(2)-C(3)-H(3A)	109.5	C(12)-C(11)-C(8)	122.1(5)	C(17)-C(22)-H(22)	121.0
S(2)-C(3)-H(3B)	109.5	C(13)-C(12)-C(11)	121.9(6)	C(21)-C(22)-H(22)	121.0
H(3A)-C(3)-H(3B)	109.5	C(13)-C(12)-H(12)	119.0	C(28)-C(23)-C(24)	117.9(5)
S(2)-C(3)-H(3C)	109.5	C(11)-C(12)-H(12)	119.0	C(28)-C(23)-C(20)	120.0(5)
H(3A)-C(3)-H(3C)	109.5	C(12)-C(13)-C(14)	119.7(6)	C(24)-C(23)-C(20)	122.1(5)
H(3B)-C(3)-H(3C)	109.5	C(12)-C(13)-H(13)	120.2	C(25)-C(24)-C(23)	119.8(6)
S(2)-C(4)-H(4A)	109.5	C(14)-C(13)-H(13)	120.2	C(25)-C(24)-H(24)	120.1
S(2)-C(4)-H(4B)	109.5	C(13)-C(14)-C(15)	119.4(6)	C(23)-C(24)-H(24)	120.1
H(4A)-C(4)-H(4B)	109.5	C(13)-C(14)-H(14)	120.3	C(26)-C(25)-C(24)	121.3(5)
S(2)-C(4)-H(4C)	109.5	C(15)-C(14)-H(14)	120.3	C(26)-C(25)-H(25)	119.4
H(4A)-C(4)-H(4C)	109.5	C(16)-C(15)-C(14)	120.1(6)	C(24)-C(25)-H(25)	119.4
H(4B)-C(4)-H(4C)	109.5	C(16)-C(15)-H(15)	119.9	C(25)-C(26)-C(27)	119.3(5)
O(4)-C(5)-C(6)	120.1(5)	C(14)-C(15)-H(15)	119.9	C(25)-C(26)-H(26)	120.4
O(4)-C(5)-C(10)	119.1(5)	C(15)-C(16)-C(11)	121.4(6)	C(27)-C(26)-H(26)	120.4
C(6)-C(5)-C(10)	120.7(5)	C(15)-C(16)-H(16)	119.3	C(28)-C(27)-C(26)	120.3(5)
C(5)-C(6)-C(7)	119.8(5)	C(11)-C(16)-H(16)	119.3	C(28)-C(27)-H(27)	119.8
C(5)-C(6)-H(6)	120.1	C(22)-C(17)-O(5)	122.9(5)	C(26)-C(27)-H(27)	119.8
C(7)-C(6)-H(6)	120.1	C(22)-C(17)-C(18)	121.3(5)	C(27)-C(28)-C(23)	121.4(5)
C(6)-C(7)-C(8)	120.6(5)	O(5)-C(17)-C(18)	115.8(5)	C(27)-C(28)-H(28)	119.3
C(6)-C(7)-H(7)	119.7	C(19)-C(18)-C(17)	118.7(5)	C(23)-C(28)-H(28)	119.3

O(7)-C(29)-C(34)	116.1(5)	C(43)-C(44)-C(47)	120.8(5)	O(6)-P(2)-O(8)	112.1(2)
O(7)-C(29)-C(30)	124.2(5)	C(45)-C(44)-C(47)	120.6(5)	N(1)-P(2)-O(8)	107.7(2)
C(34)-C(29)-C(30)	119.6(5)	C(46)-C(45)-C(44)	121.0(5)	O(7)-P(2)-O(8)	97.7(2)
C(31)-C(30)-C(29)	119.4(5)	C(46)-C(45)-H(45)	119.5	O(6)-P(2)-Na(1)	30.43(16)
C(31)-C(30)-H(30)	120.3	C(44)-C(45)-H(45)	119.5	N(1)-P(2)-Na(1)	90.14(17)
C(29)-C(30)-H(30)	120.3	C(45)-C(46)-C(41)	119.6(5)	O(7)-P(2)-Na(1)	127.28(15)
C(30)-C(31)-C(32)	122.5(5)	C(45)-C(46)-H(46)	120.2	O(8)-P(2)-Na(1)	122.09(15)
C(30)-C(31)-H(31)	118.8	C(41)-C(46)-H(46)	120.2	O(1)-Na(1)-O(6)	103.15(15)
C(32)-C(31)-H(31)	118.8	C(48)-C(47)-C(52)	118.1(5)	O(1)-Na(1)-O(2)	110.20(15)
C(31)-C(32)-C(33)	116.9(5)	C(48)-C(47)-C(44)	121.4(5)	O(6)-Na(1)-O(2)	146.22(17)
C(31)-C(32)-C(35)	122.2(5)	C(52)-C(47)-C(44)	120.5(5)	O(1)-Na(1)-O(2)#1	113.55(17)
C(33)-C(32)-C(35)	120.9(5)	C(49)-C(48)-C(47)	122.0(5)	O(6)-Na(1)-O(2)#1	90.28(15)
C(34)-C(33)-C(32)	121.3(5)	C(49)-C(48)-H(48)	119.0	O(2)-Na(1)-O(2)#1	81.47(15)
C(34)-C(33)-H(33)	119.4	C(47)-C(48)-H(48)	119.0	O(1)-Na(1)-O(3)	100.32(16)
C(32)-C(33)-H(33)	119.4	C(48)-C(49)-C(50)	119.2(6)	O(6)-Na(1)-O(3)	85.20(15)
C(29)-C(34)-C(33)	120.3(5)	C(48)-C(49)-H(49)	120.4	O(2)-Na(1)-O(3)	83.77(14)
C(29)-C(34)-H(34)	119.9	C(50)-C(49)-H(49)	120.4	O(2)#1-Na(1)-O(3)	145.94(16)
C(33)-C(34)-H(34)	119.9	C(51)-C(50)-C(49)	119.9(5)	O(1)-Na(1)-S(2)	103.53(12)
C(40)-C(35)-C(36)	117.2(5)	C(51)-C(50)-H(50)	120.1	O(6)-Na(1)-S(2)	141.54(13)
C(40)-C(35)-C(32)	120.3(5)	C(49)-C(50)-H(50)	120.1	O(2)-Na(1)-S(2)	22.51(10)
C(36)-C(35)-C(32)	122.5(5)	C(50)-C(51)-C(52)	121.2(6)	O(2)#1-Na(1)-S(2)	103.74(11)
C(37)-C(36)-C(35)	121.1(5)	C(50)-C(51)-H(51)	119.4	O(3)-Na(1)-S(2)	63.12(10)
C(37)-C(36)-H(36)	119.5	C(52)-C(51)-H(51)	119.4	O(1)-Na(1)-P(2)	112.60(11)
C(35)-C(36)-H(36)	119.5	C(51)-C(52)-C(47)	119.6(5)	O(6)-Na(1)-P(2)	19.08(10)
C(38)-C(37)-C(36)	121.1(6)	C(51)-C(52)-H(52)	120.2	O(2)-Na(1)-P(2)	131.71(13)
C(38)-C(37)-H(37)	119.5	C(47)-C(52)-H(52)	120.2	O(2)#1-Na(1)-P(2)	100.68(11)
C(36)-C(37)-H(37)	119.4	P(2)-N(1)-P(1)	130.1(3)	O(3)-Na(1)-P(2)	67.68(10)
C(37)-C(38)-C(39)	118.8(5)	S(1)-O(1)-Na(1)	128.3(2)	S(2)-Na(1)-P(2)	122.70(7)
C(37)-C(38)-H(38)	120.6	S(2)-O(2)-Na(1)	121.1(2)	O(1)-Na(1)-Na(1)#1	119.46(14)
C(39)-C(38)-H(38)	120.6	S(2)-O(2)-Na(1)#1	139.5(2)	O(6)-Na(1)-Na(1)#1	123.18(14)
C(38)-C(39)-C(40)	120.3(6)	Na(1)-O(2)-Na(1)#1	98.53(15)	O(2)-Na(1)-Na(1)#1	41.12(10)
C(38)-C(39)-H(39)	119.8	P(1)-O(3)-Na(1)	127.8(2)	O(2)#1-Na(1)-Na(1)#1	40.34(9)
C(40)-C(39)-H(39)	119.8	C(5)-O(4)-P(1)	122.0(3)	O(3)-Na(1)-Na(1)#1	118.68(13)
C(35)-C(40)-C(39)	121.5(5)	C(17)-O(5)-P(1)	125.1(3)	S(2)-Na(1)-Na(1)#1	63.46(6)
C(35)-C(40)-H(40)	119.2	P(2)-O(6)-Na(1)	130.5(2)	P(2)-Na(1)-Na(1)#1	123.97(9)
C(39)-C(40)-H(40)	119.2	C(29)-O(7)-P(2)	128.7(3)	O(1)-S(1)-C(2)	105.0(3)
C(42)-C(41)-C(46)	120.6(5)	C(41)-O(8)-P(2)	124.8(3)	O(1)-S(1)-C(1)	107.4(2)
C(42)-C(41)-O(8)	123.6(5)	O(3)-P(1)-N(1)	120.5(2)	C(2)-S(1)-C(1)	96.8(3)
C(46)-C(41)-O(8)	115.7(5)	O(3)-P(1)-O(4)	107.3(2)	O(2)-S(2)-C(3)	106.4(3)
C(41)-C(42)-C(43)	119.8(5)	N(1)-P(1)-O(4)	110.5(2)	O(2)-S(2)-C(4)	106.4(3)
C(41)-C(42)-H(42)	120.1	O(3)-P(1)-O(5)	112.7(2)	C(3)-S(2)-C(4)	97.5(3)
C(43)-C(42)-H(42)	120.1	N(1)-P(1)-O(5)	106.8(2)	O(2)-S(2)-Na(1)	36.34(14)
C(44)-C(43)-C(42)	120.7(5)	O(4)-P(1)-O(5)	96.5(2)	C(3)-S(2)-Na(1)	86.2(2)
C(44)-C(43)-H(43)	119.6	O(6)-P(2)-N(1)	120.0(2)	C(4)-S(2)-Na(1)	140.2(2)
C(42)-C(43)-H(43)	119.6	O(6)-P(2)-O(7)	106.4(2)		
C(43)-C(44)-C(45)	118.3(5)	N(1)-P(2)-O(7)	110.5(2)		

Symmetry transformations used to generate equivalent atoms:
#1 -x+1,-y,-z+1

Table 4. Anisotropic displacement parameters ($Å^2 x\ 10^3$)for 2008ZP2. The anisotropic displacement factor exponent takes the form: $-2\pi^2[\ h^2 a^{*2} U^{11} + ... + 2\ h\ k\ a^*\ b^*\ U^{12}\ ]$

	U^{11}	U^{22}	U^{33}	U^{23}	U^{13}	U^{12}
C(1)	46(3)	37(3)	25(3)	7(2)	0(2)	6(2)
C(2)	54(4)	66(5)	38(4)	7(3)	15(3)	2(3)
C(3)	41(3)	53(4)	31(3)	10(3)	8(2)	-7(3)
C(4)	36(4)	63(4)	38(3)	12(3)	13(2)	-7(3)
C(5)	30(3)	34(3)	28(3)	5(2)	-4(2)	-3(2)
C(6)	36(3)	33(3)	28(3)	3(2)	12(2)	-10(2)
C(7)	31(3)	30(3)	31(3)	5(2)	8(2)	-1(2)
C(8)	32(3)	42(3)	24(3)	4(2)	0(2)	-6(2)
C(9)	27(3)	47(4)	27(3)	4(2)	7(2)	-7(2)
C(10)	30(3)	37(3)	29(3)	4(2)	3(2)	-4(2)
C(11)	38(3)	34(3)	25(3)	0(2)	4(2)	-1(2)
C(12)	38(3)	49(4)	24(3)	2(2)	3(2)	-1(3)

C(13)	41(3)	40(3)	32(3)	1(2)	0(2)	6(2)
C(14)	57(4)	38(4)	35(3)	5(3)	-4(3)	2(3)
C(15)	51(4)	47(4)	34(3)	11(3)	2(3)	-10(3)
C(16)	35(3)	47(4)	37(3)	12(3)	2(2)	-4(2)
C(17)	32(3)	35(3)	30(3)	6(2)	15(2)	-3(2)
C(18)	34(3)	36(3)	26(3)	9(2)	6(2)	-1(2)
C(19)	30(3)	30(3)	31(3)	12(2)	6(2)	6(2)
C(20)	29(3)	31(3)	29(3)	5(2)	6(2)	-5(2)
C(21)	34(3)	35(3)	33(3)	11(2)	9(2)	3(2)
C(22)	33(3)	34(3)	24(3)	3(2)	5(2)	0(2)
C(23)	39(3)	31(3)	27(3)	8(2)	9(2)	-4(2)
C(24)	38(3)	33(3)	37(3)	4(2)	12(2)	-5(2)
C(25)	44(3)	31(3)	37(3)	2(2)	20(2)	-5(2)
C(26)	52(4)	34(3)	28(3)	5(2)	11(2)	-6(3)
C(27)	36(3)	30(3)	32(3)	3(2)	8(2)	1(2)
C(28)	36(3)	31(3)	26(3)	8(2)	-1(2)	-1(2)
C(29)	26(3)	38(3)	28(3)	12(2)	5(2)	0(2)
C(30)	30(3)	31(3)	32(3)	6(2)	6(2)	-1(2)
C(31)	31(3)	31(3)	31(3)	8(2)	5(2)	-2(2)
C(32)	32(3)	38(3)	28(3)	9(2)	8(2)	-7(2)
C(33)	33(3)	31(3)	29(3)	5(2)	9(2)	-2(2)
C(34)	36(3)	38(3)	26(3)	5(2)	11(2)	0(2)
C(35)	29(3)	33(3)	29(3)	5(2)	3(2)	-2(2)
C(36)	43(4)	38(3)	33(3)	9(2)	8(2)	-5(2)
C(37)	41(4)	44(3)	37(3)	17(3)	12(2)	1(3)
C(38)	49(4)	53(4)	28(3)	18(3)	7(2)	5(3)
C(39)	36(3)	52(4)	29(3)	9(3)	2(2)	-8(3)
C(40)	38(3)	35(3)	34(3)	10(2)	8(2)	-7(2)
C(41)	27(3)	31(3)	28(3)	8(2)	2(2)	-1(2)
C(42)	42(3)	35(3)	31(3)	8(2)	14(2)	-8(2)
C(43)	40(3)	35(3)	27(3)	12(2)	9(2)	-6(2)
C(44)	28(3)	30(3)	29(3)	5(2)	5(2)	3(2)
C(45)	42(3)	26(3)	38(3)	8(2)	2(2)	-9(2)
C(46)	36(3)	40(3)	33(3)	15(2)	7(2)	0(2)
C(47)	30(3)	32(3)	31(3)	7(2)	6(2)	-2(2)
C(48)	39(3)	34(3)	32(3)	8(2)	6(2)	-8(2)
C(49)	36(3)	37(3)	32(3)	4(2)	6(2)	3(2)
C(50)	39(3)	46(3)	29(3)	-3(3)	7(2)	-12(3)
C(51)	45(4)	33(3)	43(4)	3(2)	8(3)	-7(3)
C(52)	36(3)	33(3)	37(3)	8(2)	10(2)	3(2)
N(1)	27(3)	23(2)	31(3)	4(2)	7(2)	4(2)
O(1)	57(3)	33(2)	26(2)	9(2)	12(2)	-2(2)
O(2)	32(2)	45(3)	26(2)	9(2)	6(2)	-6(2)
O(3)	37(2)	31(2)	33(2)	9(2)	8(2)	-1(2)
O(4)	38(2)	28(2)	24(2)	4(2)	-3(2)	-10(2)
O(5)	31(2)	36(2)	29(2)	4(2)	5(2)	-2(2)
O(6)	36(2)	35(2)	31(2)	10(2)	3(2)	-2(2)
O(7)	38(2)	37(2)	26(2)	11(2)	6(2)	-1(2)
O(8)	35(2)	30(2)	28(2)	5(2)	4(2)	-8(2)
P(1)	33(2)	29(2)	24(2)	5(1)	4(1)	-4(1)
P(2)	33(2)	30(2)	25(2)	7(1)	5(1)	-5(1)
Na(1)	32(2)	36(2)	23(2)	8(1)	6(1)	-2(1)
S(1)	47(2)	31(2)	30(2)	4(1)	8(1)	-3(1)
S(2)	30(2)	40(2)	31(2)	10(1)	6(1)	-4(1)

Table 5. Hydrogen coordinates (x 10^4) and isotropic displacement parameters ($Å^2$x 10^3) for 2008ZP2.

	x	y	z	U(eq)		x	y	z	U(eq)	
H(1A)	2015	-1705	1974	56		H(3A)	1296	-1434	3957	62
H(1B)	3001	-1863	1334	56		H(3B)	254	-1517	4538	62
H(1C)	3355	-966	2096	56		H(3C)	1832	-1889	4693	62
H(2A)	5890	-1282	2445	80		H(4A)	2196	-1036	6089	68
H(2B)	5716	-2172	1680	80		H(4B)	719	-516	6033	68
H(2C)	6527	-2294	2525	80		H(4C)	2191	105	6452	68

H(6)	-1864	1356	2349	39	H(30)	3788	2675	1850	38
H(7)	-2943	2290	1513	37	H(31)	2786	3235	764	37
H(9)	-42	1519	141	42	H(33)	2997	599	-684	37
H(10)	1012	552	960	40	H(34)	3967	22	405	40
H(12)	-4222	2516	263	47	H(36)	2529	3769	-308	46
H(13)	-5048	3659	-416	48	H(37)	1500	4269	-1426	47
H(14)	-3433	4570	-823	56	H(38)	309	3160	-2567	51
H(15)	-986	4317	-531	54	H(39)	174	1523	-2583	48
H(16)	-174	3181	161	48	H(40)	1246	1008	-1476	43
H(18)	-440	3177	4036	38	H(42)	5113	1789	4361	42
H(19)	153	4192	5303	36	H(43)	5856	2801	5638	40
H(21)	3296	2497	5907	40	H(45)	7227	4858	4709	43
H(22)	2723	1449	4642	37	H(46)	6387	3877	3442	42
H(24)	446	4807	6629	43	H(48)	7496	3488	6683	42
H(25)	1335	5909	7838	44	H(49)	8434	4439	7935	43
H(26)	3738	5989	8447	46	H(50)	8634	6127	8147	49
H(27)	5266	4918	7858	40	H(51)	7873	6825	7104	50
H(28)	4425	3833	6652	39	H(52)	6907	5877	5843	42

Table 6. Torsion angles [°] for 2008ZP2.

O(4)-C(5)-C(6)-C(7)	179.0(4)	C(29)-C(30)-C(31)-C(32)	0.7(8)
C(10)-C(5)-C(6)-C(7)	-5.2(8)	C(30)-C(31)-C(32)-C(33)	-2.6(8)
C(5)-C(6)-C(7)-C(8)	0.1(8)	C(30)-C(31)-C(32)-C(35)	178.0(5)
C(6)-C(7)-C(8)-C(9)	4.1(8)	C(31)-C(32)-C(33)-C(34)	3.2(8)
C(6)-C(7)-C(8)-C(11)	-171.3(5)	C(35)-C(32)-C(33)-C(34)	-177.4(5)
C(7)-C(8)-C(9)-C(10)	-3.3(8)	O(7)-C(29)-C(34)-C(33)	179.5(5)
C(11)-C(8)-C(9)-C(10)	172.2(5)	C(30)-C(29)-C(34)-C(33)	-0.1(8)
C(8)-C(9)-C(10)-C(5)	-1.7(8)	C(32)-C(33)-C(34)-C(29)	-1.9(8)
O(4)-C(5)-C(10)-C(9)	-178.2(4)	C(31)-C(32)-C(35)-C(40)	-156.9(5)
C(6)-C(5)-C(10)-C(9)	6.0(8)	C(33)-C(32)-C(35)-C(40)	23.7(8)
C(7)-C(8)-C(11)-C(16)	137.8(6)	C(31)-C(32)-C(35)-C(36)	22.9(8)
C(9)-C(8)-C(11)-C(16)	-37.6(8)	C(33)-C(32)-C(35)-C(36)	-156.5(5)
C(7)-C(8)-C(11)-C(12)	-40.2(8)	C(40)-C(35)-C(36)-C(37)	-1.9(8)
C(9)-C(8)-C(11)-C(12)	144.5(6)	C(32)-C(35)-C(36)-C(37)	178.3(5)
C(16)-C(11)-C(12)-C(13)	-0.9(8)	C(35)-C(36)-C(37)-C(38)	1.4(9)
C(8)-C(11)-C(12)-C(13)	177.1(5)	C(36)-C(37)-C(38)-C(39)	-0.2(9)
C(11)-C(12)-C(13)-C(14)	0.7(9)	C(37)-C(38)-C(39)-C(40)	-0.6(9)
C(12)-C(13)-C(14)-C(15)	-0.1(9)	C(36)-C(35)-C(40)-C(39)	1.1(8)
C(13)-C(14)-C(15)-C(16)	-0.3(9)	C(32)-C(35)-C(40)-C(39)	-179.1(5)
C(14)-C(15)-C(16)-C(11)	0.0(9)	C(38)-C(39)-C(40)-C(35)	0.1(9)
C(12)-C(11)-C(16)-C(15)	0.5(9)	C(46)-C(41)-C(42)-C(43)	-0.6(9)
C(8)-C(11)-C(16)-C(15)	-177.5(5)	O(8)-C(41)-C(42)-C(43)	177.3(5)
C(22)-C(17)-C(18)-C(19)	1.6(8)	C(41)-C(42)-C(43)-C(44)	0.1(9)
O(5)-C(17)-C(18)-C(19)	179.6(4)	C(42)-C(43)-C(44)-C(45)	-1.2(8)
C(17)-C(18)-C(19)-C(20)	1.7(8)	C(42)-C(43)-C(44)-C(47)	-175.8(5)
C(18)-C(19)-C(20)-C(21)	-4.3(8)	C(43)-C(44)-C(45)-C(46)	2.9(9)
C(18)-C(19)-C(20)-C(23)	173.4(5)	C(47)-C(44)-C(45)-C(46)	177.4(5)
C(19)-C(20)-C(21)-C(22)	4.1(8)	C(44)-C(45)-C(46)-C(41)	-3.4(9)
C(23)-C(20)-C(21)-C(22)	-173.8(5)	C(42)-C(41)-C(46)-C(45)	2.2(9)
O(5)-C(17)-C(22)-C(21)	-179.7(5)	O(8)-C(41)-C(46)-C(45)	-175.8(5)
C(18)-C(17)-C(22)-C(21)	-1.8(8)	C(43)-C(44)-C(47)-C(48)	24.3(8)
C(20)-C(21)-C(22)-C(17)	-1.1(8)	C(45)-C(44)-C(47)-C(48)	-150.1(6)
C(19)-C(20)-C(23)-C(28)	-150.5(5)	C(43)-C(44)-C(47)-C(52)	-154.3(5)
C(21)-C(20)-C(23)-C(28)	27.2(7)	C(45)-C(44)-C(47)-C(52)	31.2(8)
C(19)-C(20)-C(23)-C(24)	26.9(8)	C(52)-C(47)-C(48)-C(49)	-2.8(8)
C(21)-C(20)-C(23)-C(24)	-155.4(5)	C(44)-C(47)-C(48)-C(49)	178.5(5)
C(28)-C(23)-C(24)-C(25)	-0.6(8)	C(47)-C(48)-C(49)-C(50)	1.0(9)
C(20)-C(23)-C(24)-C(25)	-178.0(5)	C(48)-C(49)-C(50)-C(51)	0.6(9)
C(23)-C(24)-C(25)-C(26)	0.5(9)	C(49)-C(50)-C(51)-C(52)	-0.3(9)
C(24)-C(25)-C(26)-C(27)	-0.8(9)	C(50)-C(51)-C(52)-C(47)	-1.6(9)
C(25)-C(26)-C(27)-C(28)	1.3(8)	C(48)-C(47)-C(52)-C(51)	3.0(8)
C(26)-C(27)-C(28)-C(23)	-1.4(8)	C(44)-C(47)-C(52)-C(51)	-178.3(5)
C(24)-C(23)-C(28)-C(27)	1.0(8)	C(6)-C(5)-O(4)-P(1)	-89.7(5)
C(20)-C(23)-C(28)-C(27)	178.6(5)	C(10)-C(5)-O(4)-P(1)	94.4(5)
O(7)-C(29)-C(30)-C(31)	-178.9(5)	C(22)-C(17)-O(5)-P(1)	-18.7(7)
C(34)-C(29)-C(30)-C(31)	0.7(8)	C(18)-C(17)-O(5)-P(1)	163.2(4)

C(34)-C(29)-O(7)-P(2)	-151.4(4)
C(30)-C(29)-O(7)-P(2)	28.1(7)
C(42)-C(41)-O(8)-P(2)	14.2(7)
C(46)-C(41)-O(8)-P(2)	-167.8(4)
Na(1)-O(3)-P(1)-N(1)	6.4(4)
Na(1)-O(3)-P(1)-O(4)	133.9(3)
Na(1)-O(3)-P(1)-O(5)	-121.1(3)
P(2)-N(1)-P(1)-O(3)	16.3(5)
P(2)-N(1)-P(1)-O(4)	-109.8(4)
P(2)-N(1)-P(1)-O(5)	146.4(3)
C(5)-O(4)-P(1)-O(3)	176.4(4)
C(5)-O(4)-P(1)-N(1)	-50.5(5)
C(5)-O(4)-P(1)-O(5)	60.2(4)
C(17)-O(5)-P(1)-O(3)	59.8(4)
C(17)-O(5)-P(1)-N(1)	-74.6(4)
C(17)-O(5)-P(1)-O(4)	171.6(4)
Na(1)-O(6)-P(2)-N(1)	-11.9(4)
Na(1)-O(6)-P(2)-O(7)	-138.2(3)
Na(1)-O(6)-P(2)-O(8)	116.1(3)
P(1)-N(1)-P(2)-O(6)	-14.1(5)
P(1)-N(1)-P(2)-O(7)	110.3(4)
P(1)-N(1)-P(2)-O(8)	-144.0(3)
P(1)-N(1)-P(2)-Na(1)	-20.0(4)
C(29)-O(7)-P(2)-O(6)	172.0(4)
C(29)-O(7)-P(2)-N(1)	40.1(5)
C(29)-O(7)-P(2)-O(8)	-72.1(4)
C(29)-O(7)-P(2)-Na(1)	146.9(4)
C(41)-O(8)-P(2)-O(6)	-63.2(4)
C(41)-O(8)-P(2)-N(1)	71.0(4)
C(41)-O(8)-P(2)-O(7)	-174.5(4)
C(41)-O(8)-P(2)-Na(1)	-30.7(4)
S(1)-O(1)-Na(1)-O(6)	-18.0(4)
S(1)-O(1)-Na(1)-O(2)	156.5(3)
S(1)-O(1)-Na(1)-O(2)#1	-114.2(3)
S(1)-O(1)-Na(1)-O(3)	69.4(3)
S(1)-O(1)-Na(1)-S(2)	134.0(3)
S(1)-O(1)-Na(1)-P(2)	-0.6(4)
S(1)-O(1)-Na(1)-Na(1)#1	-159.1(3)
P(2)-O(6)-Na(1)-O(1)	122.1(3)
P(2)-O(6)-Na(1)-O(2)	-48.6(5)
P(2)-O(6)-Na(1)-O(2)#1	-123.6(3)
P(2)-O(6)-Na(1)-O(3)	22.6(3)
P(2)-O(6)-Na(1)-S(2)	-10.7(4)
P(2)-O(6)-Na(1)-Na(1)#1	-98.7(3)
S(2)-O(2)-Na(1)-O(1)	-76.3(3)
Na(1)#1-O(2)-Na(1)-O(1)	112.05(18)
S(2)-O(2)-Na(1)-O(6)	94.1(3)
Na(1)#1-O(2)-Na(1)-O(6)	-77.6(3)
S(2)-O(2)-Na(1)-O(2)#1	171.6(3)
Na(1)#1-O(2)-Na(1)-O(2)#1	0.0
S(2)-O(2)-Na(1)-O(3)	22.4(3)
Na(1)#1-O(2)-Na(1)-O(3)	-149.22(17)
Na(1)#1-O(2)-Na(1)-S(2)	-171.6(3)
S(2)-O(2)-Na(1)-P(2)	74.9(3)
Na(1)#1-O(2)-Na(1)-P(2)	-96.73(17)
S(2)-O(2)-Na(1)-Na(1)#1	171.6(3)
P(1)-O(3)-Na(1)-O(1)	-122.1(3)
P(1)-O(3)-Na(1)-O(6)	-19.6(3)
P(1)-O(3)-Na(1)-O(2)	128.5(3)
P(1)-O(3)-Na(1)-O(2)#1	63.8(4)
P(1)-O(3)-Na(1)-S(2)	137.9(3)
P(1)-O(3)-Na(1)-P(2)	-11.7(2)
P(1)-O(3)-Na(1)-Na(1)#1	105.9(3)
O(6)-P(2)-Na(1)-O(1)	-63.3(3)
N(1)-P(2)-Na(1)-O(1)	106.5(2)
O(7)-P(2)-Na(1)-O(1)	-9.8(2)
O(8)-P(2)-Na(1)-O(1)	-142.4(2)
N(1)-P(2)-Na(1)-O(6)	169.8(3)
O(7)-P(2)-Na(1)-O(6)	53.5(3)
O(8)-P(2)-Na(1)-O(6)	-79.1(3)
O(6)-P(2)-Na(1)-O(2)	146.0(3)
N(1)-P(2)-Na(1)-O(2)	-44.2(2)
O(7)-P(2)-Na(1)-O(2)	-160.5(2)
O(8)-P(2)-Na(1)-O(2)	66.9(2)
O(6)-P(2)-Na(1)-O(2)#1	58.0(3)
N(1)-P(2)-Na(1)-O(2)#1	-132.25(19)
O(7)-P(2)-Na(1)-O(2)#1	111.5(2)
O(8)-P(2)-Na(1)-O(2)#1	-21.1(2)
O(6)-P(2)-Na(1)-O(3)	-155.5(3)
N(1)-P(2)-Na(1)-O(3)	14.26(19)
O(7)-P(2)-Na(1)-O(3)	-102.0(2)
O(8)-P(2)-Na(1)-O(3)	125.4(2)
O(6)-P(2)-Na(1)-S(2)	172.1(3)
N(1)-P(2)-Na(1)-S(2)	-18.15(18)
O(7)-P(2)-Na(1)-S(2)	-134.41(19)
O(8)-P(2)-Na(1)-S(2)	92.98(19)
O(6)-P(2)-Na(1)-Na(1)#1	94.1(3)
N(1)-P(2)-Na(1)-Na(1)#1	-96.17(19)
O(7)-P(2)-Na(1)-Na(1)#1	147.6(2)
O(8)-P(2)-Na(1)-Na(1)#1	15.0(2)
Na(1)-O(1)-S(1)-C(2)	63.7(4)
Na(1)-O(1)-S(1)-C(1)	-38.5(4)
Na(1)-O(2)-S(2)-C(3)	58.7(3)
Na(1)#1-O(2)-S(2)-C(3)	-134.0(4)
Na(1)-O(2)-S(2)-C(4)	161.9(3)
Na(1)#1-O(2)-S(2)-C(4)	-30.8(5)
Na(1)#1-O(2)-S(2)-Na(1)	167.2(5)
O(1)-Na(1)-S(2)-O(2)	110.3(3)
O(6)-Na(1)-S(2)-O(2)	-116.9(3)
O(2)#1-Na(1)-S(2)-O(2)	-8.5(4)
O(3)-Na(1)-S(2)-O(2)	-154.8(3)
P(2)-Na(1)-S(2)-O(2)	-121.1(3)
Na(1)#1-Na(1)-S(2)-O(2)	-6.1(3)
O(1)-Na(1)-S(2)-C(3)	-14.4(2)
O(6)-Na(1)-S(2)-C(3)	118.3(3)
O(2)-Na(1)-S(2)-C(3)	-124.7(3)
O(2)#1-Na(1)-S(2)-C(3)	-133.2(2)
O(3)-Na(1)-S(2)-C(3)	80.4(2)
P(2)-Na(1)-S(2)-C(3)	114.2(2)
Na(1)#1-Na(1)-S(2)-C(3)	-130.9(2)
O(1)-Na(1)-S(2)-C(4)	82.6(4)
O(6)-Na(1)-S(2)-C(4)	-144.6(4)
O(2)-Na(1)-S(2)-C(4)	-27.7(4)
O(2)#1-Na(1)-S(2)-C(4)	-36.2(4)
O(3)-Na(1)-S(2)-C(4)	177.5(4)
P(2)-Na(1)-S(2)-C(4)	-148.7(4)
Na(1)#1-Na(1)-S(2)-C(4)	-33.8(4)

Symmetry transformations used to generate equivalent atoms:

#1 -x+1,-y,-z+1